A STUDY OF THE MECHANISM OF VORTEX INHIBITION

by

© Shingo Ishikawa

B.S., Waseda University (1971)

B.Eng., Waseda University (1973)

S.M., Massachusetts Institute of Technology (1975)

SUBMITTED IN PARTIAL FULFILLMENT

OF THE REQUIREMENT FOR THE

DEGREE OF DOCTOR OF SCIENCE

at the

MASSACHUSETTS INSTITUTE OF TECHNOLOGY

August, 1979

Signature of Author: ....
Department of Chemical Engineering
August 10, 1979

Certified by: ....
R.C. Armstrong, Thesis Supervisor

Accepted by: ....
G.C. Williams, Chairman,
Departmental Committee on Graduate Theses

A STUDY OF THE MECHANISM OF VORTEX INHIBITION

by

Shingo Ishikawa

Submitted to the Department of Chemical Engineering on August 10, 1979, in partial fulfillment of the degree of Doctor of Science at the Massachusetts Institute of Technology.

ABSTRACT

The mechanism of vortex inhibition by dilute polymer solutions which also show drag reduction is discussed. The velocity field for a confined vortex flow of a Newtonian fluid has been determined numerically by a finite difference (ADI) technique; the results compare favorably with experimental velocity profiles found for water.

To model the behavior of dilute polymer solutions in this flow we have idealized the macromolecules as dumbbells with finitely extendable, nonlinear, elastic (FENE) connectors. An approximate constitutive equation for this model is combined with the numerically determined Newtonian velocity profiles to give the response to the polymer molecules to the vortex flow.

It is found that appreciable stretching and accompanying increase in elongational viscosity of the macromolecules occurs in the immediate vicinity of the exhaust hole. We believe that the change in stress field produced in this way is sufficient to account for vortex inhibition.

THESIS SUPERVISOR: Professor Robert C. Armstrong
Department of Chemical Engineering

Department of Chemical Engineering
Massachusetts Institute of Technology
Cambridge, Massachusetts 02139

August 10, 1979

Professor George C. Newton, Jr.
Secretary of the Faculty
Massachusetts Institute of Technology
Cambridge, Massachusetts 02139

Dear Professor Newton:

In accordance with the regulations of the faculty, I herewith submit a thesis, entitled "A Study of the Mechanism of Vortex Inhibition", in partial fulfillment of the requirements for the degree of Doctor of Science in Chemical Engineering at the Massachusetts Institute of Technology.

Respectfully submitted,

Shingo Ishikawa

ACKNOWLEDGEMENT

First, I wish to extend my sincere appreciation to my supervisor, Professor R.C. Armstrong, for suggesting the topic and his consistent interest, advice and guidance throughout this thesis investigation. I also wish to thank Professor K.A. Smith for his helpful advice and criticism. Dr. L.A. Clomburg deserves special thanks for his excellent advice on numerical simulation.

Thanks are also due to Professor Edgerton for providing the information about the strobe scope. Discussion with Dr. K.J. Wong and Mr. T.B. Irwin about the numerical calculation scheme contributed materially to the work.

The financial support from the National Science Foundation for part of this work is acknowledged.

I am indebt to my dearest friend, Keiko, who has given immeasurable encouragement with her love in the last two years. Without her continuous encouragement, this work could never have been completed. I also appreciate my brother-in-law for his long term guidance to my education.

Finally, I wish to thank my parents and the rest of my family for their continual stimulation (sometimes painful criticism) and support during my stay at M.I.T. It has been their love, patience and understanding that helped make this educational goal possible.

TABLE OF CONTENTS

LIST OF FIGURES

LIST OF TABLES

I. SUMMARY

1.1 Introduction

The viscoelastic phenomenon "vortex inhibition" was discovered by Gordon (1972) in 1972. In his experiment, a small amount of polymer in water prevents formation of a vortex in draining the solution from the bottom of a square tank (see Fig. 2.1). As shown in Fig. 2.1 this different phenomenological behavior produced by adding just small amounts of polymer indicates that the flow pattern is drastically changed due to the presence of the polymer. In order to describe vortex inhibition more explicitly, a steady state vortex flow is established by tangentially feeding the water at the outer wall of a cylindrical container with an axially uniform velocity. The steady state vortex flow is shown in Fig. 2.2. When the water is replaced by approximately 30 wppm polyethylene oxide (Polyox WSR 301) keeping the flow rate constant, the air core of the vortex is suppressed and the suppression of the air core is not steady but a randomly periodic phenomenon. Just after the air core is suppressed, it tends to extend to the bottom again. As soon as the air core reaches the bottom, it immedately is suppressed (See Fig. 2.3). This process is repeated until the polymer is degraded. During vortex inhibition, the liquid level drops by nearly 50%.

An interesting feature of vortex inhibition is that the amount of polymer added to the water is so small that the

Fig. 2.1 : Vortex Inhibition

In case of the Newtonian fluid, the vortex forms extending down to the bottom. On the other hand, if a small, critical concentration of polymer is present, the vortex is imcomplete.

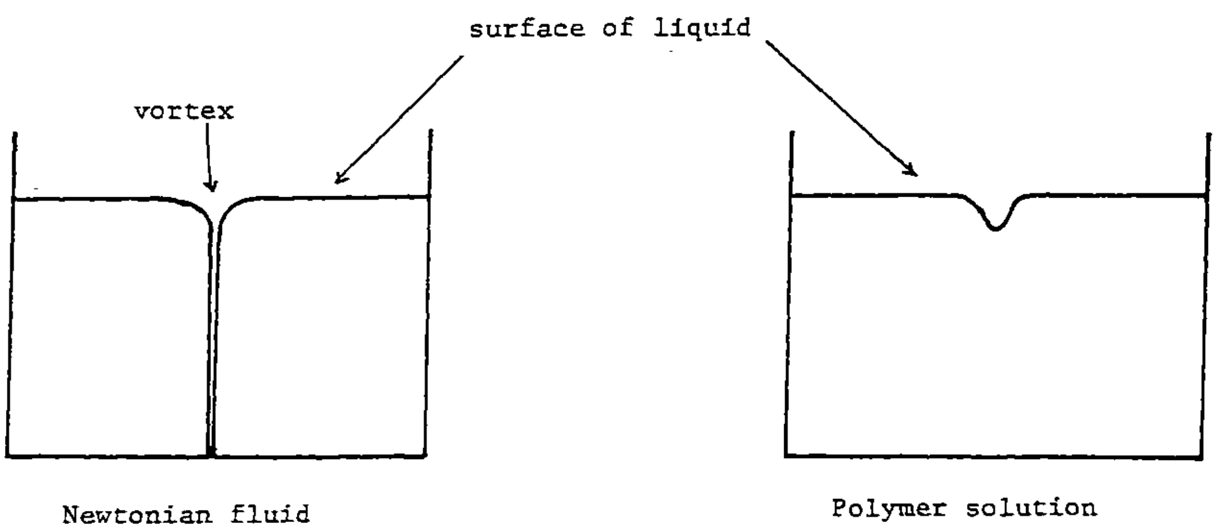

Fig. 2.2 Steady State Vortex Flow

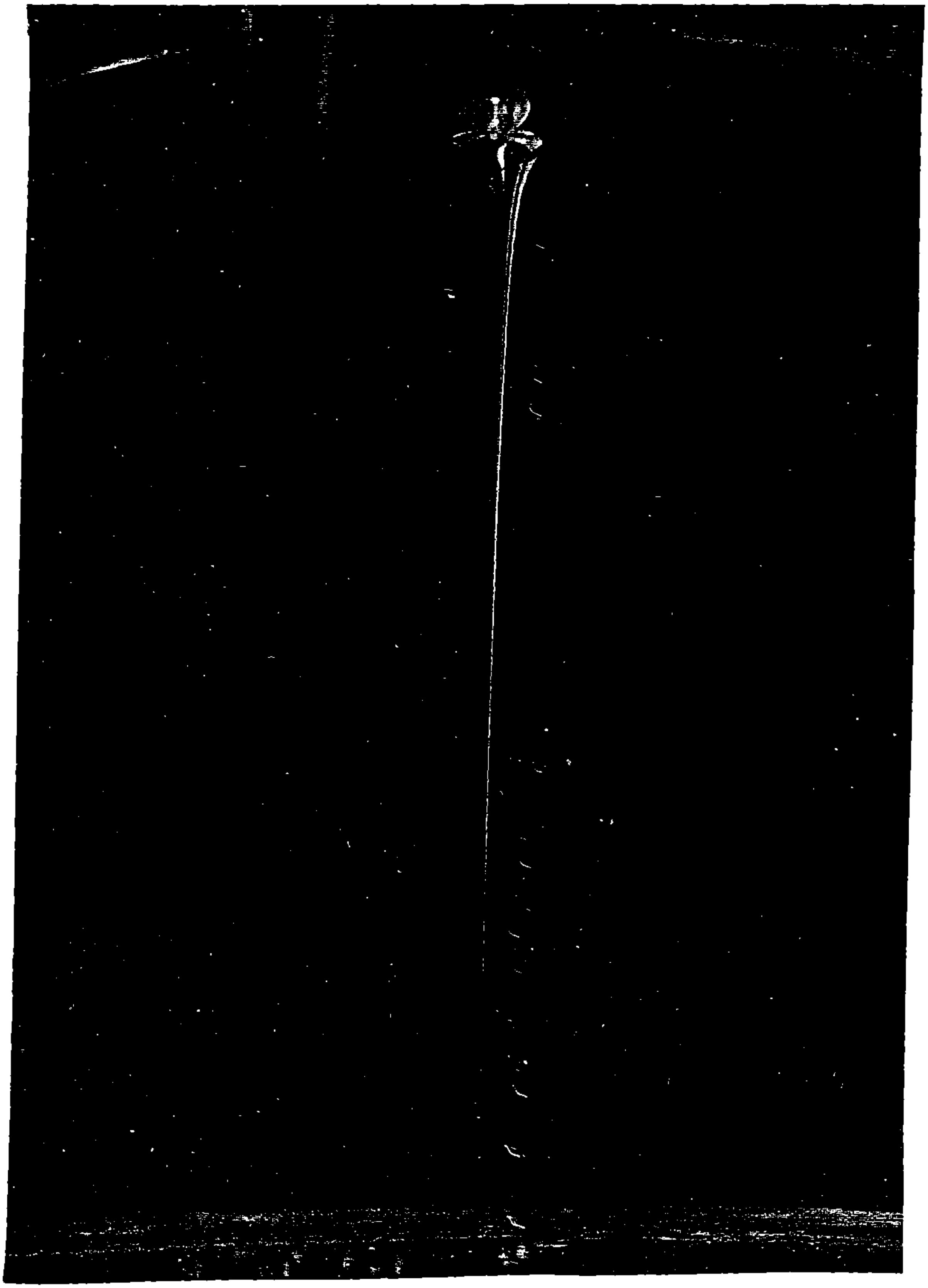

Fig. 2.3 Vortex Flow with Suppressed Air Core

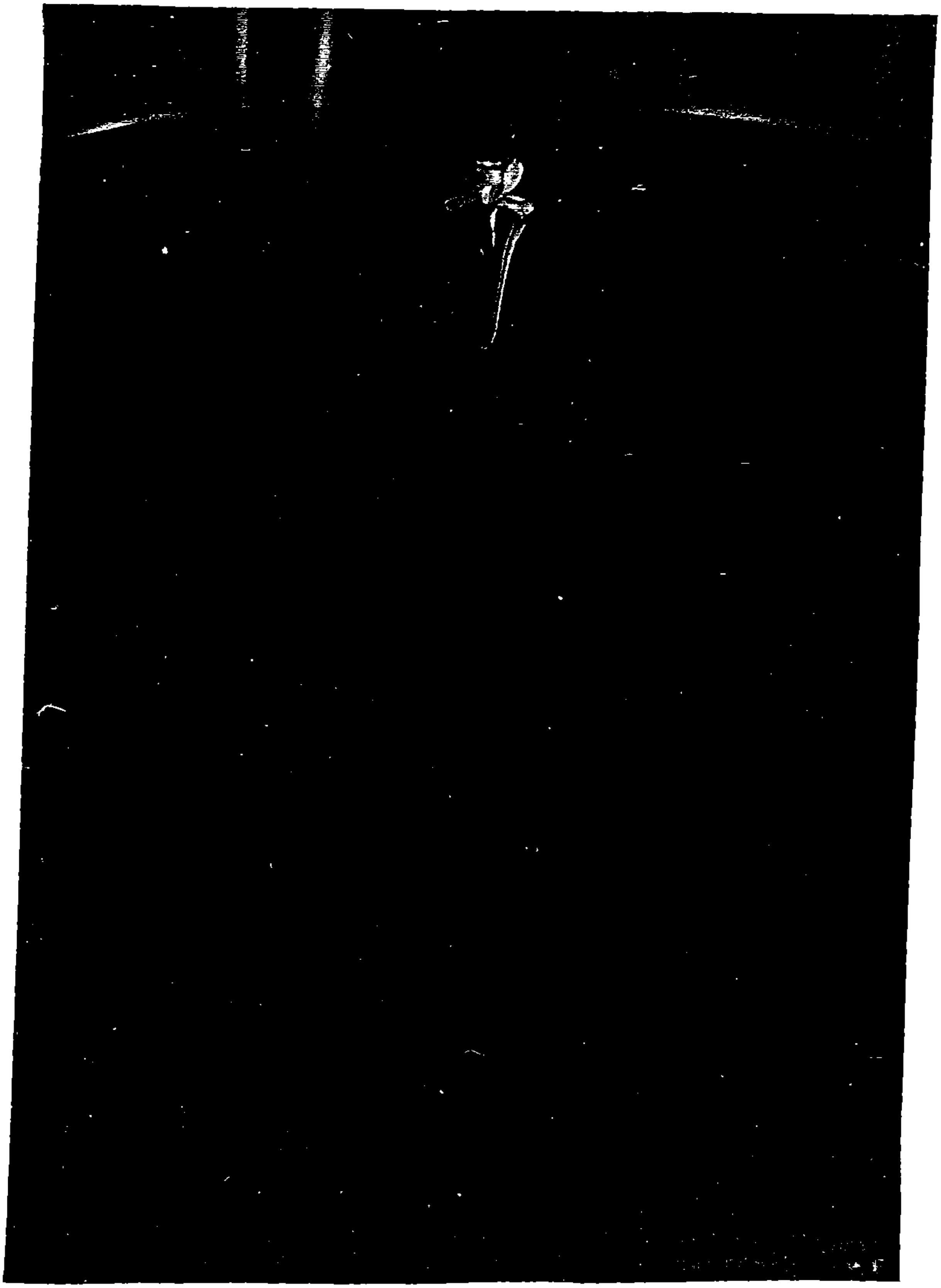

shear viscosity of the polymer solution is only slightly different from that of water itself (The relative viscosity of the solution in this study is only about 1.02). Furthermore, the macromolecules which show vortex inhibition ability are also known to be good agents for drag reduction as shown in TABLE 2.1.

Since the shear viscosity of the polymer solution is almost equal to that of water for both vortex inhibition and drag reduction, non-Newtonian rheological properties of the dilute solutions such as strain rate thickening elongational viscosity and non-zero normal stress differences in steady shear flow might be responsible for vortex inhibition. Especially the elongational viscosity is believed to be increased drastically even at moderately high elongational rate for a dilute solution. Even though no direct experimental measurements have been obtained for the elongational viscosity, the kinetic theory predicts that a high elongational viscosity is realized when a linear flexible macromolecule is stretched at almost full length due to the elongational flow field. It may, therefore, be possible to expect that the changes in flow behavior in vortex inhibition phenomenon is due to the large elongational viscosity exerted by the presence of a few macromolecules.

The objective of this thesis work is to investigate the mechanism of vortex inhibition. The study is motivated at first, by a possible correlation between vortex inhibition and drag reduction and secondly, by an interest in

TABLE 2.1

EFFECTIVE CONCENTRATIONS OF VARIOUS POLYMERS FOR V.I. AND D.R.

Polymer Designation	Polymer Type	wwpm Vortex Inhibition	wwpm Drag Reduction
Polyox FRA*	Polyethylene Oxide	7.5	9
Polyox WSR 301*	Polyethylene Oxide	30	20
Separan AP 273·	Polyacrylamide	3	5
Separan AP30·	Polyacrylamide	40	35

*Union Carbide (Manufacturer)

·Dow (Manufacturer)

Note 1: These data are from Gordon (1972).

Note 2: Effective concentration is the lowest concentration with which polymer shows the ability of vortex inhibition or drag reduction.

developing a constitutive equation (rheological equation of state) to describe dilute polymer solutions.

We can speculate from TABLE 2.1 that the mechanism of vortex inhibition may be similar to that of drag reduction. In spite of extensive studies of drag reduction, many aspects of the phenomenon are not well understood. Out of several proposed mechanisms for drag reduction, the visco-elastic nature (especially large elongational viscosity) of macromolecules in turbulent flow is proposed to be a major cause of reducing turbulent energy dissipation. According to Seyer and Metzner (1969), the bursting (Kim et al., 1971) produced by a pair of counter rotating eddies at boundary layer near the wall is characterized by stretching motion similar to elongational flow. The increased resistance to stretching due to the large elongational viscosity, thus results in less bursting and less radial momentum flox transport. However, it is not possible to make a direct test of this proposed mechanism because no precise velocity information of the fluid element is obtainable during the bursting process. The proposed mechanism for drag reduction may, in turn, be closely related to the molecular mechanism for vortex inhibition. It might be possible to infer the molecular mechanism for drag reduction from the analysis of vortex inhibition. Since the Newtonian vortex flow is treated as a laminar flow, it is much easier to be analyzed than turbulent flow.

In order to analyze vortex inhibition, a constitutive equation for a dilute polymer solution has to be introduced so that information about the stress field can be predicted.

Although a very simplified dumbbell model is used, we believe that the kinetic theory provides reasonable predictions about the differences in flow behavior resulting form molecular structures. Moreover, we can evaluate the kinetic theory constitutive equations by comparing their predictions in this flow with experimental results.

The overall picture of this study is briefly described in Fig. 1.1. The study is mainly divided into two parts; one is to investigate fluid mechanics of vortex flow and the other is to develop the constitutive equation. The study of the vortex flow is further divided into theoretical and experimental parts. The Newtonian velocity field determined from both numerical and experimental results is used for stress calculation by the constitutive equation because the Newtonian velocity field is a starting point for computing deformation of the macromolecules when the polymer solution is subjected to the flow field. The every part of study is then combined in Chapter 6 for the discussion of the results which lead to the conclusion of this study. The summary of these studies are described in the rest of this chapter.

developing a constitutive equation (rheological equation of state) to describe dilute polymer solutions.

We can speculate from TABLE 2.1 that the mechanism of vortex inhibition may be similar to that of drag reduction. In spite of extensive studies of drag reduction, many aspects of the phenomenon are not well understood. Out of several proposed mechanisms for drag reduction, the visco-elastic nature (especially large elongational viscosity) of macromolecules in turbulent flow is proposed to be a major cause of reducing turbulent energy dissipation. According to Seyer and Metzner (1969), the bursting (Kim et al., 1971) produced by a pair of counter rotating eddies at boundary layer near the wall is characterized by stretching motion similar to elongational flow. The increased resistance to stretching due to the large elongational viscosity, thus results in less bursting and less radial momentum flox transport. However, it is not possible to make a direct test of this proposed mechanism because no precise velocity information of the fluid element is obtainable during the bursting process. The proposed mechanism for drag reduction may, in turn, be closely related to the molecular mechanism for vortex inhibition. It might be possible to infer the molecular mechanism for drag reduction from the analysis of vortex inhibition. Since the Newtonian vortex flow is treated as a laminar flow, it is much easier to be analyzed than turbulent flow.

In order to analyze vortex inhibition, a constitutive equation for a dilute polymer solution has to be introduced so that information about the stress field can be predicted.

Although a very simplified dumbbell model is used, we believe that the kinetic theory provides reasonable predictions about the differences in flow behavior resulting form molecular structures. Moreover, we can evaluate the kinetic theory constitutive equations by comparing their predictions in this flow with experimental results.

The overall picture of this study is briefly described in Fig. 1.1. The study is mainly divided into two parts; one is to investigate fluid mechanics of vortex flow and the other is to develop the constitutive equation. The study of the vortex flow is further divided into theoretical and experimental parts. The Newtonian velocity field determined from both numerical and experimental results is used for stress calculation by the constitutive equation because the Newtonian velocity field is a starting point for computing deformation of the macromolecules when the polymer solution is subjected to the flow field. The every part of study is then combined in Chapter 6 for the discussion of the results which lead to the conclusion of this study. The summary of these studies are described in the rest of this chapter.

Fig. 1.1 : The Overall Picture of Vortex Inhibition Study

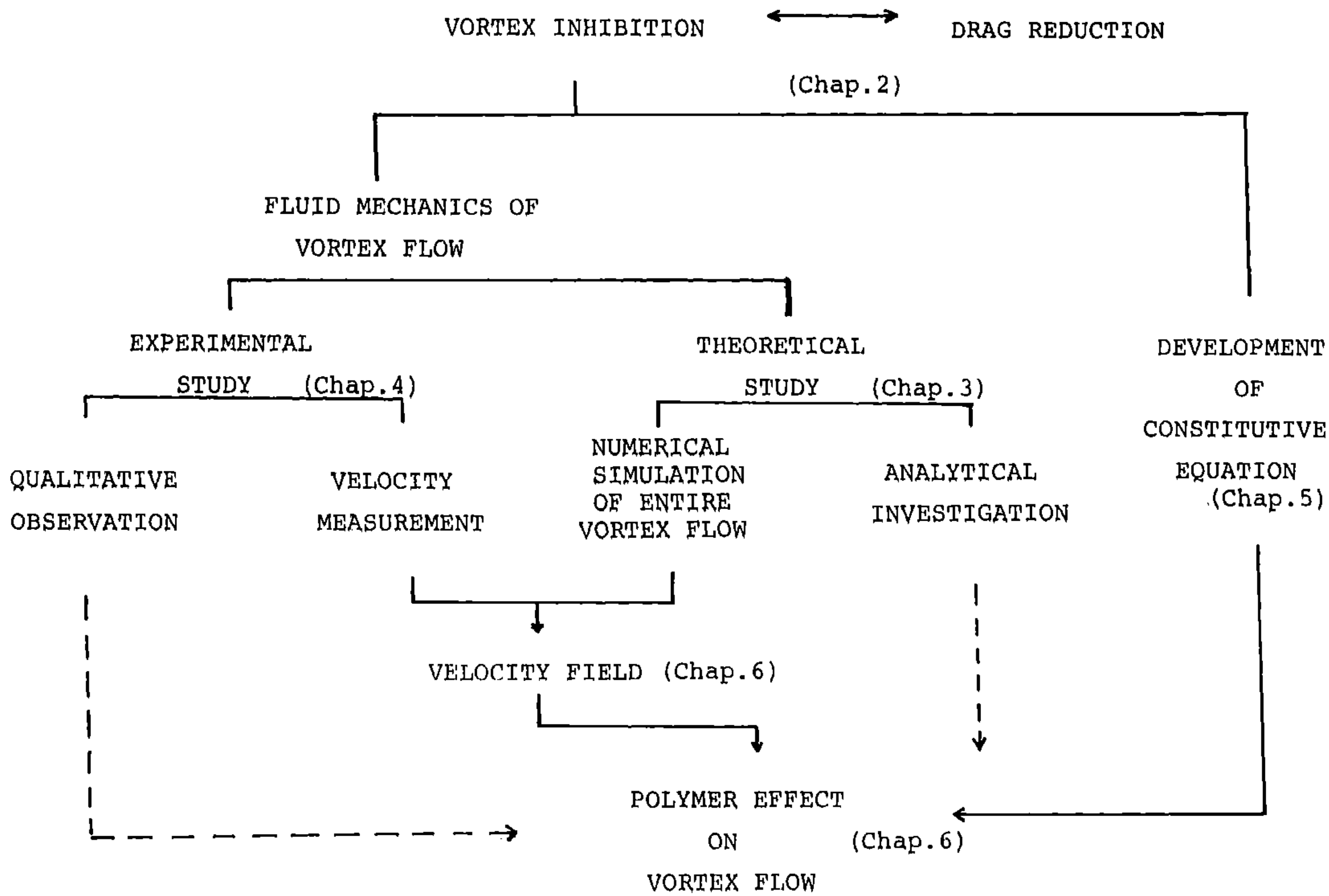

1.2 Fluid Mechanics of Vortex Flow

1.2.1 Theoretical Study

A Newtonian vortex flow has three distinct characteristics in its flow behavior. As shown in Fig. 3.1, the region I is called "free stream region" which is characterized by a potential flow. The tengential velocity V_θ is inversely proportional to the radial distance r in this region. The changes in V_θ in the z-direction is so small that the flow may be treated as one dimensional flow. The region II is called "core region" where a large amount of axial downflow exists because of the exit hole in the bottom plate. The V_θ, in turn, is proportional to the radius in this region. The centrifugal force is exactly balanced with the radial pressure gradient in both free stream and core regions (Schlichting, 1968), the balance between the two forces, however, is broken in the region III which is called "bottom boundary layer". The V_θ in the bottom boundary layer is reduced due to the drag from the bottom wall resulting in decreasing the centrifugal force. The radial pressure gradient, on the other hand, remains the same along the z-axis, this force, therefore, overcomes the centrifugal force producing a large amount of radial inflow.

The tangential velocity in the free stream and core regions is numerically solved assuming that the V_θ is independent of z. The θ-component of the equation of motion is written in terms of circulation Γ $(=rV_\theta)$,

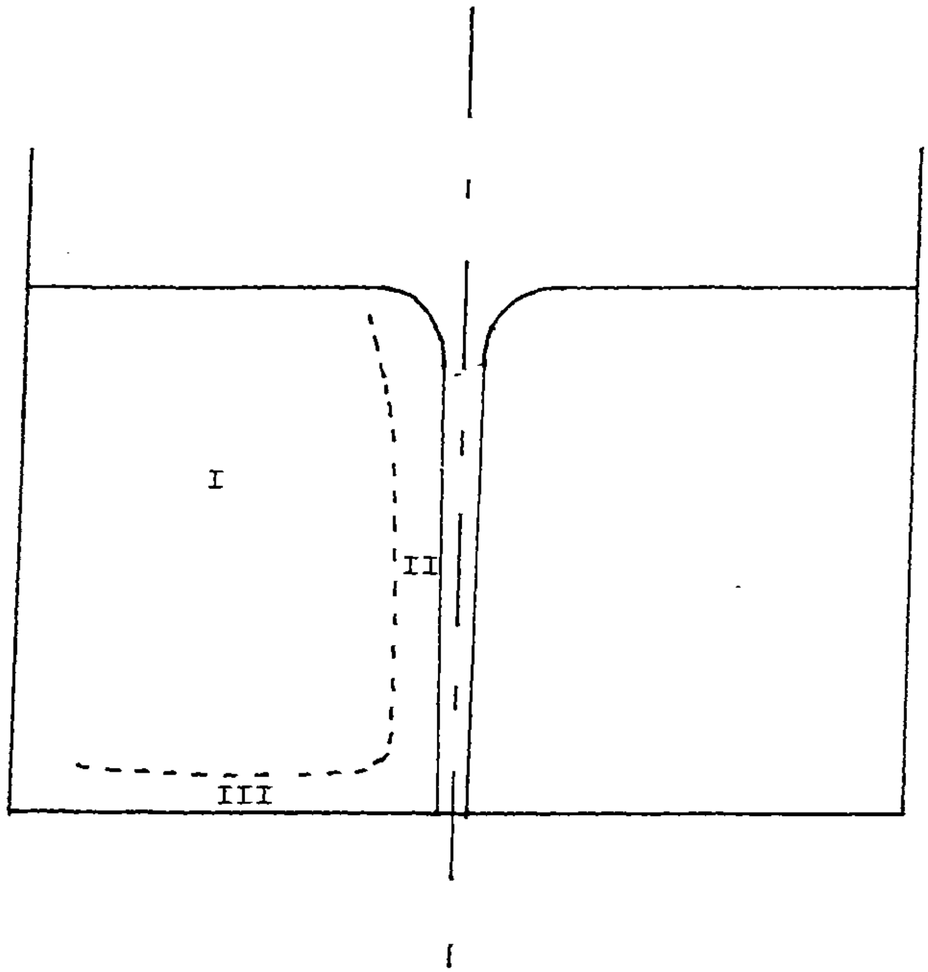

Figure 3.1

Three Different Flow Regions

in a Newtonian Vortex Flow

$$V_r \frac{d\Gamma}{dr} = \nu\left(\frac{d^2\Gamma}{dr^2} - \frac{1}{r}\frac{d\Gamma}{dr}\right) \qquad 1.1$$

where ν is kinetic viscosity. Since the radial velocity V_r is inversely proportional to r when r is large and V_r, in turn, is linear to r when r is small, Dergarabedian (1960) assumes the following functionality of V_r.

$$V_r = -\frac{\dot{\varepsilon}a^2}{2r}\left[1 - \exp\left(-\frac{r^2}{a^2}\right)\right] \qquad 1.2$$

where an elongational rate at the axis of rotation $\dot{\varepsilon}$ is defined by

$$\dot{\varepsilon} = \dot{\varepsilon}(z) = \left.\frac{\partial V_z}{\partial z}\right|_{r=0} \qquad 1.3$$

Using experimentally determined a and $\dot{\varepsilon}$ in eq. 1.2 (Chiou, 1976), eq. 1.1 is solved by a finite difference scheme with the boundary conditions $\Gamma(r=0) = 0$ and $\Gamma(r=R) = \Gamma_R$. The calculated V_θ in these regions agrees well with Chiou's experimental data (case 1 in Fig. 1.2). It is found from the numerical simulation that the tangential velocity is very sensitive to the elongational rate $\dot{\varepsilon}$. When $\dot{\varepsilon}$ is increased, the radial convection shifts the peak value of V_θ toward the axis of rotation producing a steeper V_θ- profile (case 2 in Fig. 1.2) which indicates that the increased $\dot{\varepsilon}$ intensifies the θ-component of vorticity near the axis of

Fig. 1.2

TANGENTIAL VELOCITY VS R

(With Experimental Data)

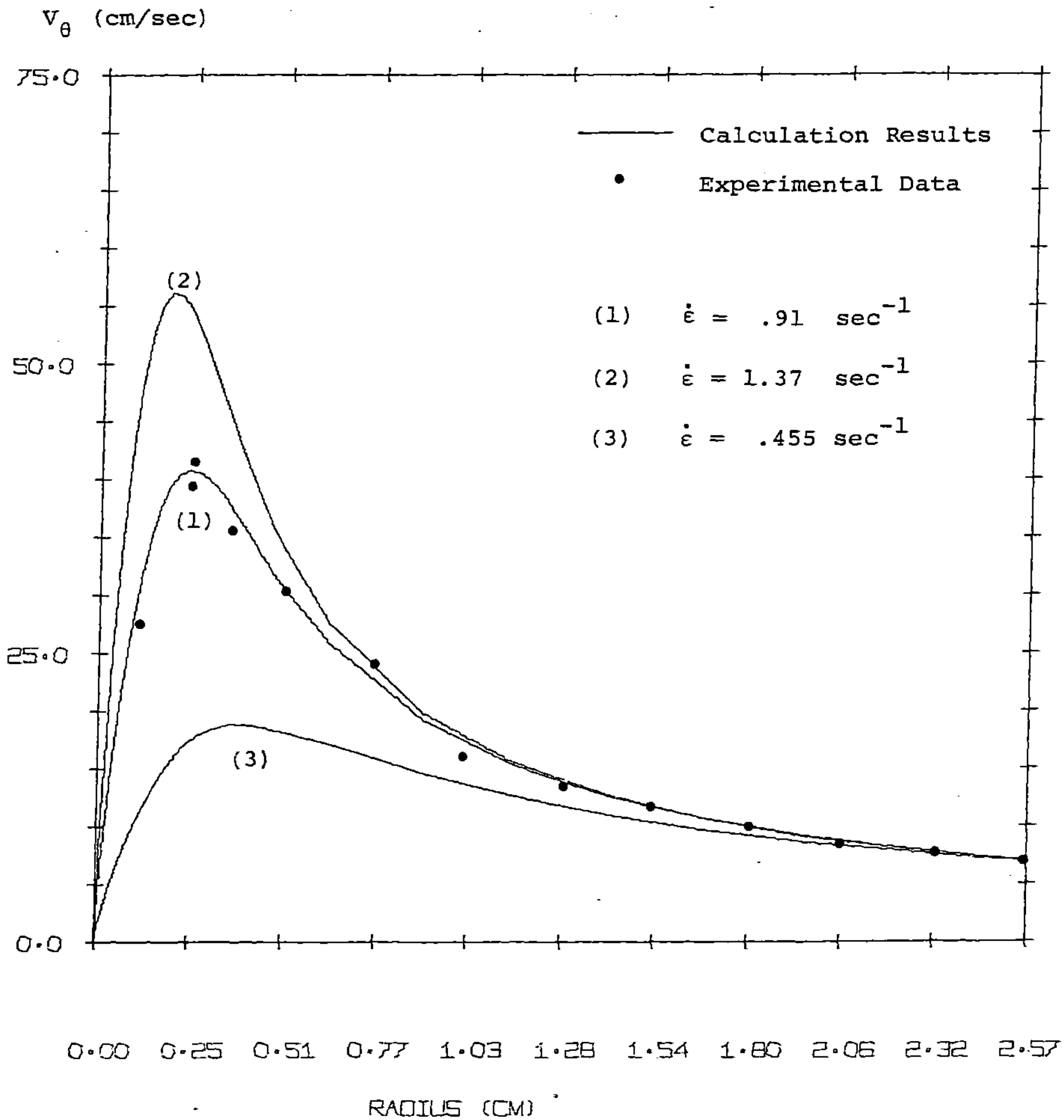

rotation. On the other hand, when $\dot{\varepsilon}$ is decreased, the vorticity is able to diffuse farther in the positive r-direction resulting in a flatter V_θ-profile (case 3 in Fig. 1.2). Since V_θ near the axis of rotation is reduced, the corresponding centrifugal force is also decreased. The radial pressure gradient which is balanced with the centrifugal force is then reduced.

The relative shape of the free surface of these vortex flows can be obtained from the tangential velocity as a function of r. Fig. 3.4 shows the calculated free surfaces with the three elongational rates corresponding to Fig. 1.2. As expected, when $\dot{\varepsilon}$ is increased (case 2 in Fig. 3.4), the free surface becomes deeper due to the larger radial pressure gradient near the center. When $\dot{\varepsilon}$, however, is decreased (case 3 in Fig. 3.4), the fluid has a flatter free surface. Vortex inhibition corresponds to the free surface shape which becomes flatter due to the polymer effect. As long as we regard the fluid as Newtonian, the above discussion suggests that vortex inhibition corresponds to a reduction in axial velocity gradient $\dot{\varepsilon}$.

It is known that large velocity gradient (strain rate) is necessary for polymers to be subject to change its conformation. Especially when the strain rate reaches the order of reciprocal of time constant λ_H, various polymer effects start revealing. Although Chiou (1976) indicated that the strain rate

Figure 3.4

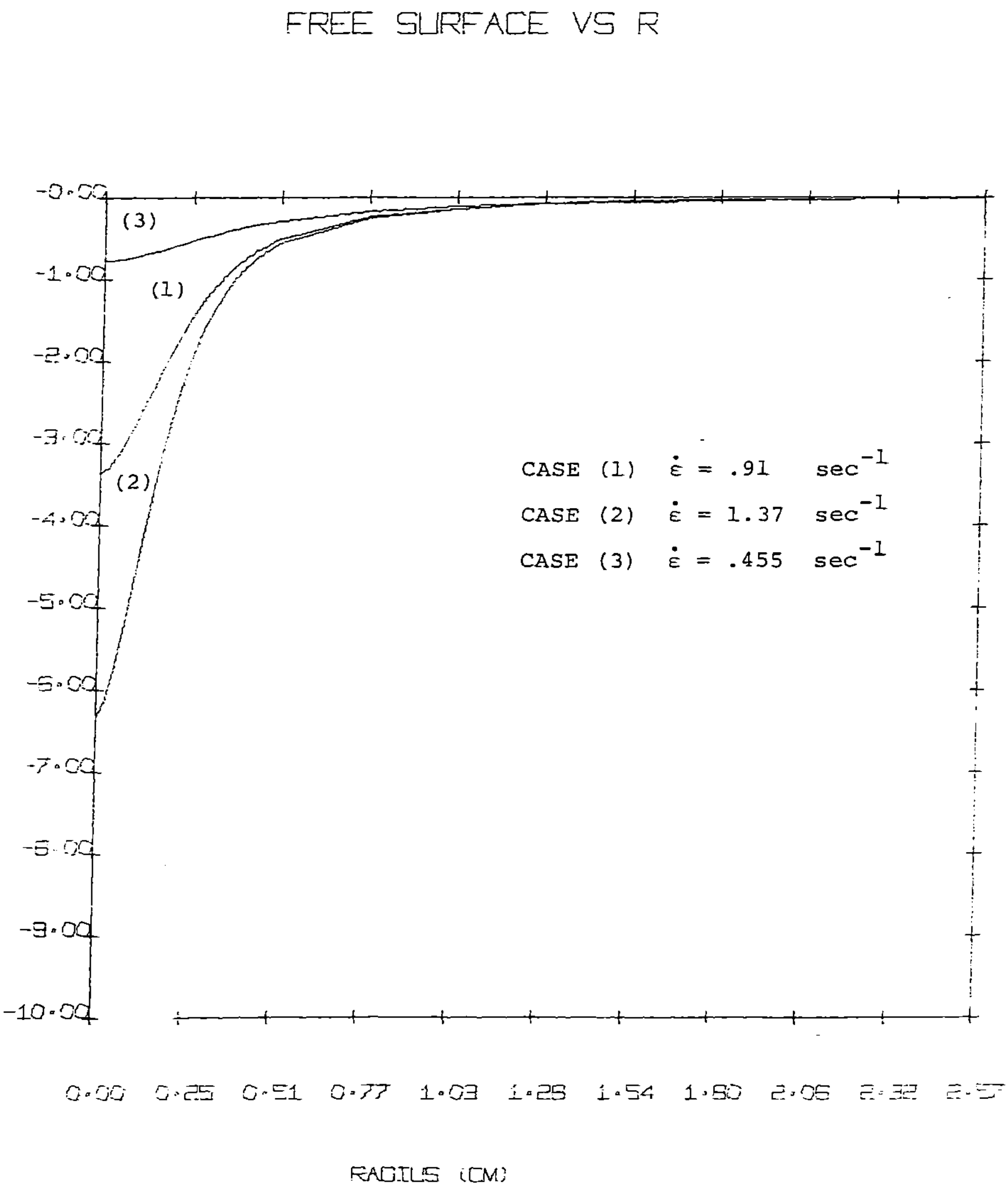
FREE SURFACE VS R
-0.00
-1.00
-2.00
-3.00
-4.00
-5.00
-6.00
-7.00
-8.00
-9.00
-10.00
(3)
(1)
(2)
CASE (1) $\dot{\varepsilon}$ = .91 sec^{-1}
CASE (2) $\dot{\varepsilon}$ = 1.37 sec^{-1}
CASE (3) $\dot{\varepsilon}$ = .455 sec^{-1}
0.00 0.25 0.51 0.77 1.03 1.28 1.54 1.80 2.06 2.32 2.57
RADIUS (CM)

$$\frac{\partial v_\theta}{\partial r}$$

would be responsible for the polymer effect causing vortex inhibition, the maximum value of the strain rate in Fig. 1.2 is at most about 60 sec^{-1} around $r=.4cm$. The figure is not large enough to realize the polymer effect because the estimated time constant for Polyox WSR 301 solution shows that the dimensionless strain rate which is the product of the time constant and strain rate will be .6. The dimensionless strain rate has to be at least more than unity to expect the polymer effect according to the rheology of polymer solution (chap. 5). The tangential velocity gradient, therefore, may not be a main cause of vortex inhibition. And this leads us to investigate the area where higher strain rates are established in the vortex flow.

The flow behavior inside the bottom boundary layer is next analyzed in order to see if the polymer effect is realized in this region. The integral method (Lewellen, 1971) is used for obtaining the boundary layer thickness and the maximum radial velocity as functions of r. The results of the method provides reasonable figures about these two variables when compared them with the results obtained by Anderson (1966). The velocity gradient estimated from the results of the integral method is then used for polymer stress tensor calculation. The constitutive equation used in this calculation is the Hookean Dumbbell model. The resulting stress tensor, however, is found to be not large enough to change the flow behavior in the bottom boundary layer when the stress terms are compared with the dominant force which is radial pressure gradient in the r-component of the equation of motion. The results of the analysis in the bottom boundary layer, thus forces us to investigate the flow behavior in the core region and in the areas near the exit hole to see if large velocity gradient is realized. In order to analyze the flow behavior in these regions, the numerical simulation is next described by solving full Navior-Stokes equations in finite difference scheme for the entire vortex tank.

For incompressible viscous flow in a confined cylindrical container, assuming that the flow is axisymmetric, the velocity field in terms of circulation, vorticity and stream function in a cylindrical coordinate (r,θ,z) are described by the following equation.

<u>CIRCULATION</u> Γ

$$\frac{\partial \Gamma}{\partial t} + V_r \frac{\partial \Gamma}{\partial r} + V_z \frac{\partial \Gamma}{\partial z} = \nu\left[\frac{\partial^2 \Gamma}{\partial r^2} + \frac{\partial^2 \Gamma}{\partial z^2} - \frac{1}{r}\frac{\partial \Gamma}{\partial r}\right] \qquad 1.4$$

<u>VORTICITY</u> ω

$$\frac{\partial \omega}{\partial t} + V_r \frac{\partial \omega}{\partial r} + V_z \frac{\partial \omega}{\partial z} - \frac{V_r \omega}{r} - \frac{1}{r^3}\frac{\partial \Gamma^2}{\partial z}$$

$$= \nu\left[\frac{\partial^2 \omega}{\partial r^2} + \frac{\partial^2 \omega}{\partial z^2} + \frac{1}{r}\frac{\partial \omega}{\partial r} - \frac{\omega}{r^2}\right] \qquad 1.5$$

STREAM FUNCTION ψ

$$\frac{\partial^2\psi}{\partial r^2} + \frac{\partial^2\psi}{\partial z^2} - \frac{1}{r}\frac{\partial\psi}{\partial r} = -r\omega \qquad 1.6$$

where ν is a kinetic viscosity. The circulation is written in terms of V_θ.

$$\Gamma = rV_\theta \qquad 1.7$$

And the relation between the vorticity and the radial and axial velocity v_r, v_z is

$$\omega = \frac{\partial V_r}{\partial z} - \frac{\partial V_z}{\partial r} \qquad 1.8$$

v_r, v_z relate to the stream function by

$$V_r = -\frac{1}{r}\frac{\partial\psi}{\partial z}$$

$$V_z = \frac{1}{r}\frac{\partial\psi}{\partial r} \qquad 1.9$$

In order to avoid the free surface as the boundary of vortex flow, a cylindrical container is assumed to have two exit holes located on the axis of rotation at each of the two walls. As shown in Fig.3.5, the vortex flow is then simulated over a quarter of the total area because of geometrical symmetry. The treatment of the free surface boundary in this way is eliminated without losing the most important characteristics of the vortex

Figure 3.5

The Model Geometry of Vortex Flow

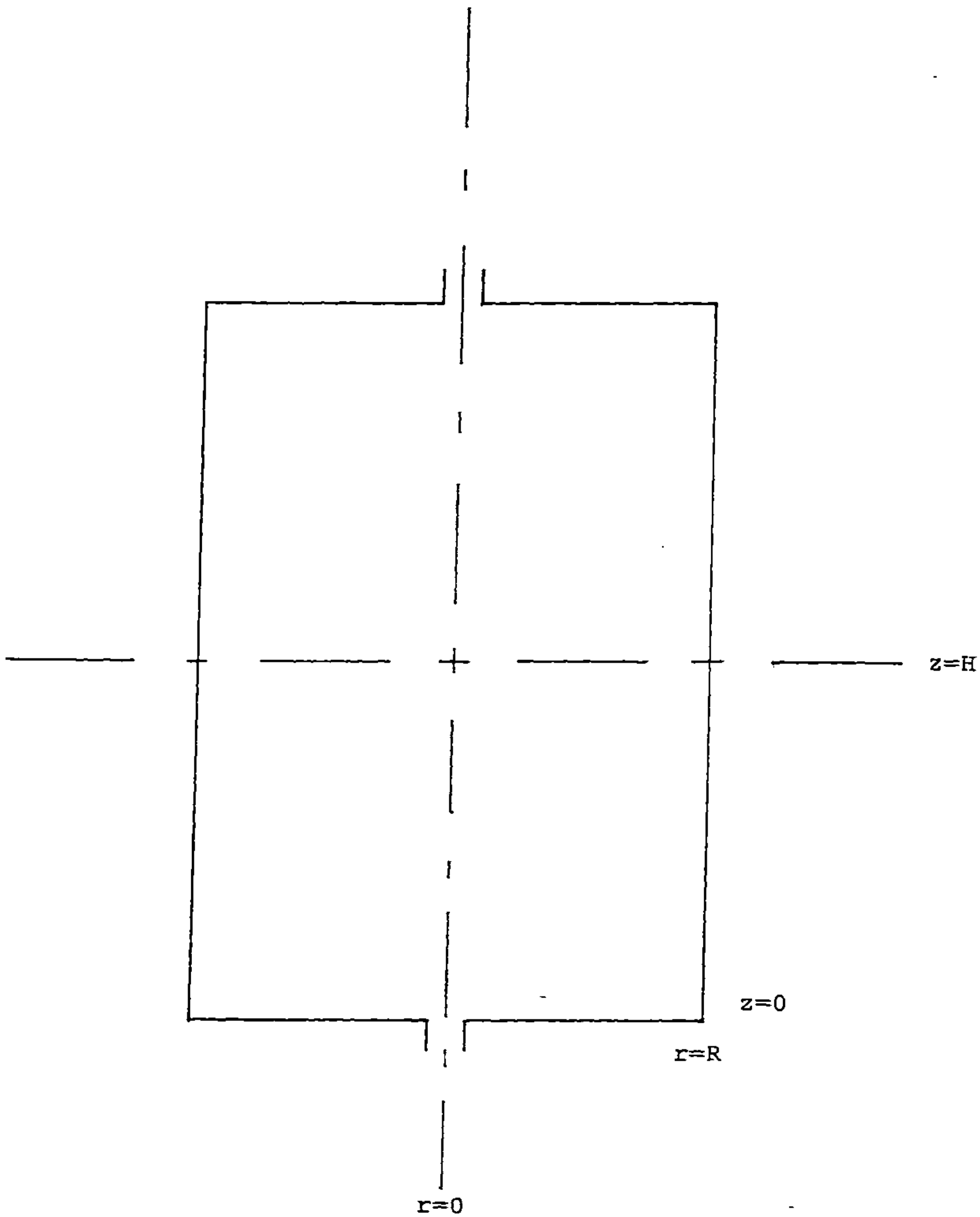

flow (Anderson, 1961). The mesh construction of the flow field is explained in Fig.3.6 according to a finite difference formula. Due to the characteristics of the vortex flow described previously, the mesh size in both the bottom boundary layer and core region is made much smaller than that in the free stream region to provide detailed information about the flow behavior in those two regions. The dot in each zone represents the spacial position of each function whose value is assumed to be uniform inside the zone. Since a zone method (Clomburg, 1971) is used for a finite difference formula, eq. 1.4 to eq. 1.6 are arranged for more suitable forms. The dimensionless forms of the equations are

<u>CIRCULATION</u> Γ

$$\frac{\partial \Gamma}{\partial t} + \frac{1}{r}\frac{\partial}{\partial r}(rv_r\Gamma) + a\frac{\partial}{\partial z}(v_z\Gamma) = \frac{1}{Re_\theta}\left[\frac{\partial^2\Gamma}{\partial r^2} + a^2\frac{\partial^2\Gamma}{\partial z^2} - \frac{1}{r}\frac{\partial\Gamma}{\partial r}\right] \tag{1.10}$$

<u>VORTICITY</u> ω

$$\frac{\partial \omega}{\partial t} + \frac{1}{r}\frac{\partial}{\partial r}(rv_r\omega) + a\frac{\partial}{\partial z}(v_z\omega) - v_r\omega - a\frac{1}{r^3}\frac{\partial\Gamma^2}{\partial z} = \frac{1}{Re_\theta}\left[\frac{\partial^2\omega}{\partial r^2} + a^2\frac{\partial^2\omega}{\partial z^2} + \frac{1}{r}\frac{\partial\omega}{\partial r} - \frac{\omega}{r^2}\right] \tag{1.11}$$

<u>STREAM FUNCTION</u> ψ

Figure 3.5

The Model Geometry of Vortex Flow

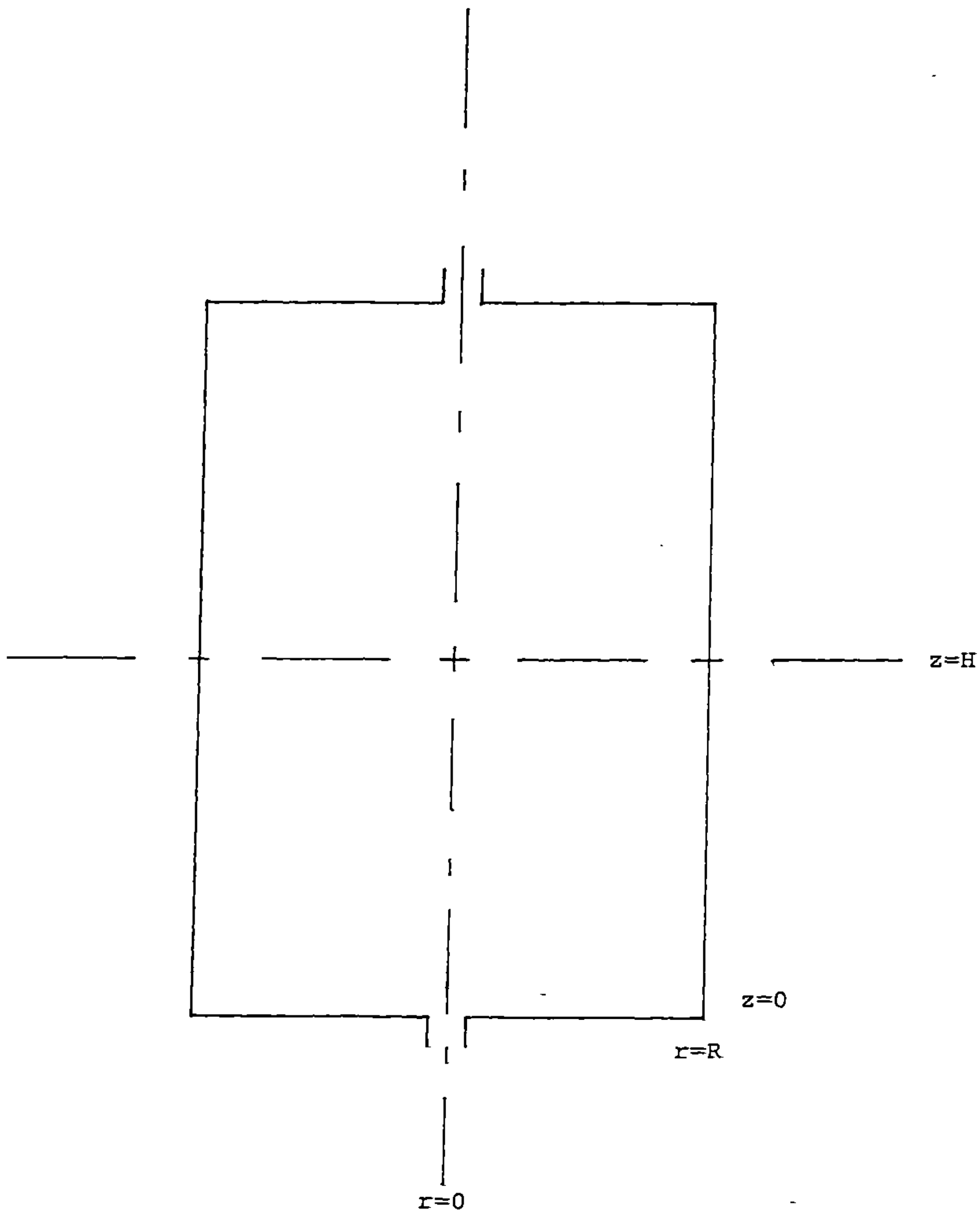

flow (Anderson, 1961). The mesh construction of the flow field is explained in Fig.3.6 according to a finite difference formula. Due to the characteristics of the vortex flow described previously, the mesh size in both the bottom boundary layer and core region is made much smaller than that in the free stream region to provide detailed information about the flow behavior in those two regions. The dot in each zone represents the spacial position of each function whose value is assumed to be uniform inside the zone. Since a zone method (Clomburg, 1971) is used for a finite difference formula, eq. 1.4 to eq. 1.6 are arranged for more suitable forms. The dimensionless forms of the equations are

CIRCULATION Γ

$$\frac{\partial \Gamma}{\partial t} + \frac{1}{r}\frac{\partial}{\partial r}(r v_r \Gamma) + a\frac{\partial}{\partial z}(v_z \Gamma) = \frac{1}{Re_\theta}\left[\frac{\partial^2 \Gamma}{\partial r^2} + a^2 \frac{\partial^2 \Gamma}{\partial z^2} - \frac{1}{r}\frac{\partial \Gamma}{\partial r}\right] \qquad 1.10$$

VORTICITY ω

$$\frac{\partial \omega}{\partial t} + \frac{1}{r}\frac{\partial}{\partial r}(r v_r \omega) + a\frac{\partial}{\partial z}(v_z \omega) - v_r\omega - a\frac{1}{r^3}\frac{\partial \Gamma^2}{\partial z} = \frac{1}{Re_\theta}\left[\frac{\partial^2 \omega}{\partial r^2} + a^2 \frac{\partial^2 \omega}{\partial z^2} + \frac{1}{r}\frac{\partial \omega}{\partial r} - \frac{\omega}{r^2}\right] \qquad 1.11$$

STREAM FUNCTION ψ

Figure 3.6

The Mesh Construction of Vortex Flow

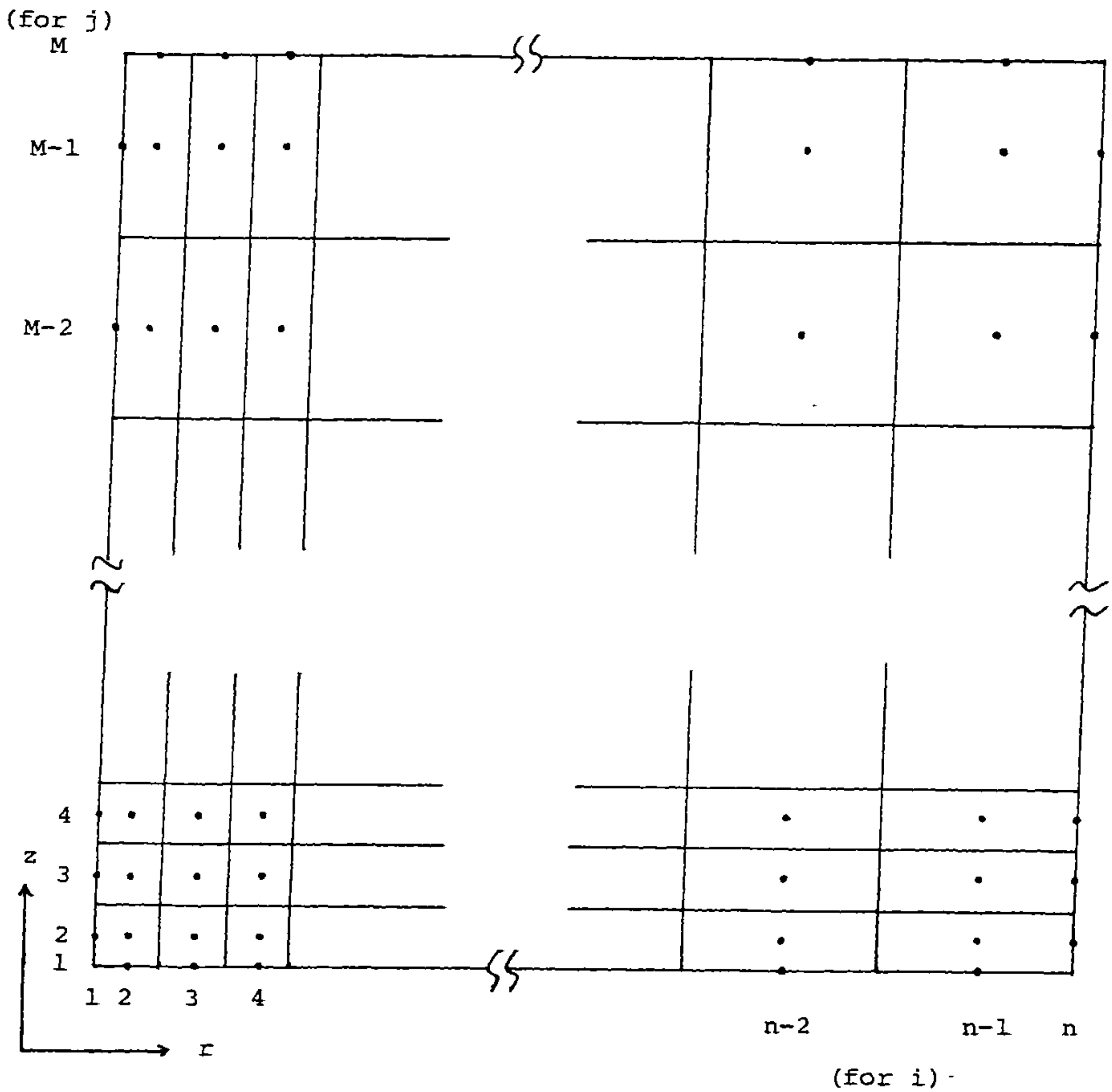

$$\frac{\partial^2\psi}{\partial r^2} + a^2 \frac{\partial^2\psi}{\partial z^2} - \frac{1}{r}\frac{\partial\psi}{\partial r} = \frac{a}{SS} r\omega \qquad 1.12$$

And dimensionless radial and axial velocities v_r and v_z are written by

$$v_r = SS\frac{1}{r}\frac{\partial\psi}{\partial z}$$

$$v_z = -\frac{SS}{a}\frac{1}{r}\frac{\partial\psi}{\partial r} \qquad 1.13$$

The dimensionless variables are defined by (dimensional counterparts are marked by asterisk)

$$\psi = \frac{\psi^*}{v_R RH}, \quad \Gamma = rv_\theta = \frac{\Gamma^*}{Rv_{\theta R}}, \quad \omega = \frac{\omega^*}{v_{\theta R}/R}$$

$$v_r = \frac{r^*}{v_{\theta R}}, \quad v_z = \frac{{v_z}^*}{v_{\theta R}}, \quad r = \frac{r^*}{R}$$

$$z = \frac{z^*}{H}, \quad t = \frac{t^*}{R/v_{\theta R}}, \quad a = \frac{R}{H}$$

Two parametres, Reynolds number (tangential) Re_θ and the ratio of v_R to $v_{\theta R}$, SS, are defined by

$$Re_\theta = \frac{R\ v_{\theta R}}{\nu} \qquad 1.14$$

$$SS = \frac{v_R}{v_{\theta R}} \qquad 1.15$$

The boundary conditions are described in TABLE 1.1. The vorticity at the bottom wall ω_b is estimated from non-slip

TABLE 1.1

THE BOUNDARY CONDITIONS FOR A CONFINED VORTEX FLOW WITH FINITE DIFFERENCE EXPRESSIONS

	STREAM FUNCTION ψ	CIRCULATION Γ	VORTICITY ω
THE AXIS OF ROTATION $r=0$ $(1 \leq j \leq M)$	TOTAL FLOW $\psi_{1,j} = 1$	ZERO $\Gamma_{1,j} = 0$	ZERO $\omega_{1,j} = 0$
THE OUTER WALL $r=1$ $(1 \leq j \leq M)$	V_r is constant V_z is zero $\psi_{N,j} = z_j$	CONSTANT $\Gamma_{N,j} = 1$	ZERO $\omega_{N,j} = 0$
LIQUID LEVEL $z=1$ $(1 \leq i \leq N)$	TOTAL FLOW $\psi_{i,M} = 1$	SHEAR FREE *2	ZERO $\omega_{i,M} = 0$
THE EXIT HOLE *1 $z=0$ $(1 \leq i \leq 3)$	SHEAR FREE $\psi_{i,1} = \psi_{i,2}$	SHEAR FREE $\Gamma_{i,1} = \Gamma_{i,2}$	SHEAR FREE $\omega_{i,1} = \omega_{i,2}$
THE BOTTOM PLATE $z=0$ $(4 \leq i \leq N)$	V_r and V_z are zero $\psi_{i,1} = 0$	ZERO $\Gamma_{i,1} = 0$	NON-SLIP CONDITION eq.1.16

*1 Since nothing is known in the exit hole, all conditions are reasonably assumed.

*2 The finite difference expression is

$$\Gamma_{i,M} = \frac{1}{8}(9\Gamma_{i,M-1} - \Gamma_{i,M-2})$$

condition. ω_b is then written by

$$\omega_b = SS\frac{9}{R_i}\,\frac{25\psi_{i,1} - \psi_{i,2}}{2\ DZ_2^{\,2}} \qquad 1.16$$

for $4 \leq i \leq N$

The stream function is first solved by S.O.R. (Successive over relaxation). The velocity v_r and v_z are then determined from the interpolated stream function assigned at four corners of each zone in Fig.3.6 by the descretized form of eq.1.13. The time advanced circulation is then solved by A.D.I. (Alternating-direction implicit method). Using the new calculated circulation, the vorticity is calculated also by A.D.I. The whole iteration procedure is summarized in Fig. 3.12. A very small time increment increases the stability of calculation because it makes a strong diagonally dominant matrix but it takes an excessive amount of calculation time. When a very large time increment is taken, however, the calculation becomes unstable so that the results are physically meaningless. The optimal time increment is determined by a trial and error approach. The iteration is terminated when the residual of each difference equation becomes sufficiently small when compared with the dominant terms in the equation for the entire geometry.

Figure 3.12

The Iteration Procedure for Vortex Flow Calculation

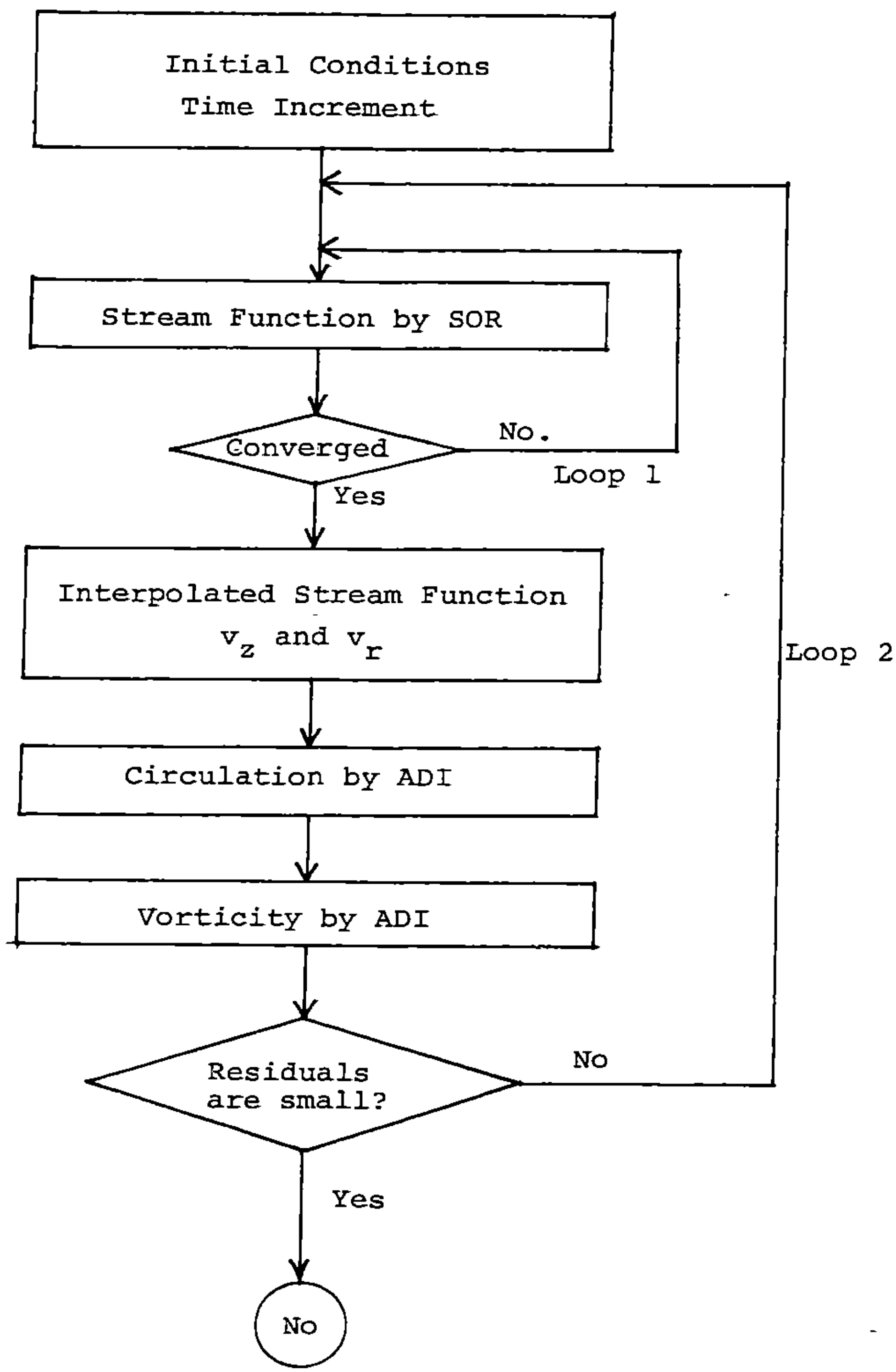

1.2.2 Experimental Study

The continuous steady state vortex flow is established by tangentially introducing fluid inside the outer wall of the vortex tank with an equal flow rate of draining fluid from the tank. The detailed description of the vortex tank is shown in Fig. 4.2 where the exit hole is located at the center of the bottom wall.

Tangential velocity V_θ at the free stream region, axial velocity V_z along the axis of rotation are quantitatively measured by photographic tracer technique. These velocity components are determined from time lapse photographs of small particles suspended in a thin section of fluid which is illuminated by a collimated beam of light. A light source used in the measurement is the strobe light (1540 strobolume, 1540-P1 oscilator, 1540-P2 Lump made by GenRad) which can flash up to 400 times per second and the duration of each flush is only 1 μsec. The tangential velocity V_θ in the free stream region is measured at different radial positions and at two different axail positions. The V_θ data at two axial positions are enough to represent V_θ in the free stream region because V_θ is almost independent of axial position. The V_θ is calculated from a particles's dot trajectory on the bottom view photograph using a horizontally collimated light (See Fig. 4.5). A number of dots can be controlled by adjusting both the flash rate and the exposure time of camera (Nikomat F 2.0).

Fig. 4.5 A Photograph for Measuring V_θ

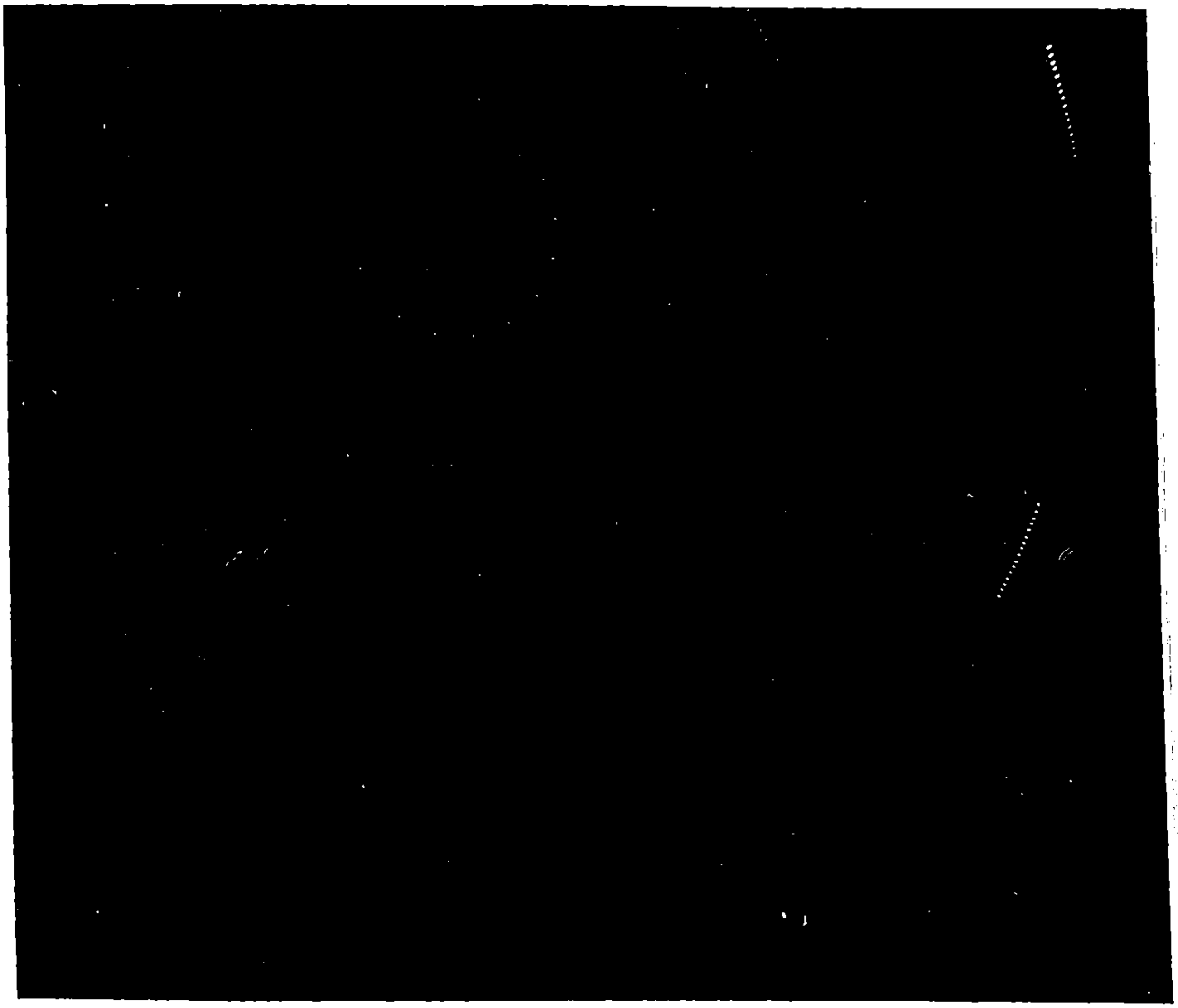

The axial velocity measurement in the core region is very difficult with the present photographic technique because the reflection of light from the air core is so strong that it makes the particles near the air core impossible to detect. Incomplete vortex flow (the word "incomplete" indicates that the air core does not extend down to the exit hole) thus is established so that V_z at the axis of rotation can be measured from the side view photograph. Fig. 4.8 is a typical photograph from which V_z at the axis of rotation is approximately determined by dividing the distance between two adjacent dots by a time span of two flashes.

The experimental procedure for the measurement of V_θ in the free stream region and V_z along the axis of rotation for both a Newtonion fluid (room temperatured water) and a polymer solution are briefly summarized as follows. After calibration, the fluid starts circulating the vortex flow system. Once a steady state vortex flow is established, the volumetric flow rate and the liquid level are determined. The small amount of seeding particles are then added in the flow system for the purpose of reflecting the light. V_z long the axis of rotation is measured followed by V_θ measurement at two different axial positions. During the velocity measurement, the flow rate and the liquid level are also measured.

The concentrated polymer solution prepared at least two days before use is then added to the flow system to make about 30 wppm polymer solution. As soon as the polymer

Fig. 4.8 A Photograph for Measuring V_z

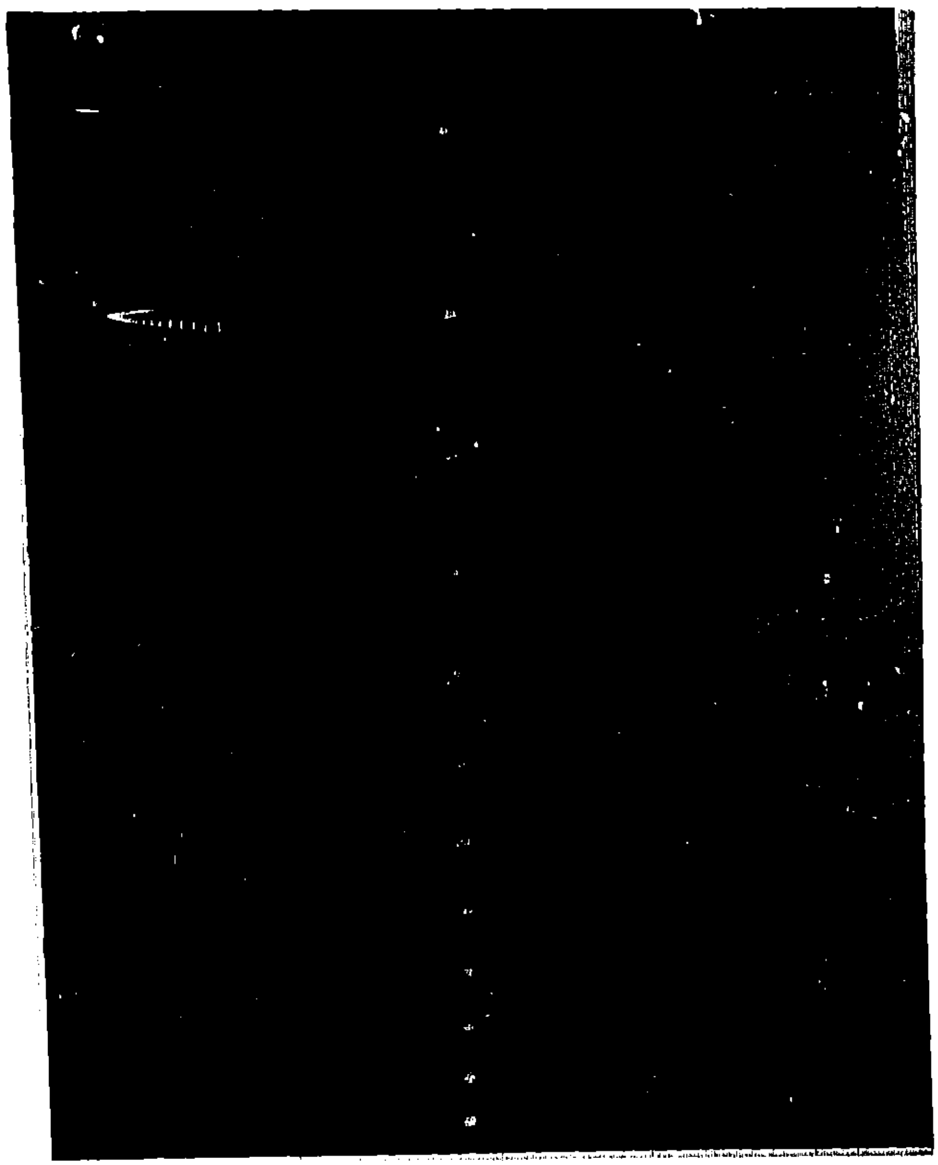

effect, that is the small fluctuation of the air core and the liquid levels falling is observed, the onset behavior of vortex inhibition is measured by taking pictures for V_θ data. All the pictures are taken within 30 seconds after the onset. The important feature of the onset behavior measurement is to be able to observe how the V_θ is changed by introducing the polymer solution into the Newtonian flow pattern. And the information is very useful for the analytical study of vortex inhibition because a numerical simulation is done for the situation where the Newtonian fluid is suddenly replaced by polymer solution to see how the resulting stress field changes due to the presence of the macromolecules. After a couple of minutes, the vortex flow completely shifts to a new quite different flow status which is the vortex flow of the polymer solution. The procedure of V_z measurement along the axis of rotation which immediately follows the V_z measurement for the Newtonian fluid is the same as that of V_θ measurement for polymer solution.

Four kinds of qualitative observations are done for studying the characteristics of vortex flow for both Newtonian and polymer fluid. The complete vortex flow is used because the air core does not disturb the observations. The flow behavior of the core region is studied by using dyed solution. When the dyed polymer solution (about 50 wppm Polyox WSR 301) is dropped on the free surface of the Newtonian vortex flow near the axis of rotation, the vortex is immediately inhibited. When dropped in the free stream region, the polymer dyed solution behaves as if it were a Newtonian fluid and the vortex is not inhibited. This observation indicates that the tangential velocity V_θ in the core region is reduced due to the presence of the macromolecules and that the polymer effect may be dominant somewhere in the core region.

The flow behavior of the bottom boundary layer is studied by injecting the Newtonian dyed solution through a very small hole (its diameter is .04 cm) located in the bottom wall to see the differences in the flow behavior between a Newtonian fluid and polymer solution. For the Newtonian fluid, the streak of the dye is very smooth and almost all of the dye goes directly out through the exit hole. For the polymer solution, however, the dye is randomly scattered around the exit hole. From this observation, the polymer effect may be important in the area near the exit hole because of the apparent difference in flow behavior between the Newtonian fluid and polymer solution.

When a small tube is installed right above the exit hole, the Newtonian vortex flow is heavily disturbed because the tube prevents a radial inflow in the bottom boundary layer from going out through the exit hole. The distinguishing feature of this observation is that installing the tube lowers the liquid level substantially while keeping the flow rate constant (See Fig. 4. 16 (a)). When the liquid level is raised up to the previous level, the flow rate has to be increased about 6%. When the liquid level reaches the

Fig. 4.16 THE EFFECT OF THE CAP EXPERIMENT

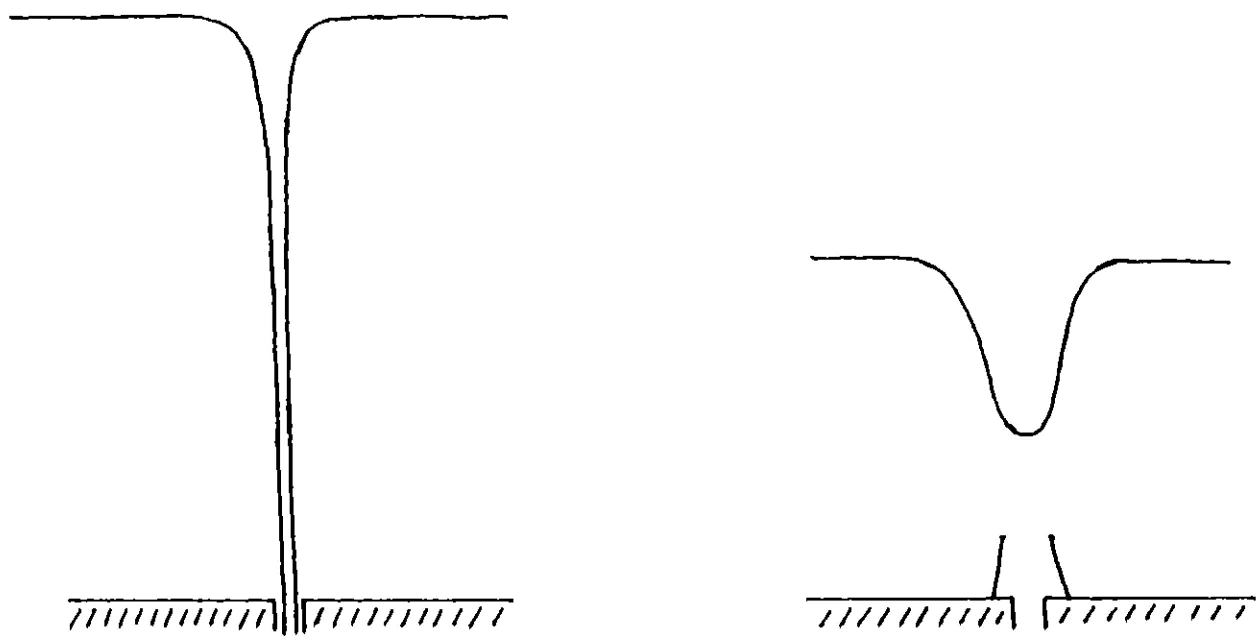

previous point, the vortex is inhibited in a very similar way to vortex inhibition by Polyox WSR 301. This experimental observation also emphasizes the importance of the flow behavior in the vicinity of the exit hole.

The vortex flows of Newtonian fluids with different viscosity are observed in terms of the air core width and liquid level. The fluids used for the observation are water, glycerin-water solution A (the relative viscosity is 1.068) and glycerin-water solution B (the relative viscosity is 1.227). Both glycerin solution A and B are found to form very similar vortex flow to that by water with respect to the shape of the air core, liquid level and flow rate. From the fact that the relative viscosity of the glycerin solution A and 30 wppm Polyox solution are almost equal, we can conclude that vortex inhibition cannot be explained solely by viscous effect but it has to be due to the elastic nature of the macromolecules.

1.3 Development of Constitutive Equation

In order to investigate the polymer effect on the flow, an approximate constitutive equation for a dilute polymer solution is needed to see how the stress tensor changes due to the existence of the macromolecules. A new constitutive equation for a dilute solution of flexible macromolecules is developed from the kinetic theory. The main difficulty associated with the kinetic theory of dilute polymeric fluids so far is that it can provide complete information about the stress tensor only for small rates of strain and a few material functions of high strain rates. The reason for the difficulty stems from being unsuccessful in solving the differential equation for the distribution function (called the diffusion equation). Although Giesekus(1966) showed that full information about the stress tensor can be obtained for the Hookean Dumbbells model without solving the diffusion equation, this model has two serious shortcomings which are shear rate independent visometric functions and an unbounded elongational viscosity even for moderately high elongational rates.

The constitutive equation developed in this study not only eliminates the shortcomings associated with the Hookean Dumbbell model but also is simple enough to be manipulated for any kind of homogenous flow at all strain rates. And it shows that shear thinning (viscosity decreases with increasing shear rate), non-zero primary normal stress coefficient and a bounded elongational viscosity for high elongational rates. The new constitutive equation called the Modified Nearly Hookean Dumbbell model (MNHD) is constructed by matching it with the Nearly Hookean Dumbbell (Armstrong and Ishikawa, 1979) for a flow where the macromolecule is neither very stretched nor oriented and with the model which Tanner (1975) developed for a flow where the macromolecule is strongly oriented and stretched. The Spring law used in the MNHD is FENE (Warner, 1972) spring law.

The main results of tests for the MNHD are shown in Fig. 6.7, Fig. 2.4, Fig. 6.9 and Fig. 6.10 by using two simple flow patterns, shear flow and elongational flow. Fig. 6.7 shows the comparison of intrinsic viscosity as a function of shear rate between available experimental data and the model prediction. The macromolecule used in the experimental data is polystyrene of various molecular weights. From the figure, the MNHD is seen to show the shear thinning phenomenon. It is also found that the mdoel shows a linear relation between $[\eta]$ and $\log \dot{\gamma}$ for higher shear rate ($\lambda_e < 2$, $\lambda_H = (5\varepsilon+1)\lambda_e$). By comparison with a wide variety of polystyrene solutions, the parameter ε which is associated with the maximum length of the macromolecule R_o falls into the range between .02 and .005, which agrees with the prediction by Christiansen and Bird (1977). This range of parameter ε may, therefore, be a proper choice for polymer stress tensor field calculation. Fig. 2.4 shows the comparison of steady state elongational viscosity between the exact solution of FENE model (Bird and et al., 1977) and the MNHD's prediction. The rapid

Fig. 6.7

$[\eta]$ vs $\lambda_e\dot{\gamma}$ with Experimental Data (1) (Polystyrene in benzene at 30 °C)

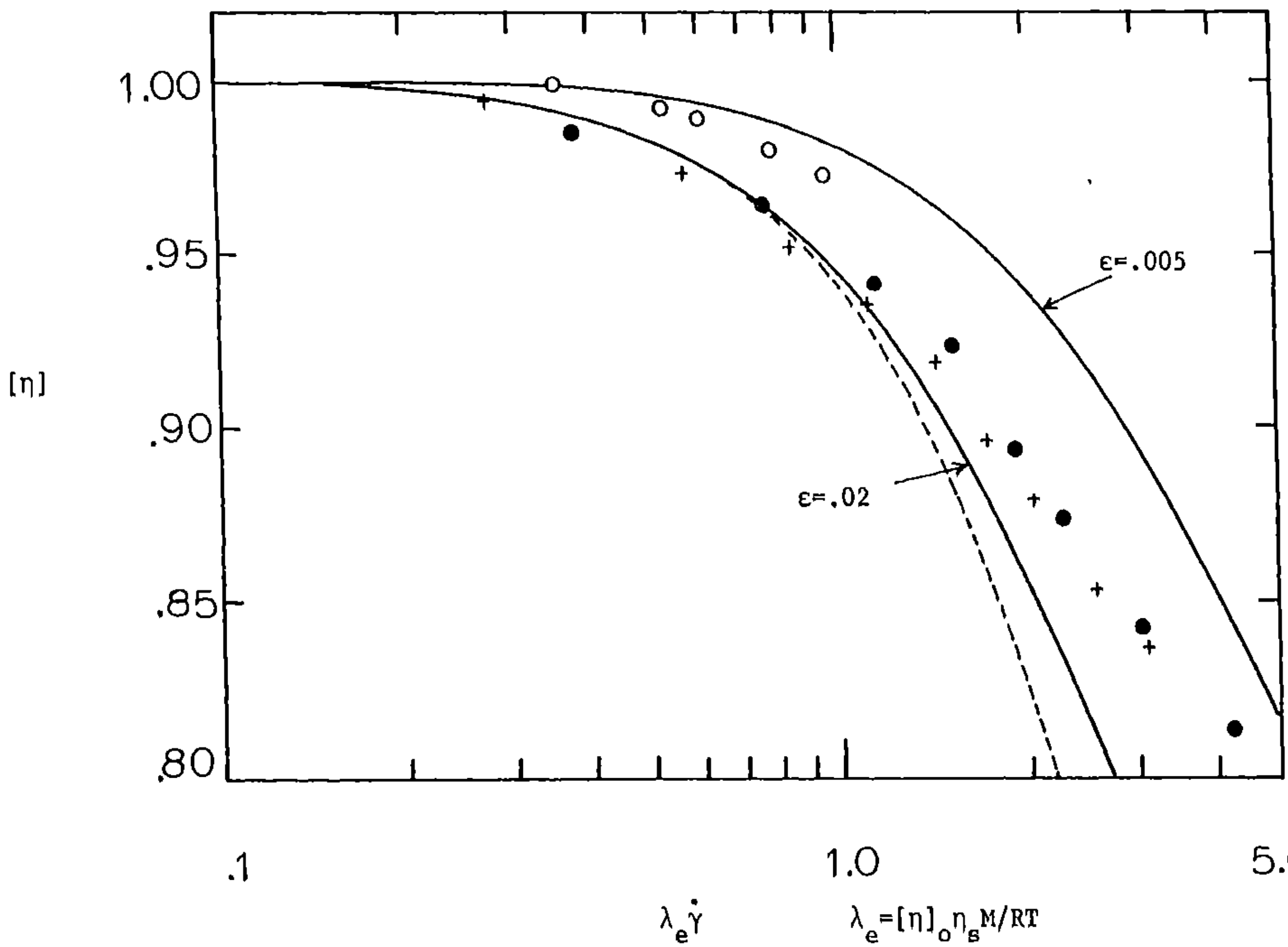

o M_w=3.16x10^6
● M_w=7.14x10^6
+ M_w=6.00x10^6

– – – – – Perturbed solution with ε=.02

Fig. 2.4 : Elongational Viscosity Predicted by MNHD

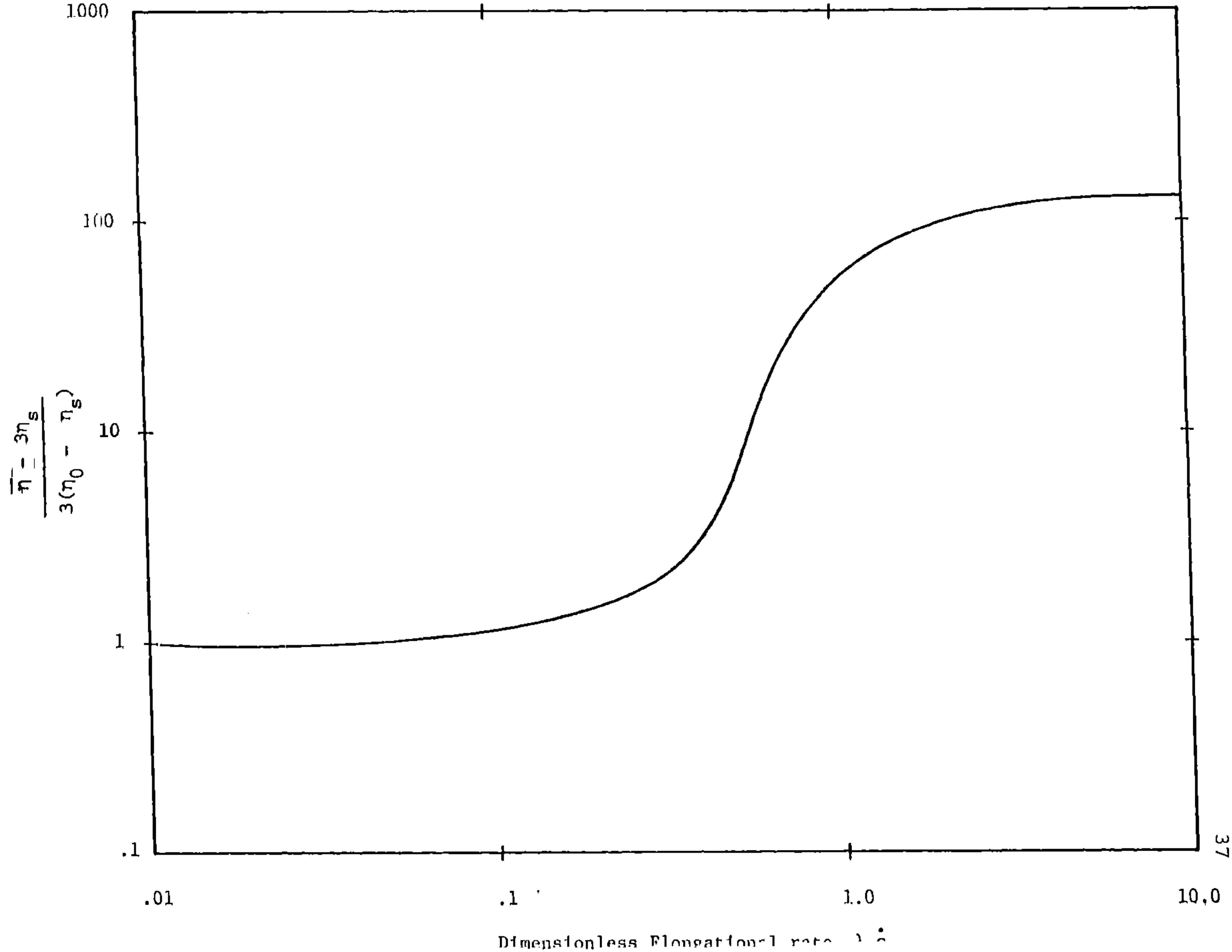

increase of elongational viscosity observed at the moderate elongational rates corresponds the nearly full extension of the macromolecules which, then, show higher resistance to be stretched out above those elongational rates. Both models eventually approach the same large asymptotic elongational viscosity at high elongational rates. It is found from Fig. 2.4 that the MNHD represents the FENE model very well over the entire range of elongational rate.

The stress growth and relaxation of elongational viscosity are plotted with different scaled dimensionless time in Fig. 6.9 and Fig. 6.10. As shown in Fig. 6.9, as the elongational rate $\lambda_H\dot{\varepsilon}$ increases, the time required for reaching a steady state becomes much shorter. This characteristic is quite different from the growth behavior of shear viscosity shown in Chap. 5 where the time to reach steady state is about $t/\lambda_H = 4$ for all shear rates. Unlike shear flow, the macromolecules subjected to elongational flow are stretched directly by hydrodynamic force and oriented to the direction of the flow. The time scale for molecular response to this flow, therefore, may be related to the elongational rate $\dot{\varepsilon}$. This is clearly explained when the elongational viscosity is plotted with the dimensionless time scaled by $1/\dot{\varepsilon}$ in Fig. 6.10 where the time to reach steady state is about $\dot{\varepsilon}t = 3$ for higher elongational rates. The shorter response time for high elongational rate is important for vortex inhibition. The residence time of fluid element is very short in the area where large velocity gradient is estab-

Fig. 6.9

Dynamic Behavior of Elongational Viscosity

with Time Scaled by λ_H

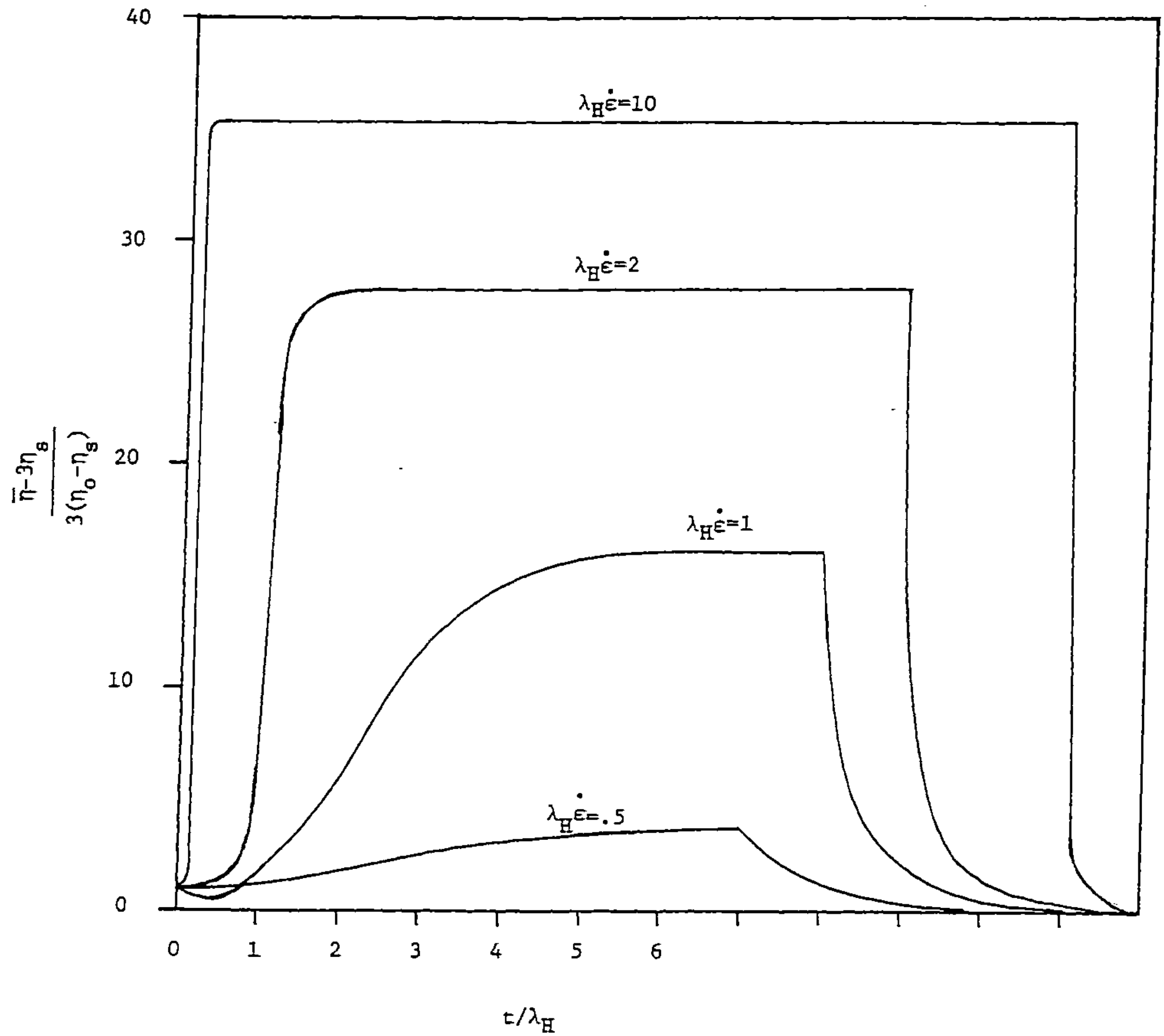

Fig. 6.10

Dynamical Behavior of Elongational Viscosity with Time Scaled by ε^{-1}

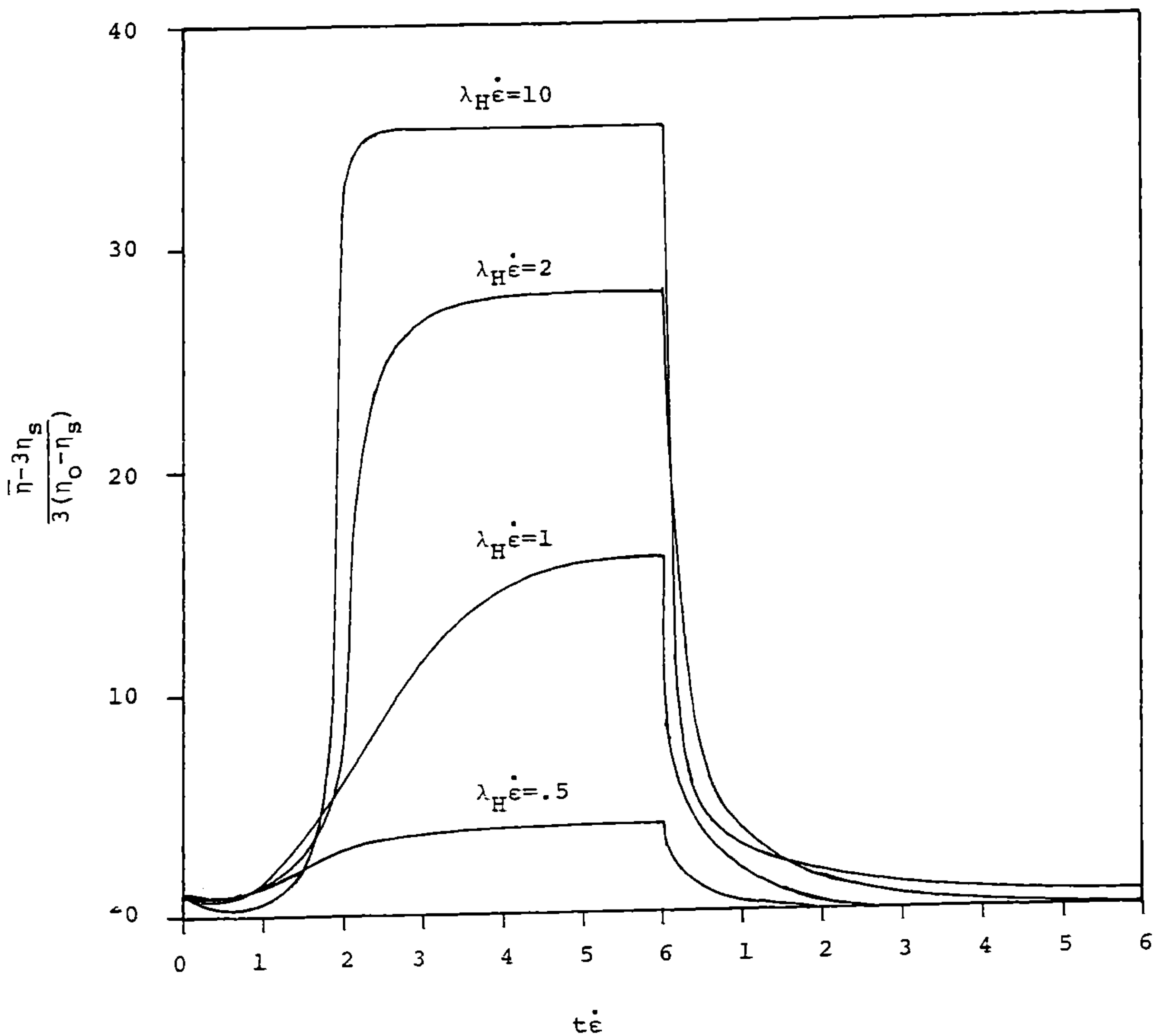

lished because the velocity of the fluid is usually very high. Unless the macromolecules are excited within the residence time of the fluid element, it would be carried away from the area of high strain rates before polymer effect appears. Thus it is necessary for realizing the polymer effect on the flow field that the response time for high elongational rates must be very short besides large elongational viscosity.

Judging from these results, the MNHD seems to be suitable for vortex inhibition analysis. The MNHD is used as a constitutive equation for the analysis of stress field in the next section because first, its form is so simple that any kind of locally homogeneous flow can be applied, and secondly, the elongational viscosity predicted by the model is as good as that by the FENE model.

1.4 The Analysis of the Onset Behavior of Vortex Inhibition

The mechanism of the onset behavior of vortex inhibition is analyzed by the following sequence. First, the Newtonian vortex flow is discussed by the results of the numerical calculation with locally obtained experimental velocity data. Secondly, the experimental observation about the onset behavior of vortex inhibition is described. Two important characteristics are emphasized there. Third, the stress tensor for polymer solution is calculated along the stream lines by the MNHD. The velocity field for the calculation is the Newtonian vortex flow. Finally, the polymer effect, namely how the flow behavior changes due to the resulting polymer stress tensor, is analyzed by an approximate method to explain the experimental findings qualitatively.

The velocity field of Newtonian vortex flow is calculated by A.D.I. for higher tangential Reynolds number Re_θ. The general flow behavior of a confined vortex flow is well described by stream lines. Fig. 6.1 and Fig. 6.2 show the results of the numerical calculation which described the stream lines representing both the radial and axial velociites for lower and higher tangential Reynolds number respectively. Each fluid element also makes swirl motion due to the tangential velocity besides moving along the stream lines. As shown in Fig. 6.1, for $Re_\theta = 10$, most of fluid elements supplied at the outer wall move toward the exit hole in taking almost the shortest distance. No reverse (due to positive v_r) or up

Fig. 6.1

Stream Lines for Low Reynolds Number $Re_\theta=10$, SS=-1

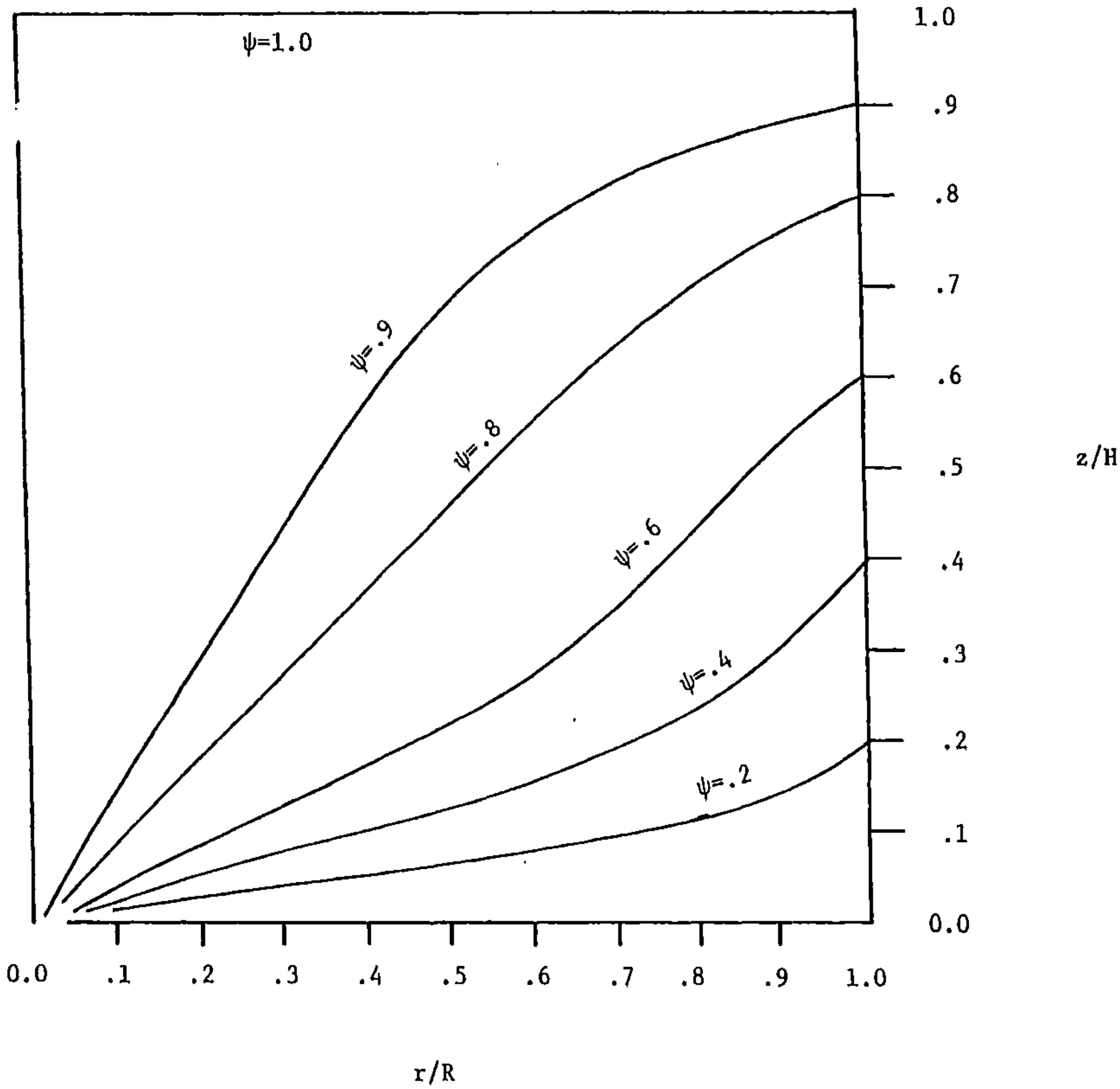

Fig. 6.2

Stream Lines for High Reynolds Number

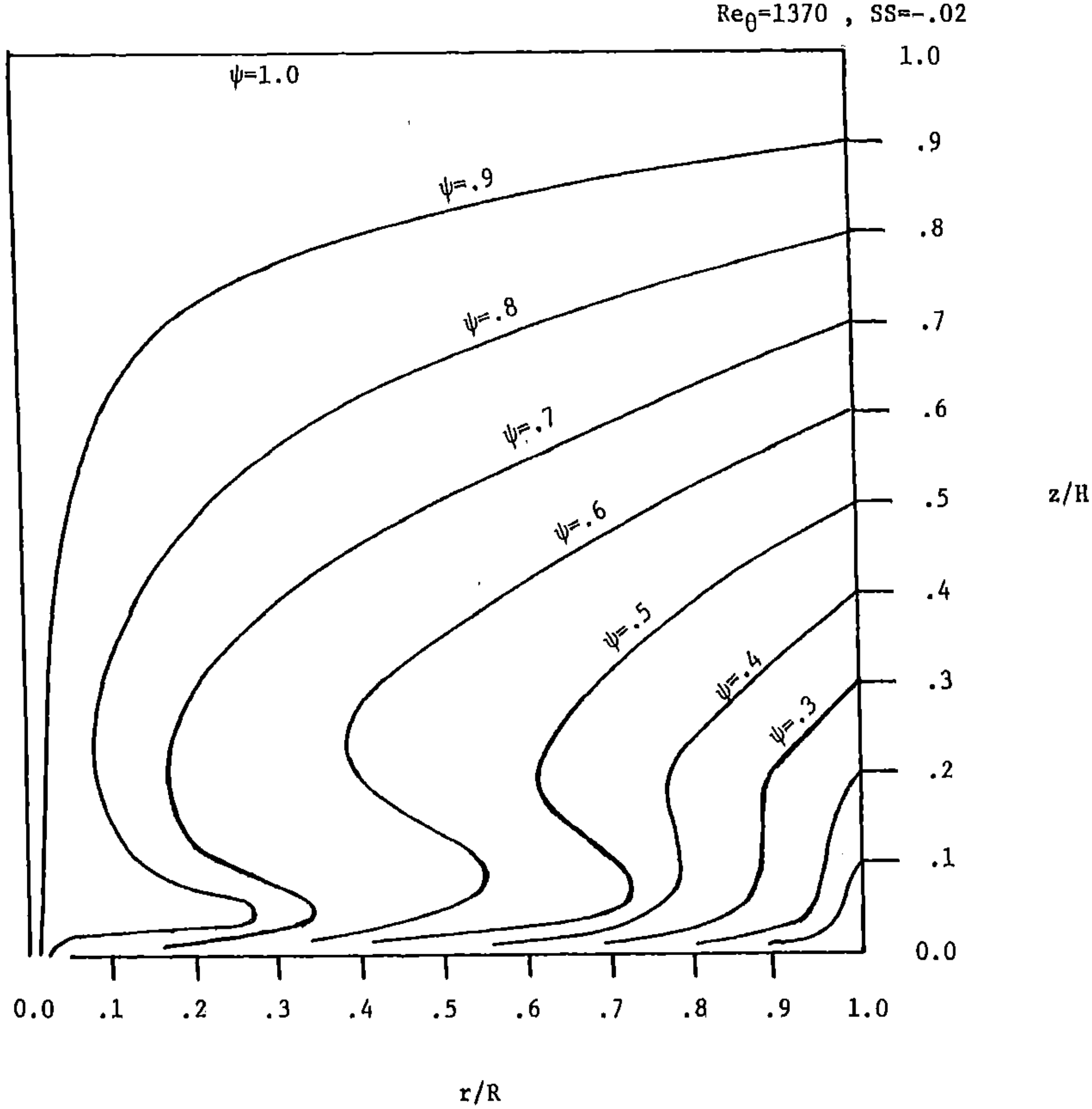

(due to positive v_z) flow is observed for such a low Re_θ. For higher Re_θ (=1370), however, the flow behavior turns out quite different. For example, taking the stream line $\psi = .8$ in Fig. 6.2 representing 80% of total flow rate, the fluid element initially moves toward the exit hole but after passing the point (r,z) = (.1,.2), the fluid starts moving back and eventually goes into the bottom boundary layer. As shown in Fig. 6.2, the bottom boundary layer is formed for high Re_θ and 80% of total flow rate is come from this thin boundary layer region. The radial velocity in the layer is much larger than that above the layer because the stream lines are very dense. The core region is also recognized by the stream line $\psi = .9$ in Fig 6.2. Unlike Fig. 6.1 the stream $\psi = .9$ is much closer to the axis of rotation and this indicates that higher axial velocity forms the core region. And the flow from the bottom boundary layer interacts with the flow from the core region near the exit hole. Tangential velocity at the free stream region is measured for various Re_θ. Although the measurement in v_θ is taken both at $z = 4.0$ cm and $z = 10.0$ cm, the difference in v_θ at these two positions is negligible. Fig. 6.3 and Fig. 6.4 show comparison between the experimentally measured v_θ and numerically calculated v_θ for two different Re_θ and SS. The numerical results show excellent agreement with experimental data for both cases. Fig. 6.5 and Fig. 6.6 show the comparison of v_z at the axis of rotation. As shown in these figures, the calculated v_z corrected by factor 2.8 predicts

Fig. 6.3

The Comparison between the Experimentally Measured V_θ and Numerically Calculated V_θ (1)

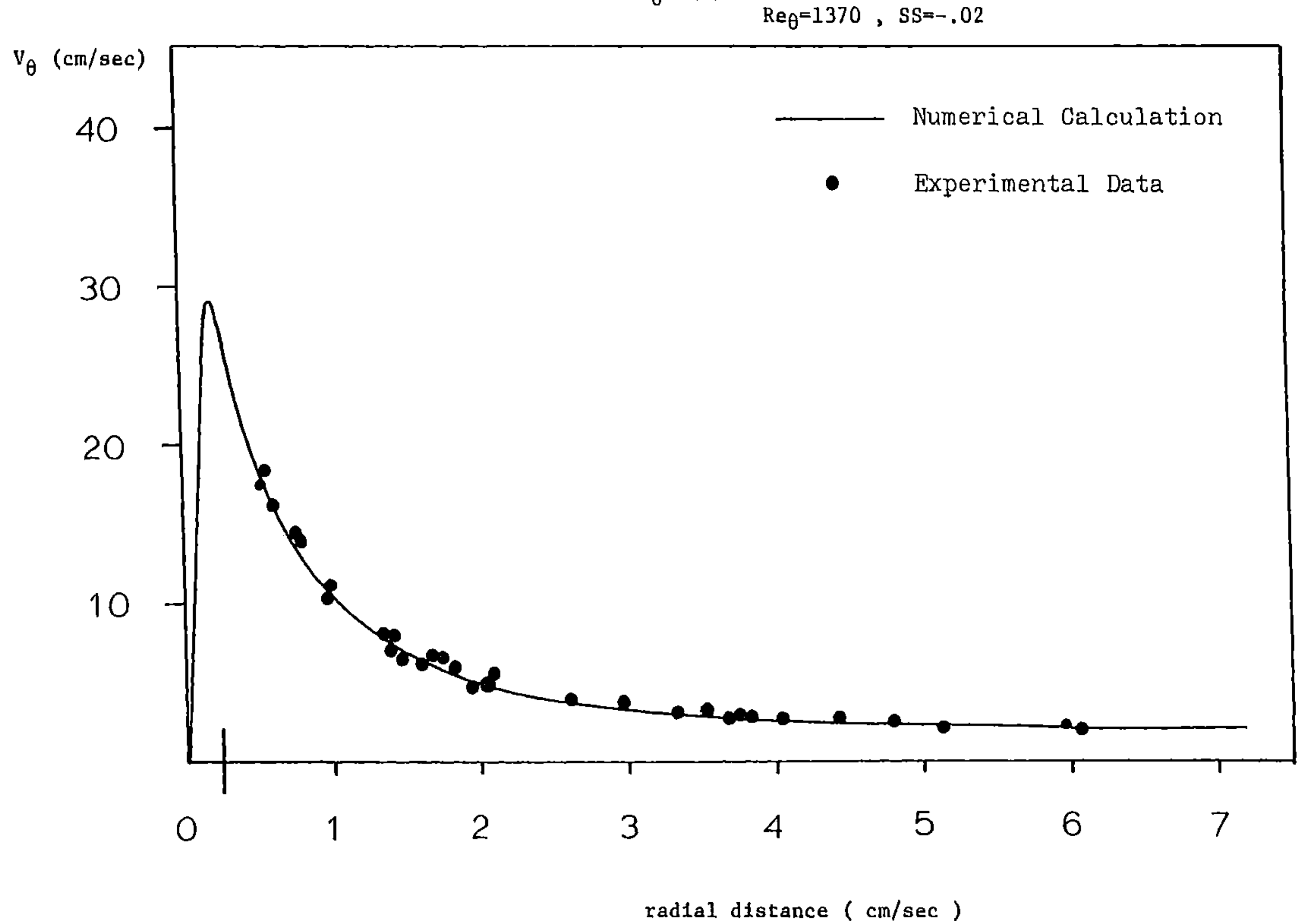

Fig. 6.4

The Comparison between the Experimentally Measured V_θ and Numerically Calculated V_θ (2)

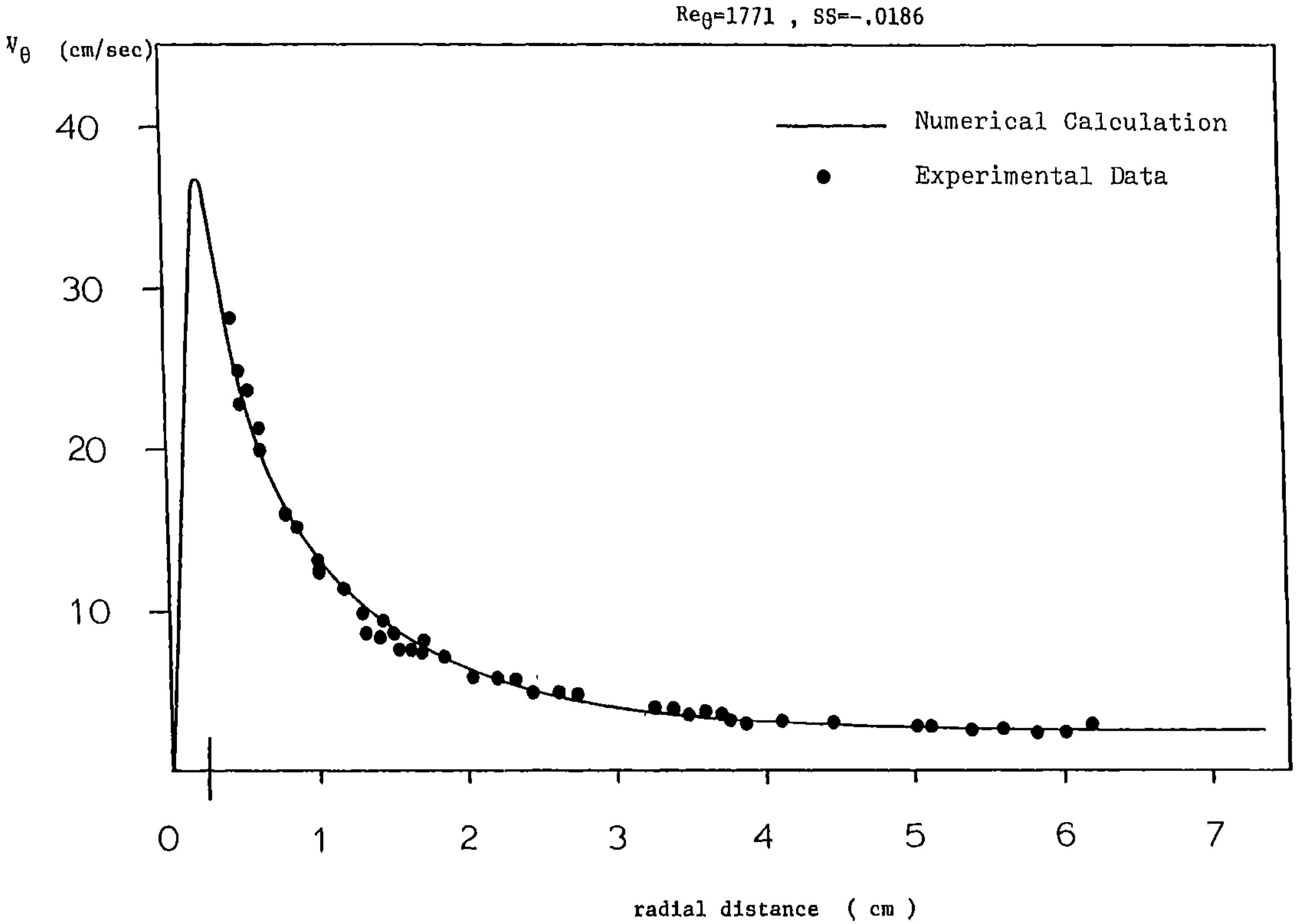

Fig. 6.5

The Comparison of V_z at $r = 0$

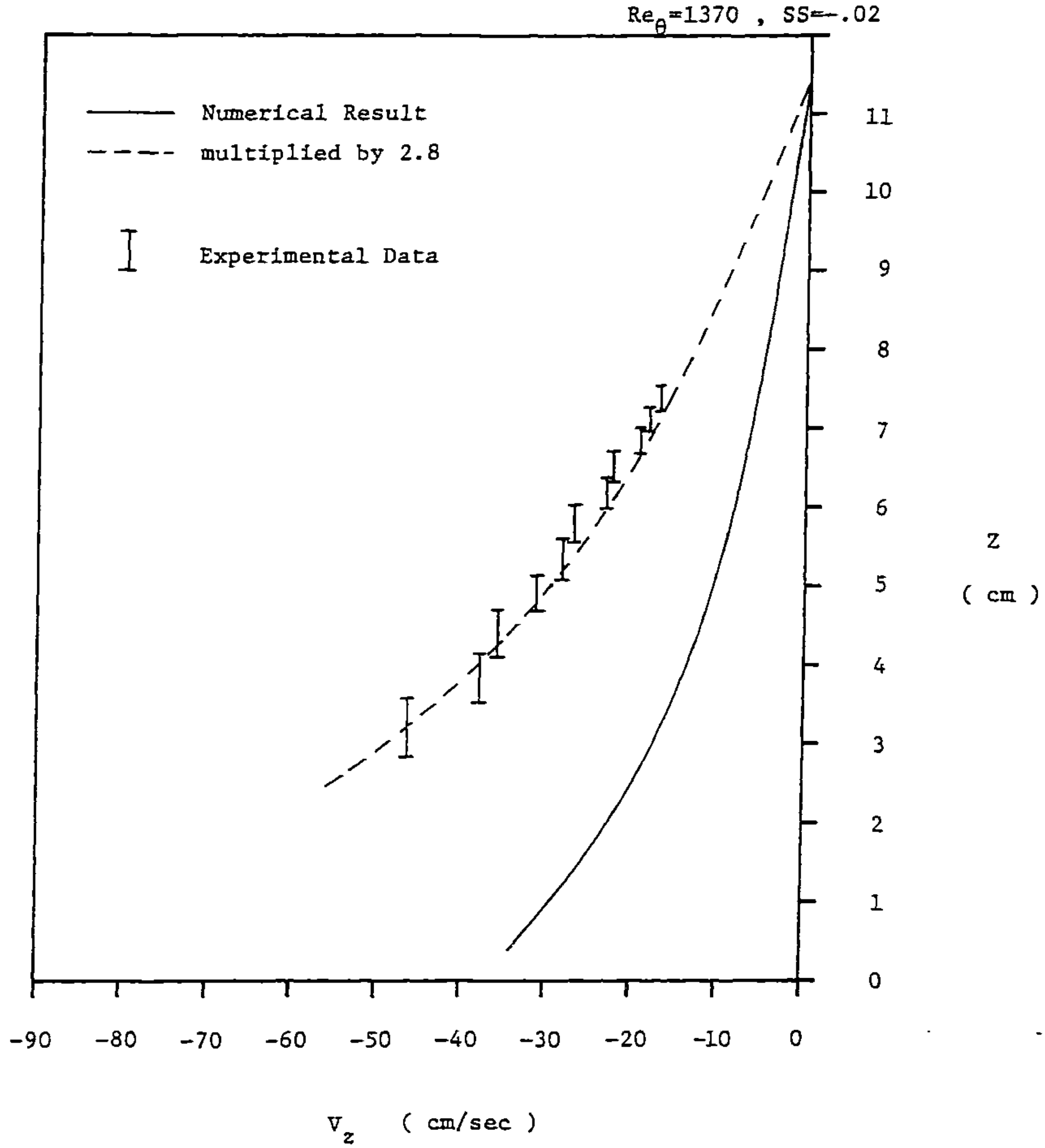

Fig. 6.6

The Comparison of V_z at r = 0

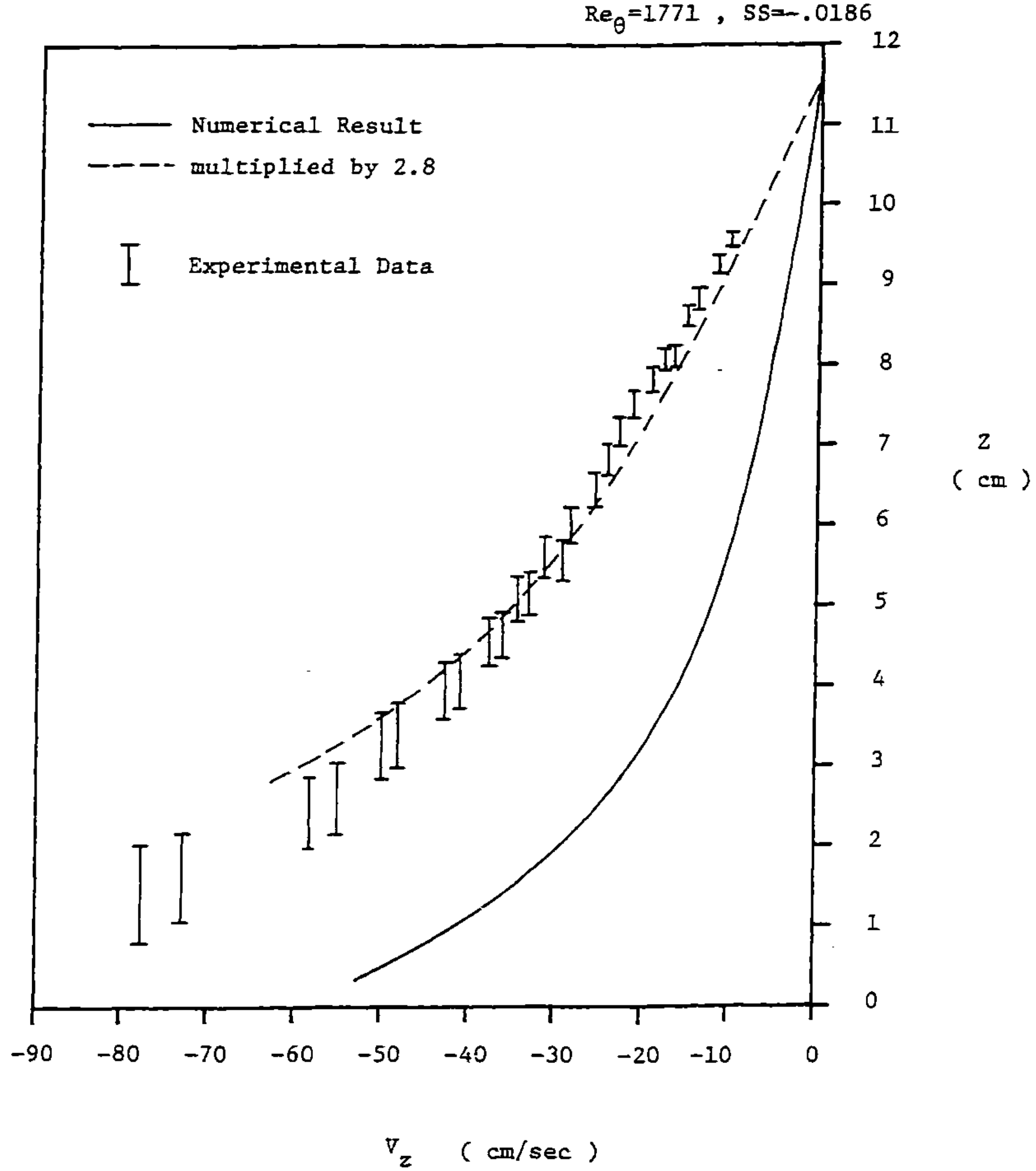

experimentally determined v_z profile very well. The correcting factor may be explained mainly by the discrepancy in the radius of the exit hole between calculation and experiment. In the calculation, the location of radius r_e has to be matched with the point at the canter of the zone. This condition makes r_e about 1.5 times larger than the real location. From the continuity of the fluid, the average value of v_z over the exit hole has to be increased 2.13 times larger for the real case. The axial velocity at the axis of rotation is increasing in almost linear fashion from the liquid surface, but as the fluid gets close to the exit hole, v_z is accelerated. This is observed from both figures. It is also found from the calculation results that v_z is further increased so rapidly especially when the fluid interacts with the flow from the bottom boundary layer to produce large velocity gradient

$$\frac{\partial V_z}{\partial z} .$$

The results of the comparison with experimental measurement show that the numerical simulation describes the vortex flow reasonably well. The confined geometry of the vortex tank does not give any significant difference from the open free surface vortex flow in terms of velocity field. Since the numerical simulation provides full information about velocity field for the entire vortex geometry and the calculated velocity field reasonably well represents the real velocity field, it is employed for stress tensor calculation for polymer solution.

The information about the onset behavior is very important for analysis of vortex inhibition because it provides the transient flow behavior from Newtonian to polymer solution. As shown in Fig. 6.11, after several minutes, the vortex flow completely shifts to a new, quite different flow status which is fully developed vortex flow of the polymer solution. The analysis of the fully developed vortex flow of the polymer solution seems to be irrelevant for this study because of the following reasons.

First, the fluctuation of the air core is very large and random so that it is almost impossible to obtain consistent velocity data especially for v_z at $r=0$. Secondly, since the liquid level is dropped to about 50% of its original figure and the total flow rate is not changed very much (see number in Fig 6.11), a much higher tangential velocity is established and this explains the broadening of the air core. This larger tangential velocity, however, may not directly be caused by the polymer effect but rather is due to the decrease of the liquid level while flow rate is almost unchanged. To investigate the polymer effect on the vortex flow, it is, therefore, more sensible to measure the onset behavior of vortex inhibition rather than the fully developed vortex flow. Besides these two reasons, the measurement of the onset behavior is more consistent with the numerical simulation which calculates the polymer stress thensor by the MNHD. The

Fig. 6.11

The Difference between the Newtonian Vortex Flow and

A Fully Developed Vortex Flow of Polymer Solution

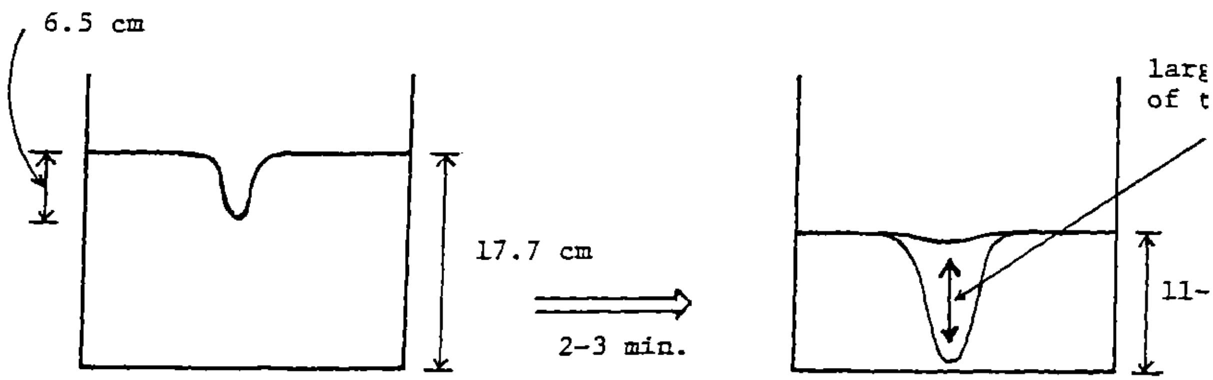

The Newtonian
vortex flow

flow rate: 33.5 cc/sec

A fully developed
vortex flow of
polymer solution

flow rate: 30.0 cc/sec

calculation simulates a physical situation where the Newtonian fluid is suddenly replaced by the polymer solution in order to see how the stress field changes due to the presence of the macromolecules.

Fig. 6.12 shows the tangential velocity measured during the onset. The tangential velocity in the free stream region is not appreciably changed when compared with that of the Newtonian fluid. Several velocity data, however are found near the axis of rotation (the core region). In v_θ measurements for the Newtonian fluid, no data could be obtained at the core region because of large axial velocity. These data indicate the reduction of v_z in the core region due to the fluctuation of the air core.

The axial velocity data on the axis of rotation is shown in Fig. 6.13 during the onset along with the Newtonian data. The v_z data for the polymer solution are obtained from different pictures taken during the onset. At each time, different v_z data is obtained because of the fluctuation of the air core. The figure indicates that v_z at $r=0$ is always lower than the case of the Newtonian fluid from any of the data. This seems to be inconsistent with the fact that the liquid level is falling during the onset. The average v_z over the exit hole must be increased to explain the liquid level's falling, v_z at $r=0$, on the other hand, seems to decrease at the exit hole form Fig. 6.13.

Thus, two experimental findings during the onset of vortex inhibition should be emphasized. First, he averaged

Fig. 6.12 The Tangential Velocity Profile before and during the Onset

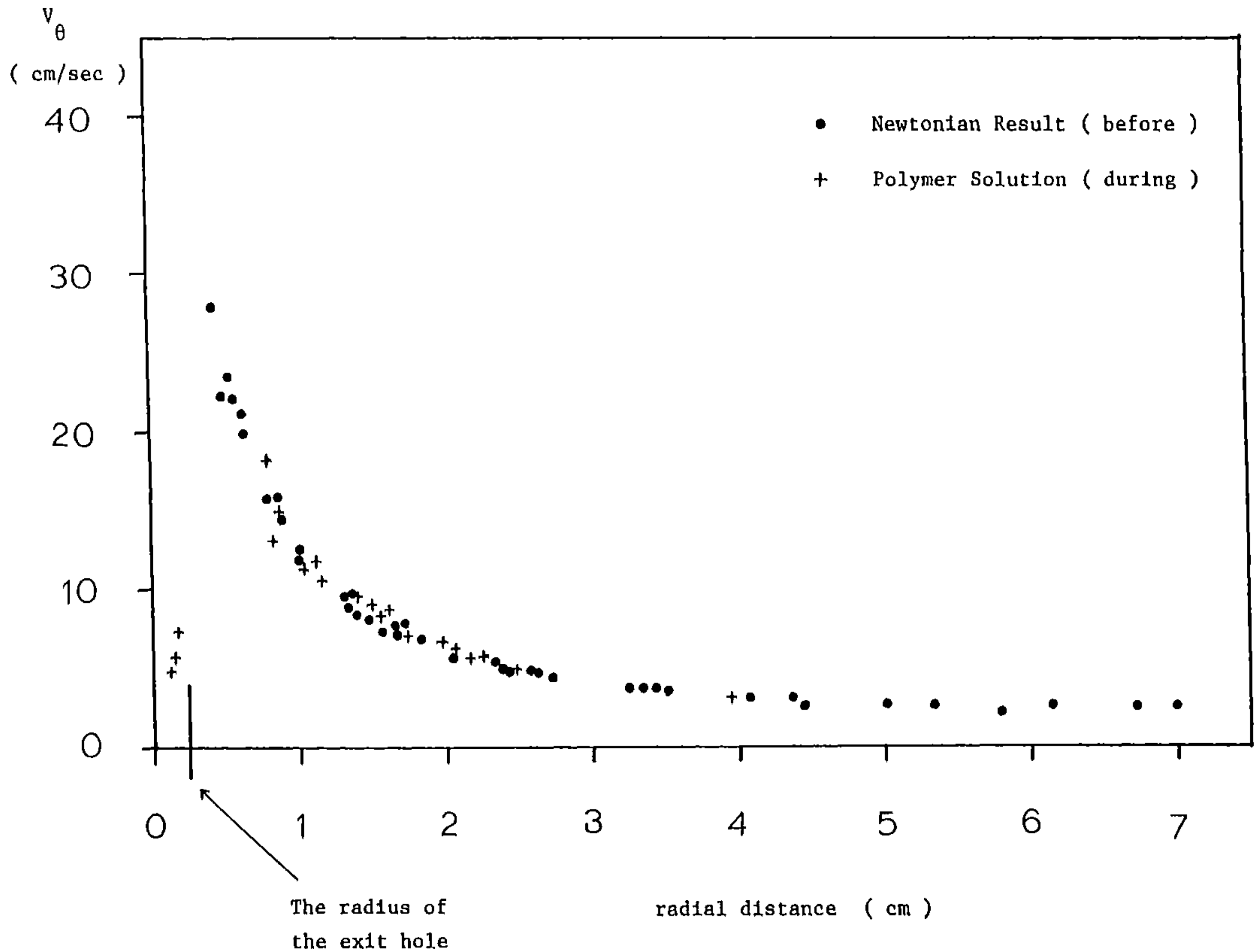

Fig. 6.13

Axial Velocity Measured before and during the Onset

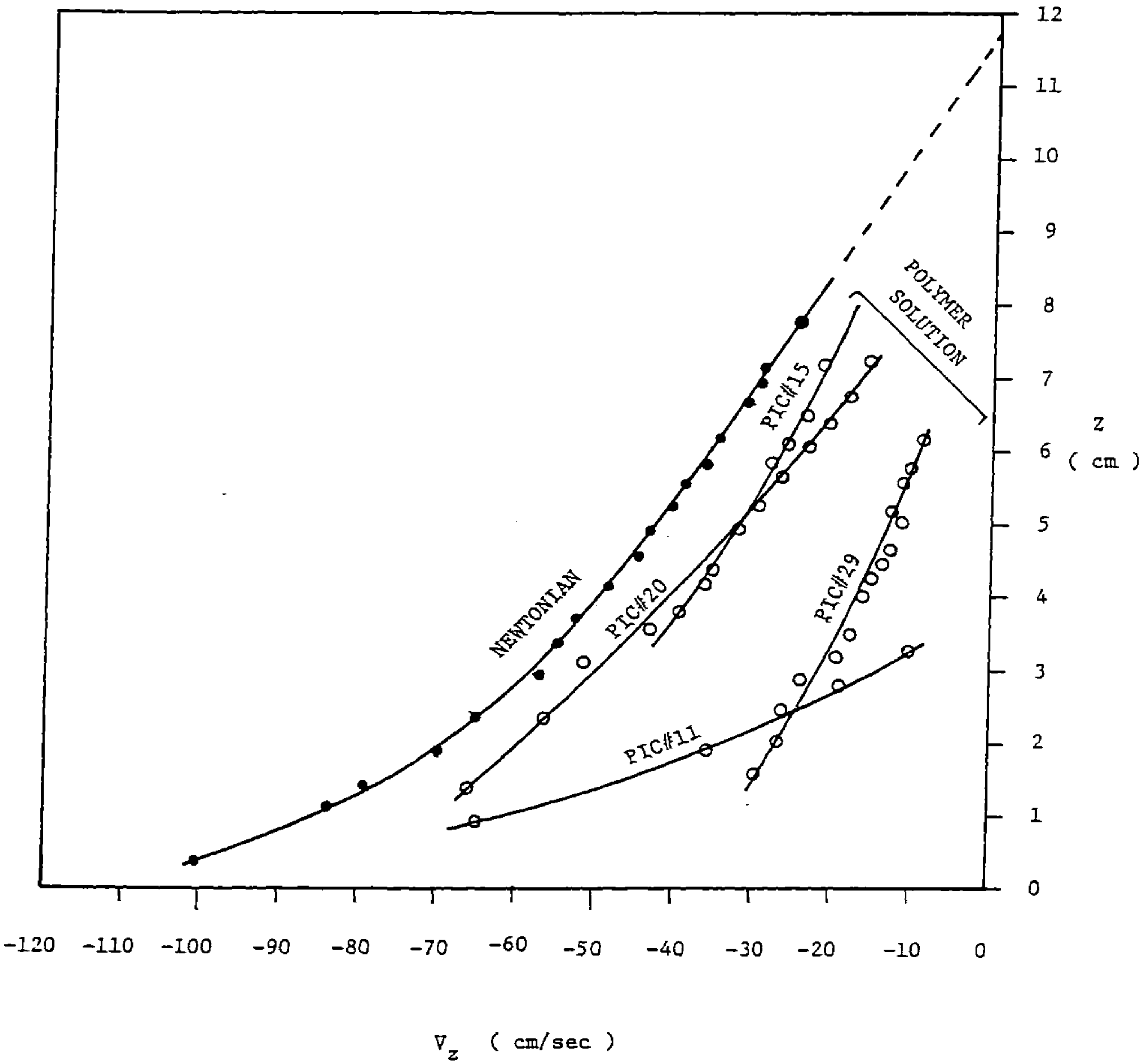

axial velocity over the exit hole is increased. Secondly, the axial velocity at the axis of rotation seems to be decreased at the exit hole. These two findings characterize the onset behavior of vortex inhibition and these are analyzed in the later parts of this chapter.

The stress tensor is calculated by using the MNHD as a constitutive equation along the stream lines obtained previously. Since the onset behavior is the transient state from the Newtonian vortex flow to the fully developed vortex flow of the polymer solution, the information about the velocity gradient may be obtained from the results of the Newtonian vortex calculation. The calculation of the stress tensor is limited to the area near the exit hole. Because the simple speculation in section 1.2 indicates that the velocity gradient is too small to excite the macromolecules until the fluid element approaches this area where the velocity gradients seem to become very large. Fig. 6.14 is a detailed picture of Fig. 6.2 of the stream lines near the exit hole. Once the fluid element reaches the square area enclosed by the lines of $r/R = .1$ and $z/H = .1$, the calculation begins. For example, the stress calculation of $\psi = .8$ starts from the point $(r/R, z/H) = (.1, .025)$. The stress tensor is then numerically calculated at the point 1. Every component of the velocity gradient tensor needed for the calculation is approximately determined from the velocity field at the point 1. This calculation procedure is repeated until the fluid element reaches the point 4 where the large velocity

Fig. 6.14

Stream Lines near the Exit Hole

Re_θ=1370 , SS=-.02

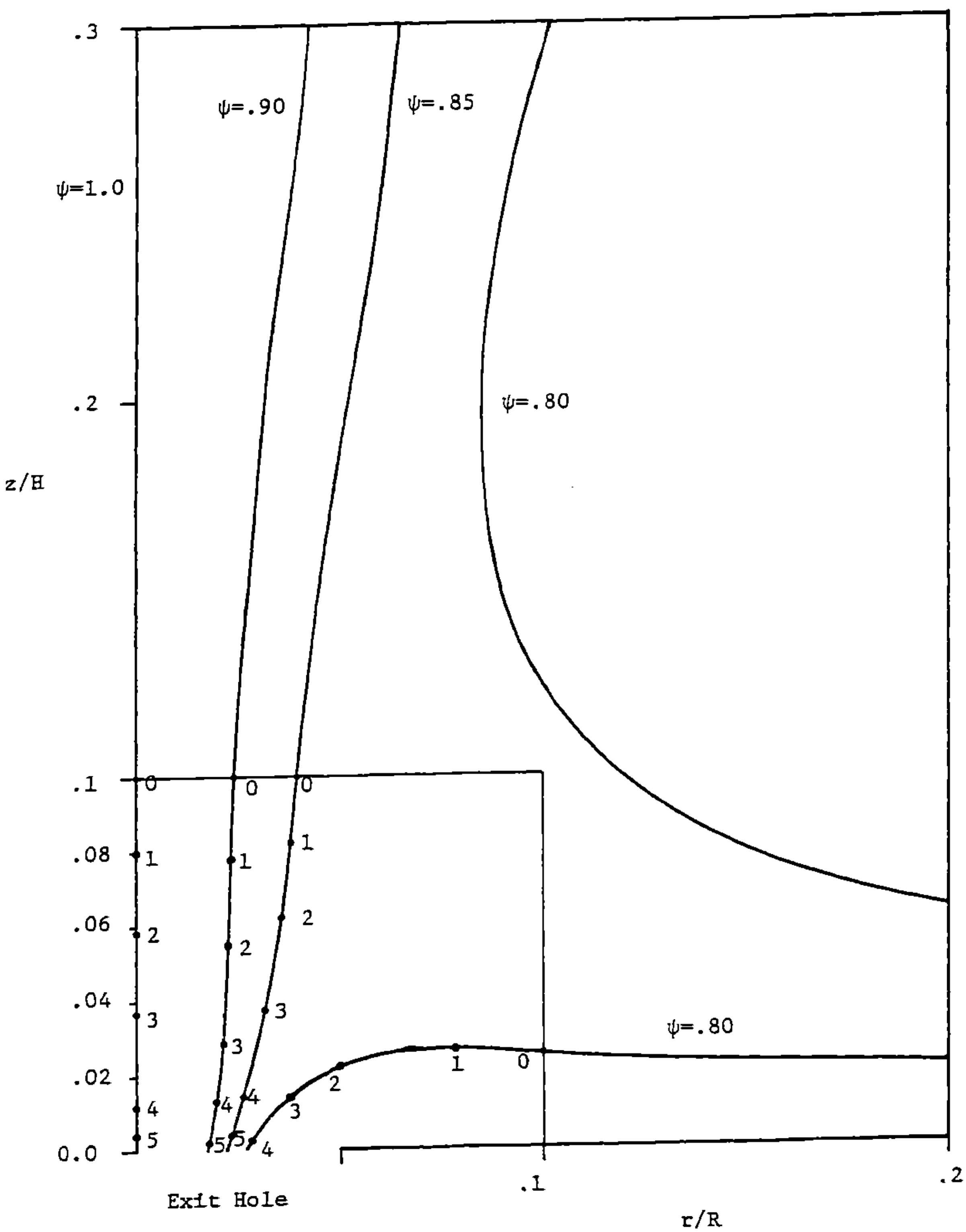

gradient is expected. The stress tensor is also calculated in this way for $\psi = .85$, $\psi = .9$ and $\psi = 1.0$. TABLE 1.2 shows the calculated stress tensor component $\tau_{p,zz}$ at each stream line. No other stress components are found to be insignificant. It is found from TABLE 1.2 that $\tau_{p,zz}$ increases extremely rapidly very near the exit hole for $\psi = .85$ and $\psi =.8$. This is due to the large velocity gradient especially

$$\frac{\partial V_z}{\partial z}$$

established at the exit hole. And the macromolecules are suddenly stretched out in the z-direction nearly to the maximum length R_o (see the column $<(R/R_o)^2>$ in the table). The study of the MNHD shows that the molecular response time is very short when the velocity gradient is very large, the macromolecule has enough time to be stretched extensively even in a very short period of time. The macromolecules flowing along the stream lines $\psi = 1.0$ and $\psi = .9$, on the other hand, are not stretched substantially. $\tau_{p,zz}$ at $\psi = 1.0$ is less than the half of the Newtonian stress component even at the point 5. The fluid element along the $\psi = 1.0$ may not be influenced by the presence of the macromolecules.

From the analysis of the Newtonian velocity field, it is found that the dominant forces in the Newtonian flow in the z-direction very near the exit hole are pressure gradient

TABLE 1.2

$\tau_{p,zz}$ ALONG THE STREAM LINES

$\psi = 1.0$			$\psi = .9$		
A	B	C	A	B	C
1 (.01)	0	.0146	1 (.02)	-.259 (-.084)	.0207
2 (.02)	-.027 (-.04)	.0153	2 (.04)	-.431 (-.266)	.0241
3 (.03)	-.045 (-.24)	.0157	3 (.06)	-.645 (-.64)	.0280
4 (.04)	-.147 (-.68)	.0182	4 (.07)	-9.158 (-3.02)	.1660
5 (.043)	-.203 (-.96)	.0194	5 (.075)	-23.618 (-3.02)	.3183
$\psi = .85$			$\psi = .8$		
A	B	C	A	B	C
1 (.04)	-2.322 (-.112)	.1185	1 (.03)	-.069 (-.02)	.0172
2 (.08)	-8.183 (-.398)	.2175	2 (.07)	-2.575 (-.7)	.1704
3 (.12)	-3.844 (-.504)	.0948	3 (.09)	-47.004 (-2.12)	.6769
4 (.15)	-44.899 (-2.08)	.4869	4 (.097)	-171.198 (-5.28)	.8019
5 (.155)	-96.449 (-3.08)	.6819			

* Column A is point number with (real time)[sec]

* Column B is $\tau_{p,zz}$ with (Newtonian counterpart) [$gcm/sec^2 \cdot cm^2$]

* Column C is $\langle (R/R_0)^2 \rangle$ where $\underline{R}$ is the end-to-end vector of macromolecule and R_0 is the maximum length.

and the corresponding inertia forces. The viscous force, therefore, does not contribute effectively to the force balance. In order to cope with these dominant forces, $\tau_{p,zz}$ must be much larger than the Newtonian stress. As shown in the case of $\psi = .85$ and $\psi = .8$, $\tau_{p,zz}$ very near the exit hole becomes much larger than the Newtonian case, it may, therefore, be possible that this stress component influences the flow behavior. To investigate the influence of $\tau_{p,zz}$ on the flow behavior, the force balance (the equation of motion) in the z-direction has to be considered with the polymer contribution to the stress terms.

The force balance in the z-direction is written by

$$\rho\left(v_r \frac{\partial v_z}{\partial r} + v_z \frac{\partial v_z}{\partial z}\right) = - \frac{\partial p}{\partial z} - \frac{1}{r}\frac{\partial}{\partial r}(r\tau_{rz}) + \frac{\partial \tau_{zz}}{\partial z} + \rho g \qquad 1.17$$

TABLE 6.6 shows the magnitude of each term in eq.1.17 with the orientation of forces around the point $(r/R, z/H) = (.03, .01)$ for the case $Re_\theta = 1370$ and $SS = -.02$. When the $\tau_{p,zz}$ is used for the stress term in eq.1.17, it becomes about 20% of the dominant force (pressure gradient) and the direction of this force turns out to the negative. This indicates that the new force produced by the macromolecules tends to push fluid downward, that is, the axial velocity at this point may be increased. Qualitatively speaking, this is consistent with the decrease of the liquid level during the onset. Although nothing can be said about the magnitude of increased axial velocity unless the equation of motion is solved with the polymer stress tensor, it may be a reasonable outcome that the polymer effect appears near the exit hole especially around $r/R = .03$ and causes the liquid level's falling.

In order to see how the flow behavior changes by the presence of the macromolecules, one must solve the equation of motion with the polymer stress tensor expression (the constitutive equation). This, however, requires a tremendous amount of calculation. Nine non-linear partial differential equations (three from the equation of motion and six from the constitutive equation) are to be solved simultaneously. The calculation is much more difficult and involved than the case of Newtonian flow problem. Instead of pursuing this difficult calculation, the polymer effect may be roughly estimated simply by changing the boundary condition at the exit hole in the Newtonian vortex flow calculation. This method comes from the previous results that the polymer stress tensor becomes significant only for the area very near the exit hole. The calculation procedure, thus, is briefly described as follows. First, the axial velocity at the exit hole is estimated by $\tau_{p,zz}$. Secondly, the boundary condition of the stream function is fixed according to the estimated v_z. Third, the velocity field for the entire vortex flow is calculated by A.D.I for a short period of time. The initial state of the calculation is the case of $Re_\theta = 1370$ and $SS = -.02$. And finally the polymer stress tensor is again calculated along the newly calculated stream lines to see the tendency of stress field. In this way, we could at least see an initial stage of flow change which may correspond to the onset behavior of vortex inhibition.

Fig. 6.15 shows the newly calculated axial velocity at the axis of rotation. The v_z at $r=0$ slightly decreases from the Newtonian case especially when z is less than 5 cm. Even for a short period of time (.286 seconds), the axial velocity responds to the change in the boundary condition which is substitution of the polymer effect at the exit hole. The decrease of the axial velocity at $r=0$ seems to correspond to one of the experimental findings during the onset behavior of vortex inhibition. The calculated tangential velocity, on the other hand, is not appreciably changed at all from the initial state especially outside the hole region. This is also consistent with the experimental fact (See Fig. 6.12).

Fig. 6.16 shows the stream lines obtained from the calculation. The dotted lines are the stream lines for the initial state. The flow pattern as a whole is not so different in the two calculations. However, the stream lines above the boundary layer shift to the right to some extent. This shift also explains the reduction of v_z at $r=0$ because the radial distance between $\psi = 1.0$ and $\psi = .9$ becomes wider. The polymer stress tensor is calculated along the each of the stream lines and the results are listed in TABLE 1.3. Again $\tau_{p,zz}$ very near the exit hole is increased dramatically for $\psi = .8$ and $\psi = .85$. The magnitude of $\tau_{p,zz}$ in both lines are a little larger than before. $\tau_{p,zz}$ along the stream

Fig. 6.15

Axial Velocity Profile after Imposing Polymer Effect

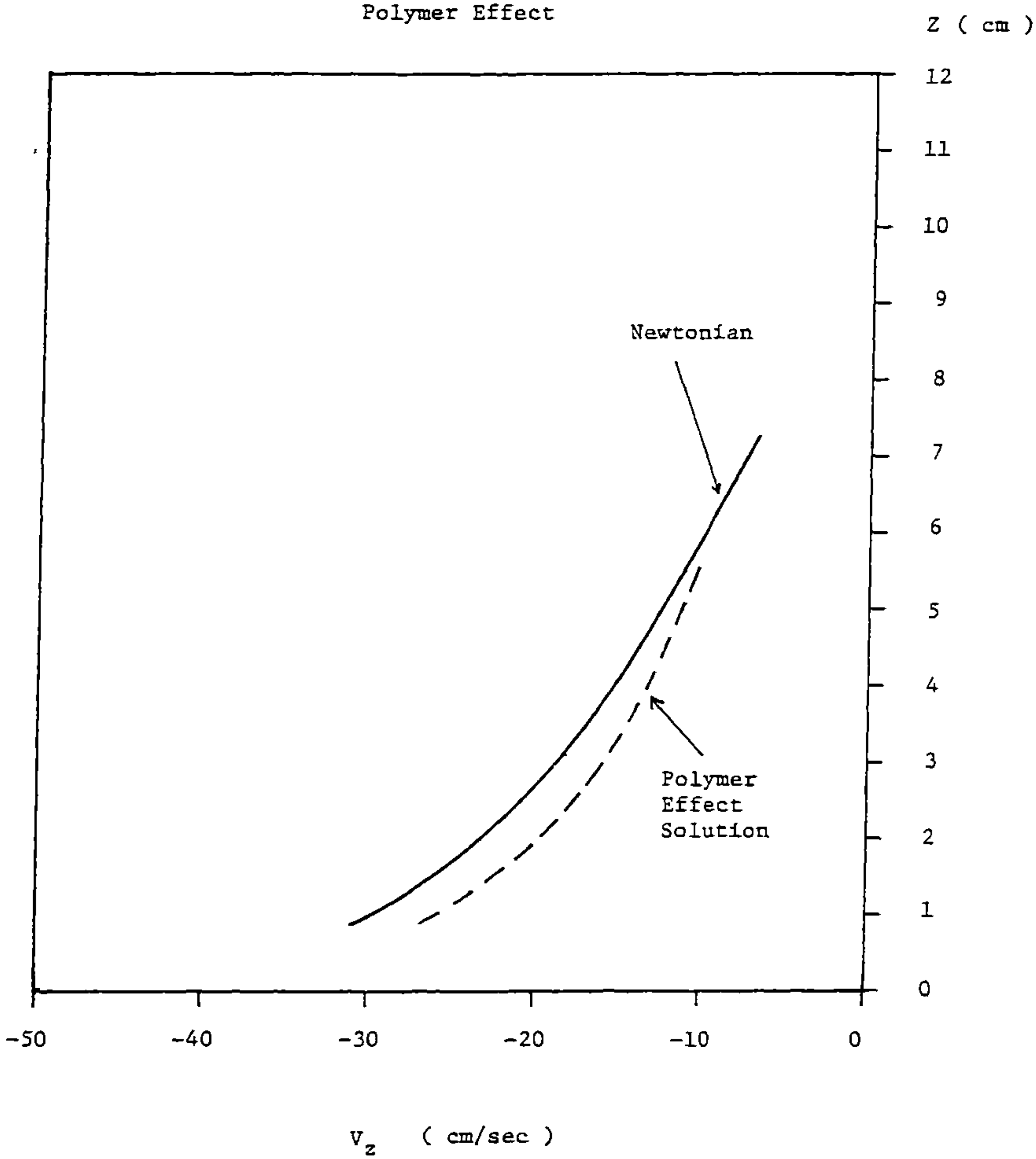

Fig. 6.16
Stream Lines near the Exit Hole after
Imposing the Polymer Effect

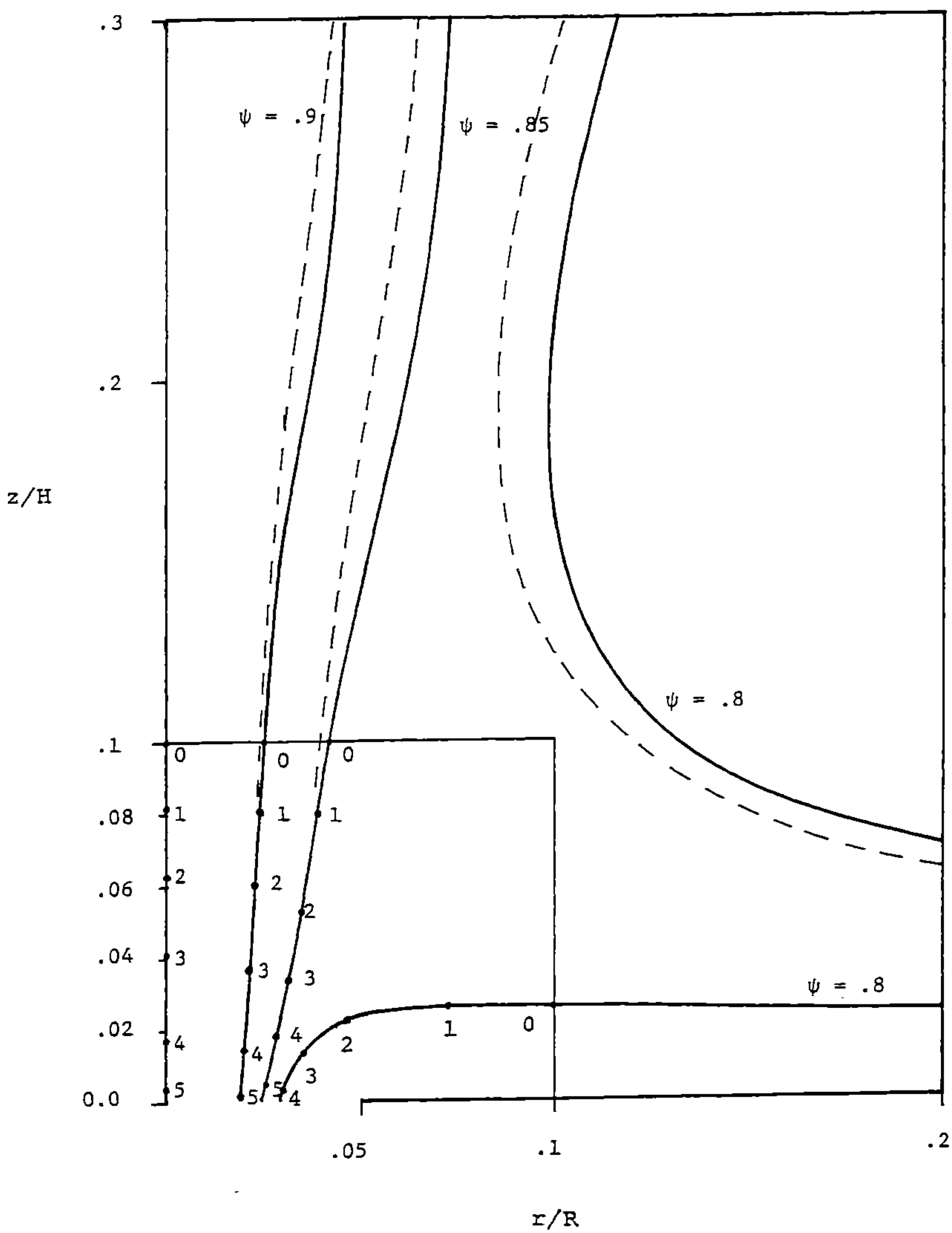

TABLE 1.3

$\tau_{p,zz}$ ALONG THE NEWLY CALCULATED STREAM LINES

$\psi = 1.0$			$\psi = .9$		
A	B	C	A	B	C
1 (.01)	-.015	.0150	1 (.02)	-.204	.0194
2 (.02)	-.042	.0156	2 (.04)	-.291	.0214
3 (.03)	-.054	.0159	3 (.06)	-.298	.0209
4 (.04)	-.152	.0183	4 (.075)	-1.247	.0394
5 (.045)	-.230	.0201	5 (.081)	-5.045	.1056
$\psi = .85$			$\psi = .8$		
A	B	C	A	B	C
1 (.05)	-2.505	.2313	1 (.04)	-.143	.0395
2 (.10)	-7.402	.3456	2 (.08)	-6.286	.2217
3 (.13)	-23.532	.4180	3 (.20)	-34.717	.4478
4 (.15)	-40.625	.4551	4 (.106)	-177.127	.8097
5 (.16)	-131.810	.7526			

* Column A is point number with (real time) [sec]

* Column B is $\tau_{p,zz}$ [$gcm/sec^2 \cdot cm^2$]

* Column C is $\langle (R/R_0)^2 \rangle$ where $\underline{R}$ is the end-to-end vector of macromolecule and R_0 is the maximum length.

lines $\psi = 1.0$ and $\psi = .9$ is not increased enough to cope with the dominant force and the macromolecules are not stretched at all. The tendency of the polymer stress tensor observed before is even more emphasized in this calculation. $\tau_{p,zz}$ along $\psi = .8$ and $\psi = .85$ still becomes large enough to be comparable to the dominant force so that the fluid may be pushed downward again. From the sequence of calculations, we found that the initial effect of the polymers, that is, to increase v_z at the exit hole around $r/R = .03$, keeps its trend as time proceeds because the increased v_z also increases the responsible velocity gradient

$$\frac{\partial v_z}{\partial z}$$

producing higher stress tensor component. From the analysis of $\tau_{p,zz}$, it is found that the dramatic increase of $\tau_{p,zz}$ along the stream lines $\psi = .85$ and $\psi = .8$ very near the exit hole seems to explain qualitatively experimental characteristics of the onset behavior of vortex inhibition, namely, the liquid level's falling and the reduction of v_z at $r = 0$.

1.5 Conclusions

Three major conclusions are drawn from the results of this study. They are:

1) The numerical calculation for the confined Newtonian vortex flow provides reasonable velocity field for the entire vortex tank geometry. The calculated velocity field reasonably agrees with experimentally measured V_θ at the free stream region and V_z along the axis of rotation by photographic tracer technique. The consistency in the comparison may make the velocity information reliable for the area near the exit hole and for the bottom boundary layer. The vortex flow studied in the thesis is highly non-linear (Re_θ is up to 2000) and has a singularity at the exit hole. The alternating-direction implicit method with the zone formulation is found to be suitable for this kind of complicated flow problem.

2) The Modified Nearly Hookean Dumbbell Model seems to be an appropriate constitutive equation for the vortex inhibition study. The model can predict a bounded large elongational viscosity which may change the flow behavior at high strain rates as well as shear thinning. The MNHD also has a simple form so that any kind of locally homogeneous flow can be applied for obtaining the polymer stress field. It is found from dynamical studies of the model that the time to reach steady state in start-up of elongational flow is well scaled by the reciprocal of elongational rate $\dot{\varepsilon}^{-1}$. This

result is quite different from that of shear flow which is scaled by the time constant λ_H.

3) A highly elongational type of flow, namely very high velocity gradient $\frac{\partial V_z}{\partial z}$, is established in the vicinity of the exit hole according to the results of the numerical calculation. This large velocity gradient may be a cause of the onset behavior of vortex inhibition. The application of the velocity field to the MNHD shows that the macromolecules moving along the stream lines passing the bottom boundary layer and outside the core region (see ψ=.8 and ψ=.85 in Fig. 6.14) seem to be almost stretched out to the maximum length R_O very near the exit hole. The stretched macromolecules produce large stress tensor which seems to explain qualitatively the characteristics of the onset behavior of vortex inhibition.

II. INTRODUCTION

2.1 The Description of Vortex Inhibition

Vortex inhibition was discovered by Gordon (1972) in 1972. In his experiment, a small amount of polymer in water prevents formation of a vortex in draining the solution from the bottom of a square tank. A square tank filled with tap water is prepared. After stirring the water vigorously with a paddle and then removing the plug from the center of the bottom, a stable vortex forms extending down to the bottom of the container. When this is repeated with a dilute polymer solution, the vortex is incomplete (see Fig. 2.1). This different phenomenological behavior produced by adding just a small amount of polymer inidcates that the flow pattern is drastically changed due to the presence of the polymer. The vortex inhibition may be explained clearly by using a steady state vortex flow. A steady state vortex flow is obtained by tangentially feeding the water at the outer wall of a cylindrical container with an axially uniform velocity. Fig. 2.2 shows the steady state vortex flow. When the water is replaced by about 30 wwpm polyethylene oxide (Polyox 301) keeping the flow rate constant, the air core of the vortex is suppressed and the suppression of the air core is not steady but a randomly periodic phenomenon. Just after the air core is suppressed, it tends to extend to the bottom again. As soon as the air core reaches the

Fig. 2.1 : Vortex Inhibition

In case of the Newtonian fluid, the vortex forms extending down to the bottom. On the other hand, if a small, critical concentration of polymer is present, the vortex is imcomplete.

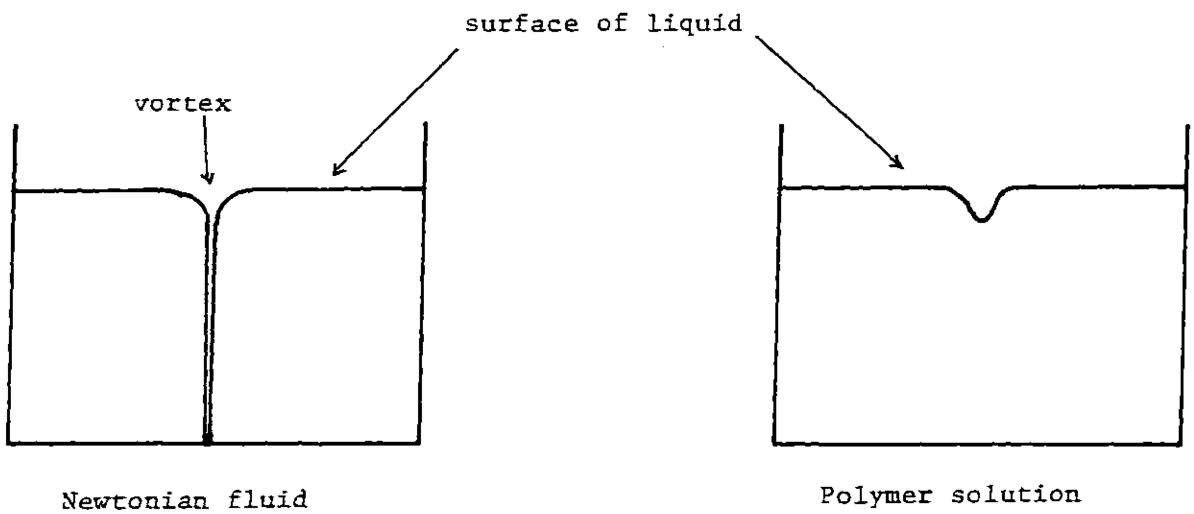

Fig. 2.2   Steady State Vortex Flow

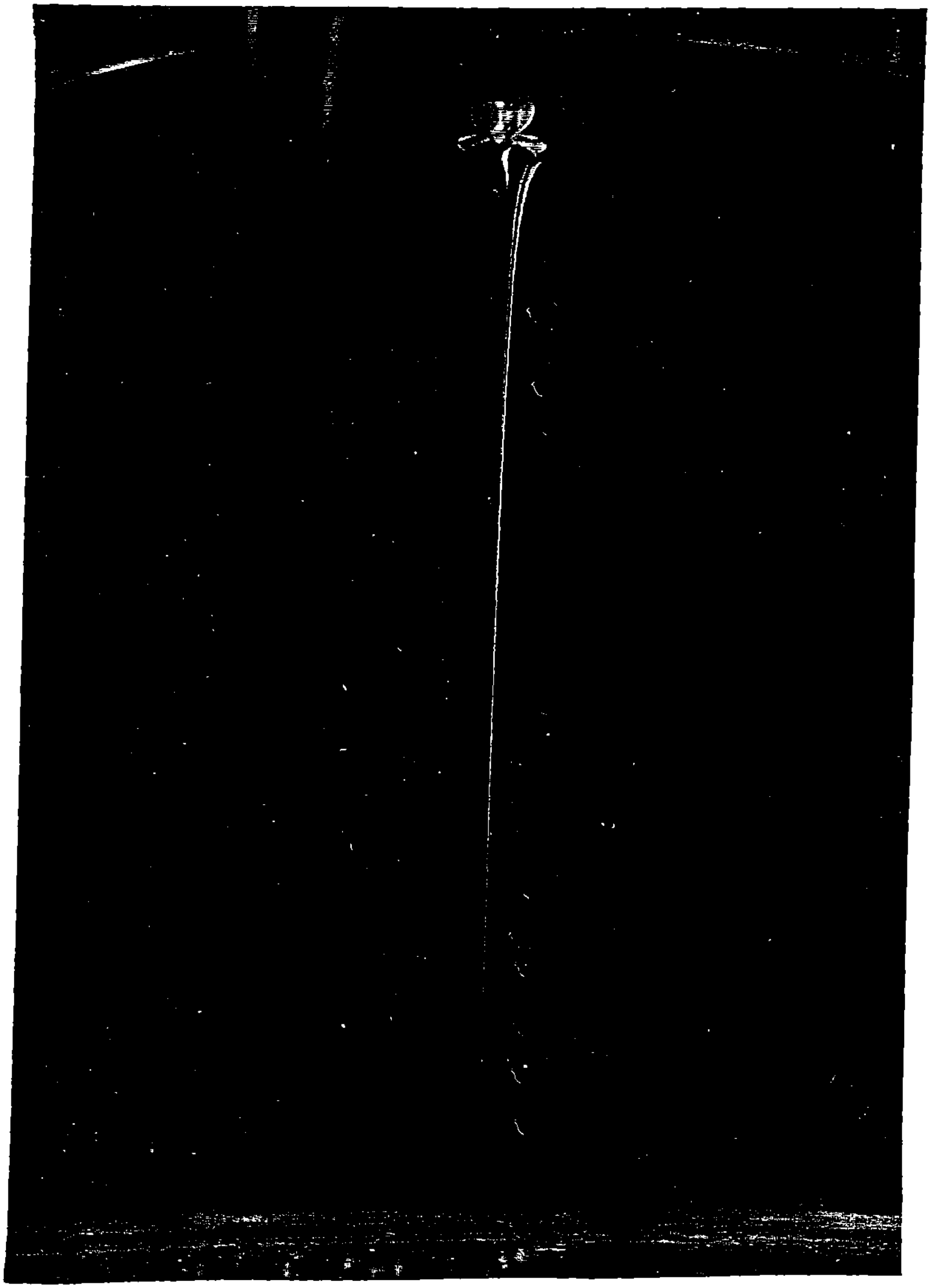

bottom, it immediately is suppressed (see Fig 2.3). This process is repeated until the polymer is degraded. During vortex inhibition, the liquid level, falls substantially (by nearly 50%).

A particularly interesting feature of vortex inhibition is that the amount of polymer added to the water is so small that the shear viscosity of the polymer solution is only slightly different from that of water itself. The relative viscosity of the polymer solution used in this study is only about 1.02.

Furthermore, Gordon (1972) showed that the macromolecules which show vortex inhibition ability are also good agents for drag reduction. As Table 2.1 shows, the same ordering in terms of effective concentration also seems to hold for both the vortex inhibition and drag reduction.

Since the viscosity of the polymer solution is almost equal to that of water for both vortex inhibition and drag reduction, non-Newtonian rheological properties of the dilute polymer solutions such as strain rate thickening elongational viscosity and non-zero normal stress differences in steady shear flow might be responsible for vortex inhibition. The elongational viscosity is believed to be increased drastically even at moderately high elongational rate for a dilute polymer solution. For instance, as shown in Fig. 2.4 the modified nearly Hookean Dumbbells model (developed in Chapter 5) shows a sudden increase of elonga-

Fig. 2.3 Vortex Flow with Suppressed Air Core

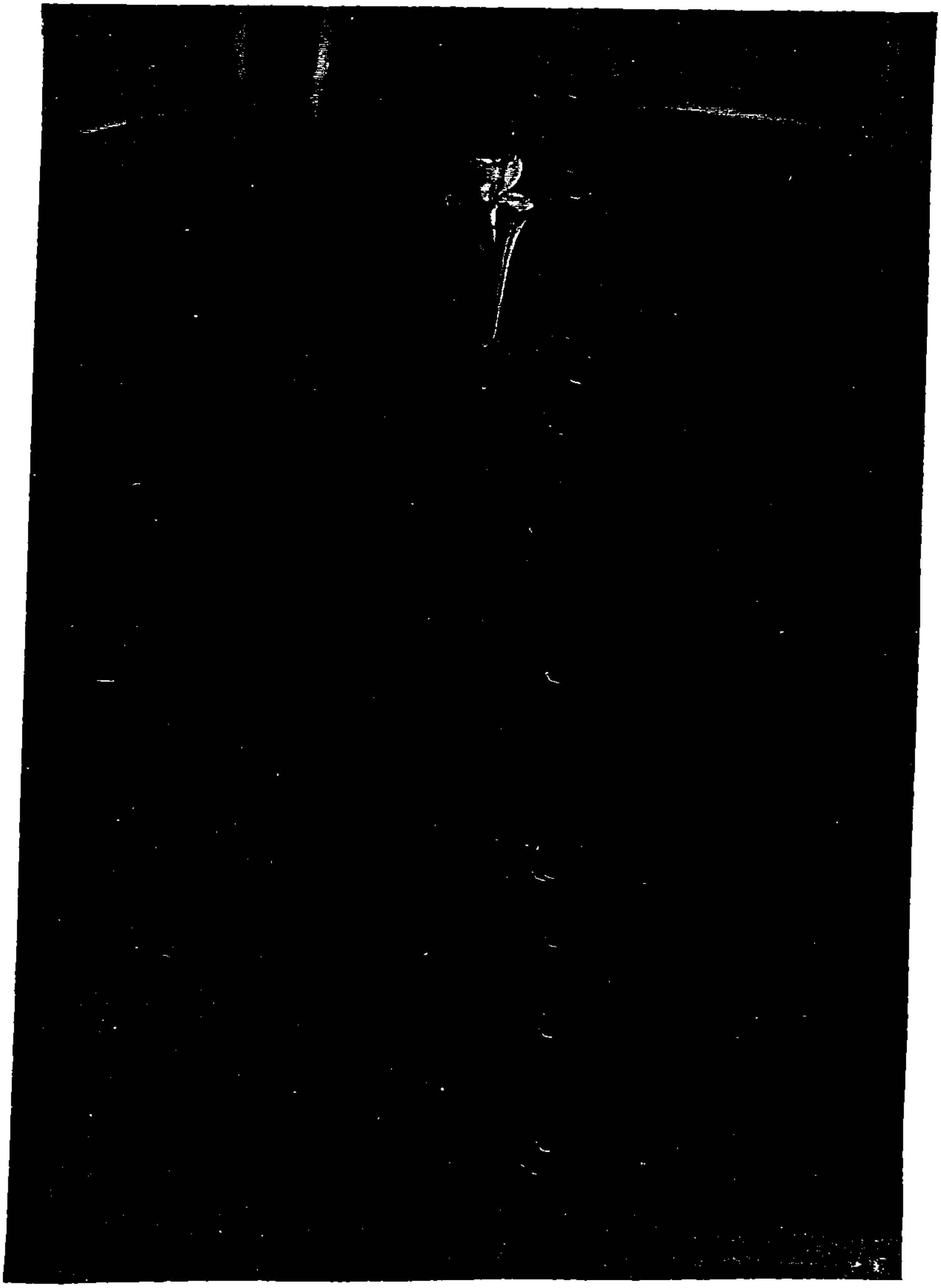

TABLE 2.1

EFFECTIVE CONCENTRATIONS OF VARIOUS POLYMERS FOR V.I. AND D.R.

Polymer Designation	Polymer Type	wwpm Vortex Inhibition	wwpm Drag Reduction
Polyox FRA*	Polyethylene Oxide	7.5	9
Polyox WSR 301*	Polyethylene Oxide	30	20
Separan AP 273•	Polyacrylamide	3	5
Separan AP30•	Polyacrylamide	40	35

*Union Carbide (Manufacturer)

•Dow (Manufacturer)

Note 1: These data are from Gordon (1972).

Note 2: Effective concentration is the lowest concentration with which polymer shows the ability of vortex inhibition or drag reduction.

Fig. 2.4 : Elongational Viscosity Predicted by MNHD

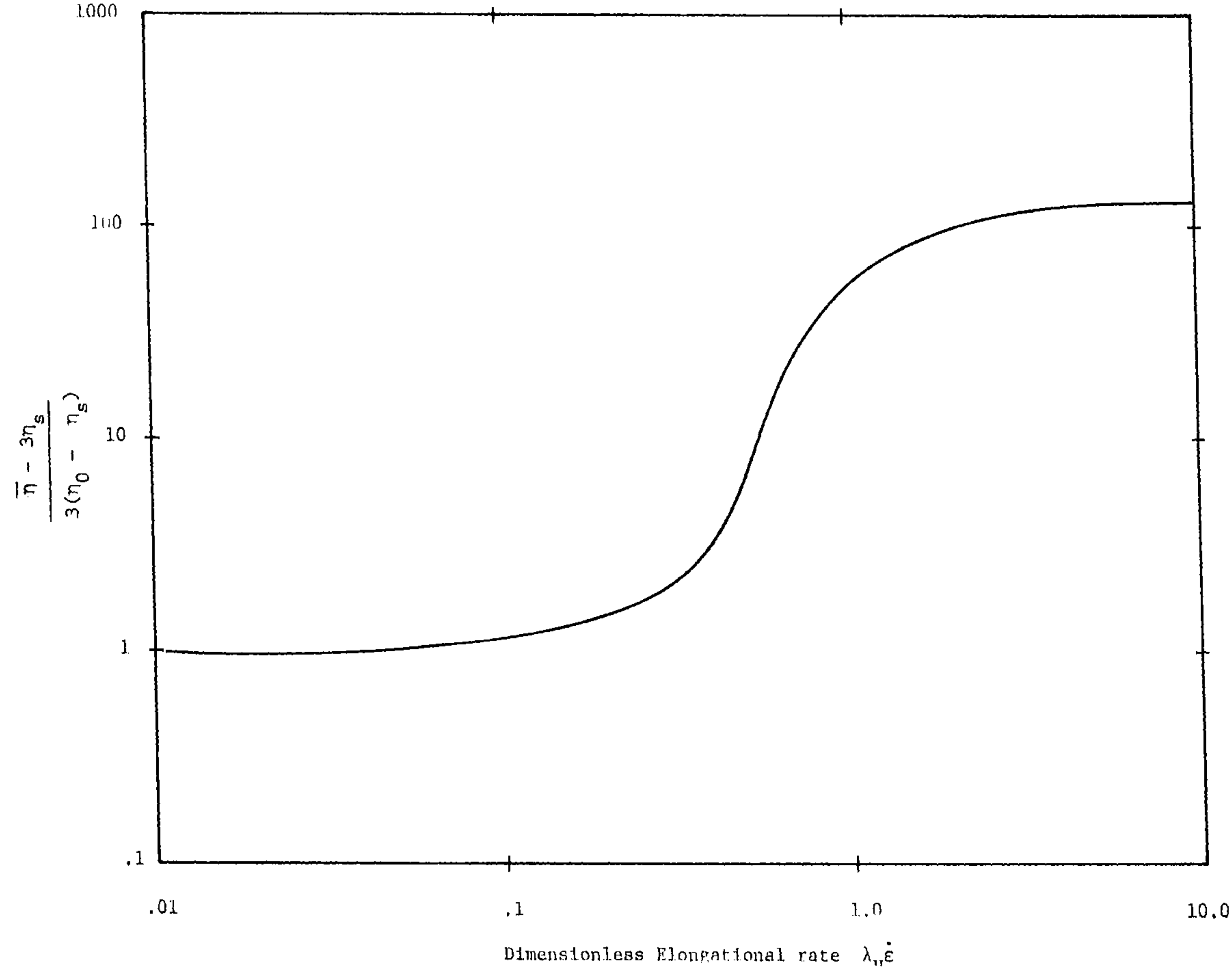

tional viscosity when the domensionless elongational is of order unity. The elongational viscosity increases up to several orders of magnitude higher than that of solvent alone. Even though no direct experimental measurements have been obtained for the elongational viscosity for a dilute polymer solution, the kinetic theory predicts that a high elongational viscosity is realized when a linear flexible polymer is stretched at almost full length due to the elongational flow field. It may, therefore, be possible to expect that the changes in flow behavior in vortex inhibition phenomenon is due to the large elongational viscosity exerted by the presence of a few macromolecules.

2.2 Objective and Motivations

The objective of this thesis work is to investigate the mechanism of vortex inhibition. The study is motivated at first, by a possible correlation between vortex inhibition and drag reduction and secondly, by an interest in developing a constitutive equation (rheological equation of state) to describe dilute polymer solutions.

We can speculate from Table 2.1 that the mechanism of vortex inhibition may be similar to that of drag reduction. Although drag reduction has been extensively studied in recent years, there are many aspects of the phenomenon which are not well understood (Lumely, 1973; Virk et al., 1967; Virk, 1975). Out of several proposed mechanism for drag reduction, the viscoelastic nature (especially large elongational viscosity) of macromolecules in turbulent flow is proposed to be a major cuase for reducing turbulent energy dissipation (Little et al., 1975; Seyer and Metzner, 1969; Gordon and Everage, 1971). According to Seyer and Metzner (1969), the bursting (Kim et al., 1971) produced by a pair of counter rotating eddies at boundary layer near the wall is characterized by stretching motion similar to elongational flow. The increased resistance to stretching due to the large elongational viscosity, thus results in less bursting and less radial momentum flux transport. However it is not possible to make a direct test of this proposed mechanism because no precise velocity information of the fliud element is obtainable during the bursting process. The proposed mechanism for drag reduction may, in turn, be closely related to the molecular mechanism of vortex inhibition. It might be, therefore, possible to infer the molecular mechanism for drag reduction from the analysis of vortex inhibition. The Newtonian vortex flow is treated as a laminar flow so that it is much easier to be analyzed than turbulen flow.

In order to analyze vortex inhibition, rheological equation of state (a constitutive equation) for a dilute polymer solution has to be introduced so that information about the stress field can be predicted. Although an extremely simplified model (beads and spring bumbbell model) is being used, we believe that the kinetic theory provides reasonable predictions about differences in flow behavior resulting from molecular structures. Moreover, we can evaluate the kinetic theory constitutive equations by comparing their predictions in the flow with experimental results.

2.3 Approach and Previous Work

Approach

A study of vortex inhibition is carried out in the following way. First, the Newtonian vortex flow is extensively studied in Chapter 3. The information about the velocity field of the Newtonian vortex flow is necessary for analyzing vortex inhibition because it provides a starting point for computing deformation of the marcomolecules when the polymer solution is subjected to the flow field. At first, various regions of the vortex flow are analytically studied and then the complete Navior-Stokes equations, with a singularity (the presence of the exit hole at the center of the bottom wall), are numerically solved by finite difference scheme for various values of tangential Reynolds number.

Secondly, the experimental part of vortex inhibition is described in Chapter 4. The velocity components (tangential and axial velocity) are measured by a photographic tracer technique. The velocity measurement not only provides the characteristic of the Newtonian vortex flow but also gives a check on the results of numerical simulation which is given in Chapter 6. Besides the velocity measurements, a series of qualitative observations about the flow behavior of both the Newtonian and polymer vortex flow are conducted to help understand the nature of vortex inhibition.

An approximate constitutive equation (rheological equation of state) for dilute polymer solutions is developed from kinetic theory in Chapter 5. The model is then tested for shear flow and elongational flow with various strain rates to evaluate the material functions such as shear viscosity, the primary normal stress coefficient and elongational viscosity.

Finally in Chapter 6, the results of the numerical simulation are used for the polymer solution stress field calculation by use of the constitutive equation developed in Chapter 5. With the calculated stress field, an attempt is made to explain vortex inhibition, that is, the dramatic differences in flow behavior between the Newtonian and polymer solution with the aid of the experimental study.

<u>Previous Work</u>

The major contributions of this thesis work are hydrodynamics of the Newtonian vortex flow and development of constitutive equation, whose prediction for elongational viscosity is especially important, for polymer solutions. There have been a number of theoretical studies of confined vortex flow in past because of its broad application in fluid dynamics, heat transfer, power generation and meterology. Lewellen (1971, 1964, 1962) has used similarity transformations and asymptotic expressions to describe the flow. Integral methods are used for analysis of the boundary layer by Rott and Lewellen (1966). Anderson (1966) has studied the flow behavior of the bottom boundary layer by reducing the boundary layer equations to ordinary differential equations based on the method developed by Smith and Cutler (1963). Farris et al. (1969) and Pao (1970) have numerically solved the full Navior-Stokes equations for confined vortex flow. These approaches, however, do not provide velocity information about the flow behavior in the vicinity of the exit hole which, in turn, plays a very important role for the analysis of vortex inhibition.

The experimental contribution to the analysis of the Newtonian vortex flow is due to Kendall (1962) and Taylor (1974). Kendall has measured radial and tangential velocity components of gases inside the bottom boundary layer and the profiles of both velocity components of liquid are qualitatively observed by Taylor. Chiou (1976) has used a photographic tracer technique for determining V_θ and V_z especially near the axis of rotation outside the bottom boundary layer. His study for vortex inhibition is also limited for the area away above the bottom wall.

There have been many models suggested for polymeric fluids from the kinetic theory (Bird, 1977). Out of these models, the idea of using a dumbbell (two beads jointed by a connector) to simulate a macromolecule is focused on this study (Bird et al., 1977). Even though the dumbbell models are oversimplified representation of polymers and the results obtained from them do not have a wide range of applicability, many of the mathematical manipulations can be performed because of the simplicity of the models. Table 2.2 shows several kinds of dumbbell model for a flexible macromolecule. The simplest one is the Hookean Dumbbell model whose connector is described by Hooke's law. The Hookean Dumbbell is the model from which the constitutive equations can be derived without solving the diffusion equation so that the polymer stress tensor can easily be calculated from any types of homogeneous flow. The model; however, has serious defects such as shear independent viscosity and unbounded elongational viscosity for high elongational rate because of the linearity in the connector force law. The connector force law developed by Warner

(1972) represents a macromolecule a little more realistically. The connector force is getting stiffer and stiffer as the end-to-end vector $\underline{R}$ becomes close to the maximum length R_o. The model shows the shear thinning, non-zero primary normal stress coefficient and bounded elongational viscosity. The mathematical manipulation, however, is limited only for small strain rates and a few material functions for high strain rates. As to the prediction of elongational viscosity at high elongational rates, Stevenson and Bird (1971) has numerically calculated bounded elongational viscosity using inverse-Langevin-Spring dumbbell model. The bounded elongational viscosity is also found by Tanner (1971) with a use of linear locked spring model. The experimental contribution to the rheology of a dilute polymer solution, however, is far behind the theory.

TABLE 2.2

CONNECTOR FORCE LAW OF DUMBBELL MODELS

Name	Connector Force Law	Comment
Hooke	$\underline{F} = H\underline{R}$	The connector is infinitely stretchable.
Tanner (1971)	$\underline{F} = H\underline{R} \quad R < R_o$	The "linear-locked" springs can stretch as far as R_o, for $R < R_o$ they are described by Hooke's law.
Warner (1972)	$\underline{F} = \frac{H}{1-(R/R_o)^2}\underline{R} \quad R < R_o$	The "finitely extendable nonlinear elastic" (FENE) connector has an upper limiting length $R = R_o$.

III. STEADY NEWTONIAN VORTEX FLOW OVER A SOLID WALL

3.1 Introduction

A newtonian vortex flow has three distinct characteristics in its flow behavior. As shown in Fig. 3.1, the region I is called 'free stream region', which is characterized by a potential flow. The tangential velocity v_θ is inversely proportional to the radial distance r (the distance from the axis of rotation) in the free stream region. The change in v_θ in the z-direction is so small that the flow may be treated as one dimensional. When the tangential Reynolds number

$$Re_\theta = \frac{Rv_{\theta R}}{\nu} ,$$

however, becomes larger, the flow eventually forms a cell and this case makes one treat it as three dimensional flow problem . It is possible that the vortex flow in the free stream region makes more than single cell (Donaldson and Sullivan, 1960).

The region II is called 'core region' where a large amount of downflow exists because of the exit hole in the bottom plate. The tangential velocity v_θ , in turn, is proportional to the radium because stress component

$$\tau_{r\theta} = -\mu r \frac{\partial}{\partial r}\left(\frac{v_\theta}{r}\right)$$

has to be vanished at the axis of rotation.

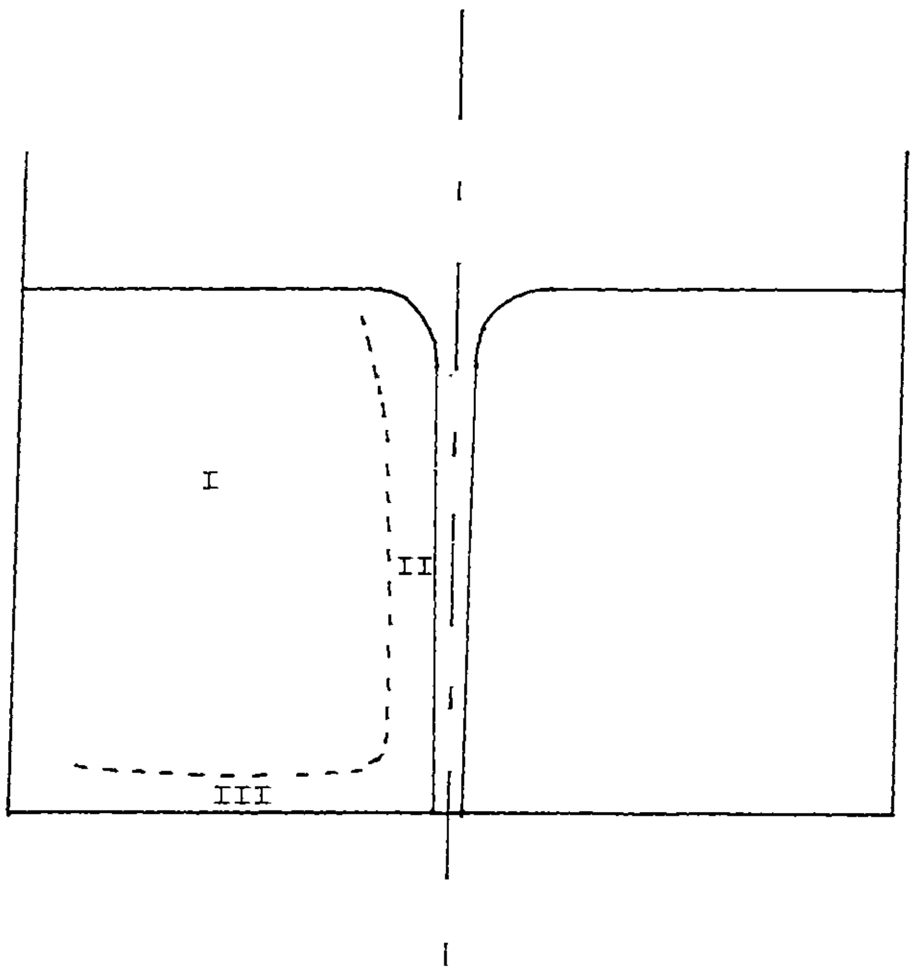

Figure 3.1

Three Different Flow Regions

in a Newtonian Vortex Flow

The relationship between the centrifugal force and the radial pressure gradient is known in both the free stream and core regions. The centrifugal force

$$-\rho \frac{v_\theta^{\,2}}{r}$$

is exactly balanced with the radial pressure gradient

$$-\frac{\partial p}{\partial r}$$

in these regions (Schlichting, 1968) but the balance between the two forces is broken in region III which is called "bottom boundary layer".

In the bottom boundary layer, the tangential velocity v_θ is reduced due to the drag from the bottom wall resulting in decreasing the centrifugal force. On the other hand, the radial pressure gradient remains the same along the z-axis (Schlichting, 1968), this force, therefore, overcomes the centrifugal force producing a large amount of radial inflow (Taylor, 1972). The amount of fluid passing through the bottom boundary layer is the same order as the total flow rate (Lewellen, 1971).

In this chapter, the tangential velocity v_θ in both the free stream and core regions is determined by using an empiracal expression of the radial velocity v_r and the flow behavior in the bottom boundary laver is approximatelv analyzed. The impact of the axial downflow from the core region on the radial inflow from the bottom boundary layer occurs near the exit hole. The flow behavior in this area is not well known because of its complicated nature (Lewellen, 1971). A numerical simulation for the entire vortex flow, therefore, is needed to investigate the flow behavior in the region near the exit hole. The simulation is seeking for the exact solution of the full Navior-Stokes equations for a confined vortex flow. The treatment of an open-free surface vortex flow such as used in the V.I. study has not been studied. Such a problem is very difficult to manipulate because the shape of the free surface must be determined as part of the solution. Dergarabedian (1960) treats a time-dependent emptying process of vortex flow although he does not consider the effect of the bottom boundary layer. Even though the confined vortex flow is different from the open-free surface vortex flow, the essential feature of the V.I. study may well be characterized by the confined vortex flow.

3.2 One Dimensional Vortex Flow

In this section the tangential velocity in the core and free stream regions is numerically solved as a one-dimensional problem and the results will agree with available experimental data. In these two regions, v_θ is assumed to be independent of z, so that the θ-component of the equation of motion becomes

$$v_r \frac{\partial \Gamma}{\partial r} = \nu\left(\frac{\partial^2 \Gamma}{\partial r^2} - \frac{1}{r}\frac{\partial \Gamma}{\partial r}\right) \qquad 3.1$$

where the circulation Γ is defined by

$$\Gamma = v_\theta \cdot r \qquad 3.2$$

Since the radial velocity v_r is inversely proportional to the radius r when r is large and v_r is, in turn, linear to r when r is small, Dergarabedian (1961) assumes the following functionality of v_r.

$$v_r = -\frac{\dot{\varepsilon} a^2}{2r}\left[1- \exp(-\frac{r^2}{a^2})\right] \qquad 3.3$$

where an elongational rate at the axis of rotation $\dot{\varepsilon}$ is defined by

$$\dot{\varepsilon} = \dot{\varepsilon}(z) = \left.\frac{\partial v_z}{\partial z}\right|_{r=0} \qquad 3.4$$

From eq. 3.3,

$$\left.\begin{aligned} v_r &\propto 1/r & \qquad r \to 0 \\ v_r &\propto r & \qquad r \to \infty \end{aligned}\right\} \qquad 3.5$$

As the desired axial velocity v_z is then given by the continuity equation,

$$v_z = v_z\Big|_{r=0} \quad \exp(-\frac{r^2}{a^2}) \qquad 3.6$$

Chiou (1976) experimentally determines the parameter a and v_z along the axis of rotation. eq. 3.1 is solved by a finite difference scheme. eq. 3.1 is discretized according to the finite difference formula and the circulation Γ at each discrete point is solved implicitly using the boundary conditions

$$\Gamma(r=0) = 0$$

and

$$\Gamma(r=R) = \Gamma_R .$$

The result of the calculation with Chiou's experimental data is shown in Fig. 3.2. The calculated v_θ agrees well with the data. After numerical simulation, it is found that the tangential velocity v_θ is very sensitive to the elongational rate $\dot{\varepsilon}$. As shown in Fig. 3.3, when $\dot{\varepsilon}$ is increased, the radial convection shifts the peak value of v_θ toward the axis of rotation producing a steeper v_θ - profile (case

3.2 One Dimensional Vortex Flow

In this section the tangential velocity in the core and free stream regions is numerically solved as a one-dimensional problem and the results will agree with available experimental data. In these two regions, v_θ is assumed to be independent of z, so that the θ-component of the equation of motion becomes

$$v_r \frac{\partial \Gamma}{\partial r} = \nu\left(\frac{\partial^2 \Gamma}{\partial r^2} - \frac{1}{r}\frac{\partial \Gamma}{\partial r}\right) \qquad 3.1$$

where the circulation Γ is defined by

$$\Gamma = v_\theta \cdot r \qquad 3.2$$

Since the radial velocity v_r is inversely proportional to the radius r when r is large and v_r is, in turn, linear to r when r is small, Dergarabedian (1961) assumes the following functionality of v_r.

$$v_r = -\frac{\dot{\varepsilon} a^2}{2r}\left[1 - \exp\left(-\frac{r^2}{a^2}\right)\right] \qquad 3.3$$

where an elongational rate at the axis of rotation $\dot{\varepsilon}$ is defined by

$$\dot{\varepsilon} = \dot{\varepsilon}(z) = \left.\frac{\partial v_z}{\partial z}\right|_{r=0} \qquad 3.4$$

From eq. 3.3,

$$\left.\begin{array}{ll} v_r \propto 1/r & r \to 0 \\ v_r \propto r & r \to \infty \end{array}\right\} \quad 3.5$$

As the desired axial velocity v_z is then given by the continuity equation,

$$v_z = v_z\Big|_{r=0} \quad \exp\left(-\frac{r^2}{a^2}\right) \qquad 3.6$$

Chiou (1976) experimentally determines the parameter a and v_z along the axis of rotation. eq. 3.1 is solved by a finite difference scheme. eq. 3.1 is discretized according to the finite difference formula and the circulation Γ at each discrete point is solved implicitly using the boundary conditions

$$\Gamma(r=0) = 0$$

and

$$\Gamma(r=R) = \Gamma_R .$$

The result of the calculation with Chiou's experimental data is shown in Fig. 3.2. The calculated v_θ agrees well with the data. After numerical simulation, it is found that the tangential velocity v_θ is very sensitive to the elongational rate $\dot{\varepsilon}$. As shown in Fig. 3.3, when $\dot{\varepsilon}$ is increased, the radial convection shifts the peak value of v_θ toward the axis of rotation producing a steeper v_θ - profile (case

Figure 3.2

TANGENTIAL VELOCITY VS R

ELONGATIONAL RATE = .91 sec^{-1}

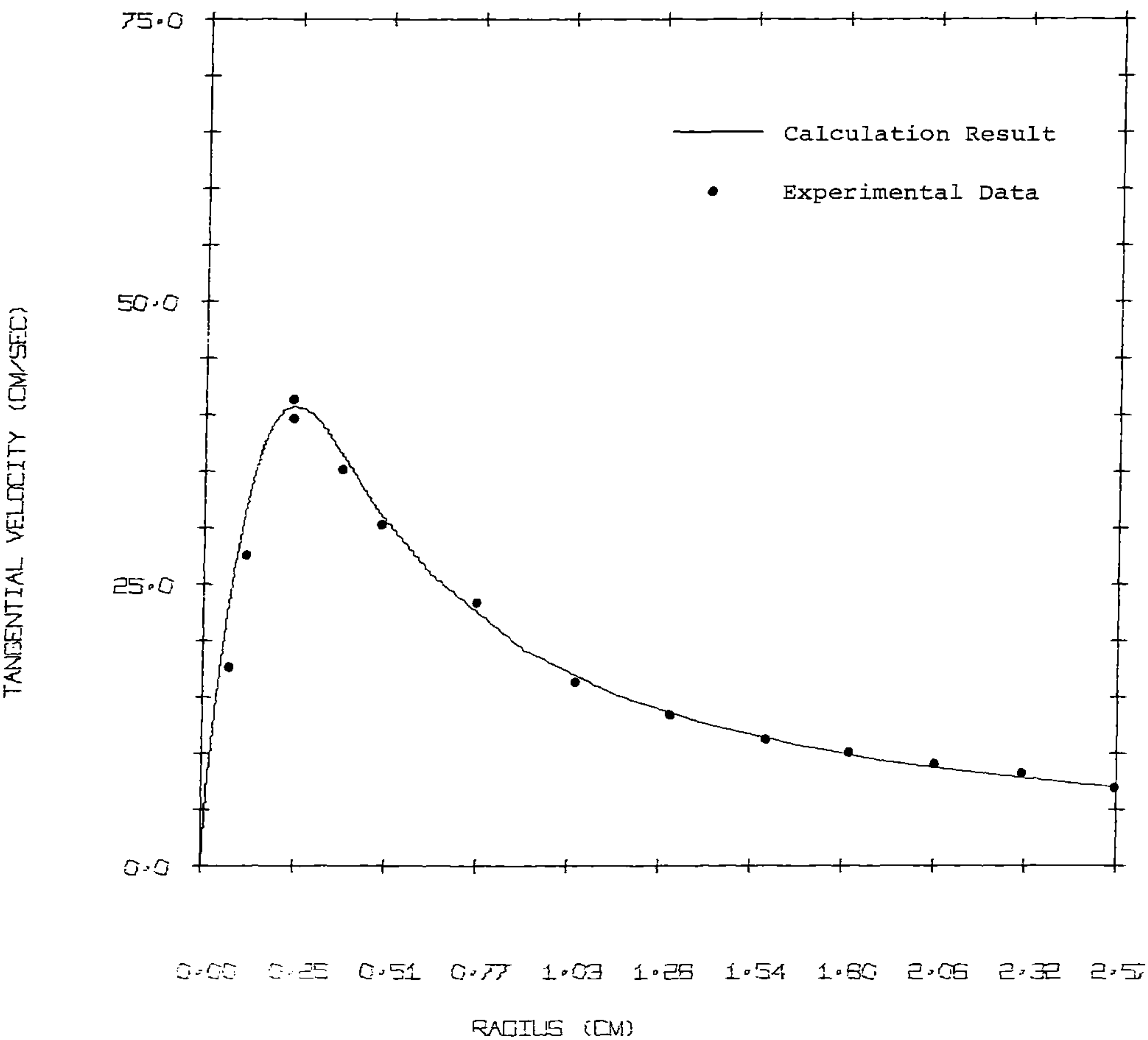

2 in Fig. 3.3). The case 2 indicates that the increased $\dot{\varepsilon}$ intensifies the θ - component of vorticity near the axis of rotation. On the other hand, when $\dot{\varepsilon}$ is decreased, the vorticity is able to diffuse farther in the direction resulting in a flatter v_θ -profile (case 3 in Fig. 3.3). Since v_θ near the axis of rotation is reduced, the corresponding centrifugal force is also decreased. The radial pressure gradient which is balanced with the centrifugal force is then reduced.

The relative shape of the free surface of these vortex flows can be obtained from the tangential velocity v_θ as a function of the radius r. From the r- and z-components of the equation of motion, the pressure gradients are

$$-\frac{\partial p}{\partial r} = -\rho\frac{v_\theta^{\,2}}{r} \qquad 3.7$$

$$\frac{\partial p}{\partial z} = -\rho z \qquad 3.8$$

Pressure is an analytic function of position (Bird and et al., 1960),

$$dp = \frac{\partial p}{\partial r}dr + \frac{\partial p}{\partial z}dz \qquad 3.9$$

An integration of eq. 3.9 along the free surface gives

$$p(r=R,S(R)) - p(r=r,S(r)) = \int_r^R \frac{\partial p}{\partial r}dr + \int_{S(r)}^{S(R)} \frac{\partial p}{\partial z}dz \qquad 3.10$$

Figure 3.3

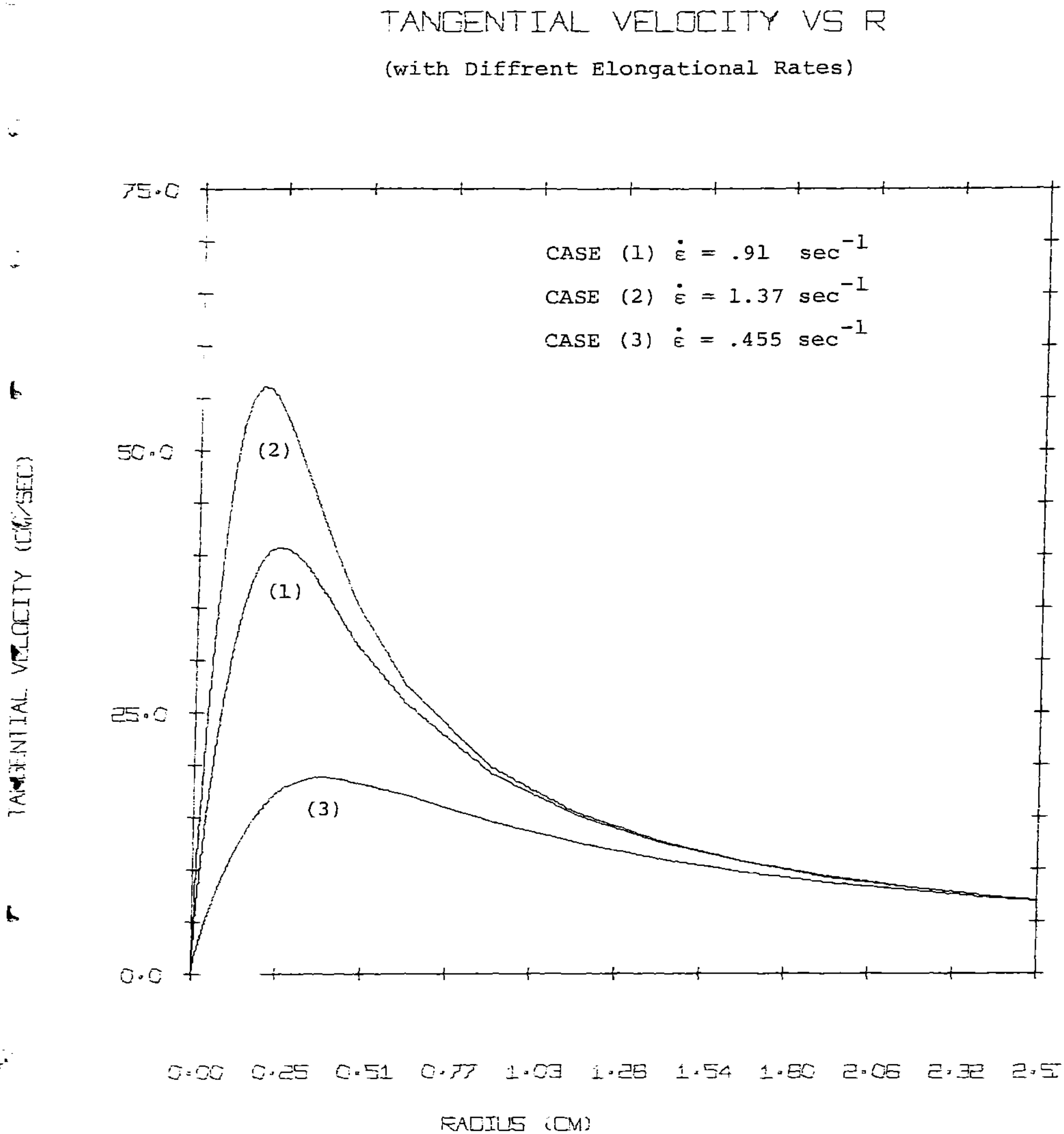
TANGENTIAL VELOCITY VS R
(with Diffrent Elongational Rates)
CASE (1) $\dot{\varepsilon}$ = .91 sec^{-1}
CASE (2) $\dot{\varepsilon}$ = 1.37 sec^{-1}
CASE (3) $\dot{\varepsilon}$ = .455 sec^{-1}
75.0
50.0
25.0
0.0
(1)
(2)
(3)
TANGENTIAL VELOCITY (CM/SEC)
0.00
0.25
0.51
0.77
1.03
1.28
1.54
1.80
2.06
2.32
2.5
RADIUS (CM)

where $S(r)$ the z-position of the free surface at r. $S(r)$ can be calculated in eq. 3.10 by knowing that the pressure is equal along the free surface. The depth of the free surface relative to that at the outer boundary $(r=R)$ is then given by

$$S(r) - S(R) = -\frac{1}{\rho g}\int_r^R \rho\frac{v_\theta^2}{r}dr \qquad 3.11$$

Fig. 3.4 shows the relative shape of the free surface with various elongational rate corresponding to Fig. 3.3 as the result of numerical integration of eq. 3.11. As expected, when the elongational rate $\dot{\varepsilon}$ is increased (case 2), the free surface becomes sharper due to the higher radial pressure gradient near the center. When the elongational rate $\dot{\varepsilon}$, however, is decreased, the fluid has a flatter free surface.

Vortex inhibition corresponds to the free surface shape's becoming flatter. As long as we regard the fluid as Newtonian, the above calculation suggests that vortex inhibition corresponds to a reduction in axial velocity gradient $\dot{\varepsilon}$.

It is known that large velocity gradient (strain rate) is necessary for polymer to be subject to change its conformation. Especially when the strain rate reaches the order of reciprocal of time constant λ_H, various polymer effects start revealing (the rheology of polymer solutions will be discussed in Chap. 5). Chiou (1976) indicated that the

Figure 3.4

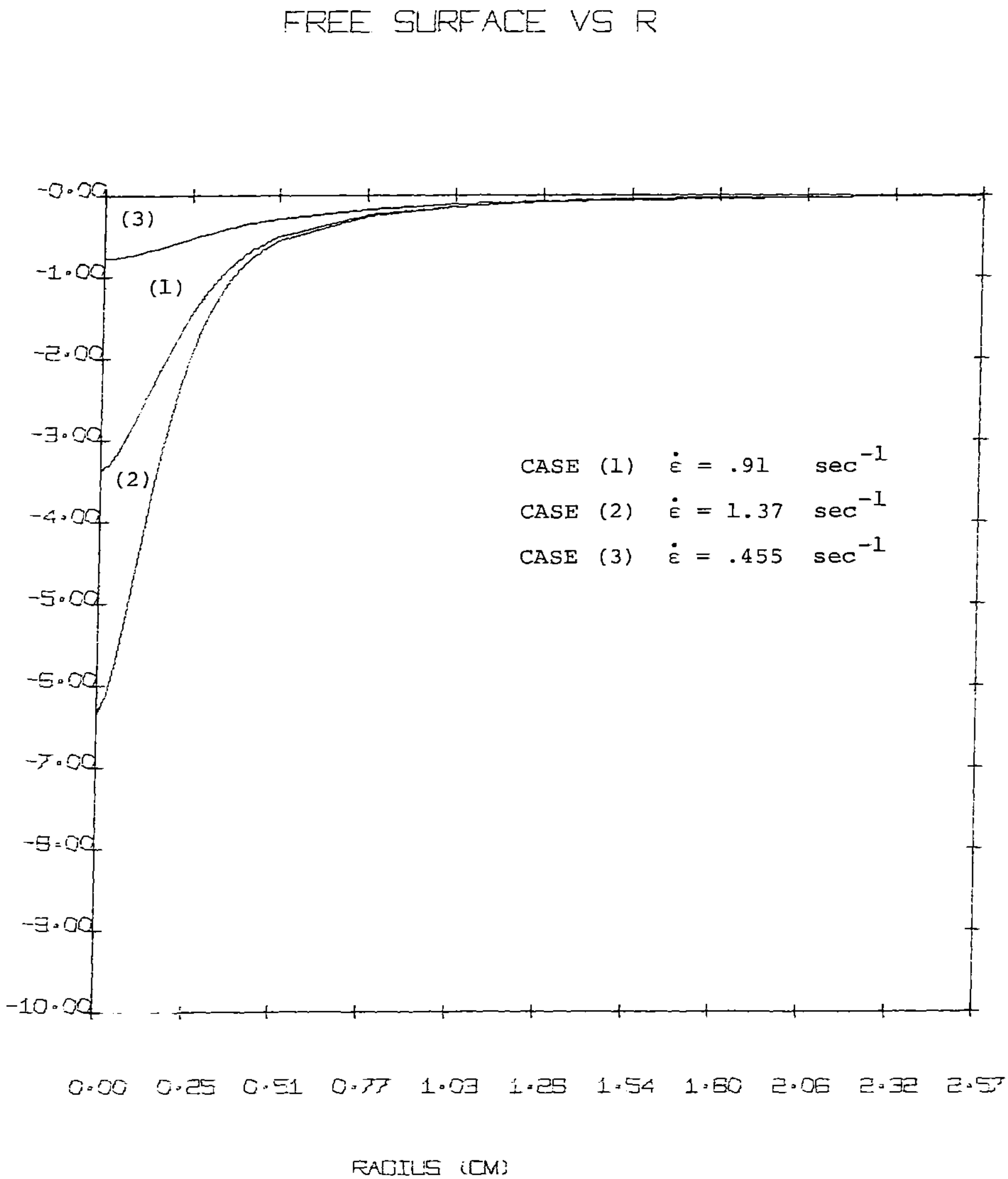
FREE SURFACE VS R
-0.00
-1.00
-2.00
-3.00
-4.00
-5.00
-6.00
-7.00
-8.00
-9.00
-10.00
(3)
(1)
(2)
CASE (1) $\dot{\varepsilon}$ = .91 sec^{-1}
CASE (2) $\dot{\varepsilon}$ = 1.37 sec^{-1}
CASE (3) $\dot{\varepsilon}$ = .455 sec^{-1}
0.00 0.25 0.51 0.77 1.03 1.28 1.54 1.80 2.06 2.32 2.57
RADIUS (CM)

strain rate

$$\frac{\partial v_\theta}{\partial r}$$

would be responsible for the polymer effect causing vortex inhibition, the maximum value of

$$\frac{\partial v_\theta}{\partial r}$$

in Fig. 3.2 is, however, at most about 60 sec^{-1} around $r = .4$ cm. This figure of

$$\frac{\partial v_\theta}{\partial r}$$

is not large enough to realize the polymer effect because the estimation of the time constant (See Appendix B) shows that the dimensionless strain rate

$$\lambda H \frac{\partial v_\theta}{\partial r}$$

will be .6. The dimensionless strain rate has to be at least more than unity to expect the polymer effect according to the results obtained in Chap. 5. The strain rate

$$\frac{\partial v_\theta}{\partial r} \quad ,$$

therefore, may not be a main cause of vortex inhibition. And this leads us to investigate the area where higher strain rates are established in vortex flow.

3.3 The Analysis of Flow Behavior Inside the Bottom Boundary Layer

Since the polymer effect reveals when velocity gradient is very large, the flow behavior inside the bottom boundary layer in analyzed by the integral method (Lewellen, 1971). A large deformation rate is expected in the bottom boundary layer because the velocity vanishes at the bottom wall. In this section, the boundary layer thickness δ and the maximum radial velocity $v_{r,max}$ in the bottom boundary layer are approximately calculated as functions of radial distance r in order to estimate the velocity gradient.

The following assumptions are made in the integral method.

1. The tangential velocity $v_{\theta,\infty}$ in the free stream region is irrotational, that is,

$$v_{\theta,\infty} = \Gamma/r$$

where Γ is a function of r only.

2. The radial velocity in the free stream region is negligible.
3. The tangential and radial velocities's profiles inside the bottom boundary layer are chosen as (Taylor, 1950)

$$v_\theta = v_{\theta,\infty}\, f(\tfrac{z}{\delta}) = v_{\theta,\infty}\left[2(\tfrac{z}{\delta}) - (\tfrac{z}{\delta})^2\right] \qquad 3.12$$

$$v_r = v_{r,max}\, g(\tfrac{z}{\delta}) = v_{r,max}\left[\frac{27}{4}(\tfrac{z}{\delta})(1-\tfrac{z}{\delta})^2\right] \qquad 3.13$$

After an order of magnitude analysis, the equations of motion to be solved are reduced to θ-component of the equations of motion:

$$v_z \frac{\partial v_\theta}{\partial z} = \nu \frac{\partial^2 v_\theta}{\partial z^2} \qquad 3.14$$

r-component of the equation of motion:

$$v_r \frac{\partial v_r}{\partial r} - \frac{v_\theta^{\,2}}{r} + v_z \frac{\partial v_r}{\partial t} = -\frac{1}{\rho}\frac{\partial p}{\partial r} + \frac{\partial^2 v_r}{\partial z^2} \qquad 3.15$$

The continuity equation is

$$\frac{\partial}{\partial r}(r v_r) + \frac{\partial}{\partial z} v_z = 0 \qquad 3.16$$

The radial pressure gradient in eq. 3.15 can be replaced by the centrifugal force in the free stream region.

$$-\frac{1}{\rho}\frac{\partial p}{\partial r} = -\frac{v_{\theta,\infty}^{\,2}}{r} \qquad 3.17$$

Integrations of eq.3.14 and 3.15 from $z = 0$ to $z = \delta(r)$ using eq. 3.12, eq.3.13, eq.3.16 and eq.3.17 give two equations having the boundary layer thickness $\delta(r)$ and the maximum radial velocity $v_{r,max}$ as two unknowns. The two equations are

$$\delta(r) = \left[\frac{-\lambda_7 \cdot v_{r,max}}{\lambda_4 \cdot v_{r,max}^{\,2} + \lambda_5 \cdot v_{\theta,\infty}^{\,2}}\, r\right]^{\frac{1}{2}} \qquad 3.18$$

$$\frac{d}{dr}(v_{r,max})^2 + 2C_1 \frac{(v_{r,max})^2}{r} = \frac{2C_2}{r^3} \qquad 3.19$$

where C_1 and C_2 and λ_1 to λ_7 are given by

$$\left.\begin{aligned} C_1 &= 1 - \frac{\lambda_3\lambda_4}{(\lambda_1-\lambda_2)\lambda_7} = .74 \\ C_2 &= \frac{\lambda_3\lambda_5}{(\lambda_1-\lambda_2)\lambda_7} = -.287 \end{aligned}\right\} \quad 3.20$$

$$\lambda_1 = \int_0^1 f(\tfrac{z}{\delta})g(\tfrac{z}{\delta})d(\tfrac{z}{\delta}) = \frac{27}{80}$$

$$\lambda_2 = \int_0^1 f(\tfrac{z}{\delta})d(\tfrac{z}{\delta}) = \frac{9}{16}$$

$$\lambda_3 = \frac{d}{d(\frac{z}{\delta})} g(\tfrac{z}{\delta})\Big|_{z=0} = 2$$

$$\lambda_4 = \int_0^1 f^2(\tfrac{z}{\delta})d(\tfrac{z}{\delta}) = \frac{243}{560} \qquad 3.21$$

$$\lambda_5 = \int_0^1 [g^2(\tfrac{z}{\delta}) - 1]d(\tfrac{z}{\delta}) = -\frac{7}{15}$$

$$\lambda_6 = \frac{d}{d(\frac{z}{\delta})} f(\tfrac{z}{\delta})\Big|_{z=0} = \frac{27}{4}$$

$$\lambda_7 = \frac{2\lambda_3\lambda_4}{\lambda_1-\lambda_2} - \lambda_6 = -14.46$$

Eq. 3.19 is solved with the boundary condition $v_{r,max} = 0$ at the outer wall (r=R). The boundary layer thickness $\delta(r)$ is then obtained from eq. 3.18. From eq. 3.19, $v_{r,max}$ is

$$v_{r,max} = \frac{C_2}{C_1-1} \Gamma^2 \left\{\frac{1}{r^2} - \frac{1}{R^2} \left(\frac{R}{r}\right)^{2C_2}\right\}^{\frac{1}{2}} \qquad 3.22$$

The results of a sample calculation are shown in TABLE 3.1 with the results by Anderson (1966). Both $v_{r,max}$ and $\delta(r)$ calculated by the two different methods are well agreed.

Although the velocity profies of v_θ and v_r are assumed in the method, reasonable results are about the boundary layer thickness and the maximum velocity are obtained when they are compared with Anderson's results. This method as well as Anderson's technique; however, can not be extended to the region near the exit hole because the tangential velocity above the boundary layer turns out to be a rigid rotational flow and the radial velocity induced by a strong downflow above the exist hole is not negligible anymore outside the bottom boundary layer. The assumptions made are, therefore, no longer appropriate. The flow behavior around the exist hole is much more complicated because the radial inflow from the bottom boundary layer interacts with the axial down flow from the core region. In order to analyze the flow behavior, a numerical simulation for an entire vortex flow will be described in the later section. Before this, stress tensor contributed by polymer additive in the bottom boundary layer is calculated in order to see if the flow behavior is influenced by the resulting polymer stress tensor.

TABLE 3.1

THE COMPARISON OF INTEGRAL METHOD AND ANDERSON'S TECHNIQUE

$r^* = r/R$	$v_{\theta,\infty}$ (cm/sec)	$v_{r,max}$ (cm/sec)		δ (cm)	
		INTEGRAL METHOD	ANDERSON'S TECHNIQUE	INTEGRAL METHOD	ANDERSON'S TECHNIQUE
1	4.00	0	0	0	0
.9	4.44	-1.08	-1.0	.28	.28
.8	5.00	-1.74	-1.5	.31	.31
.7	5.71	-2.47	-2.2	.32	.32
.6	6.67	-3.38	-3.0	.31	.32
.5	8.00	-4.62	-4.2	.28	.32
.4	10.00	-6.46	-5.9	.26	.28
.3	13.33	-9.55		.22	
.2	20.00	-15.82		.17	

* The boundary condition: $v_{rmax} = 0$, $\delta = 0$ at $r = R$

* The data used is $\Gamma = 20\ cm^2/sec$, $R = 5cm$

3.4 Influence of Polymer Additive in the Bottom Boundary Layer

To test polymer effect, the simplest Hookean Dumbbell model (Bird, et al., 1977) is used as a constitutive equation. Since no polymer effect exists in the free stream region as described in the last section because velocity gradient is too small to excite macromolecules, the bottom boundary layer is analyzed. The stress field in the region is numerically calculated using Anderson's velocity profiles (1966) and approximately calculated using the results obtained in section 3.3.

Anderson uses the following equations in the bottom boundary layer.

θ - component of equation of motion:

$$v_r \frac{\partial v_\theta}{\partial r} + \frac{v_r v_\theta}{r} + v_z \frac{\partial v_\theta}{\partial z} = \nu \frac{\partial^2 v_\theta}{\partial z^2} \qquad 3.23$$

r - component of equation of motion:

$$v_r \frac{\partial v_r}{\partial r} - \frac{v_\theta^2}{r} + v_z \frac{\partial v_r}{\partial z} = -\frac{1}{\rho}\frac{\partial p}{\partial r} + \nu \frac{\partial^2 v_z}{\partial z^2} \qquad 3.24$$

These equations are then transformed into a new coordinate system where the numerical calculation starts from the outside wall. Using the method similar to that used by Smith and Cutter (1963), the partial differential equations are reduced to a set of ordinary differential equations which can be easily solved. In this method, r-direction derivative in a finite difference formula is approximated by using only previously obtained values.

The stress field is calculated considering an imaginary situation. If a Newtonian fluid is replaced by polymer solution all of a sudden, the resulting stress field due to the polymer solution must be different. And if the difference of the stress field between the polymer solution and the Newtonian fluid is large enough to change flow pattern, it may be said that polymer effect appears. To examine the situation, the stress field is numerically calculated using the Newtonian velocity profile. Since changes in z-direction are important, the mesh points used in the calculation are 6x24 for r and z directions in the area

$$.4 \leq r/R \leq 1 \quad , \quad 0 \leq z/\delta \leq 1 \quad ,$$

where R and δ are the radius of the outer wall and the boundary layer thickness.

The constitutive equation used here is Hookean Dumbbell model.

$$\underline{\underline{\tau}}_p + \lambda_H \underline{\underline{\tau}}_{p(1)} = -nkT\lambda_H \dot{\underline{\underline{\gamma}}} \qquad 3.25$$

where $\dot{\underline{\underline{\tau}}}_p$: polymer cotribution to stress tensor

$\dot{\underline{\underline{\gamma}}}$: The rate of strain tensor $\dot{\underline{\underline{\gamma}}} = \nabla\underline{v} + (\nabla\underline{v})^+$

$\nabla\underline{v}$: Velocity gradient tensor

$(\nabla\underline{v})^+$: Transverse of $\nabla\underline{v}$

n: number density

k: Boltzman constant

T: Absolute temperature

$$\underline{\underline{\tau}}_{p(1)} \equiv \frac{D}{Dt}\underline{\underline{\tau}}_p - (\nabla\underline{v})^{+}\cdot\underline{\underline{\tau}}_p - \underline{\underline{\tau}}_p\cdot\nabla\underline{v}$$

The calculated stress field is then substituted into the r-component of the equation of motion to see if there are significant changes in an r-direction force balance. The r-component of the equation of motion is most important in the boundary layer because a strong radial inflow exists. Each stress term is calculated for both polymer and Newtonian solutions in several radial distances. TABLE 3.2 shows those results evaluated at the bottom wall where stress terms have their maximum values. Although polymer contribution appears in stress terms, these forces are not large enough to change flow pattern when compared with the radial pressure gradient which is one of the dominant forces in the r-direction force balance.

In order to see the polymer effect further down to r/R=.2. the stress field at the bottom wall can be estimated by using the results obtained in section 3.3. Two important components of velocity gradient

$$\left.\frac{\partial v_r}{\partial z}\right|_{z=0}$$

and

TABLE 3.2 <u>THE COMPARISON OF FORCE TERMS IN R-COMPONENT OF THE EQUATION OF MOTION</u>

r/R R = 5cm	$-\frac{\partial p}{\partial r} = -\rho\frac{(v_{\theta,\infty})^2}{r}$	$-\frac{\partial}{\partial r}\tau_{rr}$		$-\frac{\tau_{rr}-\tau_{\theta\theta}}{r}$	
		Polymer Solution	Newtonian Fluid	Polymer Solution	Newtonian Fluid
.4	-50.00	-1.918	0	.597	0
.6	-14.83	-.292	0	.033	0
.8	-6.25	-.040	0	.006	0

* The unit of the force terms is $g \cdot cm/sec^2/cm^3$.

* The polymer solution is considered as 30wppm Polyethylene oxide. (See Appendix B for constants used in the calculation)

* Newtonian Fluid is water at 25°C.

$$\left.\frac{\partial v_\theta}{\partial z}\right|_{z=0}$$

are expressed as

$$\frac{27}{4\delta} v_{r,max}$$

and

$$\frac{2}{\delta} v_{\theta\infty}$$

respectively according to the definitions in section 3.3. It is reasonable to assume that other components of velocity gradient tensor

$$\frac{\partial v_\theta}{\partial r} \quad , \quad \frac{\partial v_r}{\partial r} \; ,$$

etc. are small enough to be neglected when compared with the two large components. The velocity gradient

$$\frac{\partial v_r}{\partial z}$$

appears rz-component of eq. 3.25 as a forcing term. After eliminating unimportant terms in eq. 3.25, τ_{rz} is

$$\tau_{rz} \fallingdotseq - nkT\lambda_H \left.\frac{\partial v_r}{\partial z}\right|_{z=0} \qquad 3.26$$

and τ_{rz} effects τ_{rr} in rr-component of eq. 3.25, τ_{rr} is then

$$\tau_{rr} \doteq -2nkT \left(\lambda_H \frac{\partial v_r}{\partial z}\bigg|_{z=0}\right)^2 \qquad 3.27$$

In the same way as above, $\tau_{z\theta}$ is obtained from $z\theta$ - component,

$$\tau_{z\theta} \doteq - nkT \;\; \lambda_H \frac{\partial v_\theta}{\partial z}\bigg|_{z=0} \qquad 3.28$$

and $\theta\theta$ - component, $\tau_{\theta\theta}$ becomes

$$\tau_{\theta\theta} \doteq -2nkT \left(\lambda_H \frac{\partial v_\theta}{\partial z}\bigg|_{z=0}\right)^2 \qquad 3.29$$

The polymer contribution to τ_{rr} and $\tau_{\theta\theta}$ at the bottom wall are tabulated in TABLE 3.3 and compared with the numerical results using Anderson's velocity porfile. τ_{rr} and $\tau_{\theta\theta}$ from the two methods reasonably agree to each other. The values obtained by method 2 always exceed those estimated by method 1. They differ by factor about 2 for τ_{rr} and 1.5 for $\tau_{\theta\theta}$. The parenthesized values at $r/R=.2$ and $r/R=.3$ are extrapolated by multiplying the results from method 1 by the factor 1.91 for τ_{rr} and 1.43 for $\tau_{\theta\theta}$ based on averaging over the range between $r/R=.4$ and .8. Overall the two methods can well provide stress components τ_{rr} and $\tau_{\theta\theta}$ in spite of their quite different approaches. The force terms in r-component of the equation of motion is then calculated and tabulated in TABLE 3.4. Even though the force terms due to the polymer solution increase as r/R decreases, the radial pressure gradient is still a domonant force in r-component force balance at small

TABLE 3.3 THE ESTIMATION OF τ_{rr} AND $\tau_{\theta\theta}$ AT THE BOTTOM WALL

r/R	τ_{rr} [g·cm/sec^2 cm^2]		$\tau_{\theta\theta}$ [g cm/sec^{2}cm^2]	
R = 5cm	METHOD 1	METHOD 2	METHOD 1	METHOD 2
.2	-7.891	(-15.100)	-1.107	(-1.583)
.3	-3.345	(-6.356)	-.294	(-.420)
.4	-.563	-1.350	-.116	-.157
.6	-.108	-.155	-.037	-.056
.8	-.029	-.055	-.021	-.030

* METHOD 1: Analytically solved using the velocity gradient from Integral Method.

* METHOD 2: Numerically solved using the velocity gradient from Anderson's technique.

* τ_{rr}, $\tau_{\theta\theta}$ Contributed by Newtonian fluid are zero.

TABLE 3.4. THE COMPARISON OF FORCE TERMS DUE TO POLYMER SOLUTION BY TWO DIFFERENT METHODS

r/R R = 5cm	$-\frac{\partial p}{\partial r} = -\rho\frac{(v_{\theta,\infty})^2}{r}$	$-\frac{\partial}{\partial r}\tau_{rr}$ METHOD 1	$-\frac{\partial}{\partial r}\tau_{rr}$ METHOD 2	$-\frac{\tau_{rr}-\tau_{\theta\theta}}{r}$ METHOD 1	$-\frac{\tau_{rr}-\tau_{\theta\theta}}{r}$ METHOD 2
.2	-400.0	-9.092	(-17.488)	6.784	(13.517)
.3	-117.9	-7.328	(-13.750)	2.034	(5.936)
.4	-50.0	-3.097	(-5.965)	.224	.597
.6	-14.83	-.194	-.292	.024	.033
.8	-6.25	-.040	-.093	.002	.006

* ( ) are calculated using extrapolated values in TABLE 3.3.

* The unit of force terms is g cm/sec^2/cm^3.

* METHOD 1 and 2 are the same as in TABLE 3.3.

r/R because the stress forces are less than 5% of the dominant force. Again, although the stress field raised by the polymer solution grows in the bottom boundary layer, it is too small to change Newtonian flow behavior. This conclusion forces us to investigate the flow behaviors in the core region and in the area near the exit hole to see if large velocity gradient is realized. In order to analyze the flow behavior of these regions, the numerical simulation by solving a full Navior-Stokes equation for the entire vortex tank is described in the next section.

3.5 A Numerical Simulation for Entire Vortex Flow Field

3.5.1 The Governing Equations.

For an incompressible viscous flow in a confined cylindrical container, assuming that the flow is axisymmetric, the velocity field in terms of circulation, vorticity and stream function in a cylindrical coordinate (r,θ,z) are described by the following equations.

CIRCULATION Γ

$$\frac{\partial \Gamma}{\partial t} + v_r \frac{\partial \Gamma}{\partial r} + v_z \frac{\partial \Gamma}{\partial z} = \nu\left(\frac{\partial^2 \Gamma}{\partial r^2} + \frac{\partial^2 \Gamma}{\partial z^2} - \frac{1}{r}\frac{\partial \Gamma}{\partial r}\right) \qquad 3.30$$

VORTICITY ω

$$\frac{\partial \omega}{\partial t} + v_r \frac{\partial \omega}{\partial r} + v_z \frac{\partial \omega}{\partial z} - \frac{v_r \omega}{r} - \frac{1}{r^3}\frac{\partial \Gamma^2}{\partial z}$$

$$= \nu\left(\frac{\partial^2 \omega}{\partial r^2} + \frac{\partial^2 \omega}{\partial z^2} + \frac{1}{r}\frac{\partial \omega}{\partial r} - \frac{\omega}{r^2}\right) \qquad 3.31$$

STREAM FUNCTION ψ

$$\frac{\partial^2 \psi}{\partial r^2} + \frac{\partial^2 \psi}{\partial z^2} - \frac{1}{r}\frac{\partial \psi}{\partial r} = -r\omega \qquad 3.32$$

where ν is a kinetic viscosity. The circulation is written in terms of v_θ.

$$\Gamma = r v_\theta \qquad 3.33$$

and the relation between the vorticity and the radial and axial velocity v_r, v_z is

$$\omega = \frac{\partial v_r}{\partial z} - \frac{\partial v_z}{\partial r} \qquad 3.34$$

v_r, v_z relate to the stream function by

$$v_r = -\frac{1}{r}\frac{\partial \psi}{\partial z}$$
$$\qquad 3.35$$
$$v_z = \frac{1}{r}\frac{\partial \psi}{\partial r}$$

Since a zone method (Clomberg,1971) is used for a finite difference formula, the eq.3.30 to eq.3.32 are arranged for more suitable terms. The dimensionless forms of the equations are

<u>CIRCULATION</u> Γ

$$\frac{\partial \Gamma}{\partial t} + \frac{1}{r}\frac{\partial}{\partial r}(r v_r \Gamma) + a\frac{\partial}{\partial z}(v_z \Gamma)$$

$$= \frac{1}{Rer}\left(\frac{\partial^2 \Gamma}{\partial r^2} + a^2\frac{\partial^2 \Gamma}{\partial z^2} - \frac{1}{r}\frac{\partial \Gamma}{\partial r}\right) \qquad 3.30A$$

<u>VORTICITY</u> ω

$$\frac{\partial \omega}{\partial t} + \frac{1}{r}\frac{\partial}{\partial r}(r v_r \omega) + a\frac{\partial}{\partial z}(v_z \omega) - v_r \omega - S\frac{a}{r^3}\frac{\partial}{\partial z}\Gamma^2$$

$$= \frac{1}{Rer}\left(\frac{\partial^2 \omega}{\partial r^2} + a^2\frac{\partial^2 \omega}{\partial z^2} + \frac{1}{r}\frac{\partial \omega}{\partial r} - \frac{\omega}{r^2}\right) \qquad 3.31A$$

<u>STREAM FUNCTION</u> ψ

$$\frac{\partial^2\psi}{\partial r^2} + a^2\,\frac{\partial^2\psi}{\partial z^2} - \frac{1}{r}\frac{\partial\psi}{\partial r} = -ar\omega \qquad 3.32A$$

The dimensionless variables (no marks) are related to the dimensional counterparts (marked by asterisks) in the following way:

$$\psi = \frac{\psi^*}{RHv_R} \quad , \quad \Gamma = rv_\theta = \frac{\Gamma^*}{Rv_R} \quad , \quad \omega = \frac{\omega^*}{v_r/R}$$

$$v_r = \frac{v_r^*}{v_R} \quad , \quad v_z = \frac{v_z^*}{v_R} \quad , \quad r = \frac{r^*}{R}$$

$$z = \frac{z^*}{H} \quad , \quad t = \frac{t^*}{R/v_R} \quad , \quad a = \frac{R}{H}$$

where v_R and $v_{\theta R}$ are the radial and tangential velocities at the outer wall, R and H are the radius and height of the container respectively. Two important parameters, the radial Reynolds number Rer and swirl parameter S are defined by

$$Rer \equiv \frac{Rv_R}{\nu} \qquad 3.36$$

$$S \equiv \left(\frac{v_{\theta R}}{v_R}\right)^2 \qquad 3.37$$

Eq.3.28 is rewritten by

$$v_r = -\frac{1}{r}\frac{\partial\psi}{\partial z} \qquad 3.35A$$

$$v_z = \frac{1}{a} \frac{1}{r} \frac{\partial \psi}{\partial r} \tag{3.35A}$$

3.5.2 Finite Difference Formula (zone method)

In order to avoid the free surface as the boundary of vortex flow, a cylindrical container is assumed to have two exit holes located on the axis of rotation at each of the two end walls. As shown in Fig.3.5, the vortex flow is then simulated over a quarter of the total area because of geometrical symmetry. The treatment of the free surface boundary in this way is eliminated without losing the most important characteristics of the vortex flow (Anderson,1961).

The geometry of the flow field is explained in Fig.3.6. Due to the characteristics of the vortex flow described previously, the mesh size in both the bottom boundary layer and core region is made much smaller than that in the free stream region to provide detailed information about the flow behavior in those two regions. The zone construction is described in Fig. 3.7 where the dot in each zone represents the spacial position of a dependent variable F which is assumed to be uniform inside the zone (F is one of Γ, ω or ψ). The velocities v_r and v_z are calculated using linearly interpolated stream function ψ^{IN} at the corners of each zone. The $\psi^{IN}{}_{i,j}$ in Fig.3.7, for example, is calculated by

Figure 3.5

The Model Geometry of Vortex Flow

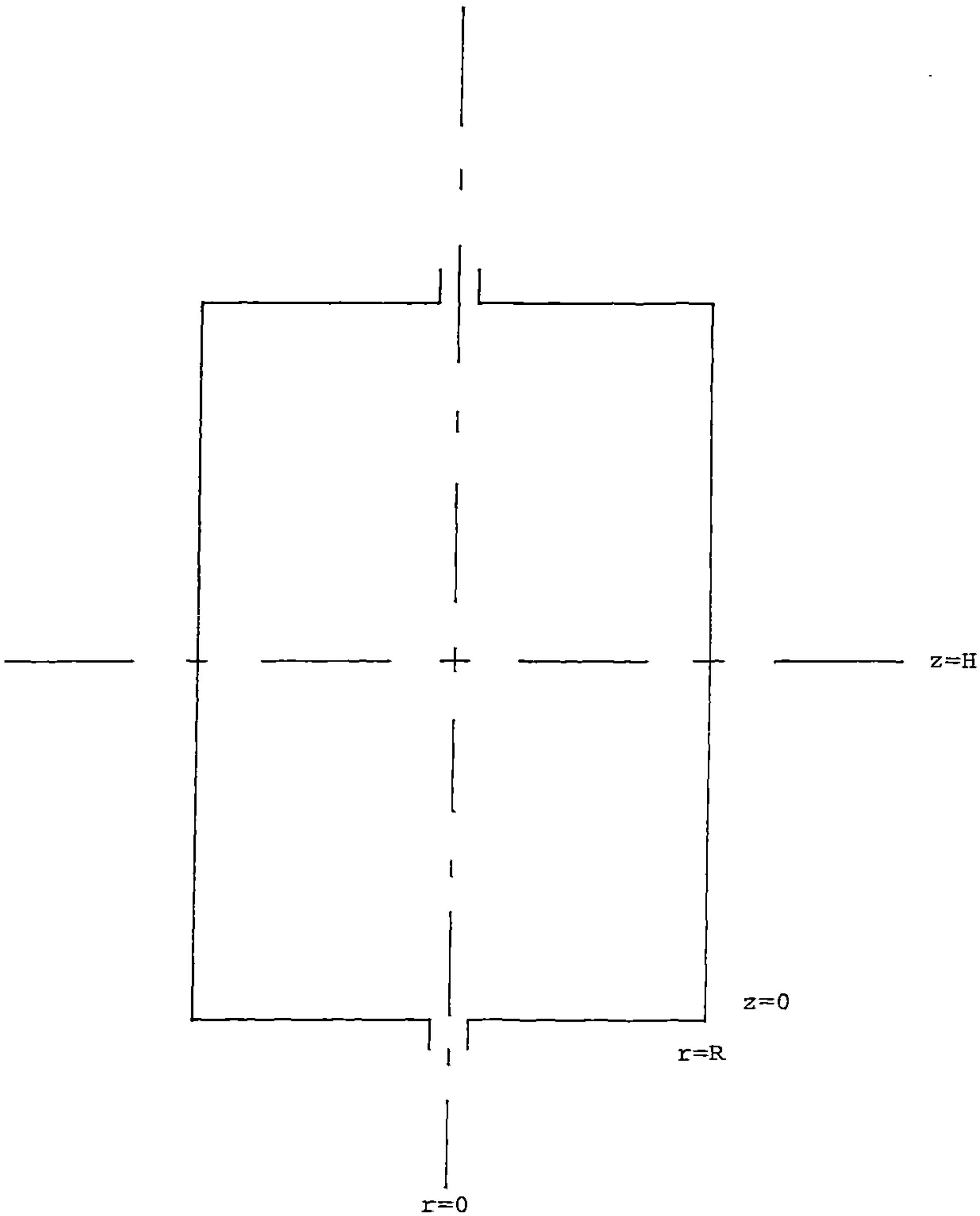

Figure 3.6

The Mesh Construction of Vortex Flow

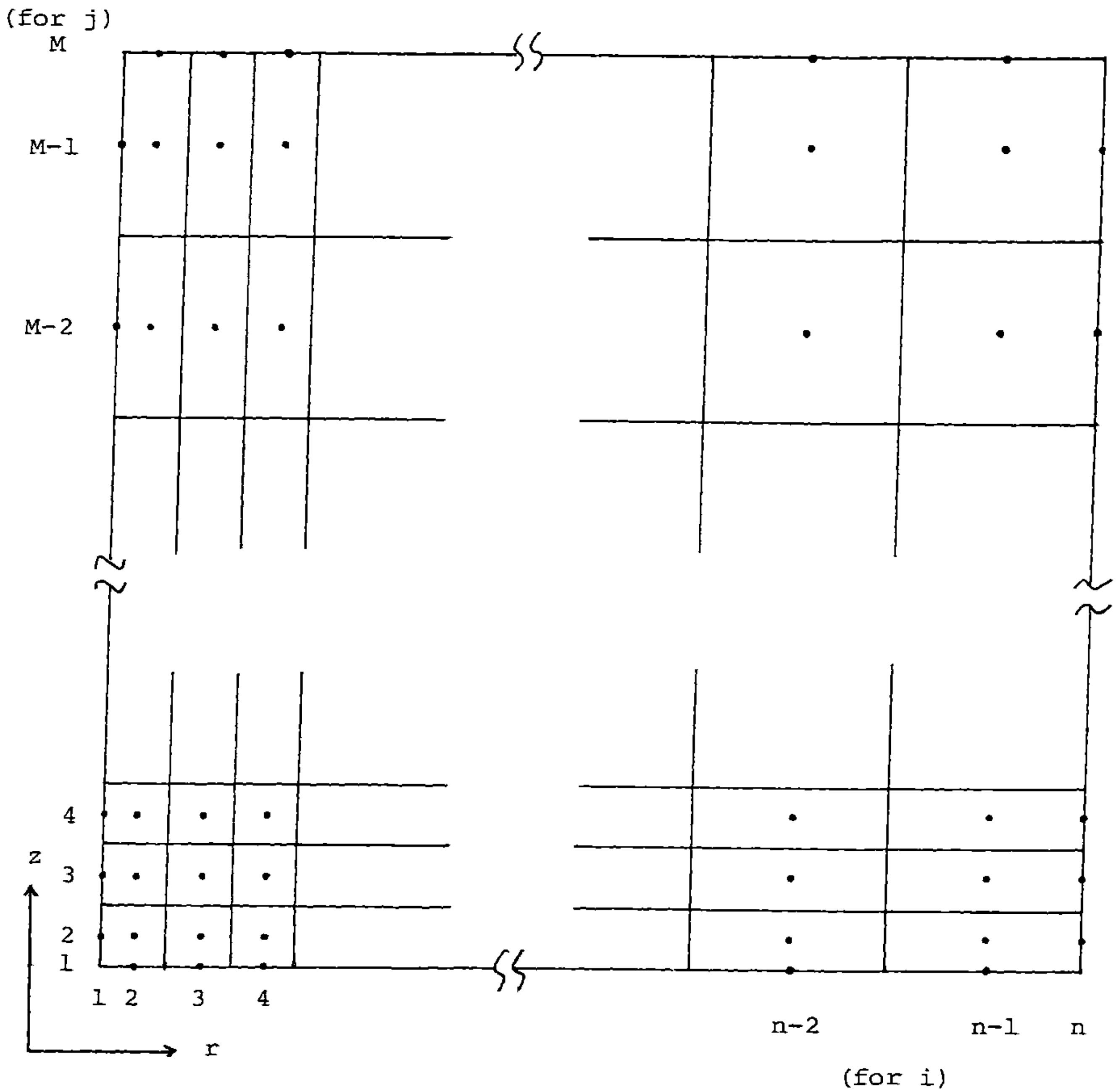

Figure 3.7

The Zone Construction

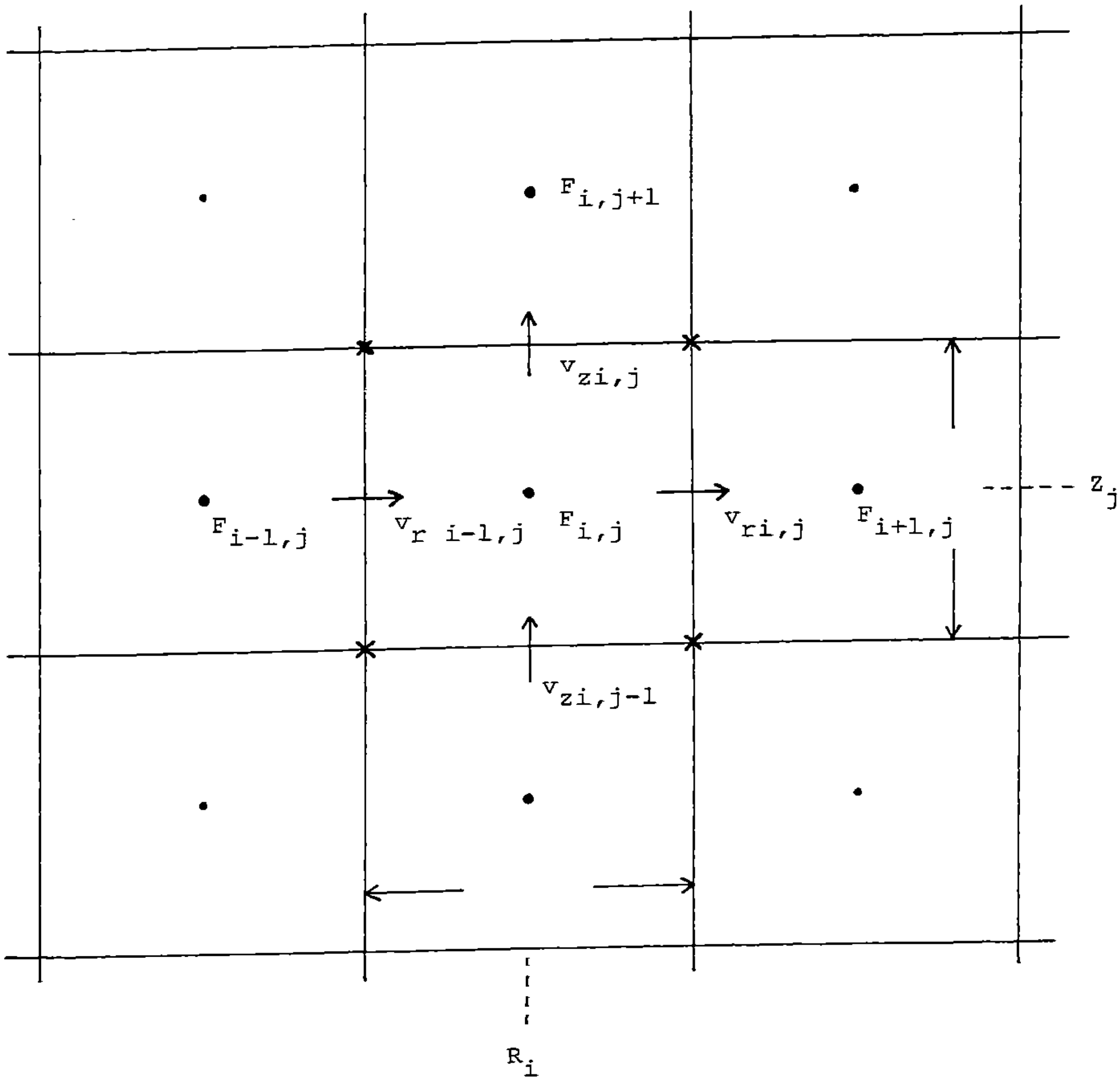

$$\psi^{IN}_{i,j} = \left(\frac{\psi_{i+1,j+1} \cdot DZ_j + \psi_{i+1,j} \cdot DZ_{j+1}}{DZ_j + DZ_{j+1}} \cdot DR_i \right.$$

$$\left. + \frac{\psi_{i,j+1} \cdot DZ_j + \psi_{i,j} \cdot DZ_{j+1}}{DZ_j + DZ_{j+1}} \cdot DR_{i+1} \right) \Big/ (DR_i + DR_{i+1})$$

$$2 \leq i \leq N \qquad \qquad 3.38$$

$$2 \leq j \leq M$$

According to eq.3.35A, the velocities $v_{r\ i,j}$ and $v_{z\ i,j}$ are approximated by

$$v_{r\ i,j} = -\frac{1}{(R_i + \frac{DR_i}{2})} \cdot (\psi^{IN}_{i,j} - \psi^{IN}_{i,j-1})/DZ_j$$

$$3.39$$

$$v_{z\ i,j} = \frac{1}{a \cdot R_i} \cdot (\psi^{IN}_{i,j} - \psi^{IN}_{i-1,j})/DR_i$$

In order to increase the stability of the calculation, in other words, to make a diagonally dominant matrix (see Appendix D), the convective terms in eq.3.30A and eq.3.31A are approximated in the following way:

$$\frac{\partial}{\partial r}(rv_rF)_{i,j} = \left[\frac{v_{r\ i,j} + |v_{r\ i,j}|}{2} (R_i + \frac{DR_i}{2}) F_{i,j} \right.$$

$$+ \frac{v_{r\ i,j} - |v_{r\ i,j}|}{2} (R_i + \frac{DR_i}{2}) F_{i+1,j}$$

$$- \frac{v_{r\ i-1,j} + |v_{r\ i-1,j}|}{2} (R_i - \frac{DR_i}{2}) F_{i-1,j} -$$

$$\frac{v_{r\ i-1,j} - |v_{r\ i-1,j}|}{2}(R_i - \frac{DR_i}{2}) F_{i,j}\Bigg] \Big/ DR_i \qquad 3.40$$

When circulation (or vorticity) is transported across a zone boundary by convection, eq.3.40 is devised such that it tends to decrease the rate of circulation change in the zone from which it comes and to increase it in the zone to which it flows to conserve circulation (or vorticity). The proper approximation of the convective terms is one of the critical factors for the stability of the calculation especially when Reynolds number and the swirl parameter are increased, that is, when the magnitude of the convective terms becomes comparable with that of the diffusion terms.

The second and first derivatives are approximated by

$$\left(\frac{\partial^2}{\partial r^2}F\right)_{i,j} = \left[\frac{F_{i+1,j} - F_{i,j}}{\left(\frac{DR_i + DR_{i+1}}{2}\right)} - \frac{F_{i,j} - F_{i-1,j}}{\left(\frac{DR_i + DR_{i-1}}{2}\right)}\right]$$

$$\div \left(\frac{R_{i+1} - R_{i-1}}{2}\right) \qquad 3.41$$

$$\left(\frac{\partial F}{\partial r}\right)_{i,j} = \frac{F_{i+1,j} - F_{i,j}}{\left(\frac{DR_i + DR_{i+1}}{2}\right)} \quad \text{or} \quad \frac{F_{i,j} - F_{i-1,j}}{\left(\frac{DR_i + DR_{i-1}}{2}\right)} \qquad 3.42$$

The choice between forward and backward approximations for the first derivative in eq.3.42 is determined so as to make a more digonally dominant matrix for the calculation.

The boundary conditions due to the geometry of the confined vortex flow is tabulated in TABLE 3.5. The circulation at the axis of rotation becomes zero although the tangential velocity v_θ may be finite at $r = 0$ because of its definition (see eq.3.33). The vorticity also vanishes at $r = 0$. The radially directed momentum flux τ_{rz} must be zero at $r = 0$ because of the axisymmetric nature of the vortex flow. From the definition of τ_{rz} for Newtonian fluids,

$$\tau_{rz} = -\mu\left(\frac{\partial v_z}{\partial r} + \frac{\partial v_r}{\partial z}\right) \qquad 3.43$$

where μ is viscosity. In order to satisfy the condition for τ_{rz} at $r = 0$, both velocity gradient components

$$\frac{\partial v_z}{\partial r} \quad \text{and} \quad \frac{\partial v_r}{\partial z}$$

in eq.3.43 have to be zero. It is also confirmed experimentally that

$$\frac{\partial v_z}{\partial r}$$

becomes zero at $r = 0$ (Chiou,1976). The boundary condition $\omega = 0$ at $r = 0$ is thus reasonable. The stream function at the outer wall is proportional to the height of the container based on the reasonable assumption that the radial velocity at tha outer wall is constant along with the height. By considering the confined vortex flow, the boundary condition at liquid level ($z = 1$) are simply placed by the shear free condition

TABLE 3.5 THE BOUNDARY CONDITIONS FOR A CONFINED VORTEX FLOW

	STREAM FUNCTION	CIRCULATION	VORTICITY
THE AXIS OF ROTATION	TOTAL FLOW	ZERO (but v_θ is finite)	ZERO
THE OUTER WALL	v_r is constant v_z is zero	CONSTANT	ZERO
LIQUID LEVEL	TOTAL FLOW	SHEAR FREE	ZERO
THE EXIT * HOLE	SHEAR FREE	SHEAR FREE	SHEAR FREE
THE BOTTOM PLATE	V_r and v_z are zero	ZERO	NON-SLIP CONDITION

* Since nothing is known in the exist hole, all conditions are reasonably assumed.

for the z-direction for the circulation and the zero vorticity because of the symmetry of the flow system. The shear free condition mentioned above is defined so that the first derivative of the circulation with respect to the z-direction is zero. The boundary conditions thus become much simpler when compared them with a curved-shaped free surface boundary condition. The simpligication of the free surface boundary condition really makes the calculation feasible. The values of vorticity at the bottom plate are determined from non-slip condition. Since the stream function vanishes at the bottom plate, the vorticity ω_b at $z = 0$ is simplified from eq. 3.32A.

$$\omega_b = - \frac{a}{r} \left. \frac{\partial^2 \psi}{\partial z^2} \right|_{z=0} \qquad 3.44$$

The second derivative of the stream function at $z = 0$ is approximated in terms of $\psi(\Delta z)$ and $\psi(2 \cdot \Delta z)$ using Taylor's expansion near $z = 0$. $\psi(\Delta z)$ and $\psi(2 \cdot \Delta z)$ are then

$$\psi(\Delta z) = \psi(0) + \psi'(0) \cdot \Delta z + \psi''(0) \frac{\Delta z^2}{2} + \psi'''(0) \frac{\Delta z^3}{6} + \ldots \qquad 3.45$$

$$\psi(2 \cdot \Delta z) = \psi(0) + \psi'(0)(2 \cdot \Delta z) + \psi''(0) \frac{(2 \cdot \Delta z)^2}{2}$$

$$+ \psi'''(0) \frac{(2 \cdot \Delta z)^3}{6} + \ldots \qquad 3.46$$

Since

$$\psi(0) = \psi'(0) = 0,$$

the second derivative is

$$\psi''(0) = \frac{8\cdot\psi(2\cdot\Delta z) - \psi(\Delta z)}{2\cdot\Delta z^2} + 0(\Delta z^2) \qquad 3.47$$

The truncation error of eq.3.47 is of order Δz^2. The flow behavior at the exit hole is not known at all. The shear free condition for the three functions (Γ,ω,ψ) may be a good choice. The boundary conditions are rewritten in terms of finite difference formulation in TABLE 3.6. The solving methods for the governing equations are described in the following two sections. The first method is called relaxation method which is suitable for low Reynolds number and the ADI method for high Reynolds number follows.

3.5.3 The solving Method for Low Reynolds Number

Using finite difference scheme, eq.3.23A to eq.3.25A are approximated for a steady state flow. The equations are summerized in a general expression.

$$C1\ F_{i,j} + C2\ F_{i+1,j} + C3\ F_{i,j+1} + C4\ F_{i-1,j} + C5\ F_{i,j-1} = C6 \qquad 3.48$$

where C1,C2,C3,C4,C5 are coefficients of the dependent variable F (ψ,Γ,ω) at zones (i,j), (i+1,j), (i,j+1), (i-1,j), (i,j-1) respectively and C6 is a forcing function. If, for

TABLE 3.6 THE BOUNDARY CONDITIONS IN FINITE DIFFERENCE EXPRESSION

		ψ	Γ	ω
$r = 0$	$(1 \leq j \leq M)$	$\psi_{1,j} = 1$	$\Gamma_{1,j} = 0$	$\omega_{1,j} = 0$
$r = 1$	$(1 \leq j \leq M)$	$\psi_{N,j} = Z_j$	$\Gamma_{N,j} = 1$	$\omega_{N,j} = 0$
$Z = 1$	$(1 \leq i \leq N)$	$\psi_{i,M} = 1$	$\Gamma_{i,M} = \frac{1}{8}(9\Gamma_{i,M-1} - \Gamma_{i,M-2})$	$\omega_{i,M} = 0$
$Z=0$	$(1 \leq i \leq 3)$	$\psi_{i,1} = \psi_{i,2}$	$\Gamma_{i,1} = \Gamma_{i,2}$	$\omega_{i,1} = \omega_{i,2}$
	$(4 \leq i \leq N)$	$\psi_{i,1} = 0$	$\Gamma_{i,1} = 0$	$\begin{pmatrix} \text{eq.3.44} \\ \text{eq.3.47} \end{pmatrix}$

example, eq.3.48 is applied to the equation for circulation, the coefficient C1 is expressed by

$$C1 = \Big[(v_{r\,i,j}+|v_{r\,i,j}|)(R_i+\frac{DR_i}{2}) - (v_{r\,i-1,j}+|v_{r\,i-1,j}|)(R_i-\frac{DR_i}{2})\Big]$$

$$\times \frac{1}{2\ DR_i} + \Big[(v_{z\,i,j}+|v_{z\,i,j}|) - (v_{z\,i,j-1}-|v_{z\,i,j-1}|)\Big]$$

$$\times \frac{a^2 \cdot R_i}{2\ DZ_j} + \frac{4}{Rer}\Bigg[\frac{R_i^{\,2}}{R_{i+1}-R_{i-1}}\Bigg\{\frac{2}{(DR_i+DR_{i+1})(R_i+R_{i+1})}$$

$$+ \frac{2}{(DR_i+DR_{i-1})(R_i+R_{i-1})}\Bigg\}$$

$$+ \frac{a^2\ R_i}{Z_{j+1}-Z_{j-1}}\left(\frac{1}{DZ_j+DZ_{j+1}} + \frac{1}{DZ_j+DZ_{j-1}}\right)\Bigg] \qquad 3.49$$

First of all, eq.3.49 is rearranged and

$$F_{i,j}^{N}\ ,\quad F_{i+1,j}^{N}\ ,\quad F_{i-1,j}^{N}$$

(N indicates a newly calculated) are implicitly solved for the r-direction by

$$C4\ F_{i-1,j}^{N} + C1\ F_{i,j}^{N} + C2\ F_{i+1,j}^{N}$$

$$= -C3\ F_{i,j+1} - C5\ F_{i,j-1} + C6 \qquad \text{for} \quad 2 \le i \le N-1 \qquad 3.50$$

This is represented in each Z-point ($2 \le j \le M-1$).

$$F_{i,j}^{N} \ , \quad F_{i,j+1}^{N} \ , \quad F_{i,j-1}^{N}$$

are then solved implicitly for the z-direction by

$$C5\ F_{i,j-1}^{N} + C1\ F_{i,j}^{N} + C3\ F_{i,j+1}^{N}$$

$$= -C2\ F_{i+1,j} - C4\ F_{i-1,j} + C6 \qquad \text{for } 2 \le j \le M-1 \qquad 3.51$$

Again eq.3.51 repeated for each R-point ($2 \le i \le N-1$). Once the value of F^N is calculated from eq.3.50 or eq.3.51, the new value is assigned to F by averaging the newly calculated value and old value with a relaxation factor to avoid a sudden change which induces instability (Schultz and Shah, 1975). The newly relaxed value of F is then used in the right hand side of eq.3.50 and eq.3.51 as a known value.

The stream function (eq.3.32A) is first calculated and the radial and axial velocities are then determined from the interpolated stream function. Using the values of the velocities, the circulation (eq.3.30A)and then the vorticity (eq. 3.31A) are manipulated. This whole procedure is repeated until the three variables reach a steady state. The calculation is terminated when all of the variables have steady values at each spacial point. The two parameter Rer and S are increased gradually from Rer = 1 and S = 1 to the experimental condition where Reynolds number is about 20 and the swirl parameter is about 2500. And the results of the previous calculation, namely the case which has a lower Rer and S, is used as an initial condition for a higher Rer and S case to make an initial error from a new steady state as small as possible. The results of the case Re = 10 and S = 40 after 60 iterations are graphically shown in Fig.3.8 to Fig.3.11. From these figures, the velocity gradient components near the exit hole are found to be extremely large when compared with those in other regions. For instance, the circulation Γ at $r = .03$ in Fig.3.8 increases dramatically as it goes down to the bottom plate. The highest value of Γ at $z = .03$ is about 20 times as much as its value at $z = 1$. The velocity gradient

$$\frac{\partial v_\theta}{\partial z}$$

therefore, is very large especially within $z = .1$. The radial velocity v_r inside the bottom boundary layer shown in Fig.3.10 is also accelerated as the fluid flows toward the axis of rotation producing a high deformation gradient

$$\frac{\partial v_r}{\partial r} .$$

The axial velocity v_z in Fig.3.11 in the core region grows very rapidly especially near the exit hole. The high velocity gradient components

$$\frac{\partial v_r}{\partial z} \qquad \text{and} \qquad \frac{\partial v_z}{\partial r}$$

Figure 3.8

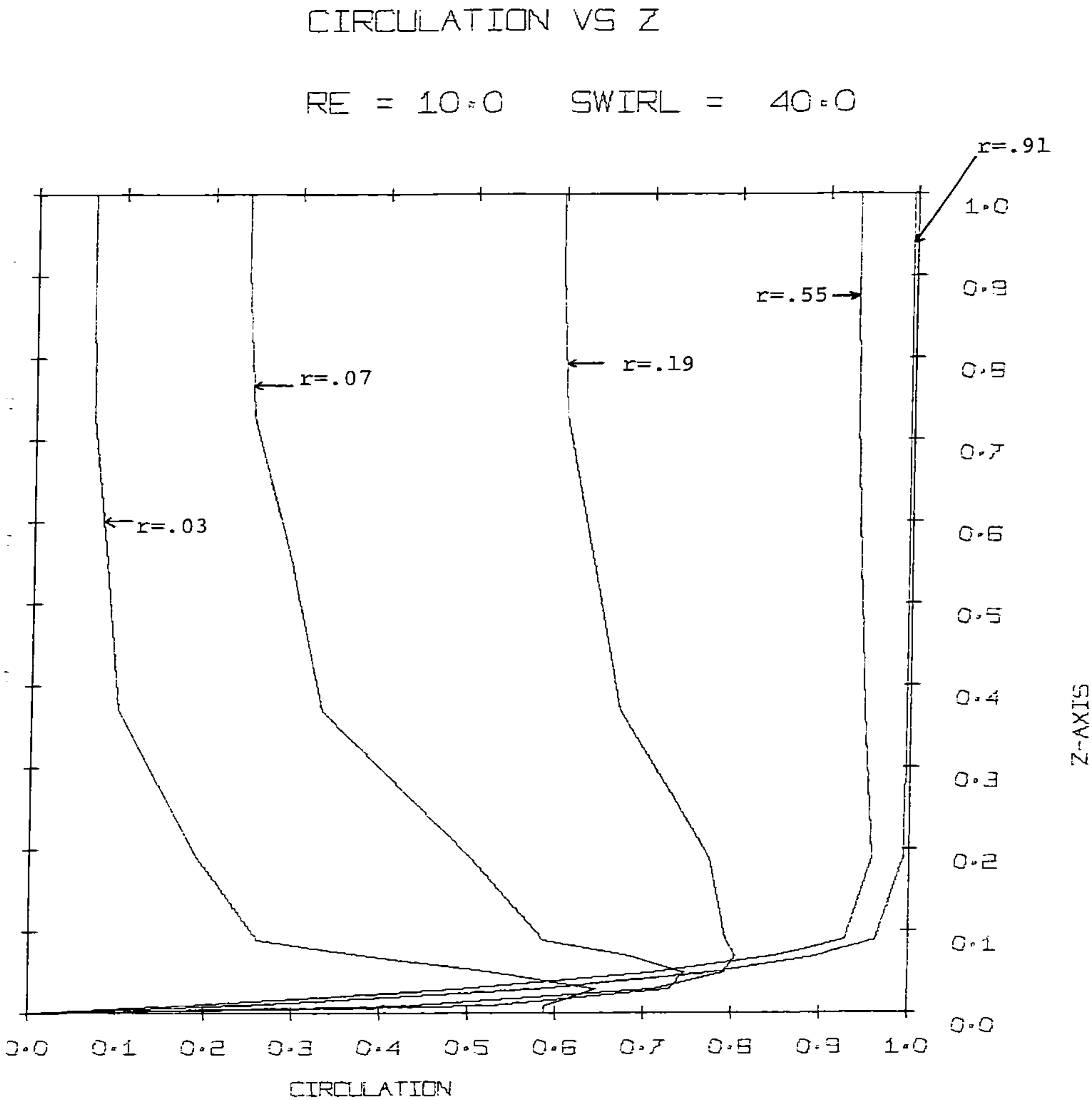
CIRCULATION VS Z
RE = 10.0 SWIRL = 40.0
r=.91
r=.55
r=.19
r=.07
r=.03
1.0
0.9
0.8
0.7
0.6
0.5
0.4
0.3
0.2
0.1
0.0
Z-AXIS
0.0
0.1
0.2
0.3
0.4
0.5
0.6
0.7
0.8
0.9
1.0
CIRCULATION

Figure 3.9

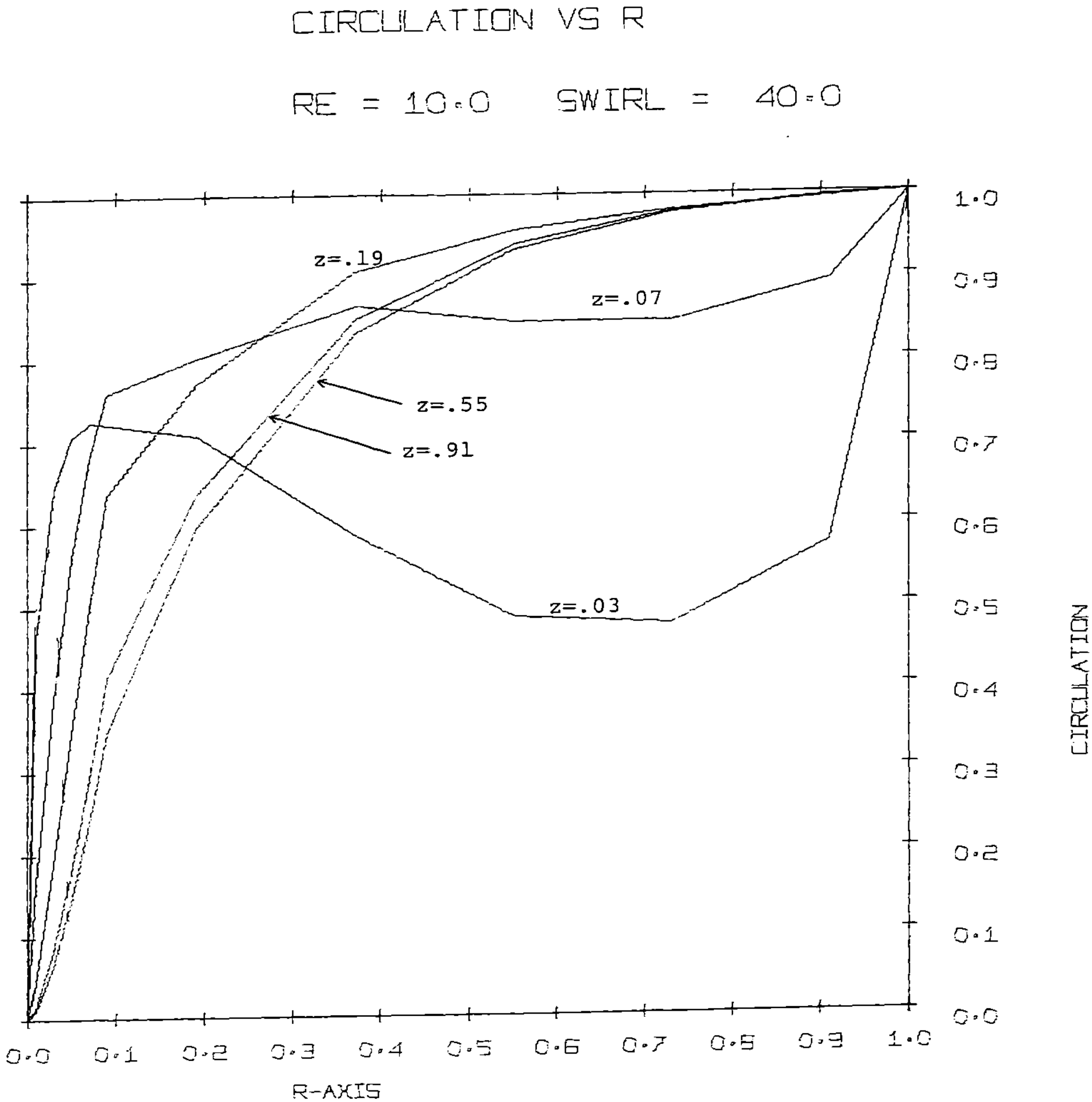
CIRCULATION VS R
RE = 10.0 SWIRL = 40.0
z=.19
z=.07
z=.55
z=.91
z=.03
0.0
0.1
0.2
0.3
0.4
0.5
0.6
0.7
0.8
0.9
1.0
R-AXIS
CIRCULATION

Figure 3.10

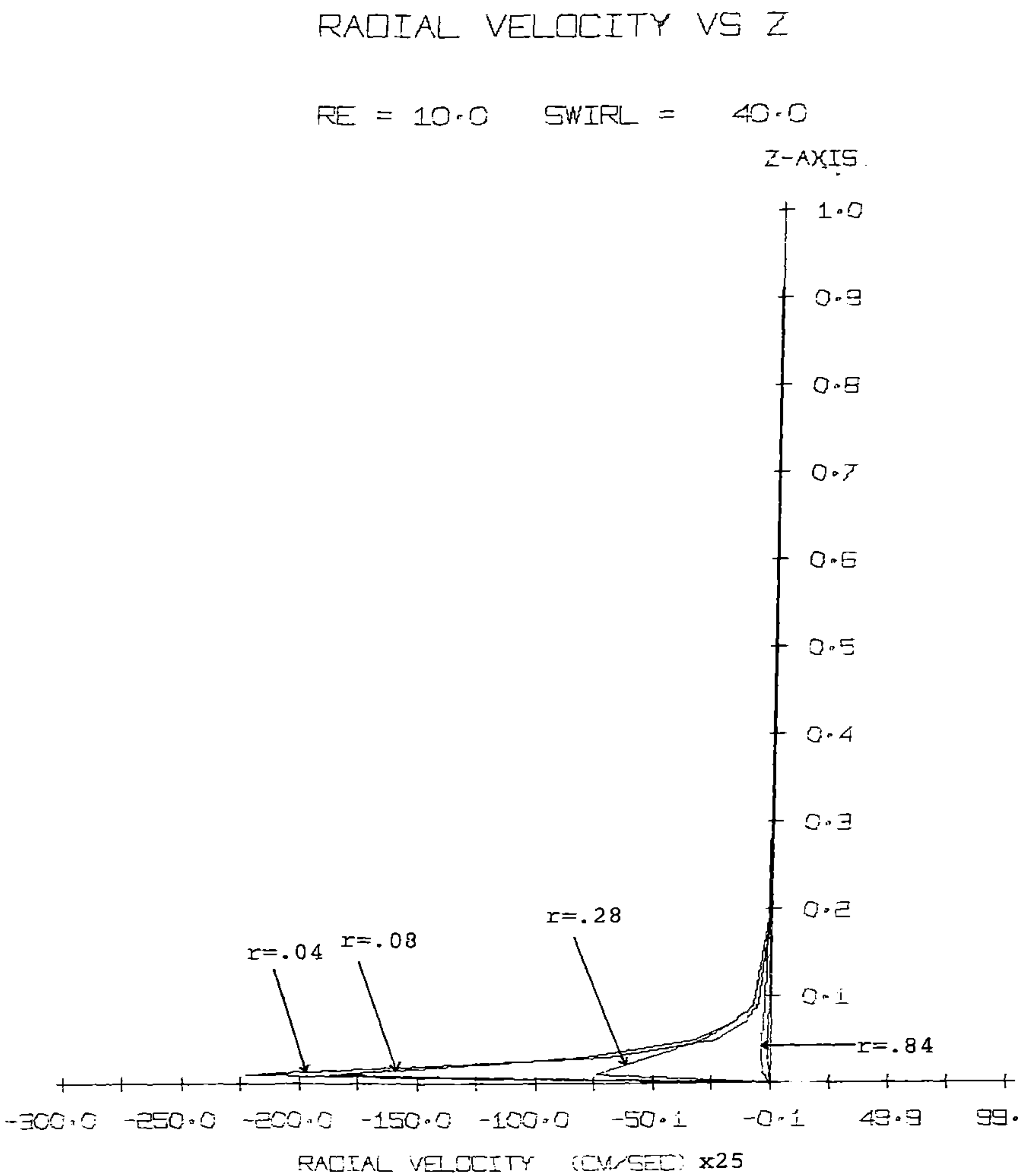
RADIAL VELOCITY VS Z
RE = 10.0 SWIRL = 40.0
Z-AXIS
1.0
0.9
0.8
0.7
0.6
0.5
0.4
0.3
0.2
0.1
r=.04
r=.08
r=.28
r=.84
-300.0
-250.0
-200.0
-150.0
-100.0
-50.1
-0.1
49.9
99.
RADIAL VELOCITY (CM/SEC) x25

Figure 3.11

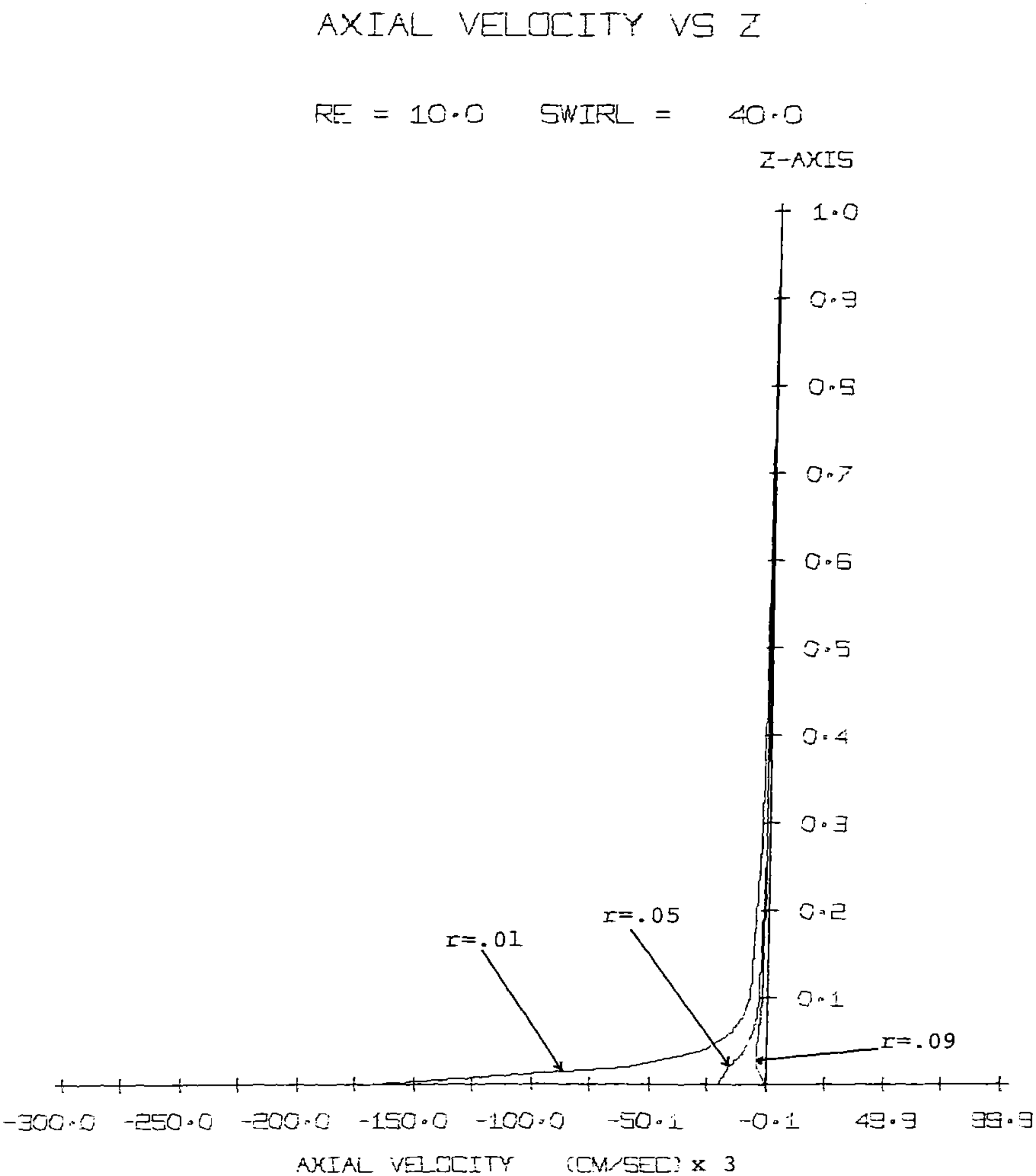
AXIAL VELOCITY VS Z
RE = 10·0 SWIRL = 40·0
Z-AXIS
1·0
0·9
0·8
0·7
0·6
0·5
0·4
0·3
0·2
0·1
r=.01
r=.05
r=.09
-300·0
-250·0
-200·0
-150·0
-100·0
-50·1
-0·1
49·9
99·9
AXIAL VELOCITY (CM/SEC) x 3

are expected in this region. On the whole, even for the case $Re = 10$ and $S = 40$, it is apparent that the significance of the flow behavior near the exit hole is emphasized because there exist much higher velocity gradients which may induce the polymer effect.

The method described in this section is found to be incapable of solving the equations for higher Reynolds number and swirl parameter case where non-linear convective terms in the circulation and vorticity equations become dominant forces. The dependent variables never reach a steady state even though very small relaxation factors and hundreds of iterations are applied. Another approach, therefore, is used to solve the non-linear partial differential equations (eq.3.30 to eq.3.32), and this approach is described in the following section.

3.5.4 The Solving Method for High Reynolds Number

The method used in this section is the alternating-direction implicit method (A.D.I.) developed by Peacman and Rachford (1955). The main difference between ADI and the relaxation method described in the last section is that ADI includes the time derivative terms in the equations so that the problem is categorized as an initial value problem. By choosing an appropriate time increment, this iteration method shows a great advantage over the relaxation method especially for large Reynolds number.

The equations (eq.3.30 to eq.3.32) are again rearranged into suitable dimensionless forms.

CIRCULATION Γ

$$\frac{\partial \Gamma}{\partial t} + \frac{1}{r}\frac{\partial}{\partial r}(rv_r\Gamma) + a\frac{\partial}{\partial z}(v_z\Gamma)$$

$$= \frac{1}{Re_\theta}\left(\frac{\partial^2\Gamma}{\partial r^2} + a^2\frac{\partial^2\Gamma}{\partial z^2} - \frac{1}{r}\frac{\partial\Gamma}{\partial r}\right) \qquad 3.30B$$

VORTICITY ω

$$\frac{\partial \omega}{\partial t} + \frac{1}{r}\frac{\partial}{\partial r}(rv_r\omega) + a\frac{\partial}{\partial z}(v_z\omega) - v_r\omega - a\frac{1}{r^3}\frac{\partial \Gamma^2}{\partial z}$$

$$= \frac{1}{Re_\theta}\left(\frac{\partial^2\omega}{\partial r^2} + a^2\frac{\partial^2\omega}{\partial z^2} + \frac{1}{r}\frac{\partial\omega}{\partial r} - \frac{\omega}{r^2}\right) \qquad 3.31B$$

STREAM FUNCTION ψ

$$\frac{\partial^2\psi}{\partial r^2} + a^2\frac{\partial^2\psi}{\partial z^2} - \frac{1}{r}\frac{\partial\psi}{\partial r} = \frac{a}{SS}r\omega \qquad 3.32B$$

And the dimensionless radial and axial velocities v_r and v_z are written by

$$\left.\begin{aligned} v_r &= SS\frac{1}{r}\frac{\partial\psi}{\partial z} \\ v_z &= -\frac{SS}{a}\frac{1}{r}\frac{\partial\psi}{\partial r} \end{aligned}\right\} \qquad 3.52$$

The dimesionless variables are defined by (dimensional counterparts are marked by asterisk)

$$\psi = \frac{\psi^*}{v_R RH} \quad , \quad \Gamma = rv_\theta = \frac{\Gamma^*}{Rv_{\theta R}} \quad , \quad \omega = \frac{\omega^*}{v_{\theta R}/R}$$

$$v_r = \frac{r^*}{v_{\theta R}} \quad , \quad v_z = \frac{v_z^*}{v_{\theta R}} \quad , \quad r = \frac{r^*}{R}$$

$$z = \frac{z^*}{H} \quad , \quad t = \frac{t^*}{R/v_{\theta R}} \quad , \quad a = \frac{R}{H}$$

Two parameters, Reynolds number (tangential) Re_θ and the ratio of v_R to $v_{\theta R}$, SS, are defined by

$$Re_\theta = \frac{R \cdot v_{\theta R}}{\nu} \qquad 3.53$$

$$SS = \frac{v_R}{v_{\theta R}} \qquad 3.54$$

The boundary conditions in TABLE 3.6 can be used for this formulation except for the vorticity at the bottom wall ω_b. ω_b is written by

$$\omega_b = SS\frac{9}{R_i}\,\frac{25\psi_{i,1} - \psi_{i,2}}{2 \cdot DZ_2{}^2} \qquad 3.55$$

$$\text{for} \quad 4 \leq i \leq N$$

The stream function is first solved by the relaxation method as described in the last section. The velocities v_r and v_z are then determined from the interpolated stream function ψ^{IN} by the descretized form of eq.3.52.

Using operator notation, eq.3.30B is expressed by

$$\frac{\partial \Gamma}{\partial t} = L_r \Gamma + L_z \Gamma \qquad 3.56$$

where the differential operations for the r and z direction are given by

$$\left.\begin{aligned} L_r \Gamma &= \frac{1}{Re_\theta}\left(\frac{\partial^2 \Gamma}{\partial r^2} - \frac{1}{r}\frac{\partial \Gamma}{\partial r}\right) - \frac{1}{r}\frac{\partial}{\partial r}(r v_r \Gamma) \\ L_z \Gamma &= \frac{1}{Re_\theta}\left(a^2 \frac{\partial^2}{\partial r^2}\Gamma\right) - a\frac{\partial}{\partial z}(v_z \Gamma) \end{aligned}\right\} \qquad 3.57$$

The time derivative and the operands are descretized by finite formulas. The circulation advanced by one time step (N+1) are then solved implicitly for the r-direction by

$$\frac{\Gamma^{N+1}}{\Delta t} - L_r^* \Gamma^{N+1} = \frac{\Gamma^N}{\Delta t} + L_z^* \Gamma^N \qquad 3.58$$

where L_r^* and L_z^* are descretized forms of L_r and L_z. The further time advanced circulation Γ^{N+2} is next solved implicitly for the z-direction using the previously obtained Γ^{N+1},

$$\frac{\Gamma^{N+2}}{\Delta t} - L_z^* \Gamma^{N+2} = \frac{\Gamma^{N+1}}{\Delta t} + L_r^* \Gamma^{N+1} \qquad 3.59$$

The vorticity is next calculated by ADI.

The whole iteration procedure (Pao, 1970) is summarized in Fig.3.12. Choosing appropriate initial conditions and time

Figure 3.12

The Iteration Procedure for Vortex Flow Calculation

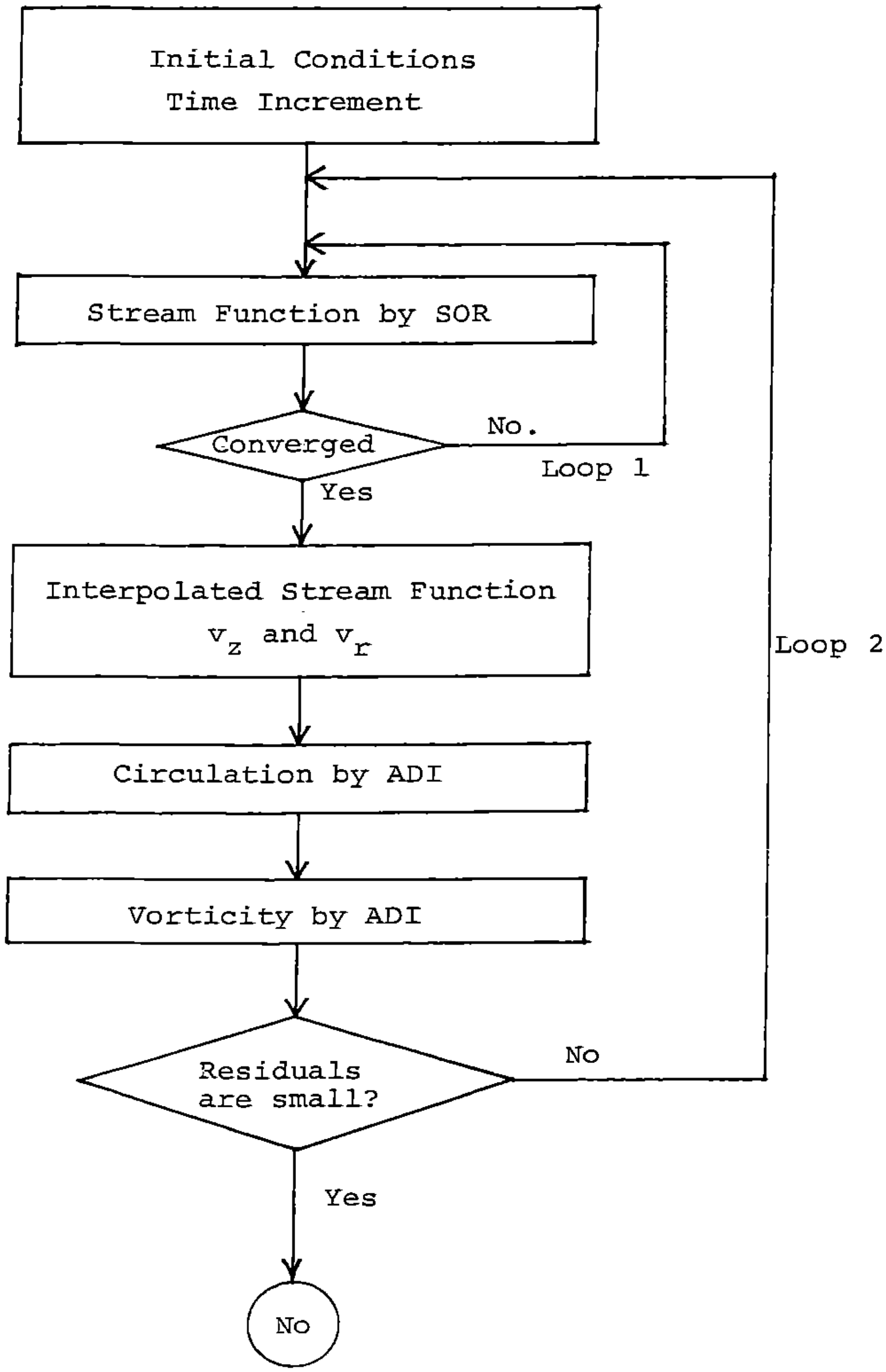

increment, the stream function is iterated until it converges. The convergence criterion for the stream function is

$$\frac{|\psi_{i,j}^{NEW} - \psi_{i,j}^{OLD}|}{\psi_{i,j}^{NEW}} < .05 \qquad 3.60$$

$$\text{for} \quad \begin{array}{l} 2 \leq i \leq N-1 \\ 2 \leq j \leq M-1 \end{array}$$

After convergence, the time advanced circulation is calculated followed by the vorticity calculation. A very small time increment increases the stability because it makes a strong diagonally dominant matrix but it takes an excessive amount of calculation time. When a very large time increment is taken, however, the calculation becomes unstable so that the results are physically meaningless. The optimal time increment is determined by a trial and error approach. Von Neuman stability analysis (Clomburg, 1971) obviously does not work for the case where the non-linear convective terms are dominant in the equations. The time increment is usually decreased when the calculation results approach a desired steady state to ensure the stability near the steady state.

The iteration is terminated when the residual of each difference equation becomes sufficiently small when compared with the dominant terms in the equation for the entire geometry. The detailed information about the calculation is found in Appendix A along with a complete listing of program.

IV. EXPERIMENTAL STUDY

4.1 Introduction

A steady state vortex flow system is constructed in the vortex inhibition study although the original experimental study conducted by Gordon (1972) used a batch vortex flow with a square shaped tank. The two advantages of the steady state vortex flow system are that it provides time-independent velocity data and makes it much easier to observe several qualitative features of the flow. A measurement of velocity in the steady state vortex flow becomes very reliable when compared with a batch system because it requires a certain amount of time to get velocity data by a photographic tracer technique described in the later section.

The macromolecule (polymer) used in the study is polyethylene oxide (Union Carbide, brand name - Polyox 301) because it shows the vortex inhibition phenomenon more distinctively than other types of polymers. For example, Separan AP-273 (high molecular weight polyacrylamide) has relatively large intrinsic viscosity (Clarke, 1970) so that it is very hard to distinguish between polymer effect and viscous effect.

A large fluctuation (in the velocity components for polymer solution) associated with the vortex inhibition makes the quantitative measurement of them very difficult. Most of the velocity measurements are thus done for

Newtonian fluid and several qualitative observations are done for both the Newtonian fluid and the polymer solution.

As mentioned in chapter 3, the flow characterization of the Newtonian vortex flow is very complicated and still not known completely. The velocity measurement of the Newtonian vortex flow, therefore, not only provides very important information about the rate of strain for the vortex inhibition study but also gives some useful understanding for confined vortex flow.

The total flow system of the steady state vortex flow is described in the next section followed by an explanation of the photographic tracer technique. Experimental procedure for the measurement of velocity components in several regions are then explained in detail. Finally four kinds of qualitative observations are portrayed.

4.2 The Flow System

The continuous steady state vortex flow is established by tangentially introducing a fluid inside the outer wall of the vortex tank with an equal flow rate of draining fluid from the tank. Fig. 4.1 shows the total flow system of the steady state vortex flow. By keeping the head of a fluid constant in the constant head tank, any desired feed rate is obtainable by adjusting the three valves, valve 1, 2, and 3. Once a steady state flow rate is established, that is, the liquid level in the vortex tank becomes stationary, the flow rate is determined by measuring the amount of the fluid leaving the vortex tank in a certain time period. The fluid drained from the vortex tank is then sent to the feed tank where excess fluid from the constant head tank is also collected. The fluid in the feed tank is brought up to the constant head tank for recycling. The pump used in the flow system is Moyno Pump (1L2-CDQ). The Moyno pump is a screw conveyor type of pump with rounded flights so that it reduces degradation substantially when compared with centrifugal or gear types of pump. Recycling the fluid is permitted for only Newtonian fluid because a polymer solution is eventually degraded when used for recycle. The macromolecules are degraded especially when a high shear rate is imposed. Since the fluid experiences high deformation rate at the valves and pump, the degradation of the macromolecules is inevitable in this kind of experimental study. The polymer degradation

Fig. 4.1 THE TOTAL FLOW SYSTEM

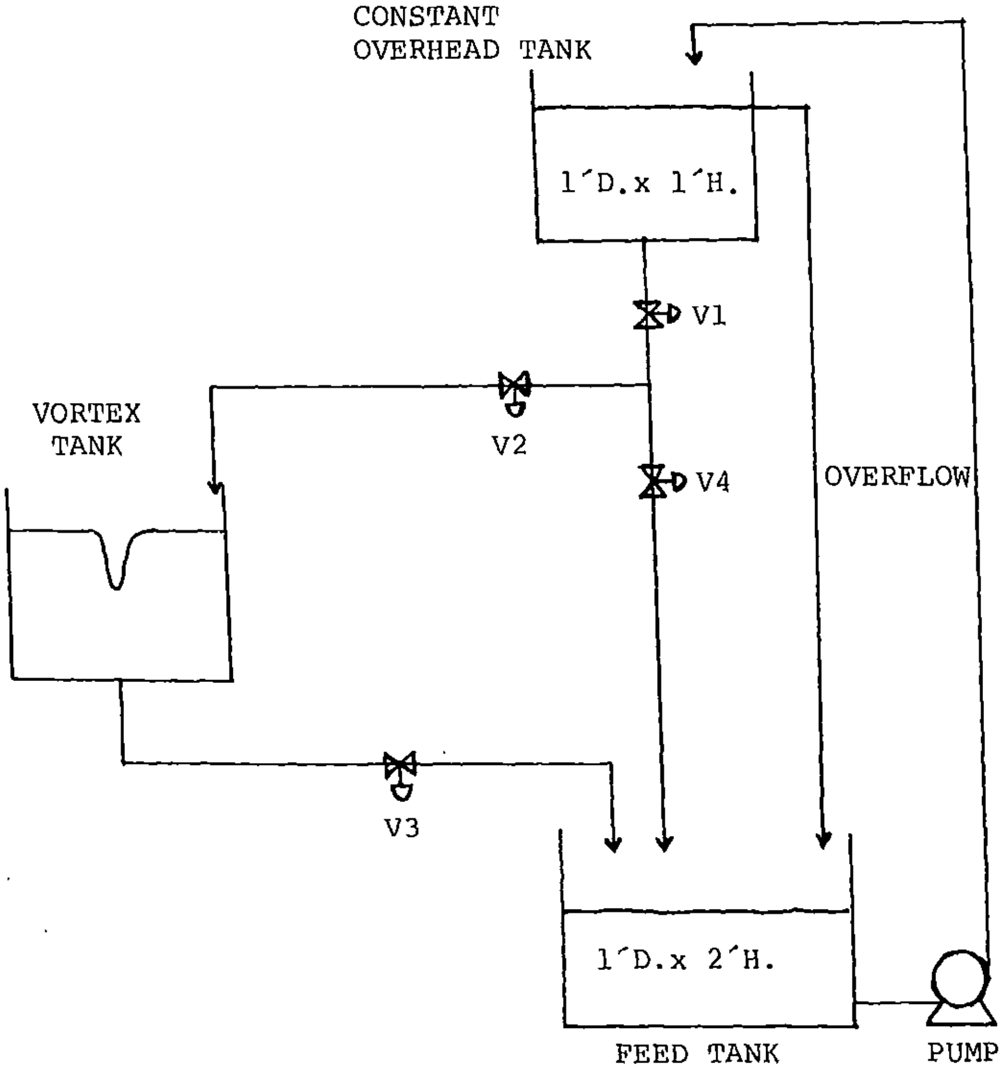

is one of the reasons why quantitative velocity measurements are difficult for the polymer solution.

A detailed sketch and photograph of the vortex tank are shown in Fig. 4.2 and Fig. 4.3 respectively. The open ended vortex tank made by plexiglas has a special inlet section. The fluid is first fed into a small tube from the constant head tank. The small tube is equipped with 39 equally spaced small holes of .32 cm diameter along its entire height. The fluid then flows into a thin channel through these small holes. A flow straightener made by a pile of many small tubes is located at the end of the channel. The fluid come through the flow straightener enters tangentially at the side wall of the vortex tank with nearly flat velocity profile from the bottom to the liquid level. Although a viscous boundary layer forms near the side wall, it does not disturb a main flow because the boundary layer thickness is very small. The exit hole is located at the center of the bottom wall. The diameter of the exit hole is .48 cm and this is about 3% of that of the vortex tank. It takes about one to two hours to get a steady state vortex flow in this flow system.

Fig. 4.2 THE VORTEX TANK

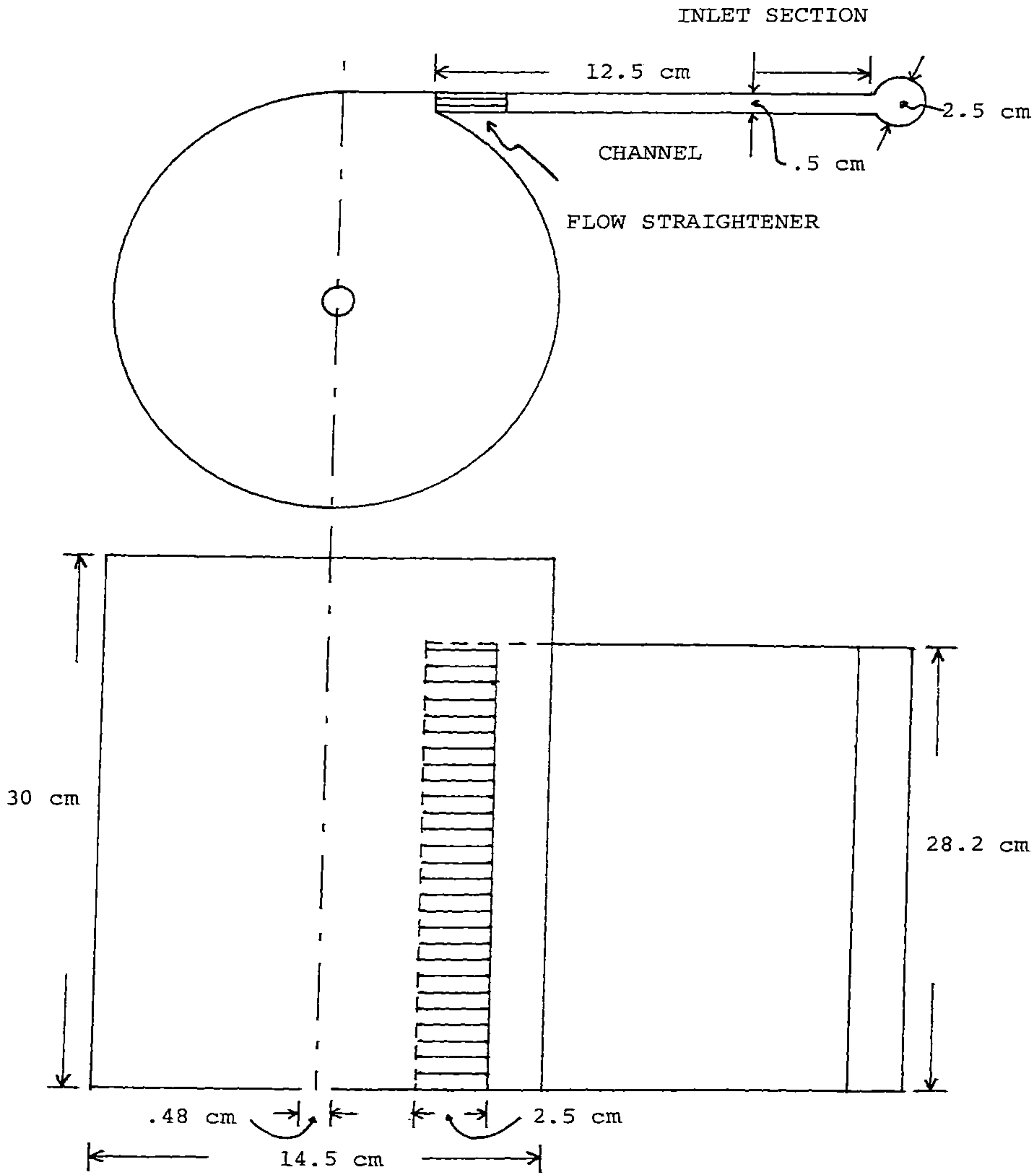

is one of the reasons why quantitative velocity measurements are difficult for the polymer solution.

A detailed sketch and photograph of the vortex tank are shown in Fig. 4.2 and Fig. 4.3 respectively. The open ended vortex tank made by plexiglas has a special inlet section. The fluid is first fed into a small tube from the constant head tank. The small tube is equipped with 39 equally spaced small holes of .32 cm diameter along its entire height. The fluid then flows into a thin channel through these small holes. A flow straightener made by a pile of many small tubes is located at the end of the channel. The fluid come through the flow straightener enters tangentially at the side wall of the vortex tank with nearly flat velocity profile from the bottom to the liquid level. Although a viscous boundary layer forms near the side wall, it does not disturb a main flow because the boundary layer thickness is very small. The exit hole is located at the center of the bottom wall. The diameter of the exit hole is .48 cm and this is about 3% of that of the vortex tank. It takes about one to two hours to get a steady state vortex flow in this flow system.

Fig. 4.2 THE VORTEX TANK

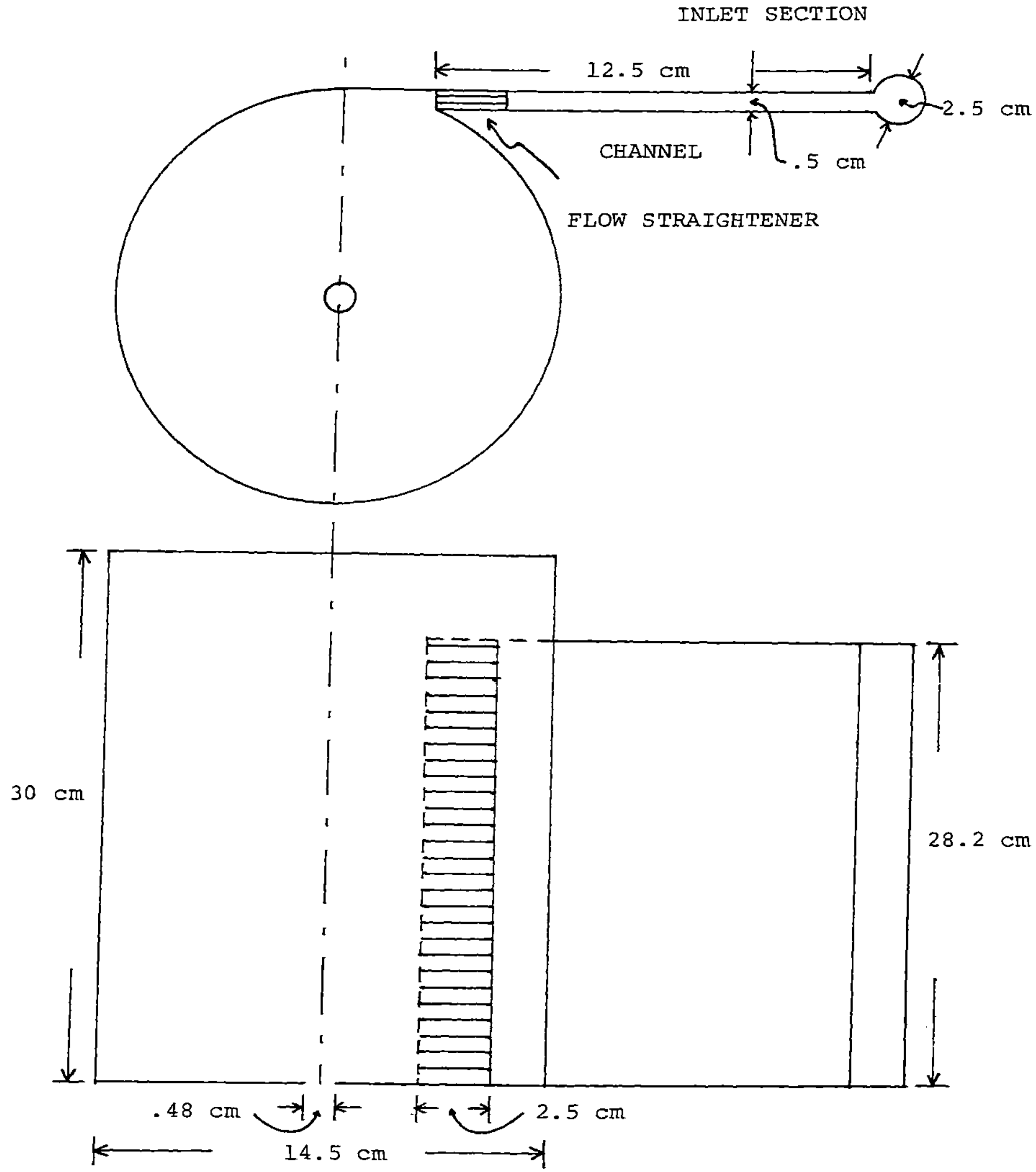

Fig. 4.3

A Photograph of the Vortex Tank

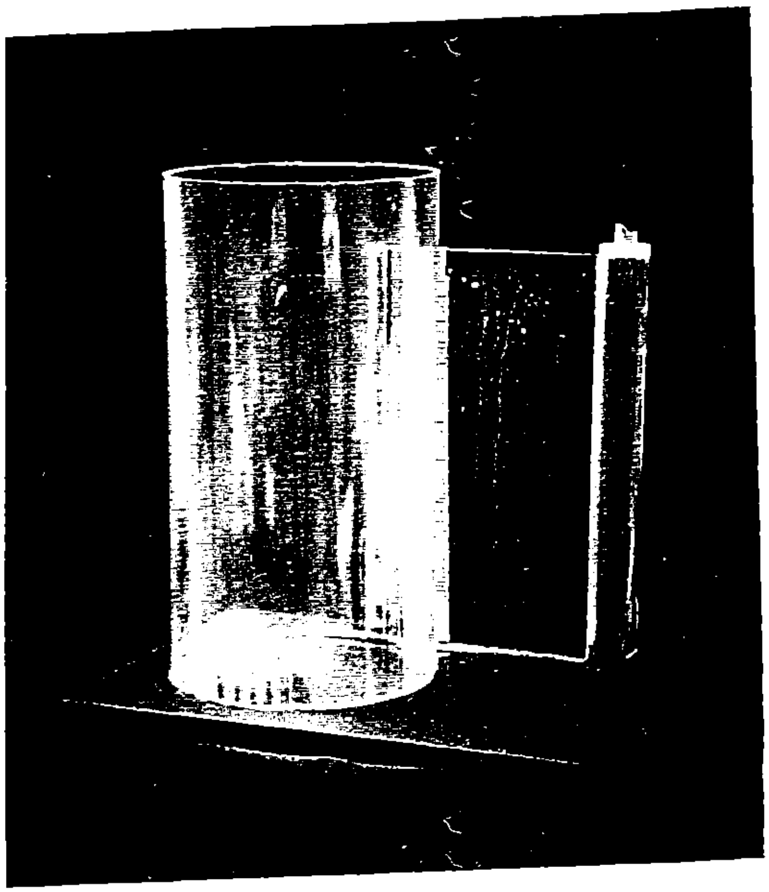

4.3 Photographic Tracer Technique

Tangential velocity V_θ at the free stream region, axial velocity V_z along the axis of rotation and axial velocity near the exit hole are quantitatively measured by this technique. These velocity components are determined from time lapse photographs of small particles suspended in a thin section of the fluid which is illuminated by a collimated beam of light (Hill, 1969 and Chiou, 1970). A strobe light (1540 strobolume, 1540-P1 oscilator, 1540-P2 lump, Genrad) can flash up to about 400 times per second and the duration of each flash is only about 1μ sec. All measurements are calibrated by photographs of scale.

The tangential velocity V_θ in the free stream region is measured at different radial positions. The measurement is done at two different axial positions. The V_θ-data at two axial positions is enough to represent V_θ in the free stream region because the tangential velocity is almost independent of axial position. The V_θ is calculated from a particle's dot trajectory on the bottom view photograph using a horizontally collimated light. The camera (Nikomat FTN F2.0) is located underneath the vortex tank so that a distortion due to free surface is eliminated. The setup of V_θ measurement is shown in Fig. 4.4. Fig. 4.5 shows the picture of a typical particle's dot trajectory. A number of dots can be controlled by adjusting both the flash rate of strobe light and the exposure time of camera. The axis of rotation on the photograph is determined by shifting a

Fig. 4.4 EXPERIMENTAL ARRANGEMENT

FOR V_θ MEASUREMENT

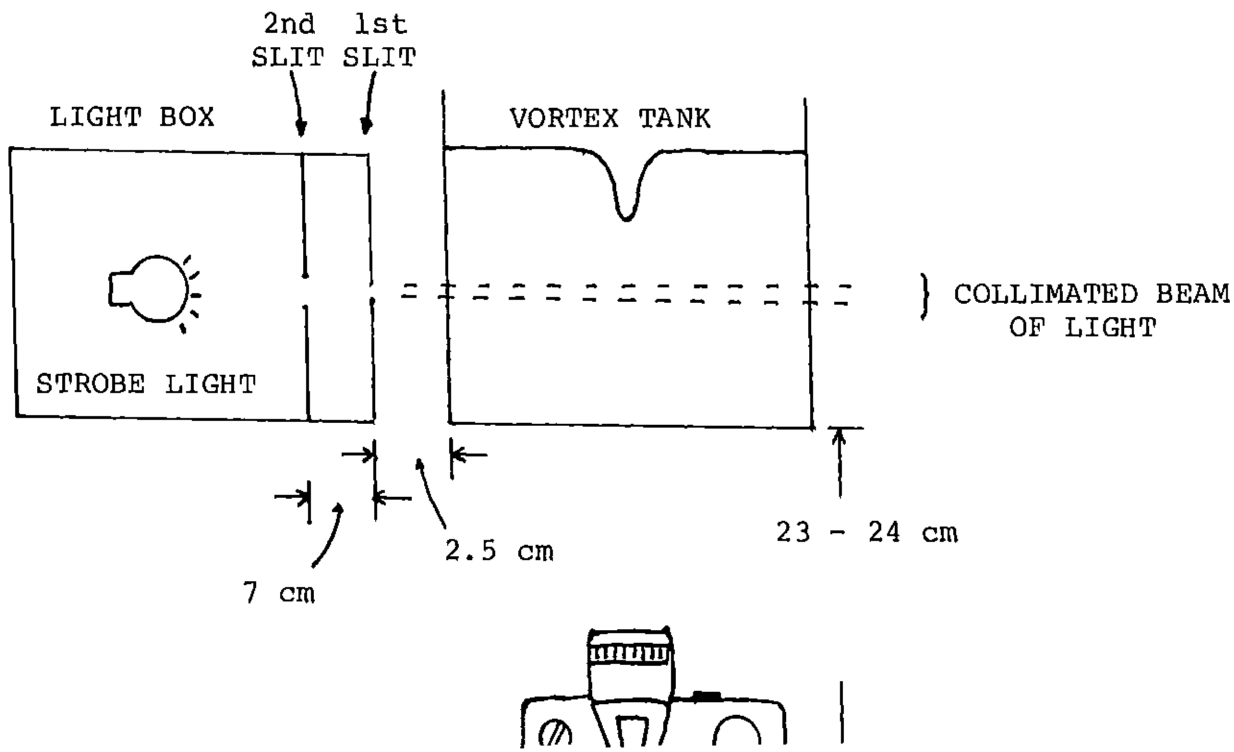

Fig. 4.5

A Photograph for Measuring V_θ

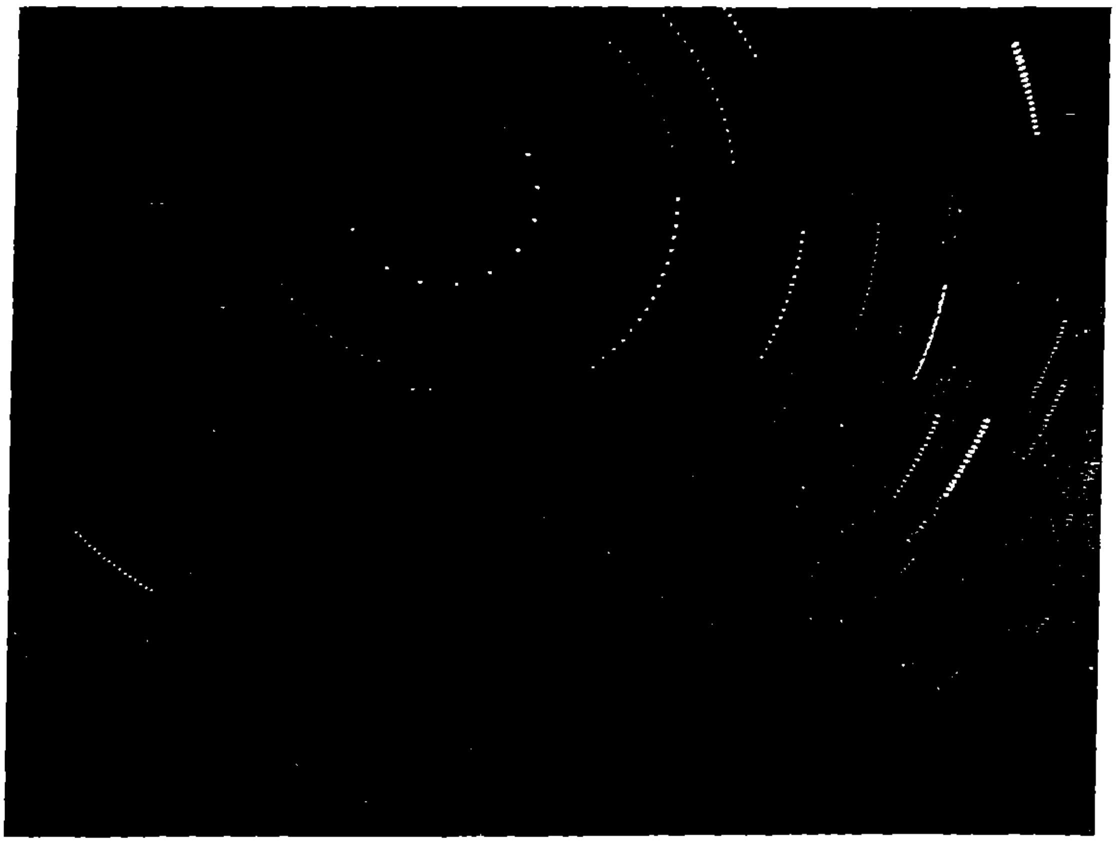

a transparency paper on which a number of concentric circles are drawn until the particles' trajectories coincide with the circles. The center of these circles on the transparency paper then indicates the axis of rotation on the photograph. Although radial velocity V_r exists in the free stream region, its value is so small when compared it with V_θ that it is hardly determined from the photograph. In Fig. 4.6, V_θ is approximately calculated by

$$V_\theta = \frac{r_1 + r_2}{2} \frac{\theta_2 - \theta_1}{\Delta t} \qquad 4.1$$

where

$$\left.\begin{aligned} r_i &= \sqrt{x_i^2 + y_i^2} \\ \theta_i &= \tan^{-1} \frac{y_i}{x_i} \end{aligned}\right\} \quad i = 1.2 \qquad 4.2$$

Since each dot in Fig. 4.6 corresponds to individual flash, Δt is determined by

$$\Delta t = nd/r_f \qquad 4.3$$

where nd is a number of dots and r_f is flash rate.

The axial velocity measurement in the core region is very difficult with the present photographic technique because the reflection of light from the air core is so strong that it makes the particles near the air core impossible to see. Incomplete vortex flow (the word 'incomplete'

Fig. 4.6 DOTS SHOWING THE TRAJECTORY OF SEED PARTICLES FOR V_θ MEASUREMENT

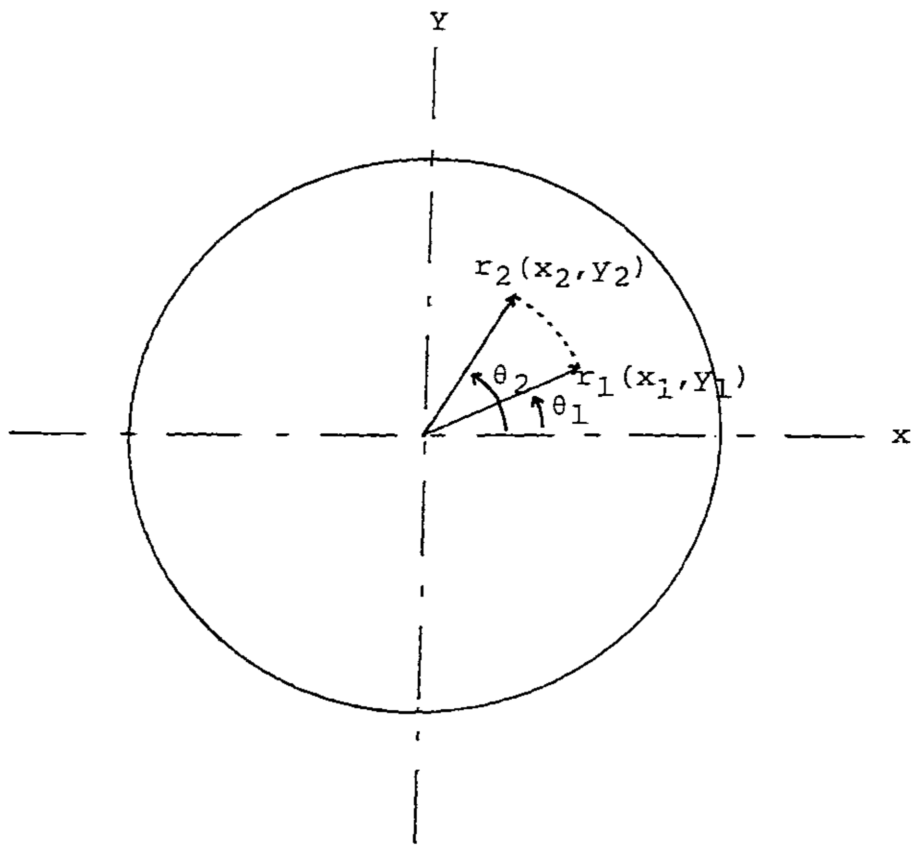

indicates that the air core does not extend down to the exit hole.) thus is established so that V_z at the axis of rotation can be measured from the side view photograph. A vertically collimated beam of light which includes the axis of rotation is used for V_z measurement. As shown in Fig. 4.7, the first slit width is 1.2 cm and the camera is located so that it can detect the scattered lights which makes a right angle with the beam of light source. Fig. 4.8 is a photograph from which V_z at the axis of rotation is calculated. V_z is approximately determined by dividing the distance between two adjacent dots by a time span for two flashes. Averaging the axial positions of the dots gives that of the calculated V_z.

When the axial velocity V_z is measured near the exit hole, a black painted disk with a hole at the center, whose diameter is the same as that of the exit hole, is placed on the bottom wall of the vortex tank so that the reflection of light from the bottom is substantially reduced. Fig. 4.9 is a photograph which shows the flow behavior near the exit hole. From the particle's trajectory in Fig. 4.10, V_z as a function of radial position near the exit hole, is approximately calculated by

$$V_z = \frac{z_1 - z_2}{\Delta t} \qquad \text{at } r_m \qquad 4.4$$

where

Fig. 4.7 EXPERIMENTAL ARRANGEMENT

FOR V_z MEASUREMENT

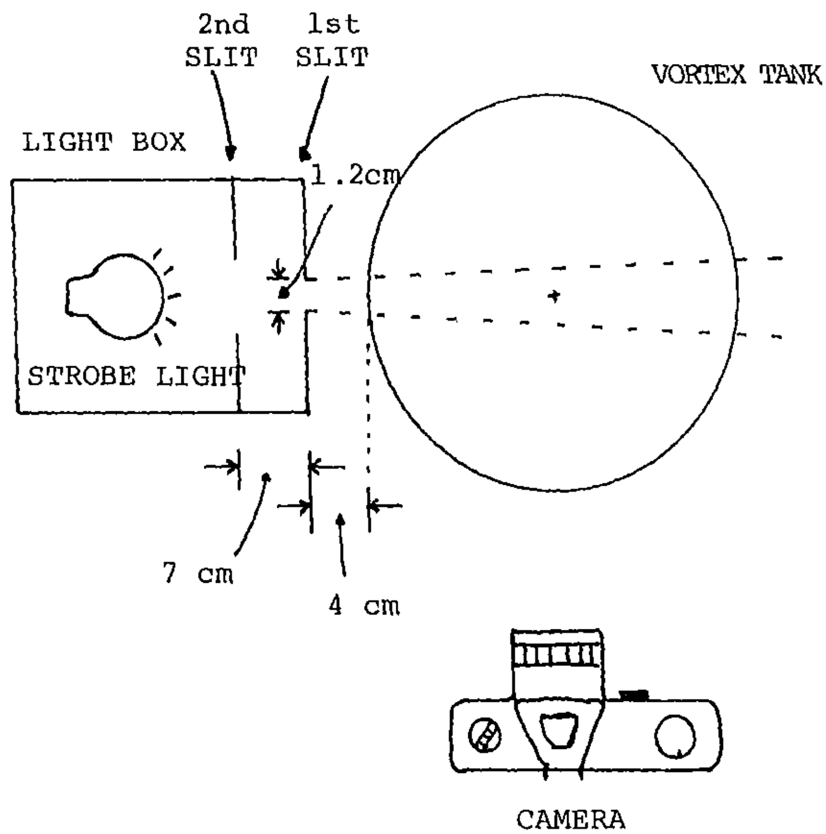

Fig. 4.8

A photograph for Measuring V_z

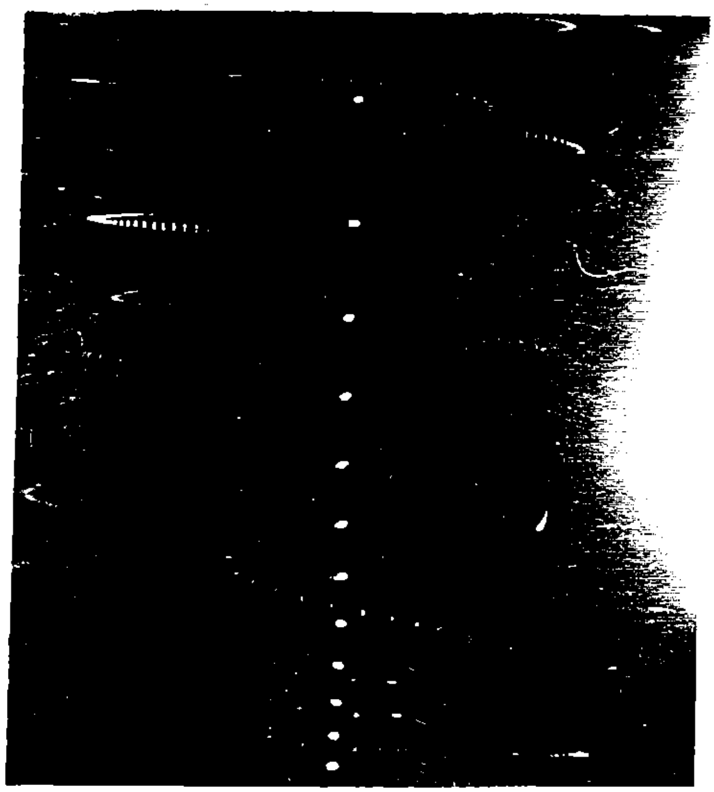

Fig. 4.9

A Photograph Showing the Flow Behavior near the Exit Hole

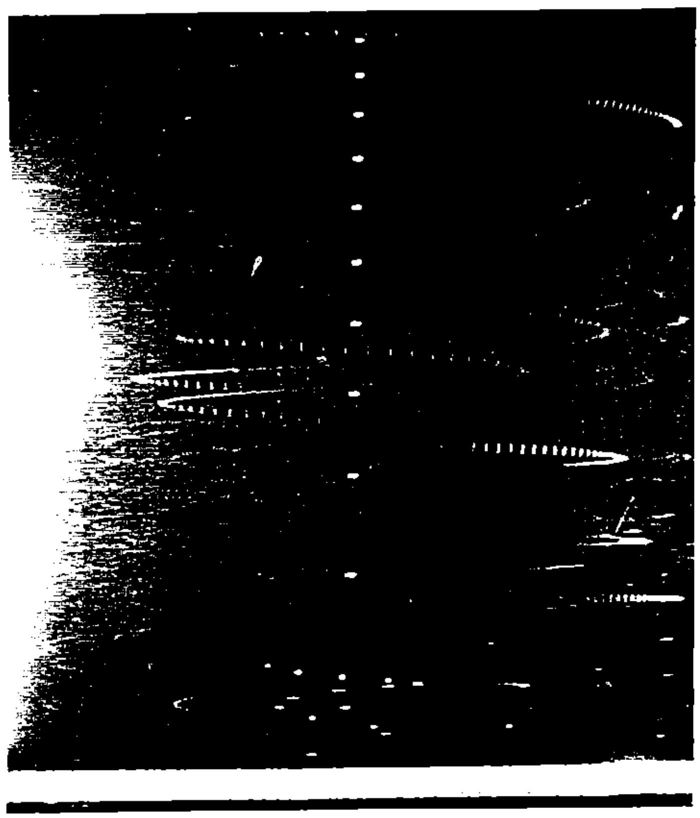

Fig. 4.10 DOTS SHOWING THE TRAJECTORY OF SEED PARTICLES FOR V_z MEASUREMENT

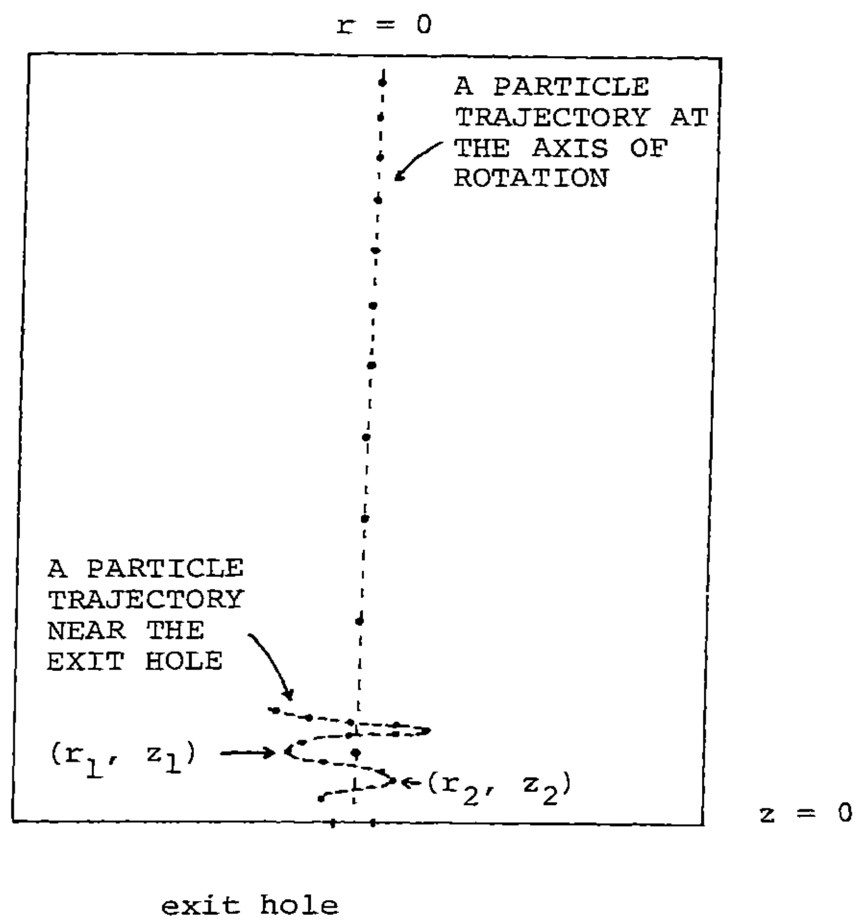

$$r_m = \frac{r_1 + r_2}{2} \qquad 4.5$$

Since the magnitude of radial velocity V_r becomes comparable to that of V_θ in this region, the particle moves appreciably towards the axis of rotation even in a very short time period (Δt = .045 sec in Fig. 4.10). Two radial positions r_1 and r_2, however, are not so different, the approximation (eq. 4.5) may thus be acceptable.

4.4 Experimental Procedure

Several kinds of experiments are done depending on the kind of velocity data to be measured. The experimental procedure for the measurement of the tangential velocity in the free stream region and the axial velocity along the axis of rotation for both a Newtonian fluid (room terperatured water) and a polymer solution are summerized as follows:

1. Calibration: After filling water in the vortex tank, the pictures of scale are taken, first at the two axial position (z_1, z_2) for V_θ calibration. Even though the axis of rotation does not coincide exactly with the center line, the error associated with this is negligible.
2. Flow Circulation: Turn on the pump to circulate the water. The valve 1 in Fig. 4.1 is wide open and at the same time valve 4 is closed. By controlling valve 2 and 3, any desired steady state is obtained. Establishing a steady state flow is determined when the fluctuation of the liquid level in the vortex tank becomes within ±.5 cm. The liquid level is usually between 15 cm and 20 cm.
3. Flow Rate and Liquid Level Measurement: After a steady state vortex flow is established, the volumetric flow rate is determined by measuring the amount of the fluid from the vortex tank in a certain time period. The measurement is repeated at least 6 times to ensure the system has reached a steady state. The liquid level is also recorded.
4. Seeding Small Particles (Chiou, 1976): The seeding particles are made from PLIOLITE (Goodyear product: Solution Regin

type S6B Lot 42-13-D1). The PLIOLITE is crushed in a mortar and pestal until a desired particle diameter range is obtained. The diameter of the particle used in the study varies between 208 μm and 425 μm. The optimal particle density is determined by trial and error. The highly concentrated particle solution is first prepared. The particle solution is then added to the feed tank little by little through a pipette. After the particles are well distributed in the whole fluid (it takes about 20 min.), the appropriateness of the particle density is judged by looking through the finder of the camera.

5. V_z Measurement Along the Axis of Rotation: The pictures for the particle behavior at the center of the vortex tank are taken by the method delineated in Fig. 4.7 The aperture and exposure time of the camera are F4.0 and .5 sec. respectively. The flash rate of strobe is 4000 times per minute. The film used for the velocity measurement is Kodak Tri-X pan with ASA 400. Twenty to thirty pictures are taken for V_z measurement.

6. Flow Rate and Liquid Level Measurement: The flow rate and the liquid level are measured again in the way described in procedure 3.

7. V_θ Measurement at z_1 and z_2: After setting up the apparatus as described in Fig. 4.4, the pictures for the particles' behavior at two different horizontal plains (z_1 and z_2) in the free stream region are taken. Due to the characteristics of the tangential velocity profile, 4 different flush rates (1000, 2000, 3000, and 4000 times per minute) are used

depending on how fast the particles move in the region of interest. The aperture and exposure time of the camera are F2.0 and ¼, ½, 1 sec. About 20 pictures are taken at each plane.

8. Flow Rate and Liquid Level Measurement: The flow rate and the liquid level are measured to see if there is any significant change in the steady state flow during the course of the experiment.

The V_θ measurement for a Newtonian fluid is terminated here. For a polymer solution, the procedure is continued to the following:

9. V_θ measurement for a polymer solution: A concentrated polymer solution is prepared at least 2 days before use. A certain amount of polymer (Polyethyrene oxide: Polyox 301 made by Union Carbide) is weighed carefully and dissolved in about 30 cc of isopropanol (Paterson and Abernathy, 1970) in a beaker. 1 g of Polyox 301 makes about 30 w. ppm solution for the system. After the powder of the polymer is well scattered in the isopropanol, water is gently poured into the beaker until the solution reaches 1000 cc. The beaker is then covered and allowed to stand until the polymer dissolves completely in the water.

The concentrated polymer solution is poured into the feed tank. As soon as the polymer effect begins. That is, the small fluctuation of the air core is observed. The pump is stopped running so that the degradation of the polymer is avoided to some extent. The onset behavior of the V.I. is then measured by taking pictures for V_θ. All the pictures are taken within 30 seconds after the onset of vortex inhibition. The importance of measurement of the onset behavior is to be able to observe how the V_θ is changed by introducing the polymer solution into the Newtonian flow pattern. And the information is very useful for the analytical study of vortex inhibition (in Chapter 6) because a numerical simulation is done for the situation where the Newtonian fluid is suddenly replaced by polymer solution to see how the resulting stress field calculated by use of the Newtonian flow behavior changes due to the presence of the macromolecules. After a couple of minutes, the vortex flow completely shifts to a new quite different flow status which is the vortex flow of the polymer solution. The flow rate and liquid level are then measured.

The procedure for the measurement of axial velocity along the axis of rotation for polymer solution is to follow the procedure 9 with the setup for V_z measurement described in Fig. 4.7.

The V_z measurement procedure near the exit hole is essentially the same as that for V_z along the axis of rotation except that the camera's position is lowered down to the bottom plate of the vortex tank. Since a black painted disk is placed on the bottom wall in order to reduce the reflection of the light from the bottom plate as much as possible, the procedure 7 and 8 are not done for the measurement.

4.5 Oualitative Observations

Four kinds of oualitative observations are done for studying the characteristics of vortex flow for both Newtonian and polymer cases. In this section, the descriptions and results are briefly mentioned. The detailed results with photographs are also presented. The complete vortex flow (the air core extends down to the exit hole) is used because the air core does not disturb the observations.

1. The flow behavior of the core region: A dyed water is used for showing the existence of the core region. When the dyed dolution is dropped from a pipette on the free surface of the Newtonian vortex flow near the axis of rotation, it immediately indicates the existence of a core region near the axis of rotation (Fig. 4.11 (a),(b),(c)). It drains out very rapidly. When it is dropped, however, far away from the axis rotation, the dyed solution makes a very slow swirl motion around the air core keeping its radial distance constant and stays inside the vortex tank much longer than the case of dropping it near the axis of rotation. The observation clearly shows the existence of the air core region where the axial velocity is much faster than that in the free stream region.

A dyed polymer solution (its concentration is about 50 ppm) is then dropped into the core region, the vortex is immediately inhibited (Fig. 4.12 (a),(b)). If dropped in the free stream region, the polymer dyed solution behaves as if it were a Newtonian fluid. The vortex is not inhibited

Fig. 4.11 (a) THE CORE REGION FOR A NEWTONIAN FLUID

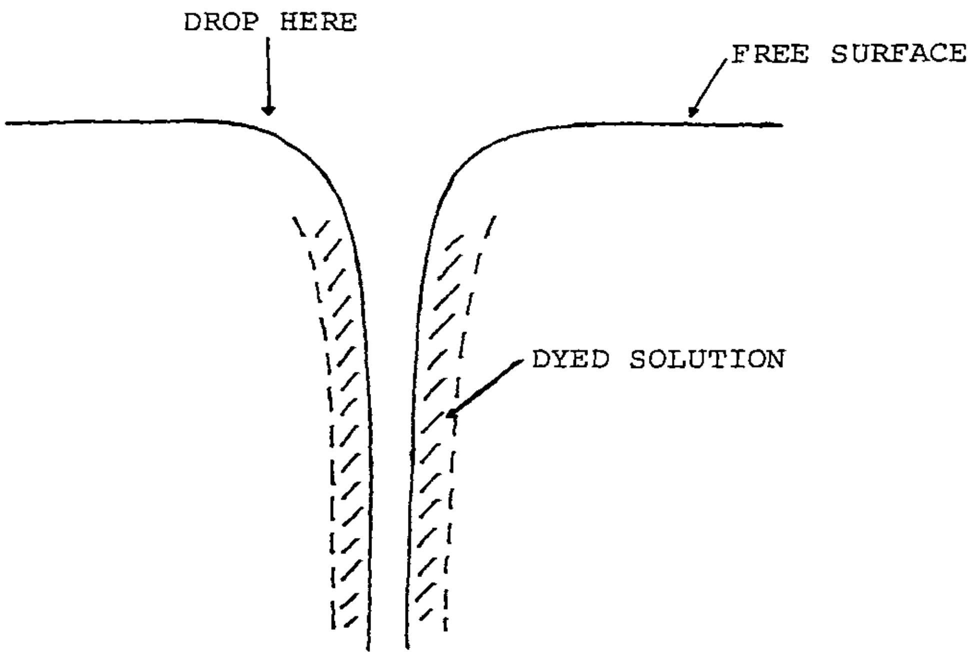

Fig. 4.11 (b)

A Photograph of Newtonian Vortex Flow

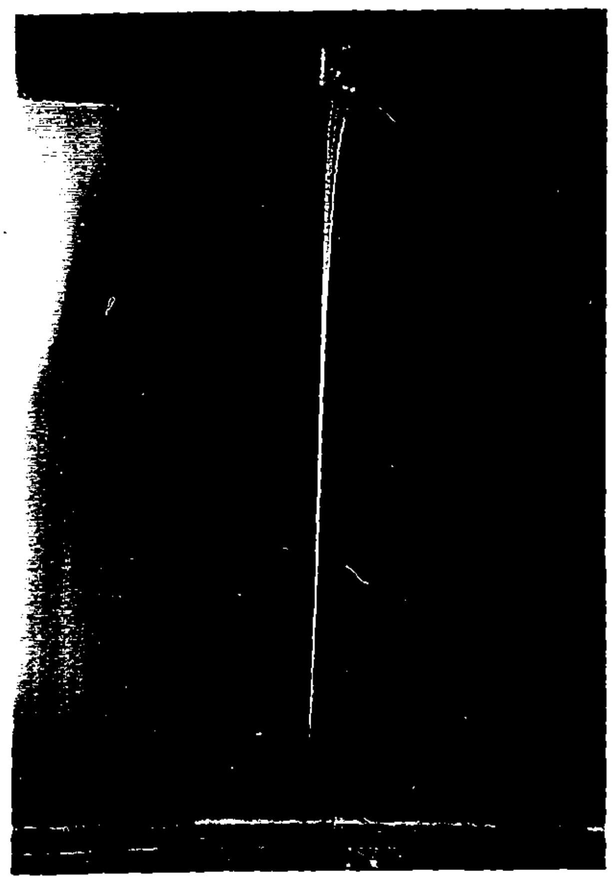

Fig. 4.11 (c)

A Photograph of Newtonian Vortex Flow
with Newtonian Dyed Solution

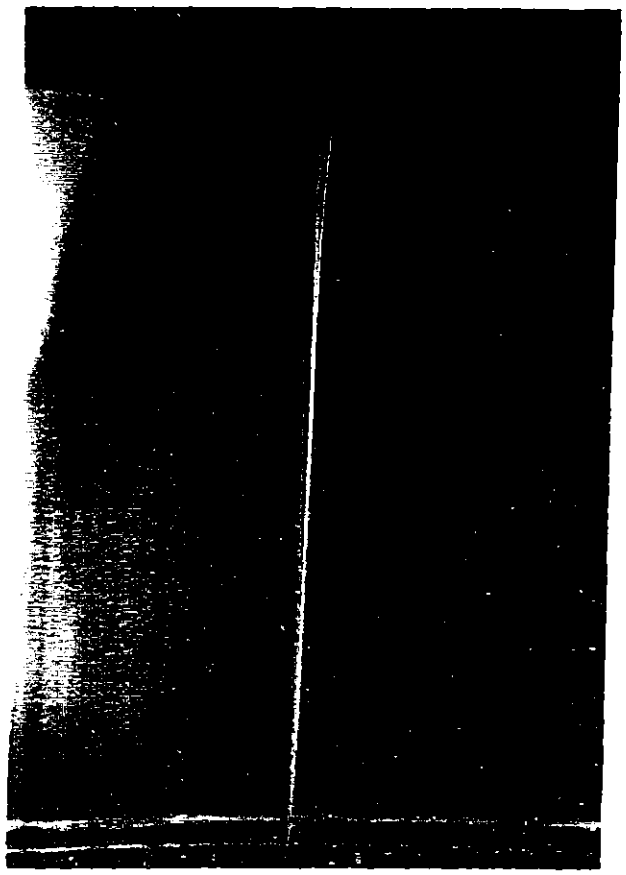

Fig. 4.12 (a) THE CORE REGION FOR A POLYMER SOLUTION

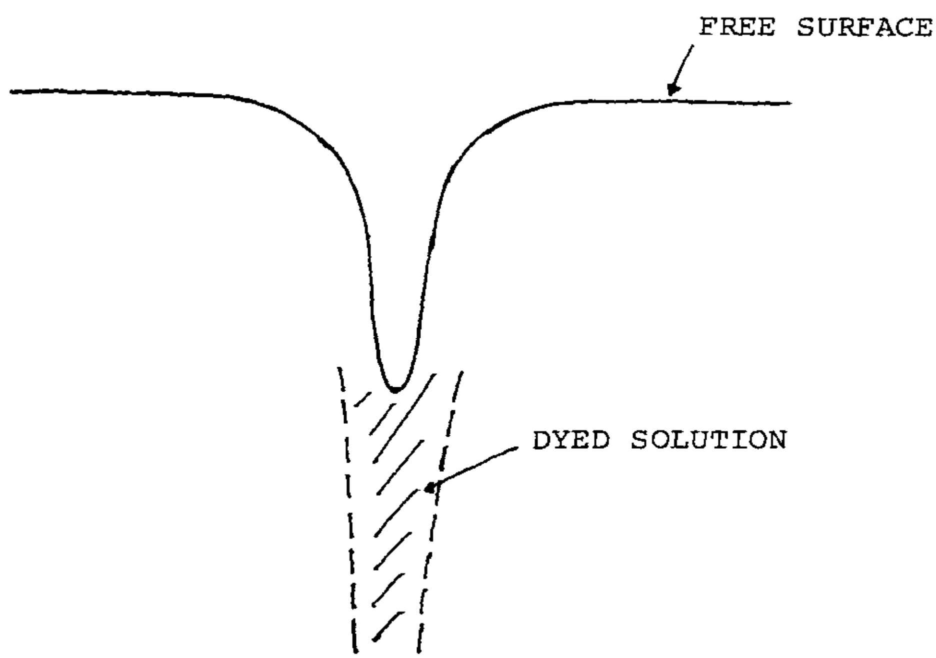

Fig. 4.12 (b)

A Photograph of Newtonian Vortex Flow with Polymer Dyed Solution

because it does not reach the core region. The observation indicates that the tangential velocity V_θ in the core region is reduced due to the presence of the macromolecules and that the polymer effect may be dominant somewhere in the core region. This observation provides quite important information for the vortex inhibition study because it indicates that a large deformation of fluid may take place in the core region.

2. The flow behavior of the bottom boundary layer: The Newtonian dyed solution is injected through a very small hole (its diameter is .04 cm) located in the bottom wall to see the difference in flow behaviors in the bottom boundary layer between a Newtonian fluid and polymer solution. For the Newtonian fluid, the streak of the dye is very smooth and almost all of the dye injected goes directly out through the exit hole (Fig. 4.13 (a),(b)).

For the polymer solution, however, the dye is randomly scattered around the exit hole. Some part of the dye drains but some of it stays near the exit hole for a while. The flow behavior is very random and no obvious streak line is observed (Fig. 4.14 (a),(b)). It may be said that the polymer effect is important in this area because of the apparent difference in flow behavior between the Newtonian fluid and polymer solution.

3. A cap experiment--near the exit hole: When a small tube is installed right above the exit hole (Fig. 4.15), the Newtonian vortex flow is heavily disturbed because the tube

Fig. 4.13 (a) THE FLOW BEHAVIOR OF THE BOTTOM BOUNDARY LAYER FOR A NEWTONIAN FLUID

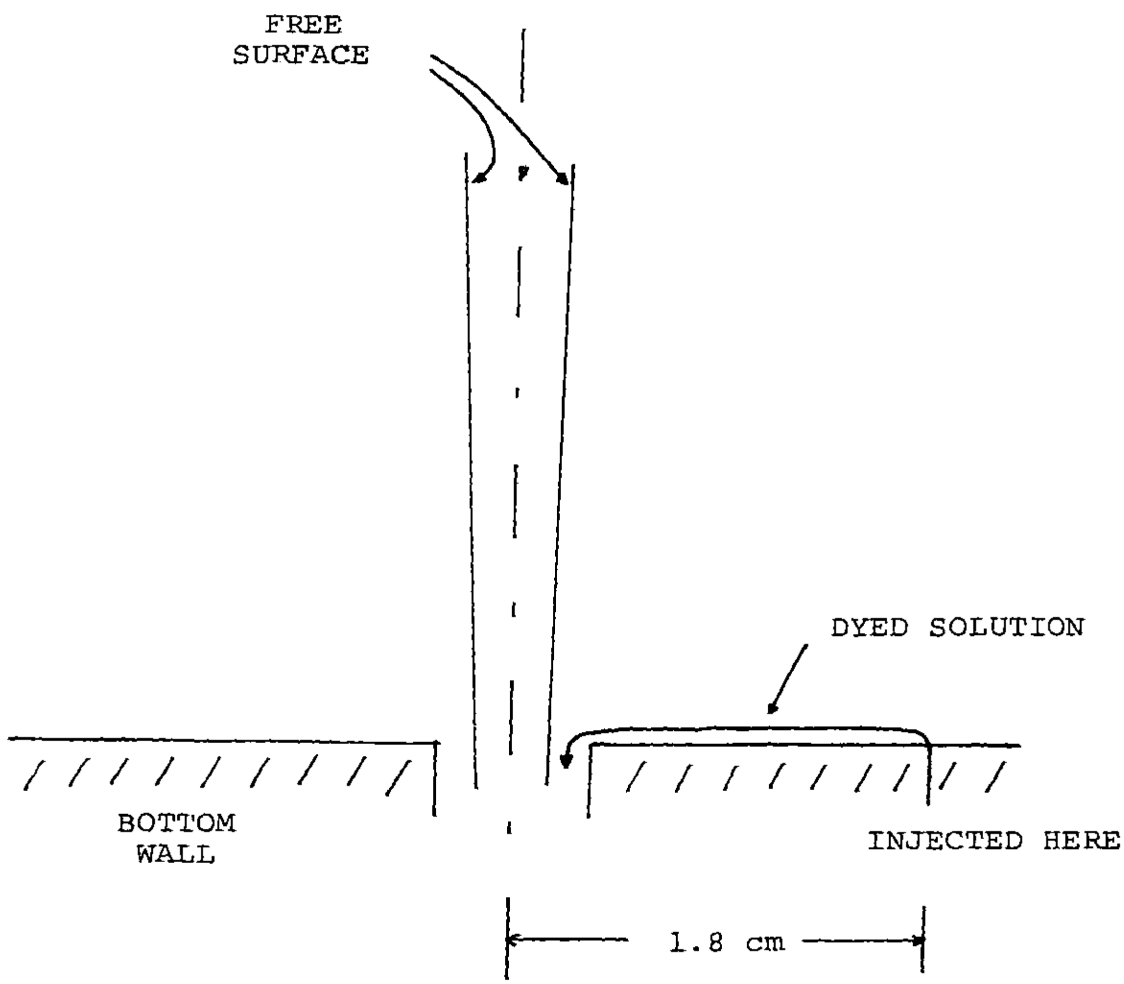

Fig. 4.13 (b)

A Photograph for a Newtonian Fluid

Fig. 4.14 (a) THE FLOW BEHAVIOR OF THE BOTTOM BOUNDARY LAYER FOR A POLYMER SOLUTION

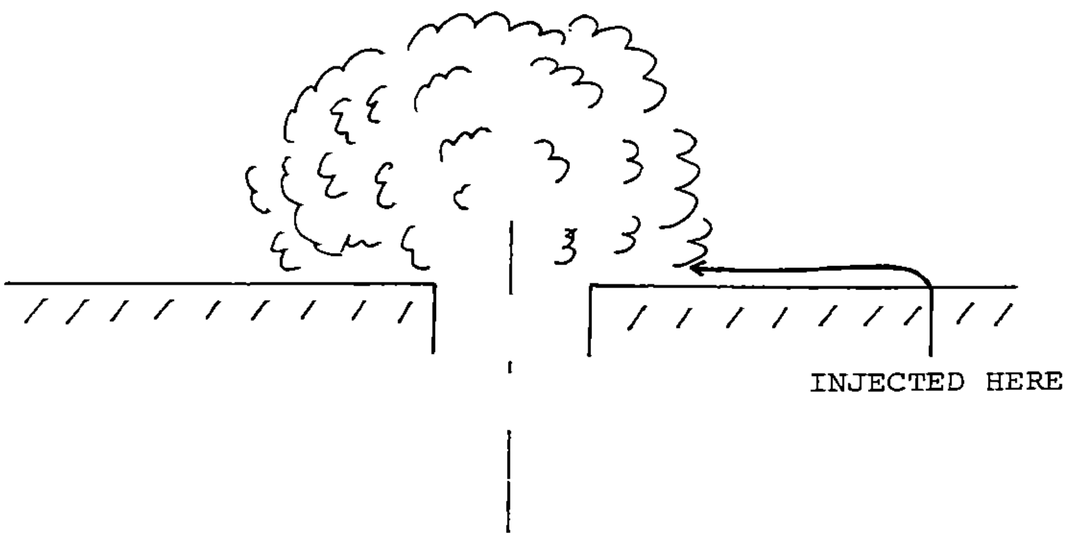

Fig. 4.14 (b)

A Photograph for a Polymer Solution

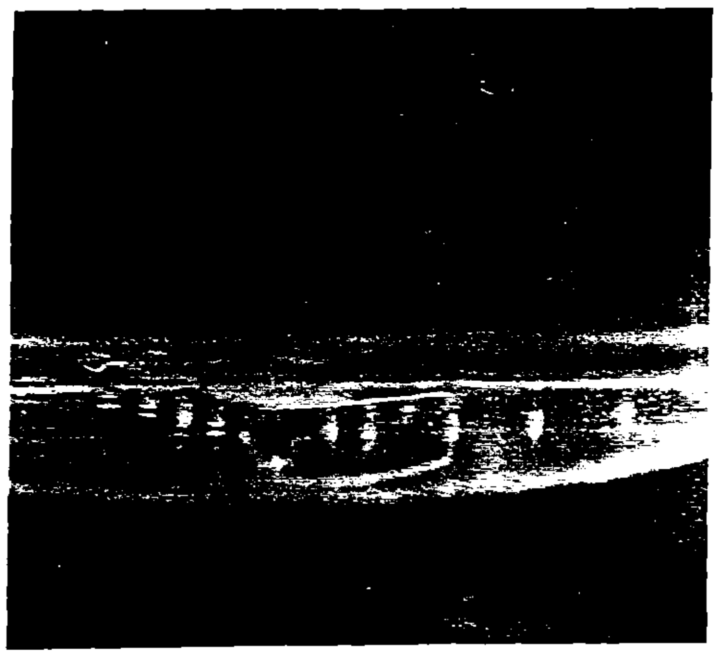

Fig. 4.15 THE DIMENSIONS OF THE CAP

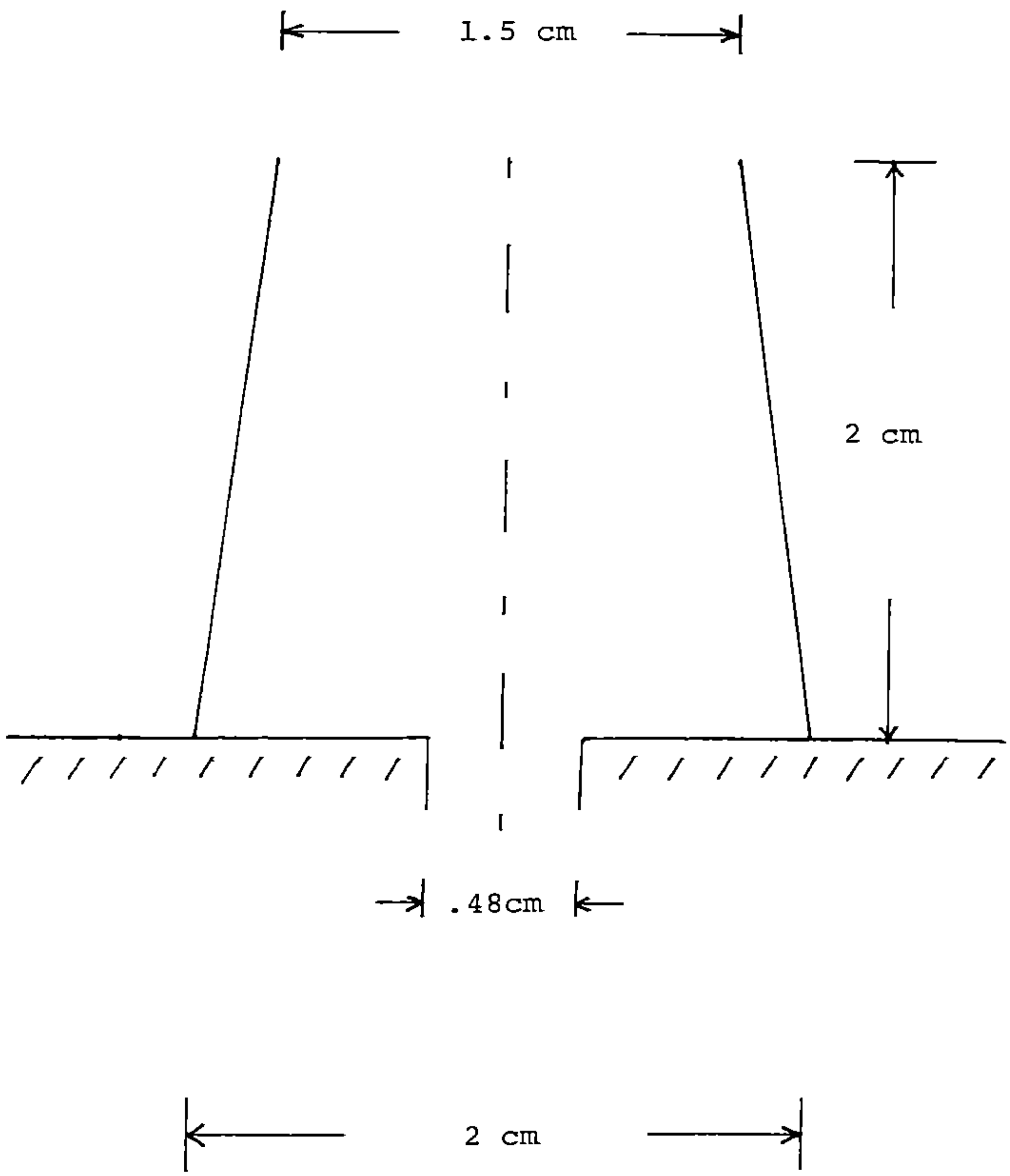

prevents a radial inflow in the bottom boundary layer region from going out through the exit hole. The distinguishing feature of this observation is that installing the cap lowers the liquid level substantially while keeping the flow rate constant (Fig 4.16 (a),(b),(c)). If the liquid level is raised up to the previous level, the flow rate has to be increased about 6%. When the liquid level reaches the previous point, the vortex is inhibited in a very similar way to vortex inhibition by Polyox 301. This experimental observation also emphasizes the importance of the flow behavior near the exit hole.

4. The vortex flow of Newtonian fluids with different viscosity: The width of the air core is measured for Newtonian fluids with different viscosity. As shown in Fig. 4.17 (a), (b),(c), the air core width is not sensitive to changes in viscosity. The fluids used for the observation are water-glycerine solutions (TABLE 4.1). Flow rate and liquid level are also not changed so much by changing viscosity. Both glycerine solution A and B form very similar vortex flow to that by water with respect to the shape of the air core, liquid level and flow rate (Fig. 4.17). Glycerine solution A and 30 wppm polymer solution (Polyox 301) have almost equal relative viscosity. From this, we can conclude that vortex inhibition can not be explained solely by viscous effect, but it has to be due to the elastic nature of the macromolecules.

Fig. 4.16 THE EFFECT OF THE CAP EXPERIMENT

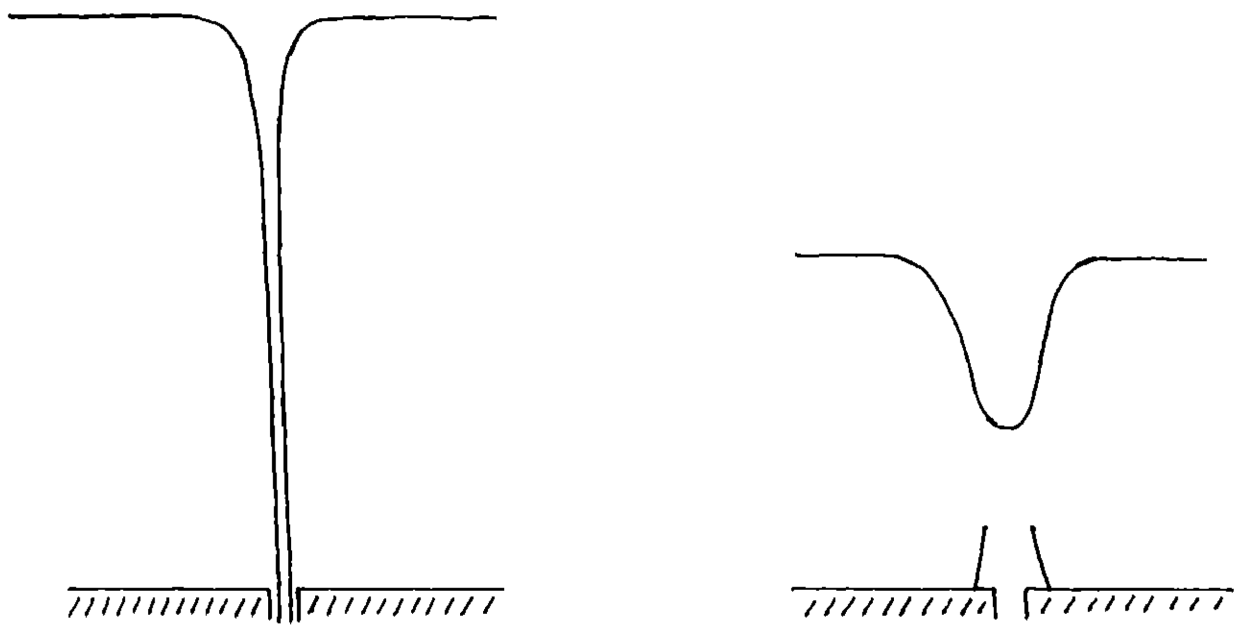

Fig. 4.16 (b)

Without the Cap

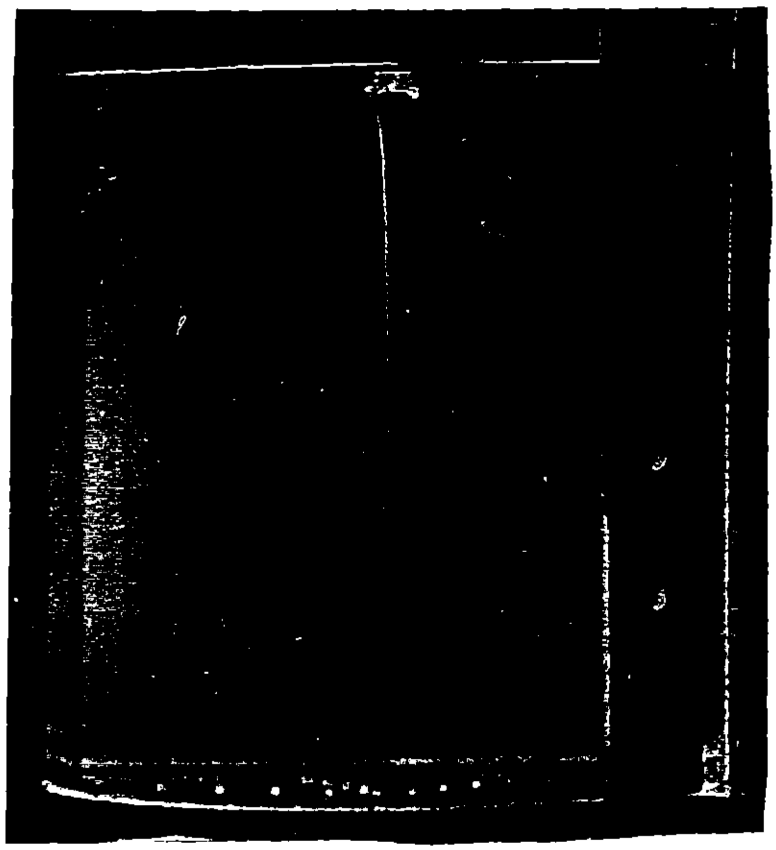

Fig. 4.16 (c)

With the Cap

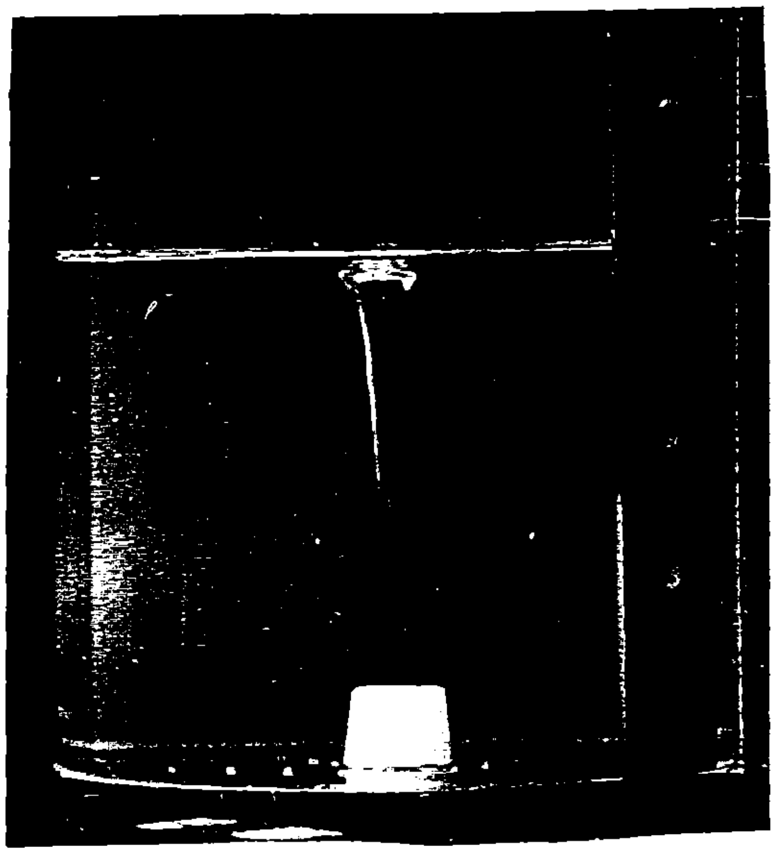

TABLE 4.1

The Vortex Flow of Glycerin Solutions

fluid	relative viscosity μrel (25°C)	liquid level h (cm)	the air core width (cm)	flow rate (cc/sec)
water	1.000	17.0	.38	36.5
glycerin-water A	1.068	16.5	.41	34.8
glycerin-water B	1.227	16.0	.42	34.6

Fig. 4.17 (a)

Water

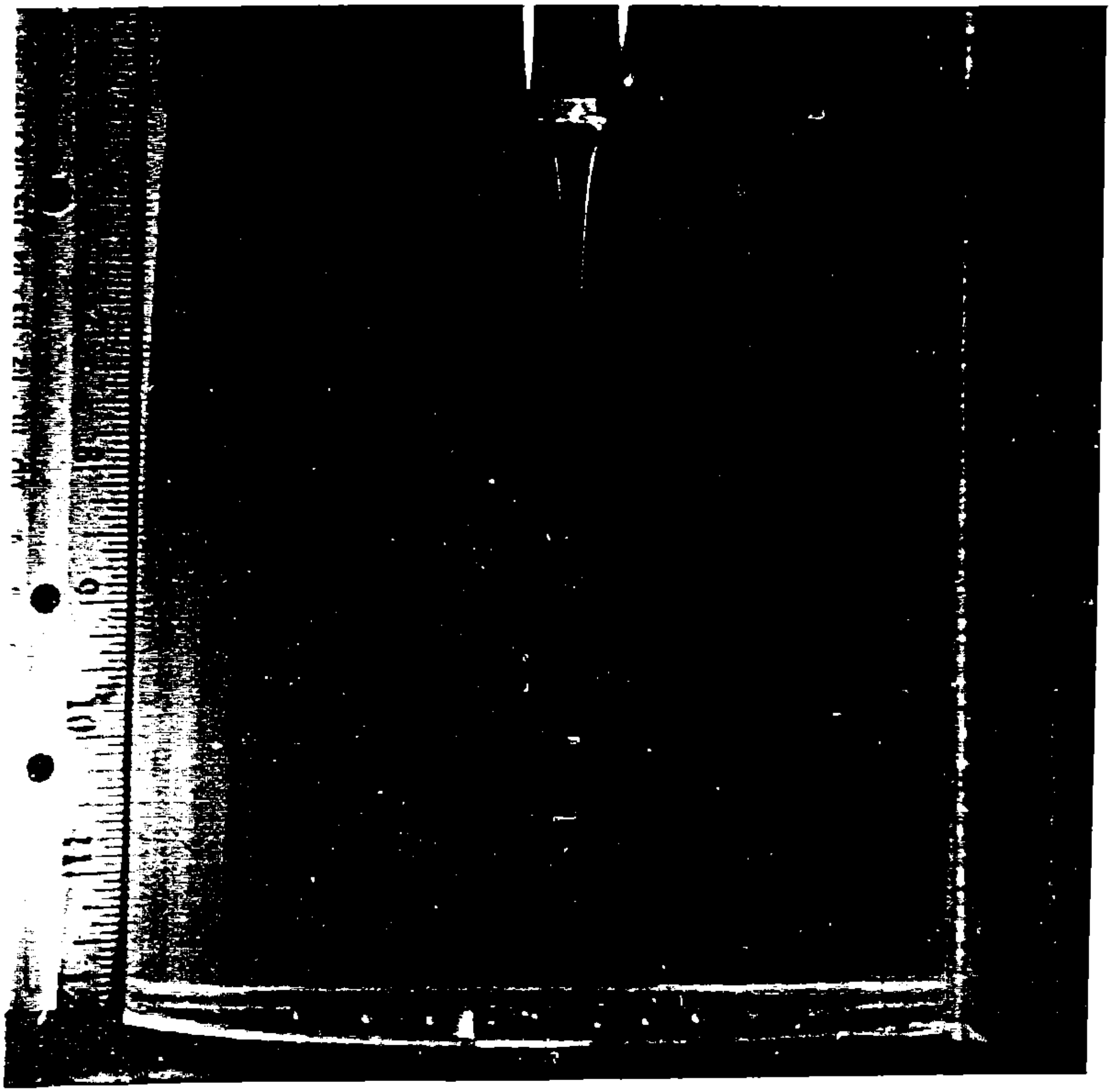

Fig. 4.17 (b)

Glycerin-Water A

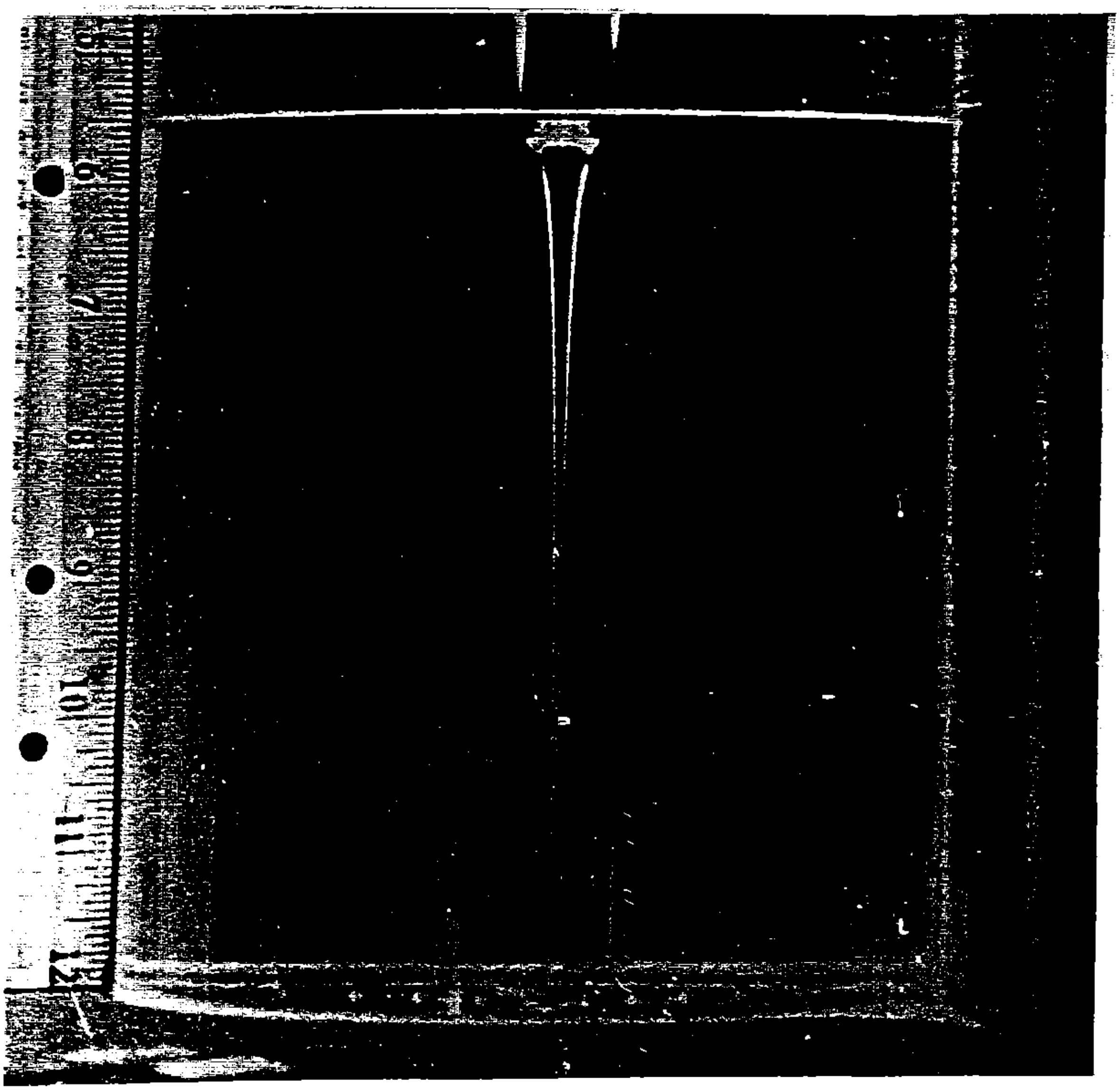

Fig. 4.17 (c)

Glycerin-Water B

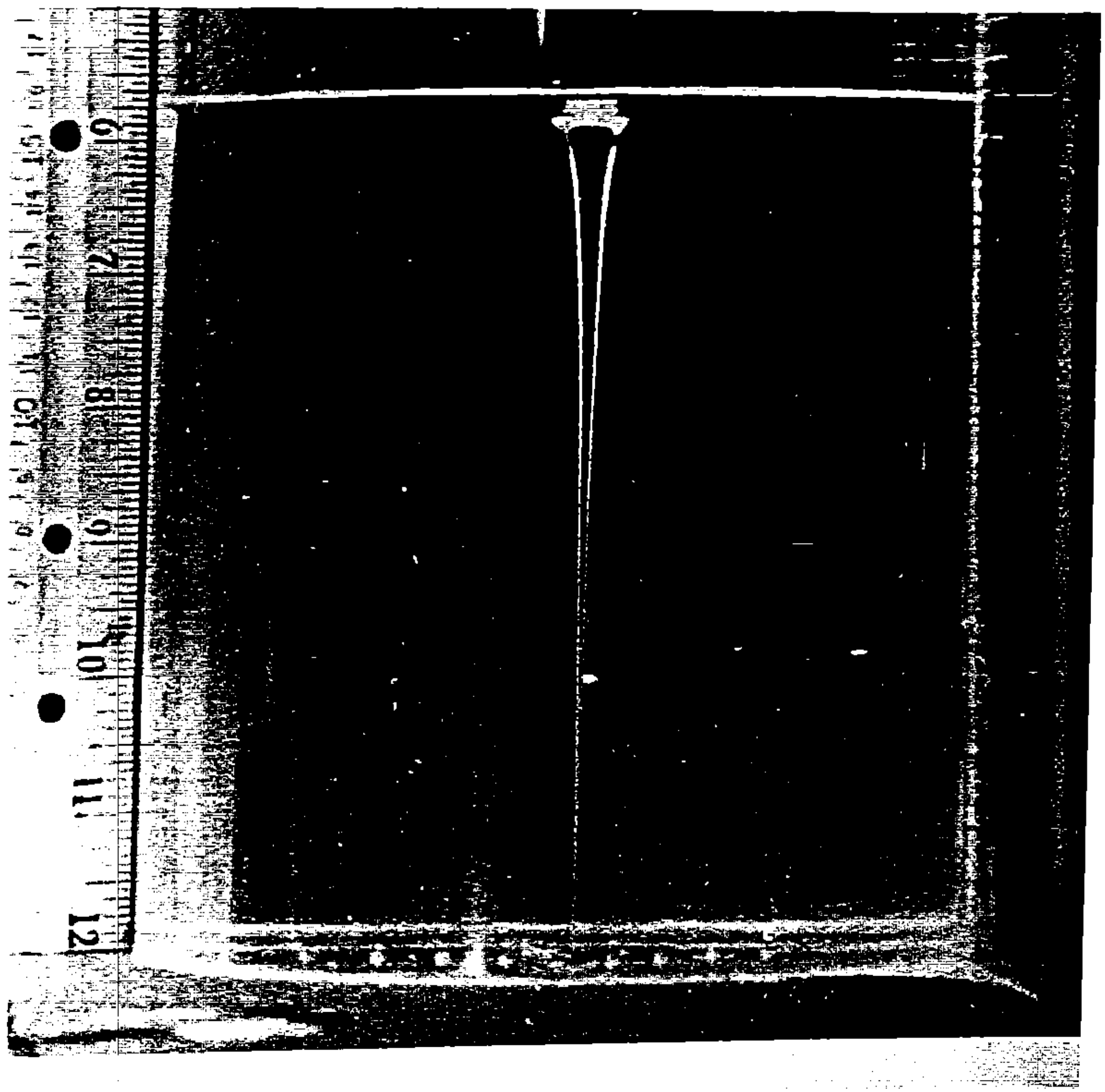

Fig. 4.17 (b)

Glycerin-Water A

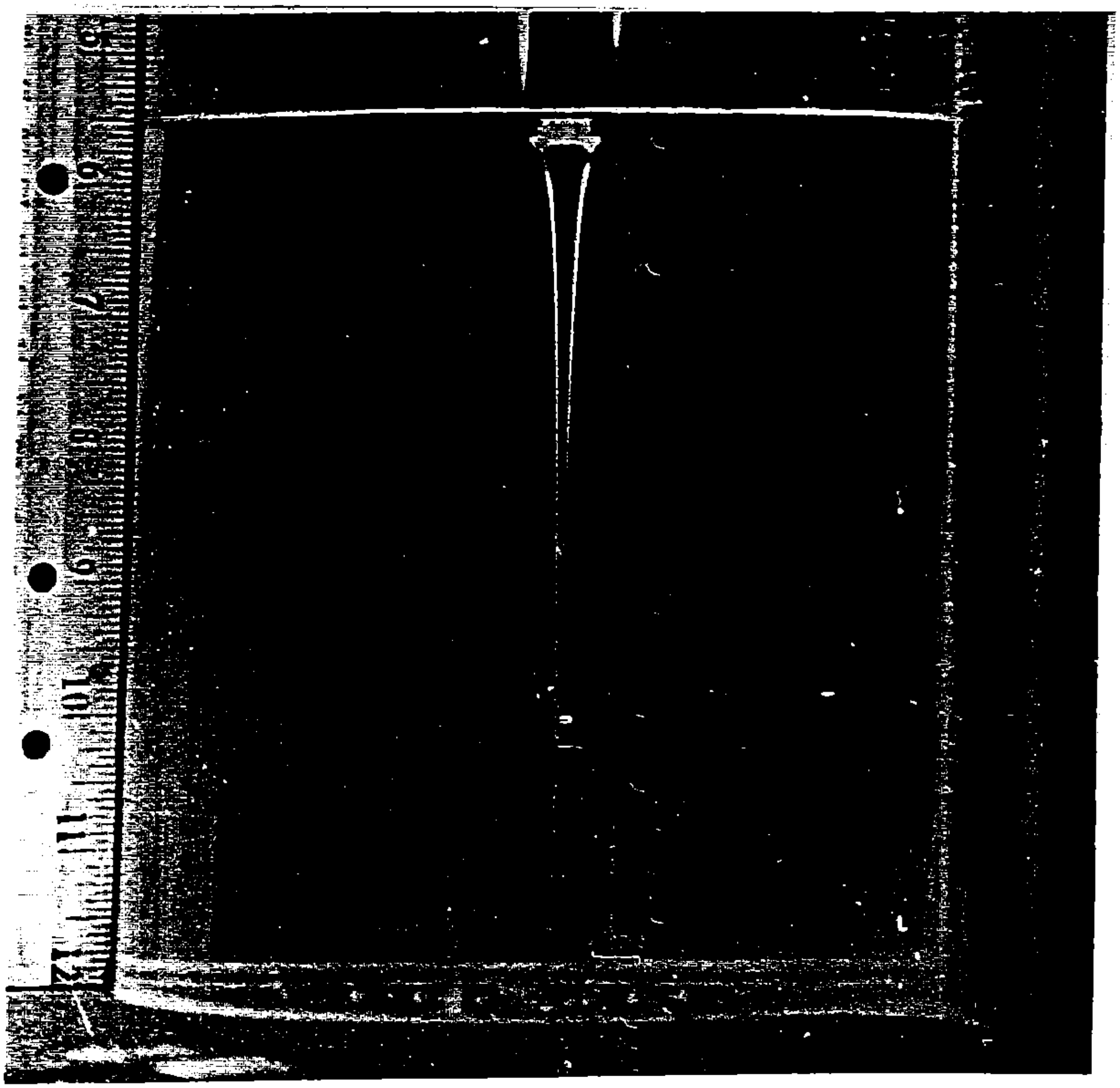

Fig. 4.17 (c)

Glycerin-Water B

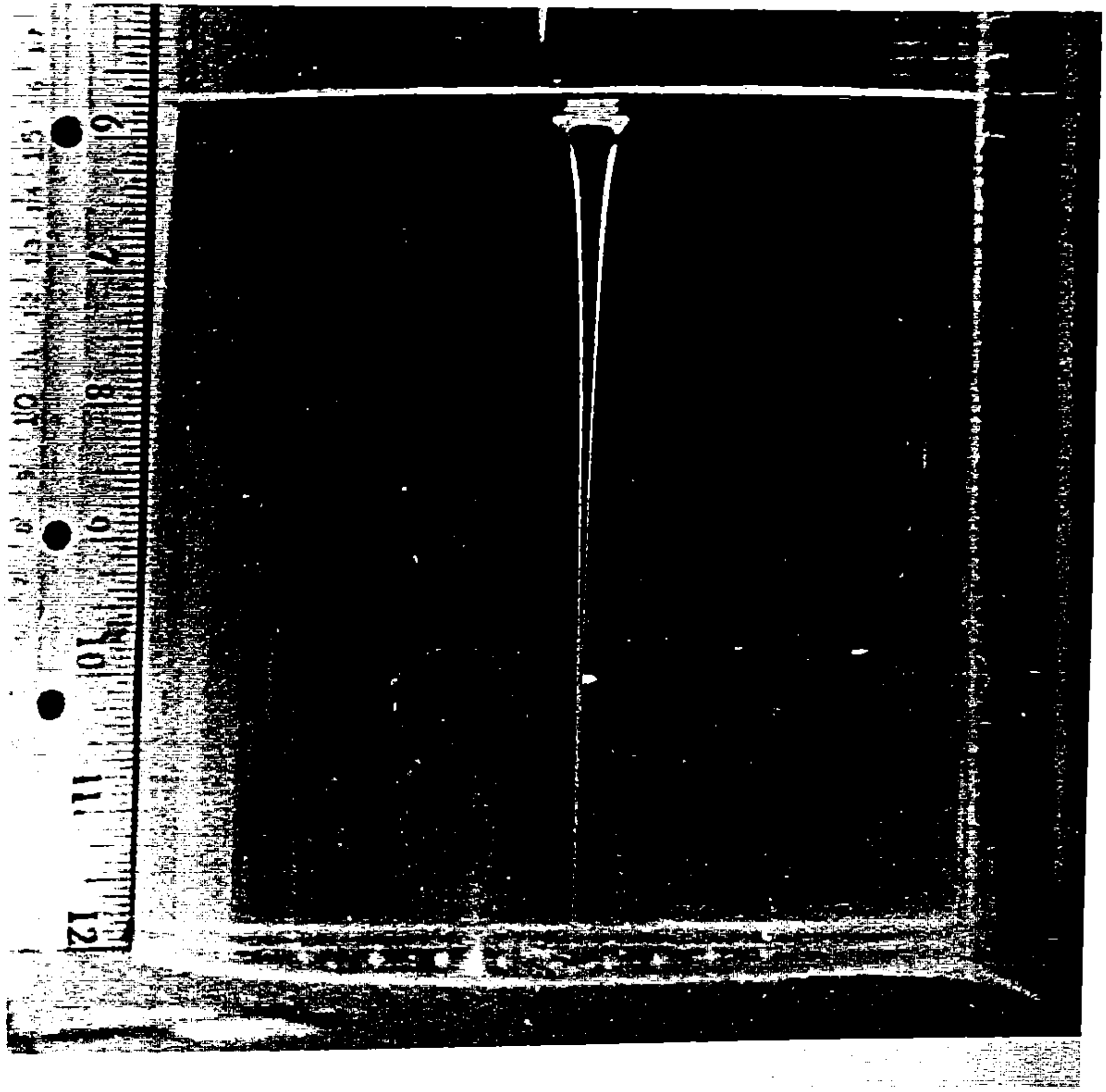

V. THE MODIFIED NEARLY HOOKEAN DUMBBELL MODEL

5.1 Introduction

In order to investigate the polymer effect on the flow, an approximate constitutive equation for a dilute polymer solution is needed to see how the stress tensor changes due to the existence of the macromolecules. In this chapter, a new constitutive equation of a dilute solution of flexible macromolecules is developed from the kinetic theory. The main difficulty associated with the kinetic theory of dilute polymeric fluids so far is that it can provide complete information about the stress tensor only for small rates of strain and a few material functions for high strain rates. The reason for the difficulty stems from being unsuccessful in solving the differential equation for the distribution function (called the diffusion equation). Although Giesekus showed that full information about the stress tensor can be obtained for the Hookean dumbbells model without solving the diffusion equation, this model has two serious shortcomings which are shear rate independent viscometric functions and an unbounded elongational viscosity even for moderately high elongational rate.

The constitutive equations studied here not only eliminate the shortcomings associated with the Hookean dumbbell model but also are simple enough to be manipulated for any kind of homegenous flow at all strain rates. And it shows that shear thinning (viscosity decreases with increasing shear rate), non-zero primary normal stress difference coefficient and and a bounded elongational viscosity for high elongational rate.

The new constitutive equation called the Modified Nearly Hookean Dumbbell model (MNHD) is derived in the next section. The model is constructed by matching it with the Nearly Hookean Dumbbell (Armstrong, 1979) (good for a flow where the macromolecule is neither very stretched nor oriented)and with the model which Tanner (1975) developed for a flow where the macromolecule is strongly oriented and stretched. The result of tests for the Modified Nearly Hookean Dumbbell model is then shown by using two simple flow patterns, shear flow and elongational flow. From these tests, the MNHD seems to be a suitable constitutive equation for the vortex inhibition study especially because it predicts an elongational viscosity well when compared with FENE (Warner, 1972) model's results. A good prediction for the elongational viscosity is very important to this study because vortex inhibition is believed due to a drastic increase of the elongational viscosity at a moderate elongational rate.

5.2 Kinetic Theory and the Modified Nearly Hookean Dumbbell Model

A dilute solution of the flexible macromolecules is modeled according to the kinetic theory. The detailed description of the kinetic theory and the dumbbell model is given by Bird, Hassager, Armstrong and Curtiss (1977). Each macromolecule in the dilute polymer solution is idealized as an elastic dumbbell consisting of two spherical beads joined by a non-bendable spring. There are n dumbbells per unit volume, suspended in a Newtonian solvent with viscosity η_s. It is assumed that n is so small that no interaction among the macromolecules occurs. The beads experience a hydrodynamic drag given by Stoke's law with friction coefficient ζ. The configurational distributional function ψ $(\underline{R},t)$ is defined as a probability density of finding a dumbbell with an end-to-end vector $\underline{R}$. A partial differential equation (diffusion equation) from which the distribution function is determined is then derived from the equation of motions for the beads and the continuity of the distribution function. The polymer contribution to stress tensor $\underline{\underline{\tau}}_p$ is then expressed in terms of expectation values using the distribution function.

For an arbitrary, time-dependent, homogeneous flow with velocity gradient $\nabla\underline{v}^{+} = \underline{\underline{\kappa}}(t)$, the kinetic theory provides the following equations.

$$<\underset{\sim}{R}\ \underset{\sim}{R}>_{(1)} \equiv \frac{D}{Dt} <\underset{\sim}{R}\ \underset{\sim}{R}> - \{\underset{\approx}{\kappa} \cdot <\underset{\sim}{R}\ \underset{\sim}{R}>\} - \{<\underset{\sim}{R}\ \underset{\sim}{R}> \cdot \underset{\approx}{\kappa}^{+}\}$$

$$= \frac{4kT}{\zeta} \underset{\approx}{\delta} - \frac{4}{\zeta} <\underset{\sim}{R}\ \underset{\sim}{F}^{(c)}> \qquad 5.1$$

$$\underset{\approx}{\tau} = -\eta_s \dot{\underset{\approx}{\gamma}} + \underset{\approx}{\tau}_p \qquad 5.2$$

$$\underset{\approx}{\tau}_p = -n <\underset{\sim}{R}\ \underset{\sim}{F}^{(c)}> = nkT\underset{\approx}{\delta} \qquad 5.3$$

or

$$\underset{\approx}{\tau}_p = \frac{n\zeta}{4} <\underset{\sim}{R}\underset{\sim}{R}>_{(1)} \qquad 5.4$$

In these equations, $_{(1)}$ is contravariant codeformational differentiation, $\underset{\approx}{\delta}$ is the unit tensor, $\underset{\sim}{F}^{(c)}$ is a force vector produced by the spring connector, < > is an expectation value with respect to the distribution function, $\dot{\underset{\approx}{\gamma}} = \nabla\underset{\sim}{v} + \nabla\underset{\sim}{v}^{+}$ is the rate of strain tensor, $\underset{\approx}{\tau}$ is stress tensor of a given polymer solution, k is Boltzmann constant and T is temperature.

In order to manipulate these equations, information about spring force vector is necessary. The "finitely extendable nonlinear elastic" (or FENE) connector force law studied by Warner (1972) is

$$\underset{\sim}{F}^{(c)} = \frac{H_o}{1-(\frac{R}{R_o})^2} \underset{\sim}{R} \qquad R < R_o \qquad 5.5$$

where R_o is the maximum length of the dumbbell. A spring with the force law in eq. 5.5 will be linear for small extensions, but will get stiffer and stiffer as the spring is more extended and finally it will become infinitely stiff at R_o.

Tanner (1975) considers that when a polymer solution is under a strong flow where macromolecules are almost fully stretched due to high strain rate, all of the macromolecules may orient in only one direction and may have a unique end-to-end vector $\underline{\tilde{R}}$. A mathematical interpretation of his idea is that the distribution function may be expressed as Dirac's delta function, namely

$$\psi\ (\underline{R},t) \propto \delta(\underline{R} - \underline{\tilde{R}}) \qquad 5.6$$

From the normalization condition of the distribution function (an integration of it over the configurational space must be unity)

$$\psi\ (\underline{R},t) = \delta(\underline{R} - \underline{\tilde{R}}) \qquad 5.7$$

By using eq. 5.7, eq. 5.1 is rewritten with FENE force law.

$$\underline{\tilde{R}}\ \underline{\tilde{R}}_{(1)} = \frac{4kT}{\zeta}\underline{\underline{\delta}} - \frac{4}{\zeta}\ \underline{\tilde{R}}\ \underline{\tilde{R}}\ \frac{H_o}{1 - (\frac{\tilde{R}}{R_o})^2} \qquad 5.8$$

Introducing a dimensionless structure tensor $\underline{\underline{\alpha}} = nH_o <\underline{R}\ \underline{R}>$, eq. 5.8 is rewritten

$$\lambda_H \underline{\underline{\alpha}}_{(1)} = nkT\underline{\underline{\delta}} - \frac{1}{1 - \epsilon\frac{tr\underline{\underline{\alpha}}}{nkT}}\ \underline{\underline{\alpha}} \qquad 5.9$$

$$\underline{\underline{\tau}}_p = \lambda_H \underline{\underline{\alpha}}_{(1)} \qquad 5.4$$

where the time constant λ_H and the dimensionless small constant ε are defined as $\lambda_H = \frac{\zeta}{4H}$ and $\varepsilon = \frac{kT}{H_o R_o^2}$ respectively.

The use of $\underline{\underline{\alpha}} = nH_o \tilde{\underline{R}}\, \tilde{\underline{R}}$ and $\mathrm{tr}\underline{\underline{\alpha}} = \frac{\tilde{R}^2}{nH}$ are also made in obtaining eq. 5.9. Eq. 5.9 along with eq. 5.4 may be a suitable constitutive equation for a dilute polymer solution in which the macromolecules are under a strong flow so that they have a unique end-to-end vector $\tilde{\underline{R}}$.

When macromolecules are under a weak flow where the strain rate is not large enough to stretch them, eq. 5.9 is no longer appropriate because the distribution function can not be described by eq. 5.7. Armstrong, Ishikawa, and Essandoh (1979) studied the Nearly Hookean Dumbbell model for a weak flow regime. The spring force law of this model is

$$\underline{F}^{(c)} = H_o \left(1 + \varepsilon \frac{HR^2}{kT}\right) \underline{R} \qquad 5.10$$

In such a weak flow, the parameter ε should be very small and indicates the deviation of the spring tension from linear behavior which is described by the Hookean Dumbbell model. We assume that the distribution function is expanded in power of ε,

$$\psi = \psi_o + \varepsilon\, \psi_1 + \varepsilon^2 \psi_2 + \cdots \qquad 5.11$$

In eq. 5.11, Ψ_o gives the distribution function of the Hookean Dumbbell model and Ψ_1 represents a deviation caused by eq. 5.10 from the linear behavior. In the same way, the structure tensor and stress tensor are also expanded as

$$nH_o \langle \underline{R}\ \underline{R} \rangle = \underline{\underline{\alpha}}_o + \varepsilon\ \underline{\underline{\alpha}}_1 + \varepsilon^2\ \underline{\underline{\alpha}}_2 + \cdot\ \cdot\ \cdot \tag{5.12}$$

$$(nH_o)^2 \langle R^2 \underline{R}\ \underline{R} \rangle = \underline{\underline{\beta}}_o + \varepsilon \underline{\underline{\beta}}_1 + \varepsilon^2 \underline{\underline{\beta}}_2 + \cdot\ \cdot\ \cdot \tag{5.13}$$

$$\underline{\underline{\tau}}_p = \underline{\underline{\tau}}_o + \varepsilon\ \underline{\underline{\tau}}_1 + \varepsilon^2 \underline{\underline{\tau}}_2 + \cdot\ \cdot\ \cdot \tag{5.14}$$

where $\underline{\underline{\beta}} = (nH_o)^2 \langle R^2\ \underline{R}\ \underline{R} \rangle$ is an additional structure tensor. The use of a regular perturbation method gives the stress tensor in terms of $\underline{\underline{\alpha}}$ and $\underline{\underline{\beta}}$, for ε^o order.

$$\lambda_H \underline{\underline{\alpha}}_{o(1)} = nkT\underline{\underline{\delta}} - \underline{\underline{\alpha}}_o \tag{5.15}$$

$$\underline{\underline{\tau}}_o = \lambda_H\ \underline{\underline{\alpha}}_{o(1)} \tag{5.16}$$

for ε^1 order,

$$\lambda_H \underline{\underline{\alpha}}_{1(1)} = -\underline{\underline{\alpha}}_1 - \frac{\underline{\underline{\beta}}_o}{nkT} \quad 5.17 \qquad \underline{\underline{\tau}}_1 = \lambda_H\ \underline{\underline{\alpha}}_{1(1)} \tag{5.18}$$

where $\underline{\underline{\beta}}_o = (\mathrm{tr}\underline{\underline{\alpha}}_o)\ \underline{\underline{\alpha}}_o + 2\{\underline{\underline{\alpha}}_o \cdot \underline{\underline{\alpha}}_o\}$. Eq. 5.16 is easily solved for a given flow field and the result is equivalent to that from the Hookean Dumbbell model. The Nearly Hookean Dumbbell model is obtained by combining eq. 5.15 with eq. 5.17 and the result is

$$\lambda_H \underline{\underline{\alpha}}_{(1)} = nkT\underline{\underline{\delta}} - \underline{\underline{\alpha}} - \frac{\varepsilon}{nkT} \underline{\underline{\beta}}_o$$

$$= nkT\underline{\underline{\delta}} - \underline{\underline{\alpha}} - \frac{\varepsilon}{nkT} [(tr\underline{\underline{\alpha}}_o)\underline{\underline{\alpha}}_o + 2(\underline{\underline{\alpha}}_o \cdot \underline{\underline{\alpha}}_o)]$$

$$= nkT\underline{\underline{\delta}} - \underline{\underline{\alpha}} - \frac{\varepsilon}{nkT} [(tr\underline{\underline{\alpha}})\underline{\underline{\alpha}} + 2(\underline{\underline{\alpha}} \cdot \underline{\underline{\alpha}})] + 0(\varepsilon^2)$$

5.19

$$\underline{\underline{\tau}}_p = \lambda_H \underline{\underline{\alpha}}_{(1)} \qquad 5.4$$

To compare the result of the Nearly Hookean Dumbbell model with Tanner's result, eq. 5.9 is expanded for small

$$\varepsilon \frac{tr\underline{\underline{\alpha}}}{nkT},$$

$$\lambda_H \underline{\underline{\alpha}}_{(1)} = nkT\underline{\underline{\delta}} - \underline{\underline{\alpha}} - \frac{\varepsilon}{nkT} tr\underline{\underline{\alpha}} \cdot \underline{\underline{\alpha}} + 0(tr\underline{\underline{\alpha}}^2) \qquad 5.20$$

The only difference is that eq. 5.19 contains an additional term $-\frac{2\varepsilon}{nkT}(\underline{\underline{\alpha}} \cdot \underline{\underline{\alpha}})$. Since eq. 5.20 is good for only a weak flow regime, the macromolecule is not extended substantially. And this indicates the following important condition

$$<\varepsilon \frac{H_o\ R^2}{kT}> = \frac{\varepsilon}{nkT} tr\underline{\underline{\alpha}} <<1 \qquad 5.21$$

In other words, the expectation value of the non-linear contribution to the spring force law in eq. 5.10 must be small.

One possible method for combining eq. 5.19 with eq. 5.9 is as follows:

$$\lambda_H \underline{\underline{\alpha}}_{(1)} = nkT\underline{\underline{\delta}} - \frac{\underline{\underline{\alpha}}}{1 - \frac{\varepsilon}{nkT} \operatorname{tr}\underline{\underline{\alpha}}} - \left(1 - \frac{\varepsilon}{nkT} \operatorname{tr}\underline{\underline{\alpha}}\right) \frac{2\varepsilon}{nkT} (\underline{\underline{\alpha}} \cdot \underline{\underline{\alpha}}) \tag{5.22}$$

Equation 5.22 is known as the Modified Nearly Hookean Dumbbell model. For a strong flow regime where all of the macromolecules are lined-up in the same direction and stretched extensively, the term $\frac{\varepsilon}{nkT} \operatorname{tr}\underline{\underline{\alpha}}$ is nearly unity. Eq. 5.22 thus becomes eq. 5.9 which is the Tanner's model. For a weak flow regime where eq. 5.21 is valid, eq. 5.22 is reduced to the Nearly Hookean Dumbbell model by expanding eq. 5.22 for small $\varepsilon \frac{1}{nkT} \operatorname{tr}\underline{\underline{\alpha}}$. A summary of these three models are shown in Table 5.1

TABLE 6.1

A SUMMARY OF THE THREE CONSTITUTIVE EQUATIONS.

Constitutive Equation	The form of Equation	Applicable flow regime
Modified Nearly Hookean Dumbbell Model (M1) Eq. 5.22	$\lambda_H \underline{\underline{\alpha}}_{(1)} = nkT\underline{\underline{\delta}} - \dfrac{\underline{\underline{\alpha}}}{1 - \dfrac{\varepsilon}{nkT}\,\mathrm{tr}\underline{\underline{\alpha}}} - \left(1 - \dfrac{\varepsilon}{nkT}\,\mathrm{tr}\underline{\underline{\alpha}}\right)\dfrac{2\varepsilon}{nkT}\,(\underline{\underline{\alpha}} \cdot \underline{\underline{\alpha}})$	any kind of flow
Tanner's Model (M2) Eq. 5.9	$\lambda_H \underline{\underline{\alpha}}_{(1)} = nkT\underline{\underline{\delta}} - \dfrac{\underline{\underline{\alpha}}}{1 - \dfrac{\varepsilon}{nkT}\,\mathrm{tr}\underline{\underline{\alpha}}}$	a strong flow $\dfrac{\varepsilon}{nkT}\,\mathrm{tr}\underline{\underline{\alpha}} \approx 1$
Nearly Hookean Dumbbell Model (M3) Eq. 5.19	$\lambda_H \underline{\underline{\alpha}}_{(1)} = nkT\underline{\underline{\delta}} - \left(1 + \dfrac{\varepsilon}{nkT}\,\mathrm{tr}\underline{\underline{\alpha}}\right)\underline{\underline{\alpha}} - \dfrac{2\varepsilon}{nkT}\,(\underline{\underline{\alpha}} \cdot \underline{\underline{\alpha}})$	a weak flow $\dfrac{\varepsilon}{nkT}\,\mathrm{tr}\underline{\underline{\alpha}} \ll 1$
The stress tensor expression	$\underline{\underline{\tau}}_p = \lambda_H \underline{\underline{\alpha}}_{(1)}$	

5.3 The predictions of the models

In order to gain physical insight about the three models discussed in the last section, two kinds of simple flow are applied to them to see the behavior of material functions calculated from the models. The stress growth and relaxation for shear flow are numerically calculated for shear stress and the primary normal stress difference. The shear rate dependence of the material functions for a steady shear flow are also calculated. The models are tested for elongational flow to analyze elongational behavior as a function of time and elongational rate.

5.3.1 Shear flow

First shear flow is considered to study viscosity and the primary normal stress difference. The shear flow is given by $v_x = \dot{\gamma}(t)y$, $v_y = v_z = 0$, where $\dot{\gamma}(t)$ is a time dependent rate of strain (shear rate). Stress Growth(denoted by + sign for material function).

For the stress growth behavior, the shear rate is described by

$$\left.\begin{array}{ll} \dot{\gamma}(t) = 0 & \text{for } t \leq 0 \\ \dot{\gamma}(t) = \dot{\gamma}(\text{constant}) & \text{for } t > 0 \end{array}\right\} \qquad 5.22$$

The normalized intrinsic viscosity $[\eta^+]/[\eta]$ and the normalized primary normal stress coefficient $\Psi_1{}^+/\Psi_1$ are calculated by the 4-th order Runge-Cutta method. $[\eta]$ and

Ψ_1 are values at steady state.

Intrinsic viscosity $[\eta]$ is defined by

$$[\eta] = \lim_{c \to o} \frac{\eta - \eta_s}{c\eta} \qquad 5.23$$

where non-Newtonian viscosity η is defined as $\tau_{yx} = -\eta(\dot{\gamma})\dot{\gamma}$ and c is the concentration of polymer solution. One can also define the primary normal stress coefficient Ψ_1 as $\tau_{xx} - \tau_{yy} = -\Psi_1(\dot{\gamma})\dot{\gamma}^2$. Note that these material functions depend on the shear rate. Some results are shown in Fig. 5.1 to Fig. 5.12

General trends for the stress growth are

1. Stress overshoot is found only for high shear rate (S = 10. in figures).
2. The peak value of the overshoot is smaller for smaller ε (for example, Fig. 5.1 and Fig. 5.2).
3. It takes longer to reach the peak for smaller ε.
4. The material functions get to their steady state values faster for higher shear rate.
5. There is little difference between S = .1 and S = .01 for both η^+ and Ψ^+.

As to the difference between η^+ and Ψ_1^+:

1. It takes longer to reach steady state for Ψ_1^+.
2. For higher stear rate (S = 10.0) the peak value of the overshoot is larger and the time required for the peak is shorter for η^+.

Fig. 5.1 to Fig. 5.12

STRESS GROWTH BEHAVIOR OF

THE THREE MODELS FOR SHEAR FLOW

The following notation is used.

M1	Modified Nearly Hookean Dumbbell	eq. 5.22
M2	Tanner's model	eq. 5.9
M3	Nearly Hookean Dumbbell	eq. 5.19

E1	$\varepsilon = .02$
E2	$\varepsilon = .005$

VISCOSITY $[\eta^+]/[\eta]$

STRESS DIFFERENCE $\Psi_1{}^+/\Psi_1$

DIMENSIONLESS TIME t/λ_H (t is real time [sec])

S dimensionless shear rate $\lambda_H\dot{\gamma}$

Fig. 5.1

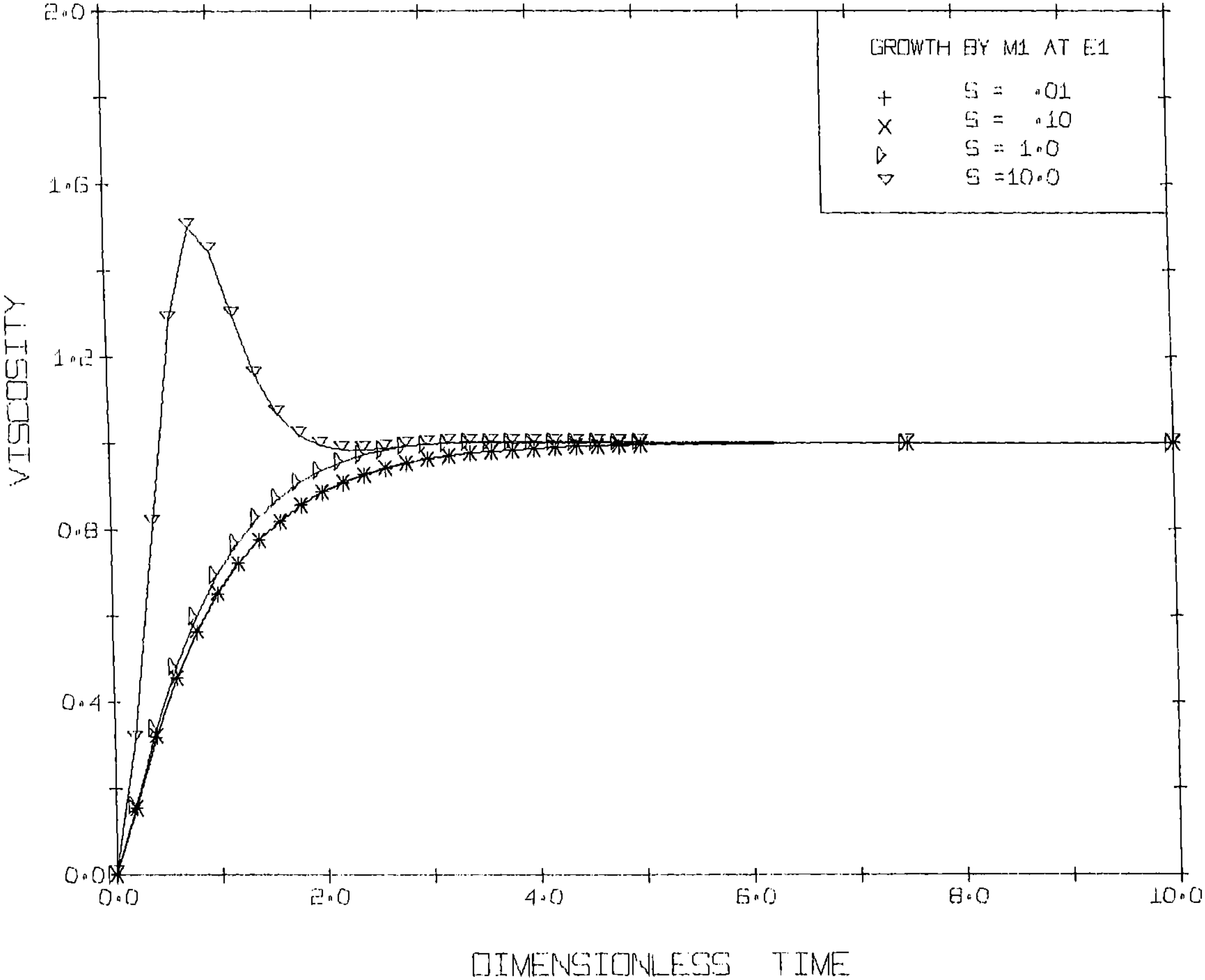
GROWTH BY M1 AT E1
S = ·01
S = ·10
S = 1·0
S =10·0
VISCOSITY
DIMENSIONLESS TIME
0·0
0·4
0·8
1·2
1·6
2·0
0·0
2·0
4·0
6·0
8·0
10·0

Fig. 5.2

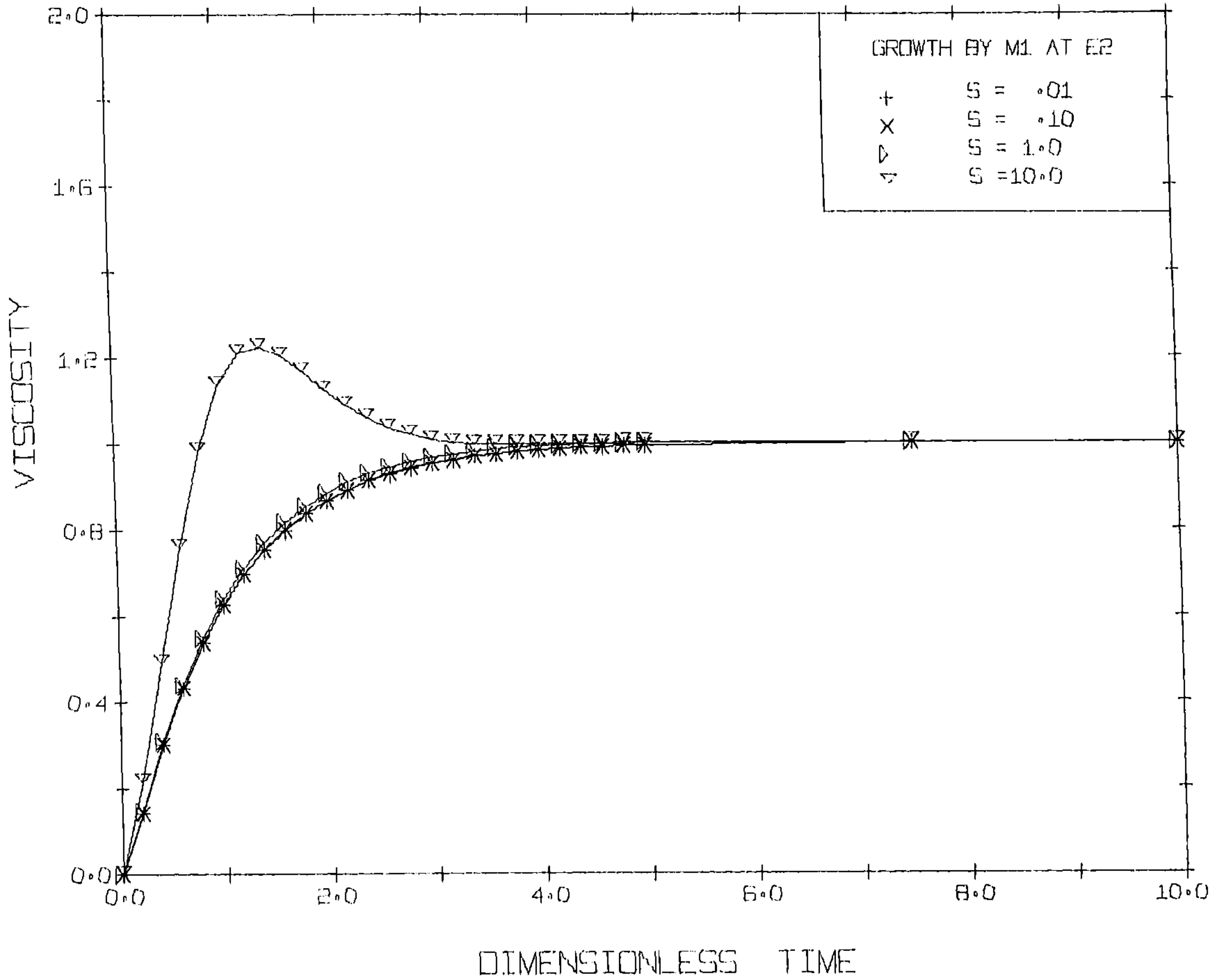
GROWTH BY M1 AT E2
S = ·01
S = ·10
S = 1·0
S =10·0
2·0
1·6
1·2
0·8
0·4
0·0
0·0
2·0
4·0
6·0
8·0
10·0
VISCOSITY
DIMENSIONLESS TIME

Fig. 5.3

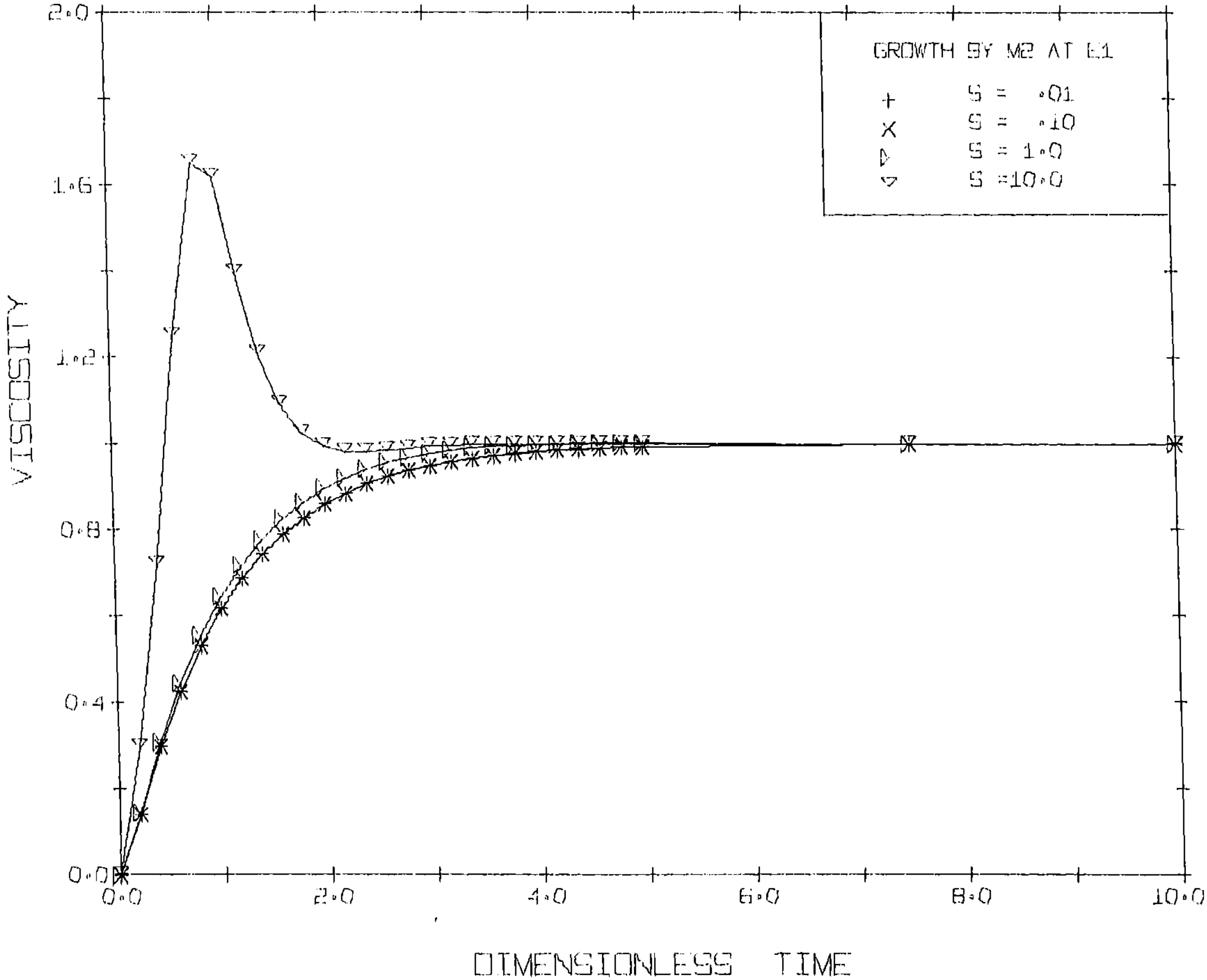

GROWTH BY M2 AT E1
S = ·01
S = ·10
S = 1·0
S =10·0
VISCOSITY
DIMENSIONLESS TIME
0·0
0·4
0·8
1·2
1·6
2·0
2·0
4·0
6·0
8·0
10·0

Fig. 5.4

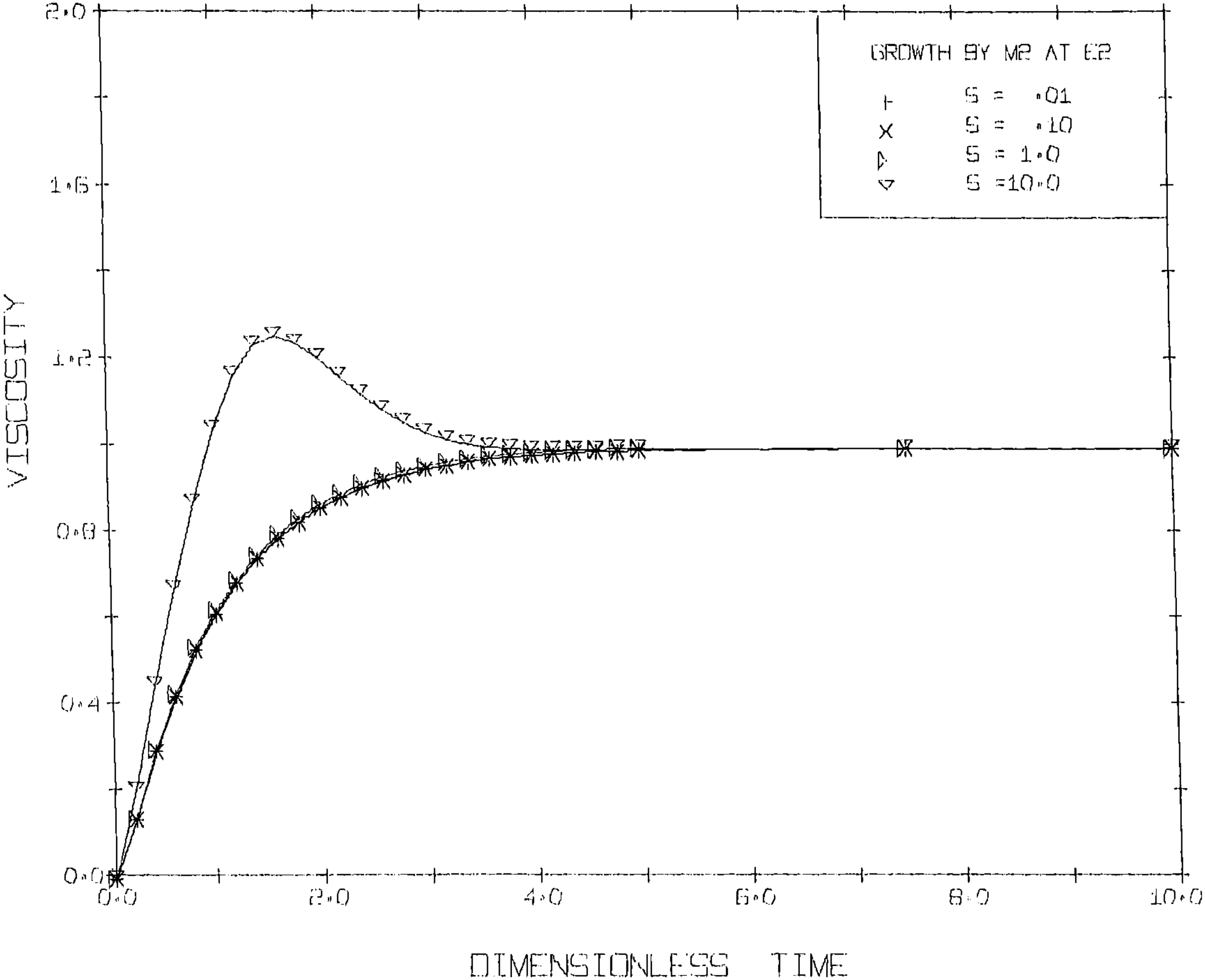

GROWTH BY M2 AT E2
S = ·01
S = ·10
S = 1·0
S =10·0
2·0
1·6
1·2
0·8
0·4
0·0
VISCOSITY
0·0
2·0
4·0
6·0
8·0
10·0
DIMENSIONLESS TIME

Fig. 5.5

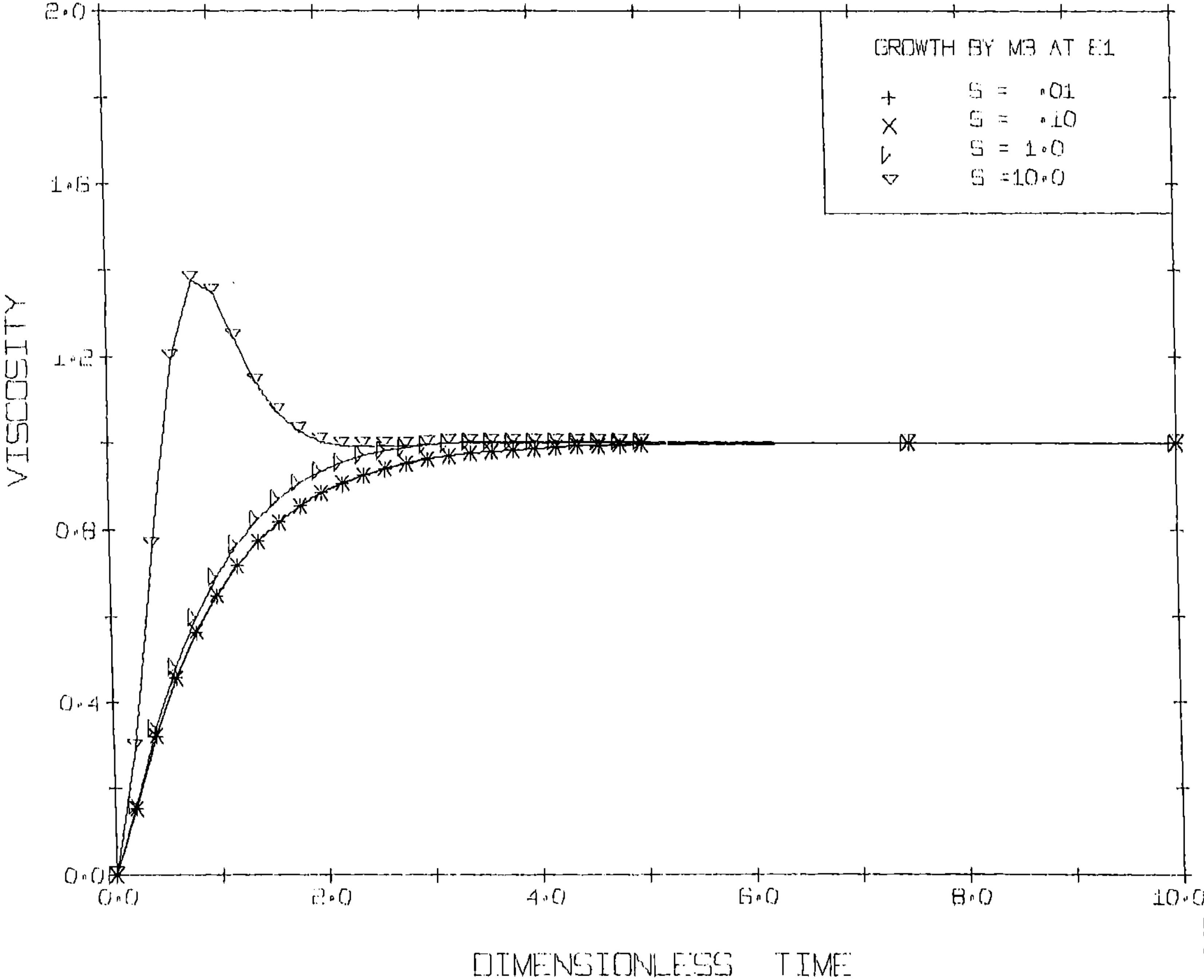

GROWTH BY M3 AT E1
S = ·01
S = ·10
S = 1·0
S =10·0
2·0
1·6
1·2
0·8
0·4
0·0
VISCOSITY
0·0
2·0
4·0
6·0
8·0
10·0
DIMENSIONLESS TIME

198

Fig. 5.6

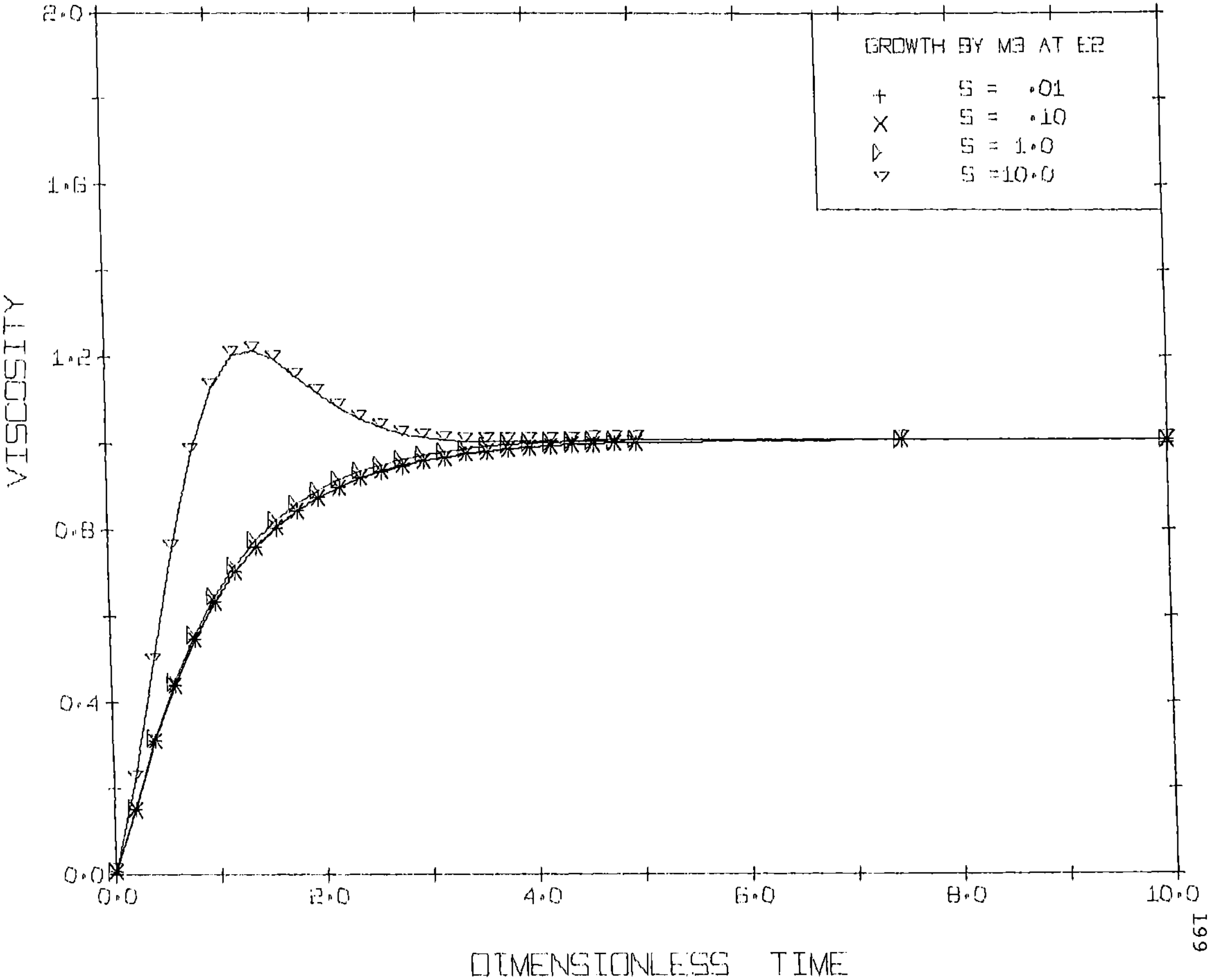

GROWTH BY M3 AT E2
S = .01
S = .10
S = 1.0
S = 10.0
VISCOSITY
DIMENSIONLESS TIME
0.0
0.4
0.8
1.2
1.6
2.0
2.0
4.0
6.0
8.0
10.0

Fig. 5.7

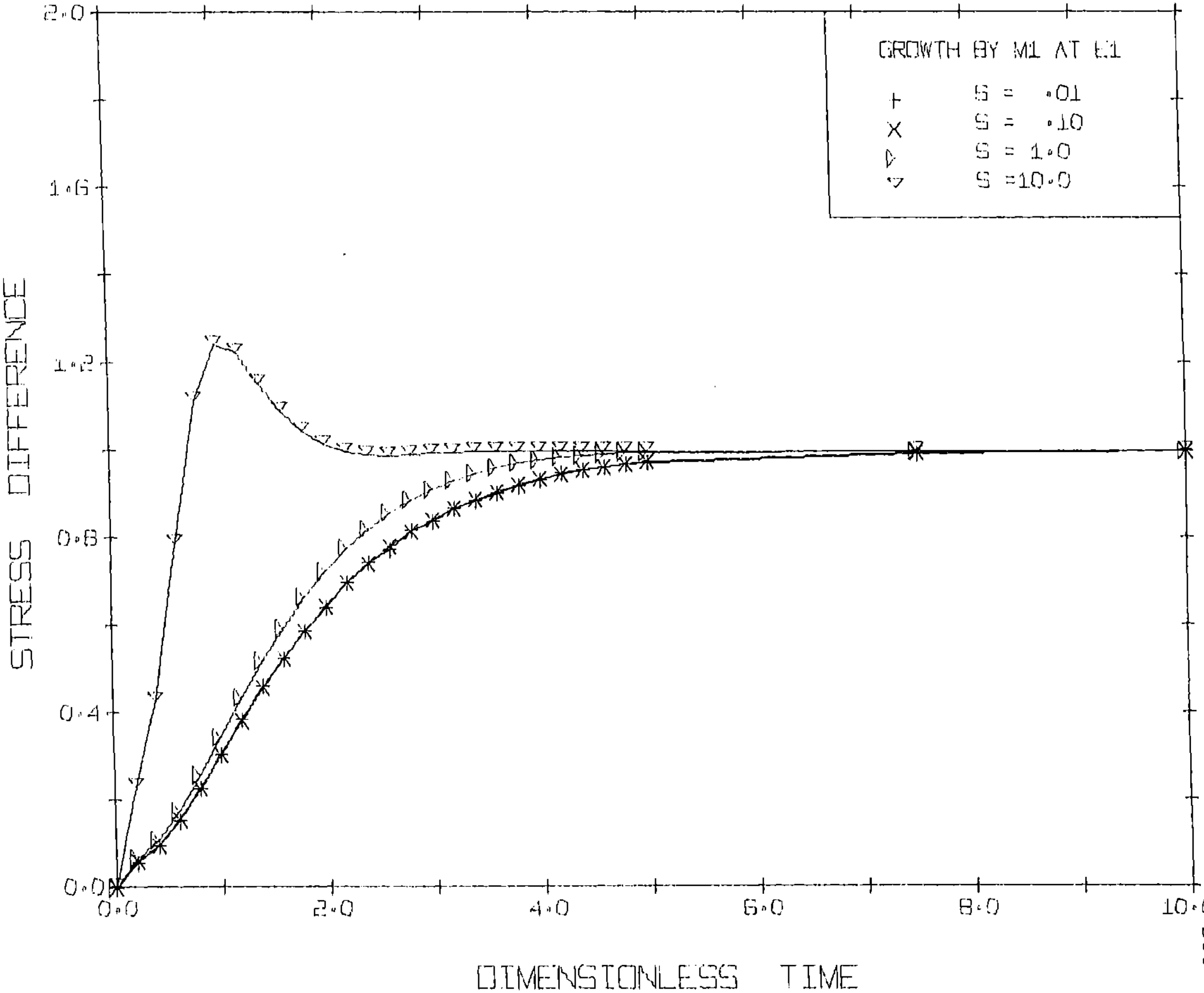
GROWTH BY M1 AT E1
S = ·01
S = ·10
S = 1·0
S =10·0
STRESS DIFFERENCE
DIMENSIONLESS TIME
0·0
0·4
0·8
1·2
1·6
2·0
0·0
2·0
4·0
6·0
8·0
10·0

200

Fig. 5.8

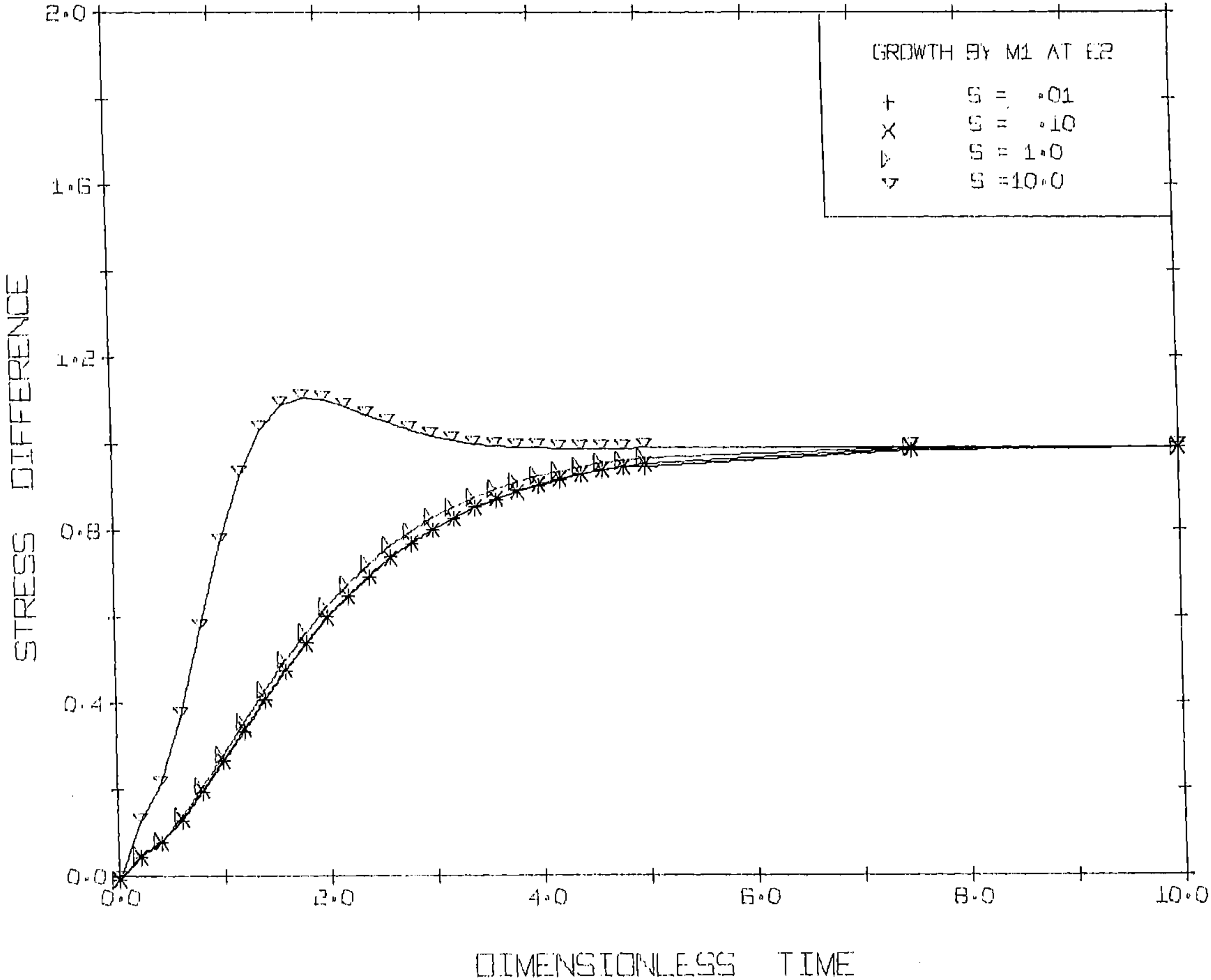

GROWTH BY M1 AT E2
S = ·01
S = ·10
S = 1·0
S =10·0
STRESS DIFFERENCE
DIMENSIONLESS TIME
2·0
1·6
1·2
0·8
0·4
0·0
0·0
2·0
4·0
6·0
8·0
10·0

Fig. 5.9

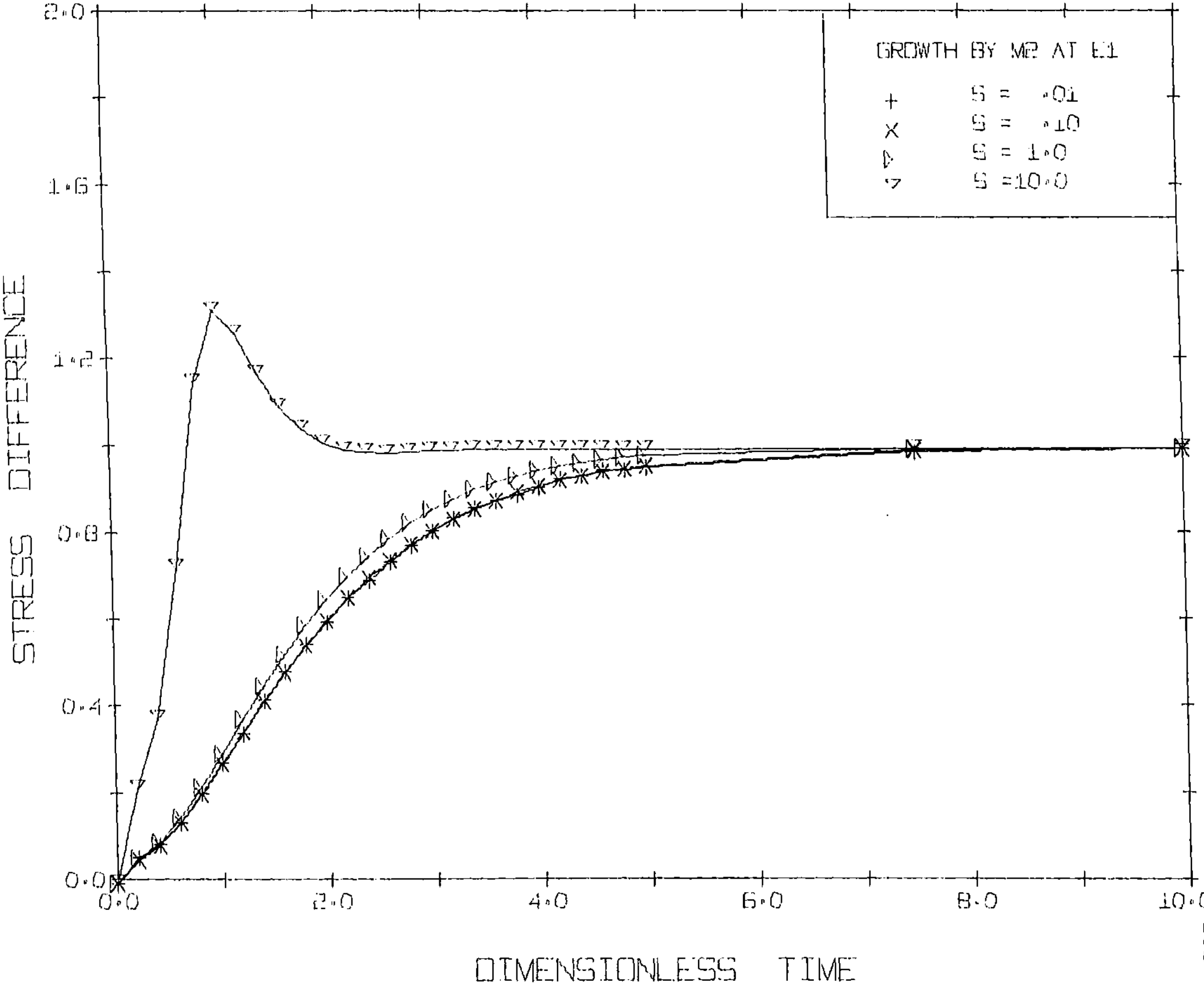
GROWTH BY M2 AT E1
S = .01
S = .10
S = 1.0
S =10.0
STRESS DIFFERENCE
DIMENSIONLESS TIME
2.0
1.6
1.2
0.8
0.4
0.0
0.0
2.0
4.0
6.0
8.0
10.0

Fig. 5.10

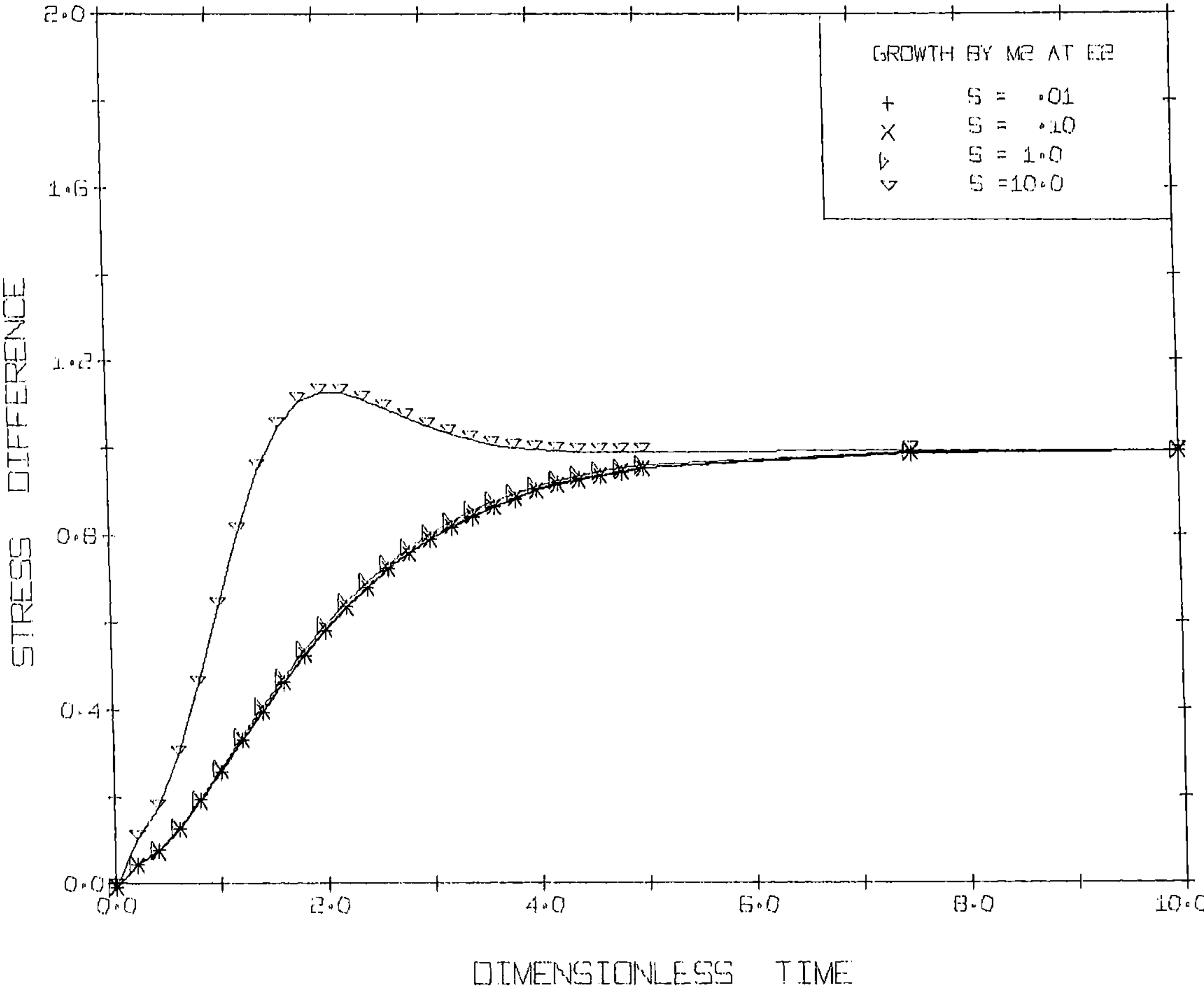
GROWTH BY M2 AT E2
+ S = ·01
X S = ·10
▷ S = 1·0
▽ S =10·0
STRESS DIFFERENCE
0·0
0·4
0·8
1·2
1·6
2·0
0·0
2·0
4·0
6·0
8·0
10·0
DIMENSIONLESS TIME

Fig. 5.11

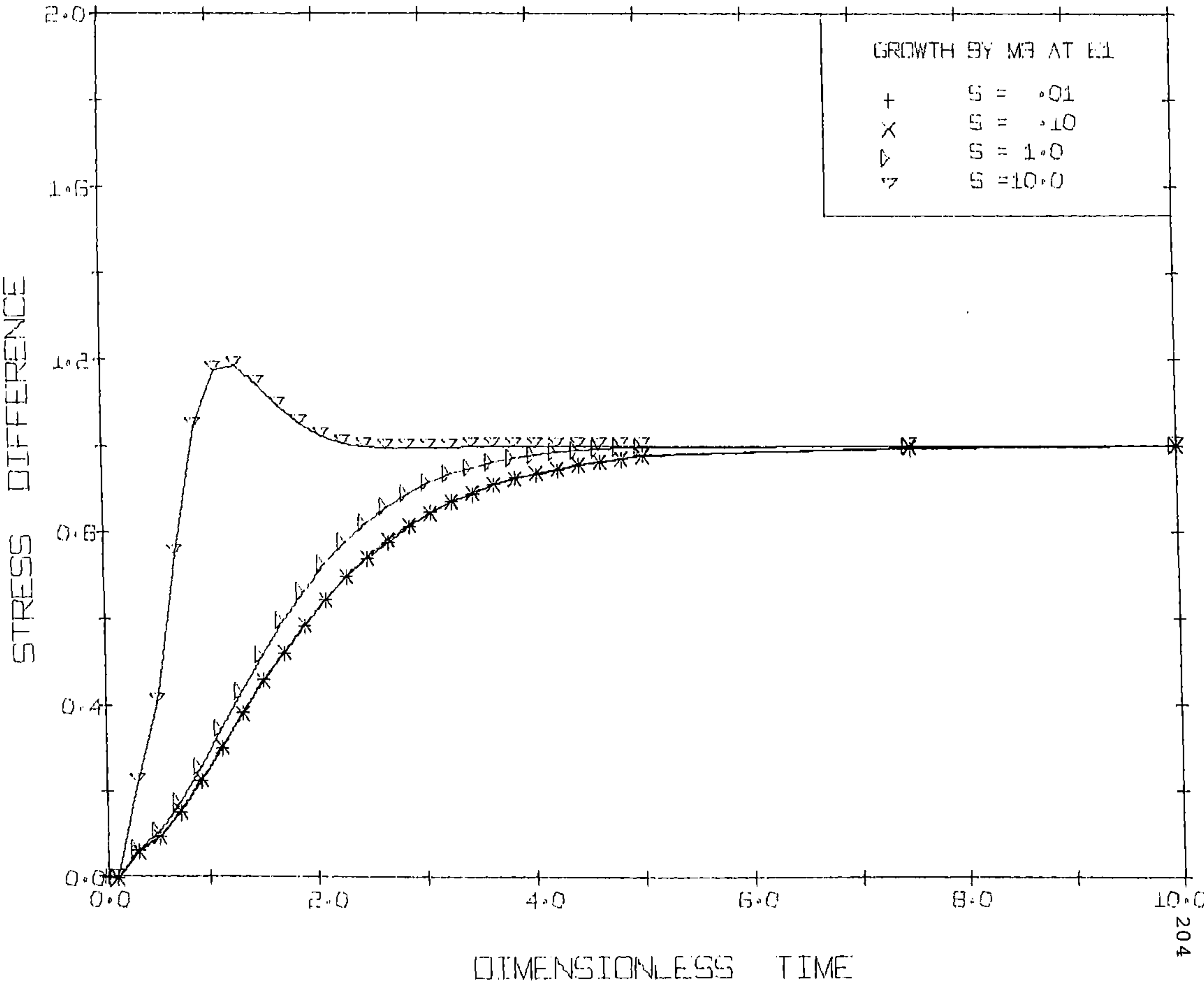
GROWTH BY M3 AT E1
S = ·01
S = ·10
S = 1·0
S =10·0
2·0
1·6
1·2
0·8
0·4
0·0
STRESS DIFFERENCE
0·0
2·0
4·0
6·0
8·0
10·0
DIMENSIONLESS TIME

Fig.5.12

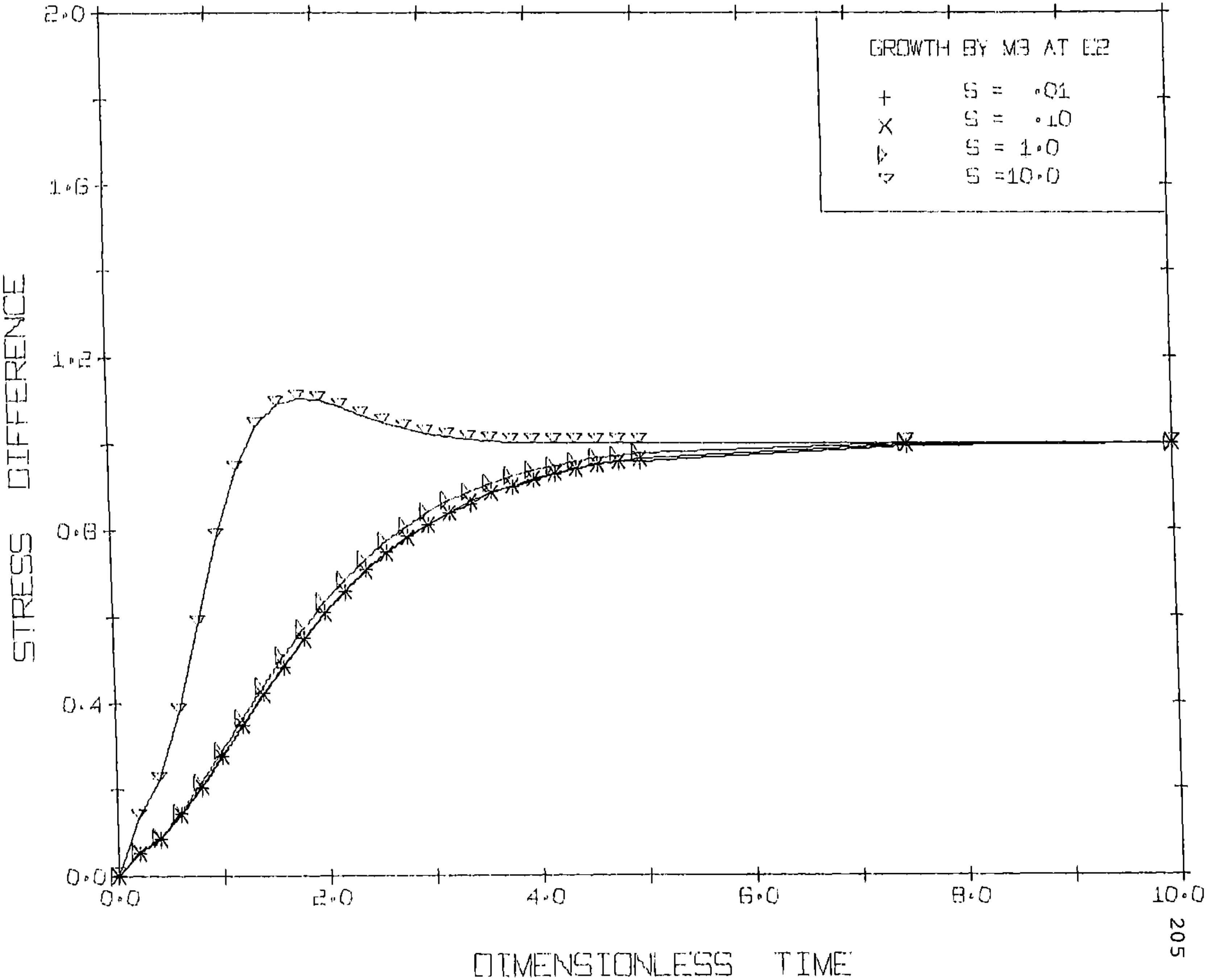
GROWTH BY M3 AT E2
+ S = ·01
X S = ·10
S = 1·0
S =10·0
STRESS DIFFERENCE
DIMENSIONLESS TIME
0·0
0·4
0·8
1·2
1·6
2·0
2·0
4·0
6·0
8·0
10·0

<u>Stress Relaxation</u> (denoted - sign for material functions)

The shear rate for the stress relaxation calculation is described by

$$\left.\begin{array}{lll}\dot{\gamma}(t) = \dot{\gamma} & \text{(constant)} & t \leq 0 \\ \dot{\gamma}(t) = 0 & & t > 0\end{array}\right\} \qquad 5.23$$

The steady state values of the material function (which will be discussed later in this chapter) are used as initial condition. The results of the calculation are plotted in Fig. 5.13 to Fig. 5.24.

The general tendencies of the relaxation behavior are

1. The higher the shear rate, the faster the stresses relax.
2. The larger ε, the faster η^- and Ψ_1^- decay.
3. No difference is found between cases $S = .01$ and $S = .1$.
4. It is also found that the relaxation behaviors of η^- and Ψ_1^- are exactly equal for each of the three models because of the structure of the models.

Fig. 5.13 to Fig. 5.24

STRESS RELAXATION BEHAVIOR OF THE
THREE MODELS FOR SHEAR FLOW

The following notation is used:

M1	Modified Nearly Hookean Dumbbell	eq. 5.22
M2	Tanner's model	eq. 5.9
M3	Nearly Hookean Dumbbell	eq. 5.19

E1 $\varepsilon = .02$

E2 $\varepsilon = .005$

VISCOSITY $[\eta^-]/[\eta]$

STRESS DIFFERENCE Ψ_1^-/Ψ_1

DIMENSIONLESS TIME t/λ_H

S dimensionless shear rate

Fig. 5.13

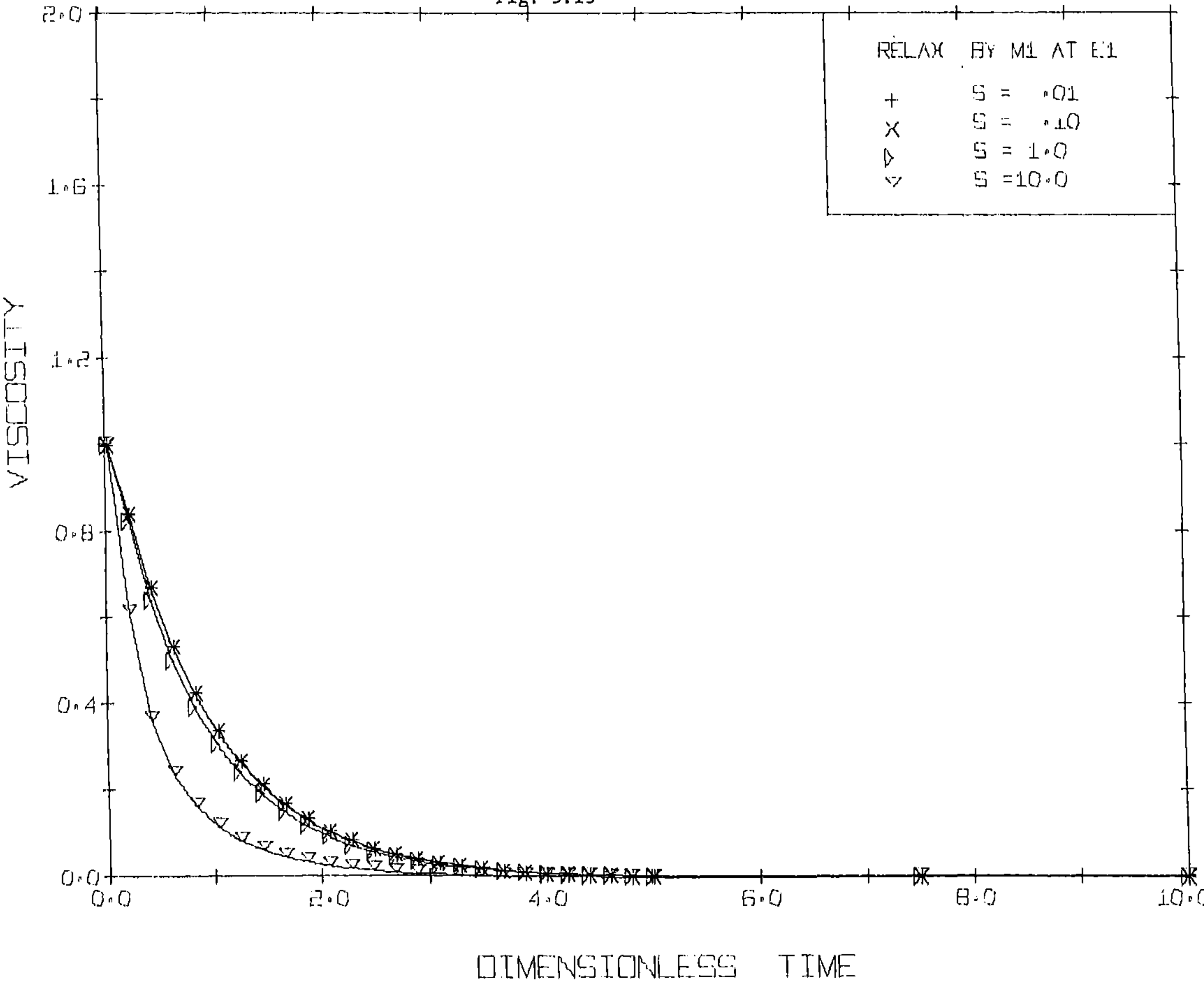
RELAX BY M1 AT E1
+ S = ·01
X S = ·10
▷ S = 1·0
▽ S =10·0
VISCOSITY
DIMENSIONLESS TIME
2·0
1·6
1·2
0·8
0·4
0·0
0·0
2·0
4·0
6·0
8·0
10·0

Fig. 5. 14

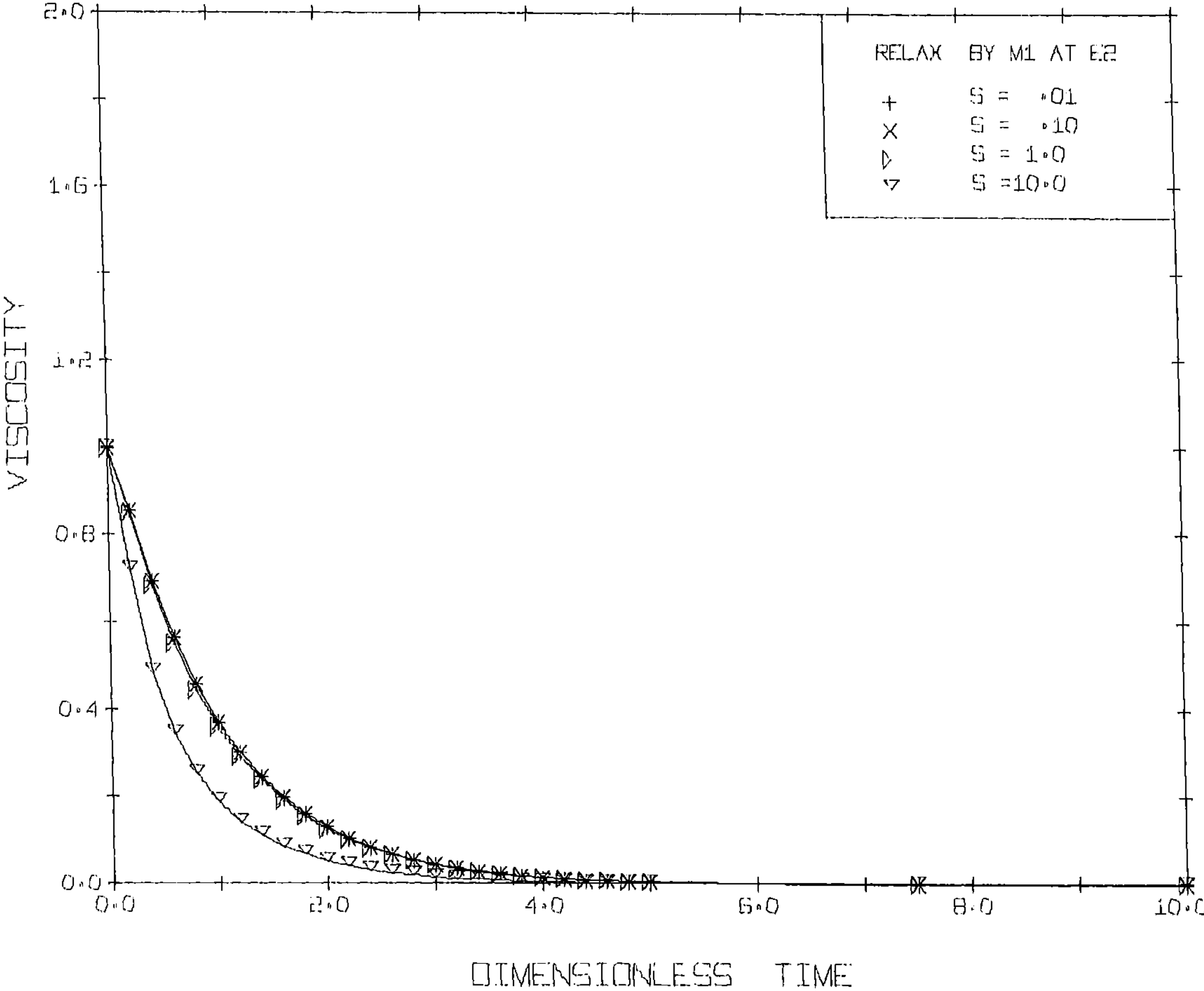

RELAX BY M1 AT E2
+ S = ·01
X S = ·10
▷ S = 1·0
▽ S =10·0
VISCOSITY
DIMENSIONLESS TIME
2·0
1·6
1·2
0·8
0·4
0·0
0·0
2·0
4·0
6·0
8·0
10·0

Fig. 5.15

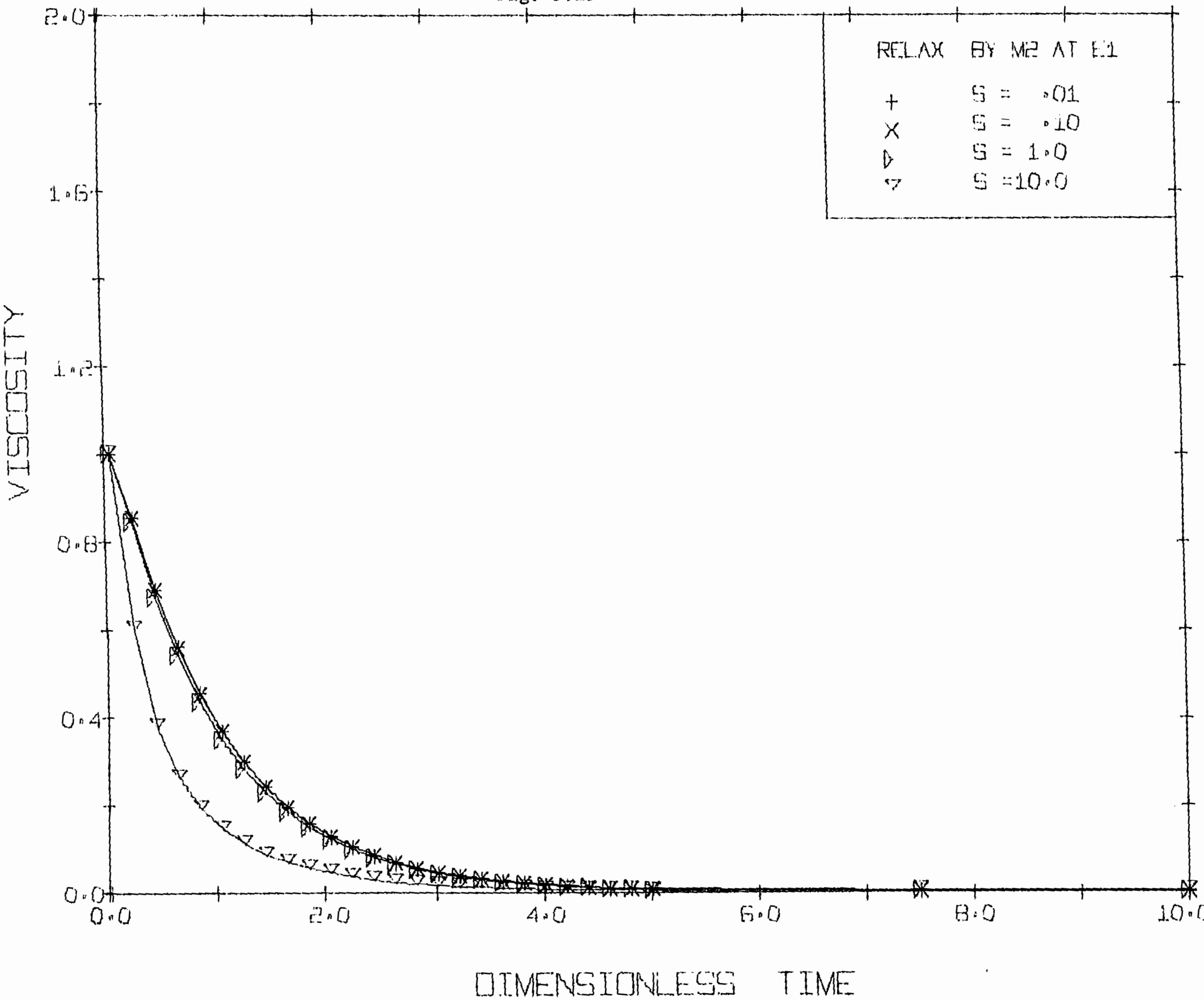
RELAX BY M2 AT E1
S = ·01
S = ·10
S = 1·0
S =10·0
VISCOSITY
DIMENSIONLESS TIME
2·0
1·6
1·2
0·8
0·4
0·0
0·0
2·0
4·0
6·0
8·0
10·0

210

Fig. 5.16

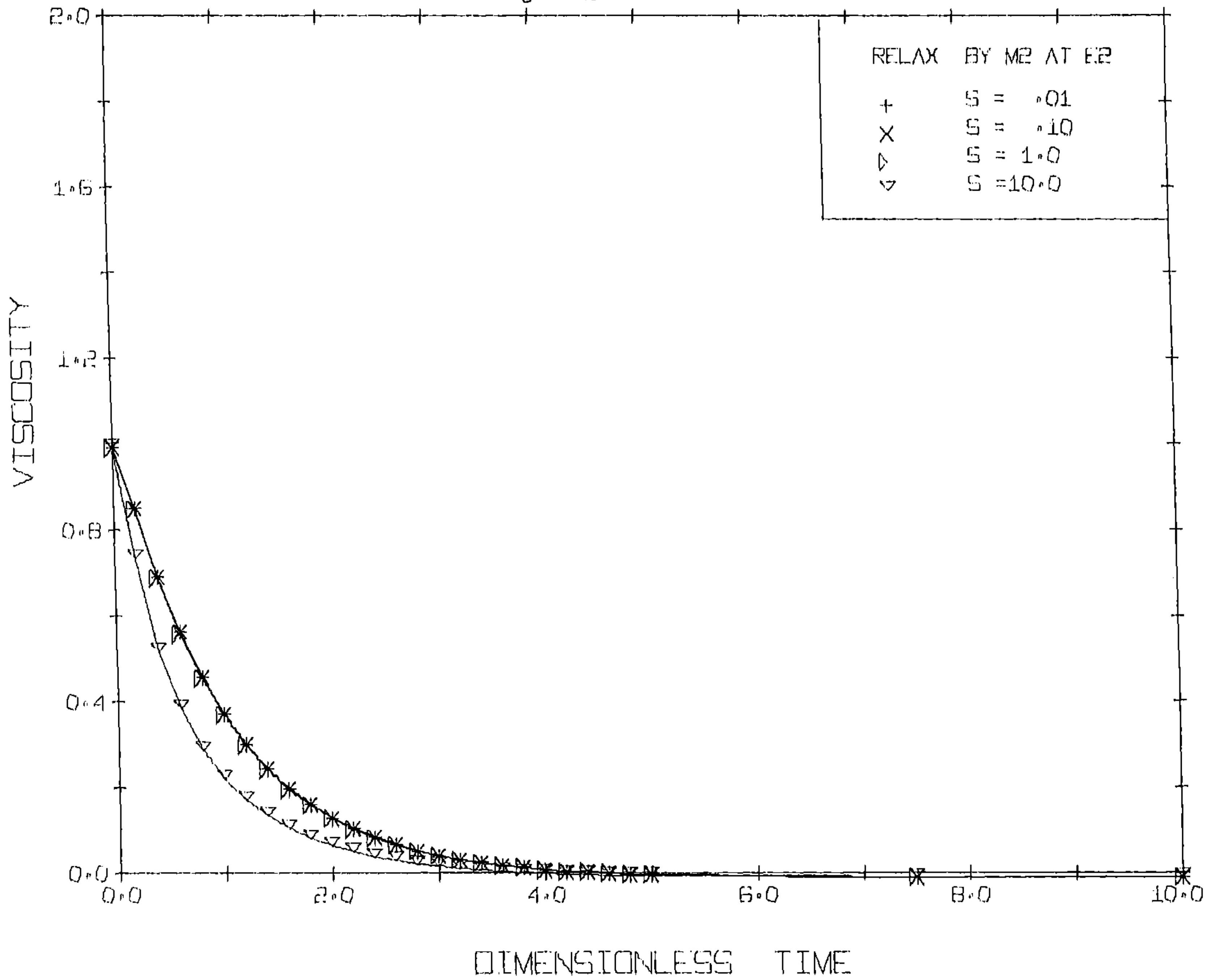
RELAX BY M2 AT E2
S = ·01
S = ·10
S = 1·0
S =10·0
VISCOSITY
DIMENSIONLESS TIME
0·0
0·4
0·8
1·2
1·6
2·0
2·0
4·0
6·0
8·0
10·0

Fig. 5.17

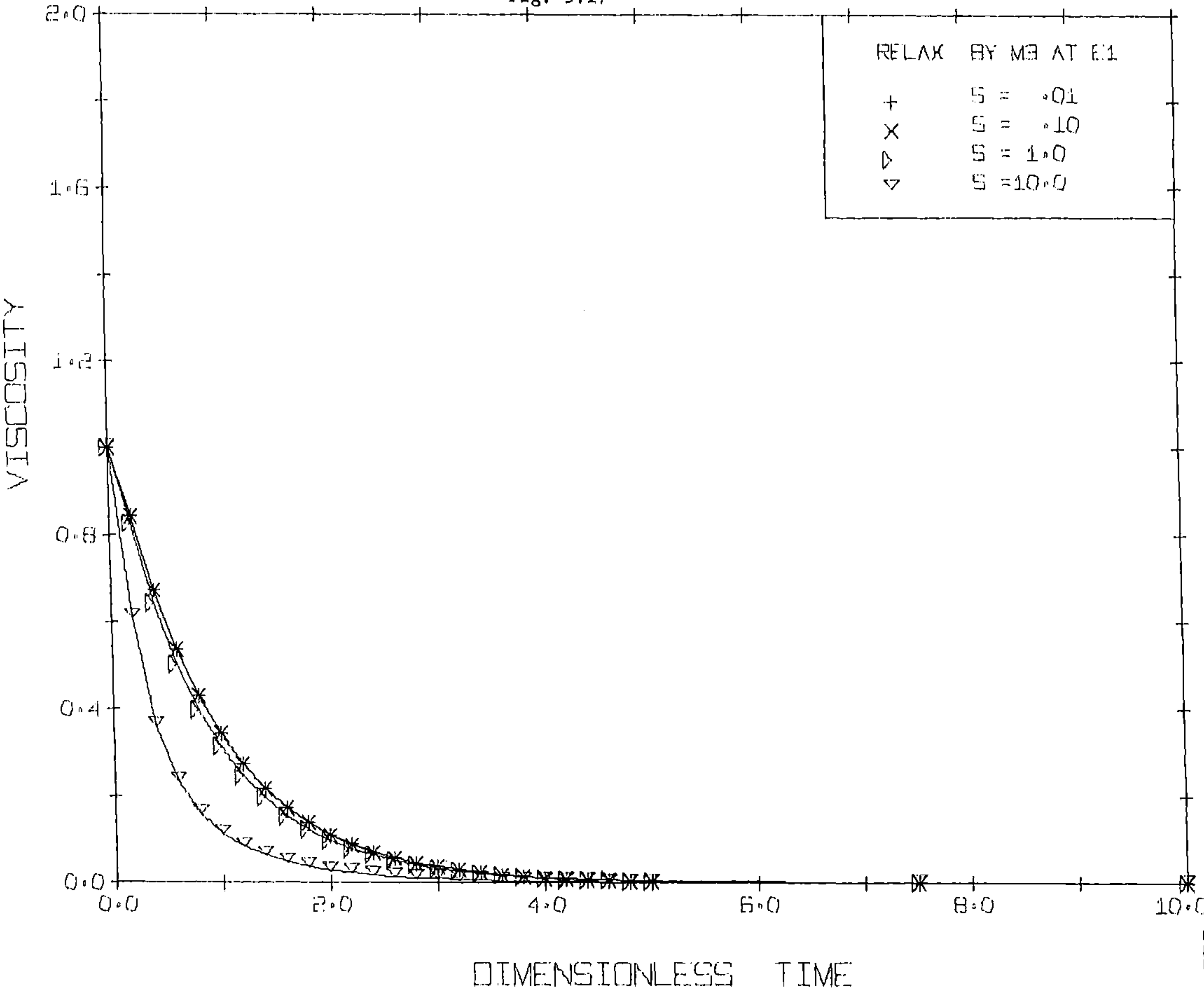
RELAX BY M3 AT E1
+ S = .01
X S = .10
▷ S = 1.0
▽ S = 10.0
VISCOSITY
DIMENSIONLESS TIME
0.0
0.4
0.8
1.2
1.6
2.0
2.0
4.0
6.0
8.0
10.0

Fig. 5.18

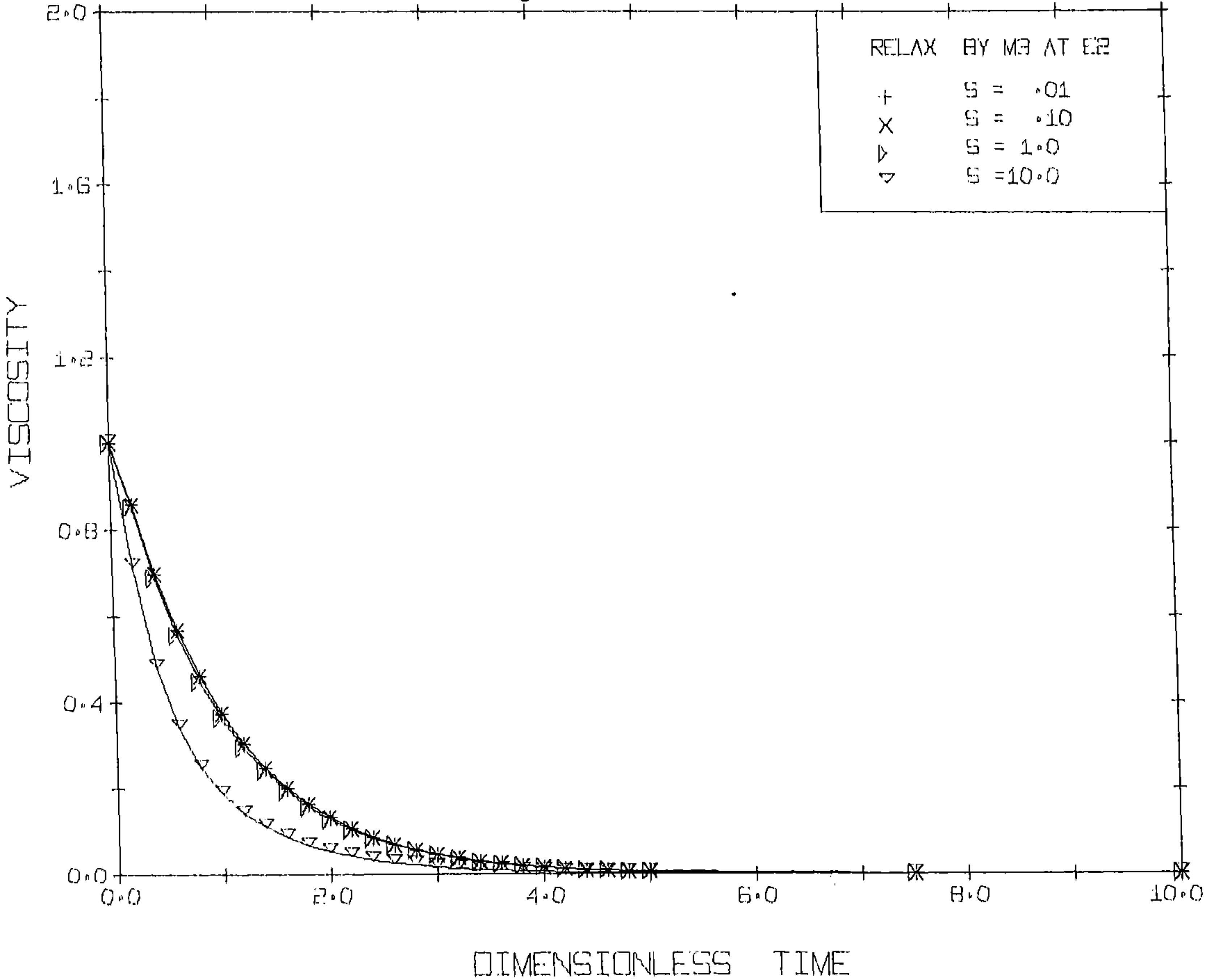
RELAX BY M3 AT E2
S = ·01
S = ·10
S = 1·0
S =10·0
VISCOSITY
DIMENSIONLESS TIME
2·0
1·6
1·2
0·8
0·4
0·0
0·0
2·0
4·0
6·0
8·0
10·0

Fig. 5.19

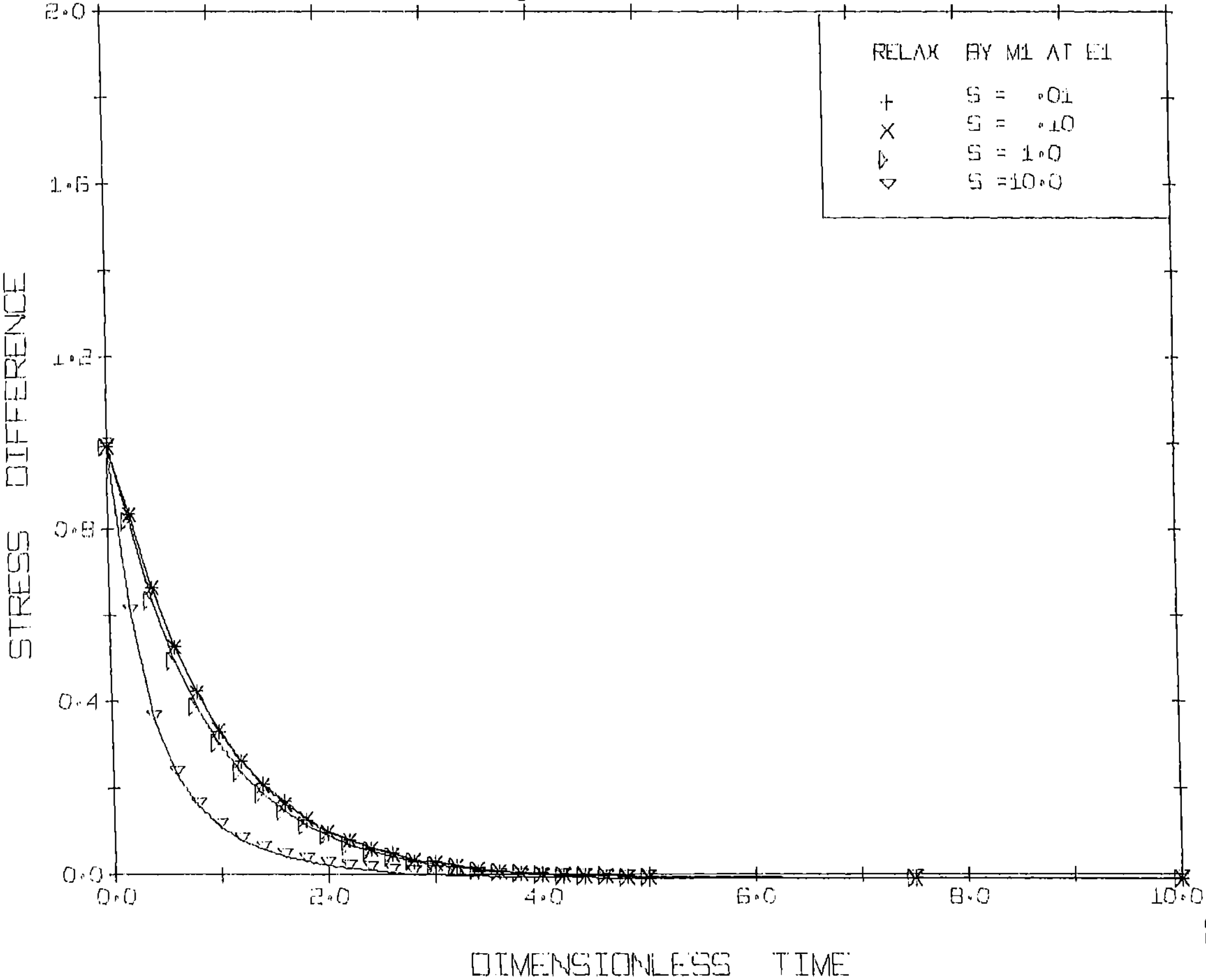

RELAX BY M1 AT E1
S = ·01
S = ·10
S = 1·0
S =10·0
STRESS DIFFERENCE
DIMENSIONLESS TIME
2·0
1·6
1·2
0·8
0·4
0·0
0·0
2·0
4·0
6·0
8·0
10·0

Fig. 5.20

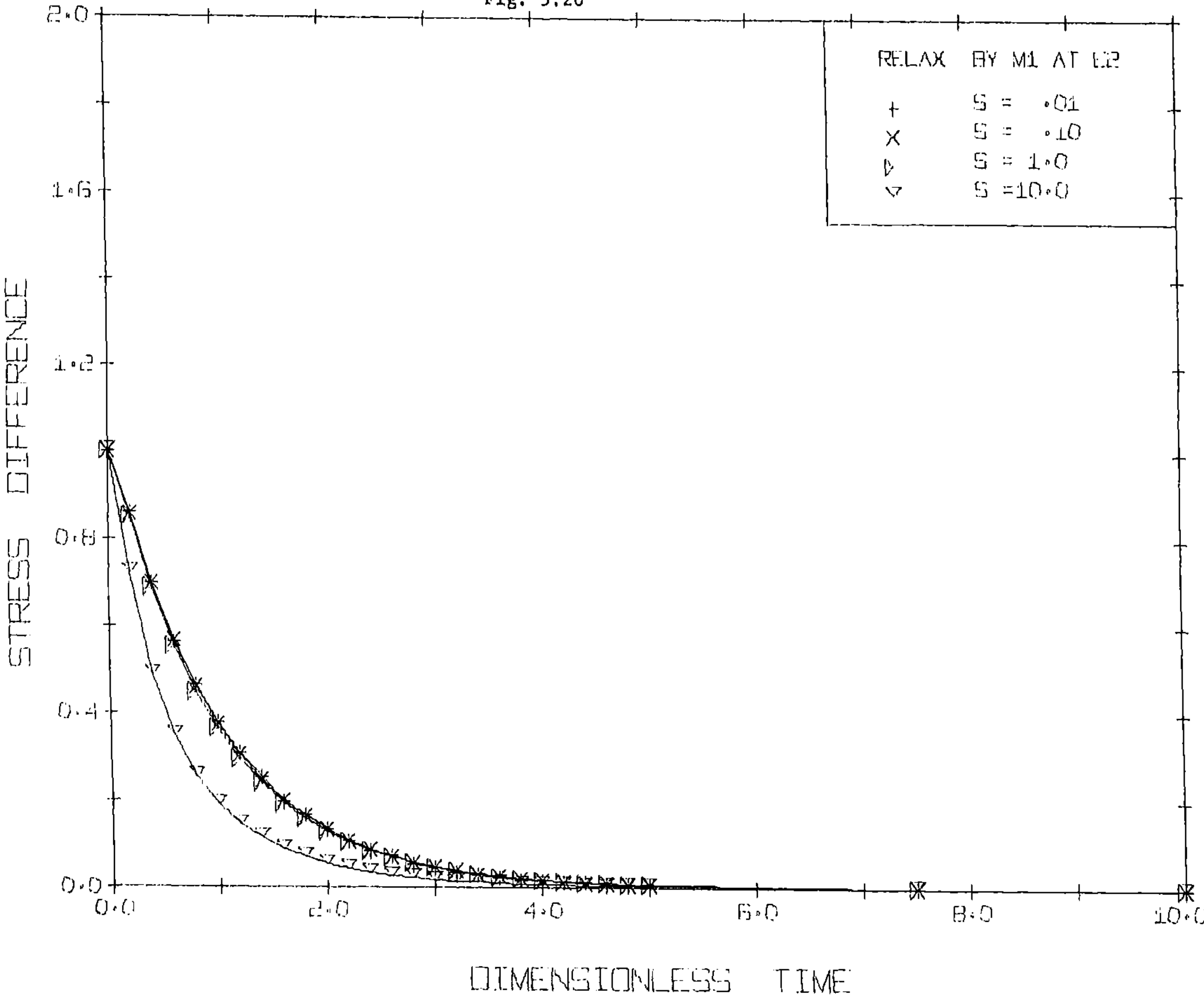
RELAX BY M1 AT E2
+ S = ·01
X S = ·10
▷ S = 1·0
▽ S =10·0
STRESS DIFFERENCE
2·0
1·6
1·2
0·8
0·4
0·0
0·0
2·0
4·0
6·0
8·0
10·0
DIMENSIONLESS TIME

Fig. 5.21

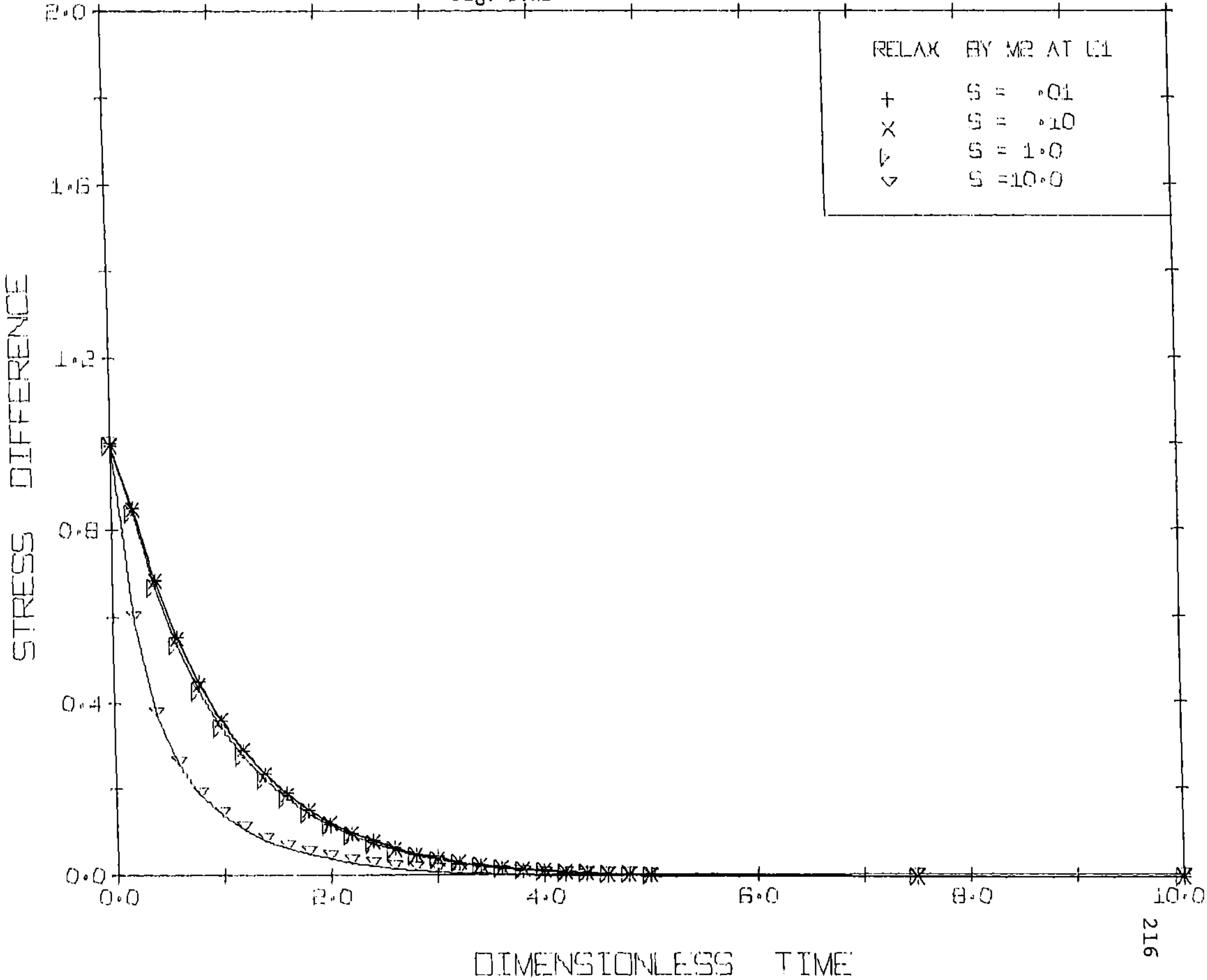

RELAX BY M2 AT C1
+ S = ·01
X S = ·10
S = 1·0
S =10·0
STRESS DIFFERENCE
DIMENSIONLESS TIME
0·0
0·4
0·8
1·2
1·6
2·0
0·0
2·0
4·0
6·0
8·0
10·0

Fig. 5.22

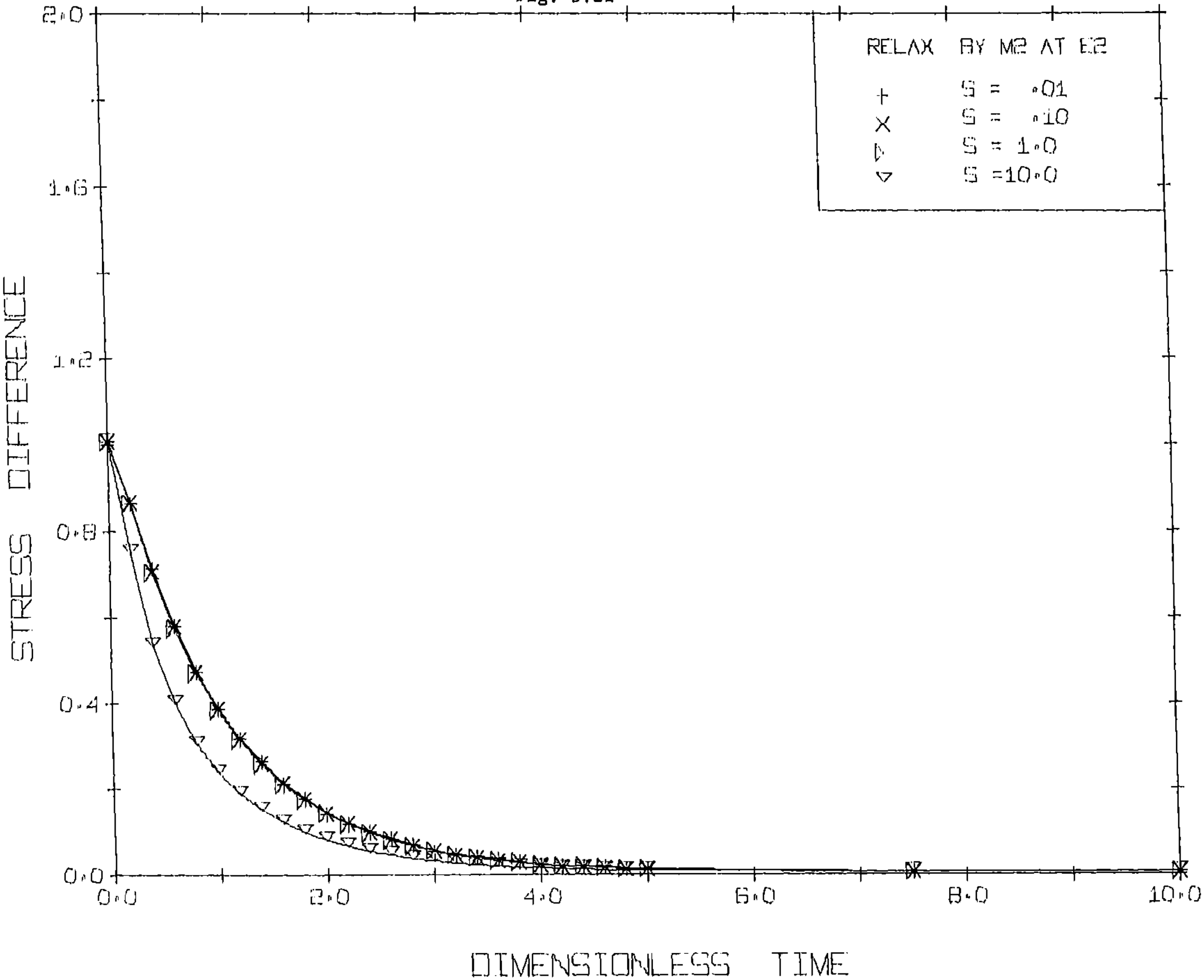
RELAX BY M2 AT E2
S = ·01
S = ·10
S = 1·0
S =10·0
STRESS DIFFERENCE
DIMENSIONLESS TIME
0·0
0·4
0·8
1·2
1·6
2·0
2·0
4·0
6·0
8·0
10·0

Fig. 5.23

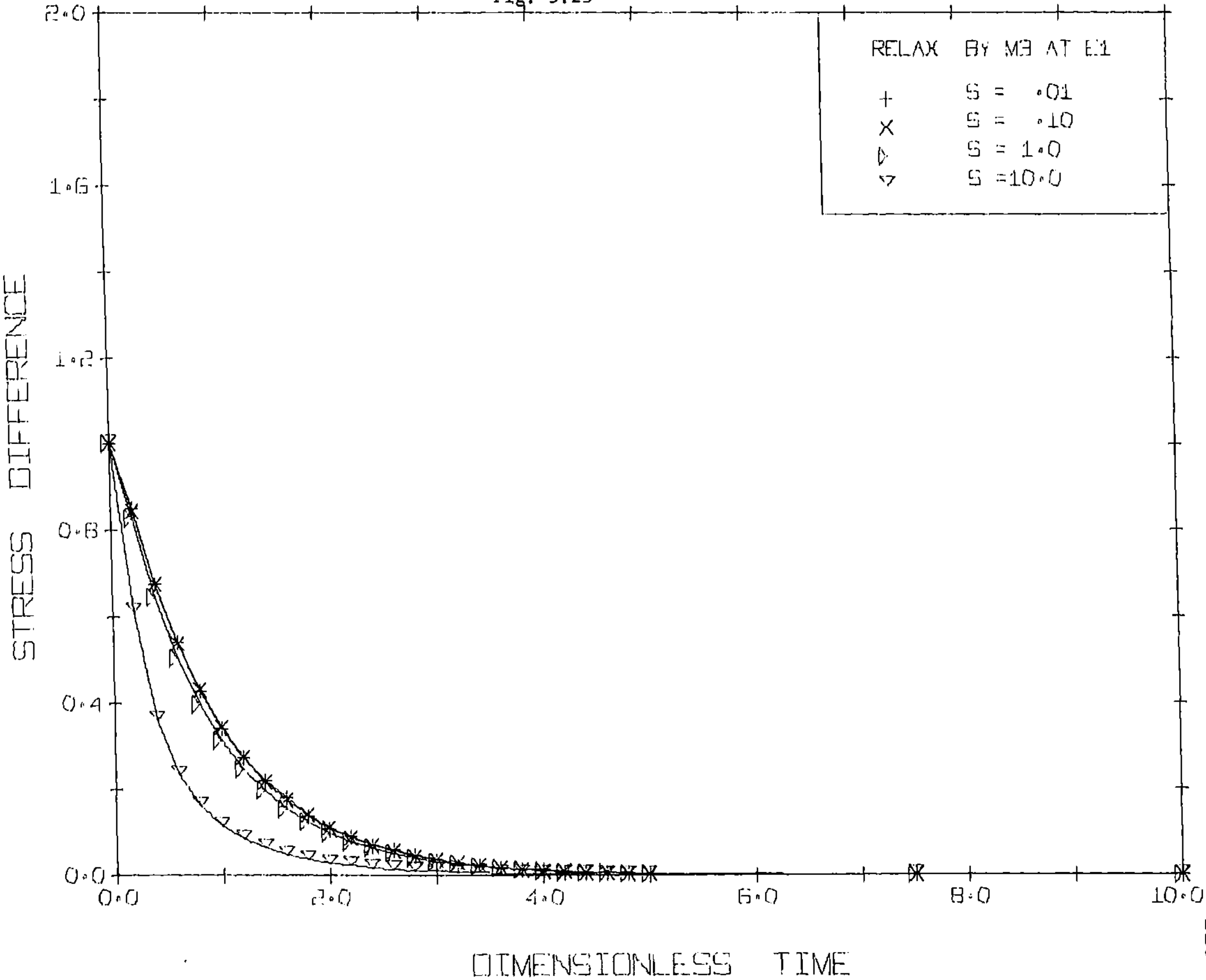

RELAX BY M3 AT E1
S = ·01
S = ·10
S = 1·0
S =10·0
STRESS DIFFERENCE
DIMENSIONLESS TIME
2·0
1·6
1·2
0·8
0·4
0·0
0·0
2·0
4·0
6·0
8·0
10·0

Fig. 5.24

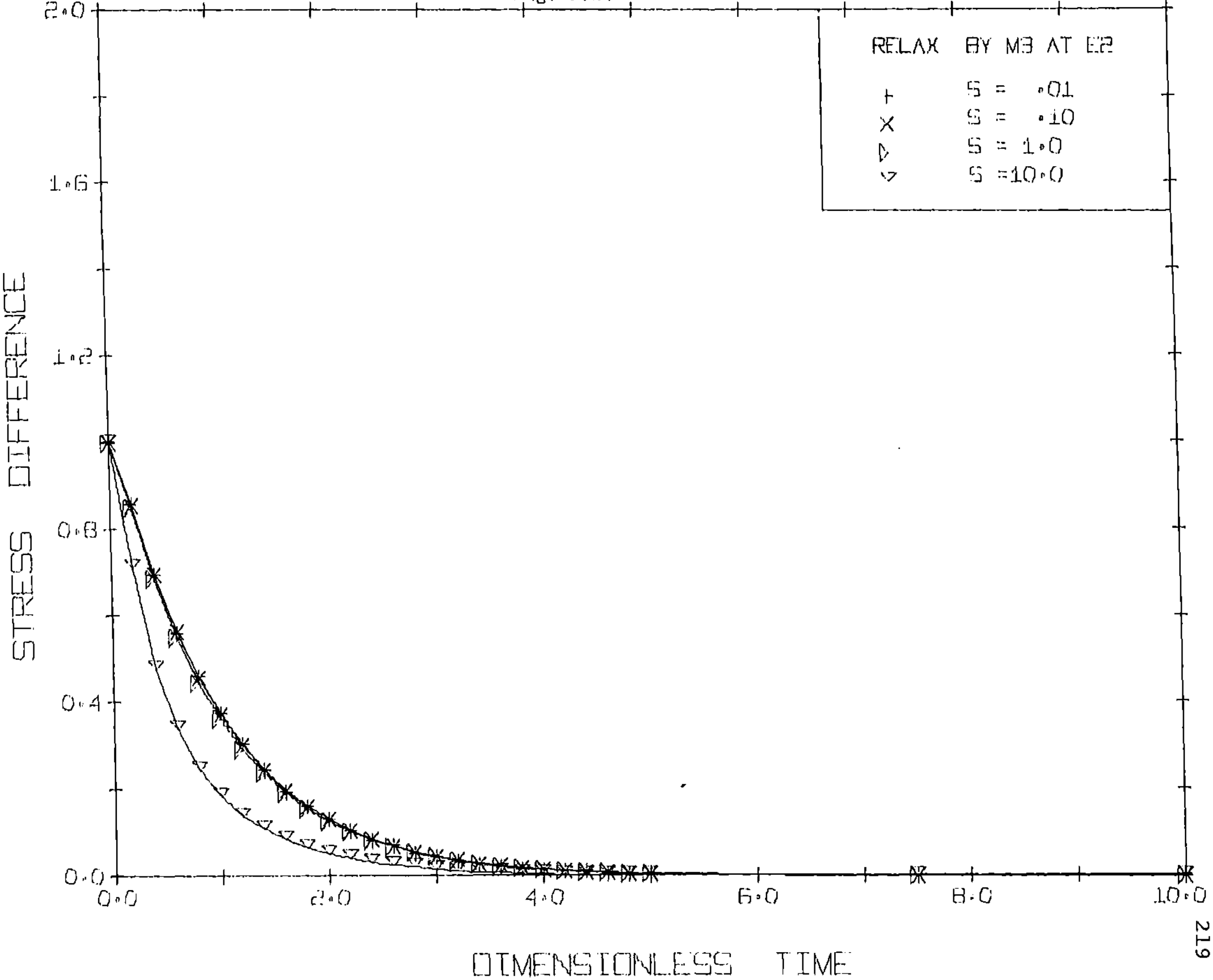
RELAX BY M3 AT E2
S = ·01
S = ·10
S = 1·0
S =10·0
STRESS DIFFERENCE
DIMENSIONLESS TIME
2·0
1·6
1·2
0·8
0·4
0·0
0·0
2·0
4·0
6·0
8·0
10·0

The Comparison of the Models

Fig. 5.25 to Fig. 5.36 show the comparison among the three models. The viscosity and the primary normal stress coefficient are compared for growth and relaxation behavior at various shear rate and ε.

For η^+ comparison, the three models show almost the same result at the lowest shear rate (Fig. 5.25). At moderate shear rate, however, the response of Tanner's model is a little shower (Fig. 5.26). Tanner's model gives the highest peak value at high shear rate and M1 and M3 have almost the same peak values (Fig. 5.27). However, the time required for reaching the peak is equal for the three models. M3 gives a little higher steady state value than those of other two models.

As to η^- comparison, M1 and M3 behave in an almost identical manner (Fig. 5.28) and they decay slightly faster than M2 does (Fig. 5.29 and Fig. 5.30). It is also found that the primary stress coefficient ($\Psi_1{}^+$, $\Psi_1{}^-$) has the same trends as viscosity ($[\eta^+]$, $[\eta^-]$) does for both growth and relaxation behavior (Fig. 5.31, Fig. 5.32, Fig. 5.34, Fig. 5.35, Fig. 5.36). At high shear rate ($S = 10$ and $\varepsilon = .005$), however, $\Psi_1{}^+$ by M2 has higher steady state value and the time required for the peak of overshoot becomes slower (Fig. 5.33). Roughly speaking, the three models predict the same trends. Up to moderate shear rate ($S = .01$, $S = .1$ and $S = 1.0$), the behavior of M1 and M3 are very similar and the prediction by

Fig 5.25 to Fig. 5.36

THE COMPARISON AMONG THE

THREE MODELS FOR SHEAR FLOW

The following notation is used:

M1	Modified Nearly Hookean Dumbbell	eq. 5.22
M2	Tanner's model	eq. 5.9
M3	Nearly Hookean Dumbbell	eq. 5.19

E1 $\varepsilon = .02$

E2 $\varepsilon = .005$

VISCOSITY	$[\eta^{+}]$	for growth
	$[\eta^{-}]$	for relaxation
STRESS DIFFERENCE	Ψ_1^{+}	for growth
	Ψ_1^{-}	for relaxation
DIMENSIONLESS TIME	t/λ_H	

S1 $S = \lambda_H \dot{\gamma} = .01$

S2 $S = \lambda_H \dot{\gamma} = .1$

S3 $S = \lambda_H \dot{\gamma} = 1.$

S4 $S = \lambda_H \dot{\gamma} = 10.$

Fig. 5.25

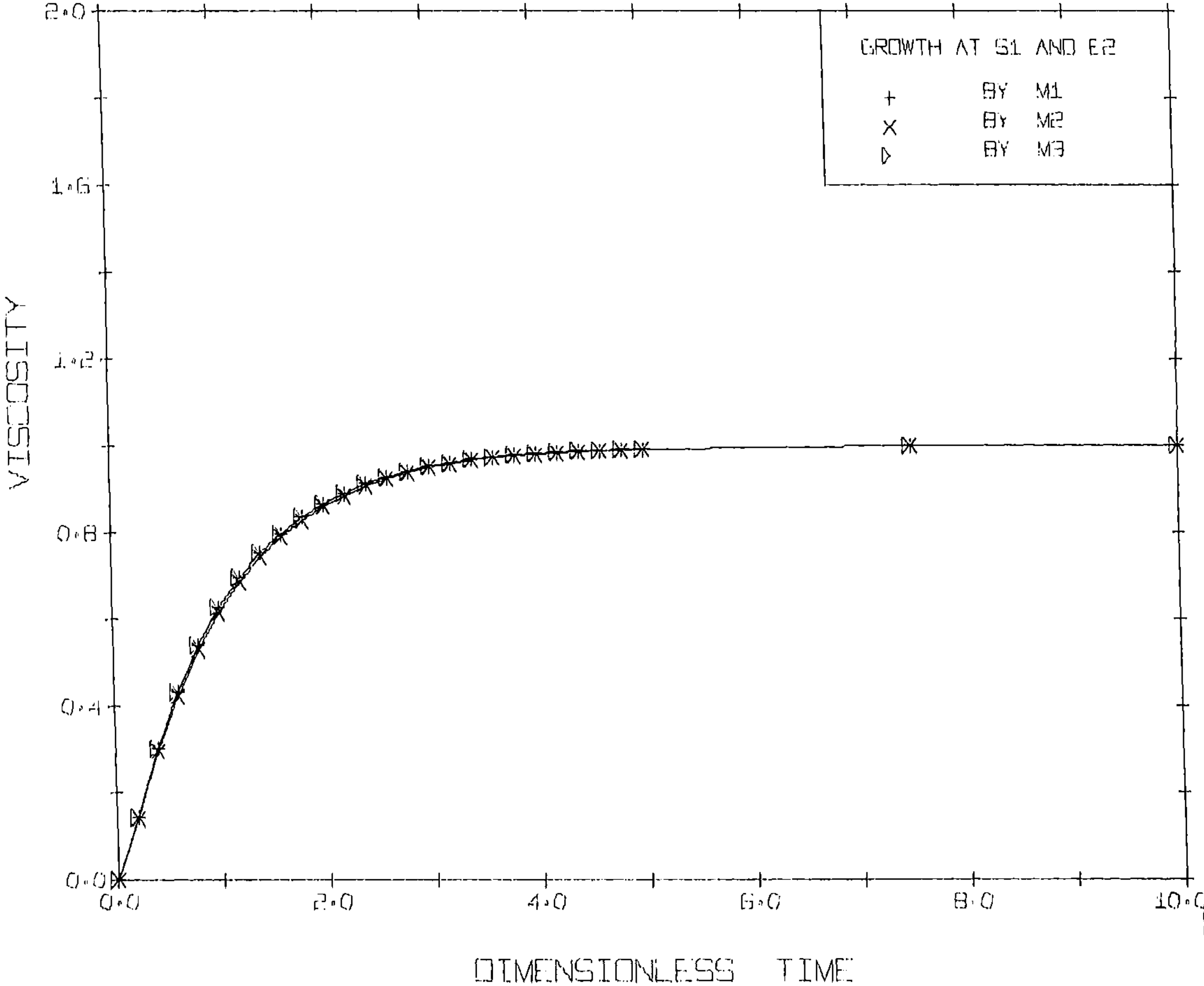

GROWTH AT S1 AND E2
+ BY M1
X BY M2
▷ BY M3
VISCOSITY
DIMENSIONLESS TIME
2.0
1.6
1.2
0.8
0.4
0.0
0.0
2.0
4.0
6.0
8.0
10.0

Fig. 5.26

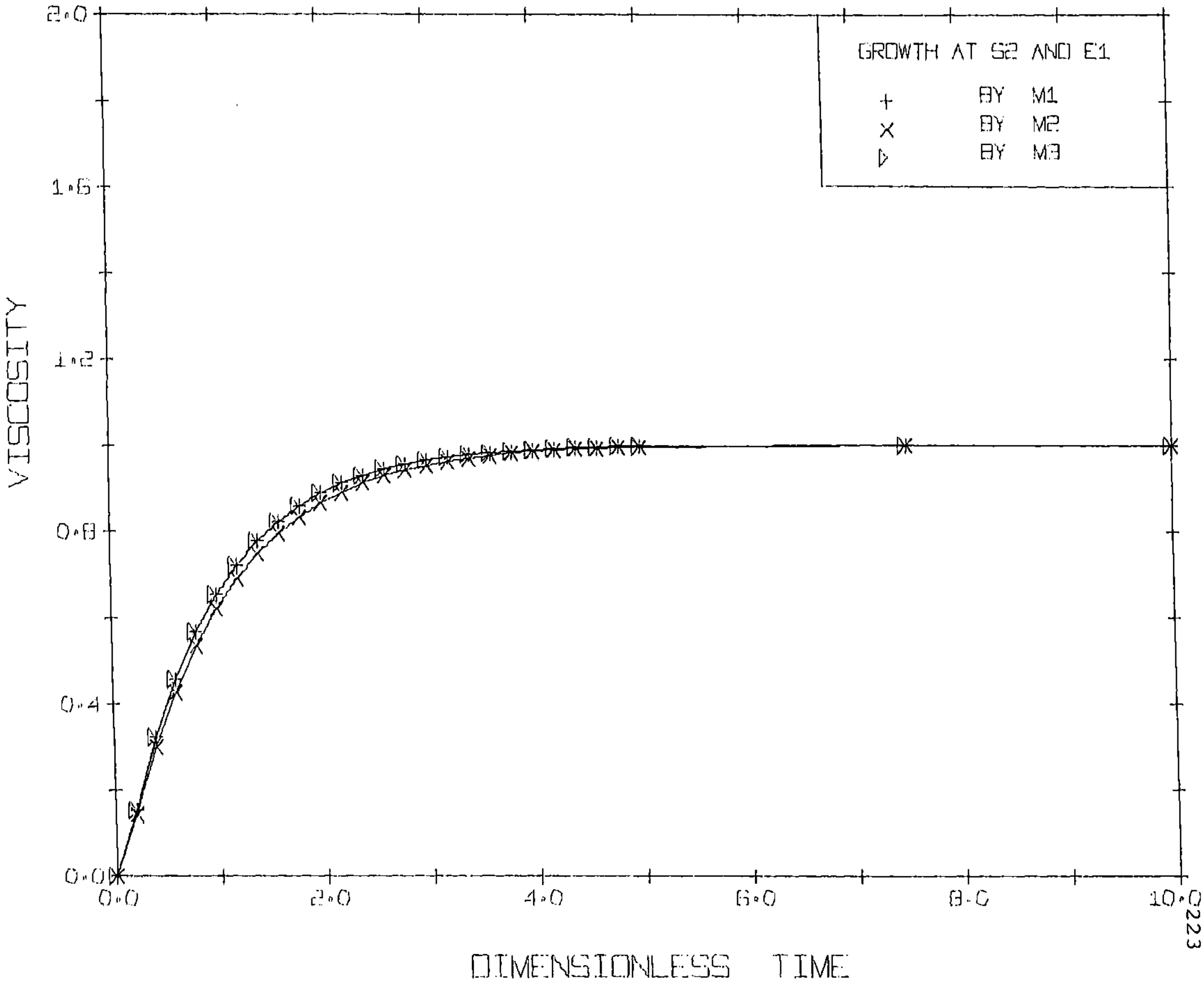
GROWTH AT S2 AND E1
BY M1
BY M2
BY M3
VISCOSITY
DIMENSIONLESS TIME
0·0
0·4
0·8
1·2
1·6
2·0
2·0
4·0
6·0
8·0
10·0

Fig. 5.27

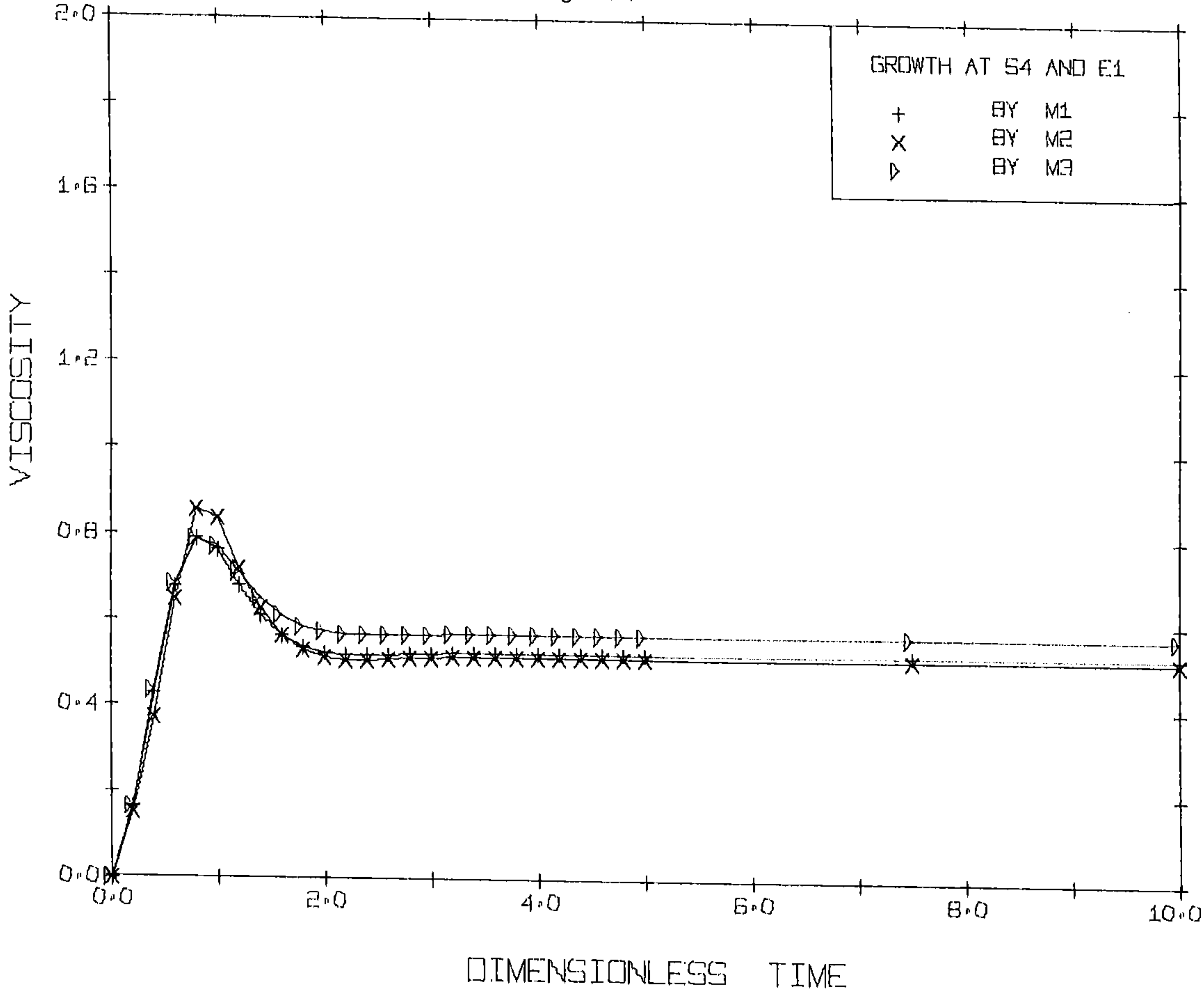
GROWTH AT S4 AND E1
BY M1
BY M2
BY M3
VISCOSITY
DIMENSIONLESS TIME
0·0
0·4
0·8
1·2
1·6
2·0
2·0
4·0
6·0
8·0
10·0

Fig. 5.28

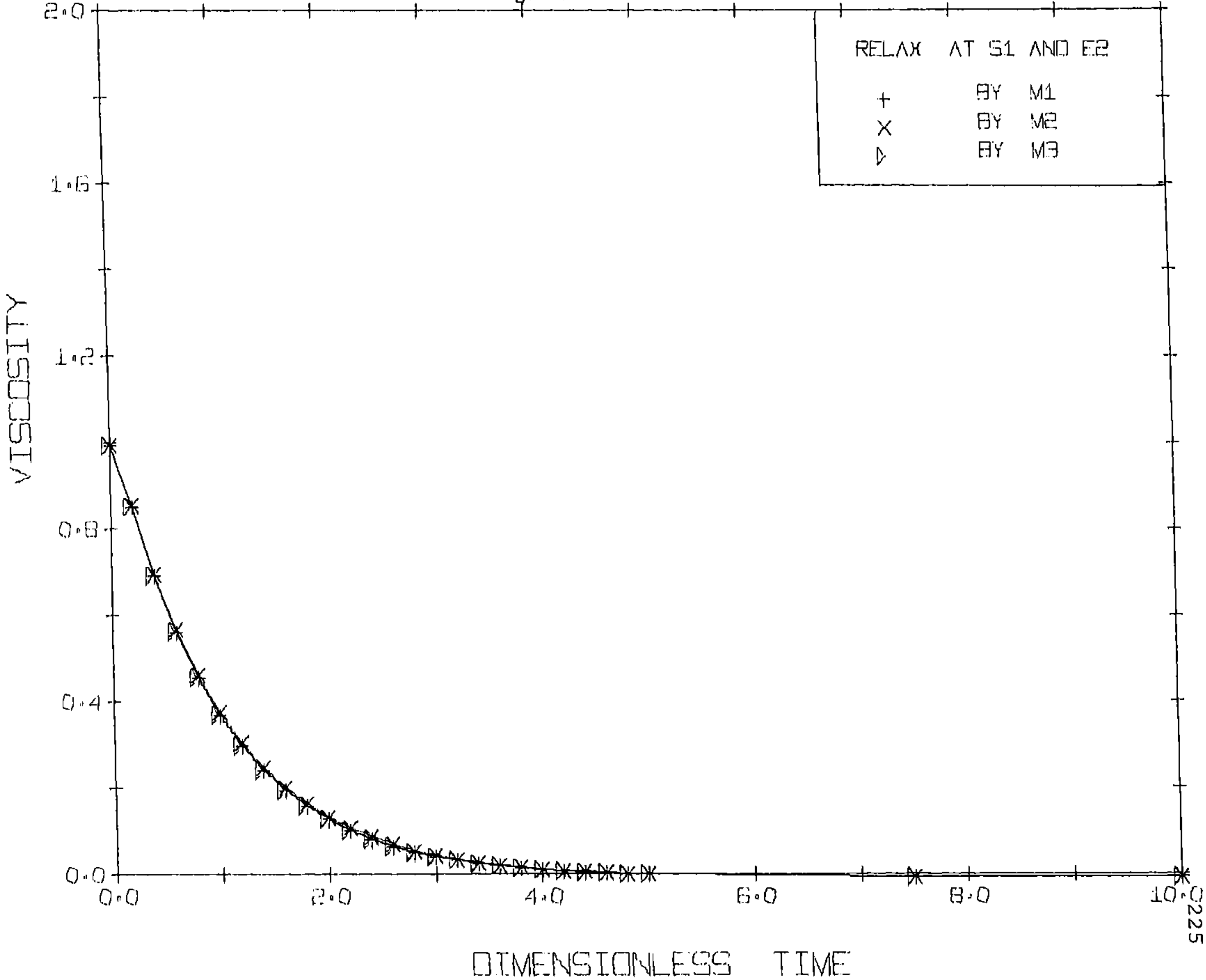
RELAX AT S1 AND E2
+ BY M1
X BY M2
▷ BY M3
VISCOSITY
DIMENSIONLESS TIME
2.0
1.6
1.2
0.8
0.4
0.0
0.0
2.0
4.0
6.0
8.0
10.0

Fig. 5.29

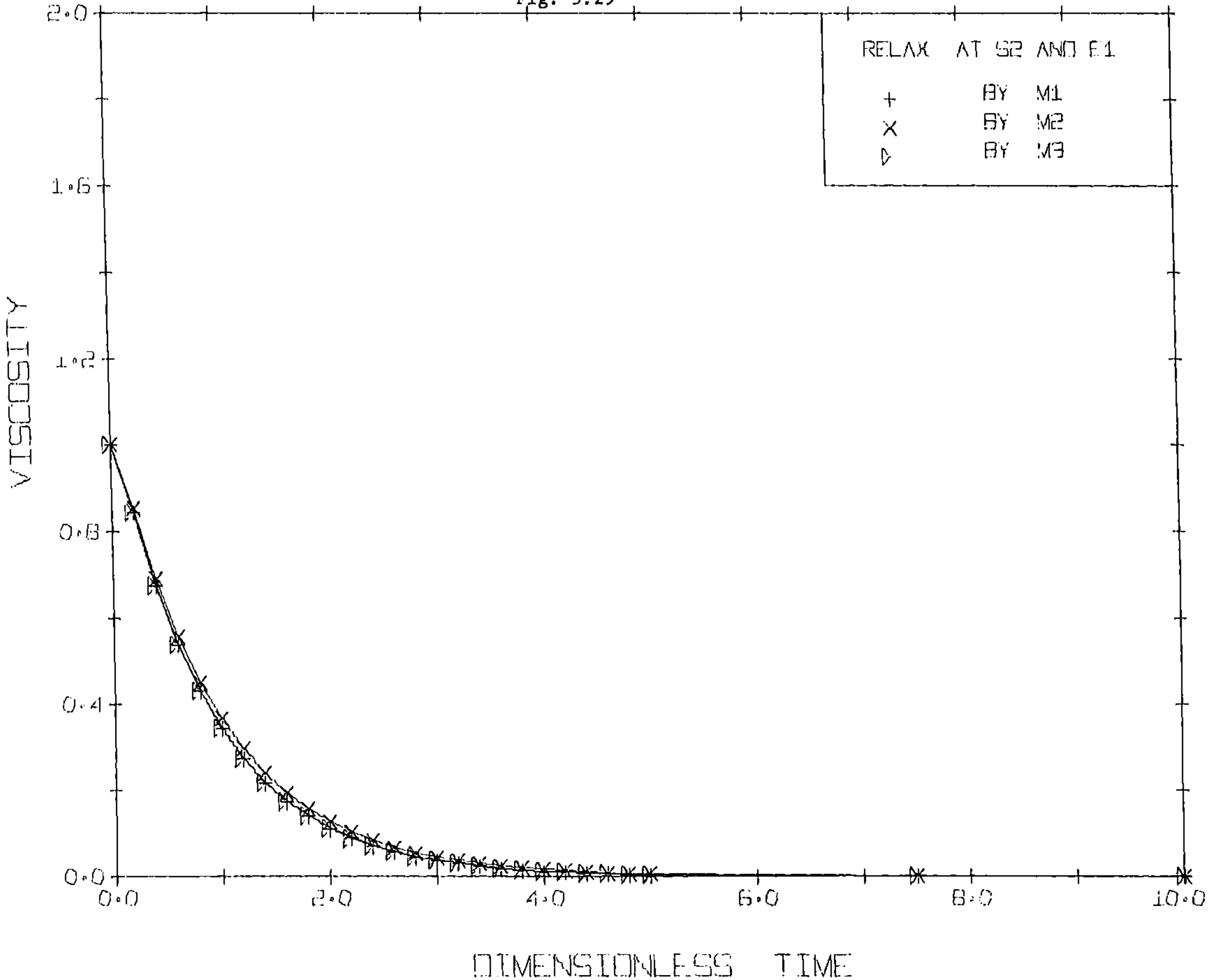

RELAX AT S2 AND E1
+ BY M1
X BY M2
▷ BY M3
2.0
1.6
1.2
0.8
0.4
0.0
VISCOSITY
0.0
2.0
4.0
6.0
8.0
10.0
DIMENSIONLESS TIME

Fig. 5.30

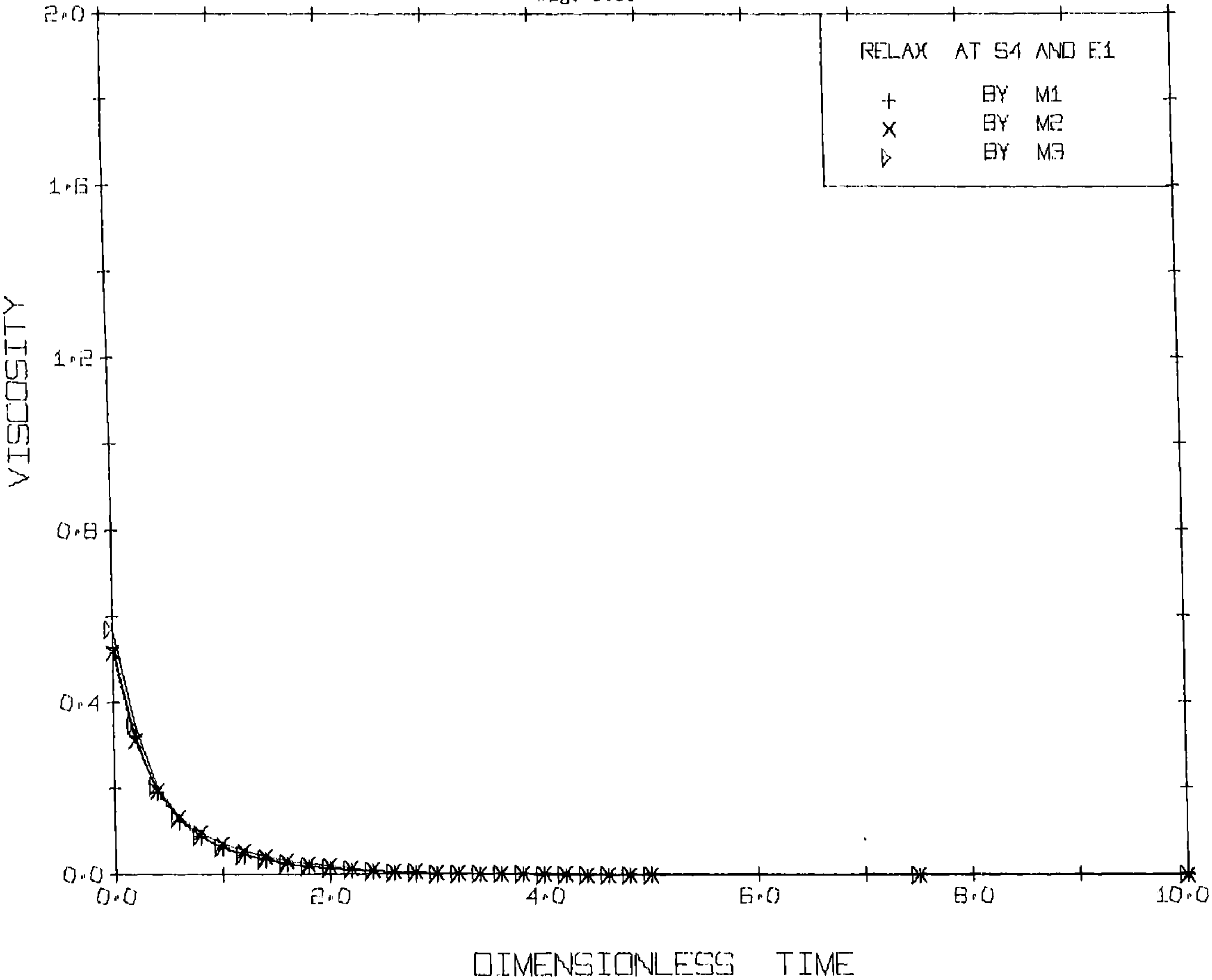
RELAX AT S4 AND E1
+ BY M1
X BY M2
▷ BY M3
VISCOSITY
DIMENSIONLESS TIME
2·0
1·6
1·2
0·8
0·4
0·0
0·0
2·0
4·0
6·0
8·0
10·0

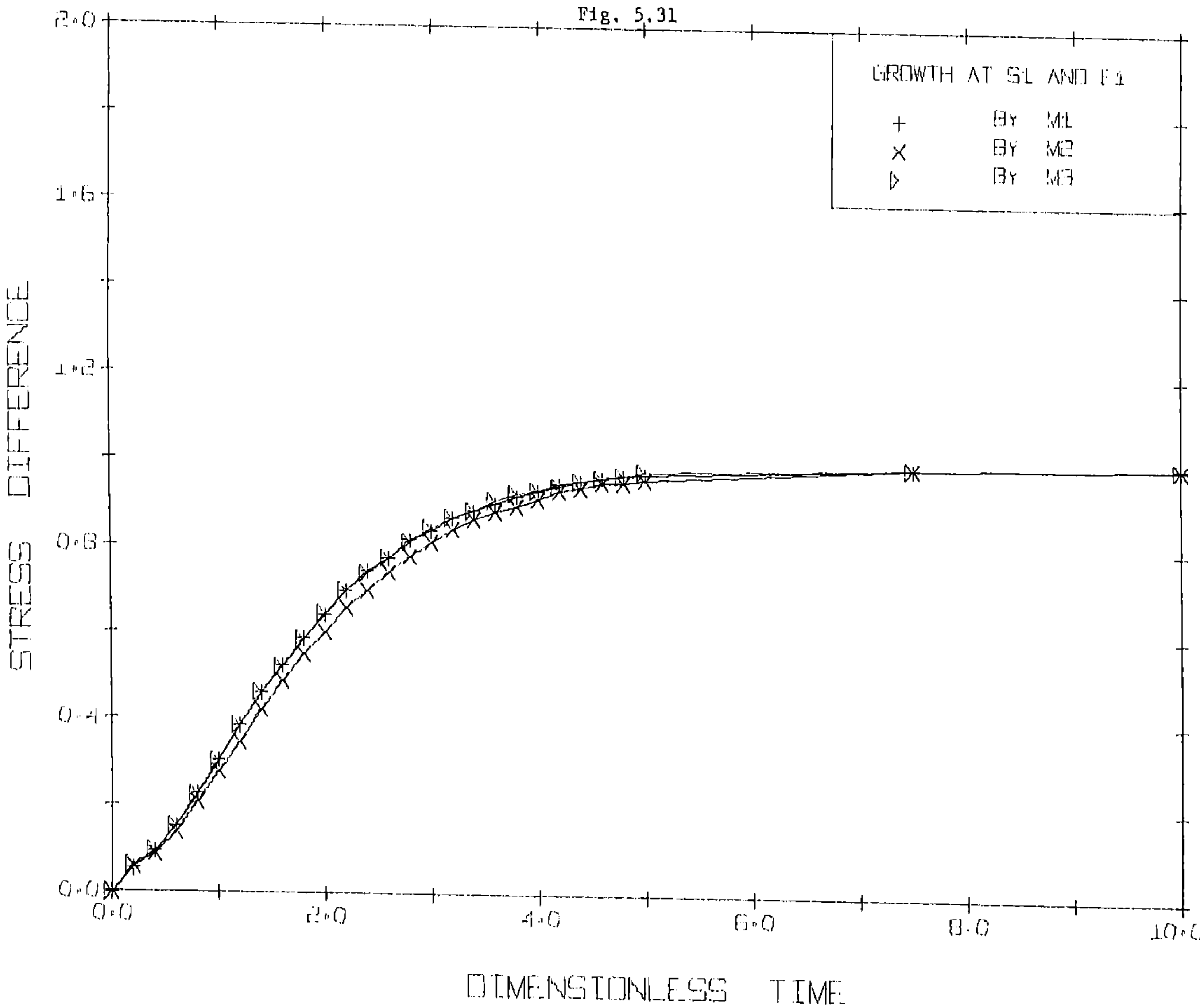
Fig. 5.31
GROWTH AT S1 AND F1
+ BY M1
× BY M2
▷ BY M3
STRESS DIFFERENCE
DIMENSIONLESS TIME
0.0
0.4
0.8
1.2
1.6
2.0
0.0
2.0
4.0
6.0
8.0
10.0

Fig. 5.32

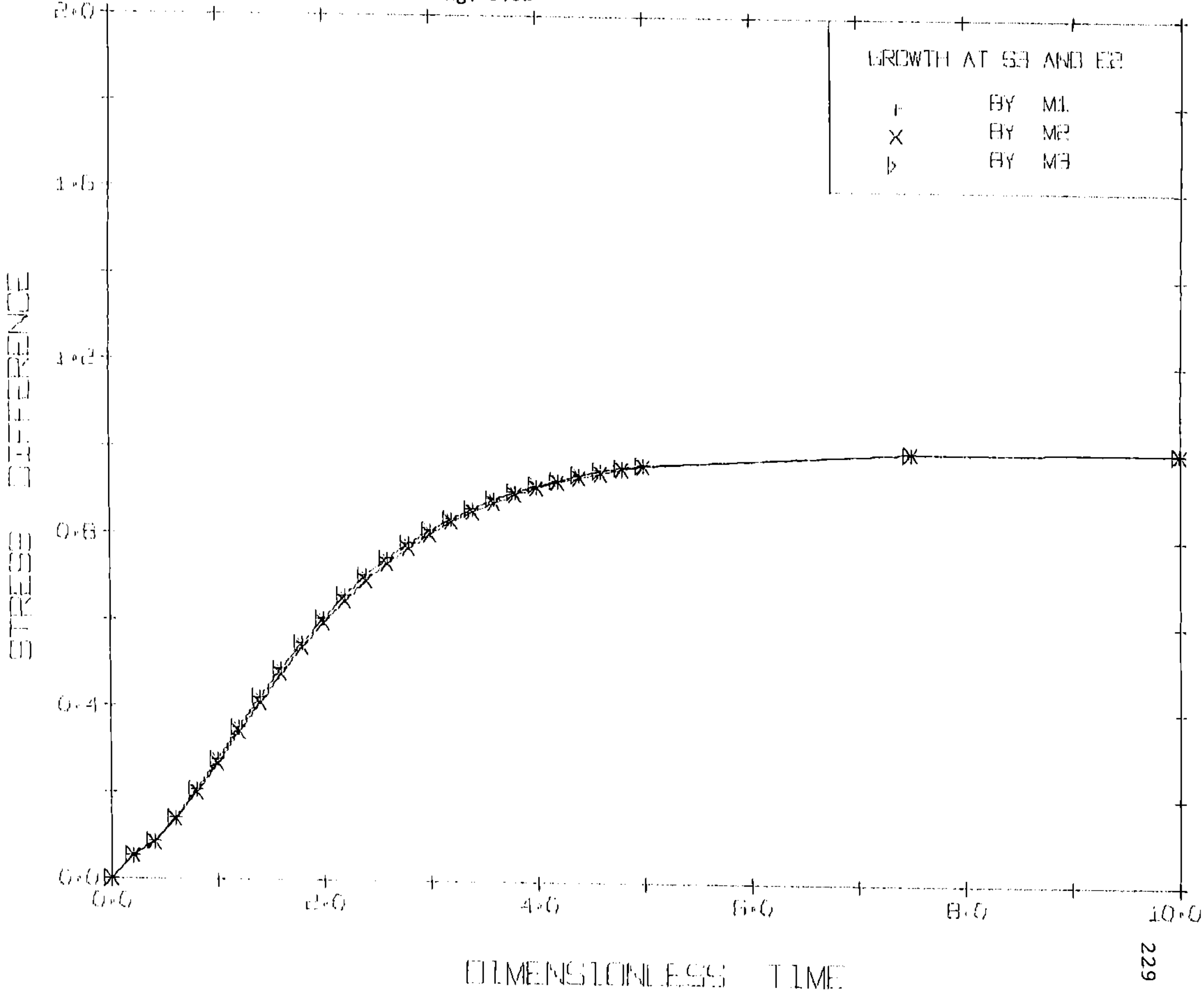
GROWTH AT S3 AND E2
+ BY M1
X BY M2
▷ BY M3
STRESS DIFFERENCE
DIMENSIONLESS TIME
0.0
0.4
0.8
1.2
1.6
2.0
2.0
4.0
6.0
8.0
10.0

Fig. 5.33

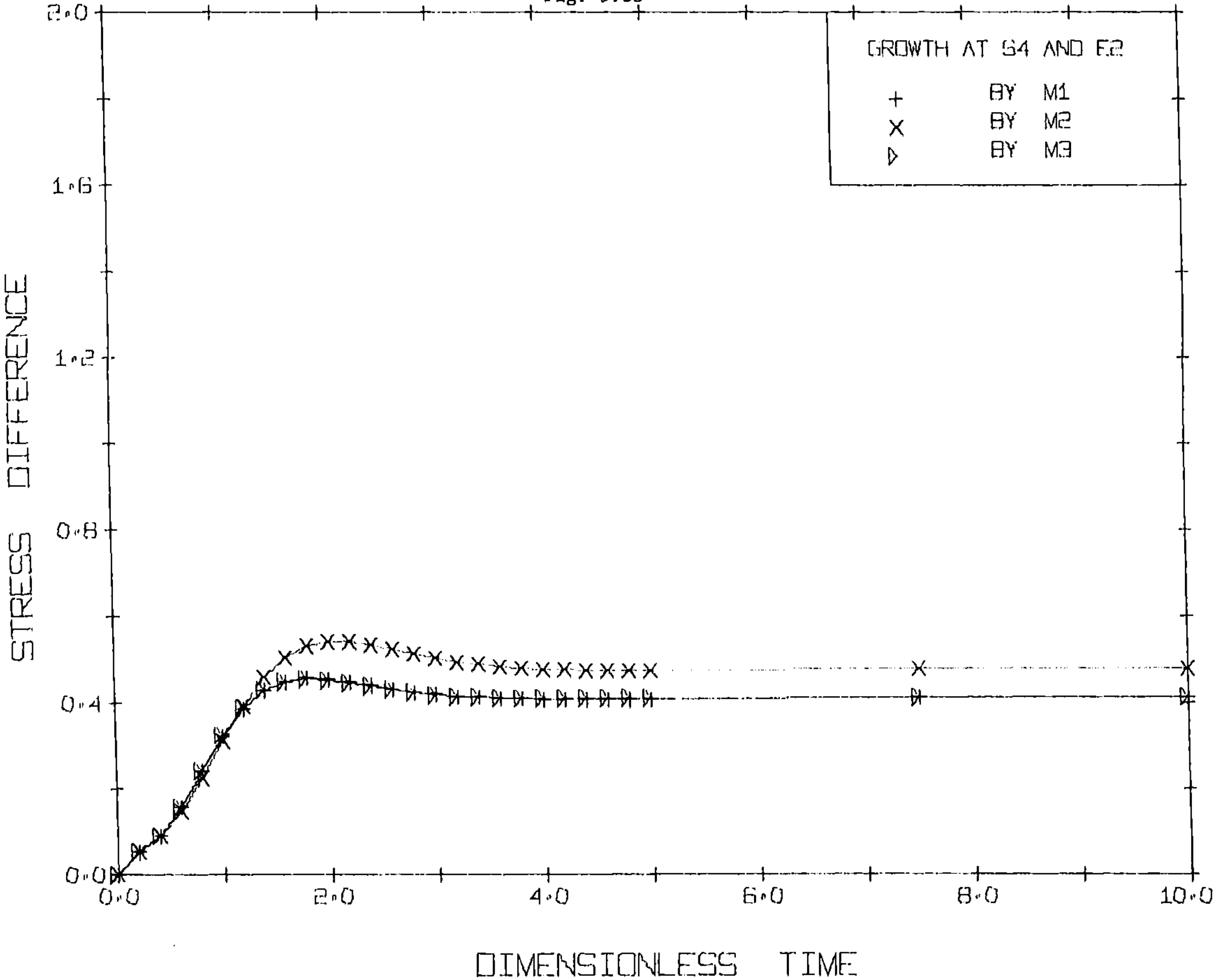
GROWTH AT S4 AND E2
BY M1
BY M2
BY M3
2·0
1·6
1·2
0·8
0·4
0·0
0·0
2·0
4·0
6·0
8·0
10·0
STRESS DIFFERENCE
DIMENSIONLESS TIME

Fig. 5.34

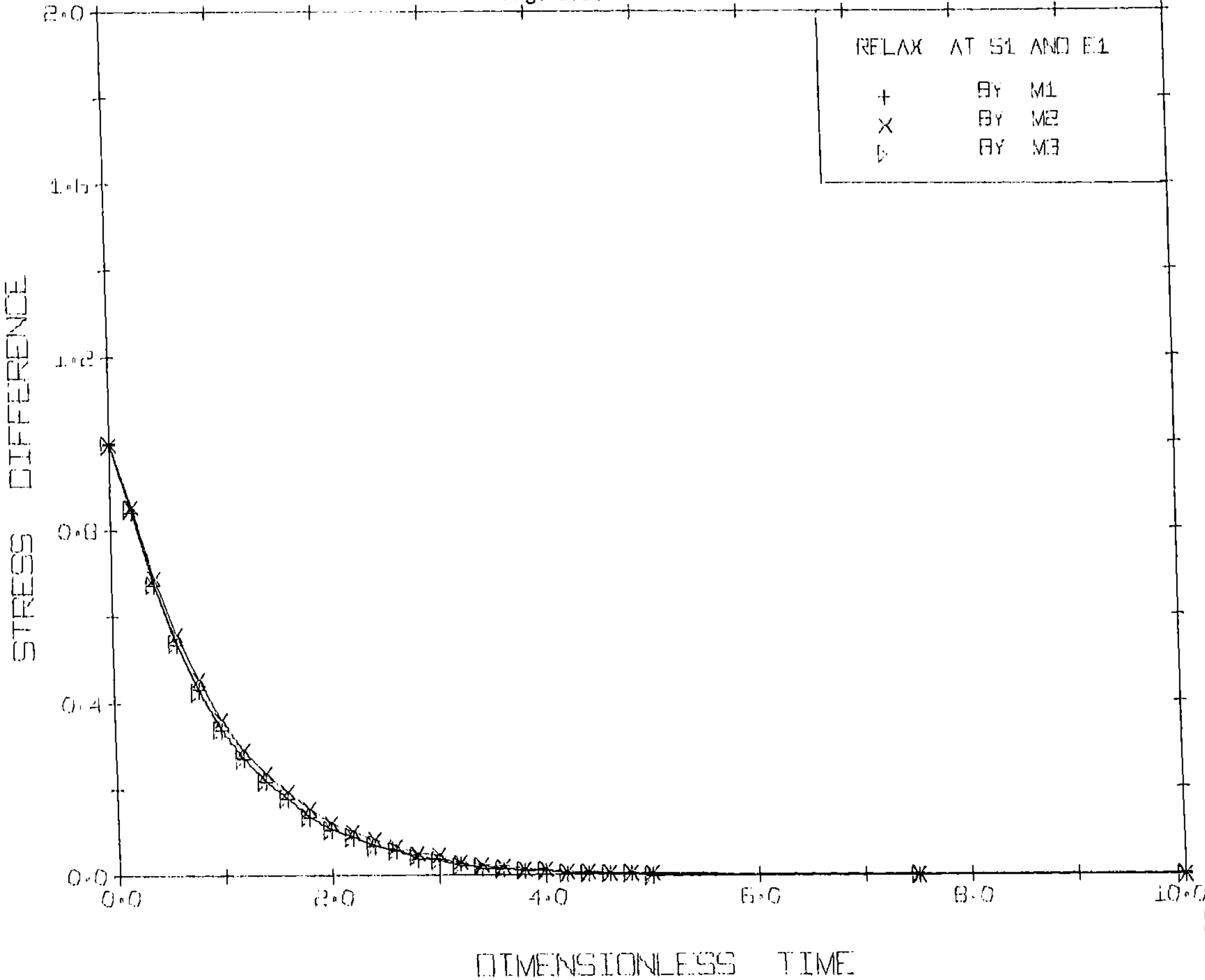
RELAX AT S1 AND E1
BY M1
BY M2
BY M3
STRESS DIFFERENCE
DIMENSIONLESS TIME
2.0
1.6
1.2
0.8
0.4
0.0
0.0
2.0
4.0
6.0
8.0
10.0

Fig. 5.35

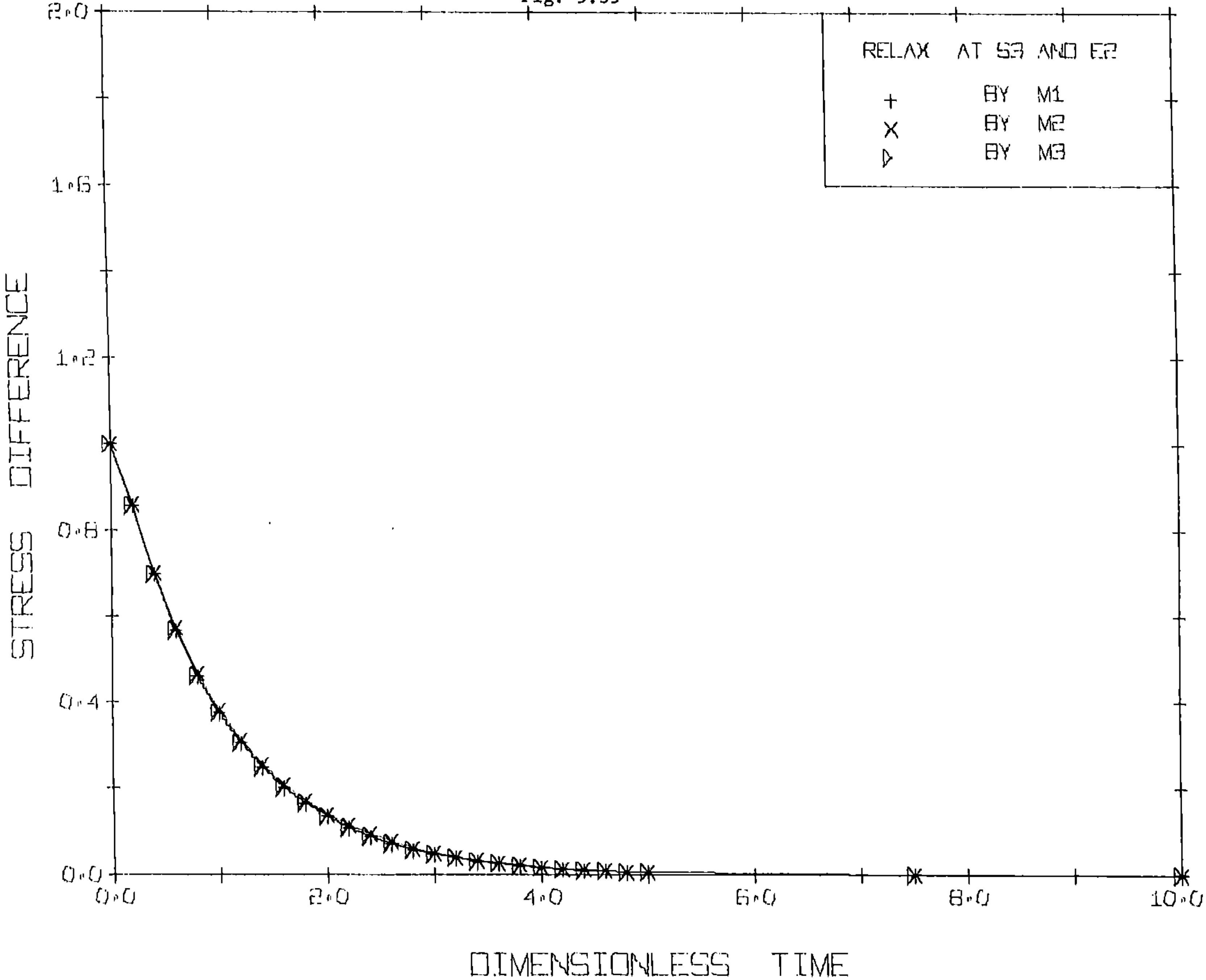

RELAX AT S3 AND E2
BY M1
BY M2
BY M3
STRESS DIFFERENCE
DIMENSIONLESS TIME
2·0
1·6
1·2
0·8
0·4
0·0
0·0
2·0
4·0
6·0
8·0
10·0

Fig. 5.36

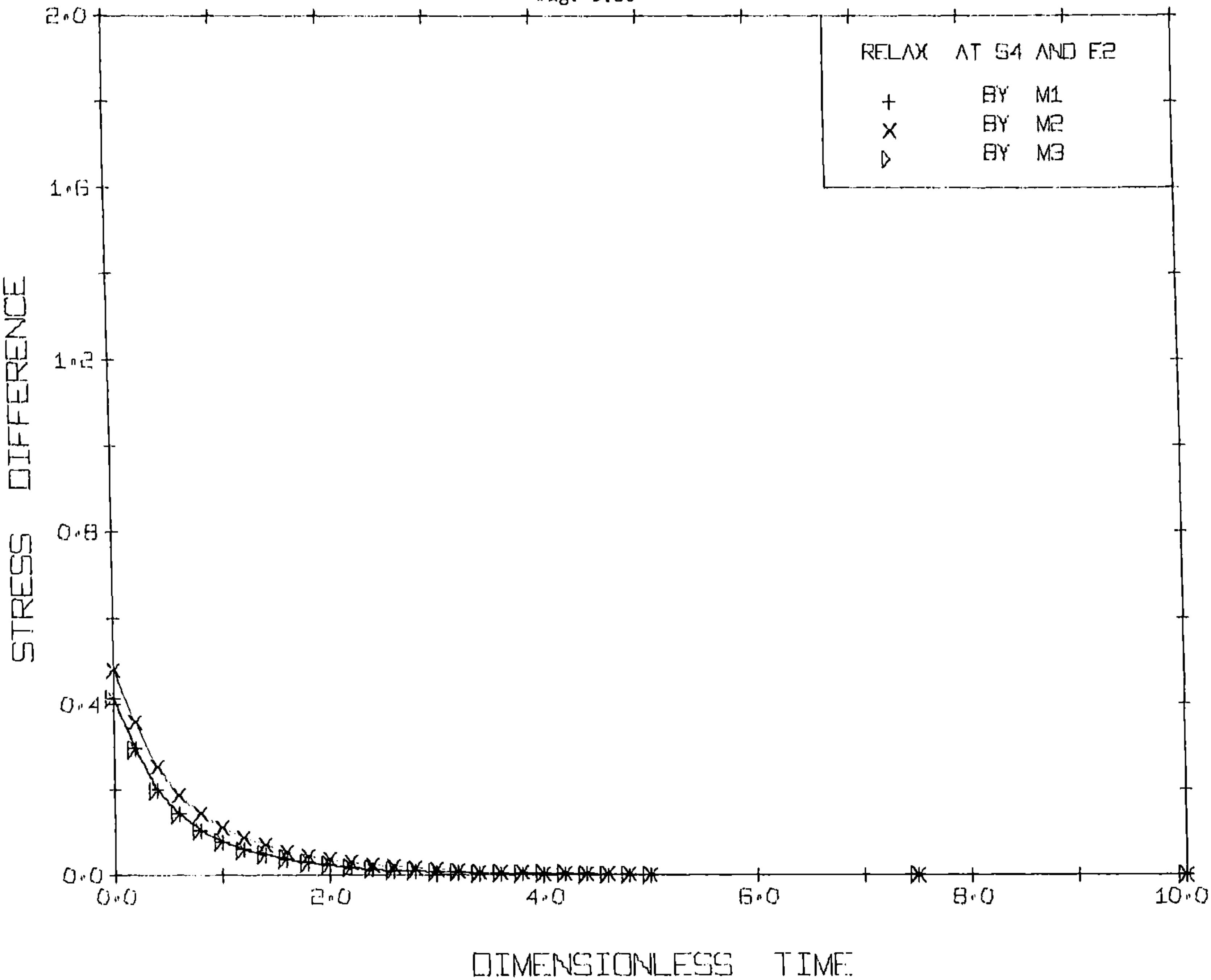
RELAX AT S4 AND E2
BY M1
BY M2
BY M3
STRESS DIFFERENCE
DIMENSIONLESS TIME
2.0
1.6
1.2
0.8
0.4
0.0
0.0
2.0
4.0
6.0
8.0
10.0

M2 slightly deviates from them. At high shear rate (S = 10.), differences in steady state values between the models are observed.

Steady Shear Flow

The steady state material functions as functions of shear rate are plotted in Fig. 5.37 to Fig. 5.40. Shear thinning for both viscosity and the primary normal stress coefficient is observed for the three models. Both onset of shear thinning and slope of decreasing curve are similar between them.

To sum up the performance of the models for shear flow, they provide fairly good predictions like shear thinning and stress overshoot and have very similar trends. Qualitatively speaking, M2 shows a small deviation from M1 and M3 whose predictions are extremely similar.

Fig. 5.37 to Fig. 5.40

THE STEADY STATE VALUES OF VISCOSITY AND THE PRIMARY NORMAL STRESS COEFFICIENT FOR SHEAR FLOW

The following notation is used:

M1	Modified Nearly Hookean Dumbbell	eq. 5.22
M2	Tanner's model	eq. 5.9
M3	Nearly Hookean Dumbbell	eq. 5.19

E1 $\varepsilon = .02$

E2 $\varepsilon = .005$

VISCOSITY $[\eta]/[\eta]_o$

STRESS DIFFERENCE $\Psi_1/\Psi_{1.o}$

SHEAR RATE $\lambda_H\dot{\gamma}$

Fig. 5.37

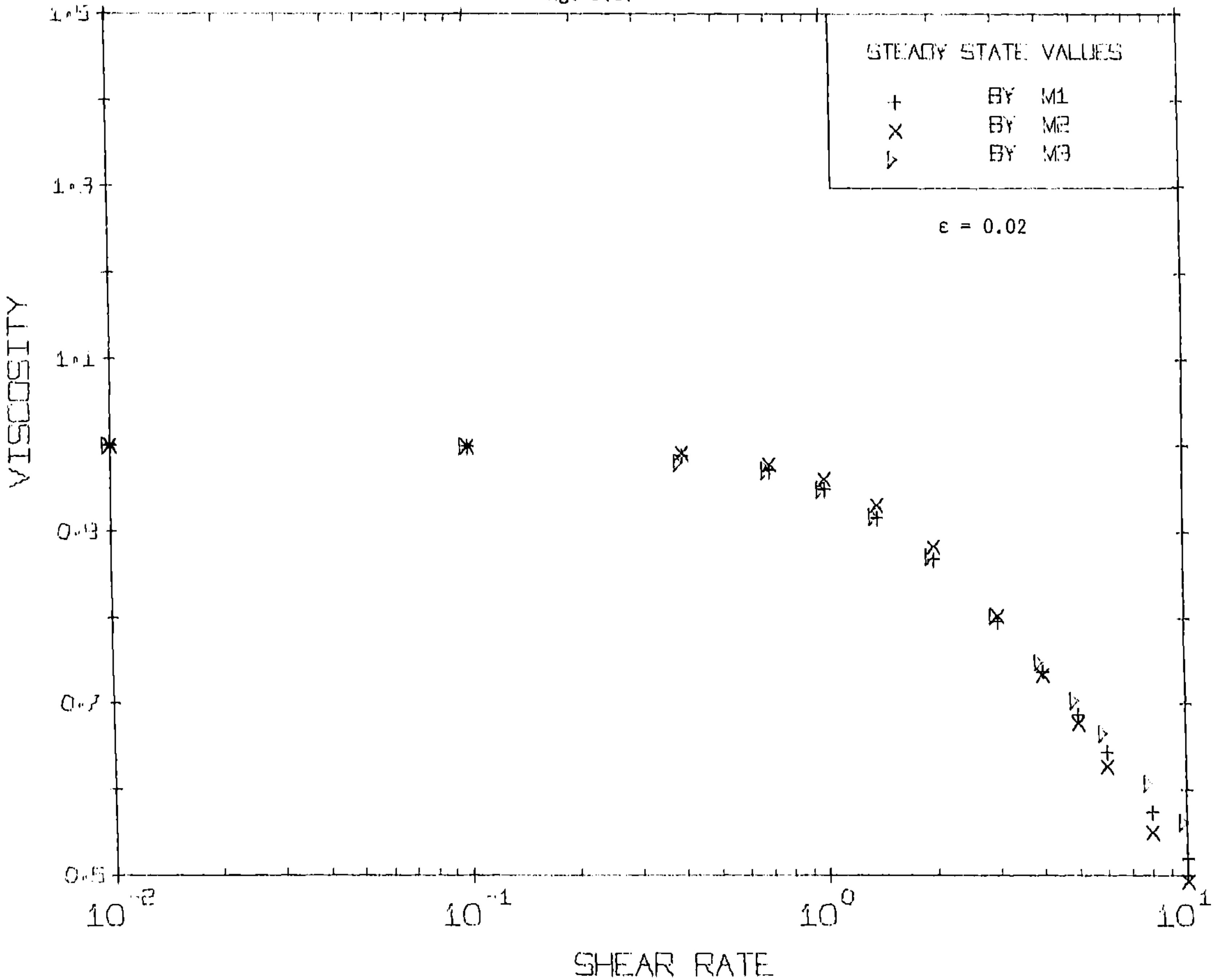
STEADY STATE VALUES
BY M1
BY M2
BY M3
ε = 0.02
VISCOSITY
SHEAR RATE
1.5
1.3
1.1
0.9
0.7
0.5
10^{-2}
10^{-1}
10^{0}
10^{1}

Fig. 5.38

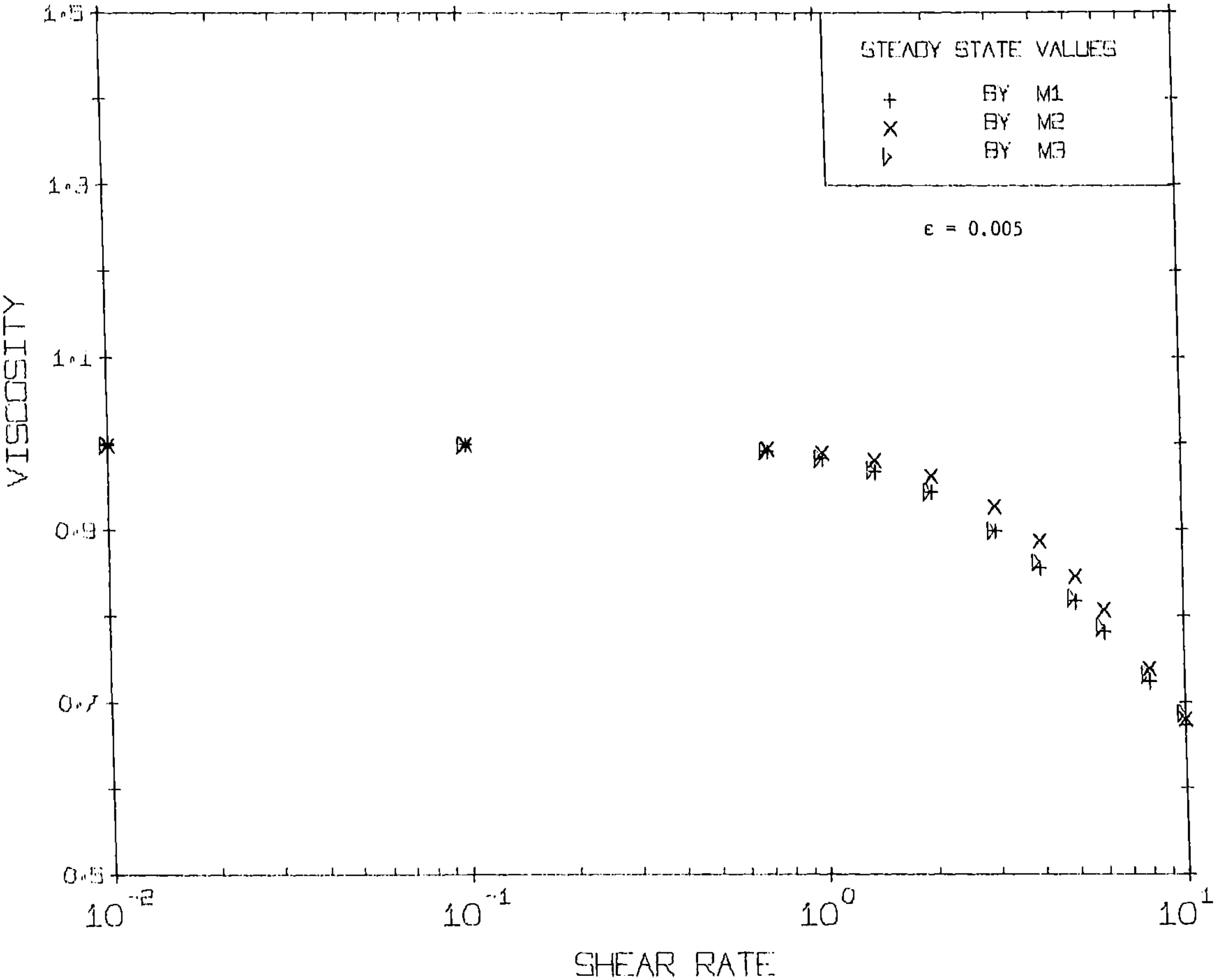

STEADY STATE VALUES
BY M1
BY M2
BY M3
ε = 0.005
VISCOSITY
SHEAR RATE
1.5
1.3
1.1
0.9
0.7
0.5
10^{-2}
10^{-1}
10^{0}
10^{1}

Fig. 5.39

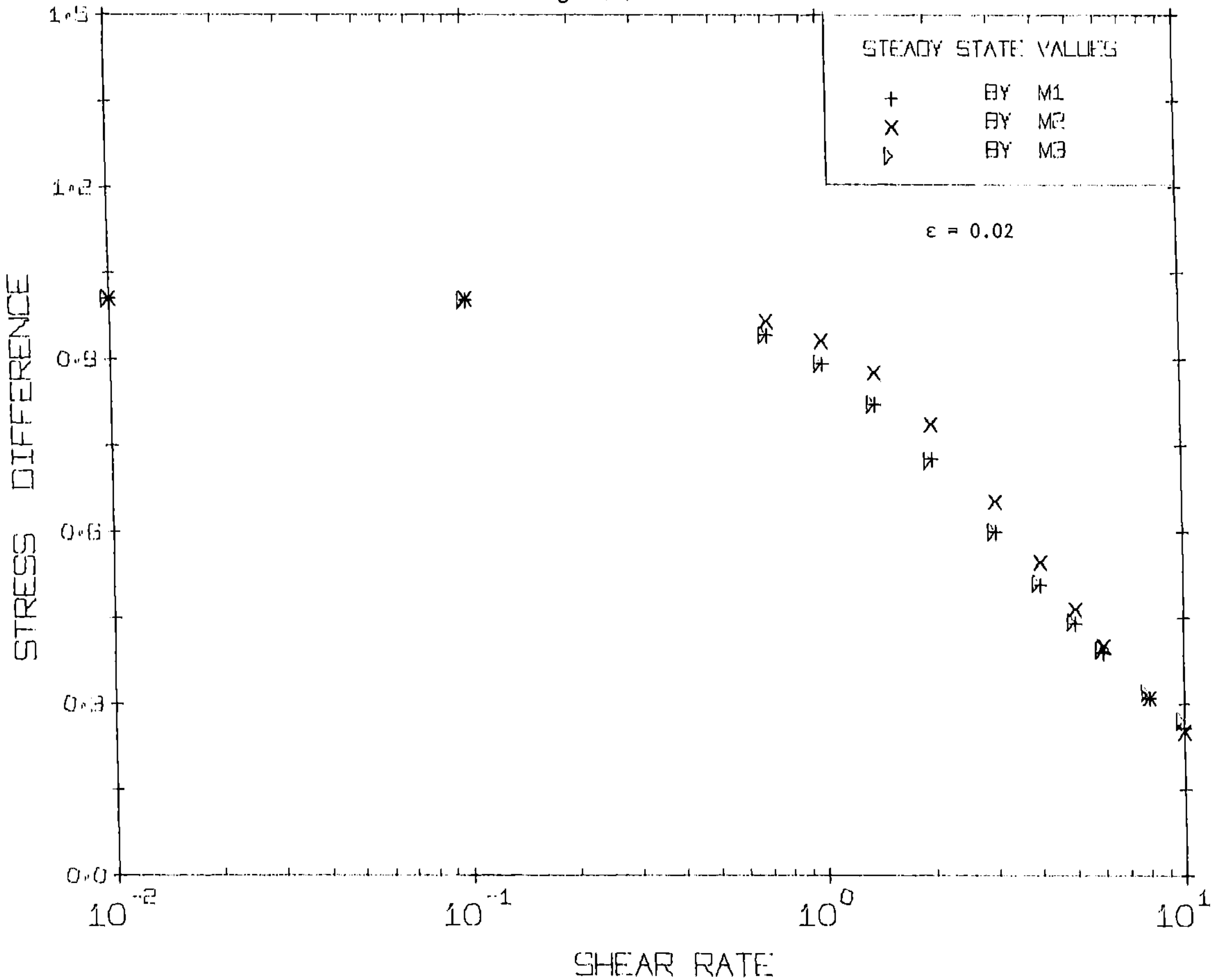
STEADY STATE VALUES
+ BY M1
X BY M2
▷ BY M3
ε = 0.02
1.5
1.2
0.9
0.6
0.3
0.0
STRESS DIFFERENCE
10^{-2}
10^{-1}
10^{0}
10^{1}
SHEAR RATE

Fig. 5.40

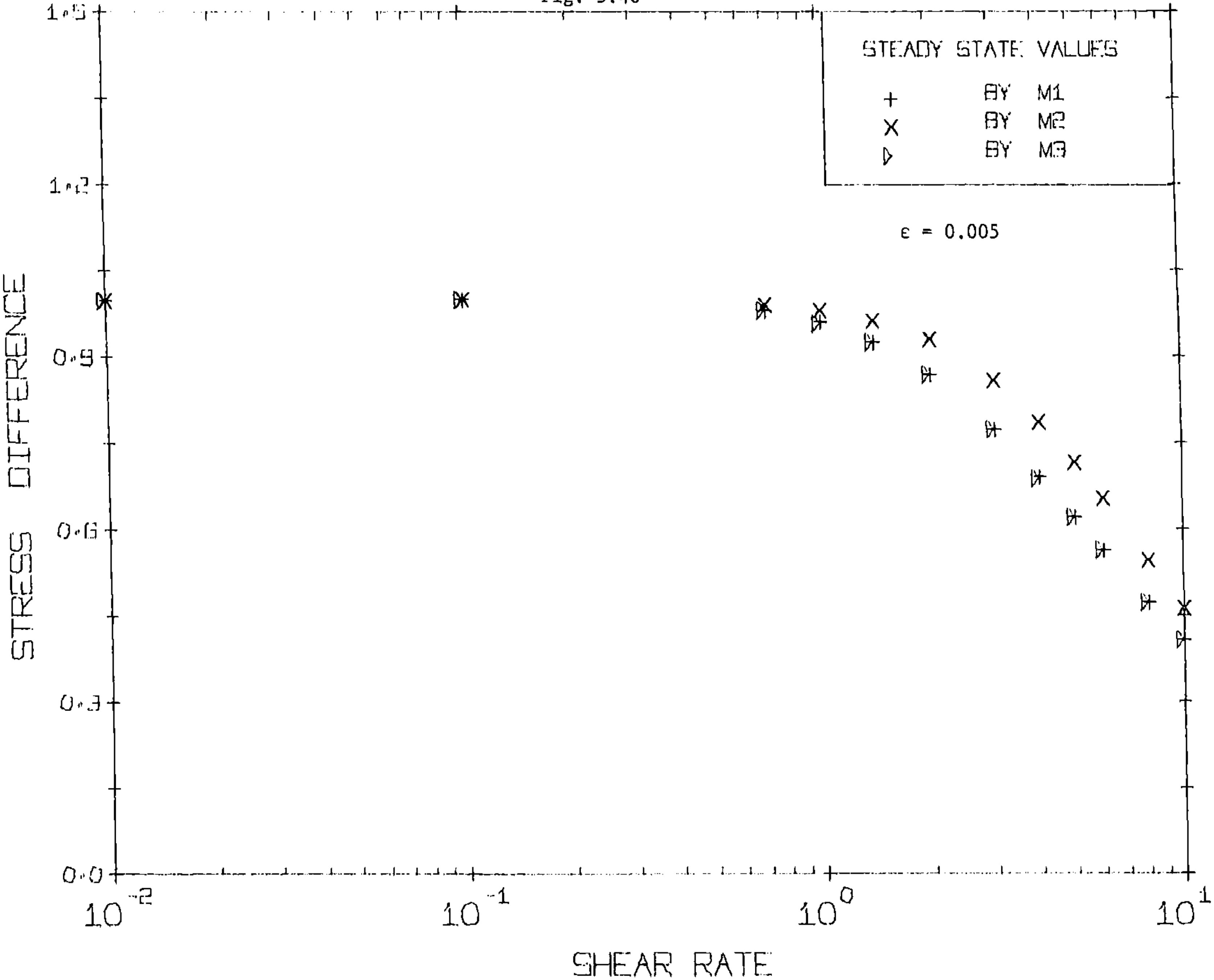

STEADY STATE VALUES
BY M1
BY M2
BY M3
ε = 0.005
STRESS DIFFERENCE
SHEAR RATE
1.5
1.2
0.9
0.6
0.3
0.0
10^-2
10^-1
10^0
10^1

5.3.2 Elongational Flow

The stress growth of elongational viscosity $\bar{\eta}^{+}$ is calculated by using the models. The elongational flow is described by

$$\left.\begin{aligned} \dot{\underline{\underline{\gamma}}} &= \begin{bmatrix} -1 & 0 & 0 \\ 0 & -1 & 0 \\ 0 & 0 & 2 \end{bmatrix} \dot{\varepsilon} \qquad && \text{for } t > 0 \\ \dot{\underline{\underline{\gamma}}} &= 0 && \text{for } t \leq 0 \end{aligned}\right\} \qquad 5.24$$

where $\dot{\varepsilon}$ is called elongational rate. The elongational viscosity is defined as $\bar{\eta} = (\tau_{yy} - \tau_{zz})/\dot{\varepsilon}$. The results of calcluation are shown in Fig. 5.41 to Fig. 5.46. It is found from these figures the three models behave similarly at low elongational rates (S = .01, S = .1).

Since macromolecules are in an almost equilibrium at this low range of elongational rates, the Brownian motion ($nkT\underline{\underline{\delta}}$) of the beads and spring force ($<\underline{R}\ \underline{F}^{(c)}>$) of the connector are two dominant contributions to stress tensor $\underline{\underline{\tau}}_p$ and these two forces are conterbalanced. No hydrodynamic force obviously is important in such low elongational rates. No matter what kind of distribution function is used, namely δ - function for M2 and perturbed solution of the diffusion equation ($\psi = \psi_o + \varepsilon\psi_1$ in eq. 5.11) for M3 (Armstrong, 1979), the results of calculation shows that there is no difference between M2 and M3.

However, once the hydrodynamic force becomes significant

Fig 5.41 to Fig. 5.46

THE STRESS GROWTH BEHAVIOR

FOR ELONGATIONAL FLOW

M1	Modified Nearly Hookean Dumbbell	eq. 5.22
M2	Tanner's model	eq. 5.9
M3	Nearly Hookean Dumbbell	eq. 5.19

E1 $\varepsilon = .02$

E2 $\varepsilon = .005$

VISCOSITY normalized elongational viscosity

$(\bar{\eta}^{+} - 3\eta_s)/3(\eta_o - \eta_s)$

η_o: viscosity at zero shear rate

DIMENSIONLESS TIME t/λ_H

S dimensionless elongational rate $\lambda_H\dot{\varepsilon}$

Fig. 5.41

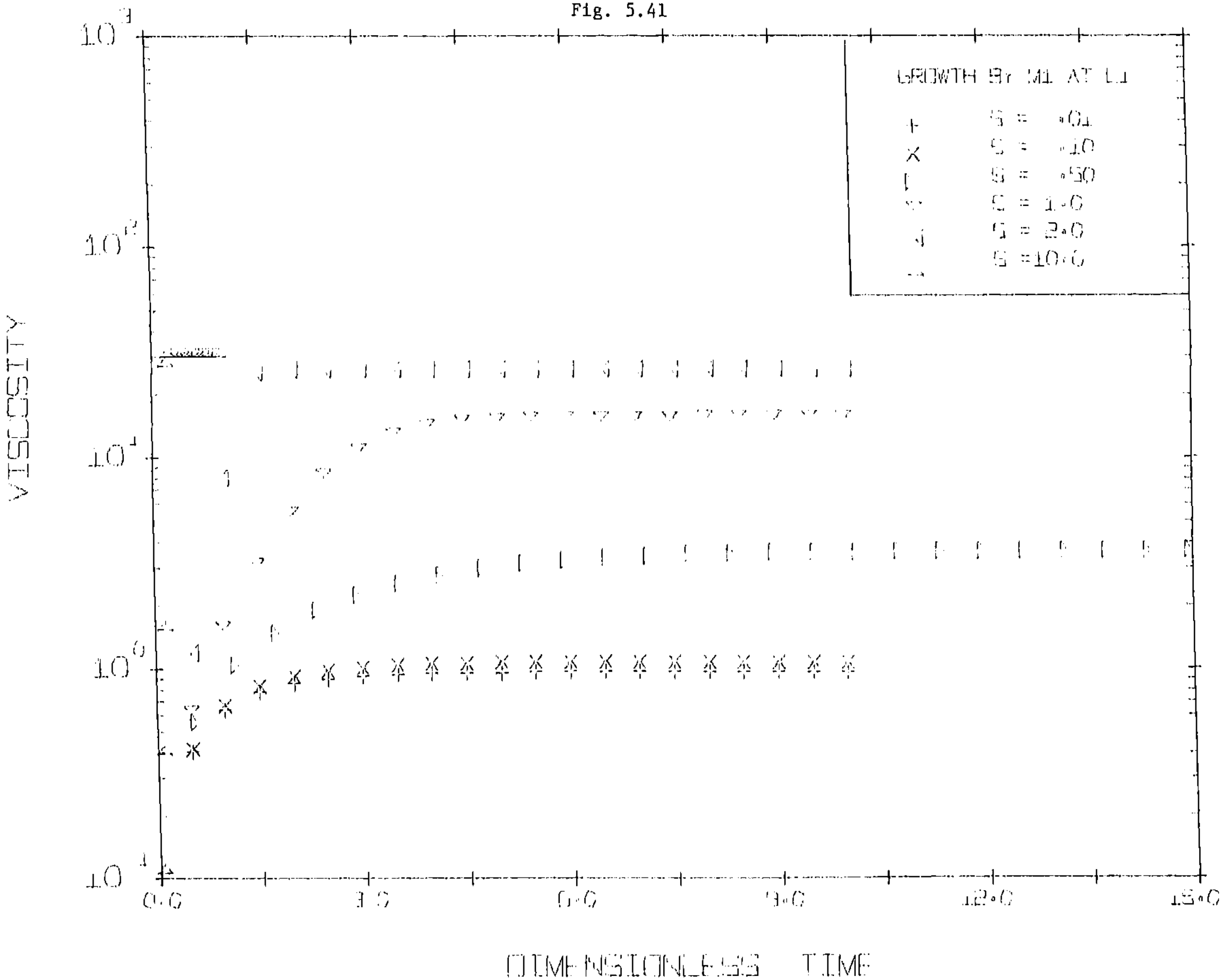
GROWTH BY M1 AT L1
S = .01
S = .10
S = .50
S = 1.0
S = 2.0
S = 10.0
VISCOSITY
DIMENSIONLESS TIME
0.0
3.0
6.0
9.0
12.0
15.0

Fig. 5.42

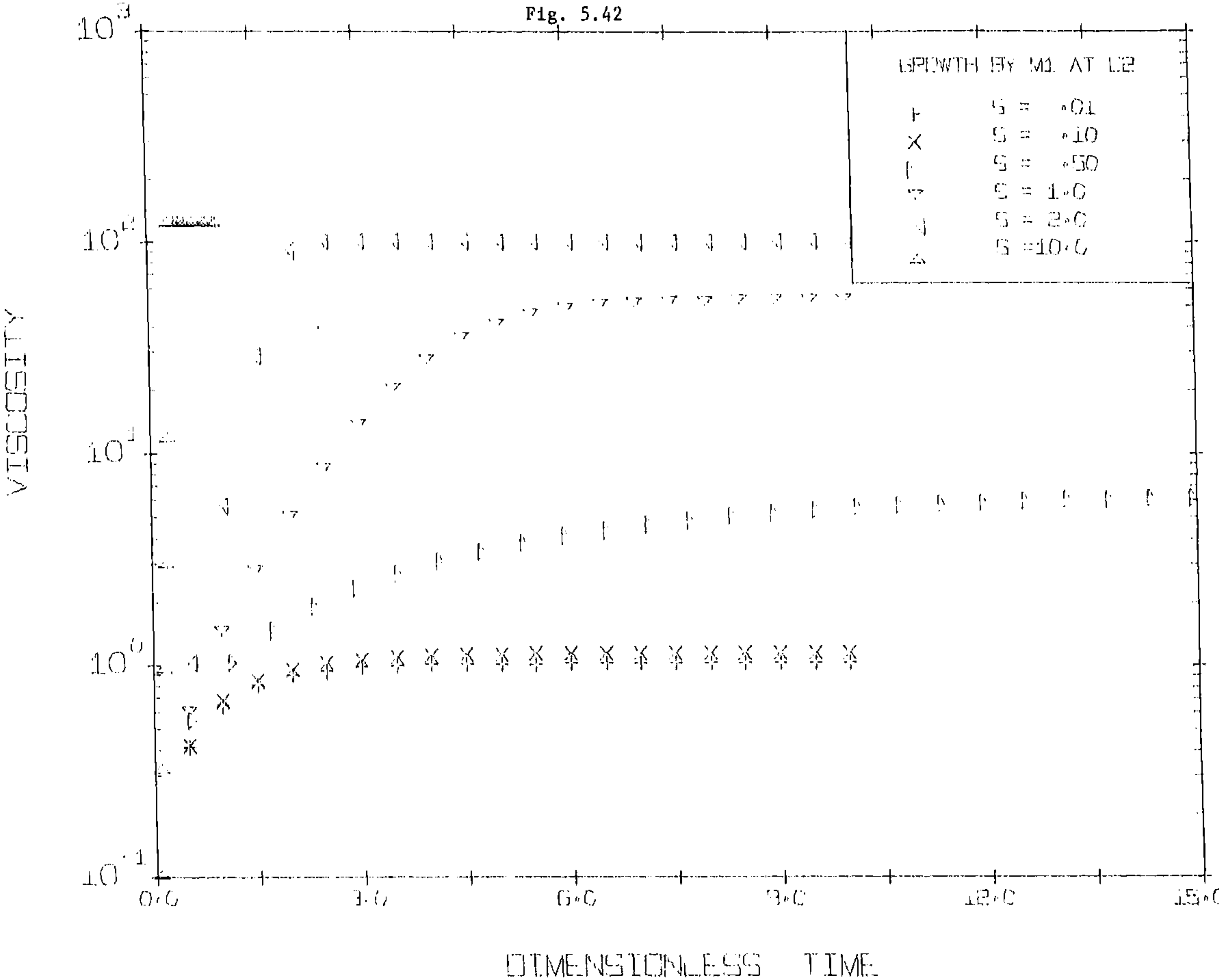
GROWTH BY M1 AT L2
S = .01
S = .10
S = .50
S = 1.0
S = 2.0
S =10.0
VISCOSITY
DIMENSIONLESS TIME
0.0
3.0
6.0
9.0
12.0
15.0

Fig. 5.43

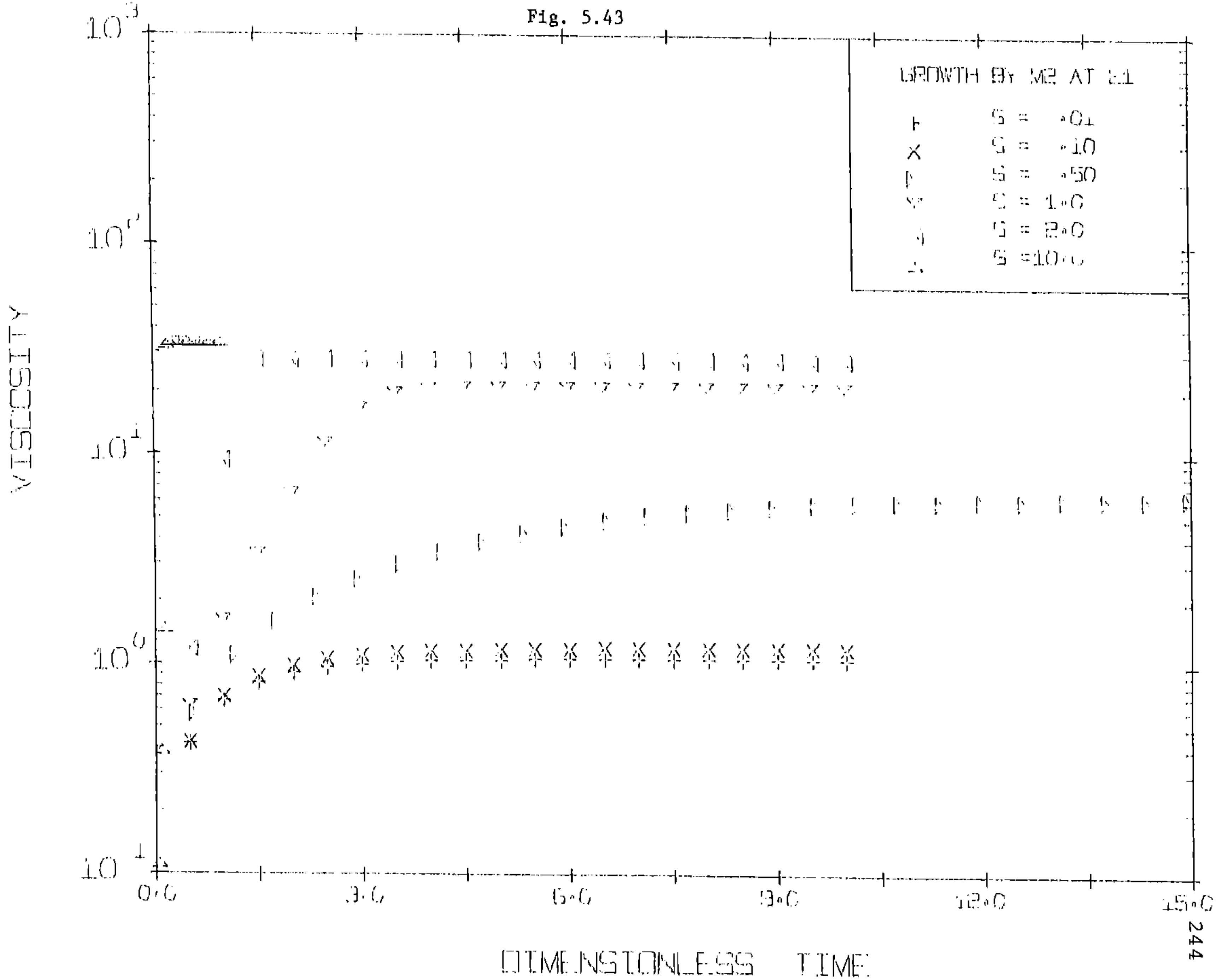
GROWTH BY M2 AT 1.1
S = .01
S = .10
S = .50
S = 1.0
S = 2.0
S =10.0
VISCOSITY
DIMENSIONLESS TIME
0.0
3.0
6.0
9.0
12.0
15.0

Fig. 5.44

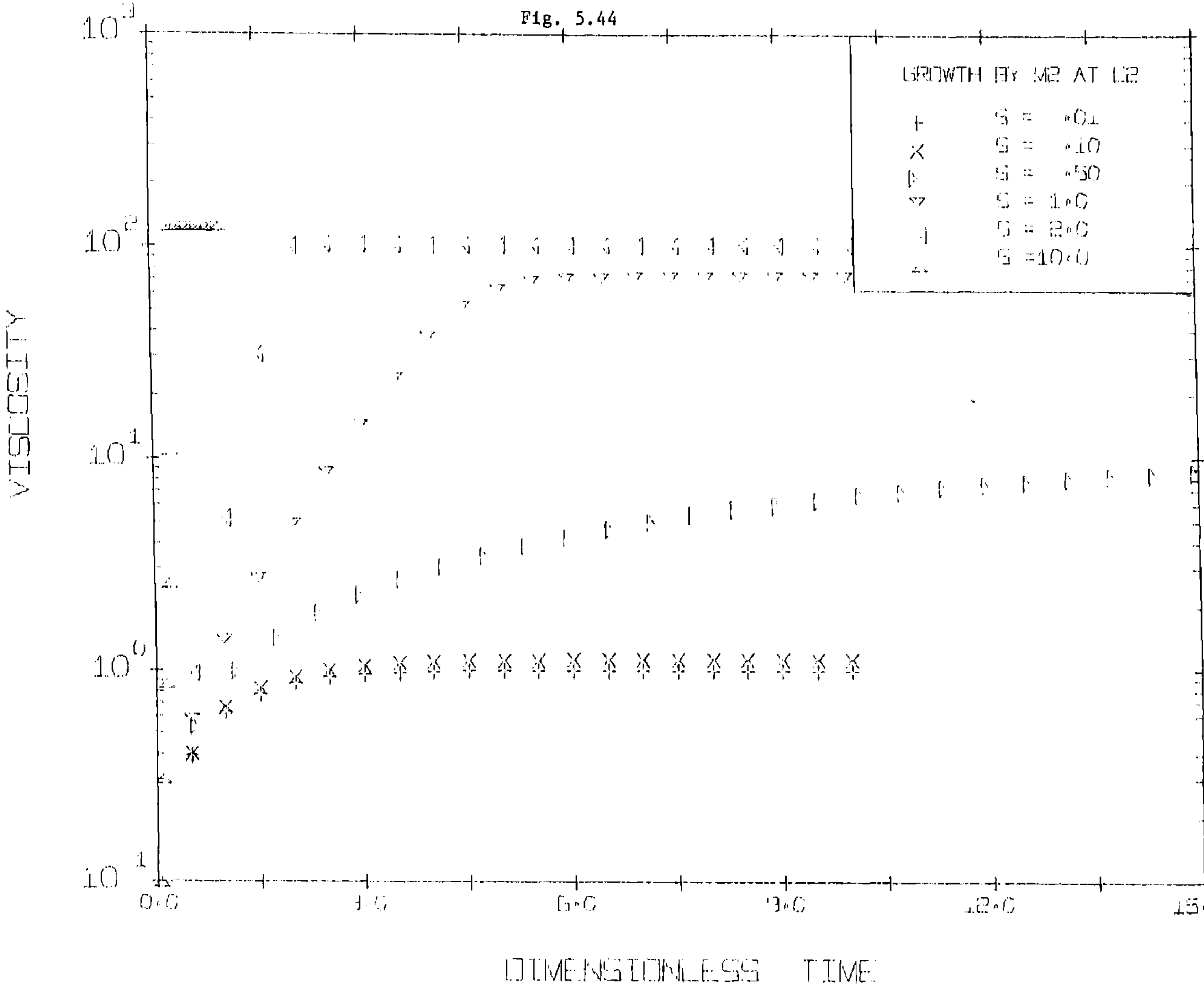
GROWTH BY M2 AT L2
S = .01
S = .10
S = .50
S = 1.0
S = 2.0
S =10.0
VISCOSITY
DIMENSIONLESS TIME
0.0
3.0
6.0
9.0
12.0
15.0

Fig. 5.45

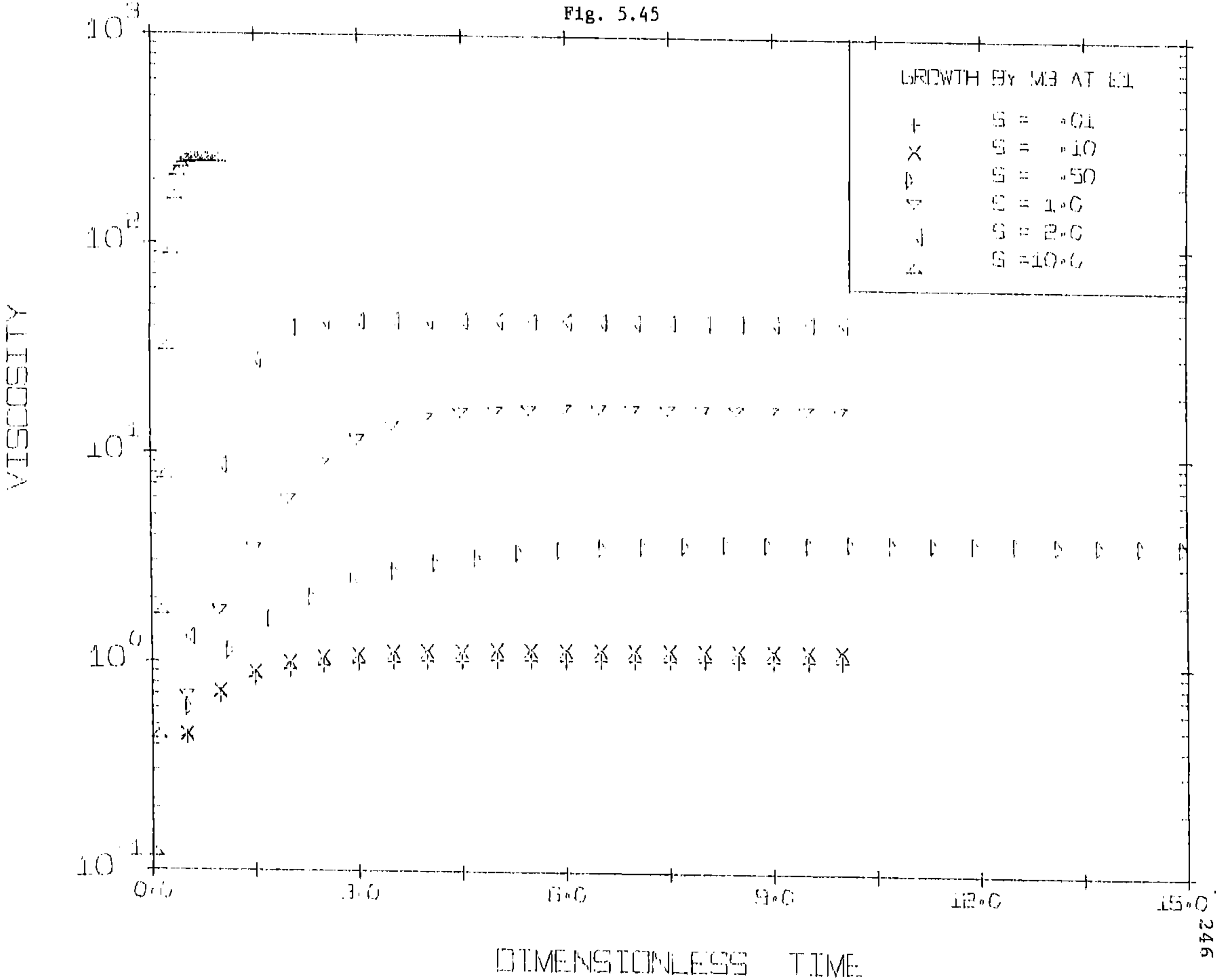

GROWTH BY M3 AT E1
S = .01
S = .10
S = .50
S = 1.0
S = 2.0
S = 10.0
VISCOSITY
DIMENSIONLESS TIME

Fig. 5.44

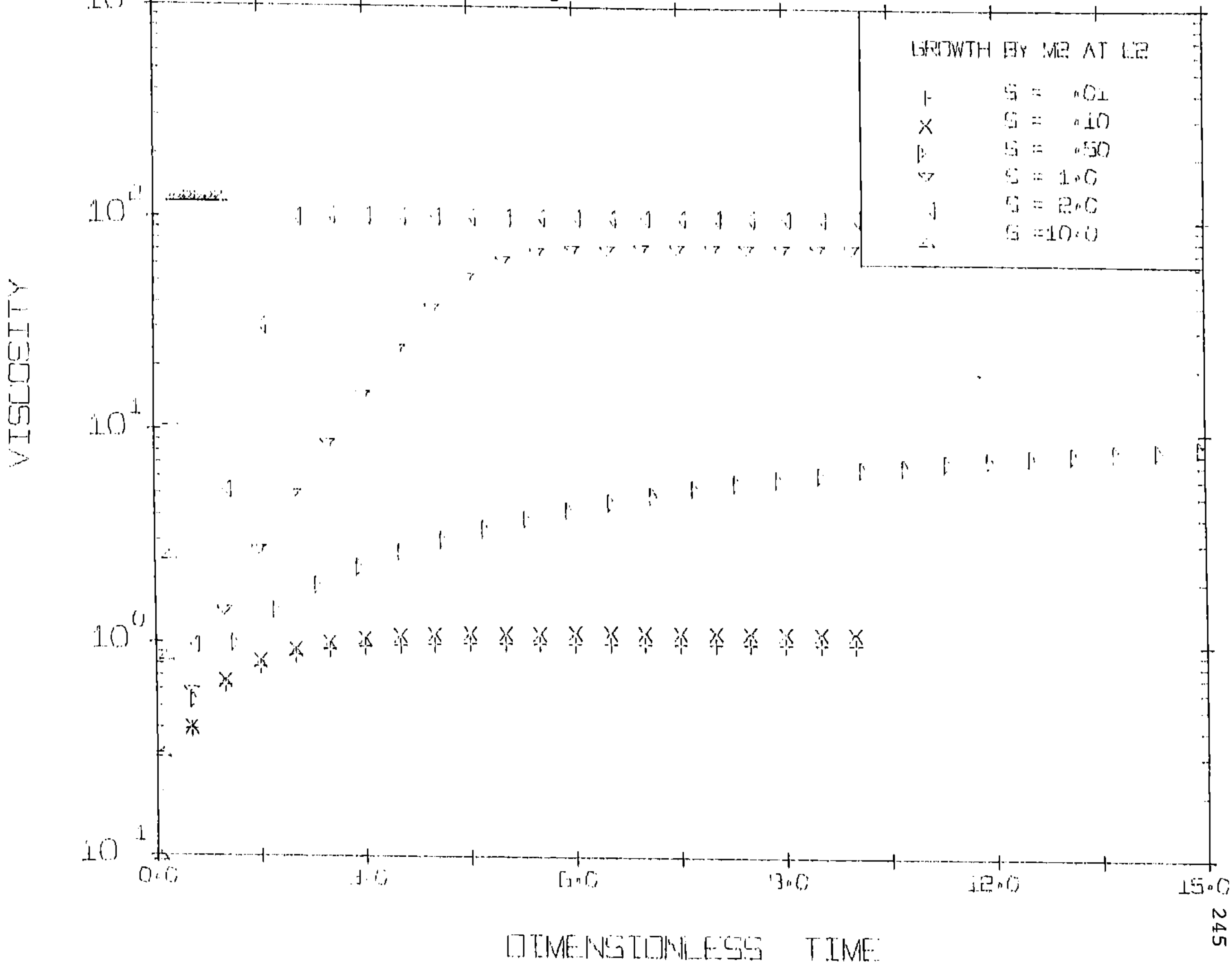

GROWTH BY M2 AT C2
S = .01
S = .10
S = .50
S = 1.0
S = 2.0
S =10.0
VISCOSITY
DIMENSIONLESS TIME
0.0
6.0
9.0
12.0
15.0

Fig. 5.45

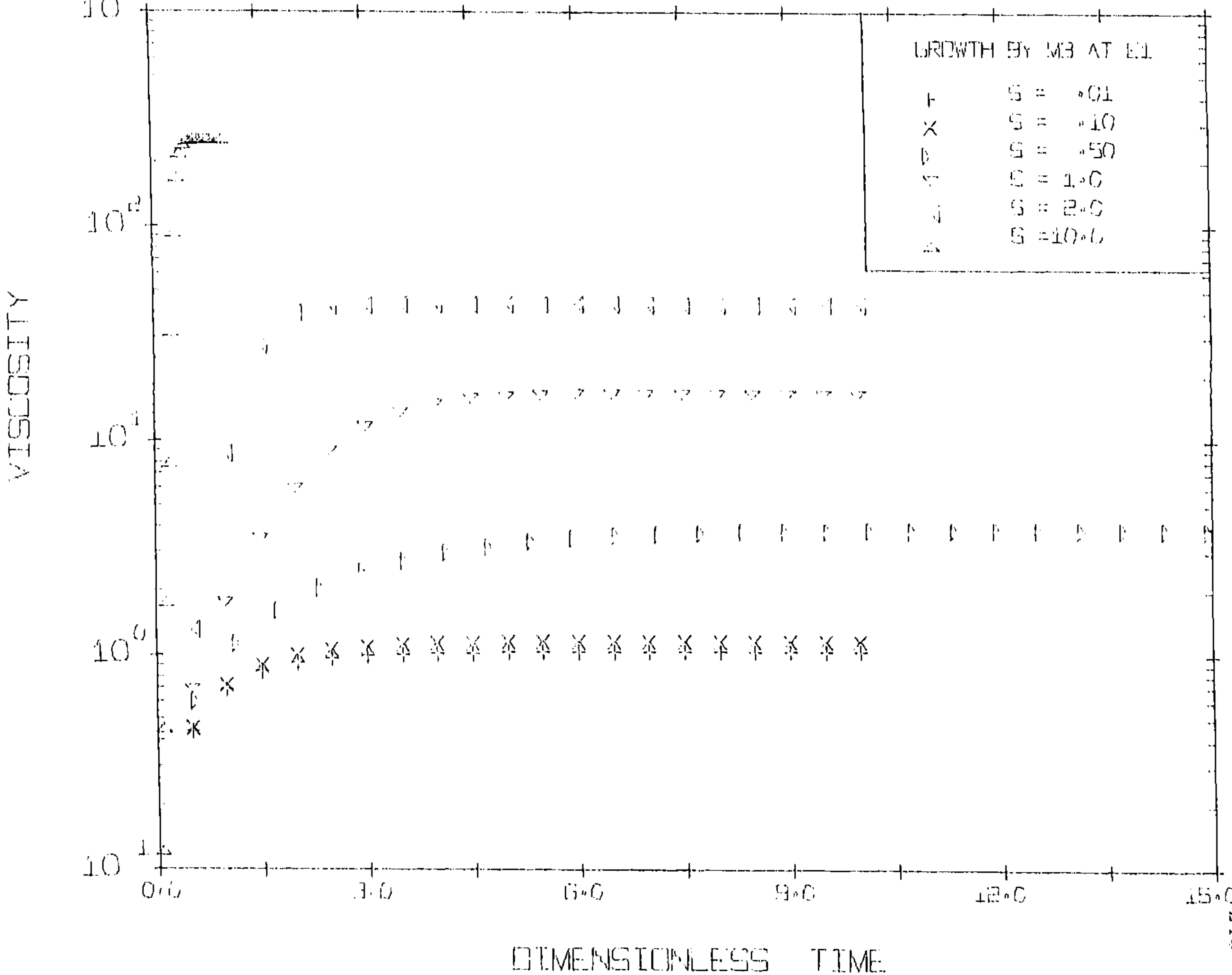
GROWTH BY MB AT E1
S = .01
S = .10
S = .50
S = 1.0
S = 2.0
S = 10.0
VISCOSITY
DIMENSIONLESS TIME
0.0
3.0
6.0
9.0
12.0
15.0

Fig. 5.46

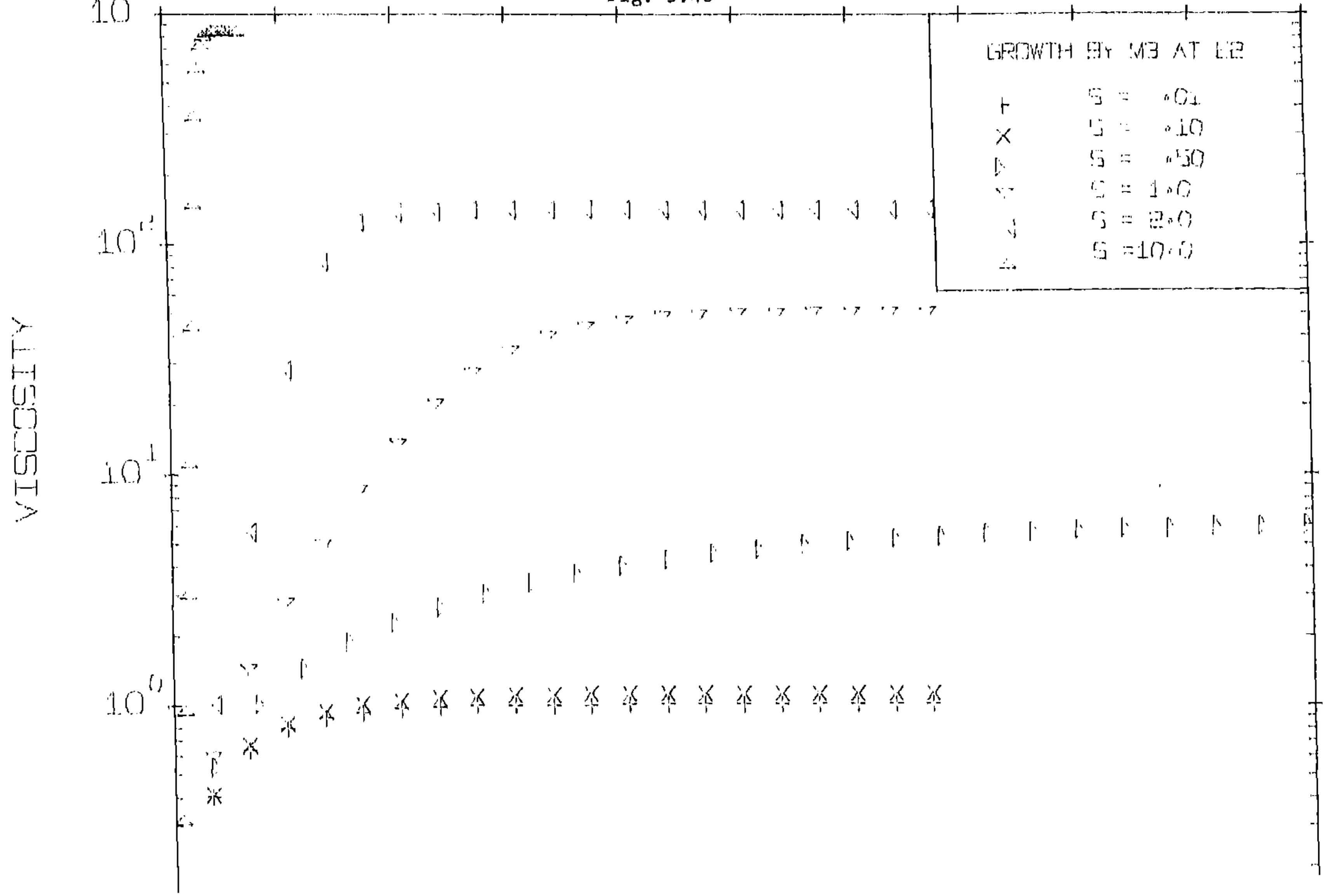

VISCOSITY
10^3
10^2
10^1
10^0
GROWTH BY M3 AT E2
S = .01
S = .10
S = .50
S = 1.0
S = 2.0
S =10.0

at intermediate elongational rates ($S = .5$, $S = 1.0$), M2 shows difference from M1 and M3. And M1 and M2 give almost the same results while the results of M3 deviate from them at high elongational rates ($S = 2.0$, $S = 10.$). These tendencies of the three models at both intermediate and high elongational rates can be expected from the previous section where M1 was derived. The qualitative behavior of the three models are explained more explicitly by the results of steady state elongational viscosity.

The steady state elongational viscosity at various elongational rates is calculated and plotted in Fig. 5.47 and Fig. 5.48. Up to $S = .3$ the three models give quite similar results and from $S = .3$ M2 starts deviating from M1 and M3, while M1 and M2 give almost equal results up to $S = 1.0$. Then M2 curve gets close to M1 curve and finally they become identical and bounded at high elongational rates. M3 is still increasing and may go to infinite when the elongational rate is further increased. As expected, M1 matches M2 and have the same asymptotic value at high elongational rate. M2 gives higher results than that of M1 in the range $S = .3 \sim 1$. As in Fig. 5.47 the asymptotic value given by M1 and M3 goes up 100. The rapid increase of elongational viscosity observed at the moderate elongational rate corresponds the nearly full extension of the macromolecules which, then, show high resistance to be stretched out above those elongational rates.

Fig. 5.47 to Fig. 5.48

THE STEADY STATE VALUES

OF ELONGATIONAL VISCOSITY

The following notation is used:

M1	Modified Nearly Hookean Dumbbell	eq. 5.22
M2	Tanner's model	eq. 5.9
M3	Nearly Hookean Dumbbell	eq. 5.19

E1	$\varepsilon = .02$
E2	$\varepsilon = .005$

VISCOSITY	normalized elongational viscosity
	$(\bar{\eta} - 3\eta_S)/3(\eta_o - \eta_S)$
ELONGATIONAL RATE	$\lambda_H \dot{\varepsilon}$

Fig. 5.47

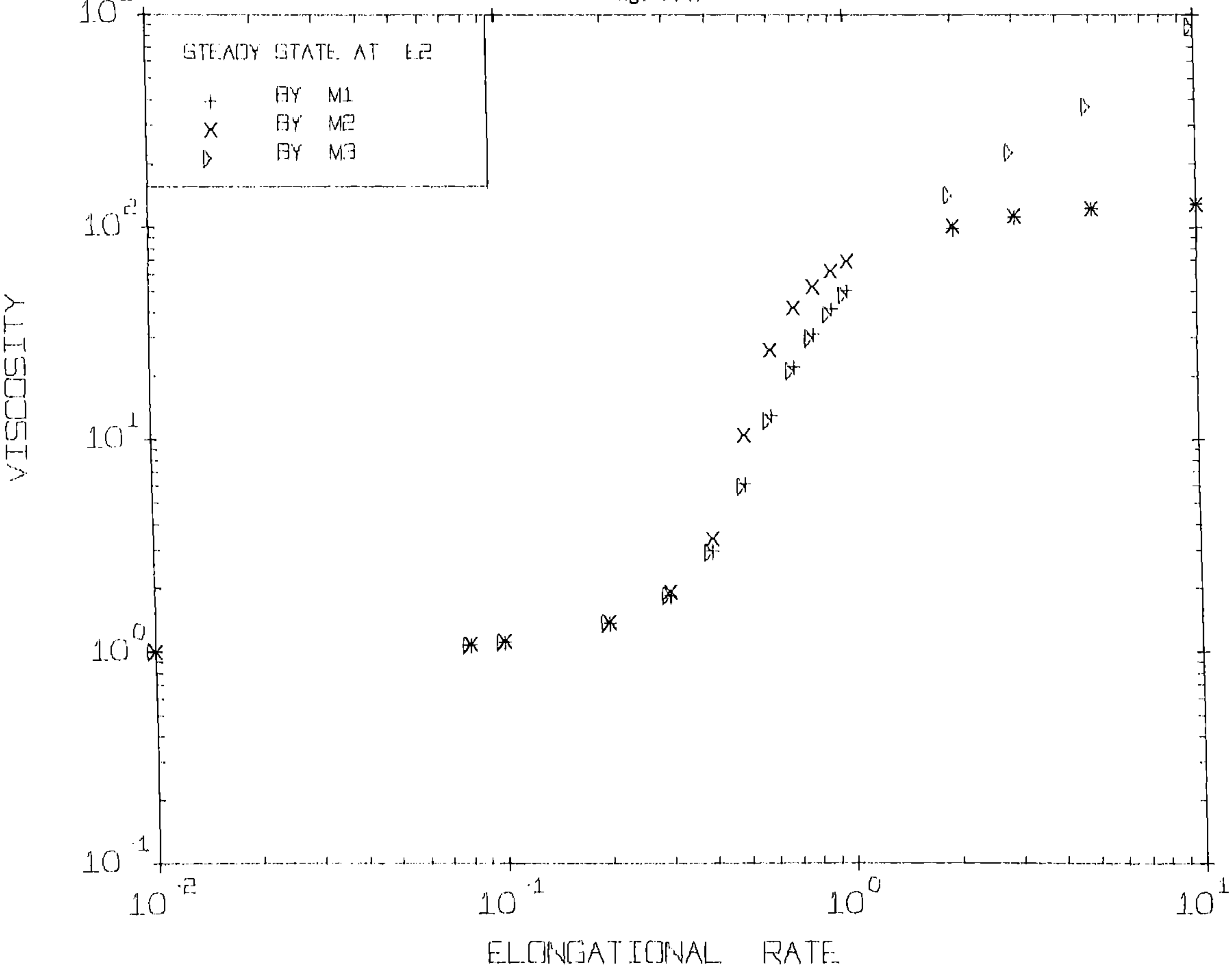

STEADY STATE AT E2
BY M1
BY M2
BY M3
VISCOSITY
ELONGATIONAL RATE
10^{3}
10^{2}
10^{1}
10^{0}
10^{-1}
10^{-2}
10^{-1}
10^{0}
10^{1}

Fig. 5.48

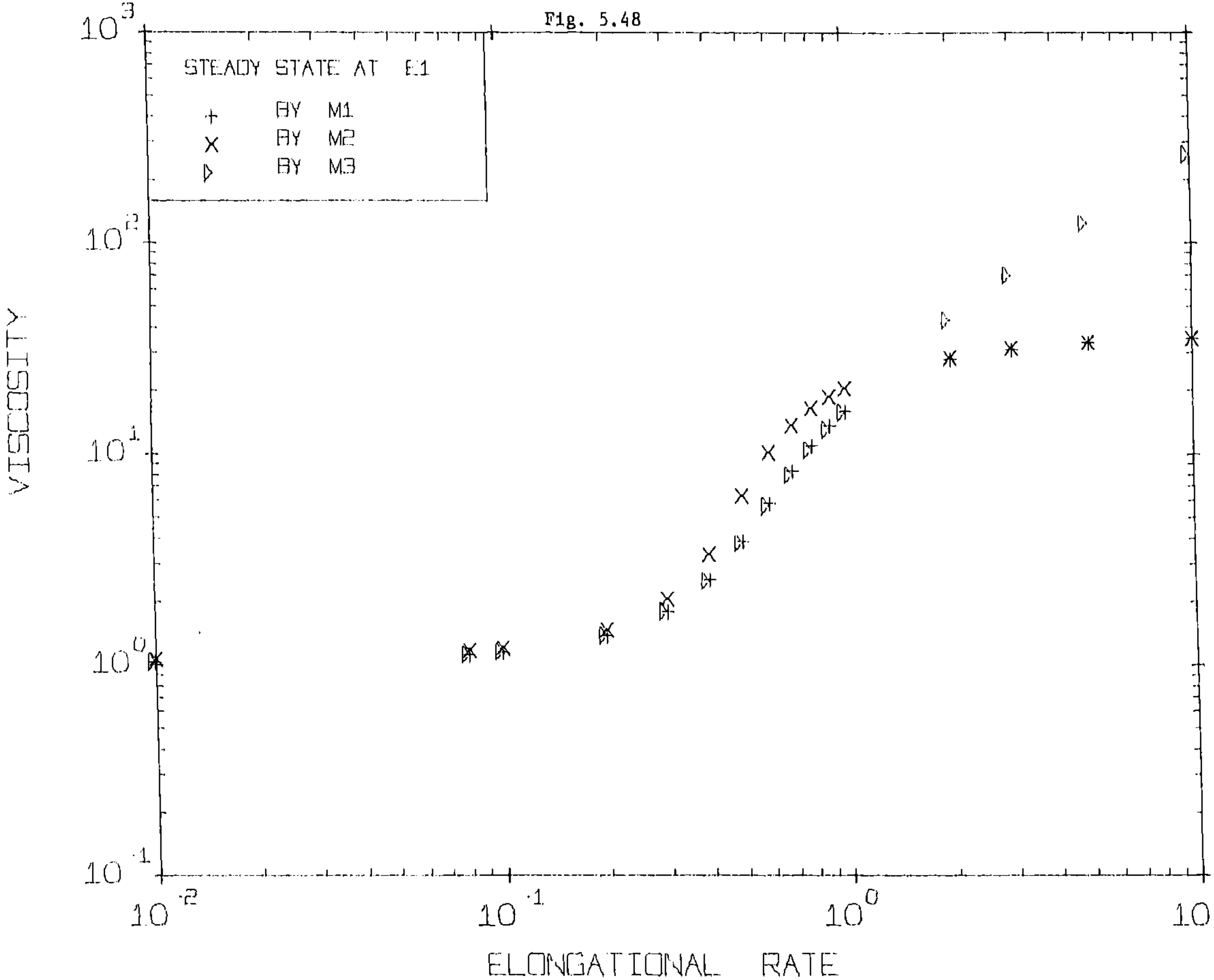
STEADY STATE AT E1
BY M1
BY M2
BY M3
VISCOSITY
ELONGATIONAL RATE
10^{3}
10^{2}
10^{1}
10^{0}
10^{-1}
10^{-2}
10^{-1}
10^{0}
10^{1}

Fig. 5.49 and Fig. 5.50 show the comparison between the exact solution of FENE model, M1 and M2. The elongational viscosity given by FENE model (Bird, et al., 1977) is

$$\bar{\eta}=3\eta_S + \frac{n\zeta}{4}\frac{\int_0^{\frac{\pi}{2}}\int_0^{R_o} R^2 \ (\frac{1}{2}\sin^2\theta + 2\cos^2\theta)\Psi'eq.\phi'_{fl} \ R^2 dR \sin\Theta \ d\Theta}{\int_0^{\frac{\pi}{2}}\int_0^{R_o} \Psi'eq.\phi'_{fe} \ dR \sin\Theta \ d\Theta} \qquad 5.25$$

where

$$\psi'eq. = [1 - (\frac{R}{R_o})^2]^{\frac{1}{2\varepsilon}} \qquad 5.26$$

$$\phi'_{fe} = \exp\ [-\frac{1}{2\varepsilon}\ (\frac{R}{R_o})^2\ (1 - 3\cos^2\theta)\lambda_H\dot{\varepsilon}] \qquad 5.27$$

Eq. 5.25 with eq. 5.26 and eq. 5.27 was numerically integrated over the configuration space in order to obtain Fig. 5.49 and Fig. 5.50. At $\varepsilon = .02$ (Fig. 5.49), M1 represents the FENE model well especially at moderately high elongational rates. On the other hand, M2 overestimates the FENE model at those rates. The three models eventually approach the same asymptotic elongational viscosity at high elongational rates. M2 turns out, however, to be closer to the FENE results when $\varepsilon = .005$ (Fig. 5.50), at range $S = .7$ to $S = 1.0$. This indicates that the macromolecules are oriented to a fix direction with smaller elongational rates when they are more flexible. By judging from Fig. 5.49 and Fig. 5.50, the Modified Nearly Hookean Dumbbell (M1) seems to be suitable for vortex inhibition analysis because it predicts the elongational viscosity well when it is compared with the FENE model's prediction. The FENE model is known experimentally to describe intrinsic viscosity for some dilute polymer solution (Christiansen and Bird, 1977/1978).

As mentioned repeatedly so far, one of the very important part of the vortex inhibition study is to find a constitutive equation (approximate if necessary) which can describe the elongational viscosity reasonably well. The use of MNHD, thus, may give reasonable information about the stress field in chapter 6 because first, it has a very simple form so that any kind of locally homogeneous flow can be applied, and, secondly, the elongational viscosity predicted by the model is as good as for the FENE model.

Fig. 5.49 and Fig. 5.50

THE COMPARISON BETWEEN M1, M2 AND FENE MODEL

The following notation is used:

M1	Modified Nearly Hookean Dumbbell	eq. 5.22
M2	Tanner's Model	eq. 5.9
FENE	FENE Model	eq. 5.25

E1 $\varepsilon = .02$

E2 $\varepsilon = .005$

VISCOSITY $(\bar{\eta}-3\eta_s)/3(\eta_o-\eta_s)$

ELONGATIONAL RATE $\lambda_H\dot{\varepsilon}$

Fig. 5.49

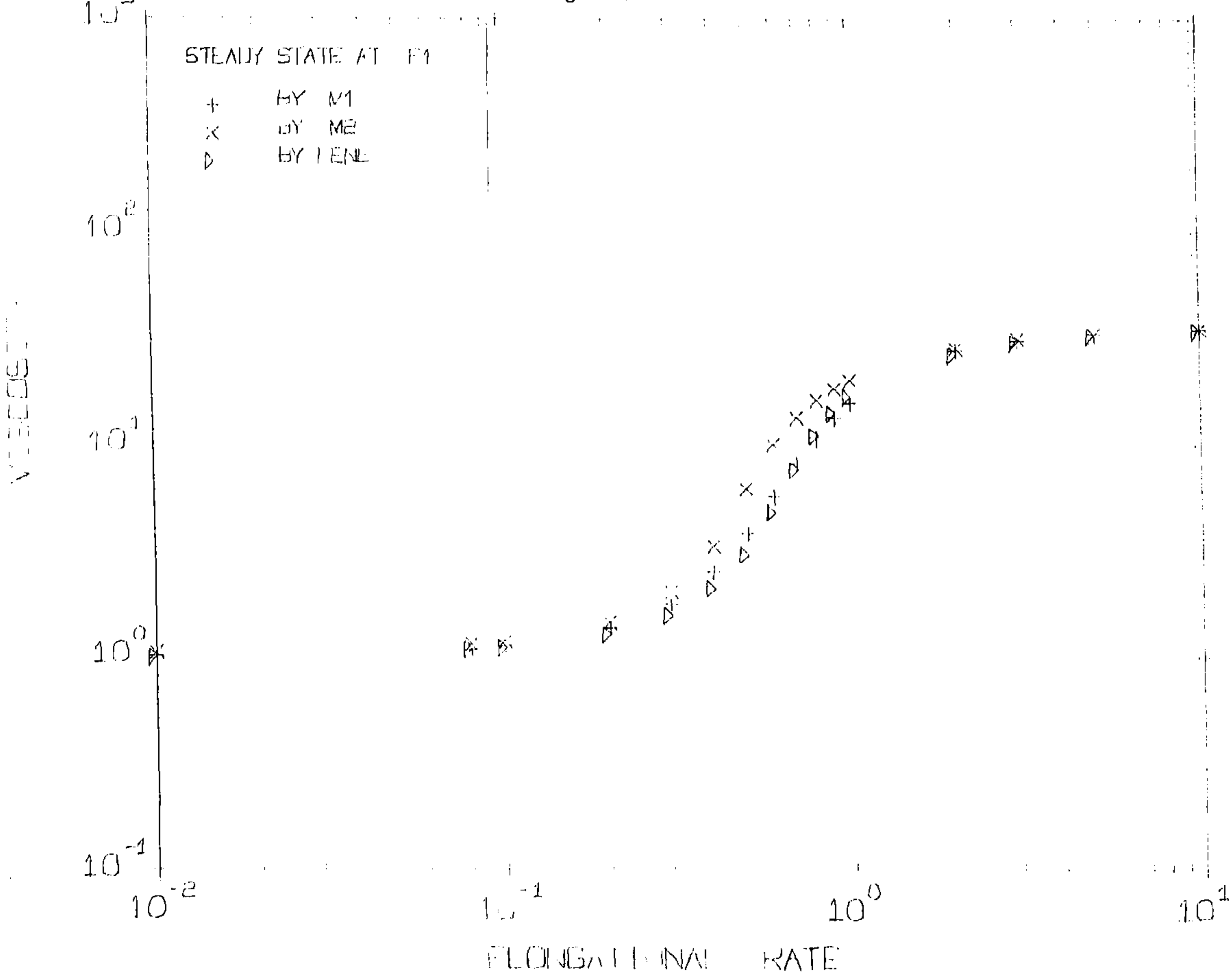

Fig. 5.50

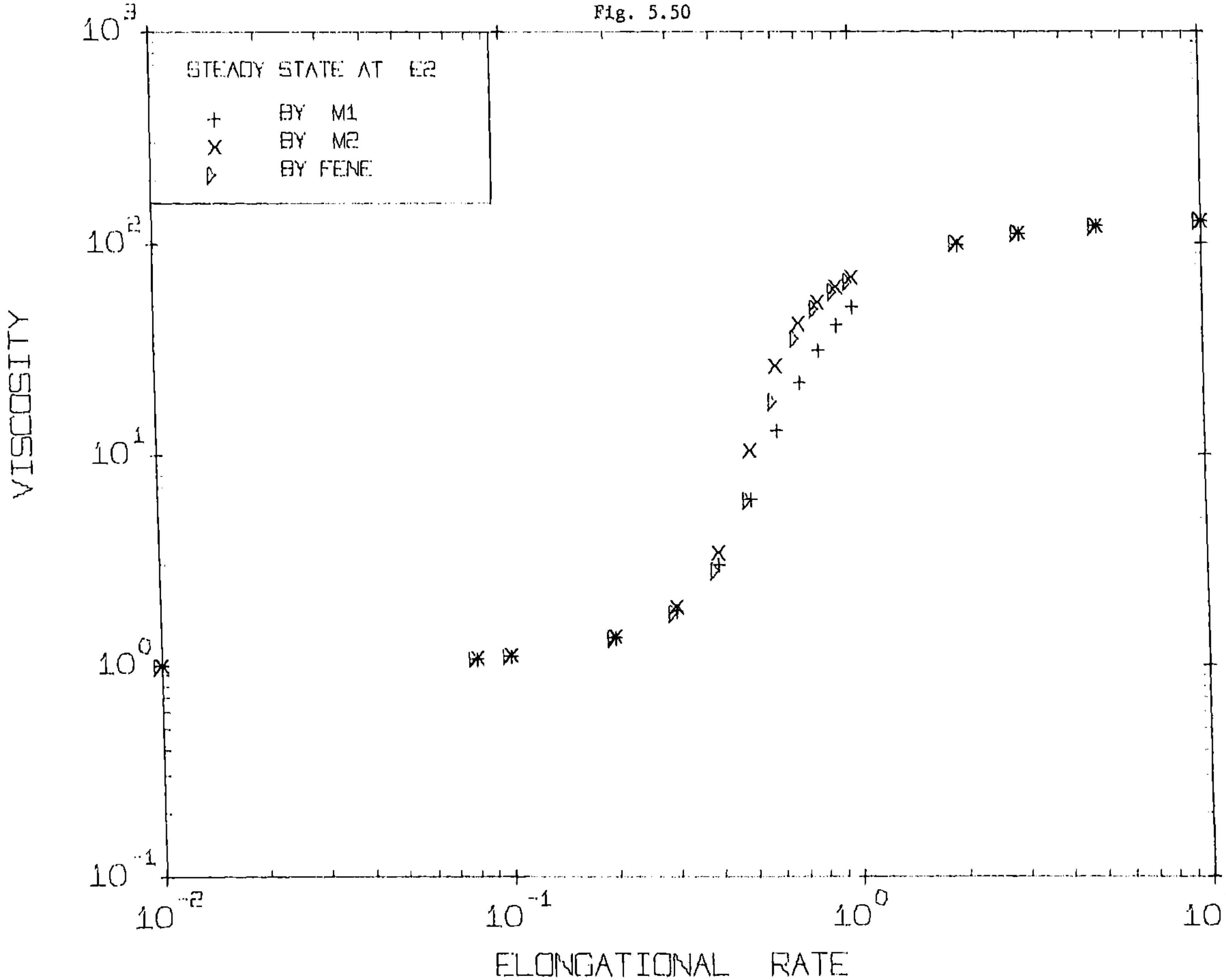

STEADY STATE AT E2
+ BY M1
X BY M2
▷ BY FENE
VISCOSITY
ELONGATIONAL RATE
10^{3}
10^{2}
10^{1}
10^{0}
10^{-1}
10^{-2}
10^{-1}
10^{0}
10^{1}

VI. THE ANALYSIS OF THE ONSET BEHAVIOR OF VORTEX INHIBITION

In this chapter, the mechanism of the onset behavior of vortex inhibition is analyzed by the following sequence. First, the Newtonian vortex flow is discussed by the results of the numerical calculation which is described in Chap. 3 with locally obtained experimental data. Secondly, a few remarks are added on the constitutive equation (the Modified Nearly Hookean Dumbbell) studied in Chap. 5 because the MNHD is used for calculating the polymer contribution to the stress tensor in polymer solution. Third, the experimental observation about the onset behavior of vortex inhibition is described. Two important characteristics are emphasized in the section. Fourth, the stress tensor for polymer solution is calculated along the stream lines by the MNHD. The velocity field used for the calculation is the Newtonian vortex flow. Finally, the polymer effect, namely how the flow behavior changes due to the resulting polymer stress tensor, is analyzed by an approximate method to explain the experimental findings qualitatively. A proposed mechanism of vortex inhibition is then briefly discussed.

6.1 The Velocity Field of Newtonian Vortex Flow

The velocity field of Newtonian vortex flow is calculated by the method described in Chap. 3 for higher tangantial Reynolds number Re_θ. The detailed calculation procedure, the complete program listings and full information about the velocity field in terms of Γ, v_r, v_z are found in Appendix A. The velocity component v_θ and v_z are locally measured as described in Chap. 4 and compared with those obtained by the numerical simulation.

The general flow behavior of a confined vortex flow is well described by stream lines. Fig. 6.1 and Fig. 6.2 show the results of the numerical calculation which describes the stream lines representing both the radial and axial velocities for lower and higher tangential Reynolds number respectively. Each fluid element also makes swirl motion due to the tangential velocity besides moving along the stream lines. As shown in Fig. 6.1, for $Re_\theta = 10$, most of fluid elements supplied at the outer wall move toward the exit hole in taking almost the shortest distance. No reverse (due to positive v_r) or up (due to positive v_z) flow is observed for such a low Re_θ . For higher Re_θ (= 1370.), however, the flow behavior turns out quite different. For example, taking the stream line $\psi = .8$ in Fig. 6.2, representing 80% of total flow rate, the fluid element initially moves toward the exit hole but after passing the point $(r,z) = (.1,.2)$, the fluid starts moving back and eventually goes

6.1 The Velocity Field of Newtonian Vortex Flow

The velocity field of Newtonian vortex flow is calculated by the method described in Chap. 3 for higher tangantial Reynolds number Re_θ. The detailed calculation procedure, the complete program listings and full information about the velocity field in terms of Γ, v_r, v_z are found in Appendix A. The velocity component v_θ and v_z are locally measured as described in Chap. 4 and compared with those obtained by the numerical simulation.

The general flow behavior of a confined vortex flow is well described by stream lines. Fig. 6.1 and Fig. 6.2 show the results of the numerical calculation which describes the stream lines representing both the radial and axial velocities for lower and higher tangential Reynolds number respectively. Each fluid element also makes swirl motion due to the tangential velocity besides moving along the stream lines. As shown in Fig. 6.1, for $Re_\theta = 10$, most of fluid elements supplied at the outer wall move toward the exit hole in taking almost the shortest distance. No reverse (due to positive v_r) or up (due to positive v_z) flow is observed for such a low Re_θ . For higher Re_θ (= 1370.), however, the flow behavior turns out quite different. For example, taking the stream line $\psi = .8$ in Fig. 6.2, representing 80% of total flow rate, the fluid element initially moves toward the exit hole but after passing the point (r,z) = (.1,.2), the fluid starts moving back and eventually goes

Fig. 6.1

Stream Lines for Low Reynolds Number $Re_\theta=10$, SS=-1

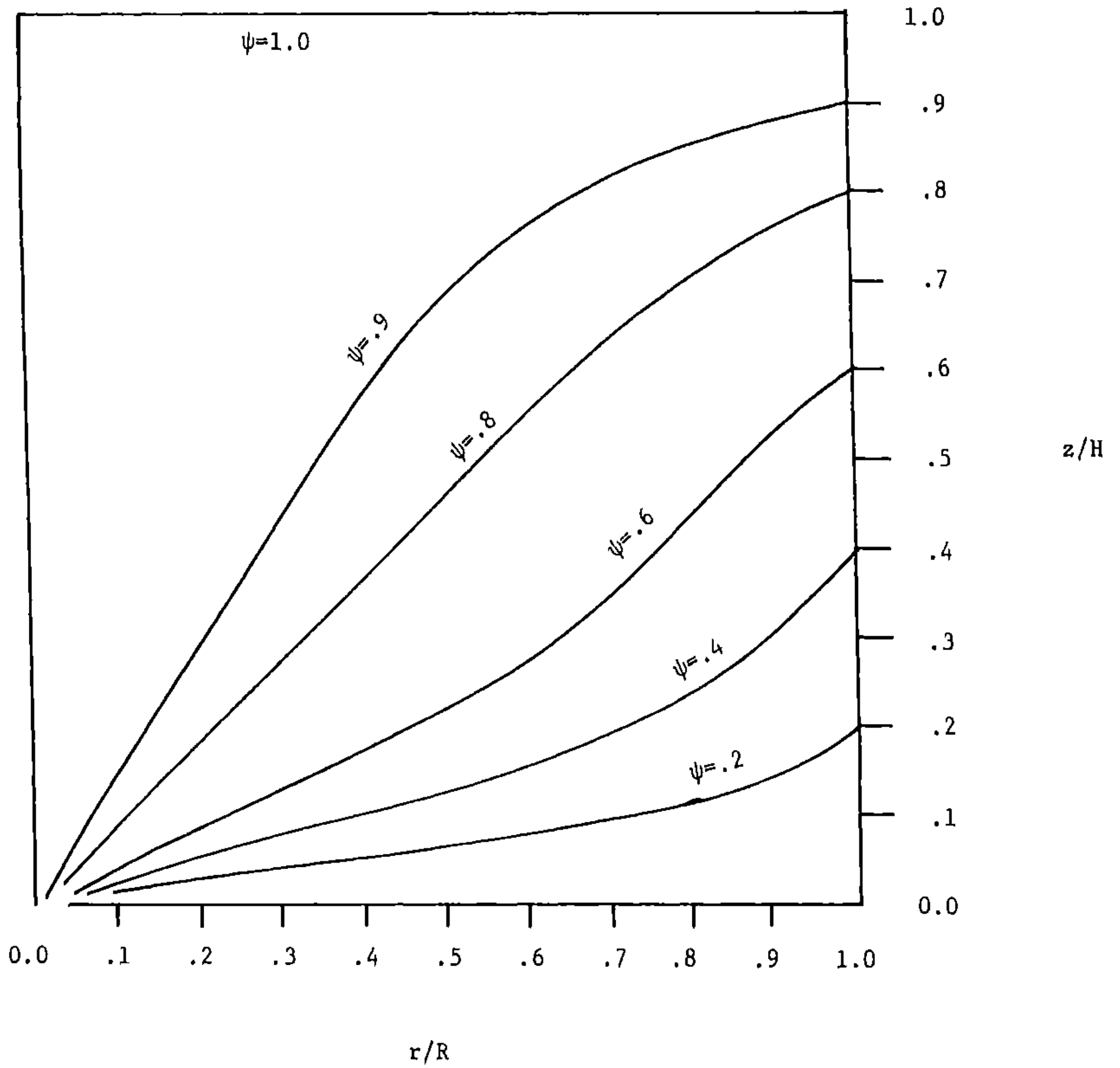

Fig. 6.2

Stream Lines for High Reynolds Number

Re_θ=1370 , SS=-.02

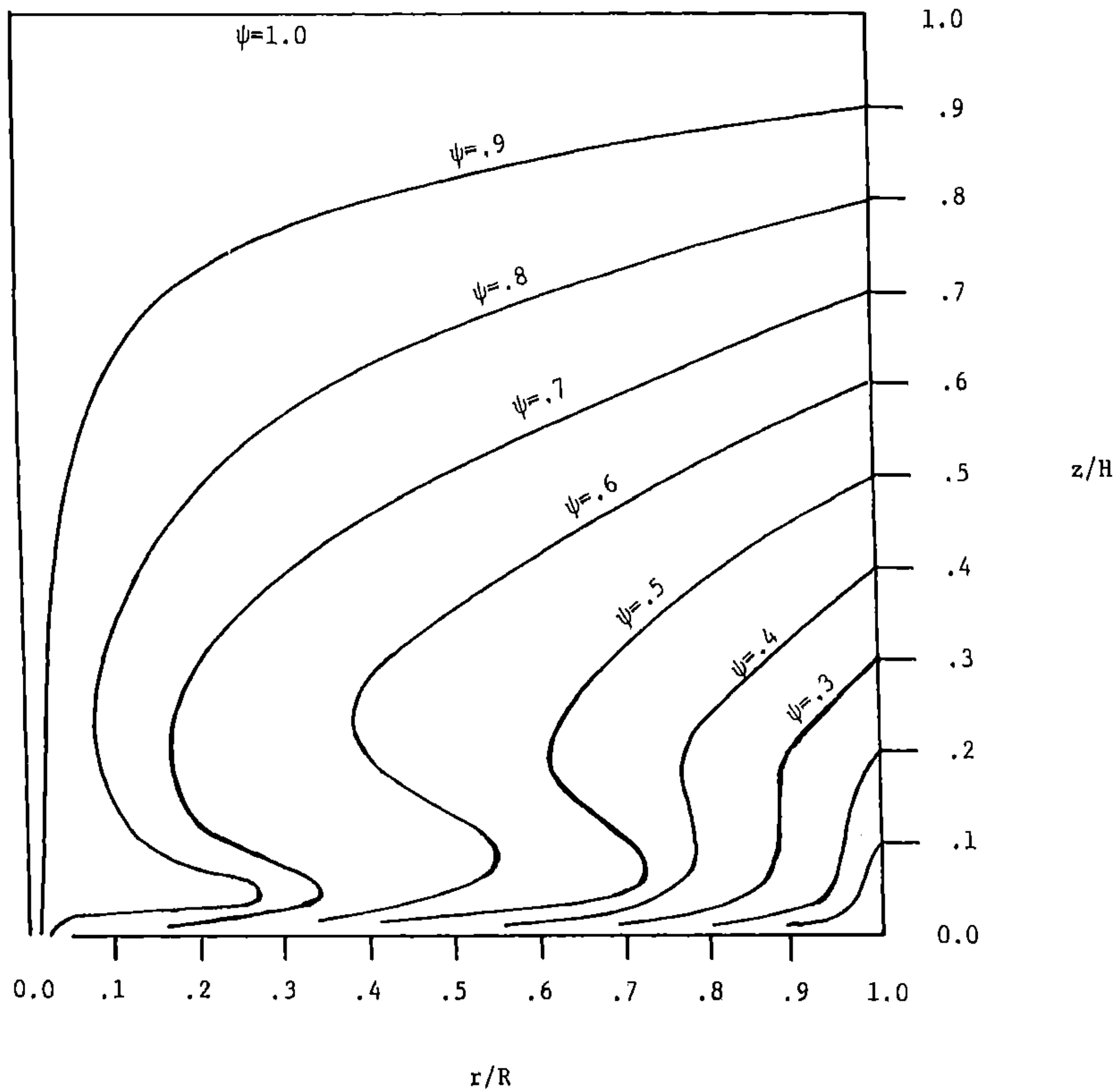

into the bottom boundary layer. As shown in Fig. 6.2, the bottom boundary layer is formed for high Re_θ and 80% of total flow rate is come from this thin boundary layer ragion. The radial velocity in the bottom boundary layer is much larger than that above the layer because the stream lines are very dense. The core region is also recognized by the stream line $\psi = .9$ in Fig. 6.2. Unlike Fig. 6.1 the stream line $\psi = .9$ is much closer to the axis of rotation and this indicates that higher axial velocity forms the core region. And the flow from the bottom boundary layer interacts with the flow from the core region near the exit hole. These qualitative features of vortex flow can also be seen by dye experiment (for the bottom boundary layer and the core region) described in Chap. 4.

Tangential velocity at the free stream region (above the bottom boundary layer) is measured for various Re_θ. Although the measurement is taken both at $z = 4.0$ cm and $z = 10.0$ cm, the difference in v_θ at these two positions is negligible. This agrees with the results of the numerical calculation (See Appendix A). Fig. 6.3 and Fig. 6.4 show comparison between the experimentally measured v_θ and numerically calculated v_θ for two different Re_θ and SS. The numerical results show excellent agreement with experimental data for both cases. The velocity data near the axis of rotation (the core region) cannot be obtained by the present measurement method because the fluid does not stay in a horizontal thin section which is illuminated by collimated

Fig. 6.3

The Comparison between the Experimentally Measured V_θ and Numerically Calculated V_θ (1)

Re_θ=1370 , SS=-.02

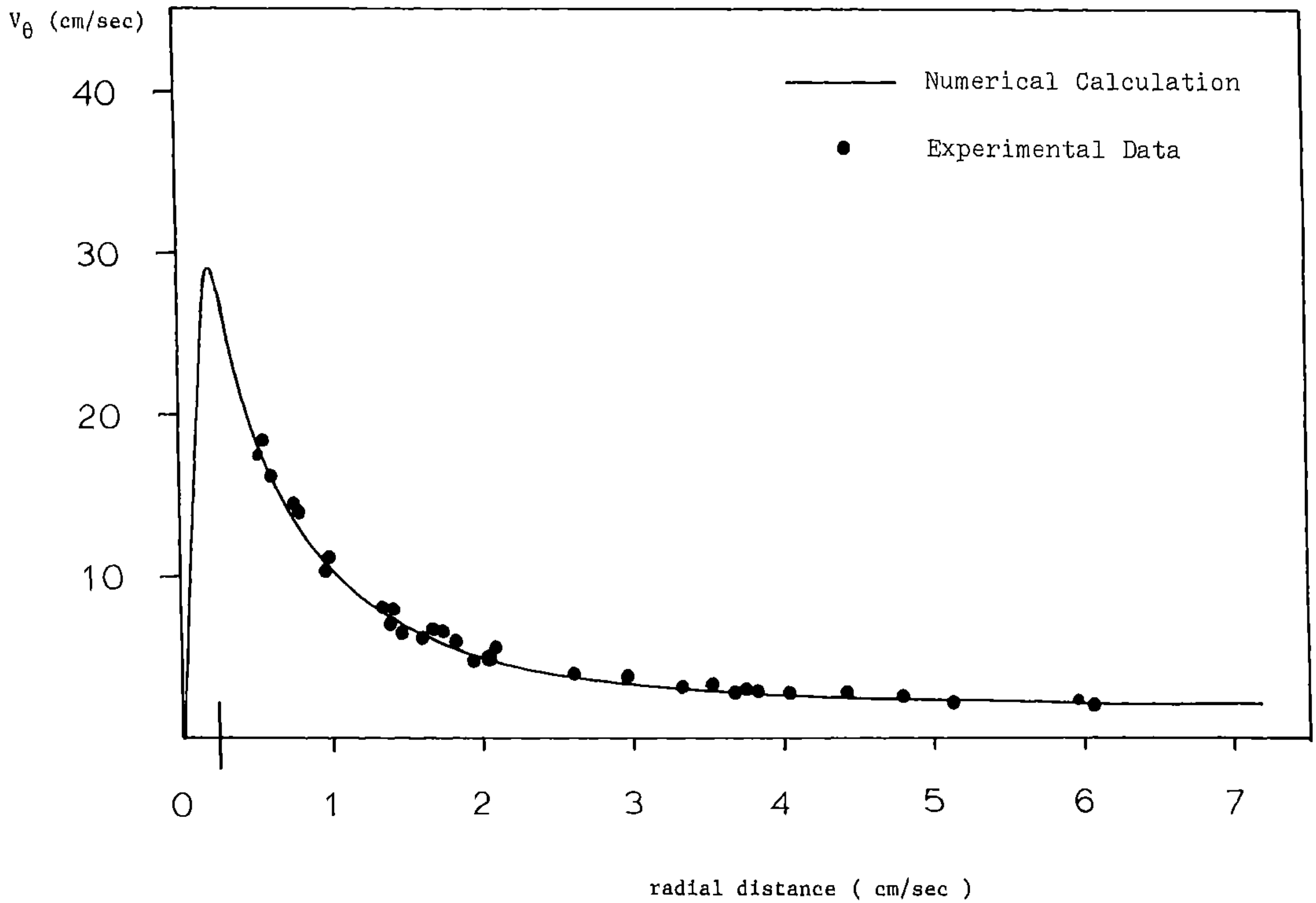

Fig. 6.4

The Comparison between the Experimentally Measured V_θ and Numerically Calculated V_θ (2)

Re_θ=1771 , SS=-.0186

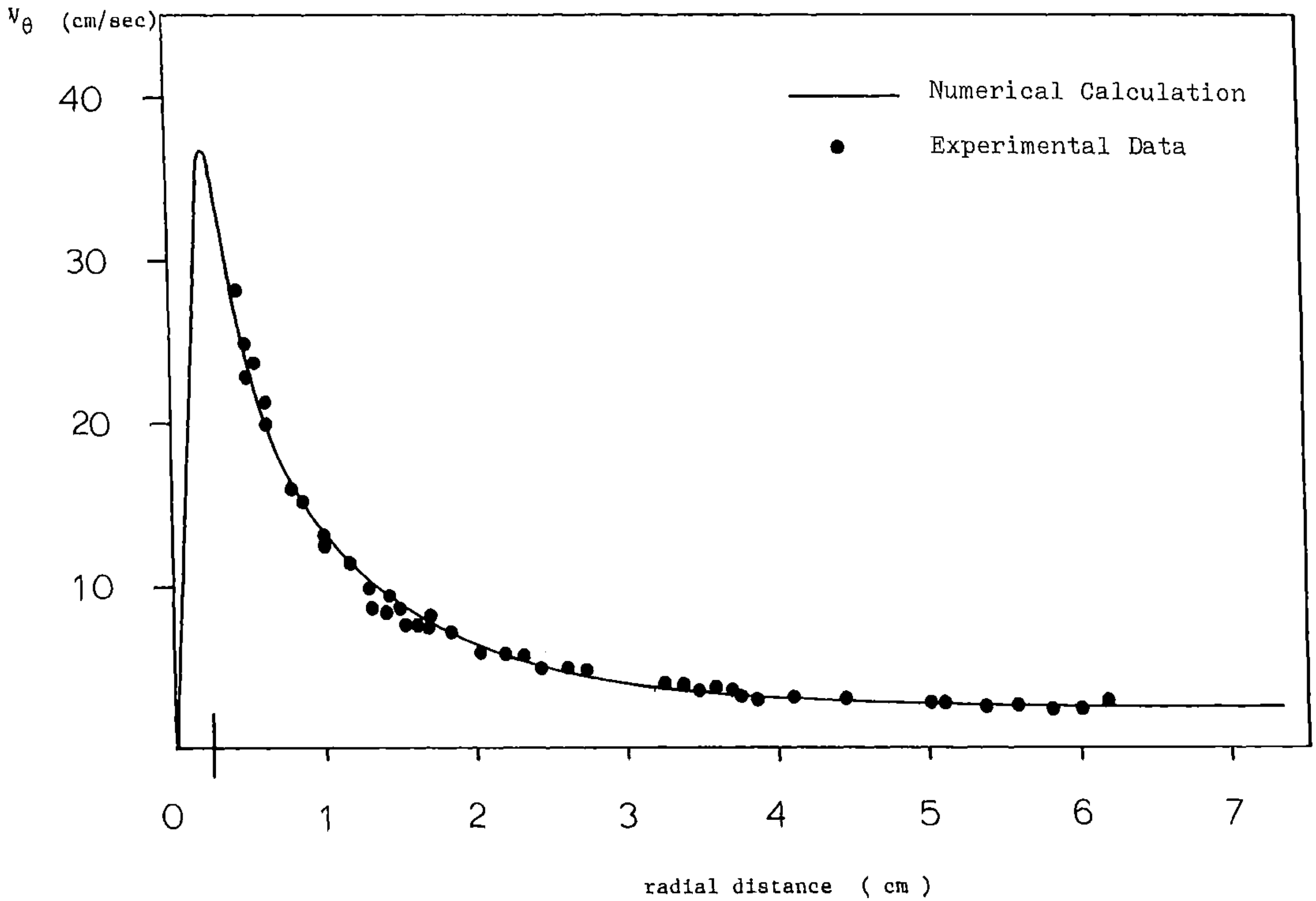

illuminated by a collimated light beam, long enough to be detected by the camera due to the higher axial velocity in this region. However, the agreement between theoretical and experimental results for $r > .5$ cm makes this calculated v_θ in the core region reasonable. The v_θ profile for both cases are very similar except that higher Re_θ gives higher v_θ over the entire range of radius. The v_θ in both figures reaches its maximum value at about $r = .24$ cm which is radius of the exit hole.

Fig. 6.5 and Fig. 6.6 show the comparison of v_z at the axis of rotation. As shown in these figures, although the calculated v_z predicts the tendency of v_z profile very well, there is discrepancy between theoretical calculation and experimental data. There seems three reasons to explain these differences. First, the zone size (especially in the r-direction) may be too large to provide the detailed information about v_z at $r = 0$. And the velocity information from the calculation is v_z at $r/R = .01$ due to the difficulties in handling at $r = 0$. In other words, the calculated v_z is the averaged value between $r/R = 0.$ and $r/R = .02$ because the zone size in the core region $\Delta(r/R)$ is .02. v_z at $r = 0$ is, therefore, larger than v_z at $r/R = .01$. Secondly, the radius of the exit hole r_e can not be described correctly in the simulation because the radius r_e has to be matched with the point at the center of the zone. This condition makes r_e in the simulation about 1.5 times larger than the real location of r_e. From the continuity of

Fig. 6.5

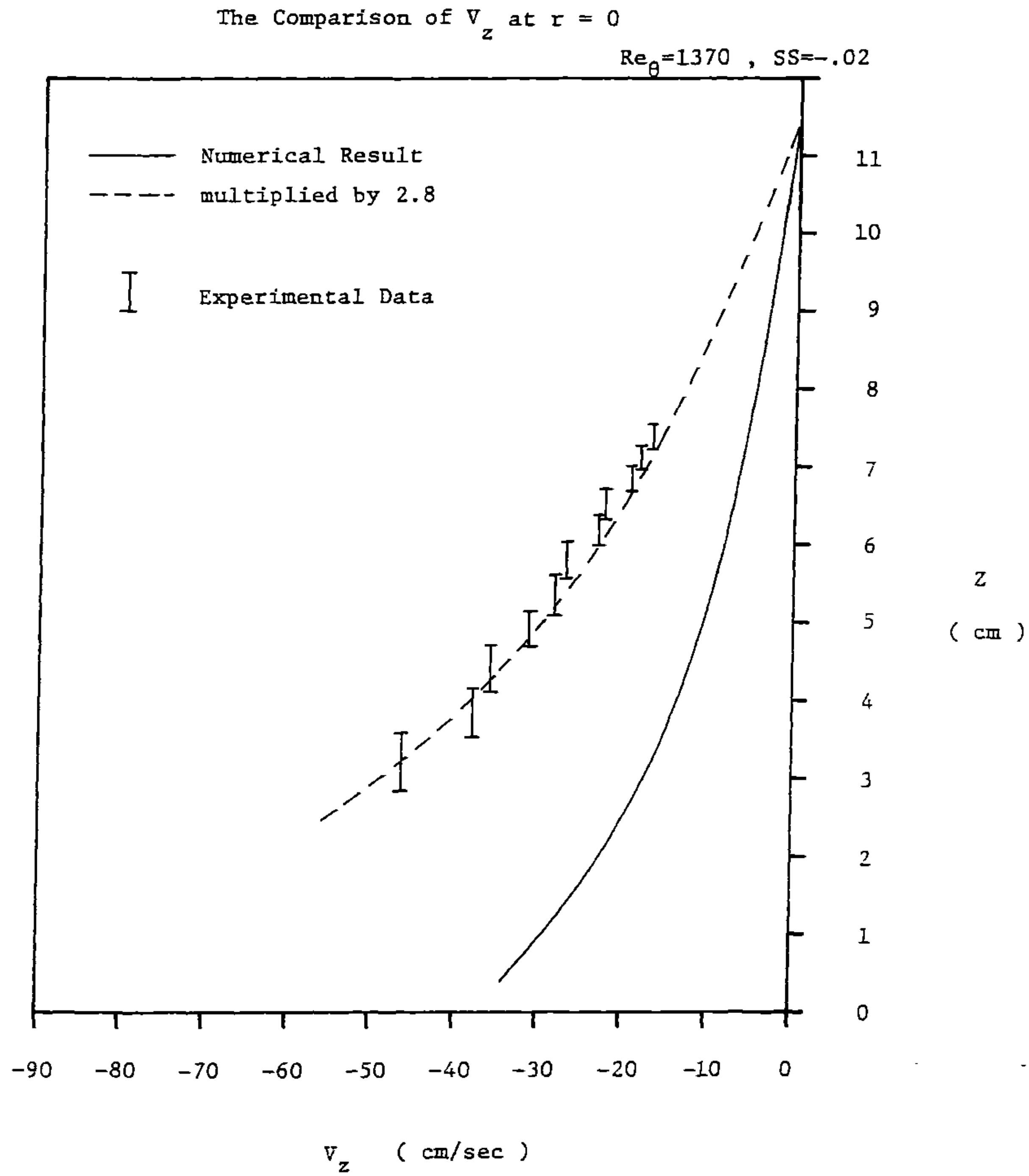
The Comparison of V_z at r = 0
Re_θ=1370 , SS=-.02
Numerical Result
multiplied by 2.8
Experimental Data
11
10
9
8
7
6
5
4
3
2
1
0
Z
(cm)
-90
-80
-70
-60
-50
-40
-30
-20
-10
0
V_z (cm/sec)

Fig. 6.6

The Comparison of V_z at $r = 0$

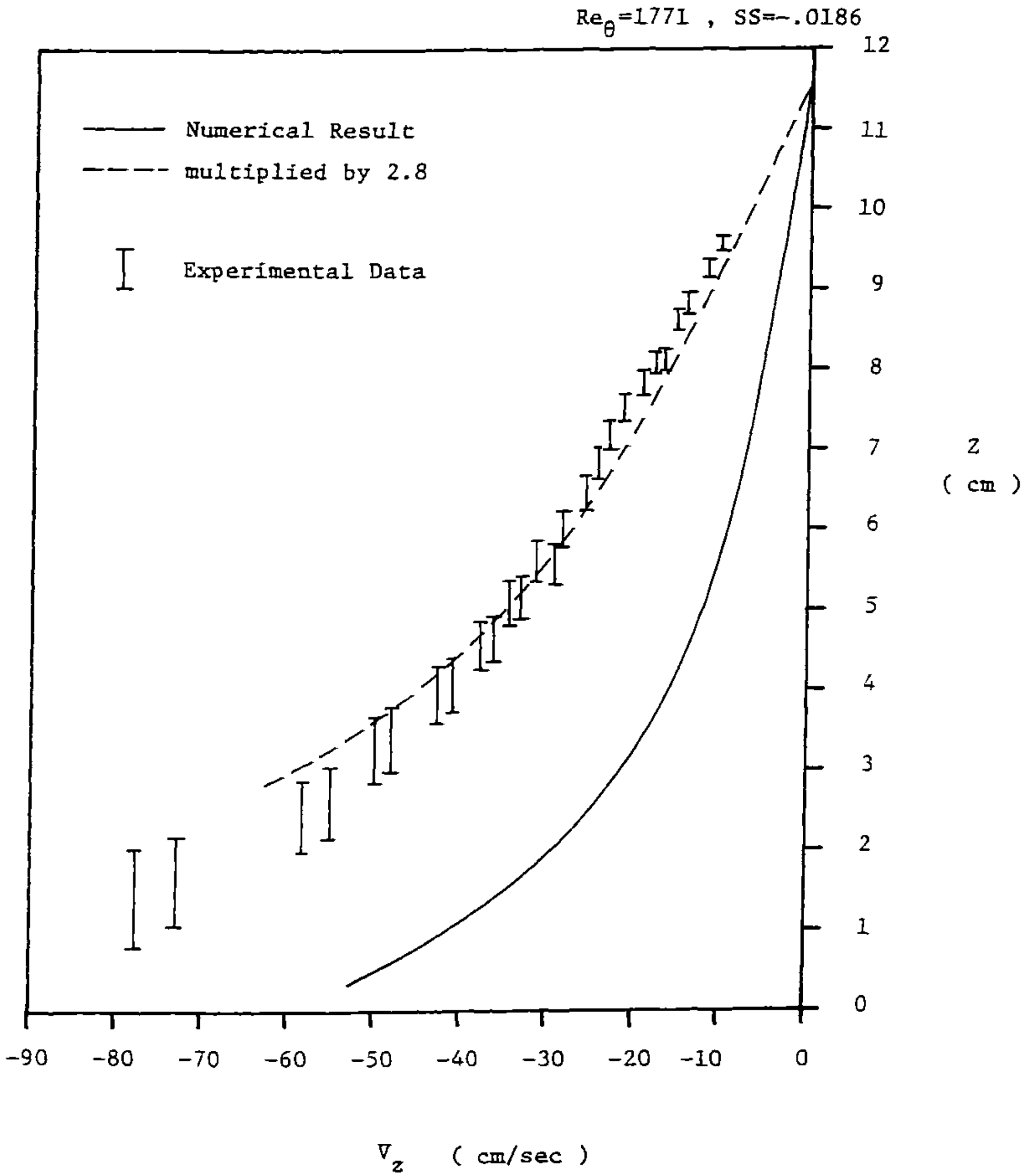

the fluid, the average value of v_z over the exit hole has to be increased 2.13 times larger for the real case. This is well explained in these figures because the correction factor 2.8 seems to fit the calculation results to the experimental data very well for both cases. Third, the numerical simulation is based on the geometry of a confined vortex flow so that no free surface is considered. However, this may not cause such a difference in v_z because the calcu= lated v_θ is matched with experimental data. Therefore, the first two reasons seem to explain the discrepancy. The discrepancy in v_z at $r = 0$ is not an essential defect mainly because the size of the exit hole is not described correctly. By reducing the r-direction zone size and locating r_e correctly, the numerical simulation may provide more precise v_z information.

The axial velocity at the axis of rotation is increasing in almost linear fashion from the liquid surface, but as the fluid gets close to the exit hole, v_z is accellerated. This is observed from both figures. It is also found from the calculation results that v_z is further increased so rapidly especially when the fluid interacts with the flow from the bottom boundary layer to produce large velocity gradient

$$\frac{\partial V_z}{\partial z} .$$

The results of the comparison with experimental measurement show that the numerical simulation certainly describes the vortex flow reasonably well. And the confined geometry of the vortex tank does not give any significant difference from the open free surface vortex flow in terms of velocity field. Since the numerical simulation provides full information about velocity field for the entire vortex geometry and the calculated velocity field reasonably well represents the real velocity field, it is employed for stress tensor calculation for polymer solution in later section.

6.2 Additional Remarks on the Modified Nearly Hookean Dumbbell Model

The Modefied Nearly Hookean Dumbbell model developed in Chap. 5 is used as a constitutive equation for stress tensor calculation of polymer solutions in the later section. In this section, two important characteristics of the MNHD model are described. The proper estimation of parameter ε from the comparison with available experimental data and the relaxation time for stress growth of elongational viscosity are very important factors for analysis of polymer contribution to stress tensor field.

Fig. 6.7 and Fig. 6.8 show the comparison of intrinsic viscosity as a function of shear rate between experimental data obtained by Christiansen and Bird (1977) and the model predictions. The macromolecule used in the experimental data is polystyrene of various molecular weights and at various temperatures. From these figures, the MNHD is seen to show the shear thinning phenomenon. It is also found taht the model shows a linear relation between $[\eta]$ and $\log \dot{\gamma}$ for higher shear rate

$$(\lambda e\dot{\gamma} > 2,\ \lambda_H = (5\varepsilon+1)\ e).$$

By comparison with a wide variety of polystyrene solutions, the parameter ε which is associated with the maximum length of the macromolecule R_o falls into the range between .02 and .005, which agrees with the prediction by Christiansen and Bird (1977). This range of the parameter

Fig. 6.7

$[\eta]$ vs $\lambda_e\dot{\gamma}$ with Experimental Data (1) (Polystyrene in benzene at 30 °C)

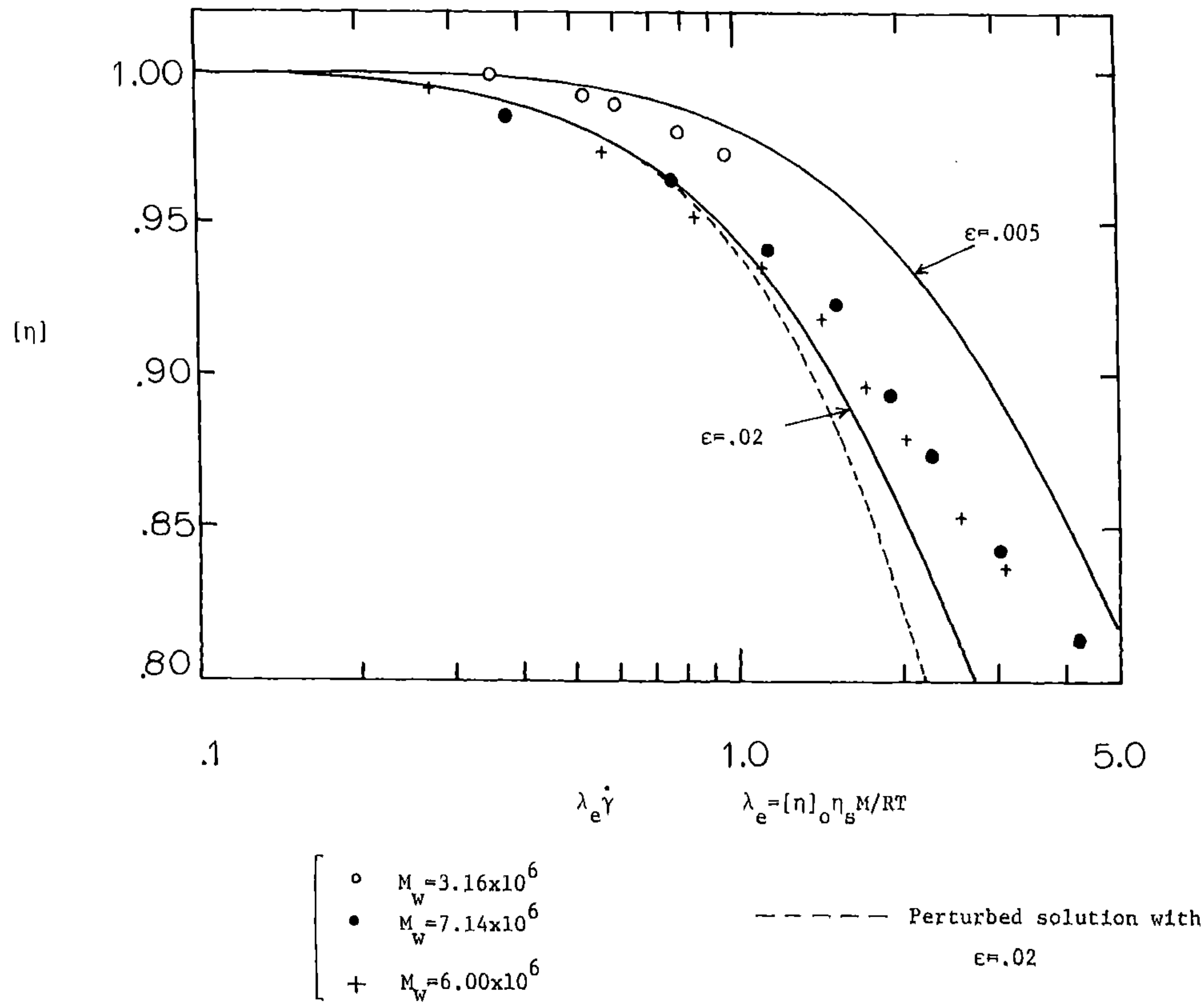

Fig. 6.8

$[\eta]$ vs $\lambda_e\dot{\gamma}$ with Experimental Data (2) (Polystyrene in toluene $Mn=10^7$)

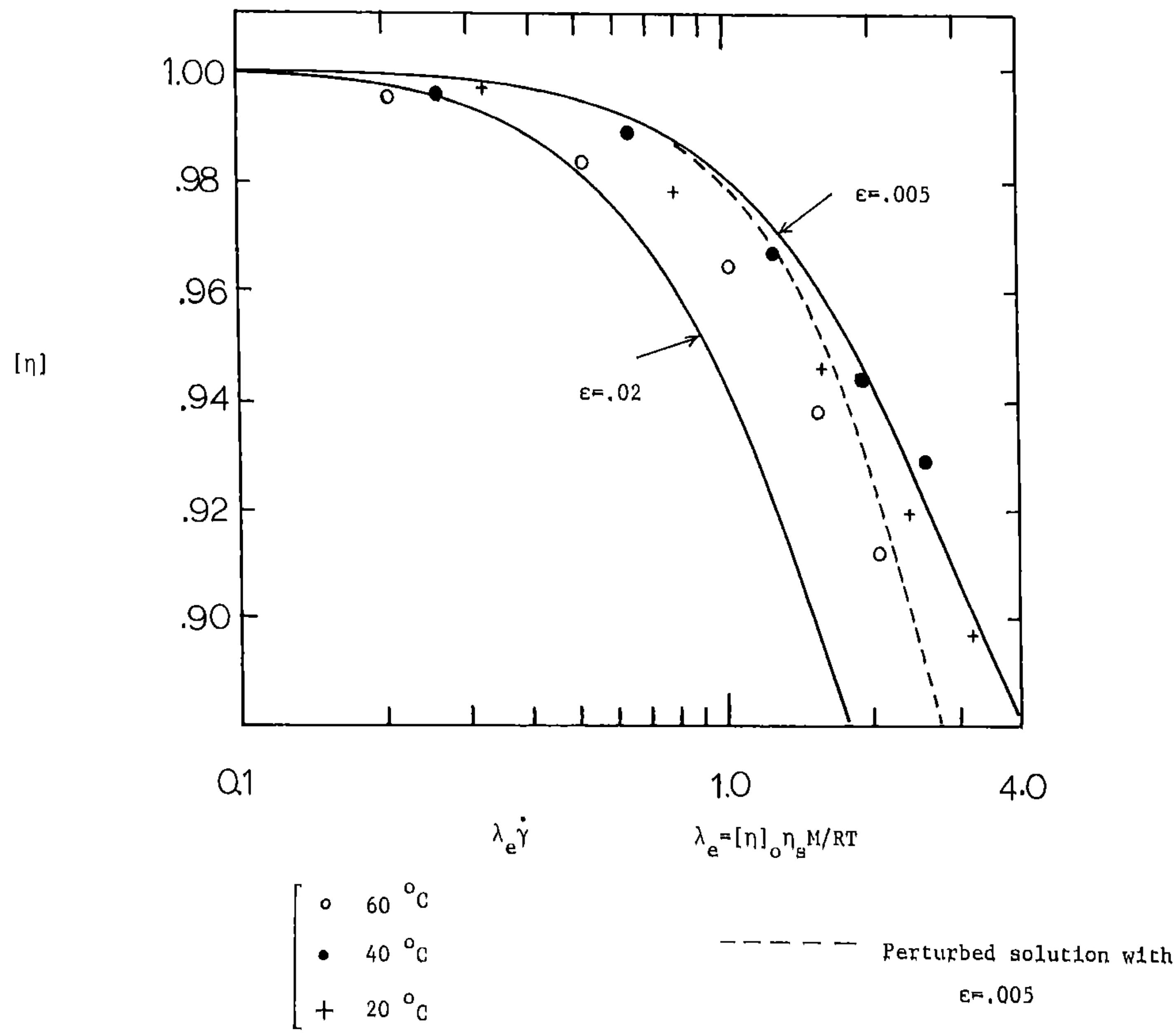

ε may, therefore, be a proper choice for polymer stress tensor field calculation.

The stress growth and relaxation of elongational viscosity are plotted with different scaled dimensionless time in Fig. 6.9 and Fig. 6.10. As shown in Fig. 6.9, as the elongational rate $\lambda_H \dot{\varepsilon}$ increases, the time required for raching a steady state becomes much shorter. This characteristic is quite different from the growth behavior of shear viscosity shown in Chap. 5 where the time to reach steady state is about $t/\lambda_H = 4$ for all shear rates. Unlike shear flow, the macromolecules subjected to elongational flow are stretched directly by hydrodynamic force and oriented to the direction of the flow. The time scale for molecular response to this flow, therefore, may be related to the elongational rate $\dot{\varepsilon}$. This is clearly explained when the elongational viscosity is plotted with the dimensionless time scaled by $1/\dot{\varepsilon}$ in Fig. 6.10 where the time to reach steady state is about $\dot{\varepsilon}t = 3$ for higher elongational rate $\lambda_H \dot{\varepsilon}$. As will be described in the later section, the shorter response time for higher elongational rate is important for vortex inhibition. The residence time of fluid element is very short in the area where large velocity gradient is established becasue the velocity of the fluid is usually very high. Unless the macromolecules are excited within the residence time of the fluid element, it would be carried away from the area of large velocity gradient before polymer effect appears. Thus it is necessary for realizing the polymer

Fig. 6.9

Dynamic Behavior of Elongational Viscosity

with Time Scaled by λ_H

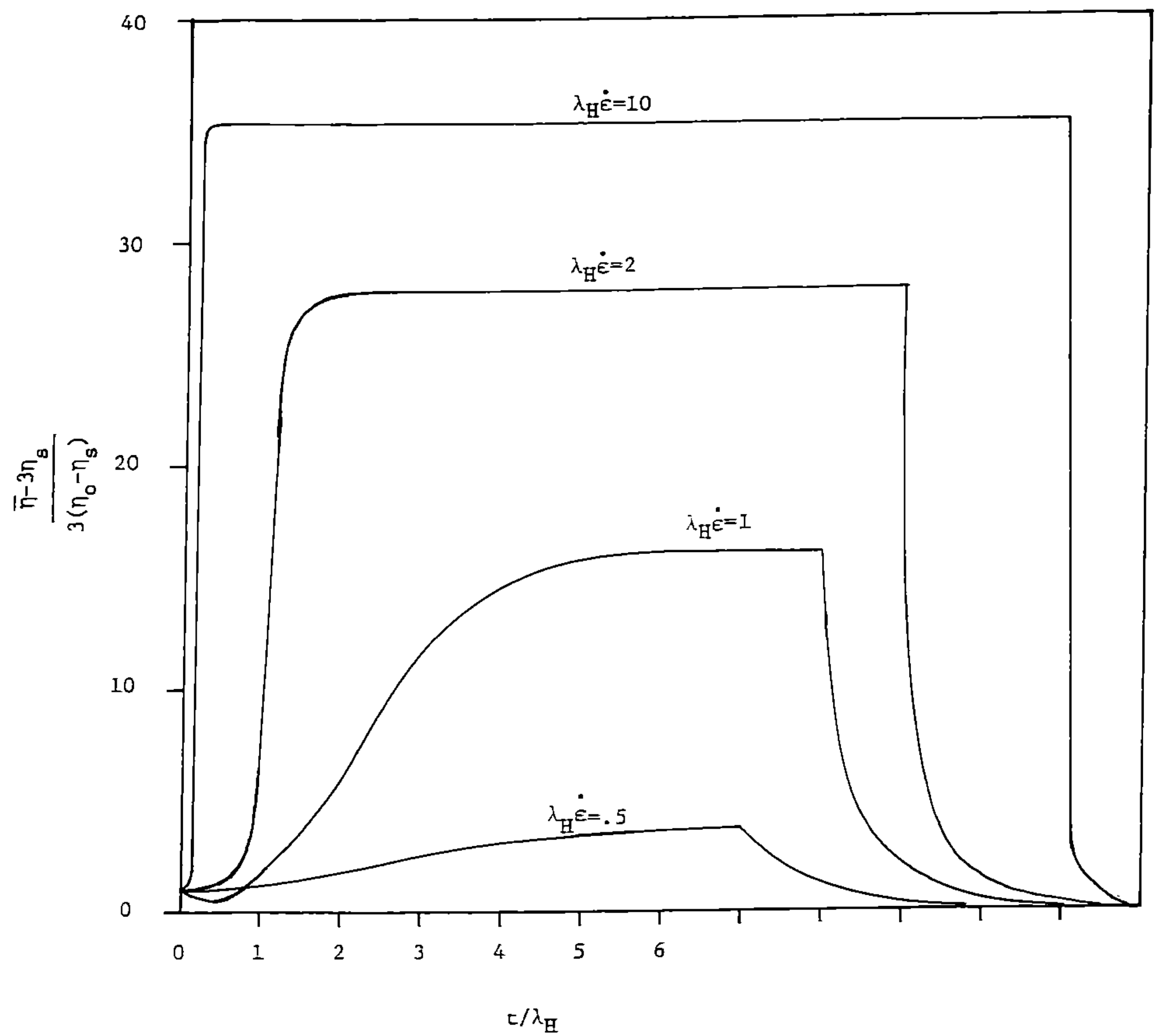

Fig. 6.10

Dynamical Behavior of Elongational Viscosity with Time Scaled by ε^{-1}

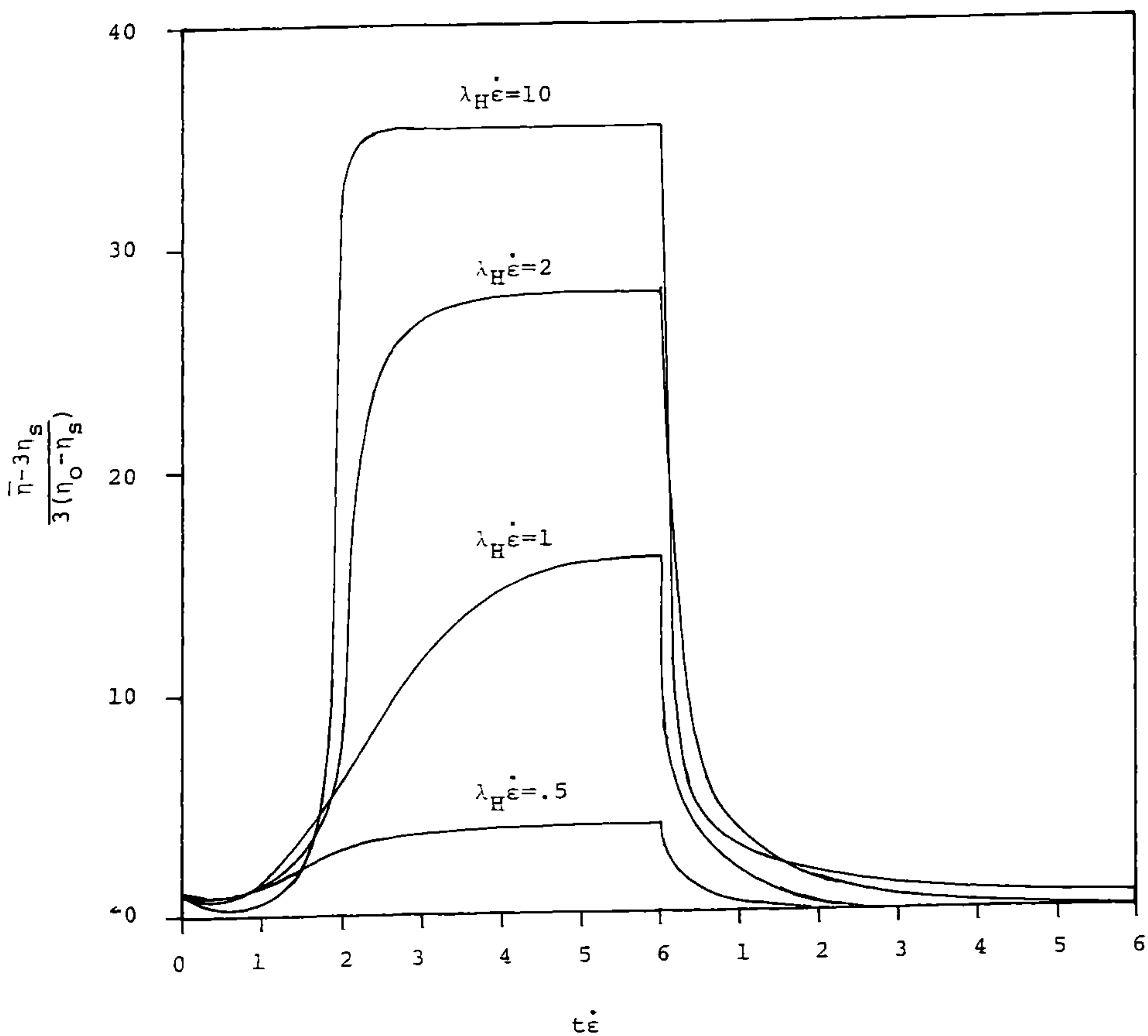

effect on the flow field that the response time for high elongational rate must be short besides high elongational viscosity which is emphasized in chap. 5.

6.3 Experimental Observation of the Onset Behavior of Vortex Inhibition

The onset behavior of vortex inhibition which is explained in Chap. 4 is described in this section. The information about the onset behavior is very important for analysis of vortex inhibition because it provides the transient flow behavior from Newtonian fluid to polymer solution. Shortly after concentrate polymer solution is poured into the feed tank, the polymer effect appears, that is, a small fluctuation of the air core is observed and the liquid level starts decreasing. This onset behavior of vortex inhibition is measured in terms of the tangential velocity v_θ and axial velocity at the axis of rotation $v_z|r = 0$. These variables are measured 30 seconds after the onset. As shown Fig. 6.11, after a couple of minutes, the vortex flow completely shifts to a new quite different flow status which is a fully developed vortex flow of the polymer solution. The flow rate and liquid level are measured. The analysis of the fully developed vortex flow of the polymer solution seems to be irrelevant for this study because of the following reasons. First, the fluctuation of the air core is very large and random so that it is almost impossible to obtain consistent velocity data especially for v_z at $r = 0$. Secondly, since the liquid level is dropped to about 50% of its original figure and the total flow rate is not changed very much (see number in Fig. 6.11), a much higher tangential

Fig. 6.11

The Difference between the Newtonian Vortex Flow and

A Fully Developed Vortex Flow of Polymer Solution

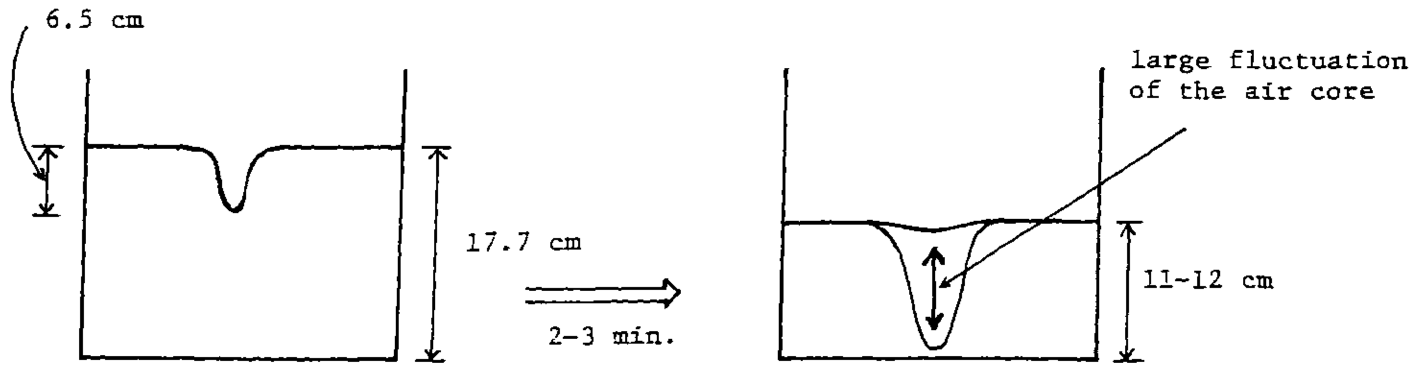

The Newtonian vortex flow

flow rate: 33.5 cc/sec

A fully developed vortex flow of polymer solution

flow rate: 30.0 cc/sec

velocity is established and this explains the broadening of the air core. This larger tangential velocity, however, may not directly be caused by the polymer effect but rather is due to the decrease of the liquid level while the flow rate is almost unchanged. To investigate the polymer effect on the vortex flow, it is, therefore, more sensible to measure the onset behavior of vortex inhibition rather than the fully developed vortex flow. Besides these two reasons, the measurement of the onset behavior is more consistent with the simulation which will be discussed in the next section where the polymer stress tensor field is calculated by the MNHD based on the Newtonian velocity field obtianed in section 6.1. The calculation simulates a physical situation where the Newtonian fluid is suddenly replaced by the polymer solution in order to see how the stress field changes due to the presence of the macromolecules.

Fig. 6.12 shows the tangential velocity measured during the onset of vortex inhibition. The tangential velocity in the free stream region is not appreciably changed when compared with that of the Newtonian fluid. Several velocity data, however, are found near the axis of rotation (the core region). In v_θ measurement for the Newtonian fluid, no data could be obtained at the core region because of large axial velocity (see section 6.1). These data indicate the reduction of v_z in the core region due to the fluctuation of the air core. Fig. 6.12 may suggest that the polymer

Fig. 6.12 The Tangential Velocity Profile before and during the Onset

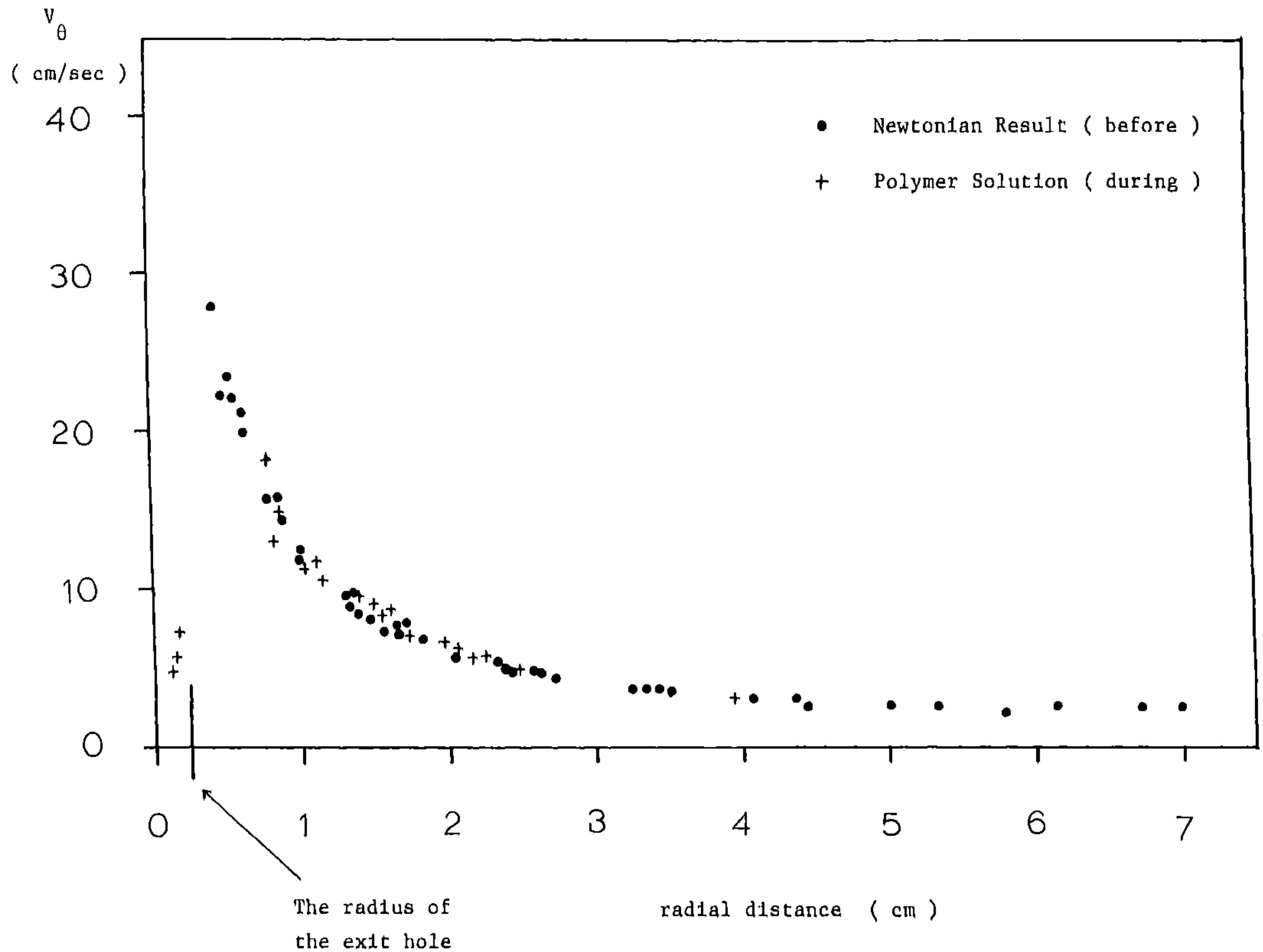

effect appears in the core region while nothing is changed in the free stream region during the onset of vortex inhibition as far as v_θ profile concerns.

The axial velocity data on the axis of rotation is shown in Fig. 6.13 during the onset along with the Newtonian data. The v_z data for the polymer solution are obtained from different pictures taken during the onset. The picture number in Fig. 6.13 indicates that the lower the number is, the earlier the picture is taken. The picture number, however, does not correspond to the precise sequence of the onset behavior. At each time, different v_z data is obtained because of the fluctuation of the air core. For example, the data of PIC #11 shows that the velocity becomes almost zero about $z = 4$ cm which is quite different from that of the Newtonian fluid. Fig. 6.13 indicates that v_z at $r = 0$ is always lower than the case of the Newtonian fluid from any of the data. This seems to be inconsistent with the fact that the liquid level is falling during the onset of vortex inhibition. The averaged v_z over the exit hole must be increased to explain the liquid level's falling, v_z at $r = 0$, on the other hand, seems to decrease at the exit hole from Fig. 6.13.

Thus two experimental findings during the onset of vortex inhibition should be emphasized in this section. First, the averaged axial velocity over the exit hole is increased

Fig. 6.13

Axial Velocity Measured before and during the Onset

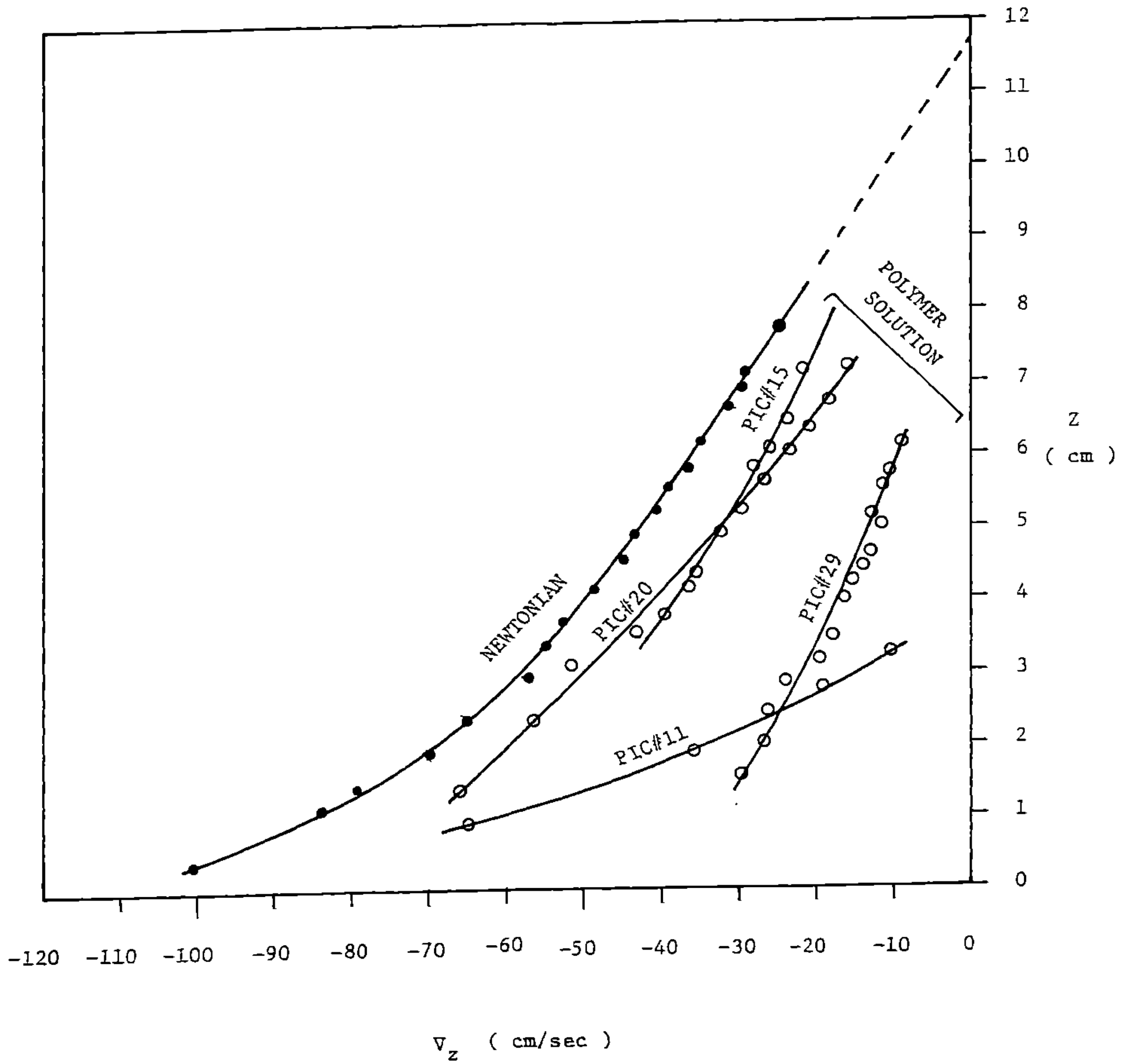

because the liquid level is decreasing while the total flow rate is not changed appreciably. Secondly, the axial velocity at the axis of rotation seems to be decreased at the exit hole from the extrapolation of the experimental data. These two findings characterize the onset behavior of vortex inhibition and these are analyzed in the following sections.

6.4 The Polymer Contribution to Stress Tensor Along the Stream Lines (Based on the result of the case $Re_\theta = 1370$ and ss = -.02)

In this section, the stress tensor is calculated by using the constitutive equation (the Modified Nearly Hookean Dumbell) along the stream line obtained in the previous section. Since the onset behavior of vortex inhibition is the transient state from the Newtonian vortex flow to the fully developed vortex flow of the polymer solution, the information about the velocity gradient may be obtained from the results of the Newtonian vortex calculation. The advantage of the numerical calculation of the Newtonian vortex flow is to provide full information about every component of the velocity gradient tensor for the entire region. In this way, the stress tensor field is calculated along the stream lines. By following the fluid element on each of the stream lines, the complicated calculation of the convective terms in the MNHD can be avoided. The six equations of the structure tensor derived from the MNHD are

rr-component

$$\lambda_H \frac{D}{Dt}\alpha_{rr} = 2\lambda_H \frac{\partial v_r}{\partial r}\alpha_{rr} + 2\lambda_H \frac{\partial v_r}{\partial z}\alpha_{rz} - 2\lambda_H \frac{v_\theta}{r}\alpha_{r\theta}$$

$$- \frac{\alpha_{rr}}{A} - \frac{2\varepsilon A}{nkT}(\alpha_{rr}{}^2 + \alpha_{r\theta}{}^2 + \alpha_{rz}{}^2) + nkT \qquad 6.1$$

$\theta\theta$-component

$$\lambda_H \frac{D}{Dt}\alpha_{\theta\theta} = 2\lambda_H \frac{v_r}{r}\alpha_{\theta\theta} + 2\lambda_H \frac{\partial v_\theta}{\partial r}\alpha_{r\theta} + 2\lambda_H \frac{\partial v_\theta}{\partial z}\alpha_{z\theta}$$

$$- \frac{\alpha_{\theta\theta}}{A} - \frac{2\varepsilon A}{nkT}(\alpha_{r\theta}^2 + \alpha_{\theta\theta}^2 + \alpha_{\theta z}^2) + nkT \qquad 6.2$$

zz-component

$$\lambda_H \frac{D}{Dt}\alpha_{zz} = 2\lambda_H \frac{\partial v_z}{\partial z}\alpha_{zz} + 2\lambda_H \frac{\partial v_z}{\partial r}\alpha_{rz}$$

$$- \frac{\alpha_{zz}}{A} - \frac{2\varepsilon A}{nkT}(\alpha_{rz}^2 + \alpha_{\theta z}^2 + \alpha_{zz}^2) + nkT \qquad 6.3$$

rθ-component

$$\lambda_H \frac{D}{Dt}\alpha_{r\theta} = \lambda_H\left(\frac{\partial v_r}{\partial r} + \frac{v_r}{r}\right)\alpha_{r\theta} + \lambda_H \frac{\partial v_\theta}{\partial r}\alpha_{rr} - \lambda_H \frac{v_\theta}{r}\alpha_{\theta\theta}$$

$$+ \lambda_H \frac{\partial v_r}{\partial z}\alpha_{\theta z} + \lambda_H \frac{\partial v_\theta}{\partial z}\alpha_{rz} - \frac{\alpha_{r\theta}}{A} - \frac{2\varepsilon A}{nkT}(\alpha_{rr}\alpha_{r\theta} + \alpha_{r\theta}\alpha_{\theta\theta} + \alpha_{rz}\alpha_{\theta z}) \qquad 6.4$$

rz-component

$$\lambda_H \frac{D}{Dt}\alpha_{rz} = \lambda_H\left(\frac{\partial v_r}{\partial r} + \frac{\partial v_z}{\partial z}\right)\alpha_{rz} + \lambda_H \frac{\partial v_z}{\partial r}\alpha_{rr} + \lambda_H \frac{\partial v_r}{\partial z}\alpha_{zz}$$

$$- \lambda_H \frac{v_\theta}{r}\alpha_{\theta z} - \frac{\alpha_{rz}}{A} - \frac{2\varepsilon A}{nkT}(\alpha_{rr}\alpha_{rz} + \alpha_{r\theta}\alpha_{\theta z} + \alpha_{rz}\alpha_{zz}) \qquad 6.5$$

θz-component

$$\lambda_H \frac{D}{Dt}\alpha_{\theta z} = \lambda_H\left(\frac{\partial v_z}{\partial z} + \frac{v_r}{r}\right)\alpha_{\theta z} + \lambda_H \frac{\partial v_\theta}{\partial r}\alpha_{rz} + \lambda_H \frac{\partial v_z}{\partial r}\alpha_{r\theta}$$

$$+ \lambda_H \frac{\partial v_\theta}{\partial z}\alpha_{zz} - \frac{\alpha_{\theta z}}{A} - \frac{2\varepsilon A}{nkT}(\alpha_{r\theta}\alpha_{rz} + \alpha_{\theta\theta}\alpha_{\theta z} + \alpha_{\theta z}\alpha_{zz}) \qquad 6.6$$

The symbol A in these equations is given by

$$A = 1 - \frac{\varepsilon}{nkT}(\alpha_{rr}+\alpha_{\theta\theta}+\alpha_{zz}) \tag{6.7}$$

The polymer stress tensor $\underline{\underline{\tau}}_p$ is then obtained from the structure tensor $\underline{\underline{\alpha}}$.

$$\tau_{p,rr} = \lambda_H \frac{D}{Dt}\alpha_{rr} - 2\lambda_H \frac{\partial v_r}{\partial r}\alpha_{rr} - 2\lambda_H \frac{\partial v_r}{\partial z}\alpha_{rz} + 2\lambda_H \frac{v_\theta}{r}\alpha_{r\theta} \tag{6.8}$$

$$\tau_{p,\theta\theta} = \lambda_H \frac{D}{Dt}\alpha_{\theta\theta} - 2\lambda_H \frac{\partial v_\theta}{\partial r}\alpha_{r\theta} - 2\lambda_H \frac{\partial v_\theta}{\partial z}\alpha_{z\theta} - 2\lambda_H \frac{v_r}{r}\alpha_{\theta\theta} \tag{6.9}$$

$$\tau_{p,zz} = \lambda_H \frac{D}{Dt}\alpha_{zz} - 2\lambda_H \frac{\partial v_z}{\partial z}\alpha_{zz} - 2\lambda_H \frac{\partial v_z}{\partial r}\alpha_{rz} \tag{6.10}$$

$$\begin{aligned}\tau_{p,r\theta} = {} & \lambda_H \frac{D}{Dt}\alpha_{r\theta} - \lambda_H\left(\frac{\partial v_r}{\partial r} + \frac{v_r}{r}\right)\alpha_{r\theta} - \lambda_H \frac{\partial v_\theta}{\partial r}\alpha_{rr} \\ & + \lambda_H \frac{v_\theta}{r}\alpha_{\theta\theta} - \lambda_H \frac{\partial v_r}{\partial z}\alpha_{\theta z} - \lambda_H \frac{\partial v_\theta}{\partial z}\alpha_{rz}\end{aligned} \tag{6.11}$$

$$\begin{aligned}\tau_{p,rz} = {} & \lambda_H \frac{D}{Dt}\alpha_{rz} - \lambda_H\left(\frac{\partial v_r}{\partial r} + \frac{\partial v_z}{\partial z}\right)\alpha_{rz} - \lambda_H \frac{\partial v_z}{\partial r}\alpha_{rr} \\ & - \lambda_H \frac{\partial v_r}{\partial z}\alpha_{zz} + \lambda_H \frac{v_\theta}{r}\alpha_{\theta z}\end{aligned} \tag{6.12}$$

$$\tau_{p,\theta z} = \lambda_H \frac{D}{Dt}\alpha_{\theta z} - \lambda_H\left(\frac{\partial v_z}{\partial z} + \frac{v_r}{r}\right)\alpha_{\theta z} - \lambda_H \frac{\partial v_\theta}{\theta r}\alpha_{rz}$$

$$- \lambda_H \frac{\partial v_z}{\partial r}\alpha_{r\theta} - \lambda_H \frac{\partial v_\theta}{\partial z}\alpha_{zz} \qquad 6.13$$

The calculation is supposed to start from the outer wall where the fluid is introduced to the vortex tank. However, the simple speculation in Chap. 3 indicates that the velocity gradient is too small to excite the macromolecules until the fluid elements approach the area near the exit hole where the velocity gradients seem to become very large. So the calculation of the stress tensor is limited only to this area. Fig. 6.14 is a detailed picture of Fig. 6.2 of the stream lines near the exit hole. Once the fluid element reaches the square area enclosed by the lines of $r/R = .1$ and $z/H = .1$, the calculation begins. For example, the stress calculation of $\psi = .8$ starts from the point $(r/R, z/H) = (.1, .025)$. The structure tensor at the point 1 is obtained by a numerical integration of eq. 6.1 to eq. 6.7. The Runge-Kutta fourth order method is accurate enough for this type of integration. (The program listing is found in Appendix C). By choosing a small time step, the time advanced structure tensor is calculated up to the point 1. Every component of the velocity gradient tensor in the equations is approximately determined from the velocity field at the point 1. Once the structure tensor at the point 1 is obtained, the polymer stress tensor is calculated by eq. 6.8 to eq. 6.13.

Fig. 6.14

Stream Lines near the Exit Hole

Re_θ=1370 , SS=-.02

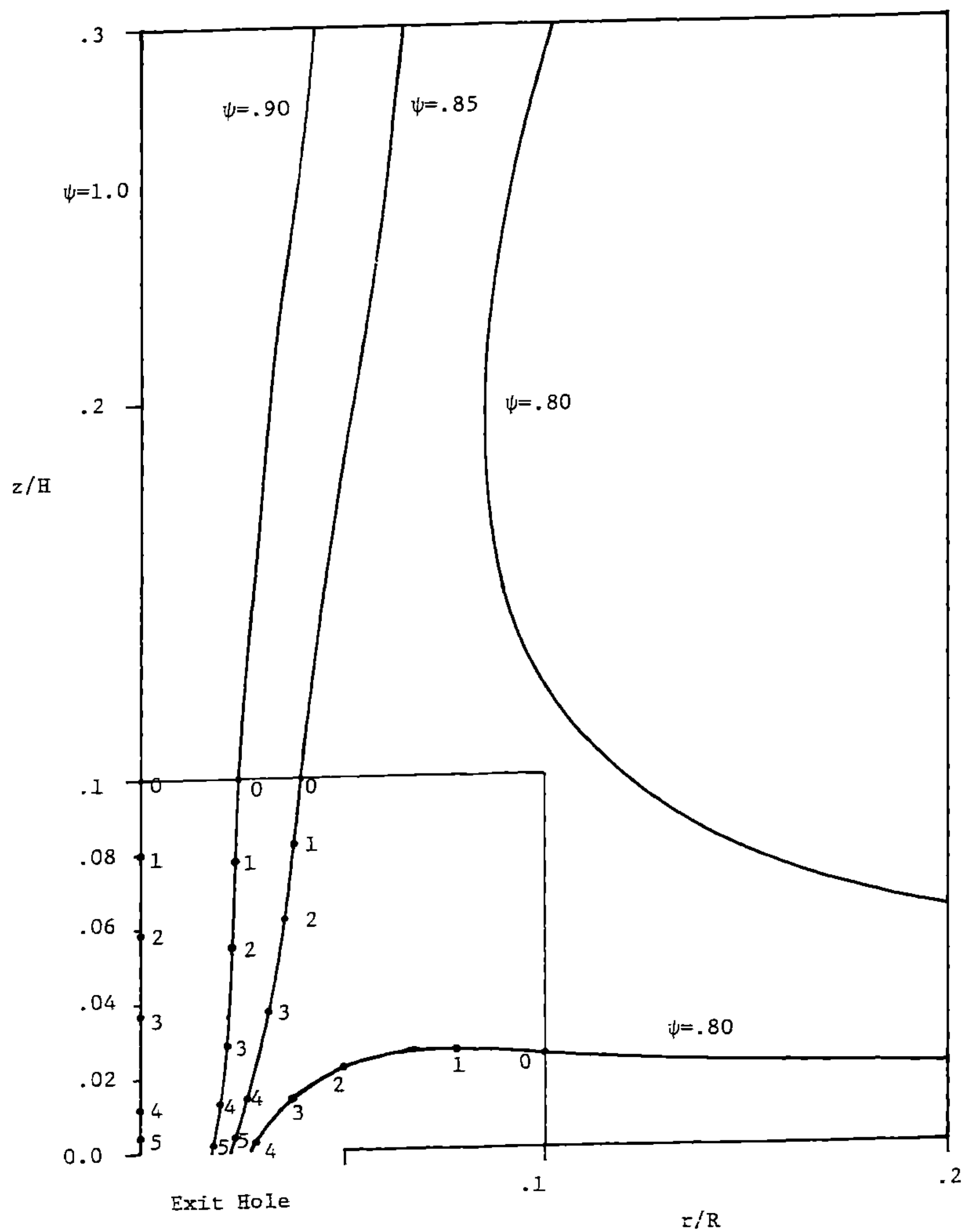

This calculation procedure is repeated until the fluid element reaches the point 4 where the large velocity gradient is expected. The structure tensor as well as the polymer stress tensor is also calculated in this way for $\psi = .85$, $\psi = .9$ and $\psi = .1.0$.

TABLE 6.1 to TABLE 6.4 show the results of the calculation. It is found from these tables that $\tau_{p,zz}$ is increased extremely rapidly very near the exit hole for the stream lines $\psi = .85$ and $\psi = .8$. This is due to the large velocity gradient especially

$$\frac{\partial V_z}{\partial z}$$

established at the exit hole. The large velocity gradient for $\psi = .8$ may easily be speculated because the fluid element from the bottom boundary layer has almost zero axial velocity and once it reaches near the exit hole, it is forced to be flowed out with a large axial velocity. The boundary layer thickness is so thin that the axial velocity has to be increased in a very short distance. And the macromolecules are suddenly stretched out in the z-direction nearly to the maximum length R_o (see the column $\langle (R/Ro)^2 \rangle$ in the tables). Since the relaxation time is very short when the velocity gradient is large according to the MNHD, the macromolecule has enough time to be stretched extensively even in a very short period of time. The macromolecules flowing along the stream lines $\psi = 1.0$ and $\psi = .9$, (TABLE 6.1 and TABLE 6.2)

TABLE 6.1

POLYMER STRESS TENSOR ALONG THE STREAM LINE $\psi = 1.0$

POINT NUMBER	TIME [SEC]	$\underline{\underline{\tau}}_p$ $[g \cdot cm/sec^2 \cdot cm^2]$						$\left\langle \left(\frac{R}{R_o}\right)^2 \right\rangle$
		$\tau_{p,rr}$	$\tau_{p,\theta\theta}$	$\tau_{p,zz}$	$\tau_{p,r\theta}$	$\tau_{p,rz}$	$\tau_{p,\theta z}$	
0	0	.000	.000	.000	.000	.000	.000	
1	.01	.000	.000	.000	.000	.000	.000	.0146
2	.02	.000	.000	-.027 (-.04)	.000	.000	.000	.0153
3	.03	.000	.000	-.045 (-.24)	.000	.000	.000	.0157
4	.04	.000	.000	-.147 (-.68)	.000	.000	.000	.0182
5	.043	.000	.000	-.203 (-.96)	.000	.000	.000	.0144

* The figures in the parenthesis are values for Newtonian fluid.

TABLE 6.2

POLYMER STRESS TENSOR ALONG THE STREAM LINE $\psi = .9$

POINT NUMBER	TIME [SEC]	$\underline{\underline{\tau}}_p$ [g·cm/sec^2·cm^2]						$\langle \left(\frac{R}{R_o}\right)^2 \rangle$
		$\tau_{p,rr}$	$\tau_{p,\theta\theta}$	$\tau_{p,zz}$	$\tau_{p,r\theta}$	$\tau_{p,rz}$	$\tau_{p,\theta z}$	
0	0	0	0	0	0	0	0	
1	.02	0	-.001	-.259 (-.084)	-.003	-.090	-.141	.0207
2	.04	.008	.012	-.431 (-.266)	-.005	-.105	-.145	.0241
3	.06	.028	.031	-.645 (-.64)	-.001	-.076	-.099	.0280
4	.07	.026	-.053	-9.158 (-3.02)	-.031	-.390	-.966	.1660
5	.075	.113	.002	-23.618 (-3.02)	.039	.338	-.991	.3183

* The figures in the parenthesis are values for Newtonian fluid.

TABLE 6.3

POLYMER STRESS TENSOR ALONG THE STREAM LINE $\psi = .85$

POINT NUMBER	TIME [SEC]	$\underline{\underline{\tau}}_p$ [g·cm/sec^2·cm^2] $\tau_{p,rr}$	$\tau_{p,\theta\theta}$	$\tau_{p,zz}$	$\tau_{p,r\theta}$	$\tau_{p,rz}$	$\tau_{p,\theta z}$	$\langle \left(\frac{R}{R_o}\right)^2 \rangle$
0	0	0	0	0	0	0	0	
1	.04	-2.368	-.442	-2.322 (-.112)	1.619	-2.352	1.481	.1185
2	.08	-3.700	-1.376	-8.183 (-.398)	2.376	-5.459	3.326	.2175
3	.12	-.301	.011	-3.844 (-.504)	.182	-.819	.261	.0948
4	.15	-1.039	-.978	-44.899 (-2.08)	-1.060	-7.088	-6.831	.4869
5	.155	.083	-.367	-96.449 (-3.80)	.061	.688	-6.077	.6819

* The figures in the parenthesis are values for Newtonian fluid.

TABLE 6.4

POLYMER STRESS TENSOR ALONG THE STREAM LINE $\psi = .8$

POINT NUMBER	TIME [SEC]	$\underline{\underline{\tau}}_p$ [g·cm/sec^2·cm^2]						$\langle \left(\frac{R}{R_o}\right)^2 \rangle$
		$\tau_{p,rr}$	$\tau_{p,\theta\theta}$	$\tau_{p,zz}$	$\tau_{p,r\theta}$	$\tau_{p,rz}$	$\tau_{p,\theta z}$	
0	0	0	0	0	0	0	0	
1	.03	-.040	.001	-.069 (-.02)	.078	-.114	.030	.0172
2	.07	-3.461	-3.315	-2.575 (-.7)	3.484	-2.997	2.805	.1704
3	.09	-35.001	-12.902	-47.004 (-2.12)	21.332	-40.598 (-2.285)	25.564	.6769
4	.097	-.306	.039	-171.298 (-5.28)	.005	-7.909 (-.97)	.646	.8019

* The figures in the parenthesis are values for Newtonian fluid.

TABLE 6.5

THE LOCATION OF EACH POINT

POINT NUMBER	ψ = 1.0		ψ = .9		ψ = .85		ψ = .8	
	r/R	z/H	r/R	z/H	r/R	z/H	r/R	z/H
0	0	.1	.025	.1	.04	.1	.1	.025
1	0	.08	.024	.078	.038	.082	.078	.026
2	0	.059	.023	.055	.036	.061	.050	.023
3	0	.037	.021	.029	.031	.038	.037	.014
4	0	.012	.02	.013	.026	.014	.028	.003
5	0	.044	.018	.002	.022	.004		

on the other hand, are not stretched substantialy. For example, at $\psi = 1$, $\tau_{p,zz}$ is less than the half of the Newtonian stress counterpart even at the point 5 so that the fluid element may not be influenced by the presence of the macromolecules. From the analysis of the Newtonian velocity field, it is found that the dominant forces in the Newtonian flow in the z-direction very near the exit hole are pressure gradient and the corresponding inertia forces. The viscous force, therefore, does not contribute effectively to the force balance. In order to cope with these dominant forces, $\tau_{p,zz}$ must be much larger than the Newtonian stress.

As shown in the case of $\psi = .85$ and $\psi = .8$, $\tau_{p,zz}$ very near the exit hole becomes much larger than the Newtonian case, it may, therefore, be possible that this stress component influences the flow behavior. To investigate the influence of $\tau_{p,zz}$ on the flow behavior, the force balance (the equation of motion) in the z-direction has to be considered with the polymer contribution to the stress tensor terms. This will be discussed in the next section.

6.5 The Analysis of Polymer Effect near the Exit Hole

As found in the last section, the dramatic increase of $\tau_{p,zz}$ is established near the exit hole for $\psi = .8$ and $\psi = .85$. This is due to elongational nature of the flow behavior which stretches the macromolecules substantially as studied in Chap. 5. In this section, we investigate how this $\tau_{p,zz}$ influences the flow behavior by using the z-direction force balance and try to explain qualitatively the onset behavior of vortex inhibition which was described in section 6.3.

The force balance in the z-direction (z-component of the equation of motion) is written by

$$\rho \left(v_r \frac{\partial v_z}{\partial r} + v_z \frac{\partial v_z}{\partial z} \right) = - \frac{\partial p}{\partial z} - \frac{1}{r} \frac{\partial}{\partial r} (r\tau_{rz}) + \frac{\partial \tau_{zz}}{\partial z} + \rho g \qquad 6.14$$

The study of the Newtonian flow field obtained in section 6.1 near the exit hole shows that the pressure gradient

$$- \frac{\partial p}{\partial z}$$

and the corresponding inertia force

$$\rho v_z \frac{\partial v_z}{\partial z}$$

are the main dominant forces and the Newtonian stress terms are too small to contribute the force balance. TABLE 6.6

TABLE 6.6

THE MAGNITUDE AND ORIENTATION OF EACH TERM IN THE FORCE BALANCE

	$\rho v_r \frac{\partial v_z}{\partial r}$	$\rho v_z \frac{\partial v_z}{\partial z}$	$-\frac{\partial p}{\partial z}$	$-\frac{1}{r}\frac{\partial}{\partial r}(r\tau_{rz})$	$-\frac{\partial}{\partial z}\tau_{zz}$	ρg
magnitude [gcm/sec^2cm^3]	953	4750	4703	3 (*1)	23 (921)	980
orientation for the z direction (+ upward, − downward)	+	+	−	+	− (−)	−

*1 The contribution of the polymer solution is less than 5% of the dominant force $-\frac{\partial p}{\partial r}$.

* The figure and sign in the parenthesis are contribution of the polymer solution estimated from TABLE 6.1 to TABLE 6.4.

* The Newtonian stress tensor is calculated by Newton's law:

$$\begin{cases} \tau_{rz} = -\mu\left(\frac{\partial v_z}{\partial r} + \frac{\partial v_r}{\partial z}\right) \\ \tau_{zz} = -2\mu \frac{\partial v_z}{\partial z} \end{cases}$$

where $\mu = .01$ [g/cmsec], $\rho = 1\ g/cm^3$ for water.

shows the magnitude of each term with the orientation of forces around the point $(r/R, z/H) = (.03, .01)$ for the case of $Re_s = 1370$, $SS = -.02$. As shown in TABLE 6.6, when the $\tau_{p,zz}$ calculated in the last section is used for the term

$$\frac{\partial}{\partial z} \tau_{zz}$$

it becomes about 20% of the pressure gradient term and the direction of this force turns out to be negative. In other words, the new force produced by the macromolecules tends to push fluid downward, that is, the axial velocity at this point may be increased. Qualitatively speaking, this is consistent with the decrease of the liquid level during the onset behavior because the average axial velocity over the exit hole is increased. Although nothing can be said about the magnitude of the increased axial velocity unless the equation of motion is solved with the polymer stress tensor, it may be a reasonable outcome that the polymer effect appears near the exit hole especially around $r/R = .03$ and causes the liquid level's falling.

In order to see how the flow behavior changes according to the presence of the macromolecules, one must solve the equation of motion with the polymer stress tensor expression (the constitutive equation). This, however, requires a tremendous amount of calculation because nine non-linear partial differential equations (three from the equation of motion and six from the constitutive equation) are to be solved simultaneously. The calculation is much more difficult and involved than the case of Newtonian flow problem. Instead of pursuing this difficult calculation, the polymer effect on the flow behavior may be roughly estimated simply by changing the boundary condition at the exit hole in the Newtonian vortex flow calculation because the polymer stress tensor becomes significant only for this area. The calculation procedure, thus, is described as follows. First, the axial velocity at the exit hole is reasonably estimated by the contribution of the polymer stress tensor. Secondly, the boundary condition of the stream function is fixed according to the estimated axial velocity. Third, the velocity field for the entire vortex flow is calculated by the method described is section 3.5 for a short period of time. And finally the stress tensor is analyzed along the newly calculated stream lines in the same way as described in section 6.4 to see the tendency of the polymer stress field. In this way, we could at least see an initial stage of flow change which may correspond to the onset behavior of vortex inhibition.

According to the results of $\tau_{p,zz}$ obtained in section 6.4, the stream function at the exit hole is estimated (see Appendix E for details). The velocity field is then calculated with this boundary condition for 20 iterations which is equivalent to .286 seconds. An initial condition used for the calculation is the velocity field of the case Re_θ = 1370, SS = 0.02 (See Appendix A for full information). Fig.

6.15 shows the axial velocity at the axis of rotation after 20 iterations. The v_z at $r = 0$ slightly decreases from the Newtonian case especially when z is less then 5 cm. Even for such a short period of time, the axial velocity responds to the change of the boundary condition which is substitution of the polymer effect at the exit hole. The decrease of the axial velocity seems to correspond to one of the experimental findings during the onset behavior of vortex inhibition. The experimental data in Fig. 6.13 is taken within 30 seconds since the polymer effect is first observed. The axial velocity is always changing from time to time because of the random fluctuation of the air core. All the v_z data in the figure, however, are lower than that of the Newtonian case. The results of calculation does indicate this tendency.

The newly calculated tangential velocity, on the other hand, is no appreciably changed at all from the initial state especially outside the hole region. This is also consistent with the experimental facts. For example, as shown in Fig. 6.12, tangential velocity data during the onset period is not different from the data taken before the onset.

Fig 6.16 shows the stream lines obtained from the calculation. The dotted lines are the stream lines for the initial state. The flow pattern as a whole is not so different in the two calculations. However, the

Fig. 6.15

Axial Velocity Profile after Imposing Polymer Effect

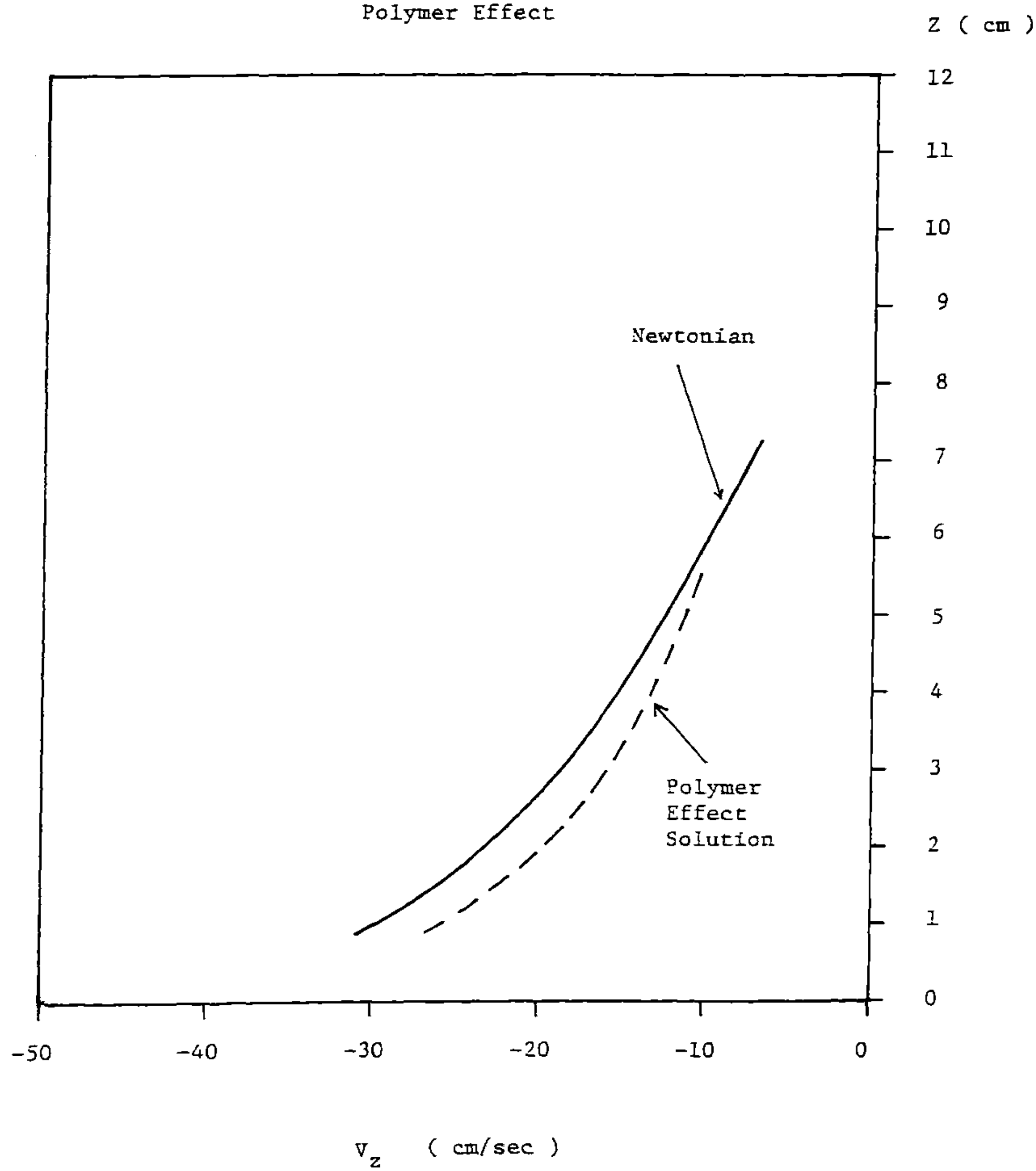

Fig. 6.16

Stream Lines near the Exit Hole after Imposing the Polymer Effect

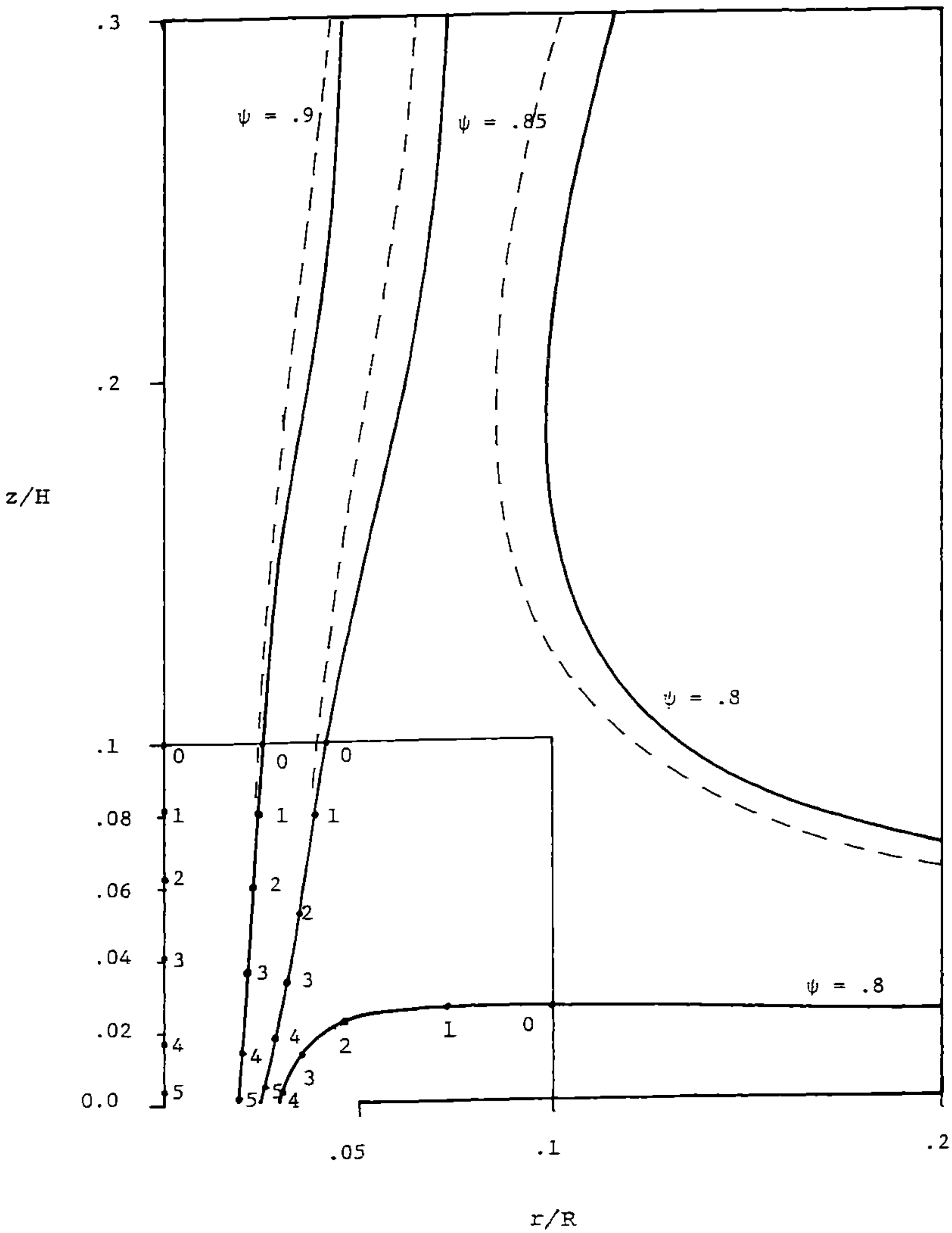

stream lines above the bottom boundary layer shift to the right to some extent. This shift also explains the reduction of v_z at $r = 0$ because the radial distance between $\psi = 1.$ and $\psi = .9$ becomes wider. The polymer stress tensor is calculated along each of the stream lines in Fig. 6.16 in the same manner as in section 6.4. The results are listed in TABLE 6.7 to TABLE 6.11. Again $\tau_{p,zz}$ very near the exit hole is increased so rapidly for $\psi = .8$ and $\psi = .85$. And the magnitude of $\tau_{p,zz}$ in both stream lines are a little larger than before. $\underline{\underline{\tau}}_p$ along the stream lines $\psi = 1.0$ and $\psi = .9$ is not increased enough to cope with dominant force of the equation of motion and the macromolecules are not stretched at all. The tendency of the polymer stress tensor observed in section 6.5 is even more emphasized in this calculation. In other words, $\tau_{p,zz}$ still becomes large enough to be comparable to the dominant force so that the fluid may be pushed downward again. It is found from the sequence of the calculations that the initial effect of the macromolecules, that is, to increase v_z at the exit hole around $r/R = .03$, keeps its tendency as time proceeds because the increased v_z also increases the responsible velocity gradient

$$\frac{\partial v_z}{\partial z}$$

producing higher stress tensor component (especially $\psi = .85$). This nature of $\tau_{p,zz}$ is important because once the polymer

TABLE 6.7

POLYMER STRESS TENSOR ALONG THE NEWLY CALCULATED STREAM LINE $\psi = 1.0$

POINT NUMBER	TIME [SEC]	$\underline{\underline{\tau}}_p$ $[g \cdot cm/sec^2 \cdot cm^2]$						$\langle \left(\frac{R}{R_o}\right)^2 \rangle$
		$\tau_{p,rr}$	$\tau_{p,\theta\theta}$	$\tau_{p,zz}$	$\tau_{p,r\theta}$	$\tau_{p,rz}$	$\tau_{p,\theta z}$	
0	0	0	0	0	0	0	0	
1	.01	0	0	-.015	0	0	0	.0150
2	.02	0	0	-.042	0	0	0	.0156
3	.03	0	0	-.054	0	0	0	.0159
4	.04	0	0	-.152	0	0	0	.0183
5	.045	0	0	-.230	0	0	0	.0201

TABLE 6.8

POLYMER STRESS TENSOR ALONG THE NEWLY CALCULATED STREAM LINE $\psi = .9$

POINT NUMBER	TIME	$\underline{\underline{\tau}}_p$						$<\left(\frac{R}{R_o}\right)^2>$
		$\tau_{p,rr}$	$\tau_{p,\theta\theta}$	$\tau_{p,zz}$	$\tau_{p,r\theta}$	$\tau_{p,rz}$	$\tau_{p,\theta z}$	
0	0	0	0	0	0	0	0	
1	.02	0	0	-.205	0	-.089	-.124	.0194
2	.04	0	0	-.291	0	-.090	-.137	.0214
3	.06	.013	.014	-.298	.002	-.081	-.124	.0209
4	.075	.064	.056	-1.247	.009	.016	-.128	.0394
5	.081	.101	.052	-5.045	.109	.109	-.100	.1056

TABLE 6.7

POLYMER STRESS TENSOR ALONG THE NEWLY CALCULATED STREAM LINE $\psi = 1.0$

POINT NUMBER	TIME [SEC]	$\underline{\underline{\tau}}_p$ $[g \cdot cm/sec^2 \cdot cm^2]$						$\left\langle \left(\frac{R}{R_o}\right)^2 \right\rangle$
		$\tau_{p,rr}$	$\tau_{p,\theta\theta}$	$\tau_{p,zz}$	$\tau_{p,r\theta}$	$\tau_{p,rz}$	$\tau_{p,\theta z}$	
0	0	0	0	0	0	0	0	
1	.01	0	0	-.015	0	0	0	.0150
2	.02	0	0	-.042	0	0	0	.0156
3	.03	0	0	-.054	0	0	0	.0159
4	.04	0	0	-.152	0	0	0	.0183
5	.045	0	0	-.230	0	0	0	.0201

TABLE 6.8

POLYMER STRESS TENSOR ALONG THE NEWLY CALCULATED STREAM LINE $\psi = .9$

POINT NUMBER	TIME	$\underline{\underline{\tau}}_p$						$\left\langle \left(\frac{R}{R_o}\right)^2 \right\rangle$
		$\tau_{p,rr}$	$\tau_{p,\theta\theta}$	$\tau_{p,zz}$	$\tau_{p,r\theta}$	$\tau_{p,rz}$	$\tau_{p,\theta z}$	
0	0	0	0	0	0	0	0	
1	.02	0	0	-.205	0	-.089	-.124	.0194
2	.04	0	0	-.291	0	-.090	-.137	.0214
3	.06	.013	.014	-.298	.002	-.081	-.124	.0209
4	.075	.064	.056	-1.247	.009	.016	-.128	.0394
5	.081	.101	.052	-5.045	.109	.109	-.100	.1056

TABLE 6.9

POLYMER STRESS TENSOR ALONG THE NEWLY CALCULATED STREAM LINE $\psi = .85$

POINT NUMBER	TIME [SEC]	$\underline{\underline{\tau}}_p$ [g·cm/sec^2·cm^2]						$<\left(\frac{R}{R_o}\right)^2>$
		$\tau_{p,rr}$	$\tau_{p,\theta\theta}$	$\tau_{p,zz}$	$\tau_{p,r\theta}$	$\tau_{p,rz}$	$\tau_{p,\theta z}$	
0	0	0	0	0	0	0	0	
1	.05	-8.917	-3.092	-2.505	5.382	-4.716	2.779	.2313
2	.10	-13.552	-5.643	-7.402	8.870	-10.018	6.470	.3456
3	.13	-8.990	-3.555	-23.532	5.775	-14.551	9.160	.4180
4	.15	-.982	-.107	-40.625	-.405	-6.585	-2.610	.4551
5	.16	-.319	-.093	-131.810	-.241	-7.394	-4.456	.7526

TABLE 6.10

POLYMER STRESS TENSOR ALONG THE NEWLY CALCULATED STREAM LINE $\psi = .8$

POINT NUMBER	TIME [SEC]	$\underline{\underline{\tau}}_p$ [g·cm/sec^2·cm^2]						$<\left(\frac{R}{R_o}\right)^2>$
		$\tau_{p,rr}$	$\tau_{p,\theta\theta}$	$\tau_{p,zz}$	$\tau_{p,r\theta}$	$\tau_{p,rz}$	$\tau_{p,\theta z}$	
0	0	0	0	0	0	0	0	
1	.04	-.0382	-.595	-.143	.574	-.243	.195	.0395
2	.08	-6.436	-.914	-6.286	2.494	-6.415	2.323	.2217
3	.10	-5.411	-.268	-34.717	-.996	-13.699	-2.922	.4478
4	.106	-2.327	-.022	-177.127	-.262	-20.540	-2.678	.8097

effect appears this effect may continue.

In this section it is found from the analysis of $\tau_{p,zz}$ that the dramatic increase of $\tau_{p,zz}$ along the stream lines $\psi = .85$ and $\psi = .8$ very near the exit hole seems to explain qualitatively experimental characteristics of the onset behavior of vortex inhibition, namely, the liquid level's falling and the reduction of v_z at $r = 0$.

The mechanism of vortex inhibition is discussed in the next section based on the main results of the previous sections.

6.6 A Proposed Mechanism of Vortex Inhibition

The results of the Newtonian vortex flow calculation indicate that the velocity gradient

$$\frac{\partial v_z}{\partial z}$$

increases significantly only near the exit hole and the experimental observations of the onset behavior suggest that the polymer effect starts with both the liquid level's falling and the reduction of v_z at $r = 0$. Since the onset behavior of vortex inhibition is a transient state from the Newtonian vortex flow to a fully developed vortex flow of polymer solution, the initial change of the polymer contribution to the stress tensor is calculated by solving the constitutive equation using the Newtonian velocity field. The dramatic increase of $\tau_{p,zz}$ very near the exit hole is found from the calculation. This increase is mainly due to the strong elongational type of flow which stretches the macromolecules. Furthermore, the simple simulation shows that the increased $\tau_{p,zz}$ seems qualitatively to explain the onset bahavior of vortex inhibition.

Although the mechanism of the fully developed vortex flow may not be precisely described because of the complicated nature of the phenomenon, we may speculate the mechanism for the fluctuation of the air core from the analysis of the onset behavior. The suppression of the air core corresponds to the decrease of v_θ in the core region and the reduction of v_θ may be due to the decrease of v_z at $r = 0$ which is one of the polymer effects discussed in the last section. The experimental measurement shows v_z at $r = 0$ is always lower than that for Newtonian case during the onset. The overall flow behavior, then, becomes more like the case of the low tangential Reynolds number (see Fig. 6.1, for example). As shown in Fig. 6.1, the flow approaches the exit hole from all directions, and a bottom boundary layer no longer exists. The flow behavior is quite different from that of high Re_θ. For high Re_θ, most of the flow (about 80%) is from the thin bottom boundary layer as shown in Fig. 6.2. The fluid element from the boundary layer has almost zero axial velocity and it is merged with the fluid from the core region near the exit hole. The fluid element is then axially accelerated rapidly within the length of the boundary layer thickness producing the large velocity gradient. This explains why $\tau_{p,zz}$ becomes very large only for the stream lines $\psi = .8$ and $\psi = .85$ ($\psi = .8$ is from the boundary layer and $\psi = .85$ is the stream line next to $\psi = .8$). Since a large velocity gradient

$$\frac{\partial v_z}{\partial z}$$

does not exist near the exit hole in the absence of the bottom boundary layer during the suppression of the air core, no polymer effect is expected. The flow system, thus, tries to go back the original Newtonian vortex flow. And the tangential velocity in the core region increases producing the extension of the air core again. This whole process may explain the fluctuation of the air core.

VII. CONCLUDING REMARKS

Three major conclusions are drawn from the results of this study. They are:

1) The numerical calculation for the confined Newtonian vortex flow provides reasonable velocity field for the entire vortex tank geometry. The calculated velocity field reasonably agrees with experimentally measured v_θ at the free stream region and v_z along the axis of rotation by photographic tracer technique. The consistency in the comparison may make the velocity information reliable for the area near the exist hole and for the bottom boundary layer. The vortex flow studied in the thesis is highly non-linear (Re_θ is up to 2000) and has a singularity at the exist hole. The alternating-direction implicit method with the zone formulation is gound to be suitable for this kind of complicated flow problem.

2) The Modified Nearly Hookean Dumbbell model seems to be an appropriate constitutive equation for the vortex inhibition study. The model can predict a boudned large elongational viscosity which may change the flow behavior at high strain rates as well as shear thinning. The MNHD also has a simple form so that any kind of locally homogeneous flow can be applied for obtaining the polymer stress field. It is found from dynamical studies of the model that the time to reach steady state in start-up of elongational flow is well scaled by the reciprocal of elongational rate $\dot{\varepsilon}^{-1}$. This result is quite different from that of shear flow which is

scaled by the time constant λ_H.

3) A highly elongational type of flow, namely very high velocity gradient

$$\frac{\partial v_z}{\partial z},$$

is established in the vicinity of the exit hole according to the results of the numerical calculation. This large velocity gradient may be a cause of the onset behavior of vortex inhibition. The application of the velocity field to the MNHD shows that the macromolecules moving along the stream lines passing the bottom boundary layer and outside the core region (See $\psi = .8$ and $\psi = .85$ in Fig. 6.14) seem to be almost stretched out to the maximum length R_o very near the exit hole. The stretched macromolecules produce large stress tensor which seems to explain qualitatively the characteristics of the onset behavior of vortex inhibition.

The following possible studies are recommended as extentions of this study.

1) To develop the solving method for the non-Newtonian velocity field by solving the constitutive equation and the equations of motion simultaneously.

2) To develop an experimental technique to measure the velocity field especially in the vicinity of the exit hole.

3) To develop an experimental technique to measure rheological properties (shear viscosity, the normal stress coefficient and hopefully elongational viscosity) of a dilute

solution of flexible linear macromolecules.

4) To establish high elongational type of flow in a simple geometry so that both measurement and calculation of the velocity field are easier. This may also confirm the importance of elongational viscosity for dilute polymer solutions.

Since the elongational viscosity seems to be responsible for the flow change of the onset behavior of vortex inhibition, the mechanism of drag reduction may also be related to the large elongational viscosity exerted by macromolecules. As to this direction,

5) To study the turbulent pipe flow to obtain detailed velocity information about the bursting process in order to investigate how the macromolecules are deformed.

VIII. APPENDICES

Appendix A: Computer Program of the Newtonian Vortex Flow Calculation.

As described in Chap. 3, this computer program is designed for solving the Navior-Stokes equations in a confined vortex flow especially for high tangential Reynolds number. The methods used in the program are lined SOR for the stream function and ADI for the circulation and vorticity. The calculation program mainly consists of six files, KEIKO, STFN, VRVZ, CIRL, VOTY and RESI. The file KEIKO controls the whole calculation procedure which is described in Fig. 3.12. It can start and cease the calculation. The initial conditions, a time increment for the circulation and vorticity, zone description and many parameters are also determined in KEIKO. The calculation data are stored or read or printed or punched in this file. KEIKO also includes several subroutines. The subroutine NONS determines the boundary values of vorticity ω_b at the bottom wall according to eq. 3.55. The subroutine KEIKO, a basic tool of both lined SOR and ADI, solves the tridiagonal system matrix.

The stream function is solved by the lined SOR in the file STFN. The interpolated stream function which defined at each corner of the zone is also calculated in this file. VRVZ determines the radial and axial velocity from the interpolated stream function at zone boundaries (See Fig. 3.7). The circulation and vorticity are solved by ADI in files CIRL and

VOTY respectively. In CIRL and VOTY, both functions are first solved implicitly in the r-direction (R-sweep) and followed by Z-sweep using the intermediate results obtained by R-sweep. After certain number of iterations (loop 2), the residuals of each function are calculated in the file RESI.

Description of Variables

Variable	Description
ST(I,J)	Stream function ψ
STN(I,J)	The intermediate stream function after R-sweep
CI(I,J)	Circulation Γ
CIN(I,J)	The intermediate circulation after R-sweep
VO(I,J)	Vorticity ω
VON(I,J)	The intermediate vorticity after R-sweep
VR(I,J)	Radial velocity v_r
VZ(I,J)	Axial velocity v_z
EX(I,J)	The interpolated stream function
R(I)	The radial position of zone center
DR(I)	Zone size for r-direction
Z(J)	The axial position of zone center
DZ(J)	Zone size for z-direction
RS(I,J)	The residual of stream function
RC(I,J)	The residual of circulation
RV(I,J)	The residual of vorticity
M	Constant for WRITE format
N	Constant for PUNCH format
L	Constant for READ format
NT	The number of variables(ψ,Γ,ω) location in r-direction
NTC	NTC = NT - 1
NTC1	NTC1 = NT - 2; The number of zones in r-direction
MT	The number of variables (ψ,Γ,ω) locations in z-direction

Variable	Description
MTC	MTC = MT - 1
MTC1	MTC1 = MT - 2; the number of zones in z-direction
NEXIT	The radial location of the radius of the exit hole
NE1	NE1 = NEXIT - 1
IM	The index number for choosing the method to determine the bottom boundary values of VORTICITY ω_b. IM = 1 ~ 4 (See subroutine NONS in file KEIKO)
IP	The number of inner iterations
IDD	The number of outer iterations
ICT	ICT = IP x IDD; The number of total iterations
RE	Tangential Reynolds number defined by eq. 3.53
SS	The ratio of v_R to $v_{\theta R}$ defined by eq. 3.54
SFAC	The relaxation factor for stream function calculation
AFER	The convergency criterion for stream function calculation described by eq. 3.60
A	The ratio of R to H
INOP	INOP = 1; Fixed boundary condition at the exit hole for stream function (This condition is used for the polymer effect calculation described in section 6.5) INOP = 2; The Newtonian calculation
IIST	Stream function data reference number for input
IICI	Circulation data reference number for input
IIVO	Vorticity data reference number for input
IOST	Stream function data reference number for output
IOCI	Circulation data reference number for output
IOVO	Vorticity data reference number for output

Program Listing

The complete listing of the six files are followed.

FILE: KEIKO   FORTRAN A   CONVERSATIONAL MONITOR SYSTEM

```
CC     THE FILE KEIKO HAS THE FOLLOWING CHARACTERISTICS.
CC       TO INPUT AND OUTPUT THE DATA.
CC       TO CONSTRUCT THE ZONE.
CC       TO DETERMINE THE ITERATION SCHEME.
CC       TO CONTROL OVERALL CALCULATION AS DESCRIBED IN
CC       FIG. 3. 12.
CC       TO DETERMINE THE BOTTOM WALL VORTICITY ( IN SUBROUTINE
CC       NONS ).
CC       TO PRINT AND PUNCH THE DATA.
CC       TO SOLVE THE TRI-DIAGONAL MATRIX.
       DEFINE FILE 10(38,120,L,I12), 15(38,120,L,I17)
       DEFINE FILE 20(38,120,L,I22)
       DEFINE FILE 61(38,120,L,I10),71(38,120,L,I15)
       DEFINE FILE 81(38,120,L,I20)
       COMMON ST(12,38),CI(12,38),VO(12,38),R(12),DR(12)
       COMMON DZ(38),Z(38)
       COMMON A,NT,MT,NTC,MTC,NTC1,MTC1,NEXIT,NE1,INOP
       COMMON RE,SWIRL,SS
       COMMON DT(10)
       COMMON SFAC,CFAC,VFAC,AFER
       COMMON EX(12,38)
       COMMON INX,INY
       COMMON DS(10)
       IIST=10
       IICI=15
       IIVO=20
       IOST=61
       IOCI=71
       IOVO=81
       M=6
       L=5
       N=9
       DO 6 I=1,10
     6 DT(I)=0.
       NT=12
       MT=38
       NTC=11
       MTC=37
       NTC1=10
       MTC1=36
       NEXIT=4
       NE1=3
       R(1)=0.
       DR(1)=0.
       DZ(1)=0.
       DR(12)=0.
       DZ(38)=0.
       Z(1)=0.
       DO 70 I=2,6
       DR(I)=.02
    70 DR(I+5)=.18
       DO 71  J=2,21
    71 DZ(J)=.01
       DO 72 J=22,37
    72 DZ(J)=.05
```

```
      DO 73 I=2,NT
   73 R(I)=R(I-1)+(DR(I)+DR(I-1))/2.
      DO 74 J=2,MT
   74 Z(J)=Z(J-1)+(DZ(J)+DZ(J-1))/2.
      IM=3
      IM=1
      IP=20
      IDD=2
      ICT=0
      WRITE(M,400)
  400 FORMAT(/,10X,'IF VZ IS PARABOLIC, INPUT 0',/,
     110X,'IF VR IS ZERO INPUT 1',/)
      READ(L,401) INOP
  401 FORMAT(I10)
      WRITE(M,312)
  312 FORMAT(/,10X,'PLEASE INPUT SS IN F10.5',/)
      READ(L,204) SS
      DO 1 J=1,MT
      READ(IIST'J,200) (ST(I,J),I=1,12)
      READ(IICI'J,200) (CI(I,J),I=1,12)
      READ(IIVO'J,201) (VO(I,J),I=1,12)
    1 CONTINUE
      ST(2,1)=.9946
      WRITE(M,320)
  320 FORMAT(10X,'IF THE SAME SS PARAMETER IS USED, INPUT 1,',/,
     110X,'IF SS AS DIFFERENT, TYPE 0 .',/)
      READ(L,280) ISS
  280 FORMAT(I10)
      IF(ISS) 13,13,14
   13 CONTINUE
      DO 3 I=1,NT
      DO 3 J=1,MT
    3 VO(I,J)=-VO(I,J)*SS
   14 CONTINUE
      WRITE(M,321)
  321 FORMAT(10X,'IF STORED INITIAL CONDITION IS USED, INPUT 1,'
     1,/,10X,'IF NEWLY INPUT INITIAL CONDITION IS USED,INPUT 0',/)
      READ(L,280) ICH
      IF(ICH) 10,10,11
   10 CONTINUE
      CI(2,MT)=.04
      CI(3,MT)=.40
      CI(4,MT)=.50
      CI(5,MT)=.5528
      CI(6,MT)=.6322
       CI(7,MT)=.6748
      CI(8,MT)=.6379
      CI(9,MT)=.6638
      CI(10,MT)=.7552
      CI(11,MT)=.91
      DO 2 I=2,11
      DO 2 J=2,MTC
    2 CI(I,J)=CI(I,MT)
      CI(2,1)=CI(2,MT)
      CI(3,1)=CI(3,MT)
```

```
   11 CONTINUE
  200 FORMAT(12F10.5)
  201 FORMAT(12E10.4)
   25 CONTINUE
      WRITE(M,307)
  307 FORMAT(/,10X,'PLEASE INPUT REYNOLS NUMBER INF10.1',/)
      READ(L,204) RE
      WRITE(M,308)
  308 FORMAT(/,10X,'PLEASE INPUT SPAC IN F10.4',/)
      READ(L,205) SPAC
  205 FORMAT(F10.4)
      WRITE(M,309)
  309 FORMAT(/,10X,'PLEASE INPUT APER IN F12.8',/)
      READ(L,206)  APER
      WRITE(M,310)
  310 FORMAT(/,10X,'PLEASE INPUT DT(1)  IN F12.8',/)
      READ(L,206) DT(1)
  206 FORMAT(F12.8)
      WRITE(M,311)
  311 FORMAT(/,10X,'PLEASE INPUT A IN F10.4',/)
      READ(L,205) A
      WRITE(M,313)
  313 FORMAT(/,10X,'PLEASE INPUT DS(1)  IN F12.8',/)
      READ(L,206) DS(1)
      IIP=0
      II=0
      WRITE(M,150) RE,SS,A
  150 FORMAT(/,10X,'REYNOLD NUMBER IS',F10.1,/,10X,
     1'SS PARAMETER IS',F10.5,/,10X,
     2'ASPECT RATION IS',F5.2,/)
CC    INITIAL CONDITION
      WRITE(M,101)
  101 FORMAT(/,10X,'INITIAL VALUES OF ST,CI AND VO',/)
      WRITE(M,300)
      CALL PPPP(ST,M,Z)
      WRITE(M,301)
      CALL PPPP(CI,M,Z)
      WRITE(M,302)
      CALL PPPP(VO,L,Z)
CC    SET UP ITERATION
   49 CONTINUE
      ICT=ICT+1
      IF(IIP-IP) 50,51,51
   51 II=II+1
      WRITE(M,103) II,ICT
  103 FORMAT(/,10X,'AFTER',I5,'    CYCLES',I5,'    ITERATIONS',//)
      WRITE(M,300)
      CALL PPPP(ST,M,Z)
      WRITE(M,650) INX,INY
  650 FORMAT(/,10X,'NUMBER OF TIMES FOR ST. IS BELOW 0',2I5,/)
      WRITE(M,301)
      CALL PPPP(CI,M,Z)
      CALL VRVZ(R,Z,DR,DZ,EX,A,SS)
      CALL RESI
      IF(II-IDD) 52,53,53
```

```
   52 IIP=0
   50 IIP=IIP+1
      CALL STFN
      CALL NONS(IM,SS)
      CALL CIRL
      CALL VOTY
      GO TO 49
   53 CONTINUE
      CALL PPPP(VO,L,Z)
      DO 30 J=1,MT
      WRITE(IOST'J,200) (ST(I,J),I=1,12)
      WRITE(IOCI'J,200) (CI(I,J),I=1,12)
   30 WRITE(IOVO'J,201) (VO(I,J),I=1,12)
      WRITE(6,305)
  305 FORMAT(/,10X,'PLEASE INPUT SS VALUE IN F10.5')
      READ(L,204) SS
  204 FORMAT(F10.5)
      IF(SS) 21,20,21
   21 CONTINUE
C     ENTER NEW RELAXATION FACTORS
      IDD=2
      ICT=0
      GO TO 25
   20 CONTINUE
  300 FORMAT(/,10X,'STREAM FUNCTION',/)
  301 FORMAT(/,10X,'CIRCULATION',/)
  302 FORMAT(/,10X,'VORTICITY',/)
      STOP
      END
      SUBROUTINE NONS(IM,SS)
      COMMON ST(12,38),CI(12,38),VO(12,38),R(12),DR(12)
      COMMON DZ(38),Z(38)
      COMMON A,NT,MT,NTC,MTC,NTC1,MTC1,NEXIT,NE1
C     THIS SUBROUTINE DETERMINES THE VALUE OF VORTICITY AT
C     THE BOTTOM WALL BY NON-SLIP CONDITION.
C     IM=1:  PRECISE METHOD
C     IM=2:  MR. WON'S METHOD
C     IM=3:  SIMPLE ONE
C     IM=4:   SIMPLE ONE NO.2
      GO TO (1,2,3,4),IM
    1 DO 10 I=NEXIT,NTC
   10 VO(I,1)=(27.*ST(I,2)-ST(I,3))/(9.*DZ(2)**2/4.)*A/R(I)*SS
      GO TO 20
    2 DO 11 I=NEXIT,NTC
   11 VO(I,1)=(25.*ST(I,2)-ST(I,3))/(8.*DZ(2)**2/4.)*A/R(I)*SS
      GO TO 20
    3 DO 12 I=NEXIT,NTC
   12 VO(I,1)=SS*(2.*ST(I,2))/(DZ(2)**2/4.)*A/R(I)
      GO TO 20
    4 DO 13 I=NEXIT,NTC
   13 VO(I,1)=SS*ST(I,2)/(DZ(2)**2/4.)*A/R(I)
   20 VINC=VO(NEXIT,1)/FLOAT(NEXIT+1)
      VO(2,1)=VINC
      DO 14 I=3,NE1
   14 VO(I,1)=2.*VINC+VO(I-1,1)
```

```
      RETURN
      END
      SUBROUTINE PCPC(AB,M)
      DIMENSION AB(12,38)
      IF(M-6) 2,3,3
    3 DO 4 K=1,38
      J=39-K
    4 WRITE(7,100)  (AB(I,J),I=1,12)
      GO TO 1
    2 DO 5 K=1,38
      J=39-K
    5 WRITE(7,101)  (AB(I,J),I=1,6)
      DO 6 K=1,38
      J=39-K
    6 WRITE(7,101)  (AB(I,J),I=7,12)
    1 CONTINUE
  100 FORMAT(12F6.3)
  101 FORMAT(6E12.3)
      RETURN
      END
      SUBROUTINE PPPP(AB,M,Z)
      DIMENSION AB(12,38),Z(38)
      IF(M-6) 2,3,3
    3 DO 4 K=1,38
      J=39-K
    4 WRITE(M,100)  (AB(I,J),I=1,11),Z(J)
      GO TO 1
    2 L=M+1
      DO 5 K=1,38
      J=39-K
    5 WRITE(L,101)  (AB(I,J),I=1,11),Z(J)
    1 CONTINUE
  100 FORMAT(12F10.5)
  101 FORMAT(11E10.3,F10.5)
      RETURN
      END
      SUBROUTINE KEIKO(A,B,C,D,X,NTT1)
      DIMENSION A(36),B(36),C(36),D(36),X(36),G(36),U(36),O(36),Y(36)
      O(1)=0.
      G(1)=B(1)
      U(1)=C(1)/G(1)
      DO 1 I=2,NTT1
      O(I)=A(I)
      G(I)=B(I)-O(I)*U(I-1)
    1 U(I)=C(I)/G(I)
      Y(1)=D(1)/G(1)
      DO 2 I=2,NTT1
    2 Y(I)=(D(I)-Y(I-1)*O(I))/G(I)
      X(NTT1)=Y(NTT1)
      DO 3 J=2,NTT1
      I=1+NTT1-J
    3 X(I)=Y(I)-X(I+1)*U(I)
      RETURN
      END
      FUNCTION DELTA(I,J)
```

```
      IF(I-J) 1,2,1                                                     KEI02760
    1 DELTA=0.                                                          KEI02770
      RETURN                                                            KEI02780
    2 DELTA=1.                                                          KEI02790
      RETURN                                                            KEI02800
      END                                                               KEI02810
```

```
CC    THE FILE STFN CONSISTS OF ONE SUBROUTINE.
CC    THE SUBROUTINE SOLVES STREAM FUNCTION BY THE LINED
CC    SOR WITH RELAXATION FACTOR SFAC. THIS ALSO
CC    CALCULATES INTERPOLATED STREAM FUNCTION FROM WHICH
CC    THE RADIAL AND AXIAL VELOCITIES ARE DETERMINED.
      SUBROUTINE STFN
      DIMENSION F(36),B(36),C(36),D(36),X(36),STN(12,38)
      COMMON ST(12,38),CI(12,38),VO(12,38),R(12),DR(12)
      COMMON DZ(38),Z(38)
      COMMON A,NT,MT,NTC,MTC,NTC1,MTC1,NEXIT,NE1,INOP
      COMMON RE,SWIRL,SS
      COMMON DT(10)
      COMMON SFAC,CFAC,VFAC,AFER
      COMMON EX(12,38)
      COMMON INX,INY
      COMMON DS(10)
      ICON=1
      NTT=1
      INX=0
      INY=0
      IIP=1
   30 CONTINUE
C    R-SWEEP OF STREAM FUNCTION
      DO 100 J=2,MTC
      DO 250 I=2,NTC
      AAA=-A*R(I)**2*VO(I,J)/SS
      DIS1=DR(I+1)+DR(I)
      DIS2=DR(I)+DR(I-1)
      DIS3=DZ(J+1)+DZ(J)
      DIS4=DZ(J)+DZ(J-1)
      DIS5=(R(I-1)+R(I))/2.
      DDDZZ=(Z(J+1)-Z(J-1))/2.
      DDDRR=(R(I+1)-R(I-1))/2.
      S1A=(1./DIS1+1./DIS2)*2./DDDRR*R(I)+2./DIS2+R(I)*DS(IIP)
      S1B=-(1./DIS3+1./DIS4)*2./DDDZZ*A**2*R(I)+R(I)*DS(IIP)
      S1AA=(1./DIS3+1./DIS4)*2./DDDZZ*A**2*R(I)
      S1A=S1A+S1AA
      S1B=R(I)*DS(IIP)
      S2=2./DIS1/DDDRR*R(I)
      S3=2./DIS3*A**2/DDDZZ*R(I)
      S4=(1.+R(I)/DDDRR)*2./DIS2
      S5=2./DIS4*A**2/DDDZZ*R(I)
CC AVOID STREAM FUNCTION BECOMES NEGATIVE
      AAA1=S3*ST(I,J+1)+S5*(1.-DELTA(2,J)*(DELTA(2,I)+DELTA(3,I))*
     1DELTA(1,INOP))*ST(I,J-1)+AAA
      IF(J-2) 70,70,250
   70 IF(I-NEXIT) 250,76,76
   76 IF(AAA1) 77,77,250
   77 AAA1=0.
      INX=INX+1
  250 CONTINUE
      ID=I-2
      IF(ID) 50,50,51
   50 F(I-1)=1.
      B(I-1)=S1A-S5*DELTA(2,J)*DELTA(1,INOP)
```

```
      C(I-1)=-S2
      D(I-1)=AAA1+S4*ST(I-1,J)
     1+S1B*ST(I,J)
      GO TO 200
   51 ID=I-NTC
      IF(ID) 52,53,53
   52 F(I-1)=-S4
      B(I-1)=S1A-S5*DELTA(2,J)*DELTA(3,I)*DELTA(1,INOP)
      C(I-1)=-S2
      D(I-1)=AAA1
     1+S1B*ST(I,J)
      GO TO 200
   53 F(I-1)=-S4
      B(I-1)=S1A
      C(I-1)=0.
      D(I-1)=AAA1+S2*ST(I+1,J)
     1+S1B*ST(I,J)
  200 CONTINUE
      CALL KEIKO(F,B,C,D,X,NTC1)
      DO 55 I=1,NTC1
   55 ST(I+1,J)=SFAC*X(I)+(1.-SFAC)*ST(I+1,J)
  100 CONTINUE
C    Z-SWEEP OF STREAM FUNCTION
      DO 300 I=2,NTC
      DO 400 J=2,MTC
      AAA=-A/SS*R(I)**2*VO(I,J)
      DIS1=DR(I+1)+DR(I)
      DIS2=DR(I)+DR(I-1)
      DIS3=DZ(J+1)+DZ(J)
      DIS4=DZ(J)+DZ(J-1)
      DIS5=(R(I-1)+R(I))/2.
      DDDRR=(R(I+1)-R(I-1))/2.
      DDDZZ=(Z(J+1)-Z(J-1))/2.
      S1B=(1./DIS3+1./DIS4)*2.*A**2*R(I)/DDDZZ+R(I)*DS(IIP)
      S1A=-(1./DIS1+1./DIS2)*2.*R(I)/DDDRR-2./DIS2+R(I)*DS(IIP)
      S1BB=S1A*(-1.)+R(I)*DS(IIP)
      S1B=S1B+S1BB
      S1A=R(I)*DS(IIP)
      S2=2./DIS1/DDDRR*R(I)
      S3=2./DIS3*A**2/DDDZZ*R(I)
      S4=(1.+R(I)/DDDRR)*2./DIS2
      S5=2./DIS4*A**2/DDDZZ*R(I)
      ID=J-2
      IF(ID) 60,60,61
   60 F(J-1)=0.
      B(J-1)=S1B-S5*(DELTA(2,I)+DELTA(3,I))*DELTA(1,INOP)
      C(J-1)=-S3
      D(J-1)=S2*ST(I+1,J)+S4*ST(I-1,J)+S5*ST(I,J-1)
     1*(1.-(DELTA(2,I)+DELTA(3,I))*DELTA(1,INOP))
     1+S1A*ST(I,J)+AAA
CC    AVOID ST. IS BELOW ZORO
      IF(I-NEXIT) 73,75,75
   75 DDD=S3*ST(I,J+1)+S5*ST(I,J-1)+AAA
      IF(DDD) 72,72,73
   72 C(J-1)=0.
```

```
CC    THE FILE STFN CONSISTS OF ONE SUBROUTINE.
CC    THE SUBROUTINE SOLVES STREAM FUNCTION BY THE LINED
CC    SOR WITH RELAXATION FACTOR SFAC. THIS ALSO
CC    CALCULATES INTERPOLATED STREAM FUNCTION FROM WHICH
CC    THE RADIAL AND AXIAL VELOCITIES ARE DETERMINED.
      SUBROUTINE STFN
      DIMENSION F(36),B(36),C(36),D(36),X(36),STN(12,38)
      COMMON ST(12,38),CI(12,38),VO(12,38),R(12),DR(12)
      COMMON DZ(38),Z(38)
      COMMON A,NT,MT,NTC,MTC,NTC1,MTC1,NEXIT,NE1,INOP
      COMMON RE,SWIRL,SS
      COMMON DT(10)
      COMMON SFAC,CFAC,VFAC,AFER
      COMMON EX(12,38)
      COMMON INX,INY
      COMMON DS(10)
      ICON=1
      NTT=1
      INX=0
      INY=0
      IIP=1
   30 CONTINUE
C   R-SWEEP OF STREAM FUNCTION
      DO 100 J=2,MTC
      DO 200 I=2,NTC
      AAA=-A*R(I)**2*VO(I,J)/SS
      DIS1=DR(I+1)+DR(I)
      DIS2=DR(I)+DR(I-1)
      DIS3=DZ(J+1)+DZ(J)
      DIS4=DZ(J)+DZ(J-1)
      DIS5=(R(I-1)+R(I))/2.
      DDDZZ=(Z(J+1)-Z(J-1))/2.
      DDDRR=(R(I+1)-R(I-1))/2.
      S1A=(1./DIS1+1./DIS2)*2./DDDRR*R(I)+2./DIS2+R(I)*DS(IIP)
      S1B=-(1./DIS3+1./DIS4)*2./DDDZZ*A**2*R(I)+R(I)*DS(IIP)
      S1AA=(1./DIS3+1./DIS4)*2./DDDZZ*A**2*R(I)
      S1A=S1A+S1AA
      S1B=R(I)*DS(IIP)
      S2=2./DIS1/DDDRR*R(I)
      S3=2./DIS3*A**2/DDDZZ*R(I)
      S4=(1.+R(I)/DDDRR)*2./DIS2
      S5=2./DIS4*A**2/DDDZZ*R(I)
CC AVOID STREAM FUNCTION BECOMES NEGATIVE
      AAA1=S3*ST(I,J+1)+S5*(1.-DELTA(2,J)*(DELTA(2,I)+DELTA(3,I))*
     1DELTA(1,INOP))*ST(I,J-1)+AAA
      IF(J-2) 70,70,250
   70 IF(I-NEXIT) 250,76,76
   76 IF(AAA1) 77,77,250
   77 AAA1=0.
      INX=INX+1
  250 CONTINUE
      ID=I-2
      IF(ID) 50,50,51
   50 F(I-1)=0.
      B(I-1)=S1A-S5*DELTA(2,J)*DELTA(1,INOP)
```

```
      C (I-1)=-S2                                                       STF00560
      D (I-1)=AAA1+S4*ST(I-1,J)                                         STF00570
     1+S1B*ST(I,J)                                                      STF00580
      GO TO 200                                                         STF00590
   51 ID=I-NTC                                                          STF00600
      IF (ID) 52,53,53                                                  STF00610
   52 F (I-1)=-S4                                                       STF00620
      B (I-1)=S1A-S5*DELTA(2,J)*DELTA(3,I)*DELTA(1,INOP)                STF00630
      C (I-1)=-S2                                                       STF00640
      D (I-1)=AAA1                                                      STF00650
     1+S1B*ST(I,J)                                                      STF00660
      GO TO 200                                                         STF00670
   53 F (I-1)=-S4                                                       STF00680
      B (I-1)=S1A                                                       STF00690
      C (I-1)=0.                                                        STF00700
      D (I-1)=AAA1+S2*ST(I+1,J)                                         STF00710
     1+S1B*ST(I,J)                                                      STF00720
  200 CONTINUE                                                          STF00730
      CALL KEIKO(F,B,C,D,X,NTC1)                                        STF00740
      DO 55 I=1,NTC1                                                    STF00750
   55 ST(I+1,J)=SFAC*X(I)+(1.-SFAC)*ST(I+1,J)                           STF00760
  100 CONTINUE                                                          STF00770
C     Z-SWEEP OF STREAM FUNCTION                                        STF00780
      DO 300 I=2,NTC                                                    STF00790
      DO 400 J=2,MTC                                                    STF00800
      AAA=-A/SS*R(I)**2*VO(I,J)                                         STF00810
      DIS1=DR(I+1)+DR(I)                                                STF00820
      DIS2=DR(I)+DR(I-1)                                                STF00830
      DIS3=DZ(J+1)+DZ(J)                                                STF00840
      DIS4=DZ(J)+DZ(J-1)                                                STF00850
      DIS5=(R(I-1)+R(I))/2.                                             STF00860
      DDDRR=(R(I+1)-R(I-1))/2.                                          STF00870
      DDDZZ=(Z(J+1)-Z(J-1))/2.                                          STF00880
      S1B=(1./DIS3+1./DIS4)*2.*A**2*R(I)/DDDZZ+R(I)*DS(IIP)             STF00890
      S1A=-(1./DIS1+1./DIS2)*2.*R(I)/DDDRR-2./DIS2+R(I)*DS(IIP)         STF00900
      S1BB=S1A*(-1.)+R(I)*DS(IIP)                                       STF00910
      S1B=S1B+S1BB                                                      STF00920
      S1A=R(I)*DS(IIP)                                                  STF00930
      S2=2./DIS1/DDDRR*R(I)                                             STF00940
      S3=2./DIS3*A**2/DDDZZ*R(I)                                        STF00950
      S4=(1.+R(I)/DDDRR)*2./DIS2                                        STF00960
      S5=2./DIS4*A**2/DDDZZ*R(I)                                        STF00970
      ID=J-2                                                            STF00980
      IF(ID) 60,60,61                                                   STF00990
   60 F(J-1)=0.                                                         STF01000
      B(J-1)=S1B-S5*(DELTA(2,I)+DELTA(3,I))*DELTA(1,INOP)               STF01010
      C(J-1)=-S3                                                        STF01020
      D(J-1)=S2*ST(I+1,J)+S4*ST(I-1,J)+S5*ST(I,J-1)                     STF01030
     1*(1.-(DELTA(2,I)+DELTA(3,I))*DELTA(1,INOP))                       STF01040
     1+S1A*ST(I,J)+AAA                                                  STF01050
CC    AVOID ST. IS BELOW ZORO                                           STF01060
      IF(I-NEXIT) 73,75,75                                              STF01070
   75 DDD=S3*ST(I,J+1)+S5*ST(I,J-1)+AAA                                 STF01080
      IF(DDD) 72,72,73                                                  STF01090
   72 C(J-1)=0.                                                         STF01100
```

```
      D(J-1)=S2*ST(I+1,J)+S4*ST(I-1,J)+S1A*ST(I,J)
      INY=INY+1
   73 CONTINUE
      GO TO 400
   61 ID=J-MTC
      IF(ID) 62,63,63
   62 F(J-1)=-S5
      B(J-1)=S1B
      C(J-1)=-S3
      D(J-1)=S2*ST(I+1,J)+S4*ST(I-1,J)
     1+S1A*ST(I,J)
     2+AAA
      GO TO 400
   63 F(J-1)=-S5
      B(J-1)=S1B
      C(J-1)=0.
      D(J-1)=S2*ST(I+1,J)+S4*ST(I-1,J)+S3*ST(I,J+1)
     1+S1A*ST(I,J)
     2+AAA
  400 CONTINUE
      CALL KEIKO(F,B,C,D,X,MTC1)
      DO 65 J=1,MTC1
   65 STN(I,J+1)=SFAC*X(J)+(1.-SFAC)*ST(I,J+1)
  300 CONTINUE
CC    CHECK CONVERGENCY
      DO 10 I=2,NTC
      DO 10 J=2,MTC
      ER=ABS((STN(I,J)-ST(I,J))/STN(I,J))
      IF(ER-AFER) 10,10,11
   10 CONTINUE
      WRITE(6,101) ICON
  101 FORMAT(10X,'THE NUMBER OF ITERATION IS',I10)
      GO TO 80
   11 CONTINUE
      DO 15 I=2,NTC
      DO 15 J=2,MTC
   15 ST(I,J)=STN(I,J)
      ICON=ICON+1
      IF(ICON-50) 81,10,10
   81 CONTINUE
      GO TO 30
   80 CONTINUE
      DO 16 I=2,NTC
      DO 16 J=2,MTC
   16 ST(I,J)=STN(I,J)
      IF(INOP-1) 650,600,650
  600 CONTINUE
      ST(2,1)=STN(2,2)
      ST(3,1)=STN(3,2)
  650 CONTINUE
CC CALCULATE INTERPOLATED STREAM FUNCTION
      DO 500 I=1,NTC
      DO 500 J=1,MTC
      EXST=(ST(I,J)*DR(I+1)+ST(I+1,J)*DR(I))/(DR(I)+DR(I+1))
     1*DZ(J+1)/(DZ(J)+DZ(J+1))
```

```
     2+(ST(I,J+1)*DR(I+1)+ST(I+1,J+1)*DR(I))/(DR(I)+DR(I+1))
     3*DZ(J)/(DZ(J)+DZ(J+1))
 500 EX(I,J)=EXST
     RETURN
     END
```

```
CC    THE FILE VRVZ HAS ONE SUBROUTINE VRVZ.
CC    THE SUBROUTINE VRVZ CALCULATES THE RADIAL AND
CC    AXIAL VELOCITIES FROM THE INTERPOLATED STREAM
CC    FUNCTION  WHICH IS DETERMINED IN THE FILE STFN.
CC    THE SUBROUTINE ALSO PRINTS THE VELOCITY DATA.
       SUBROUTINE VRVZ(R,Z,DR,DZ,EX,A,SS)
       DIMENSION R(12),Z(38),DR(12),DZ(38),EX(12,38)
       DIMENSION VR(12,38),VZ(12,38),ZZ(38)
        DO 1 I=2,11
       DO 1 J=2,37
       E1=EX(I,J)
       E2=EX(I-1,J)
       E3=EX(I,J-1)
       E4=EX(I-1,J-1)
       VR(I,J)=SS*(E1-E3)/DZ(J)/(R(I)+DR(I)/2.)
       IF(I-2) 87,87,88
   87  VR(I-1,J)=0.
       GO TO 89
   88  VR(I-1,J)=SS*(E2-E4)/DZ(J)/(R(I-1)+DR(I-1)/2.)
   89  CONTINUE
       VZ(I,J)=-SS*(E1-E2)/DR(I)/R(I)/A
       VZ(I,J-1)=-SS*(E3-E4)/DR(I)/R(I)/A
    1  CONTINUE
       DO 7 J=1,38
       VR(1,J)=0.
    7  VZ(1,J)=0.
       DO 4 I=1,37
    4  ZZ(I)=Z(I)+DZ(I)/2.
       WRITE(6,100)
  100  FORMAT(/,10X,'THE VELOCITY DATA VR AND VZ',//,
      110X,'THE RADIAL VELOCITY VR',/)
       DO 2 K=2,37
       J=39-K
    2  WRITE(6,101)  (VR(I,J),I=1,11),Z(J)
  101  FORMAT(11E10.3,F10.3)
       WRITE(6,102)
  102  FORMAT(/,10X,'THE AXIAL VELOCITY VZ',/)
       DO 3 K=1,37
       J=38-K
    3  WRITE(6,101)  (VZ(I,J),I=1,11),ZZ(J)
       RETURN
       END
```

```fortran
CC    THE FILE CIRL INCLUDES ONE SUBROUTINE CIRL.
CC    THE SUBROUTINE CIRL CALCULATES CIRCULATION BY ADI.
      SUBROUTINE CIRL
      DIMENSION P(36),B(36),C(36),D(36),X(36),CIN(12,38)
      COMMON ST(12,38),CI(12,38),VO(12,38),R(12),DR(12)
      COMMON DZ(38),Z(38)
      COMMON A,NT,MT,NTC,MTC,NTC1,MTC1,NEXIT,NE1,INOP
      COMMON RE,SWIRL,SS
      COMMON DT(10)
      COMMON SFAC,CFAC,VFAC,AFER
      COMMON EX(12,38)
      M=6
      IIP=1
C   R-SWEEP OF CIRCULATION
      DO 81 J=2,MTC
      DO 82 I=3,NTC
      E1=EX(I,J)
      E2=EX(I-1,J)
      E3=EX(I,J-1)
      E4=EX(I-1,J-1)
C   CALCULATION OF DIS AND VEL
      DIS1=DR(I+1)+DR(I)
      DIS2=DR(I)+DR(I-1)
      DIS3=DZ(J+1)+DZ(J)
      DIS4=DZ(J)+DZ(J-1)
      DIS5=R(I)+DR(I)/2.
      DIS6=R(I)-DR(I)/2.
      DIS7=(R(I)+R(I+1))/2.
      DIS8=(R(I)+R(I-1))/2.
C   CONVECTIVE TERMS: VERY IMPORTANT
      V1=SS*(E1-E3)/DZ(J)/(R(I)+DR(I)/2.)
      IF(I-2) 95,95,96
   95 V2=0.
      GO TO 97
   96 V2=SS*(E2-E4)/DZ(J)/(R(I-1)+DR(I-1)/2.)
   97 CONTINUE
      V3=-SS*(E1-E2)/DR(I)/R(I)/A
      V4=-SS*(E3-E4)/DR(I)/R(I)/A
      VEL1=V1+ABS(V1)
      VEL2=V1-ABS(V1)
      VEL3=V2+ABS(V2)
      VEL4=V2-ABS(V2)
      VEL5=V3+ABS(V3)
      VEL6=V3-ABS(V3)
      VEL7=V4+ABS(V4)
      VEL8=V4-ABS(V4)
      EXT=2./(RE*DIS2)
      DDDZZ=(Z(J+1)-Z(J-1))/2.
      DDDRR=(R(I+1)-R(I-1))/2.
      C1A=(VEL1*DIS5-VEL4*DIS6)/(2.*DR(I))
     1+2./RE/DDDRR*R(I)**2*(1./(DIS1*DIS7)+1./(DIS2*DIS8))
     1+R(I)*DT(IIP)
      C1B=-(VEL5-VEL8)/DZ(J)/2.*A*R(I)
     1-2./RE/DDDZZ*R(I)*(1./DIS3+1./DIS4)*A**2
     1+R(I)*DT(IIP)
```

```
      C2=2.*R(I)**2/(RE*DDDRR*DIS1*DIS7)-VEL2/2.*DIS5/DR(I)
      C4=2.*R(I)**2/(RE*DDDRR*DIS2*DIS8)+VEL3/2.*DIS6/DR(I)
      C3=2.*A**2/DIS3/RE/DDDZZ*R(I)-VEL6/2.*A/DZ(J)*R(I)
      C5=2.*A**2/DIS4/RE/DDDZZ*R(I)+VEL7/2.*A/DZ(J)*R(I)
      ID=I-3
      IF(ID) 10,10,3
   10 F(I-1)=0.
      B(I-1)=C1A-C4/9.
      C(I-1)=-C2
      D(I-1)=C1B*CI(I,J)+C3*CI(I,J+1)+C5*CI(I,J-1)
      GO TO 82
    3 IF(I-NZXIT) 4,11,11
    4 F(I-1)=-C4
      B(I-1)=C1A
      C(I-1)=-C2
      D(I-1)=C1B*CI(I,J)+C3*CI(I,J+1)+C5*CI(I,J-1)
      GO TO 82
   11 ID=I-NTC
      IF(ID) 12,13,13
   12 F(I-1)=-C4
      B(I-1)=C1A
      C(I-1)=-C2
      D(I-1)=C1B*CI(I,J)+C3*CI(I,J+1)+C5*CI(I,J-1)
      GO TO 82
   13 F(I-1)=-C4
      B(I-1)=C1A
      C(I-1)=0.
      D(I-1)=C1B*CI(I,J)+C3*CI(I,J+1)+C5*CI(I,J-1)
     1+C2*CI(I+1,J)
   82 CONTINUE
      DO 14 I=1,9
      F(I)=F(I+1)
      B(I)=B(I+1)
      C(I)=C(I+1)
   14 D(I)=D(I+1)
      CALL KEIKO(F,B,C,D,X,9)
      DO 15 I=1,9
   15 CIN(I+2,J)=X(I)
      CIN(2,J)=CIN(3,J)/9.
   81 CONTINUE
      DO 30 J=1,MT
      CIN(1,J)=CI(1,J)
   30 CIN(NT,J)=CI(NT,J)
      DO 31 I=1,NT
      CIN(I,1)=CI(I,1)
   31 CIN(I,MT)=CI(I,MT)
C     Z-SWEEP OF CIRCULATION
      DO 83 I=3,NTC
      DO 84 J=2,MTC
      E1=EX(I,J)
      E2=EX(I-1,J)
      E3=EX(I,J-1)
      E4=EX(I-1,J-1)
C     CALCULATION OF DIS AND VEL
      DIS1=DR(I+1)+DR(I)
```

```
      DIS2=DR(I)+DR(I-1)                                               CIR01110
      DIS3=DZ(J+1)+DZ(J)                                               CIR01120
      DIS4=DZ(J)+DZ(J-1)                                               CIR01130
      DIS5=R(I)+DR(I)/2.                                               CIR01140
      DIS6=R(I)-DR(I)/2.                                               CIR01150
      DIS7=(R(I)+R(I+1))/2.                                            CIR01160
      DIS8=(R(I)+R(I-1))/2.                                            CIR01170
C     CONVECTIVE TERMS: VERY IMPORTANT                                 CIR01180
      V1=SS*(E1-E3)/DZ(J)/(R(I)+DR(I)/2.)                              CIR01190
      IF(I-2) 87,87,88                                                 CIR01200
   87 V2=0.                                                            CIR01210
      GO TO 89                                                         CIR01220
   88 V2=SS*(E2-E4)/DZ(J)/(R(I-1)+DR(I-1)/2.)                          CIR01230
   89 CONTINUE                                                         CIR01240
      V3=-SS*(E1-E2)/DR(I)/R(I)/A                                      CIR01250
      V4=-SS*(E3-E4)/DR(I)/R(I)/A                                      CIR01260
      VEL1=V1+ABS(V1)                                                  CIR01270
      VEL2=V1-ABS(V1)                                                  CIR01280
      VEL3=V2+ABS(V2)                                                  CIR01290
      VEL4=V2-ABS(V2)                                                  CIR01300
      VEL5=V3+ABS(V3)                                                  CIR01310
      VEL6=V3-ABS(V3)                                                  CIR01320
      VEL7=V4+ABS(V4)                                                  CIR01330
      VEL8=V4-ABS(V4)                                                  CIR01340
      EXT=2./(RE*DIS2)                                                 CIR01350
      DDDRE=(R(I+1)-R(I-1))/2.                                         CIR01360
      DDDZZ=(Z(J+1)-Z(J-1))/2.                                         CIR01370
      C1B=(VEL5-VEL8)/DZ(J)/2.*A*R(I)                                  CIR01380
     1+2./RE/DDDZZ*(1./DIS3+1./DIS4)*A**2*R(I)+R(I)*DT(IIP)            CIR01390
      C1A=-(VEL1*DIS5-VEL4*DIS6)/(2.*DR(I))                            CIR01400
     1-2./RE/DDDRE*R(I)**2*(1./(DIS1*DIS7)+1./(DIS2*DIS8))             CIR01410
     1+R(I)*DT(IIP)                                                    CIR01420
      C2=2.*R(I)**2/(RE*DDDRE*DIS1*DIS7)-VEL2/2.*DIS5/DR(I)            CIR01430
      C4=2.*R(I)**2/(RE*DDDRR*DIS2*DIS8)+VEL3/2.*DIS6/DR(I)            CIR01440
      C3=2.*A**2/DIS3/RE/DDDZZ*R(I)-VEL6/2.*A/DZ(J)*R(I)               CIR01450
      C5=2.*A**2/DIS4/RE/DDDZZ*R(I)+VEL7/2.*A/DZ(J)*R(I)               CIR01460
      ID=J-2                                                           CIR01470
      IF(ID) 20,20,21                                                  CIR01480
   20 CONTINUE                                                         CIR01490
      I9=I-NEXIT                                                       CIR01500
      IF(I9) 70,71,71                                                  CIR01510
   70 A(J-1)=0.                                                        CIR01520
      B(J-1)=C1B-C5-C4/9.                                              CIR01530
      C(J-1)=-C3                                                       CIR01540
      D(J-1)=C2*CIN(I+1,J)                                             CIR01550
     1+C1A*CIN(I,J)                                                    CIR01560
      GO TO 84                                                         CIR01570
   71 A(J-1)=0.                                                        CIR01580
      B(J-1)=C1B                                                       CIR01590
      C(J-1)=-C3                                                       CIR01600
      D(J-1)=C2*CIN(I+1,J)+C4*CIN(I-1,J)+C5*CIN(I,J-1)                 CIR01610
     1+C1A*CIN(I,J)                                                    CIR01620
      GO TO 84                                                         CIR01630
   21 ID=J-MTC                                                         CIR01640
      IF(ID) 22,23,23                                                  CIR01650
```

```
   22 F(J-1)=-C5
      B(J-1)=C1B
      C(J-1)=-C3
      D(J-1)=C2*CIN(I+1,J)+C4*CIN(I-1,J)
     1+C1A*CIN(I,J)
      GO TO 84
   23 F(J-1)=-C5+C3/8.
      B(J-1)=C1B-C3*9./8.
      C(J-1)=1.
      D(J-1)=C2*CIN(I+1,J)+C4*CIN(I-1,J)
     1+C1A*CIN(I,J)
   84 CONTINUE
      CALL KEIKO(F,B,C,D,X,MTC1)
      DO 25 J=1,MTC1
   25 CI(I,J+1)=X(J)
   83 CONTINUE
      DO 19 J=2,MTC
   19 CI(2,J)=CI(3,J)/9.
      DO 18 I=2,NE1
   18 CI(I,1)=CI(I,2)
      DO 26 I=1,NT
   26 CI(I,MT)=9./8.*CI(I,MTC)-CI(I,MTC1)/8.
      RETURN
      END
```

```
CC    THE FILE VOTY INCLUDES ONE SUBROUTINE VOTY.
CC    THE SUBROUTINE VOTY SOLVES THE VOTICITY BY ADI.
      SUBROUTINE VOTY
      DIMENSION F(36),B(36),C(36),D(36),X(36),VON(12,38)
      COMMON ST(12,38),CI(12,38),VO(12,38),R(12),DR(12)
      COMMON DZ(38),Z(38)
      COMMON A,NT,MT,NTC,MTC,NTC1,MTC1,NEXIT,NE1,INOP
      COMMON RE,SWIRL,SS
      COMMON DT(10)
      COMMON SFAC,CFAC,VFAC,AFER
      COMMON EX(12,38)
      IIP=1
C     R-SWEEP OF VORTICITY
      DO 5 J=2,MTC
      DO 6 I=2,NTC
      E1=EX(I,J)
      E2=EX(I-1,J)
      E3=EX(I,J-1)
      E4=EX(I-1,J-1)
C     CALCULATION OF DIS AND VEL
      DIS1=DR(I+1)+DR(I)
      DIS2=DR(I)+DR(I-1)
      DIS3=DZ(J+1)+DZ(J)
      DIS4=DZ(J)+DZ(J-1)
      DIS5=R(I)+DR(I)/2.
      DIS6=R(I)-DR(I)/2.
      DIS7=(R(I)+R(I+1))/2.
      DIS8=(R(I)+R(I-1))/2.
C     CONVECTIVE TERMS: VERY IMPORTANT
      V1=SS*(E1-E3)/DZ(J)/(R(I)+DR(I)/2.)
      IF(I-2) 87,87,88
   87 V2=0.
      GO TO 89
   88 V2=SS*(E2-E4)/DZ(J)/(R(I-1)+DR(I-1)/2.)
   89 CONTINUE
      V3=-SS*(E1-E2)/DR(I)/R(I)/A
      V4=-SS*(E3-E4)/DR(I)/R(I)/A
      VEL1=V1+ABS(V1)
      VEL2=V1-ABS(V1)
      VEL3=V2+ABS(V2)
      VEL4=V2-ABS(V2)
      VEL5=V3+ABS(V3)
      VEL6=V3-ABS(V3)
      VEL7=V4+ABS(V4)
      VEL8=V4-ABS(V4)
      DDDZZ=(Z(J+1)-Z(J-1))/2.
      DDDRR=(R(I+1)-R(I-1))/2.
      VEXT=R(I)/RE
      VEXT2=2.*R(I)**2/(RE*DIS1)
      VEXT3=R(I)**2*(V1*DIS5+V2*DIS6)/2.
      V1A=(VEL1*DIS5-VEL4*DIS6)*R(I)**2/(2.*DR(I))
     1+(2.*R(I)**2/DDDRR*(DIS7/DIS1+DIS8/DIS2)+R(I))/RE
     1+R(I)**3*DT(IIP)
      V1B=-(VEL5-VEL8)/DZ(J)/2.*A*R(I)**3
     1-2./RE/DDDZZ*(1./DIS3+1./DIS4)*A**2*R(I)**3+R(I)**3*DT(IIP)
```

```
      V2=R(I)**2*(2.*DIS7/(RE*DIS1*DDDRR)-VEL2*DIS5/(2.*DR(I)))
      V4=R(I)**2*(2.*DIS8/(RE*DIS2*DDDRR)+VEL3*DIS6/(2.*DR(I)))
      V3=R(I)**3*(2./(RE*DIS3*DDDZZ)*A**2-VEL6/(2.*DZ(J))*A)
      V5=R(I)**3*(2./(RE*DIS4*DDDZZ)*A**2+VEL7/(2.*DZ(J))*A)
      V6=2.*A*CI(I,J)*((CI(I,J+1)-CI(I,J))/DIS3
     1+(CI(I,J)-CI(I,J-1))/DIS4)
      ID=I-2
      IF(ID) 30,30,24
   30 F(I-1)=0.
      B(I-1)=V1A
      C(I-1)=-V2
      D(I-1)=V3*VO(I,J+1)+V5*VO(I,J-1)+V4*VO(I-1,J)+V6
     1+V1B*VO(I,J)
      GO TO 6
   24 IF(I-NEXIT) 25,31,31
   25 F(I-1)=-V4
      B(I-1)=V1A
      C(I-1)=-V2
      D(I-1)=V3*VO(I,J+1)+V5*VO(I,J-1)+V6
     1+V1B*VO(I,J)
      GO TO 6
   31 ID=I-NTC
      IF(ID) 32,33,33
   32 F(I-1)=-V4
      B(I-1)=V1A
      C(I-1)=-V2
      D(I-1)=V3*VO(I,J+1)+V5*VO(I,J-1)+V6
     1+V1B*VO(I,J)
      GO TO 6
   33 F(I-1)=-V4
      B(I-1)=V1A
      C(I-1)=0.
      D(I-1)=V3*VO(I,J+1)+V5*VO(I,J-1)+V6+V2*VO(I+1,J)
     1+V1B*VO(I,J)
    6 CONTINUE
      CALL KEIKO(F,B,C,D,X,NTC1)
      DO 35 I=1,NTC1
   35 VON(I+1,J)=X(I)
    5 CONTINUE
      DO 50 J=1,MT
      VON(1,J)=VO(1,J)
   50 VON(NT,J)=VO(NT,J)
      DO 51 I=1,NT
      VON(I,1)=VO(I,1)
   51 VON(I,MT)=VO(I,MT)
C     Z-SWEEP OF VORTICITY
      DO 7 I=2,NTC
      DO 8 J=2,MTC
      E1=EX(I,J)
      E2=EX(I-1,J)
      E3=EX(I,J-1)
      E4=EX(I-1,J-1)
C     CALCULATION OF DIS AND VEL
      DIS1=DR(I+1)+DR(I)
      DIS2=DR(I)+DR(I-1)
```

```
      DIS3=DZ(J+1)+DZ(J)
      DIS4=DZ(J)+DZ(J-1)
      DIS5=R(I)+DR(I)/2.
      DIS6=R(I)-DR(I)/2.
      DIS7=(R(I)+R(I+1))/2.
      DIS8=(R(I)+R(I-1))/2.
C   CONVECTIVE TERMS: VERY IMPORTANT
      V1=SS*(E1-E3)/DZ(J)/(R(I)+DR(I)/2.)
      IF(I-2) 96,96,97
   96 V2=0.
      GO TO 98
   97 V2=SS*(E2-E4)/DZ(J)/(R(I-1)+DR(I-1)/2.)
   98 CONTINUE
      V3=-SS*(E1-E2)/DR(I)/R(I)/A
      V4=-SS*(E3-E4)/DR(I)/R(I)/A
      VEL1=V1+ABS(V1)
      VEL2=V1-ABS(V1)
      VEL3=V2+ABS(V2)
      VEL4=V2-ABS(V2)
      VEL5=V3+ABS(V3)
      VEL6=V3-ABS(V3)
      VEL7=V4+ABS(V4)
      VEL8=V4-ABS(V4)
      DDDZZ=(Z(J+1)-Z(J-1))/2.
      DDDRR=(R(I+1)-R(I-1))/2.
      VEXT=R(I)/RE
      VEXT2=2.*R(I)**2/(RE*DIS1)
      VEXT3=R(I)**2*(V1*DIS5+V2*DIS6)/2.
      V1B=(VEL5-VEL8)/DZ(J)/2.*A*R(I)**3
     1+2./RE/DDDZZ*(1./DIS3+1./DIS4)*A**2*R(I)**3+R(I)**3*DT(IIP)
      V1A=-(VEL1*DIS5-VEL4*DIS6)*R(I)**2/(2.*DR(I))
     1-(2.*R(I)**2/DDDRR*(DIS7/DIS1+DIS8/DIS2)+R(I))/RE
     1+R(I)**3*DT(IIP)
      V2=R(I)**2*(2.*DIS7/(RE*DIS1*DDDRR)
     1-VEL2*DIS5/(2.*DR(I)))
      V4=R(I)**2*(2.*DIS8/(RE*DDDRR*DIS2)
     1-VEL3*DIS6/(2.*DR(I)))
      V3=R(I)**3*(2./(RE*DIS3*DDDZZ)*A**2-VEL6/(2.*DZ(J))*A)
      V5=R(I)**3*(2./(RE*DIS4*DDDZZ)*A**2+VEL7/(2.*DZ(J))*A)
      V6=2.*CI(I,J)*A*((CI(I,J+1)-CI(I,J))/DIS3
     1+(CI(I,J)-CI(I,J-1))/DIS4)
      ID=J-2
      IF(ID) 40,41,41
   40 CONTINUE
      IF(I-NEXIT) 46,47,47
   46 F(J-1)=1.
      B(J-1)=V1B-V5
      C(J-1)=-V3
      D(J-1)=V2*VON(I+1,J)+V4*VON(I-1,J)+V6+V1A*VON(I,J)
      GO TO 8
   47 F(J-1)=0.
      B(J-1)=V1B
      C(J-1)=-V3
      D(J-1)=V2*VON(I+1,J)+V4*VON(I-1,J)+V6+V5*VON(I,J-1)
     1+V1A*VON(I,J)
```

```
      GO TO 8
   41 ID=J-MTC
      IF (ID) 42,43,43
   42 F(J-1)=-V5
      B(J-1)=V1B
      C(J-1)=-V3
      D(J-1)=V2*VON(I+1,J)+V4*VON(I-1,J)+V6
     1+V1A*VON(I,J)
      GO TO 8
   43 F(J-1)=-V5
      B(J-1)=V1B
      C(J-1)=0.
      D(J-1)=V2*VON(I+1,J)+V4*VON(I-1,J)+V6+V3*VON(I,J+1)
     1+V1A*VON(I,J)
    8 CONTINUE
      CALL KEIKO(F,B,C,D,X,MTC1)
      DO 45 J=1,MTC1
   45 VO(I,J+1)=X(J)
    7 CONTINUE
      DO 39 I=2,NE1
   39 VO(I,1)=VO(I,2)
      RETURN
      END
```

```
CC    THE FILE RESI INCLUDES TWO SUBROUTINES, RESI AND PRES.
CC    THE SUBROUTINE RESI CALCULATES THE RESIDUALS OF THE
CC    THREE FUNCTIONS AND THE SUBROUTINE PRES PRINTS THE
CC    RESULTS.
      SUBROUTINE RESI
      DIMENSION RS(12,38),RC(12,38),RV(12,38)
      COMMON ST(12,38),CI(12,38),VO(12,38),R(12),DR(12)
      COMMON DZ(38),Z(38)
      COMMON A,NT,MT,NTC,MTC,NTC1,MTC1,NEXIT,NE1,INOP
      COMMON RE,SWIRL,SS
      COMMON DT(10)
      COMMON SFAC,CFAC,VFAC
      COMMON EX(12,38)
      IIP=1
      DO 2 I=1,NT
      DO 2 J=1,MT
      RS(I,J)=0.
      RC(I,J)=0.
      RV(I,J)=0.
    2 CONTINUE
      DO 1 I=2,NTC
      DO 1 J=2,MTC
      E1=EX(I,J)
      E2=EX(I-1,J)
      E3=EX(I,J-1)
      E4=EX(I-1,J-1)
C     CALCULATION OF DIS AND VEL
      DIS1=DR(I+1)+DR(I)
      DIS2=DR(I)+DR(I-1)
      DIS3=DZ(J+1)+DZ(J)
      DIS4=DZ(J)+DZ(J-1)
      DIS5=R(I)+DR(I)/2.
      DIS6=R(I)-DR(I)/2.
      DIS7=(R(I)+R(I+1))/2.
      DIS8=(R(I)+R(I-1))/2.
C     CONVECTIVE TERMS: VERY IMPORTANT
      V1=SS*(E1-E3)/DZ(J)/(R(I)+DR(I)/2.)
      IF(I-2) 87,87,88
   87 V2=0.
      GO TO 89
   88 V2=SS*(E2-E4)/DZ(J)/(R(I-1)+DR(I-1)/2.)
   89 CONTINUE
      V3=-SS*(E1-E2)/DR(I)/R(I)/A
      V4=-SS*(E3-E4)/DR(I)/R(I)/A
      VEL1=V1+ABS(V1)
      VEL2=V1-ABS(V1)
      VEL3=V2+ABS(V2)
      VEL4=V2-ABS(V2)
      VEL5=V3+ABS(V3)
      VEL6=V3-ABS(V3)
      VEL7=V4+ABS(V4)
      VEL8=V4-ABS(V4)
      DDDZZ=(Z(J+1)-Z(J-1))/2.
      DDDRR=(R(I+1)-R(I-1))/2.
CCC   STREAM FUNCTION
```

```
      AAA=-A/SS*R(I)**2*VO(I,J)
      S1A=(1./DIS1+1./DIS2)*2./DDDRR*R(I)+2./DIS2
      S1AA=(1./DIS3+1./DIS4)*2./DDDZZ*A**2*R(I)
      S1A=S1A+S1AA
      S2=2./DIS1/DDDRR*R(I)
      S3=2./DIS3*A**2/DDDZZ*R(I)
      S4=(1.+R(I)/DDDRR)*2./DIS2
      S5=2./DIS4*A**2/DDDZZ*R(I)
      RS(I,J)=-S1A*ST(I,J)+S2*ST(I+1,J)+S3*ST(I,J+1)+S4*ST(I-1,J)
     1+S5*ST(I,J-1)+AAA
CCC   CIRCULATION
      EXT=2./(RE*DIS2)
      C1A=(VEL1*DIS5-VEL4*DIS6)/(2.*DR(I))
     1+2./RE/DDDRR*R(I)**2*(1./(DIS1*DIS7)+1./(DIS2*DIS8))
     1+R(I)*DT(IIP)
      C1B=-(VEL5-VEL8)/DZ(J)/2.*A*R(I)
     1-2./RE/DDDZZ*R(I)*(1./DIS3+1./DIS4)*A**2+R(I)*DT(IIP)
      C1A=C1A-C1B
      C2=2.*R(I)**2/(RE*DDDRR*DIS1*DIS7)-VEL2/2.*DIS5/DR(I)
      C4=2.*R(I)**2/(RE*DDDRR*DIS2*DIS8)+VEL3/2.*DIS6/DR(I)
      C3=2.*A**2/DIS3/RE/DDDZZ*R(I)-VEL6/2.*A/DZ(J)*R(I)
      C5=2.*A**2/DIS4/RE/DDDZZ*R(I)+VEL7/2.*A/DZ(J)*R(I)
      RC(I,J)=-C1A*CI(I,J)+C2*CI(I+1,J)+C3*CI(I,J+1)+C4*CI(I-1,J)
     1+C5*CI(I,J-1)
CCC    VORTICITY
      VEXT=R(I)/RE
      VEXT2=2.*R(I)**2/(RE*DIS1)
      VEXT3=R(I)**2*(V1*DIS5+V2*DIS6)/2.
      V1A=(VEL1*DIS5-VEL4*DIS6)*R(I)**2/(2.*DR(I))
     1+(2.*R(I)**2/DDDRR*(DIS7/DIS1+DIS8/DIS2)+R(I))/RE
     1+R(I)**3*DT(IIP)
      V1B=-(VEL5-VEL8)/DZ(J)/2.*A*R(I)**3
     1-2./RE/DDDZZ*(1./DIS3+1./DIS4)*A**2*R(I)**3+R(I)**3*DT(IIP)
      V1A=V1A-V1B
      V2=R(I)**2*(2.*DIS7/(RE*DIS1*DDDRR)-VEL2*DIS5/(2.*DR(I)))
      V4=R(I)**2*(2.*DIS8/(RE*DIS2*DDDRR)+VEL3*DIS6/(2.*DR(I)))
      V3=R(I)**3*(2./(RE*DIS3*DDDZZ)*A**2-VEL6/(2.*DZ(J))*A)
      V5=R(I)**3*(2./(RE*DIS4*DDDZZ)*A**2+VEL7/(2.*DZ(J))*A)
      V6=2.*A*CI(I,J)*((CI(I,J+1)-CI(I,J))/DIS3
     1+(CI(I,J)-CI(I,J-1))/DIS4)
      RV(I,J)=-V1A*VO(I,J)+V2*VO(I+1,J)+V3*VO(I,J+1)+V4*VO(I-1,J)
     1+V5*VO(I,J-1)+V6
    1 CONTINUE
CCC   PRINT RESUDUALS
      WRITE(6,100)
      CALL PRES(RS,Z)
      WRITE(6,101)
      CALL PRES(RC,Z)
      WRITE(6,102)
      CALL PRES(RV,Z)
  100 FORMAT(/,10X,'THE RESUDUAL OF EACH FUNCTION',//,10X,
     1'STREAM FUNCTION',/)
  101 FORMAT(/,10X,'CIRCULATION',/)
  102 FORMAT(/,10X,'VORTICITY',/)
      RETURN
```

```
      END                                                         RES01110
      SUBROUTINE PRES(AB,Z)                                       RES01120
      DIMENSION AB(12,38),Z(38)                                   RES01130
      DO 1 K=2,38,3                                               RES01140
      J=39-K                                                      RES01150
    1 WRITE(6,100) (AB(I,J),I=1,11),Z(J)                          RES01160
  100 FORMAT(11E10.3,F10.3)                                       RES01170
      RETURN                                                      RES01180
      END                                                         RES01190
```

The Result of Run #42 ($Re_\theta = 1370$, SS = -.02)

All the calculations are executed by CMS (Conversational Monitor System) under IBM 370 operated by IPC at MIT. The calculation starts with $Re_\theta = 10$ and SS = -1 from the situation where the fluid is completely at rest. After several hundreds of iterations, each function (ψ, Γ, ω) is fully developed. These functions are then stored as initial conditions for higher Reynolds number calculations. For the case $Re_\theta = 1370$ and SS = -.02, the experimentally measured circulation in the free stream region is input as the initial condition for the circulation calculation. The circulation in both core region and bottom boundary layer is reasonably guessed. Setting $Re_\theta = 1370$ and SS = -.02 which corresponds to the experimental condition, the iteration starts. Every fifty iterations, three functions (ψ, Γ, ω) as well as the radial and axial velocities are printed over the entire geometry. Residuals of the three functions are also calculated and printed. The whole calculation is terminated when the following requirements are satisfied.

1. The convergency of the stream function in the loop 1 is very fast, one iteration is desirable (see Fig. 3.12)
2. The circulation and vorticity do not change much in each iteration in the loop 2.
3. The residuals of the three functions are sufficiently

small over the entire geometry when they are compared with the dominant terms in the equations.

The results of each function and the radial and axial velocity after 400 iterations inthe loop 2 are followed.

STREAM FUNCTION

											z
1.00000	1.00000	1.00000	1.00000	1.00000	1.00000	1.00000	1.00000	1.00000	1.00000	1.00000	1.00000
1.00000	1.00039	1.00218	0.99994	0.99769	0.99608	0.99236	0.98893	0.98568	0.98186	0.97754	0.97500
1.00000	0.99969	0.99815	0.99251	0.98776	0.98445	0.97615	0.96660	0.95676	0.94546	0.93251	0.92500
1.00000	0.99803	0.98910	0.98009	0.97365	0.96936	0.95878	0.94385	0.92742	0.90887	0.88737	0.87500
1.00000	0.99700	0.98317	0.97123	0.96271	0.95692	0.94208	0.92079	0.89774	0.87210	0.84216	0.82500
1.00000	0.99679	0.98166	0.96681	0.95540	0.94736	0.92572	0.89709	0.86759	0.83494	0.79683	0.77500
1.00000	0.99663	0.98061	0.96221	0.94760	0.93719	0.90833	0.87229	0.83663	0.79723	0.75131	0.72500
1.00000	0.99613	0.97786	0.95506	0.93710	0.92437	0.88890	0.84615	0.80465	0.75889	0.70559	0.67500
1.00000	0.99508	0.97217	0.94483	0.92383	0.90904	0.86753	0.81863	0.77164	0.71990	0.65964	0.62500
1.00000	0.99363	0.96439	0.93271	0.90901	0.89234	0.84481	0.78977	0.73759	0.68035	0.61352	0.57500
1.00000	0.99218	0.95641	0.92090	0.89468	0.87607	0.82146	0.75974	0.70267	0.64038	0.56732	0.52500
1.00000	0.99093	0.94945	0.91037	0.88150	0.86075	0.79758	0.72864	0.66717	0.60031	0.52116	0.47500
1.00000	0.98990	0.94378	0.90122	0.86957	0.84644	0.77322	0.69692	0.63178	0.56083	0.47531	0.42500
1.00000	0.98891	0.93836	0.89229	0.85778	0.83217	0.74836	0.66547	0.59775	0.52302	0.43022	0.37500
1.00000	0.98784	0.93265	0.88346	0.84653	0.81865	0.72413	0.63607	0.56719	0.48863	0.38661	0.32500
1.00000	0.98644	0.92518	0.87381	0.83544	0.80568	0.70205	0.61188	0.54342	0.46033	0.34550	0.27500
1.00000	0.98476	0.91638	0.86430	0.82640	0.79655	0.69014	0.59773	0.53047	0.44138	0.30829	0.22500
1.00000	0.98346	0.90950	0.85803	0.82321	0.79617	0.68691	0.59279	0.52873	0.43601	0.28882	0.19500
1.00000	0.98238	0.90382	0.85402	0.82283	0.79813	0.68641	0.59207	0.52967	0.43560	0.28299	0.18500
1.00000	0.98139	0.89876	0.85015	0.82288	0.80060	0.68637	0.59223	0.53163	0.43600	0.27754	0.17500
1.00000	0.98054	0.89444	0.84649	0.82306	0.80319	0.68699	0.59370	0.53483	0.43730	0.27251	0.16500
1.00000	0.97979	0.89062	0.84284	0.82302	0.80557	0.68850	0.59680	0.53937	0.43954	0.26795	0.15500
1.00000	0.97913	0.88717	0.83912	0.82257	0.80771	0.69122	0.60170	0.54529	0.44272	0.26391	0.14500
1.00000	0.97854	0.88411	0.83533	0.82166	0.80992	0.69560	0.60839	0.55257	0.44681	0.26045	0.13500
1.00000	0.97805	0.88151	0.83151	0.82010	0.81269	0.70216	0.61674	0.56112	0.45173	0.25764	0.12500
1.00000	0.97769	0.87947	0.82771	0.81758	0.81649	0.71147	0.62655	0.57083	0.45742	0.25556	0.11500
1.00000	0.97744	0.87803	0.82410	0.81355	0.82170	0.72408	0.63751	0.58154	0.46374	0.25430	0.10500
1.00000	0.97727	0.87709	0.82098	0.80753	0.82870	0.74046	0.64923	0.59305	0.47052	0.25400	0.09500
1.00000	0.97709	0.87600	0.81896	0.80288	0.83460	0.76106	0.66121	0.60506	0.47747	0.25477	0.08500
1.00000	0.97667	0.87403	0.81810	0.80194	0.83396	0.78659	0.67279	0.61702	0.48403	0.25667	0.07500
1.00000	0.97584	0.86986	0.81634	0.80129	0.83055	0.81799	0.68292	0.62770	0.48706	0.25953	0.06500
1.00000	0.97456	0.86321	0.81211	0.80829	0.83329	0.85465	0.68957	0.63396	0.48997	0.26247	0.05500
1.00000	0.97326	0.85686	0.80131	0.82756	0.84749	0.89236	0.68776	0.62804	0.48097	0.26283	0.04500
1.00000	0.97160	0.84743	0.77801	0.83302	0.85188	0.91374	0.66342	0.59355	0.45041	0.25420	0.03500
1.00000	0.97117	0.84609	0.80880	0.80549	0.78991	0.86000	0.58503	0.50285	0.37844	0.22361	0.02500
1.00000	0.97179	0.85250	0.72851	0.64647	0.59299	0.64227	0.40686	0.32594	0.24262	0.15179	0.01500
1.00000	0.96553	0.79818	0.39230	0.26630	0.21270	0.20697	0.11126	0.07649	0.05485	0.03585	0.00500
1.00000	0.96555	0.79822	0.0	0.0	0.0	0.0	0.0	0.0	0.0	0.0	0.0
0	.01	.03	.05	.07	.09	.19	.37	.55	.73	.91	

CIRCULATION

											z
0.0	0.04786	0.43071	0.61957	0.69955	0.73514	0.74580	0.76624	0.79911	0.85143	0.93754	1.00000
0.0	0.04789	0.43097	0.61955	0.69954	0.73514	0.74580	0.76624	0.79911	0.85143	0.93753	0.97500
0.0	0.04812	0.43306	0.61940	0.69948	0.73516	0.74583	0.76626	0.79903	0.85141	0.93748	0.92500
0.0	0.04792	0.43131	0.61904	0.69954	0.73528	0.74592	0.76633	0.79912	0.85154	0.93747	0.87500
0.0	0.04750	0.42752	0.61877	0.69973	0.73547	0.74604	0.76643	0.79925	0.85164	0.93747	0.82500
0.0	0.04761	0.42847	0.61967	0.70031	0.73579	0.74622	0.76658	0.79946	0.85173	0.93748	0.77500
0.0	0.04830	0.43472	0.62164	0.70119	0.73623	0.74645	0.76678	0.79964	0.85186	0.93747	0.72500
0.0	0.04885	0.43969	0.62312	0.70201	0.73671	0.74674	0.76705	0.79990	0.85203	0.93748	0.67500
0.0	0.04903	0.44130	0.62382	0.70272	0.73725	0.74711	0.76738	0.80019	0.85226	0.93748	0.62500
0.0	0.04892	0.44024	0.62417	0.70345	0.73784	0.74755	0.76780	0.80058	0.85255	0.93751	0.57500
0.0	0.04873	0.43859	0.62480	0.70439	0.73857	0.74808	0.76831	0.80106	0.85288	0.93754	0.52500
0.0	0.04869	0.43823	0.62598	0.70550	0.73940	0.74872	0.76892	0.80161	0.85328	0.93754	0.47500
0.0	0.04888	0.43991	0.62773	0.70682	0.74033	0.74946	0.76965	0.80226	0.85375	0.93755	0.42500
0.0	0.04919	0.44269	0.62949	0.70804	0.74128	0.75030	0.77047	0.80301	0.85425	0.93758	0.37500
0.0	0.04957	0.44612	0.63108	0.70913	0.74224	0.75121	0.77139	0.80382	0.85483	0.93762	0.32500
0.0	0.04990	0.44914	0.63194	0.70950	0.74291	0.75208	0.77238	0.80472	0.85543	0.93765	0.27500
0.0	0.05042	0.45379	0.63213	0.70843	0.74310	0.75317	0.77353	0.80561	0.85593	0.93768	0.22500
0.0	0.05096	0.45862	0.63247	0.70732	0.74254	0.75336	0.77374	0.80569	0.85590	0.93770	0.19500
0.0	0.05176	0.46583	0.63320	0.70640	0.74126	0.75350	0.77395	0.80583	0.85591	0.93770	0.18500
0.0	0.05238	0.47142	0.63384	0.70545	0.74006	0.75362	0.77425	0.80606	0.85588	0.93771	0.17500
0.0	0.05287	0.47583	0.63471	0.70436	0.73903	0.75372	0.77461	0.80630	0.85582	0.93772	0.16500
0.0	0.05329	0.47963	0.63609	0.70321	0.73824	0.75381	0.77495	0.80649	0.85566	0.93774	0.15500
0.0	0.05367	0.48305	0.63800	0.70206	0.73768	0.75391	0.77524	0.80664	0.85540	0.93774	0.14500
0.0	0.05401	0.48609	0.64033	0.70098	0.73722	0.75402	0.77543	0.80676	0.85509	0.93771	0.13500
0.0	0.05430	0.48868	0.64302	0.70003	0.73674	0.75414	0.77554	0.80680	0.85475	0.93761	0.12500
0.0	0.05452	0.49069	0.64603	0.69935	0.73615	0.75425	0.77556	0.80677	0.85434	0.93747	0.11500
0.0	0.05467	0.49199	0.64926	0.69921	0.73532	0.75434	0.77550	0.80670	0.85385	0.93728	0.10500
0.0	0.05472	0.49246	0.65177	0.70039	0.73370	0.75439	0.77535	0.80654	0.85323	0.93704	0.09500
0.0	0.05472	0.49252	0.65222	0.70278	0.73109	0.75457	0.77512	0.80629	0.85241	0.93671	0.08500
0.0	0.05489	0.49403	0.65151	0.70501	0.72848	0.75498	0.77482	0.80580	0.85118	0.93619	0.07500
0.0	0.05544	0.49900	0.64960	0.70541	0.72612	0.75503	0.77446	0.80479	0.84907	0.93508	0.06500
0.0	0.05645	0.50804	0.64809	0.71036	0.72573	0.75391	0.77397	0.80237	0.84484	0.93211	0.05500
0.0	0.05818	0.52366	0.65185	0.72640	0.73532	0.75310	0.77321	0.79525	0.83530	0.92334	0.04500
0.0	0.05803	0.52227	0.66505	0.73065	0.74279	0.75028	0.76402	0.77358	0.81119	0.89989	0.03500
0.0	0.05940	0.53458	0.70495	0.71903	0.72010	0.72112	0.72380	0.71336	0.74792	0.83821	0.02500
0.0	0.06547	0.58922	0.64046	0.62458	0.61216	0.60896	0.60028	0.56182	0.58833	0.67883	0.01500
0.0	0.05561	0.50050	0.43987	0.36860	0.32343	0.30774	0.28986	0.23548	0.24173	0.30333	0.00500
0.0	0.05561	0.50050	0.0	0.0	0.0	0.0	0.0	0.0	0.0	0.0	0.0
r = 0	.01	.03	.05	.07	.09	.19	.37	.55	.73	.91	

VORTICITY

											Z
0.0	0.0	0.0	0.0	0.0	0.0	0.0	0.0	0.0	0.0	0.0	1.00000
0.0	0.471E+01	0.180E+02	-0.102E+00	-0.930E+00	-0.373E+00	-0.280E-01	-0.191E-02	0.150E-02	-0.219E-04	0.679E-03	0.97500
0.0	0.340E+01	0.118E+02	-0.456E+01	-0.307E+01	-0.111E+01	-0.925E-01	-0.762E-02	-0.954E-03	-0.133E-02	0.583E-03	0.92500
0.0	-0.839E+01	-0.146E+02	-0.116E+02	-0.562E+01	-0.193E+01	-0.161E+00	-0.149E-01	-0.548E-02	-0.252E-02	0.703E-04	0.87500
0.0	-0.157E+02	-0.351E+02	-0.170E+02	-0.788E+01	-0.269E+01	-0.229E+00	-0.221E-01	-0.852E-02	-0.247E-02	0.134E-04	0.82500
0.0	-0.182E+02	-0.409E+02	-0.205E+02	-0.997E+01	-0.345E+01	-0.315E+00	-0.307E-01	-0.100E-01	-0.300E-02	-0.877E-04	0.77500
0.0	-0.175E+02	-0.367E+02	-0.236E+02	-0.120E+02	-0.418E+01	-0.400E+00	-0.422E-01	-0.122E-01	-0.400E-02	-0.741E-04	0.72500
0.0	-0.164E+02	-0.297E+02	-0.274E+02	-0.141E+02	-0.495E+01	-0.498E+00	-0.550E-01	-0.164E-01	-0.556E-02	-0.105E-03	0.67500
0.0	-0.197E+02	-0.338E+02	-0.327E+02	-0.164E+02	-0.573E+01	-0.611E+00	-0.705E-01	-0.211E-01	-0.759E-02	-0.344E-03	0.62500
0.0	-0.280E+02	-0.506E+02	-0.391E+02	-0.188E+02	-0.655E+01	-0.745E+00	-0.911E-01	-0.276E-01	-0.951E-02	-0.496E-03	0.57500
0.0	-0.385E+02	-0.738E+02	-0.455E+02	-0.211E+02	-0.734E+01	-0.898E+00	-0.115E+00	-0.349E-01	-0.120E-01	-0.336E-03	0.52500
0.0	-0.486E+02	-0.962E+02	-0.511E+02	-0.232E+02	-0.812E+01	-0.108E+01	-0.145E+00	-0.440E-01	-0.153E-01	-0.298E-03	0.47500
0.0	-0.570E+02	-0.113E+03	-0.557E+02	-0.249E+02	-0.882E+01	-0.129E+01	-0.182E+00	-0.556E-01	-0.191E-01	-0.466E-03	0.42500
0.0	-0.645E+02	-0.127E+03	-0.596E+02	-0.265E+02	-0.956E+01	-0.153E+01	-0.225E+00	-0.697E-01	-0.239E-01	-0.729E-03	0.37500
0.0	-0.724E+02	-0.141E+03	-0.629E+02	-0.275E+02	-0.101E+02	-0.179E+01	-0.280E+00	-0.875E-01	-0.300E-01	-0.883E-03	0.32500
0.0	-0.837E+02	-0.164E+03	-0.656E+02	-0.273E+02	-0.107E+02	-0.218E+01	-0.342E+00	-0.103E+00	-0.339E-01	-0.878E-03	0.27500
0.0	-0.101E+03	-0.201E+03	-0.687E+02	-0.266E+02	-0.109E+02	-0.219E+01	-0.323E+00	-0.942E-01	-0.307E-01	-0.809E-03	0.22500
0.0	-0.110E+03	-0.229E+03	-0.714E+02	-0.253E+02	-0.950E+01	-0.223E+01	-0.385E+00	-0.119E+00	-0.371E-01	-0.103E-02	0.19500
0.0	-0.125E+03	-0.267E+03	-0.760E+02	-0.223E+02	-0.715E+01	-0.238E+01	-0.501E+00	-0.155E+00	-0.452E-01	-0.136E-02	0.18500
0.0	-0.136E+03	-0.294E+03	-0.812E+02	-0.186E+02	-0.517E+01	-0.254E+01	-0.617E+00	-0.183E+00	-0.497E-01	-0.162E-02	0.17500
0.0	-0.146E+03	-0.314E+03	-0.876E+02	-0.148E+02	-0.334E+01	-0.271E+01	-0.703E+00	-0.193E+00	-0.477E-01	-0.175E-02	0.16500
0.0	-0.155E+03	-0.331E+03	-0.951E+02	-0.117E+02	-0.188E+01	-0.291E+01	-0.740E+00	-0.188E+00	-0.396E-01	-0.166E-02	0.15500
0.0	-0.163E+03	-0.345E+03	-0.103E+03	-0.948E+01	-0.766E+00	-0.314E+01	-0.729E+00	-0.171E+00	-0.272E-01	-0.123E-02	0.14500
0.0	-0.170E+03	-0.357E+03	-0.112E+03	-0.863E+01	0.407E+00	-0.338E+01	-0.681E+00	-0.145E+00	-0.120E-01	-0.335E-03	0.13500
0.0	-0.175E+03	-0.366E+03	-0.121E+03	-0.104E+02	0.224E+01	-0.359E+01	-0.610E+00	-0.113E+00	0.606E-02	0.969E-03	0.12500
0.0	-0.178E+03	-0.371E+03	-0.129E+03	-0.165E+02	0.531E+01	-0.372E+01	-0.522E+00	-0.737E-01	0.283E-01	0.278E-02	0.11500
0.0	-0.180E+03	-0.371E+03	-0.135E+03	-0.308E+02	0.103E+02	-0.376E+01	-0.421E+00	-0.252E-01	0.577E-01	0.604E-02	0.10500
0.0	-0.181E+03	-0.368E+03	-0.136E+03	-0.608E+02	0.214E+02	-0.370E+01	-0.306E+00	0.422E-01	0.101E+00	0.135E-01	0.09500
0.0	-0.183E+03	-0.368E+03	-0.133E+03	-0.826E+02	0.325E+02	-0.364E+01	-0.164E+00	0.156E+00	0.177E+00	0.329E-01	0.08500
0.0	-0.190E+03	-0.381E+03	-0.126E+03	-0.774E+02	0.259E+02	-0.333E+01	0.493E-01	0.400E+00	0.332E+00	0.855E-01	0.07500
0.0	-0.203E+03	-0.409E+03	-0.118E+03	-0.824E+02	0.113E+02	-0.190E+01	0.496E+00	0.988E+00	0.681E+00	0.224E+00	0.06500
0.0	-0.223E+03	-0.459E+03	-0.128E+03	-0.592E+02	0.363E+00	0.150E+01	0.169E+01	0.242E+01	0.146E+01	0.567E+00	0.05500
0.0	-0.239E+03	-0.462E+03	-0.191E+03	0.413E+02	0.198E+02	0.116E+02	0.532E+01	0.540E+01	0.303E+01	0.133E+01	0.04500
0.0	-0.250E+03	-0.492E+03	-0.428E+03	0.121E+03	0.811E+02	0.434E+02	0.136E+02	0.104E+02	0.572E+01	0.280E+01	0.03500
0.0	-0.273E+03	-0.603E+03	0.121E+03	0.203E+03	0.135E+03	0.905E+02	0.259E+02	0.158E+02	0.877E+01	0.493E+01	0.02500
0.0	-0.230E+03	-0.554E+02	0.327E+03	0.241E+03	0.167E+03	0.118E+03	0.309E+02	0.131E+02	0.711E+01	0.516E+01	0.01500
0.0	-0.159E+03	0.177E+03	0.310E+03	0.135E+03	0.340E+02	-0.144E+02	-0.267E+02	-0.235E+02	-0.143E+02	-0.641E+01	0.00500
0.0	-0.159E+03	0.177E+03	-0.877E+04	-0.416E+04	-0.254E+04	-0.116E+04	-0.312E+03	-0.141E+03	-0.754E+02	-0.399E+02	0.0
x = 0	.01	.03	.05	.07	.09	.19	.37	.55	.73	.91	

THE VELOCITY DATA VR AND VZ

THE RADIAL VELOCITY VR

r =0	.02	.04	.06	.08	.1	.28	.46	.64	.82	1.0	z
0.0	0.202E-02	-0.181E-01	-0.368E-01	-0.425E-01	-0.413E-01	-0.271E-01	-0.222E-01	-0.204E-01	-0.198E-01	-0.200E-01	0.975
0.0	-0.772E-01	-0.823E-01	-0.731E-01	-0.634E-01	-0.548E-01	-0.281E-01	-0.225E-01	-0.205E-01	-0.199E-01	-0.200E-01	0.925
0.0	-0.883E-01	-0.906E-01	-0.772E-01	-0.657E-01	-0.564E-01	-0.285E-01	-0.228E-01	-0.207E-01	-0.200E-01	-0.200E-01	0.875
0.0	-0.434E-01	-0.518E-01	-0.526E-01	-0.503E-01	-0.462E-01	-0.285E-01	-0.232E-01	-0.209E-01	-0.201E-01	-0.200E-01	0.825
0.0	-0.146E-01	-0.289E-01	-0.402E-01	-0.436E-01	-0.423E-01	-0.294E-01	-0.238E-01	-0.212E-01	-0.202E-01	-0.200E-01	0.775
0.0	-0.223E-01	-0.389E-01	-0.501E-01	-0.516E-01	-0.487E-01	-0.313E-01	-0.248E-01	-0.217E-01	-0.204E-01	-0.200E-01	0.725
0.0	-0.500E-01	-0.645E-01	-0.686E-01	-0.649E-01	-0.588E-01	-0.337E-01	-0.258E-01	-0.222E-01	-0.206E-01	-0.200E-01	0.675
0.0	-0.798E-01	-0.896E-01	-0.841E-01	-0.752E-01	-0.665E-01	-0.359E-01	-0.268E-01	-0.228E-01	-0.208E-01	-0.200E-01	0.625
0.0	-0.933E-01	-0.992E-01	-0.885E-01	-0.776E-01	-0.685E-01	-0.375E-01	-0.278E-01	-0.232E-01	-0.210E-01	-0.200E-01	0.575
0.0	-0.882E-01	-0.932E-01	-0.831E-01	-0.739E-01	-0.663E-01	-0.387E-01	-0.286E-01	-0.235E-01	-0.210E-01	-0.200E-01	0.525
0.0	-0.745E-01	-0.808E-01	-0.746E-01	-0.684E-01	-0.630E-01	-0.397E-01	-0.291E-01	-0.235E-01	-0.209E-01	-0.200E-01	0.475
0.0	-0.655E-01	-0.729E-01	-0.697E-01	-0.654E-01	-0.613E-01	-0.401E-01	-0.288E-01	-0.229E-01	-0.205E-01	-0.200E-01	0.425
0.0	-0.659E-01	-0.722E-01	-0.680E-01	-0.635E-01	-0.598E-01	-0.393E-01	-0.273E-01	-0.214E-01	-0.196E-01	-0.200E-01	0.375
0.0	-0.783E-01	-0.792E-01	-0.680E-01	-0.610E-01	-0.569E-01	-0.357E-01	-0.235E-01	-0.183E-01	-0.180E-01	-0.200E-01	0.325
0.0	-0.968E-01	-0.886E-01	-0.655E-01	-0.528E-01	-0.466E-01	-0.258E-01	-0.163E-01	-0.131E-01	-0.153E-01	-0.200E-01	0.275
0.0	-0.121E+00	-0.101E+00	-0.572E-01	-0.302E-01	-0.211E-01	-0.142E-01	-0.831E-02	-0.684E-02	-0.119E-01	-0.200E-01	0.225
0.0	-0.237E+00	-0.176E+00	-0.620E-01	0.246E-02	0.149E-01	-0.704E-02	-0.218E-02	-0.144E-02	-0.885E-02	-0.200E-01	0.195
0.0	-0.320E+00	-0.233E+00	-0.685E-01	0.256E-01	0.393E-01	-0.196E-02	0.255E-02	0.226E-02	-0.688E-02	-0.200E-01	0.185
0.0	-0.280E+00	-0.211E+00	-0.609E-01	0.331E-01	0.461E-01	0.395E-02	0.738E-02	0.536E-02	-0.535E-02	-0.200E-01	0.175
0.0	-0.244E+00	-0.193E+00	-0.597E-01	0.320E-01	0.469E-01	0.120E-01	0.134E-01	0.881E-02	-0.369E-02	-0.200E-01	0.165
0.0	-0.217E+00	-0.183E+00	-0.655E-01	0.252E-01	0.449E-01	0.218E-01	0.201E-01	0.124E-01	-0.194E-02	-0.200E-01	0.155
0.0	-0.194E+00	-0.175E+00	-0.740E-01	0.187E-01	0.462E-01	0.334E-01	0.269E-01	0.160E-01	-0.140E-03	-0.200E-01	0.145
0.0	-0.168E+00	-0.166E+00	-0.840E-01	0.156E-01	0.557E-01	0.464E-01	0.336E-01	0.194E-01	0.167E-02	-0.200E-01	0.135
0.0	-0.137E+00	-0.153E+00	-0.974E-01	0.156E-01	0.751E-01	0.608E-01	0.396E-01	0.226E-01	0.349E-02	-0.200E-01	0.125
0.0	-0.102E+00	-0.136E+00	-0.116E+00	0.154E-01	0.103E+00	0.762E-01	0.448E-01	0.253E-01	0.529E-02	-0.200E-01	0.115
0.0	-0.699E-01	-0.114E+00	-0.140E+00	0.134E-01	0.139E+00	0.923E-01	0.488E-01	0.276E-01	0.704E-02	-0.200E-01	0.105
0.0	-0.575E-01	-0.886E-01	-0.132E+00	0.140E-01	0.153E+00	0.108E+00	0.513E-01	0.291E-01	0.866E-02	-0.200E-01	0.095
0.0	-0.915E-01	-0.743E-01	-0.705E-01	-0.203E-02	0.934E-01	0.124E+00	0.517E-01	0.293E-01	0.987E-02	-0.200E-01	0.085
0.0	-0.187E+00	-0.111E+00	-0.350E-01	-0.352E-01	0.205E-01	0.140E+00	0.482E-01	0.267E-01	0.997E-02	-0.200E-01	0.075
0.0	-0.323E+00	-0.210E+00	0.302E-02	0.355E-01	0.621E-01	0.152E+00	0.366E-01	0.179E-01	0.716E-02	-0.200E-01	0.065
0.0	-0.389E+00	-0.350E+00	0.936E-01	0.270E+00	0.227E+00	0.141E+00	0.563E-02	-0.605E-02	-0.292E-02	-0.200E-01	0.055
0.0	-0.467E+00	-0.624E+00	-0.781E-01	0.271E+00	0.226E+00	0.588E-01	-0.723E-01	-0.625E-01	-0.292E-01	-0.200E-01	0.045
0.0	-0.321E+00	-0.410E-01	-0.122E+00	-0.498E+00	-0.551E+00	-0.241E+00	-0.248E+00	-0.178E+00	-0.864E-01	-0.200E-01	0.035
0.0	0.130E+00	-0.555E+00	-0.197E+01	-0.278E+01	-0.260E+01	-0.943E+00	-0.570E+00	-0.371E+00	-0.189E+00	-0.200E-01	0.025
0.0	-0.134E+01	-0.581E+01	-0.796E+01	-0.698E+01	-0.585E+01	-0.201E+01	-0.978E+00	-0.586E+00	-0.312E+00	-0.200E-01	0.015
0.0	-0.151E+01	-0.147E+02	-0.169E+02	-0.107E+02	-0.810E+01	-0.244E+01	-0.100E+01	-0.547E+00	-0.296E+00	-0.200E-01	0.005

THE AXIAL VELOCITY VZ

0.0	0.0	0.0	0.0	0.0	0.0	0.0	0.0	0.0	0.0	0.0	1.000
0.0	0.202E-01	-0.127E+00	-0.149E+00	-0.851E-01	-0.407E-01	-0.101E-01	-0.391E-02	-0.285E-02	-0.247E-02	-0.228E-02	0.950
0.0	-0.752E+00	-0.419E+00	-0.258E+00	-0.134E+00	-0.632E-01	-0.171E-01	-0.762E-02	-0.567E-02	-0.489E-02	-0.453E-02	0.900
0.0	-0.164E+01	-0.729E+00	-0.359E+00	-0.179E+00	-0.843E-01	-0.240E-01	-0.114E-01	-0.845E-02	-0.728E-02	-0.675E-02	0.850
0.0	-0.207E+01	-0.929E+00	-0.467E+00	-0.241E+00	-0.117E+00	-0.338E-01	-0.154E-01	-0.112E-01	-0.962E-02	-0.892E-02	0.800
0.0	-0.222E+01	-0.107E+01	-0.593E+00	-0.318E+00	-0.159E+00	-0.455E-01	-0.195E-01	-0.139E-01	-0.119E-01	-0.110E-01	0.750
0.0	-0.244E+01	-0.126E+01	-0.738E+00	-0.398E+00	-0.200E+00	-0.569E-01	-0.234E-01	-0.164E-01	-0.140E-01	-0.130E-01	0.700
0.0	-0.294E+01	-0.152E+01	-0.891E+00	-0.475E+00	-0.238E+00	-0.673E-01	-0.270E-01	-0.188E-01	-0.161E-0[illegible]	-0.149E-01	0.650
0.0	-0.374E+01	-0.185E+01	-0.104E+01	-0.544E+00	-0.274E+00	-0.772E-01	-0.305E-01	-0.210E-01	-0.180E-01	-0.167E-01	0.600
0.0	-0.467E+01	-0.220E+01	-0.117E+01	-0.609E+00	-0.310E+00	-0.879E-01	-0.339E-01	-0.231E-01	-0.197E-01	-0.184E-01	0.550
0.0	-0.555E+01	-0.253E+01	-0.130E+01	-0.675E+00	-0.350E+00	-0.100E+00	-0.374E-01	-0.250E-01	-0.214E-01	-0.201E-01	0.500
0.0	-0.630E+01	-0.282E+01	-0.142E+01	-0.746E+00	-0.395E+00	-0.114E+00	-0.408E-01	-0.267E-01	-0.230E-01	-0.218E-01	0.450
0.0	-0.695E+01	-0.309E+01	-0.155E+01	-0.821E+00	-0.445E+00	-0.129E+00	-0.439E-01	-0.281E-01	-0.247E-01	-0.238E-01	0.400
0.0	-0.761E+01	-0.335E+01	-0.167E+01	-0.892E+00	-0.495E+00	-0.144E+00	-0.462E-01	-0.293E-01	-0.265E-01	-0.262E-01	0.350
0.0	-0.839E+01	-0.362E+01	-0.176E+01	-0.950E+00	-0.540E+00	-0.156E+00	-0.474E-01	-0.302E-01	-0.288E-01	-0.294E-01	0.300
0.0	-0.936E+01	-0.388E+01	-0.180E+01	-0.971E+00	-0.565E+00	-0.164E+00	-0.478E-01	-0.311E-01	-0.320E-01	-0.339E-01	0.250
0.0	-0.106E+02	-0.415E+01	-0.174E+01	-0.898E+00	-0.547E+00	-0.169E+00	-0.476E-01	-0.317E-01	-0.361E-01	-0.402E-01	0.200
0.0	-0.110E+02	-0.423E+01	-0.167E+01	-0.841E+00	-0.533E+00	-0.171E+00	-0.473E-01	-0.316E-01	-[illegible].370E-01	-0.417E-01	0.190
0.0	-0.117E+02	-0.433E+01	-0.157E+01	-0.753E+00	-0.512E+00	-0.174E+00	-0.468E-01	-0.316E-01	-0.381E-01	-0.435E-01	0.180
0.0	-0.122E+02	-0.442E+01	-0.147E+01	-0.663E+00	-0.490E+00	-0.176E+00	-0.461E-01	-0.316E-01	-0.393E-01	-0.454E-01	0.170
0.0	-0.127E+02	-0.452E+01	-0.139E+01	-0.576E+00	-0.467E+00	-0.177E+00	-0.452E-01	-0.317E-01	-0.406E-01	-0.475E-01	0.160
0.0	-0.132E+02	-0.462E+01	-0.132E+01	-0.491E+00	-0.439E+00	-0.176E+00	-0.443E-01	-0.319E-01	-0.421E-01	-0.497E-01	0.150
0.0	-0.136E+02	-0.472E+01	-0.127E+01	-0.406E+00	-0.404E+00	-0.173E+00	-0.434E-01	-0.324E-01	-0.436E-01	-0.521E-01	0.140
0.0	-0.139E+02	-0.483E+01	-0.124E+01	-0.316E+00	-0.356E+00	-0.169E+00	-0.427E-01	-0.330E-01	-0.453E-01	-0.547E-01	0.130
0.0	-0.142E+02	-0.494E+01	-0.123E+01	-0.215E+00	-0.287E+00	-0.163E+00	-0.423E-01	-0.338E-01	-0.471E-01	-0.575E-01	0.120
0.0	-0.144E+02	-0.506E+01	-0.126E+01	-0.973E-01	-0.186E+00	-0.157E+00	-0.425E-01	-0.346E-01	-0.489E-01	-0.605E-01	0.110
0.0	-0.145E+02	-0.516E+01	-0.134E+01	0.380E-01	-0.436E-01	-0.150E+00	-0.435E-01	-0.356E-01	-0.507E-01	-0.636E-01	0.100
0.0	-0.146E+02	-0.524E+01	-0.143E+01	0.167E+00	0.114E+00	-0.141E+00	-0.456E-01	-0.366E-01	-0.525E-01	-0.670E-01	0.090
0.0	-0.148E+02	-0.528E+01	-0.145E+01	0.225E+00	0.220E+00	-0.126E+00	-0.489E-01	-0.376E-01	-0.541E-01	-0.704E-01	0.080
0.0	-0.152E+02	-0.530E+01	-0.141E+01	0.215E+00	0.274E+00	-0.104E+00	-0.540E-01	-0.386E-01	-0.554E-01	-0.738E-01	0.070
0.0	-0.158E+02	-0.537E+01	-0.123E+01	0.253E+00	0.311E+00	-0.831E-01	-0.617E-01	-0.397E-01	-0.563E-01	-0.770E-01	0.060
0.0	-0.166E+02	-0.557E+01	-0.842E+00	0.481E+00	0.323E+00	-0.732E-01	-0.728E-01	-0.410E-01	-0.561E-01	-0.791E-01	0.050
0.0	-0.175E+02	-0.609E+01	-0.437E+00	0.858E+00	0.334E+00	-0.768E-01	-0.878E-01	-0.424E-01	-0.536E-01	-0.787E-01	0.040
0.0	-0.182E+02	-0.593E+01	-0.550E+00	0.393E+00	0.165E+00	-0.841E-01	-0.102E+00	-0.424E-01	-0.471E-01	-0.724E-01	0.030
0.0	-0.179E+02	-0.676E+01	-0.247E+01	-0.110E+01	-0.251E+00	-0.864E-01	-0.101E+00	-0.375E-01	-0.345E-01	-0.560E-01	0.020
0.0	-0.206E+02	-0.136E+02	-0.738E+01	-0.225E+01	-0.547E+00	-0.739E-01	-0.671E-01	-0.223E-01	-0.163E-01	-0.272E-01	0.010
0.0	-0.236E+02	-0.322E+02	-0.160E+02	0.0	0.0	0.0	0.0	0.0	0.0	0.0	0.0
r = 0	.01	.03	.05	.07	.09	.19	.37	.55	.73	.91	

THE RESUDUAL OF EACH FUNCTION

STREAM FUNCTION

0.0	0.409E-02	-0.202E-01	0.561E-01	0.632E-01	0.238E-01	0.130E-01	0.532E-02	-0.672E-03	-0.154E-02	-0.267E-02	0.975
0.0	0.512E-03	0.577E-01	-0.159E-01	-0.387E-01	-0.178E-01	-0.112E-01	-0.979E-03	-0.618E-02	-0.160E-01	-0.795E-02	0.825
0.0	-0.473E-02	-0.104E+00	0.144E-01	0.653E-01	0.337E-01	0.271E-01	0.126E-01	-0.220E-01	-0.372E-01	-0.220E-01	0.675
0.0	0.143E-01	0.152E+00	0.103E+00	0.732E-01	0.294E-01	0.166E-02	-0.372E-01	-0.678E-01	-0.637E-01	-0.310E-01	0.525
0.0	0.191E-02	0.116E-01	0.226E-01	0.354E-01	0.145E-01	-0.165E-01	-0.619E-01	-0.788E-01	-0.613E-01	-0.254E-01	0.375
0.0	0.884E-02	0.106E+00	0.751E-01	0.771E-01	0.312E-01	-0.117E-01	-0.322E-01	-0.183E-01	0.742E-02	0.100E-01	0.225
0.0	0.101E-01	0.133E+00	0.485E-01	-0.206E-01	0.555E-01	0.315E-02	0.496E-02	0.641E-01	0.963E-01	0.589E-01	0.175
0.0	0.809E-02	0.152E+00	-0.122E+00	-0.121E+00	-0.273E-01	0.235E-01	0.359E-01	0.108E+00	0.150E+00	0.801E-01	0.145
0.0	0.128E-02	0.101E+00	-0.229E+00	-0.195E+00	-0.482E-01	0.420E-01	0.818E-01	0.149E+00	0.166E+00	0.802E-01	0.115
0.0	-0.120E-01	-0.185E-01	-0.201E+00	-0.304E+00	0.427E-01	0.376E-01	0.121E+00	0.215E+00	0.215E+00	0.117E+00	0.085
0.0	-0.299E-01	-0.223E+00	-0.351E+00	0.139E+00	-0.154E+00	0.984E-01	0.130E+00	0.355E+00	0.309E+00	0.125E+00	0.055
0.0	-0.194E-01	-0.155E+00	-0.211E+00	-0.183E+00	-0.255E-01	0.771E-01	0.109E+00	0.321E+00	0.263E+00	0.113E+00	0.025
0.0	0.0	0.0	0.0	0.0	0.0	0.0	0.0	0.0	0.0	0.0	0.0

CIRCULATION

0.0	0.468E-02	-0.236E-01	-0.125E-01	-0.596E-02	0.209E-02	-0.112E-02	0.137E-02	0.347E-02	0.120E-01	0.720E-02	0.975
0.0	0.210E-02	-0.144E-01	-0.720E-02	-0.329E-02	0.145E-02	-0.179E-02	-0.424E-03	0.317E-02	0.158E-01	-0.790E-02	0.825
0.0	0.360E-02	-0.166E-01	-0.482E-02	0.287E-03	-0.442E-03	0.560E-03	0.311E-02	0.388E-02	0.422E-02	0.408E-01	0.675
0.0	-0.803E-03	-0.713E-02	-0.205E-02	0.141E-03	-0.615E-03	0.317E-02	0.347E-02	0.670E-02	0.378E-01	0.232E-01	0.525
0.0	0.763E-02	-0.143E-01	-0.639E-02	-0.114E-03	-0.235E-04	0.178E-02	0.131E-02	0.179E-02	0.285E-02	-0.808E-02	0.375
0.0	0.107E-01	-0.866E-02	-0.379E-03	-0.307E-03	-0.101E-02	0.210E-02	0.205E-03	-0.693E-03	0.290E-01	0.313E-01	0.225
0.0	0.490E-01	-0.149E-01	0.131E-01	0.304E-02	-0.202E-03	0.322E-03	-0.905E-03	-0.204E-02	0.187E-01	-0.339E-01	0.175
0.0	0.338E-01	-0.214E-01	-0.430E-02	0.623E-02	-0.422E-03	0.408E-03	0.751E-03	-0.331E-02	0.141E-01	-0.708E-02	0.145
0.0	0.144E-01	-0.278E-01	-0.195E-01	0.101E-01	-0.188E-02	-0.217E-02	0.144E-02	-0.352E-02	0.402E-01	0.168E-01	0.115
0.0	0.168E-01	-0.151E-01	-0.112E-01	-0.674E-02	-0.234E-02	0.260E-04	-0.240E-02	-0.698E-02	-0.383E-01	0.217E-01	0.085
0.0	0.174E+00	-0.480E-01	0.457E-01	-0.229E-01	0.118E-01	-0.369E-02	-0.372E-03	-0.825E-02	0.111E-01	0.299E-01	0.055
0.0	0.607E+00	-0.142E+00	-0.388E+00	0.962E-02	-0.396E-02	-0.251E-01	-0.385E-01	0.719E-01	0.625E-01	0.750E-01	0.025
0.0	0.0	0.0	0.0	0.0	0.0	0.0	0.0	0.0	0.0	0.0	0.0

VORTICITY

0.0	-0.275E-02	-0.135E-01	0.418E-02	0.169E-02	0.133E-03	-0.343E-03	-0.198E-03	0.665E-03	0.221E-03	0.363E-03	0.975
0.0	-0.477E-02	0.186E-01	0.132E-02	-0.177E-03	-0.499E-03	-0.259E-02	-0.192E-02	-0.257E-02	-0.156E-02	-0.159E-03	0.825
0.0	-0.699E-02	-0.292E-01	-0.151E-02	0.251E-02	0.921E-03	-0.529E-02	-0.450E-02	-0.415E-02	-0.316E-02	-0.203E-03	0.675
0.0	-0.198E-01	0.254E-01	0.137E-01	0.668E-02	0.257E-02	-0.889E-02	-0.818E-02	-0.771E-02	-0.[illegible]61E-02	-0.496E-03	0.525
0.0	-0.160E-01	-0.574E-02	-0.991E-03	0.211E-02	0.885E-03	-0.125E-01	-0.118E-01	-0.112E-01	-0.799E-02	-0.968E-03	0.375
0.0	-0.192E-01	0.421E-02	0.153E-01	0.206E-01	0.109E-01	-0.116E-01	-0.128E-01	-0.972E-02	-0.450E-02	-0.118E-02	0.225
0.0	-0.102E+00	-0.158E-01	0.846E-01	-0.945E-02	0.354E-01	-0.831E-02	-0.592E-02	-0.794E-02	0.866E-02	-0.204E-02	0.175
0.0	-0.672E-01	0.181E-02	0.739E-01	0.792E-02	0.185E-01	-0.379E-02	-0.286E-01	-0.223E-01	0.145E-01	-0.140E-03	0.145
0.0	-0.192E-01	0.183E-02	0.184E-01	0.110E+00	0.258E-01	0.939E-03	-0.436E-01	-0.193E-01	0.253E-01	0.172E-01	0.115
0.0	-0.646E-01	0.110E-01	-0.488E-01	0.417E+00	0.703E-01	-0.747E-02	-0.257E-01	0.199E-01	0.100E+00	0.680E-01	0.085
0.0	-0.169E+00	-0.112E+00	0.196E+00	-0.104E+01	-0.188E+00	0.211E+00	0.142E+00	0.303E+00	0.685E+00	0.505E+00	0.055
0.0	0.408E+00	-0.776E+00	-0.115E+02	0.118E+01	0.675E+00	0.146E+01	0.184E+01	-0.101E+01	0.432E+00	0.322E-01	0.025
0.0	0.0	0.0	0.0	0.0	0.0	0.0	0.0	0.0	0.0	0.0	0.0

Appendix B: The Measurement of Intrinsic Viscosity of Polyox WSR 301 (Polyethylene Oxide)

The intrinsic viscosity of Polyox WSR 301 is measured by Ostwald-Fenske viscometer. By keeping temperature constant (25.4 $\pm$ .05°C), the time required for the solution to fall for a certain distance is measured. The time measurement is repeated at least six times to obtain consistent data. The relative, specific and inherent viscosities are then determined by the following equations.

$$\eta_r = \frac{\eta}{\eta_s} \doteq \frac{t}{t_s} \qquad \text{B.1}$$

$$\eta_{sp} = \frac{\eta-\eta_s}{\eta_s} \doteq \frac{t-t_s}{t_s} \qquad \text{B.2}$$

$$\eta_{inh} = (\ln\eta_r)/c \qquad \text{B.3}$$

where ts and t the time required for solvent along (water) and the solution. The intrinsic viscosity is determined from the intersection of the extrapolated curves $\eta sp/c$ and η_{inh} at zero concentration. From Fig. B.1, the intrinsic viscosity is found to be between 12 and 14 [dl/g]. TABLE B.1 shows the intrinsic viscosity and weight average molecular weight obtained from several investigators. Using $[\eta]$ = 14 [dl/g] and Mw = 3.81, the number density n and the time constant λ_H are calculated. According to Bird, Hassager, Armstrong and Cirtiss (1977), the time constant for

FENE dumbbell model is determined by

$$\lambda_H = (5\varepsilon+1)\ \frac{[\eta]_o \eta_s M_w}{RT} \qquad \text{B.4}$$

where R is gas constant. Eq. B.4 with the data gives $\lambda_H = 2.36 \times 10^{-3}$ [sec]. The number density of 30 wppm of Polyox WSR 301 is 4.31×10^{12} [molecules/cm^3]. In the polymer stress calculations in chapters 3.5. and 6, the values of $\lambda_H = .01$ [sec] and $nkT = .2$ [gcm/sec^{2}cm^2] are used.

Fig. B.1

Determination of Intrinsic Viscosity

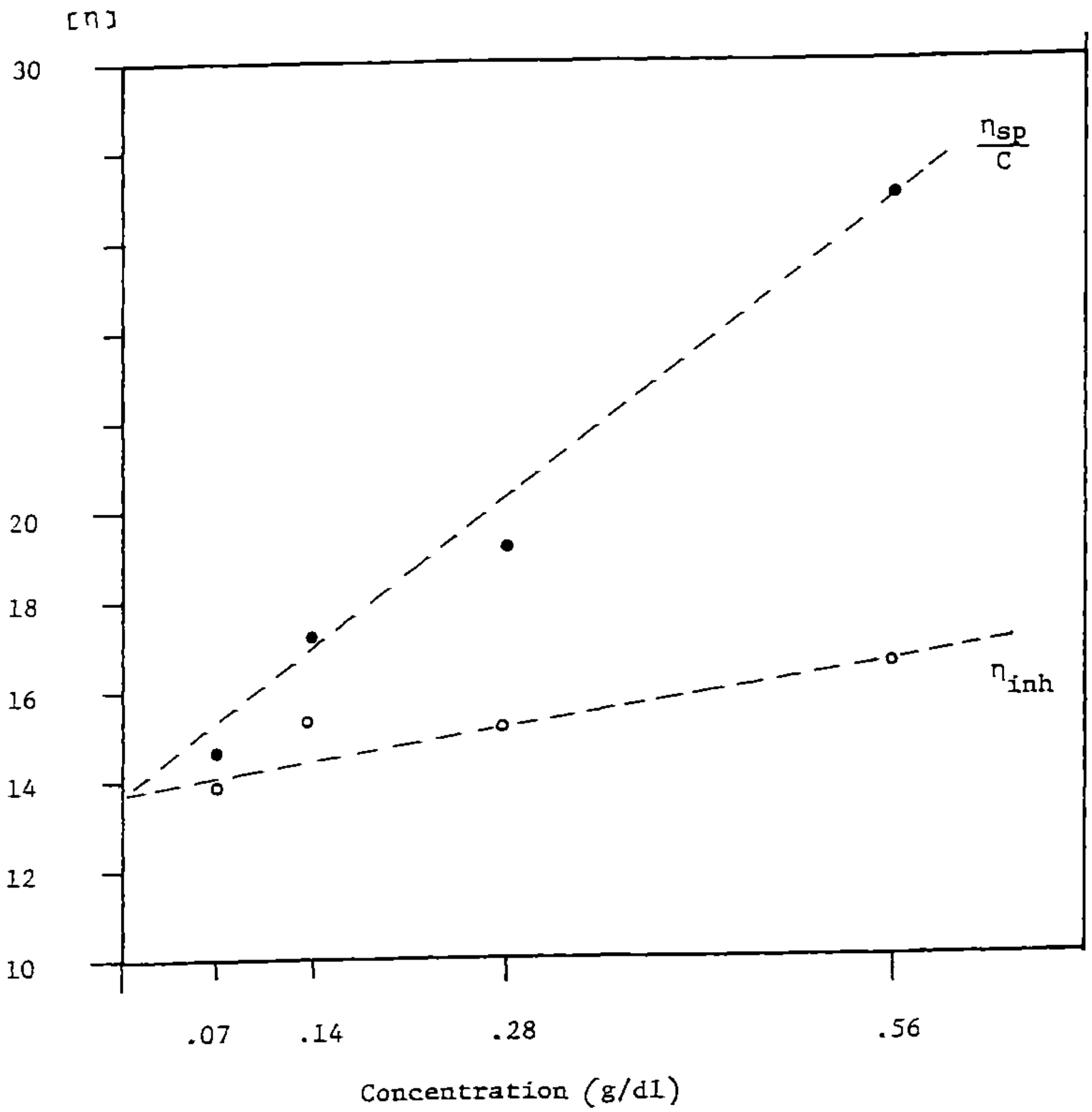

TABLE B.1

THE MOLECULAR CHARACTERISTICS OF POLYOX WSR 301

Name	$[\eta]$ [dl/g]	$M_w \times 10^{-6}$
ISHIKAWA	12-14	3.16-3.81 *
PATERSON (1970)	28	8
CHIOU (1976)	15.1	4.2 *
VIRK (1975)	20.1	6.1

* The molecular weight M_w is calculated by

$$[\eta] = (1.03 \times 10^{-4}) M_w^{0.78}$$

Appendix C: Program Listings for Polymer Stress Calculation by the MNHD

C.1 Polymer Stress Tensor Calculation in Chap. 6

The method used in this calculation is Runge-Kulla fourth order method. Since the stress tensor as well as structure tensor are calculated along the stream lines, the convective terms in the MNHD are eliminated. The equations to be solved are found in eq. 6.1 to eq. 6.13

Description of Variables and Program Listing

Variables	Description
PST (I,II)	I = 1,6 corresponds $\tau_{p,rr}$, $\tau_{p,\theta\theta}$, $\tau_{p,zz}$, $\tau_{p,r\theta}$, $\tau_{p,rz}$, $\tau_{p,\theta z}$ respectively. These components are determined at the points on the stream lines in Fig. 6.14 and Fig. 6.16 II indicates the point number in these figures.
BXX, BXXOD	The time advanced α_{rr} and α_{rr} before the integration.
TXX	$\tau_{p,rr}$ XX, YY, ZZ, XY, XZ, YZ correspond to rr, $\theta\theta$, zz, $r\theta$, rz, θz components respectively.
F1-F6	The calculated values of the right hand side of eq. 6.1 to eq. 6.6
T	Time [sec]
DT	Time increment [sec]
E	The parameter ε
VKMAX	The number of iteration
CNKT	nkT defined in chap. 5
S(1)	$\lambda_H \dfrac{\partial v_r}{\partial r}$

S(2)	$\lambda_H \frac{\partial v_r}{\partial z}$
S(3)	$\lambda_H \frac{v_r}{r}$
S(4)	$\lambda_H \frac{\partial v_z}{\partial z}$
S(5)	$\lambda_H \frac{\partial v_z}{\partial r}$
S(6)	$\lambda_H \frac{\partial v_\theta}{\partial r}$
S(7)	$\lambda_H \frac{\partial v_\theta}{\partial z}$
S(8)	$\lambda_H \frac{v_\theta}{r}$

```
CC    THIS PROGRAM CALCULATES ALL THE STRESS TRENSOR COMPONENTS
CC    ALONG THE STREAM LLINES DESCRIBED IN THE SECTION 6.4.
      DIMENSION TT(10),PST(6,10),H(6,4)
      COMMON BXX,BYY,BZZ,BXY,BXZ,BYZ
      COMMON BXXOD,BYYOD,BZZOD,BXYOD,BXZOD,BYZOD
      COMMON S(8),DT,E,CNKT,COP
      COMMON TXX,TYY,TZZ,TXY,TXZ,TYZ
      COMMON P1,P2,P3,P4,P5,P6
      CNKT=.2
      E=.005
   90 CONTINUE
      WRITE(6,100)
  100 FORMAT(/,10X,'PLEASE INPUT THE VALUE OF STREAM ',
     1'LINE IN F5.2',/)
      READ(5,200) STLN
  200 FORMAT(F5.2)
CC    INITIAL VALUE ASSIGNMENT
      BXX=1.-5.*E
      BYY=1.-5.*E
      BZZ=1.-5.*E
      BXY=0.
      BXZ=0.
      BYZ=0.
      T=0.
      II=0
   70 CONTINUE
      WRITE(6,101)
  101 FORMAT(/,10X,'PLEASE INPUT DT IN F10.5',/)
      READ(5,201) DT
  201 FORMAT(F10.5)
      WRITE(6,102)
  102 FORMAT(/,10X,'PLEASE INPUT VKMAX IN F10.5',/)
      READ(5,201) VKMAX
      KMAX=IFIX(VKMAX)
      WRITE(6,103)
      READ(5,203) S(1)
      WRITE(6,104)
      READ(5,203) S(2)
      WRITE(6,105)
      READ(5,203) S(3)
      WRITE(6,106)
      READ(5,203) S(4)
      WRITE(6,107)
      READ(5,201) S(5)
      WRITE(6,108)
      READ(5,203) S(6)
      WRITE(6,109)
      READ(5,203) S(7)
      WRITE(6,110)
      READ(5,203) S(8)
  203 FORMAT(F10.5)
  103 FORMAT(/,10X,'PLEASE INPUT VELOCITY GRAD S(1) ',
     1'IN F10.5',/)
  104 FORMAT(10X,'INPUT S(2)')
  105 FORMAT(10X,'INPUT S(3)')
```

```
  106 FORMAT(10X,'INPUT S(4)')
  107 FORMAT(10X,'INPUT S(5)')
  108 FORMAT(10X,'INPUT S(6)')
  109 FORMAT(10X,'INPUT S(7)')
  110 FORMAT(10X,'INPUT S(8)')
CC SET K IS EQUAL TC ZERO
      K=0
   51 I=1
      BXXOD=BXX
      BXYOD=BXY
      BYYOD=BYY
      BZZOD=BZZ
      BXZOD=BXZ
      BYZOD=BYZ
   50 CONTINUE
      CALL FCAL
      H(1,I)=DT*F1
      H(2,I)=DT*F2
      H(3,I)=DT*F3
      H(4,I)=DT*F4
      H(5,I)=DT*F5
      H(6,I)=DT*F6
      IF(I-1) 40,40,41
   40 I=2
      T=T+DT/2.
      BXX=BXX+H(1,1)/2.
      BXY=BXY+H(2,1)/2.
      BYY=BYY+H(3,1)/2.
      BZZ=BZZ+H(4,1)/2.
      BXZ=BXZ+H(5,1)/2.
      BYZ=BYZ+H(6,1)/2.
      GO TO 50
   41 IF(I-2) 42,42,43
   42 I=3
      BXX=BXX+H(1,2)/2.-H(1,1)/2.
      BXY=BXY+H(2,2)/2.-H(2,1)/2.
      BYY=BYY+H(3,2)/2.-H(3,1)/2.
      BZZ=BZZ+H(4,2)/2.-H(4,1)/2.
      BXZ=BXZ+H(5,2)/2.-H(5,1)/2.
      BYZ=BYZ+H(6,2)/2.-H(6,1)/2.
      GO TO 50
   43 IF(I-3) 44,44,45
   44 I=4
      T=T+DT/2.
      BXX=BXX+H(1,3)-H(1,2)/2.
      BXY=BXY+H(2,3)-H(2,2)/2.
      BYY=BYY+H(3,3)-H(3,2)/2.
      BZZ=BZZ+H(4,3)-H(4,2)/2.
      BXZ=BXZ+H(5,3)-H(5,2)/2.
      BYZ=BYZ+H(6,3)-H(6,2)/2.
      GO TO 50
   45 K=K+1
      BXX=BXXOD+(H(1,1)+2.*H(1,2)+2.*H(1,3)+H(1,4))/6.
      BXY=BXYOD+(H(2,1)+2.*H(2,2)+2.*H(2,3)+H(2,4))/6.
      BYY=BYYOD+(H(3,1)+2.*H(3,2)+2.*H(3,3)+H(3,4))/6.
```

```
      BZZ=BZZOD+(H(4,1)+2.*H(4,2)+2.*H(4,3)+H(4,4))/6.
      BXZ=BXZOD+(H(5,1)+2.*H(5,2)+2.*H(5,3)+H(5,4))/6.
      BYZ=BYZOD+(H(6,1)+2.*H(6,2)+2.*H(6,3)+H(6,4))/6.
      IF(K-KMAX) 51,60,60
   60 CONTINUE
      CALL STPP
      II=II+1
      TT(II)=T
      PST(1,II)=TXX
      PST(2,II)=TYY
      PST(3,II)=TZZ
      PST(4,II)=TXY
      PST(5,II)=TXZ
      PST(6,II)=TYZ
      WRITE(6,120) STLN,T
  120 FORMAT(/,10X,'THE RESULTS OF STREAM LINE',F5.2,
     1/,10X,'AT THE TIME ',F10.5,/)
      WRITE(6,121)
  121 FORMAT(/,10X,'ALPHA RR',2X,'ALPHA TT',2X,
     1'ALPHA ZZ',2X,'ALPHA RT',2X,'ALPHA RZ',2X,
     1'ALPHA TZ',2X,'EXTENSION RATIO')
      EXT=E*(BXX+BYY+BZZ)
      WRITE(6,122) BXX,BYY,BZZ,BXY,BXZ,BYZ,EXT
  122 FORMAT(/,10X,F8.4,6F10.4)
      WRITE(6,123)
  123 FORMAT(/,10X,'MORE CALCULATION IS NEEDED?',
     1' IF YES, INPUT 1, IF NO, INPUT 0',/)
      READ(5,204) IJD1
  204 FORMAT(I5)
      IF(IJD1) 65,65,70
   65 CONTINUE
CC    PRINT STRESS TENSOR BY THE MNHD
      WRITE(6,125)
  125 FORMAT(/,10X,'TIME',7X,'TRR',7X,'TTT',7X,
     1'TZZ',7X,'TRT',7X,'TRZ',7X,'TTZ',/)
      DO 67 J=1,II
   67 WRITE(6,126) TT(J),(PST(L,J),L=1,6)
  126 FORMAT(/,10X,F4.1,3X,6F10.3)
      WRITE(6,124)
  124 FORMAT(/,10X,'MORE CASE IS NEEDED?',
     1' IF YES, INPUT 1, IF NO, INPUT 0',/)
      READ(5,204) IJD2
      IF(IJD2) 66,66,80
   66 CONTINUE
      STOP
      END
      SUBROUTINE FCAL
CC    THIS SUBROUTINE CALCULATES THE RIGHT HAND SIDES OF EQ.6.1
CC    TO EQ.6.6.
      COMMON BXX,BYY,BZZ,BXY,BXZ,BYZ
      COMMON BXXOD,BYYOD,BZZOD,BXYOD,BXZOD,BYZOD
      COMMON S(3),DT,E,CNKT,COF
      COMMON TXX,TYY,TZZ,TXY,TXZ,TYZ
      COMMON F1,F2,F3,F4,F5,F6
      COF=1.-E*(BXX+BYY+BZZ)
```

```
      F1=2.*S(1)*BXX+2.*S(2)*BXZ-2.*S(8)*BXY
     1-BXX/COF-2.*E*(BXX**2+BXY**2+BXZ**2)*COF+1.
      F3=2.*S(3)*BYY+2.*S(6)*BXY+2.*S(7)*BYZ
     1-BYY/COF-2.*E*(BXY**2+BYY**2+BYZ**2)*COF+1.
      F4=2.*S(4)*BZZ+2.*S(5)*BXZ
     1-BZZ/COF-2.*E*(BXZ**2+BYZ**2+BZZ**2)*COF+1.
      F2=S(6)*BXX+(S(1)+S(3))*BXY-S(8)*BYY+S(2)*BYZ
     1+S(7)*BXZ
     2-BXY/COF-2.*E*(BXX*BXY+BXY*BYY+BXZ*BYZ)*COF
      F5=(S(1)+S(4))*BXZ+S(5)*BXX+S(2)*BZZ-S(8)*BYZ
     1-BXZ/COF-2.*E*(BXX*BXZ+BXY*BYZ+BXZ*BZZ)*COF
      F6=(S(4)+S(3))*BYZ+S(6)*BXZ+S(5)*BXY+S(7)*BZZ
     1-BYZ/COF-2.*E*(BXY*BXZ+BYY*BYZ+BYZ*BZZ)*COF
      RETURN
      END
      SUBROUTINE STPP
CC    THIS SUBROUTINE CALCULATES THE STRESS TENSOR FROM THE
CC    STRUCTURE TENSOR EQUATIONS ( EQ.6.8 TO EQ.6.13 ).
      COMMON BXX,BYY,BZZ,BXY,BXZ,BYZ
      COMMON BXXOD,BYYOD,BZZOD,BXYOD,BXZOD,BYZOD
      COMMON S(8),DT,E,CNKT,COF
      COMMON TXX,TYY,TZZ,TXY,TXZ,TYZ
      COMMON F1,F2,F3,F4,F5,F6
      TXX=(BXX-BXXOD)/DT-2.*S(1)*BXX-2.*S(2)*BXZ+2.*S(8)*BXY
      TYY=(BYY-BYYOD)/DT-2.*S(3)*BYY-2.*S(6)*BXY-2.*S(7)*BYZ
      TZZ=(BZZ-BZZOD)/DT-2.*S(4)*BZZ-2.*S(5)*BXZ
      TXY=(BXY-BXYOD)/DT-S(6)*BXX-(S(1)+S(3))*BXY+S(8)*BYY
     1-S(2)*BYZ-S(7)*BXZ
      TXZ=(BXZ-BXZOD)/DT-(S(1)+S(4))*BXZ-S(5)*BXX-S(2)*BZZ
     1+S(8)*BYZ
      TYZ=(BYZ-BYZOD)/DT-(S(4)+S(3))*BYZ-S(6)*BXZ-S(5)*BXY
     1-S(7)*BZZ
      TXX=TXX*CNKT
      TYY=TYY*CNKT
      TZZ=TZZ*CNKT
      TXY=TXY*CNKT
      TXZ=TXZ*CNKT
      TYZ=TYZ*CNKT
      RETURN
      END
```

C.2 The Intrinsic Viscosity for Shear Flow (in Chap. 5)

This program solves the intrinsic viscosity and the primary normal stress coefficient for shear flow by Ringe-Kutta forth order method.

Description of Main Variables and Program Listing

Variable	Description
VIS	Intrinsic Viscosity
SVIS	Intrinsic viscosity scaled by its steady state value
PSD	Primary normal stress coefficient
SPSD	Primary normal stress coefficient scaled by its steady state value
BXX	α_{xx}
BYY	α_{yy}
BZZ	α_{zz}
BXY	α_{xy}
BXZ	α_{xz}
BYZ	α_{yz}
TXX	$\tau_{p,xx}$
TYY	$\tau_{p,yy}$
TXY	$\tau_{p,xy}$
E	ε
T,T1	Time
DT	Time increment
SR	Dimensionless Shear rate $\lambda_H\dot{\gamma}$

Variable	Description
IMET	Reference number for specifying model IMET = 1; MNHD IMET = 2; TANNER IMET = 3; NHD

```
C     THIS PROGRAM CALCULATES VISCOSITY AND THE PRIMARY
C     NORMAL STRESS COEFFICIENT FOR SHEAR FLOW BY THE
C     THREE DIFFERENT METHODS.
      DIMENSION H(6,4),T1(32)
      DIMENSION SVIS(32),VIS(32),PSD(32),SPSD(32)
      DIMENSION EVI(32)
      COMMON BXX,BXY,BYY,BZZ,BXZ,BYZ
      COMMON F1,F2,F3,F4,F5,F6,SR(8),E(4),M,T,LL
      COMMON C1,IMET
      COMMON AXX,AXY,AYY
      DEFINE FILE 1(200,12,U,I01),2(200,12,U,I02)
      DEFINE FILE 3(200,12,U,I03),4(200,12,U,I04)
      DEFINE FILE 5(200,12,U,I05),6(200,12,U,I06)
      DEFINE FILE 7(200,12,U,I07),8(200,12,U,I08)
      L1=1
      L2=2
      M1=1
      M2=8
C     IMET=1:    MNHD
C     IMET=2:    TANNER'S
C     IMET=3:    NHD
      READ(2,305) IMET
  305 FORMAT(I10)
      GO TO (600,601,602),IMET
  600 WRITE(3,306)
      GO TO 604
  601 WRITE(3,307)
      GO TO 604
  602 WRITE(3,308)
  604 CONTINUE
  306 FORMAT(/,10X,'MODIFIED N.H.D. MODEL',/)
  307 FORMAT(/,10X,'TANNER MODEL',/)
  308 FORMAT(/,10X,'N.H.D. MODEL',/)
  500 CONTINUE
      READ(2,301) C1
  301 FORMAT(F10.2)
      IF(C1) 502,501,502
  502 WRITE(3,302) C1
  302 FORMAT(/,10X,'   PARAMETER C1 = ',F5.2,/)
      NN=0
      READ(2,300) N
  300 FORMAT(I5)
   25 CONTINUE
C   III=0:  STRESS GROWTH FOR SHEAR FLOW
C   III=1:  STRESS RELAXATION FOR SHEAR FLOW
C   III=2:  STRESS GROWTH FOR ELONGATIONAL FLOW
      READ(2,200) III
  200 FORMAT(I10)
      READ(2,350)
  350 FORMAT(F10.5)
      IF(III-1) 19,19,21
   19 CONTINUE
      E(1)=.02
      E(2)=.005
      COF1=1.-5.*E(1)
```

```
      SR(1)=.01/COF1
      SR(2)=.1/COF1
      SR(3)=1./COF1
      SR(4)=10./COF1
      SR(8)=8.0/COF1
      SR(7)=6.0/COF1
      SR(6)=5.0/COF1
      SR(5)=4.0/COF1
      SR(4)=3.0/COF1
      SR(3)=2.0/COF1
      SR(2)=1.4/COF1
      SR(1)=.7/COF1
      GO TO 83
   21 CONTINUE
      E(1)=.02
      E(2)=.005
      COF1=1.-5.*E(1)
      SR(1)=.01/COF1
      SR(2)=.1/COF1
      SR(3)=.5/COF1
      SR(4)=.7/COF1
      SR(5)=1./COF1
      SR(6)=2./COF1
      SR(7)=3./COF1
      SR(7)=10./COF1
   83 CONTINUE
      DO 98 LL=L1,L2
      WRITE(3,104) E(LL)
      DO 99 M=M1,M2
      WRITE(3,103) SR(M)
C  79 CONTINUE
C     INITIAL CONDITION
      IF(III) 1,1,2
    1 WRITE(3,201)
  201 FORMAT(/,10X,'STRESS GROWTH FOR SHEAR FLOW',/)
      BXX=1.-5.*E(LL)
      BXY=0.
      BYY=1.-5.*E(LL)
      BZZ=1.-5.*E(LL)
      BXZ=0.
      BYZ=0.
      VIS(1)=0.
      PSD(1)=0.
      T1(1)=0.
      GO TO 80
    2 IF(III-1) 3,3,4
    3 WRITE(3,202)
  202 FORMAT(/,10X,'STRESS RELAXATION FOR SHEAR FLOW',/)
      VIS(1)=VIS(30)
      PSD(1)=PSD(30)
      T1(1)=0.
      GO TO 80
    4 IF(III-2) 5,5,6
    5 WRITE(3,203)
  203 FORMAT(/,10X,'STRESS GROWTH FOR ELONGATIONAL FLOW',/)
```

FILE: P2   FORTRAN A   CONVERSATIONAL MONITOR SYSTEM

```
      BXX=1.-5.*E(LL)
      BXY=0.
      BYY=1.-5.*E(LL)
      BZZ=1.-5.*E(LL)
      BXZ=0.
      BYZ=0.
      EVI(1)=0.
      GO TO 80
    6 WRITE(3,204)
  204 FORMAT('1',10X,'STRESS RELAXATION FOR ELONGATIONAL FLOW',/)
   80 CONTINUE
CC THE CASE DT=.05
      J=1
      K=1
      T=0.
      DT=.1
      KK=3
      KKK=2
   51 I=1
      BXXOD=BXX
      BXYOD=BXY
      BYYOD=BYY
      BZZOD=BZZ
      BXZOD=BXZ
      BYZOD=BYZ
   50 CONTINUE
      IF(III) 7,7,8
    7 CALL SHGR
      GO TO 81
    8 IF(III-1) 9,9,10
    9 CALL SHRE
      GO TO 81
   10 IF(III-2) 11,11,12
   11 CALL ELGR1
      GO TO 81
   12 CONTINUE
   81 CONTINUE
      H(1,I)=DT*F1
      H(2,I)=DT*F2
      H(3,I)=DT*F3
      H(4,I)=DT*F4
      H(5,I)=DT*F5
      H(6,I)=DT*F6
      IF(I-1) 40,40,41
   40 I=2
      T=T+DT/2.
      BXX=BXX+H(1,1)/2.
      BXY=BXY+H(2,1)/2.
      BYY=BYY+H(3,1)/2.
      BZZ=BZZ+H(4,1)/2.
      BXZ=BXZ+H(5,1)/2.
      BYZ=BYZ+H(5,1)/2.
      GO TO 50
   41 IF(I-2) 42,42,43
   42 I=3
```

```
      BXX=BXX+H(1,2)/2.-H(1,1)/2.
      BXY=BXY+H(2,2)/2.-H(2,1)/2.
      BYY=BYY+H(3,2)/2.-H(3,1)/2.
      BZZ=BZZ+H(4,2)/2.-H(4,1)/2.
      BXZ=BXZ+H(5,2)/2.-H(5,1)/2.
      BYZ=BYZ+H(6,2)/2.-H(6,1)/2.
      GO TO 50
   43 IF(I-3) 44,44,45
   44 I=4
      T=T+DT/2.
      BXX=BXX+H(1,3)-H(1,2)/2.
      BXY=BXY+H(2,3)-H(2,2)/2.
      BYY=BYY+H(3,3)-H(3,2)/2.
      BZZ=BZZ+H(4,3)-H(4,2)/2.
      BXZ=BXZ+H(5,3)-H(5,2)/2.
      BYZ=BYZ+H(6,3)-H(6,2)/2.
      GO TO 50
   45 K=K+1
      BXX=BXXOD+(H(1,1)+2.*H(1,2)+2.*H(1,3)+H(1,4))/6.
      BXY=BXYOD+(H(2,1)+2.*H(2,2)+2.*H(2,3)+H(2,4))/6.
      BYY=BYYOD+(H(3,1)+2.*H(3,2)+2.*H(3,3)+H(3,4))/6.
      BZZ=BZZOD+(H(4,1)+2.*H(4,2)+2.*H(4,3)+H(4,4))/6.
      BXZ=BXZOD+(H(5,1)+2.*H(5,2)+2.*H(5,3)+H(5,4))/6.
      BYZ=BYZOD+(H(6,1)+2.*H(6,2)+2.*H(6,3)+H(6,4))/6.
      IF(III-1) 55,56,55
   55 CONTINUE
      TXX=(BXX-BXXOD)/DT-2.*SR(M)*BXY
      TXY=(BXY-BXYOD)/DT-SR(M)*BYY
      TYY=(BYY-BYYOD)/DT
      GO TO 57
   56 TXX=(BXX-BXXOD)/DT
      TXY=(BXY-BXYOD)/DT
      TYY=(BYY-BYYOD)/DT
   57 CONTINUE
      TXXE=(BXX-BXXOD)/DT+SR(M)*BXX
      TZZE=(BZZ-BZZOD)/DT-2.*SR(M)*BZZ
      IF(K-KK) 46,47,46
   47 J=J+1
      EVI(J)=(TXXE-TZZE)/(3.*(1.-5.*E(LL)))/SR(M)
      VIS(J)=-TXY/SR(M)/COF1
      PSD(J)=-(TXX-TYY)/SR(M)**2/(2.*(1.-12.*E(LL)))
      T1(J)=T
      IF(K-51) 60,61,61
   61 KKK=25
   60 CONTINUE
      KK=KK+KKK
   46 IF(T-15.) 51,52,52
   52 CONTINUE
      IF(III) 13,13,14
   13 CONTINUE
      DO 70 I=1,30
      SPSD(I)=PSD(I)/PSD(30)
   70 SVIS(I)=VIS(I)/VIS(30)
      GO TO 82
   14 IF(III-1) 15,15,16
```

```
   15 DO 71 I=1,30
      SPSD(I)=PSD(I)/PSD(1)
   71 SVIS(I)=VIS(I)/VIS(1)
      GO TO 82
   16 IF(III-2) 17,17,18
   17 CONTINUE
      GO TO 82
   18 CONTINUE
   82 CONTINUE
      WRITE(3,100)
      INUM=M+(LL-1)*4
      DO 20 I=1,30
      WRITE(3,101) T1(I),VIS(I),SVIS(I),PSD(I),SPSD(I)
CC    STORE THE DATA IN DISK
      IREC=I+(IMET-1)*60
      IF(III) 86,86,87
   86 WRITE(INUM'IREC) T1(I),VIS(I),SVIS(I),PSD(I),SPSD(I)
      GO TO 20
   87 WRITE(INUM'IREC+30) T1(I),VIS(I),SVIS(I),PSD(I),SPSD(I)
   20 CONTINUE
  100 FORMAT('     TIME ',12X,' VISCOSITY',12X,' N. VIS.   ',12X,
     1'STRESS DIF.',12X,'N.ST. DIF.',/)
  101 FORMAT(F7.3,4E22.4)
  103 FORMAT('1',' THE VALUE OF SHEAR RATE  = ',F9.2,/)
  104 FORMAT(/,' THE VALUE OF PERTURBATION PARAMETER = ',F9.4,/)
      IF(III) 75,75,96
   75 III=1
      WRITE(3,110)
  110 FORMAT(/,10X,'THE VALUES OF STRUCTURE TENSORS',/,10X,
     1'BXX,BXY,BYY,BXZ,BYZ,BZZ',/)
      WRITE(3,111) BXX,BXY,BYY,BXZ,BYZ,BZZ
  111 FORMAT(5X,6E15.4)
C     GO TO 79
   96 III=0
   99 CONTINUE
      IF(III-1) 24,24,97
   24 CONTINUE
      COF1=1.-5.*E(2)
      SR(1)=.01/COF1
      SR(2)=.1/COF1
      SR(3)=1./COF1
      SR(4)=10./COF1
      SR(8)=6.5/COF1
      SR(7)=6.0/COF1
      SR(6)=5.0/COF1
      SR(5)=4.0/COF1
      SR(4)=3.0/COF1
      SR(3)=2.0/COF1
      SR(2)=1.4/COF1
      SR(1)=.7/COF1
      GO TO 98
   97 COF1=1.-5.*E(2)
      SR(1)=.01/COF1
      SR(2)=.1/COF1
      SR(3)=.5/COF1
```

```
      SR(4)=.7/COF1
      SR(5)=1./COF1
      SR(6)=2./COF1
      SR(7)=3./COF1
   98 CONTINUE
      NN=NN+1
      NNN=NN-N
      IF(NNN) 25,26,26
   26 CONTINUE
      GO TO 500
  501 CONTINUE
      CALL EXIT
      END
      SUBROUTINE SHGR
CC    THIS SUBROUTINE CALCULATES THE RIGHT HAND SIDES  OF
CC    EQ.5.22, EQ.5.9, AND EQ.5.19 FOR STRESS GROWTH FOR
CC    SHEAR FLOW.
      COMMON BXX,BXY,BYY,BZZ,BXZ,BYZ
      COMMON F1,F2,F3,F4,F5,F6,SR(8),E(4),M,T,LL
      COMMON C1,IMET
      GO TO (1,2,3),IMET
C1    MNHD
    1 CONTINUE
      AA=1./(1.-E(LL)*(BXX+BYY+BZZ))
      AAA=(1./AA)**C1
      BB=2.*E(LL)*AAA
      GO TO 4
C2    TANNER'S
    2 CONTINUE
      AA=1./(1.-E(LL)*(BXX+BYY+BZZ))
      AAA=(1./AA)**C1
      BB=0.
      GO TO 4
C3    NHD
    3 CONTINUE
      AA=1.+E(LL)*(BXX+BYY+BZZ)
      BB=2.*E(LL)
    4 CONTINUE
      F1=2.*SR(M)*BXY-AA*BXX-BB*(BXX**2+BXY**2+BXZ**2)+1.
      F2=SR(M)*BYY-AA*BXY-BB*(BXX*BXY+BXY*BYY+BXZ*BYZ)
      F5=SR(M)*BYZ-AA*BXZ-BB*(BXX*BXZ+BXY*BYZ+BXZ*BZZ)
      F4=-AA*BZZ-BB*(BXZ**2+BYZ**2+BZZ**2)+1.
      F6=-AA*BYZ-BB*(BXY*BXZ+BYY*BYZ+BYZ*BZZ)
      F3=-AA*BYY-BB*(BXY**2+BYY**2+BYZ**2)+1.
      RETURN
      END
      SUBROUTINE SHRE
CC    THIS SUBROUTINE CALCULATES THE RIGHT HAND SIDES OF
CC    EQ.5.22, EQ.5.9, AND EQ.5.19 FOR STRESS RELAXATION
CC    FOR SHEAR FLOW.
      COMMON BXX,BXY,BYY,BZZ,BXZ,BYZ
      COMMON F1,F2,F3,F4,F5,F6,SR(8),E(4),M,T,LL
      COMMON C1,IMET
      GO TO (1,2,3),IMET
C1    MNHD
```

```
    1 CONTINUE
      AA=1./(1.-E(LL)*(BXX+BYY+BZZ))
      AAA=(1./AA)**C1
      BB=2.*E(LL)*AAA
      GO TO 4
C2    TANNER'S
    2 CONTINUE
      AA=1./(1.-E(LL)*(BXX+BYY+BZZ))
      AAA=(1./AA)**C1
      BB=0.
      GO TO 4
C3    NHD
    3 CONTINUE
      AA=1.+E(LL)*(BXX+BYY+BZZ)
      BB=2.*E(LL)
    4 CONTINUE
      F1=2.*SR(M)*BXY-AA*BXX-BB*(BXX**2+BXY**2+BXZ**2)+1.
     1-2.*SR(M)*BXY
      F2=SR(M)*BYY-AA*BXY-BB*(BXX*BXY+BXY*BYY+BXZ*BYZ)
     1-SR(M)*BYY
      F5=SR(M)*BYZ-AA*BXZ-BB*(BXX*BXZ+BXY*BYZ+BXZ*BZZ)
     1-SR(M)*BYZ
      F4=-AA*BZZ-BB*(BXZ**2+BYZ**2+BZZ**2)+1.
      F6=-AA*BYZ-BB*(BXY*BXZ+BYY*BYZ+BYZ*BZZ)
      F3=-AA*BYY-BB*(BXY**2+BYY**2+BYZ**2)+1.
      RETURN
      END
      SUBROUTINE ELGR1
      COMMON BXX,BXY,BYY,BZZ,BXZ,BYZ
      COMMON F1,F2,F3,F4,F5,F6,SR(8),E(4),M,T,LL
      COMMON C1,INIT
      COMMON AXX,AXY,AYY
      AA=1./(1.-E(LL)*(2.*BXX+BZZ))
      AAA=(1./AA)**C1
      BB=2.*E(LL)*AAA
      BB=0.
      F1=1.-SR(M)*BXX-AA*BXX-BB*BXX**2
      F4=1.+2.*SR(M)*BZZ-AA*BZZ-BB*BZZ**2
      F2=0.
      F3=0.
      F5=0.
      F6=0.
      RETURN
      END
```

C.3 Elongational Viscosity for Elongational Flow (in Chap. 5)

This program solves elongational viscosity by predictor-corrector method.

Description of Main Variables and Program Listing

Variable	Description
S	Elongational rate
DT	Time increment
TLIM	The maximum time limit
XI	α_{xx} after the prediction
ZI	α_{zz} after the prediction
XN, AXX	α_{xx} after the correction
ZN, AZZ	α_{zz} after the correction
EVI, EVO	Elongational viscosity

```
CC    THIS PROGRAM SOLVES ELONGATIONAL VISCOSITY BY THE
CC    THREE MODELS.  THE SOLVING METHOD IS PREDICTOR
CC    AND CORRECTOR.  THE EULER METHOD IS USED FOR PREDICTION
CC    AND NEWTON METHOD IS USED FOR CORRECTION.
      DIMENSION S(2,20),E(2)
      DIMENSION AXX(30),AZZ(30),ELO(30),TT(30)
      COMMON S,TLIM,DT,IP,I,J
      DEFINE FILE 11(360,6,U,ISH01),12(360,6,U,ISH02)
      DEFINE FILE 13(360,6,U,ISH03),14(360,6,U,ISH04)
      DEFINE FILE 15(360,6,U,ISH05),16(360,6,U,ISH06)
      DEFINE FILE 17(360,6,U,ISH07),18(360,6,U,ISH08)
      DEFINE FILE 19(360,6,U,ISH09),20(360,6,U,ISH10)
      DEFINE FILE 21(360,6,U,ISH11),22(360,6,U,ISH12)
      DEFINE FILE 23(360,6,U,ISH13),24(360,6,U,ISH14)
      DEFINE FILE 25(360,6,U,ISH15),26(360,6,U,ISH16)
      C1=1.
      M=3
      L=2
CC    READ INFORMATION
C     IMET=1:    M.N.H.D.
C     IMET=2:    TANNER'S METHOD
C     IMET=3:    N.H.D.
      READ(L,199) IMET
  199 FORMAT(I10)
      GO TO (51,52,53),IMET
   51 WRITE(M,105)
      GO TO 54
   52 WRITE(M,106)
      GO TO 54
   53 WRITE(M,107)
   54 CONTINUE
  105 FORMAT(/,10X,'M.N.H.D. METHOD',/)
  106 FORMAT(/,10X,'TANNERS METHOD',/)
  107 FORMAT(/,10X,'N.H.D. METHOD',/)
      DO 1 I=1,2
      READ(L,200) (S(I,J),J=1,8)
    1 READ(L,200) (S(I,J),J=9,16)
      READ(L,201) (E(I),I=1,2)
      READ(L,202) TLIM,T1,I1,I2,J1,J2
      LL=0
C     LL=0:    GROWTH BEHAVIOR
C     LL=1:    RELAXATION BEHAVIOR
CC    WRITE INFORMATION
      DO 2 I=I1,I2
      DO 3 J=1,16
    3 S(I,J)=S(I,J)/(1.-5.*E(I))
      DO 2 J=J1,J2
      SS=S(I,J)
      WRITE(M,101) E(I),S(I,J)
    5 CONTINUE
      IF(LL) 70,70,71
   70 CONTINUE
      WRITE(M,103)
      WRITE(M,102)
      XO=1.-5.*E(I)
```

```
      ZO=1.-5.*E(I)
      EVI=(XO+ZO*2.)/3./XO
      GO TO 72
   71 CONTINUE
      WRITE(M,104)
      WRITE(M,102)
      XO=XN
      ZO=ZN
   72 CONTINUE
      N=1
      K=0
      T=0.
      AXX(1)=XO
      AZZ(1)=ZO
      ELO(1)=EVI
      TT(1)=T
      CALL PARA1
CC    PREDICTION BY EXPLICIT SCHEME
      IF(LL) 60,60,59
   59 CONTINUE
      S(I,J)=0.
   60 CONTINUE
      GO TO (81,82,83),IMET
   81 CONTINUE
      A=1.-E(I)*(2.*XO+ZO)
      B=A**C1
      GO TO 84
   82 CONTINUE
      A=1.-E(I)*(2.*XO+ZO)
      B=0.
      GO TO 84
   83 A=1./(1.+E(I)*(2.*XO+ZO))
      B=1.
   84 CONTINUE
      XI=XO+DT*(1.-S(I,J)*XO-XO/A)
     1-DT*2.*E(I)*B*XO**2
      ZI=ZO+DT*(1.+2.*S(I,J)*ZO-ZO/A)
     1-DT*2.*E(I)*B*ZO**2
CC    CORRECTION BY IMPLICIT SCHEME (N-R METHOD)
   50 CONTINUE
      GO TO (91,92,93),IMET
   91 CONTINUE
      AI=1.-E(I)*(2.*XI+ZI)
      BI=AI**C1
      FA=2.*E(I)/AI**2
      FB=-2.*E(I)*C1*BI/AI
      GA=E(I)/AI**2
      GB=-E(I)*C1*BI/AI
      GO TO 94
   92 CONTINUE
      AI=1.-E(I)*(2.*XI+ZI)
      BI=0.
      FA=2.*E(I)/AI**2
      FB=0.
      GA=E(I)/AI**2
```

```
      GB=0.
      GO TO 94
   93 AI=1./(1.+E(I)*(2.*XI+ZI))
      BI=1.
      FA=2.*E(I)
      FB=0.
      GA=E(I)
      GB=0.
   94 CONTINUE
      F=XI+DT*S(I,J)*XI+DT*XI/AI-DT-XO
     1+2.*E(I)*DT*BI*XI**2
      G=ZI-2.*DT*ZI*S(I,J)+DT*ZI/AI-DT-ZO
     1+2.*E(I)*DT*BI*ZI**2
      F1=1.+DT*S(I,J)+DT/AI+DT*XI*FA
     1+4.*E(I)*DT*BI*XI+2.*E(I)*XI**2*DT*FB
      G1=1.-2.*S(I,J)+DT/AI+DT*ZI*GA
     1+4.*E(I)*DT*BI*ZI+2.*E(I)*ZI**2*DT*GB
      XN=XI-F/F1
      ZN=ZI-G/G1
      TEST1=ABS((XN-XI)/XI)
      TEST2=ABS((ZN-ZI)/ZI)
      IF(TEST1-T1) 10,10,11
   10 IF(TEST2-T1) 12,12,11
   11 XI=XN
      ZI=ZN
      GO TO 50
   12 T=T+DT
      TX=(XN-XO)/DT+S(I,J)*XN
      TZ=(ZN-ZO)/DT-2.*S(I,J)*ZN
      EVI=(TX-TZ)/(3.*SS*(1.-5.*E(I)))
      K=K+1
      IF(K-IP) 30,31,31
   31 CONTINUE
      T=T*1.000001
      N=N+1
      AXX(N)=XN
      AZZ(N)=ZN
      ELO(N)=EVI
      TT(N)=T
      K=0
   30 CONTINUE
      IF(T-TLIM) 20,20,21
   20 XO=XN
      ZO=ZN
      GO TO 60
   21 CONTINUE
      DO 40 II=1,N
      NR=II+LL*30+(I-1)*60+(IMET-1)*120
      JC=J+10
      WRITE(JC'NR) TT(II),ELO(II)
   40 WRITE(M,100) TT(II),AXX(II),AZZ(II),ELO(II)
      IF(LL) 41,41,42
   41 LL=1
      GO TO 5
   42 LL=0
```

```
    2 CONTINUE
  101 FORMAT('1',10X,'PERTURBATION PARAMETER = ',F10.5,
     1'  :  ELONGATIONAL RATE = ',F10.5,/)
  102 FORMAT(/,10X,'TIME',15X,'ALPHA XX',15X,'ALPHA ZZ',15X,
     1'ELONGATIONAL VISCOSITY',/)
  100 FORMAT(F14.2,2E23.3,E31.3)
  200 FORMAT(8F7.3)
  201 FORMAT(2F10.3)
  202 FORMAT(2F10.5,4I5)
  103 FORMAT(/,5X,'STRESS GROWTH',/)
  104 FORMAT(/,5X,'STRESS RELAXATION',/)
      STOP
      END
      SUBROUTINE PARA1
CC    THIS SUBROUTINE SPECIFIES TIME INCREMENT ACCORDING
CC    TO THE ELONGATIONAL RATES.
      DIMENSION S(2,20)
      COMMON S,TLIM,DT,IP,I,J
      CHECK=S(I,J)-.2
      IF(CHECK) 1,2,2
    1 TLIM=10.
      DT=.02
      IP=25
      GO TO 10
    2 CHECK=S(I,J)-1.
      IF(CHECK) 3,7,7
    3 TLIM=15.
      DT=.01
      IP=60
      GO TO 10
    7 CHECK=S(I,J)-3.
      IF(CHECK) 8,9,9
    8 TLIM=10.
      DT=.01
      IP=50
      GO TO 10
    9 CHECK=S(I,J)-5.
      IF(CHECK) 11,4,4
   11 TLIM=2.
      DT=.01
      IP=10
      GO TO 10
    4 CHECK=S(I,J)-10.
      IF(CHECK) 5,6,6
    5 TLIM=1.
      DT=.005
      IP=10
      GO TO 10
    6 TLIM=1.
      DT=.001
      IP=50
   10 CONTINUE
      RETURN
      END
```

Appendix D: The Convergency of Diagonally Dominant Matrix

Most of numerical problems in finite different scheme are reduced to solving large matrix equations. The matrix equation is written by

$$Ax = b \tag{D.1}$$

where A is the system matrix which described a physical situation, x is an unknown vector to be solved and b is a known vector. In order to understand a diagonally dominant matrix is sufficient for convergency of iterative methods, we use simple Jacobi method for demonstration. In Jacobi method, the matrix A is divided into parts.

$$A = D + C \tag{D.2}$$

The matrix D consists of diagonal elements of the matrix A and the matrix C is off-diagonal elements of the matrix A. A newly calculated vector $x^{(k+1)}$ by iteration is then expressed by

$$Dx^{(k+1)} = b - Cx^{(k)} \tag{D.3}$$

Introducing the exact solution vector $\bar{x}$ of eq. D.1, D.3 becomes

$$\delta x^{(k+1)} = M\delta x^{(k)}$$

where

$$\delta x^{(k)} = x^{(k)} - \bar{x}$$

and

$$M = -D^{-1}C,$$

Taking norm of eq. D.4 in L_∞ space,

$$\| \delta x^{(k+1)} \| \leq \| M^k \| \cdot \| \delta x^{(k)} \| \leq \|M\|^k \cdot \| \delta x^{(o)} \| \qquad \text{D.5}$$

According to eq. D.5, the error from the exact solution is reduced to zero if $\| M \|$ is less than unity and the number of iteration k is sufficiently large. The sufficient condition for convergency is thus

$$\|M\| < 1 \qquad \text{D.6}$$

The matrix M for the Jacobi method is written by

$$|m_{i,j}| = \frac{|a_{i,j}|}{|a_{i,i}|} \qquad \text{for} \quad i \neq j \qquad \text{D.7}$$

$$m_{i,j} = 0 \qquad \text{for} \quad i \neq j \qquad \text{D.8}$$

From eq. D.7 and D.9, the norm of the matrix M in L_∞ is

$$\| M\| \equiv \max_i \sum_j |m,i,j| = \max_i \sum_j \frac{|a_{i,j}|}{|a_{i,i}|} < 1 \qquad \text{D.10}$$

So if the matrix A is a diagonally dominant matrix, the iterative method (Jacobi) for eq. D.1 provides convergency.

Appendix E: The Estimation of the Stream Function at the Exit Hole

From the newly produced force

$$\frac{\partial}{\partial z}\tau_{p,zz}$$

in TABLE 6.6, v_z is expected to increase. To estimate instantaneous change of v_z, we focus on the z-component of the equation of motion around the point (r/R, z/H) = (.03, .01). The equation to be solved is arranged as following introducing time difference formula.

$$\frac{v_z^{N+1}-v_z^{N}}{\Delta t} + v_z^{N+1}\left(\frac{\partial v_z}{\partial Z}\right)^{o} + v_r^{o}\left(\frac{\partial v_z}{\partial r}\right)^{o} = -\frac{1}{\rho}\frac{\partial p}{\partial z}^{o} - \frac{1}{\rho}\frac{\partial}{\partial z}\tau_{p,zz}+g \qquad \text{E.1}$$

And v_z^N is expressed by

$$v_z^{N+1} = \left\{\left[-\frac{1}{\rho}\frac{\partial p^{o}}{\partial z} - \frac{1}{\rho}\frac{\partial}{\partial z}\tau_{p,zz} + g - v_r^{o}\left(\frac{\partial v_z}{\partial r}\right)^{o}\right] + v_z^{N}\Big/\Delta t\right\}\Bigg/ \left[1/\Delta t + \left(\frac{\partial v_z}{\partial z}\right)^{o}\right] \qquad \text{E.2}$$

where v_z^{N+1} is a time advanced velocity and ^{o} indicates the fixed values throughout the iteration. In eq. E.1 and eq. E.2, only axial velocity is assumed to be changed due to the new force

$$-\frac{1}{\rho}\frac{\partial}{\partial z}\tau_{p,zz}$$

while other variables remain constant. Although this assumption may be crude, it might give some adea about how v_z changes because the axial velocity in the dominant term

$$v_z^{N+1}\left(\frac{\partial v_z}{\partial z}\right)^o$$

is treated implicitly and the change of the velocity gradient

$$\left(\frac{\partial v_z}{\partial z}\right)^o$$

may be smaller than that of the axial velocity. The magnitude of the term

$$v_r^o \left(\frac{\partial v_z}{\partial r}\right)^o$$

is smaller than the dominant terms as shown in TABLE 6.6, the change of the term, therefore, may be insignificant.

By choosing $\Delta t = .0001$ second, eq. E.2 is repeated until the time reaches .001 seconds which is about one tenth of the time constant of polyethyrene oxide λ_H. The newly calculated v_z^{N+1} increases about 3% of the original value (at time zero). This rate of increase may be applied to the axial velocity at the point $(r/R, z/H) = (.03, 0)$. The axial velocity, thus, grows -65 cm/sec from -63.1 cm/sec. From the new value, the interpolated stream function is calculated from which the stream function is fixed as boundary condition. Since the axial velocity at $r/R = .03$ represents the average velocity in the zone which covers form $r/R = .02$ to $r/R = .04$ in the Newtonian calculation, the axial velocity used in the calculation in section 6.5 is only 1% increased velocity.

NOMENCLATURE

Symbol	Definition
A	System Matrix
a	Ratio of radius of the Vortex Tank to Liquid Level; $a = R/H$
a	Parameter Used in eq. 3.4
c	Concentration
$\underline{F}$	Force Vector Exerted by Connector Spring
F	General Expression of ψ, Γ, ω
g	Gravitational Acceleration
H	Spring Constant for Hook's Law
H	Liquid Level
k	Boltzmann Constant
Lr	Differential Operator Defined in eq. 3.57
Lz	Differential Operator Defined in eq. 3.57
Lr^*	Discretized Form of Lr
Lz^*	Discretized Form of Lz
M	Molecular Weight
n	Number Density
p	Pressure
$\underline{R}$	Dumbbell Orientation Vector
R	End-to-end Distance of a Polymer Molecule
R_o	Maximum Length of a Polymer Molecule
R	Gas Constant
R	Radius of the Vortex Tank
r	Radial Coordinate in Cylindrical Coordinates